The function of Ana1 in centrosome assembly, and the regulation of centriole growth in *Drosophila*

Saroj Saurya

Sir William Dunn School of Pathology and Lincoln College

University of Oxford

A thesis submitted for the degree of *Doctor of Philosophy*

Trinity 2018

Abstract

The function of Ana1 in centrosome assembly, and the regulation of centriole growth in *Drosophila*

Saroj Saurya

Sir William Dunn School of Pathology and Lincoln College

A thesis submitted for the degree of *Doctor of Philosophy*

Trinity 2018

Centrioles are microtubule-based structures that play a crucial role in the formation of centrosomes, cilia and flagella. Centriole defects are linked to several human diseases such as microcephaly, primordial dwarfism, cancer and ciliopathies. In *Drosophila*, Plk4, Sas-6, Ana2, Sas-4 and Asl form a conserved pathway that is essential for centriole assembly. Ana1 was identified as a potential centriole assembly protein in two genome-wide RNAi screens in *Drosophila* S2 cells, and *ana1* mutant flies are uncoordinated, and their sperm are immotile. Thus, Ana1 appeared to have an important role in centriole assembly, but it was unclear how it functioned in the context of the known assembly pathway.

The primary aim of my thesis was to characterise the function of fly Ana1 *in vivo*. I found that Ana1 is not essential for centriole assembly, but it helps recruit Asl to new-born centrioles to allow them to mature properly so that they can duplicate and organize mitotic PCM. Unexpectedly, I discovered that Ana1 also promotes centriole elongation in a dose-dependent manner. Several centriolar proteins can influence centriole length, but how they do so is unclear. In collaboration with several colleagues in the laboratory, we developed techniques that allowed us, for the first time, to monitor the kinetics of daughter centriole growth in *Drosophila* embryos. We found that Plk4 sets the size of the centriole cartwheel by enforcing an inverse relationship between the cartwheel growth rate and period. I found that Ana1 does not influence cartwheel growth, but I identified several other proteins that do so, most notably CP110 and Cep97, that normally bind to the distal end of the centrioles. These studies have provided several important new insights into how centriole length is regulated.

Acknowledgements

I would like to start by expressing my sincere gratitude to Jordan for giving me the opportunity to work in such a fantastic scientific environment, for believing in me and allowing me to complete my DPhil study alongside my full-time laboratory management work. His guidance helped me throughout my DPhil degree. My DPhil study would have been impossible without his continuous support, his patience, motivation, and immense knowledge, which he provides to all his students whenever needed. I could not have dreamt of a better expert for my DPhil study than Jordan.

I extend my thankfulness to Matthew Freeman, who guided me through the essential basics of proper scientific research, and instilled in me all the necessary qualities of a good scientist during my early scientific career spent in his lab at Cambridge.

All my mentors throughout my academic and professional career- Rameshwar Kamboj Himanshu, Anita Thomas, Rita Rath, Neeraja Sood, Neera Saxena, Rup Lal, Aparna Dixit, Virendra Upadhye, V. S. Narayanan, Harjeet Kaur Khanna, Angus McQuibban, Ariel Blocker, Adrian Hill, Sarah Gilbert, Matt Cottingham, Aroul Ramadass, Alexandre Akoulitchev and Christian Millar for showering their blessings.

I would also like to thank Ulrike Gruneberg as my graduate advisor, Oreste Acuto as my College advisor, Alberto Baena Lopez and Deborah Goberdhan as my DPhil transfer and confirmation assessors for their expert advice during my DPhil studies.

Next, I would like to thank all my fellow lab-mates, past and present Raff Lab members. Thank you for the help, advice and inspiring and stimulating lab discussions about science, for the restless nights spent working together before deadlines throughout the past years, for all the fun we had at tea breaks, lab retreats and organizing social events throughout my studies. I will fondly remember the great laughs and friendships forged over exciting “tea time” conversations. I feel privileged to have worked with very incredible people during my DPhil.

I was fortunate to learn all about confocal, live cell, 3D-SIM and STORM microscopy from Alan Wainman since my first days at the microscopy and for always trying to solve my technical problems with the microscopes, lasers and related issues. This work wouldn’t be the same without a constant source of advice, the help and endless

dedication from Alan Wainman. I was lucky to work, learn and enjoy a great deal from Zsofia Novak, especially concerning RNA preparation, injection work, helpful discussions, motivation and the fun times we had during conferences and the social activities. I thank Mustafa Aydogan for being supportive, valuable, entertaining and the driving force of the centriole elongation project. The state of the project we have now would have been unimaginable without your efforts and hard work. Thomas L. Steinacker, Laura Hankins, Mohammad Mofatteh, Isaac Wong, Sebastian Haddock, Edward Rea, Eline Vanhoutum and Iona Manley for your assistance and bringing cheerfulness into the centriole elongation team. Anna Caballe for organizing all the postdoc association events, looking after Raff lab twitter account and being so supportive and social all the time. Lisa Gartenmann, Ines Alvarez Rodrigo Andreas Haensele and Joey Fisher for making the lab a great place to work.

A special note of thanks to Paul Conduit, Richard Richens and Matthew Cottee, who helped me through my difficult phases, joined with me in my happy times and taught me a great deal. Catarina Vicente for helping me with oocyte activation experiments, bringing joy to the lab and being a great event organizer. Helio Roque, Metta Pratt and Anna Franz for teaching me EM and introducing me to the idea of enjoying life to its full extent whenever possible. Jenny Richens for helping me to settle in the lab in the first place. Nadine Muschalik, Janina Baumbach and Violet Feng for the beautiful time we had at the conference, lab retreats and all the social activities. Boris Sieber, Rachel Humphrey, Adam Volanakis, Kasia Kozyrska, Jonathan Bohlen, Oğuz Kaan Yılmaz, Fatima Arif, Zhaigen Tan, Wonsang Lee, Maria Lobo and Emile for providing the experimental assistance, and leaving an indelible mark in the short period of your stay in the lab.

The Sir William Dunn School of Pathology for providing a pleasing, friendly and enjoyable atmosphere to work. Thanks John Marriot, David and Simon Cooper, for all their IT assistance. Errin Johnson and Adam Costin for all their immense help with EM over all these years. I would especially like to thank the people at the reception, admin staff, the purchasing and finance department, the store, the workshop, the Media kitchen and the Café for all of their massive support all these years. Special thanks to Sonia Muliyil and Pradeep Barak for their continuous help, inspirations and the good times we have spent together. Also I thank all my friends at the Dunn School,

especially Jo Peel, Lucinda Risius, Melissa Wright, Michael Masih, Ashish Dhir, Somdutta Dhir, Michael Dye, Kumi Gibson, Aaron Masih, Michael Barton, Alessia Galasso, Jana Alonso Lorenzo, Lewis Arthurton, Derek Xu, Claire Hill, Sebastian Kittelmann, Ulrike Kuenzel, Patrizia Abrusci, Steven Johnson, Dawn O'Reilly, Eva Gluenz, Annemieke Kok, Philip Cobden, Samantha Knight, Michael Tellier, Clemence Levet, Marina Katash, Rita Richards, Mark Hawks, Martin Wilkins, Audra Giles, Joanne Collett, Sylvina James, Ross Griffiths, Frances Wright, James Lamerton, Gonzalo Ramirez Roman, Paul Fairchild, Elizabeth Bikoff, Fumiko Esashi, Susan Lea, Justin Deme, Ivan Fong, Ivan Boubriak, Kerryanne Crawford, Deeksha Munnur, Osamu Suyari, Nina Sulkowski, Abul Tarafder, Isabel Wassing, Marjorie Fournier, Jane Sharps, Ángela Moncada Pazos, Xin Shen, Iqbal Dulloo, Adam Grieve, Kyojiro Ikeda, Nina Jajčanin Jozić, Sam Dean, Mirvat Surhi, Mehak Mumtaz, Jane Vowles, Joan Monks, Guangyu Liu, Mariya Lobanovska, Alice Ahn, Lucas Kuhlen, Martin Reichhardt, Giulia Masi, Anna-Lisa Lanz, Gytis Jankevicius, Niloofar Karaji, Daniel Fonseca, Letitia Jean, Sreerekha S. Pillai, Nivedita Natarajan, Wayne Swan, Peter Stroud, Bruce Coppen, Martin Osgathorpe, Jason Clifton, Marcus Bottomley, Chris Norbury, Anton van der Merwe, Andrew Jefferson, Archna Shah, Anna Pielach, Michael Boemo, Pedro Carvalho, Shona Murphy, Olga Perestenko, David Vaux, Ivan Ahel, Herman Waldmann, Quentin Sattentau, Conrad Nieduszynski, Dzmitry Batrakou, Sonali Munshaw, William James, Lior Pytowski, Benjamin Dodsworth, Chris Carnie, Phoebe Oldach, Carolin Müller, Satyan Chintawar, Arun Dhillon and Nandita Bodra for their endless encouragement and assistance through out my DPhil study.

I thank the Abcam for supporting all our social activities, CRUK and Wellcome Trust for supporting our research through very generous funding.

I would also like to thank the organizers of EMBO centrosomes and spindle pole bodies conferences, BSCB conferences, and all the people I met during the meetings for their valuable suggestions on my DPhil venture. Special thanks to James Wakefield, Jeroen Dobbelaere, Renata Basto, Harish Chandra Thakur, Pavithra Chavali for coming to my poster and their valuable inputs.

I owe special thanks to an exceptional person, my husband, Shreesh for his continued love, support and understanding during my pursuit of the DPhil degree, which made completion of this thesis possible. You were always around at times I thought it was

impossible to continue, helped me to keep things in perspective and managed home while I was away for my late night experiments, conferences and lab retreats. I appreciate my fantastic son Ishaan who has been the driving force and motivation behind my DPhil studies. I much value his contribution and for always showing patience during my thesis writing. Massive thanks to my parents, Mummy and Papa, for showing their faith in me, and giving me the liberty to choose whatever I desired in my life. You have taught me to achieve my goals through hard work, patience and perseverance. Although you hardly understood what I researched on, you were always willing to support any decision I made in my life. I would also like to credit my brothers, Roshan and Rajesh for their selfless love, care and sacrifice they endured to shape my life. I appreciate my sister-in-laws Kavita, Pritha, Vandana, Siddhi and my brother-in-laws Ateesh and Amit for their support and valuable prayers. Also, I express my thanks to my nieces Sanya, Aashana, Aarshia and Samya and my nephews Arsh and Subh for their affection. My sincere regard goes to my mother-in-law for her prayers, love and moral support. Thanks to Krishan uncle, aunts -Rajo, Rani, Meeli, Bani, Bimla, Jaggo, Kaushal, cousins -Pawan, Satish, Bina and the people in my Village Baljattan for their continued encouragement.

Thanks to my friends Harsh, Kusam, Maninder, Elizabeth, Ghazala, Shweta, Arturo Reyes, Saranya, Marina, Anthony, Niki, Yadvinder, Tatiana, Petros, Yizhong, Wei, Yael, Loredana, Sunny, Simon, Sumi, Iman, Abul, Shruti, Rohit, Sumeeta, Archana, Sanjay, Seema, Pratishtha, Madhu, Anita, Jyotsna, Kavita, Vasudha, Vineeta, Pushpa, Laxmi, Anupam, Shailender, Avmeet, Subhas, Savita, Rachna, Abraham Karpas, Alla, Shashi Rattan, Alison, Farida, Faaizah, Dinesh, Mohit, Meghana, Amit, Shakti and Avnish for bringing joy to my life. Immensely grateful to Bindu Shangari for giving me the hope and confidence to carry on doing my research and writing thesis and for the positive change that she has brought into my life.

I am the luckiest in the world to have a caring family and a group of friends who are always there for me with their love and unconditional support. They have supported me financially and emotionally all my life. I could not have made all the achievements without them. I am very thankful to God for giving me the strength and patience to work with compassion throughout my life. I pray to receive the same in the future.

I would like to dedicate this thesis to my family and friends here in the UK and India.

Publications resulting from this study

Drosophila Ana1 is required for centrosome assembly and centriole elongation

Saroj Saurya, Hélio Roque, Zsofia A. Novak, Alan Wainman, Mustafa G. Aydogan, Adam Volanakis, Boris Sieber, David Miguel Susano Pinto and Jordan W. Raff. Journal of Cell Science (2016) 129, 2514-2525

A homeostatic clock sets daughter centriole size in flies

Mustafa G. Aydogan, Alan Wainman, **Saroj Saurya**, Thomas L. Steinacker, Anna Caballe, Zsofia A. Novak, Janina Baumbach, Nadine Muschalik and Jordan W. Raff. Journal of Cell Biology (2018) 217, 1233–1248

A free-running oscillator times and executes centriole biogenesis

Mustafa G. Aydogan, Thomas L. Steinacker, Mohammad Mofatteh, Lisa Gartenmann, Alan Wainman, **Saroj Saurya**, Paul T. Conduit, Felix Y. Zhou, Michael A. Boemo, Jordan W. Raff.

(Manuscript submitted for publication in Journal of Cell Biology)

Abbreviations

3D-SIM	3D structured-illumination microscopy
aa	Amino acid
ALMS1	Alstrom syndrome protein 1
Ana	Anastral
ana1^{mecB}	Mechanosensory mutant B of Ana1
ANST	Ana2-STIL
APC	Anaphase promoting complex
Asl	Asterless
AU	Arbitrary unit
BB	Basal body
BLAST	Basic Local Alignment Search Tool
BP	Base pair
BSA	Bovine serum albumin
C2CD3	Calcium-dependent lipid-binding domain of protein kinase C
CA	Centrosome amplification
CaMKII	Ca2+/calmodulin-dependent protein kinase II
CC	Coiled-coil
Cdc25	Cell division cycle 25 (also called String)
Cdk	Cyclin-dependent kinase
Centrobin	Centrosomal BRCA2 interacting protein
Cep	Centromal protein
Ce	Caenorhabditis elegans
Chk	Check-point kinase
CID	Cartwheel Inner Density
CM2	Cnn-motif 2
Cnn	Centrosomin
Co-IP	Co-immunoprecipitation
CP	Centrosomal protein
CPAP	Centromal P4.1-associated protein
CPB	Cryptic Polo Box
CR	Conserved Region

Cr	Chlamydomonas reinharttii
CT	C-terminus
CP100	Centrosomal protein of 110 kDa
DDC8	Differential display clone 8
DEST	Destination vector
DGRC	*Drosophila* Genomics Resource Centre
DNA	Deoxyribonucleic acid
DRE	Downstream regulatory element
DTT	Dithiothreitol
E	Endogenous promoter of the gene
ED	Emission discrimination mode
EDTA	Ethylenediaminetetraacetic acid
EM	Electron microscopy
EMS	Ethyl methanesulfonate
ER	Endoplasmic reticulum
ET	Electron Tomography
FBXW5	F-Box And WD-40 Repeat Domain Containing 5
FL	Full length
FRAP	Fluorescence recovery after photobleaching
FS	Fast sequential capture mode
GFP	Green fluorescent protein
GMC	Ganglion mother cell
GSC	Germline stem cell
GTU88	Gamma Tubulin antibody, Clone GTU88
H/hr/hrs	Hours
HRP	Horseradish peroxidase
IF	Immunofluorescence
IPTG	Isopropyl b-D-1-thiogalactopyranoside
K	Kilo (1000)
kDa	Kilo Dalton
KEN	Consensus sequence of KEN amino acids (Lysine,Glutamic Acid, Asparagine)
KIAA	Beginning of the gene code at Kazusa cDNA sequencing project
KIFs	Kinesin superfamily proteins
Klp10A	Kinesin-like protein at 10A

l	Litre
M	Molar
MAPs	Microtubule associated proteins
MCPH	Microcephaly Primary Hereditary (Autosomal Recessive Primary Microcephaly)
MD	Motor domain
μg	Micrograms
Min	Minutes
Ml	Millilitre
MM	Millimolar
mRNA	Messenger ribonucleic acid
MTOC	Microtubule organising centre
MTs	Microtubules
MW	Molecular Weight
Myt1	Myelin transcription factor 1
NEB	Nuclear envelope breakdown
NT	N-terminus
OFD1	Orofaciodigital Syndrome1
ORC	Origin recognition complex
PACT	Pericentrin-AKAP450 centrosome targeting domain
PAGE	Polyacrylamide gel elctrophoresis
PB	Polo box
PBS	Phosphate buffer saline
PCL	Proximal centriole-like
PCM	Pericentriolar material
PCR	Polymerase chain reaction
PICA	Present in C-terminal of Ana-1
PISA	Present in SAS-6 (motif)
Plk	Polo-like kinase
PLP	Pericentrin like protein
POC	Proteome of the centriole
PSIPRED	PSI-blast based secondary structure PREDiction
r	Spearman correction coefficient
RFP	Red fluorescent protein
RKA	Reduce Kinase activity

RNAi	RNA interference
ROI	Region of interest
RPE-1	Retinal pigment epithelial (human cells)
RT	Room temperature
S/sec	Seconds
S2	Schneider 2
SAC	Spindle assembly checkpoint
Sak	Serine/threonine-protein kinase Plk4
SAP	Dsas-6/ana2 particle
SAS	Spindle Assembly Abnormal
SCF-βTrCP	Skp, Cullin, F-box, β-transducing repeat-containing protein complex
SD	Standard deviation
SDS-PAGE	Sodium Dodecycl Sulphate- Polyacrylamide Gel Electrophoresis
SEM	Standard error of mean
SPD/Spd	Spindle defective
SPICE1	Spindle and centriole associated protein 1
STAN	STIL/Ana2 domain
STIL	SCL/TAL1 interrupting locus
TBS	Tris buffered saline
TCP	TCP10 or T-complex 10 (domain)
TEM	Transition electron microscopy
TIM	Truncated in Microcephaly
Tp	Time point
TTBK2	Tau-tubulin kinase-2
U/Ubq	Ubiquitin
U2OS	Human Bone Osteosarcoma Epithelial Cells
UAS	Upstream activating sequence
USP33	Ubiquitin Specific Peptidase 33
WD40	Short structural motif of approximately 40 amino acids, often terminating in a tryptophan-aspartic acid (W-D) dipeptide
WT	Wild type
Y2H	Yeast- two-hybrid
Zeo	Zeocin
ZYG	Zygotic defective

Table of Contents

Abstract III

Acknowledgements V

Publications resulting from this study IX

Abbreviations XI

Table of Contents XV

Chapter 1: Introduction 1

1.1: Centrioles, centrosomes and cilia 1
1.2: The architecture of centrioles, basal bodies and axonemes 3
1.3: Centriole ultrastructure 6
1.4: Core centriole duplication factors in *C. elegans*, humans and *Drosophila* 8
1.4.1: ZYG-1/Sak/Plk4 11
1.4.2: SAS-6/Sas-6 14
1.4.3: SAS-5/Ana2/STIL 16
1.4.4: SAS-4/Sas-4/CPAP 18
1.4.5: Asl/Cep152 20
1.4.6: Cep135/Bld10 22
1.5: The regulation of Centriole length 25
1.5.1: The Centriole elongation process 26
1.5.2: Proteins that promote centriole growth 28
1.5.3: Proteins that suppress centriole growth 29
1.5.4: Other potential regulators of centriole length 32
1.6: The function of Ana1/Cep295 in centriole assembly 32
1.7: *Drosophila* embryo as a model system to study centrosome formation 35
1.8: *Drosophila* testes as a model system to study centriole formation 37
1.9: Thesis Summary 40

Chapter 2: Materials and Methods 43

2.1: Fly husbandry 43
2.1.1: Fly handling 43
2.1.2: *Drosophila* stocks 43
2.1.2.1 Generation of Transgenic lines 44
2.1.2.2 Generation of Cilia rescue flies 44
2.1.3: Assessing the hatching rate of embryos 44
2.1.4: Assessing the fertility of male adult flies 45
2.2: Antibodies used in this thesis 45
2.3: Molecular Biology 46
2.3.1: Purification of genomic DNA from *Drosophila* 46
2.3.2: Cloning of vectors to generate transgenic fly lines 47
2.3.3: Plasmid mutagenesis 48
2.3.4: Construction of vectors for *in vitro* RNA production (for RNA-microinjection experiments) 49
2.4: Biochemistry 51
2.4.1: Preparation of *Drosophila* embryo, brain, wing disc and testes lysates for protein expression analysis 51
2.4.2: Electrophoresis and Western blotting 52

2.4.3: Labelling of Antibody for microinjection 53
2.4.4: Fold increase calculation of the overexpressed proteins 53
2.5: Cell Biology 54
2.5.1: Preparation of embryos or fly testes for live imaging analysis 54
2.5.2: Microinjection of antibodies or RNA into living embryos 54
2.5.3: Immunofluorescence staining of eggs or embryos 55
2.5.4: Fixation and staining of *Drosophila* tissues for immunofluorescence analysis 55
2.6: Microscopy 57
2.6.1: Live confocal imaging of *Drosophila* embryos and testes 57
2.6.2: Immunofluorescence imaging of fixed *Drosophila* eggs/embryos/brains/testes 58
2.6.3: Super-resolution imaging of fixed *Drosophila* testes 58
2.6.4: Transmission electron microscopy 59
2.7: Image analysis and statistics 59
2.7.1: Quantification of centrosomes in larval brain cells and centriole in pupal testes cells 59
2.7.2: Quantification of centriole length in testes 60
2.7.3: Quantification of *de novo* centriole formation in unfertilised eggs 60
2.7.4: Analysis of live imaging data, acquired on the Perkin Elmer ERS spinning Disc confocal system 61
2.7.5: Analysis of data acquired on the OMX V3 super-resolution imaging system 62
2.7.6: Quantification of GFP or SAPs fluorescence in live embryo or laid eggs or pupal testes 63
2.7.7: Centriole length measurement in *Drosophila* wing disc cells 64
2.7.8: Statistical analysis 64
2.7.9: Image manipulation and presentation 65

Chapter 3: The role of Ana1 in centrosome assembly 67

3.1: Introduction 67
3.2: Results 69
3.2.1: Initial characterization of the *ana1* gene and generation of transgenic lines expressing GFP-Ana1 fusion proteins 69
3.2.2: Ana1 is required for the assembly and/or maintenance of centrioles and centrosomes 72
3.2.3: The N-terminal region of Ana1 does not appear to be essential for centriole assembly and/or maintenance 74
3.2.4: The overexpression of Ana1 does not detectably drive *de novo* centriole assembly or centriole over-duplication 78
3.2.5: Ana1 does not appear to be essential for the assembly of the central cartwheel 80
3.2.6: Ana1 is required to recruit Asl to SAPs 83
3.2.7: Antibody injection experiments suggest that Ana1 helps recruit Asl specifically to newly forming mother centrioles 88
3.2.8: Ana1 molecules are asymmetrically oriented within the centriole, and the C-terminal regions of Asl and Ana1 are in close proximity 91
3.2.9: A structure/function analysis of Ana1 94
3.2.10: Attempts to narrow down the regions of Ana1 required for its centriolar localization and its ability to recruit Asl 98
3.2.11: Ana1 levels influence centriole length, and this activity requires the N-terminal region 101
3.2.12: Ana1 levels influence centriole length in wing disc cells 106
3.3: Discussion 109

Chapter 4: The regulation of centriole length 115

4.1: Introduction 115

4.2: Results **121**
4.2.1: Measuring the dynamics of daughter centriole growth in living fly embryos using a Sas-6-GFP incorporation assay 121
4.2.2: Plk4 influences the rate and period of daughter centriole growth in living fly embryos 125
4.2.3: Overexpressing Plk4 increases the period of daughter centriole growth, but does not alter the rate of growth 127
4.2.4: Reducing the kinase activity of Plk4 reduces the rate of daughter centriole growth, but does not alter the period of growth 129
4.2.5: Examining the potential role of centriole growth promoting factors in cartwheel growth dynamics. 130
4.2.6: Examining the potential role of centriole distal-end binding proteins in regulating cartwheel growth 133
4.2.7: Reducing the levels of CP110 and Klp10A changes the parameters of cartwheel growth 136
4.2.8: CP110 and Cep97 levels influence centriole cartwheel growth rate and growth period 139
4.2.9: Structure/function analysis of Klp10A 142
4.3: Discussion **145**

Chapter 5: The potential influence of cell cycle regulators on centriole cartwheel growth **153**

5.1: Introduction **153**
5.2: Results **157**
5.2.1: Centriole growth parameters appear to be influenced by the basic cell cycle oscillator in early *Drosophila* embryos 157
5.2.2: Assessing the role of the basic cell cycle machinery in regulating the parameters of cartwheel growth 159
5.2.3: Myt1, Wee1, Twine and String are not detectably concentrated at the centrioles in early *Drosophila* embryos 166
5.3: Discussion **169**

Chapter 6: Discussion **173**

6.1: The function of Ana1 in flies **173**
6.2: The regulation of centriole length in flies **176**

Publications **181**

Appendix **183**

Tables **185**

References **213**

Chapter 1: Introduction

1.1: Centrioles, centrosomes and cilia

The centriole is a microtubule (MT)-based cylinder-shaped structure that acts as a template for the formation of centrosomes, cilia and flagella in eukaryotes (Figure 1.1). Centrioles are absent from most fungi, conifers and flowering plants but are present in the male gametes of green algae, mosses, liverworts and hornworts, seedless vascular plants, cycads, and ginkgo (Azimzadeh, 2014). It is therefore thought that centrioles were present in the last eukaryotic common ancestor (LECA) but subsequently were lost in certain evolutionary phyla.

The centrosome consists of a pair of orthogonally arranged centrioles surrounded by a complex proteinaceous structure called the pericentriolar material (PCM) (Figure 1.1A). The centrosome is the principal microtubule organising centre (MTOC) in the animal cell, higher fungi and several eukaryotes and it has important roles in regulating spindle formation, chromosome segregation, cytokinesis, cell shape, polarity and motility (Bornens, 2012; Conduit and Raff, 2015; Fu et al., 2015; Nigg and Raff, 2009). Cilia play important roles in sensing and generating liquid flow, sensing the surrounding environment and they host components of several important signalling pathways (Wheway et al., 2018). Unsurprisingly, centriole defects have been linked to many human diseases, for example microcephaly, primordial dwarfism, cancer and a host of complex ciliary defects collectively termed ciliopathies (Bettencourt-Dias et al., 2011; Braun and Hildebrandt, 2017; Chavali et al., 2014; Gönczy, 2015; Schatten and Sun, 2015). It is therefore essential to understand how centrioles are assembled and how their numbers are controlled.

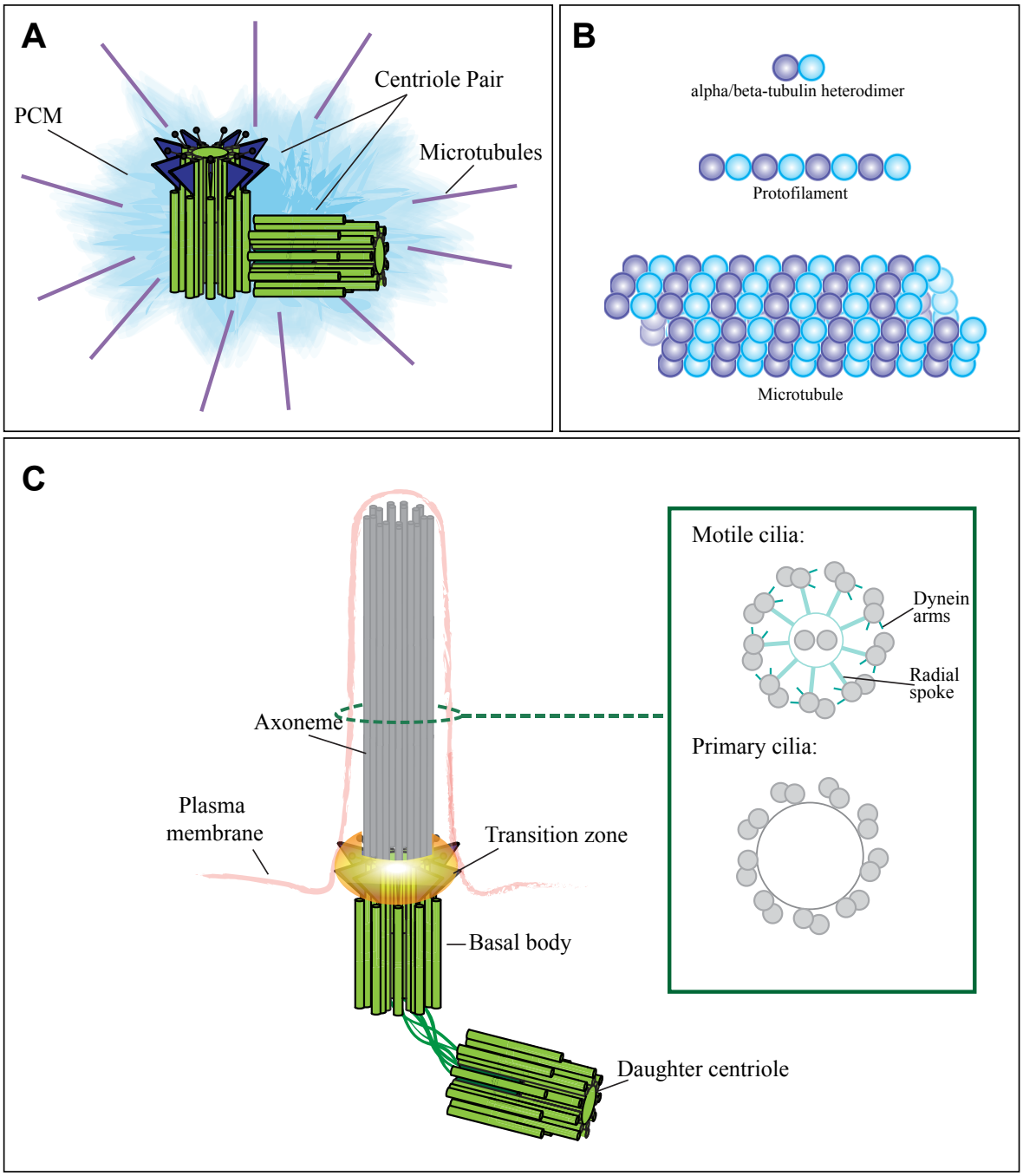

Figure 1.1: Centriole, Centrosome and cilia. (A) Schematic shows a centrosome with a central orthogonally arranged centriole pair surrounded by pericentriolar material (PCM). **(B)** Schematic shows α- and β-tubulin heterodimers (*purple* and *blue* respectively), the proto-filaments they form, and MTs that assemble from 13 protofilaments arranged into a hollow, cylindrical structure. **(C)** Schematic shows a mother centriole serving as the basal body of a cilium. The axoneme of the cilium consists of MT doublets arranged in different patterns depending on the type of cilium, as illustrated in the boxed region: Top, the 9+2 arrangement in motile cilia with dynein arms, radial spoke and a central MT pair; Bottom, the 9+0 arrangement in non-motile/primary cilia with no central pair. Illustrations are modified from original drawings of Lisa Gartenmann.

1.2: The architecture of centrioles, basal bodies and axonemes

The core structure of centrioles is highly conserved across evolution with occasional species-specific deviations (Banterle and Gönczy, 2017; Carvalho-Santos et al., 2011; Gupta and Kitagawa, 2018; Winey and O'Toole, 2014) (Figure 1.2). Centrioles usually vary in length from ~100-500nm and in width from ~100-250nm (Azimzadeh and Marshall, 2010; Gönczy, 2012; Gupta and Kitagawa, 2018; Winey and O'Toole, 2014). At their core, centrioles possess a radial nine-fold symmetrical structure known as the cartwheel that is connected to nine sets of outer MT blades arranged circumferentially as either singlets (A-tubules, Figure 1.2A), doublets (A and B tubules, Figure 1.2B) or triplets (A, B and C tubules; Figure 1.2C), depending on the species and cell type (Azimzadeh and Marshall, 2010; Delattre and Gönczy, 2004; Gönczy, 2012; Gupta and Kitagawa, 2018). These MTs are arranged with an anticlockwise twist when viewed from the proximal end (Gupta and Kitagawa, 2018; Uzbekov and Prigent, 2007). The A-tubule consists of a complete MT of 13 protofilaments, to which two successive ten protofilament B- and C-MTs are assembled (Linck and Stephens, 2007) (Figure 1.2C). Each protofilament mostly consists of α/β tubulin dimers (Figure 1.1B). The A-MT from one triplet is connected with the C-MT of the next triplet via a so-called A–C linker (Figure 1.2C).

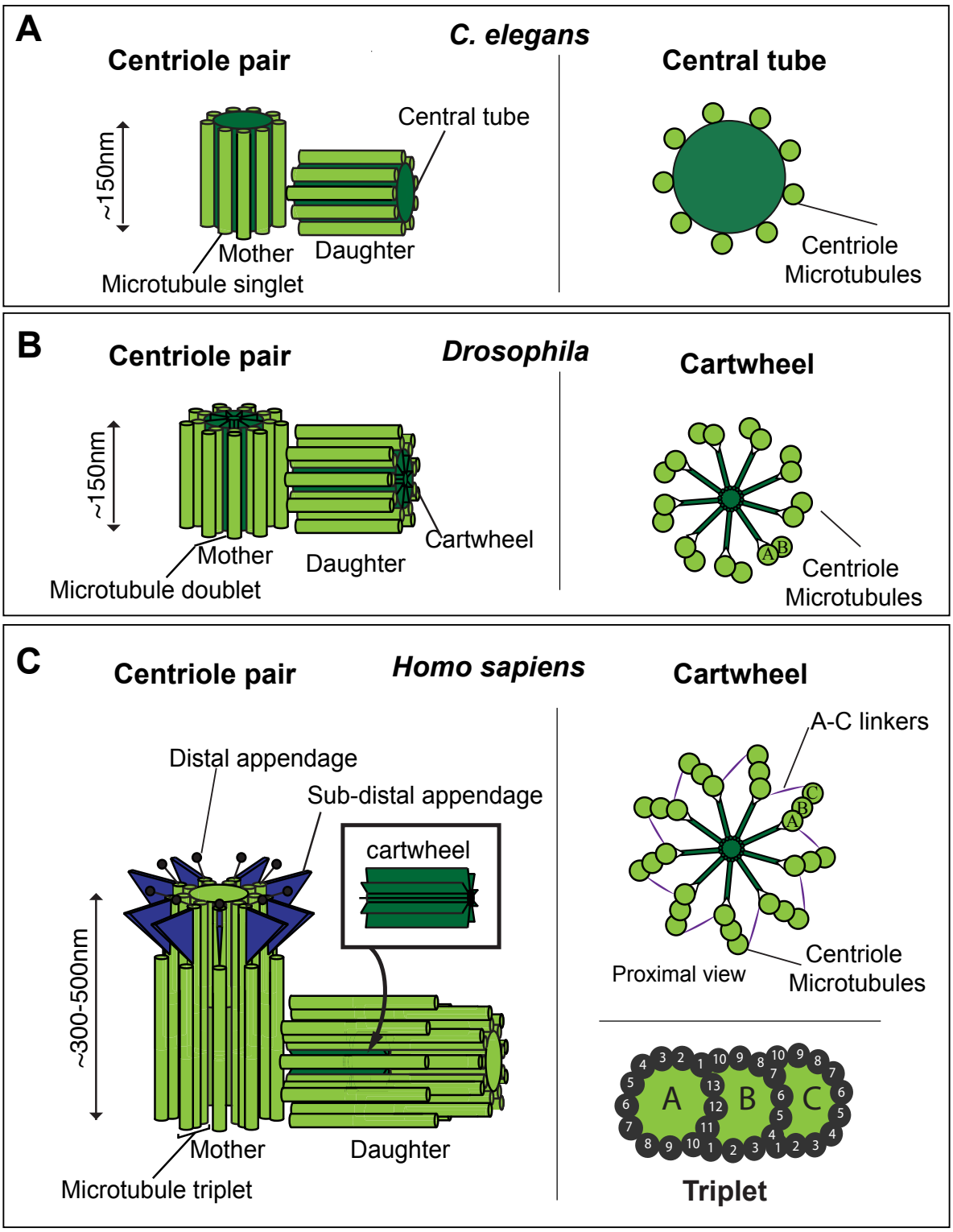

Figure 1.2: A centriole structures across various model organisms. (A) Schematic illustration of a *C. elegans* centriole pair with central tube and nine MT singlets. **(B)** Schematic illustration of a *Drosophila* centriole pair with cartwheel and nine MT doublets. **(C)** Schematic illustration of a human centriole pair with cartwheel, nine MT triplets that form doublets at the distal end, which is also decorated with distal and sub-distal appendages. Schematic at Bottom right illustrates a MT triplet: The A tubule comprises a complete cylinder made up of 13 protofilaments while the B and C tubules are incomplete and contain only 10 protofilaments. Figures have been modified from (Conduit and Raff, 2015).

In vertebrates, the distal wall of a fully mature centriole carries two sets of appendages (Figure 1.2C): sub-distal appendages, which are necessary for securing cytoskeletal MTs (Bornens, 2002; Uzbekov and Alieva, 2018) and distal appendages, which are required for membrane docking during ciliogenesis (Ishikawa et al., 2005; Uzbekov and Alieva, 2018). These structures are not detectable in the centrioles of flies or worms, although these simpler centrioles can still organise functional cilia. The fully matured centriole is called the “mother”, while the younger centriole that lacks appendages, and will only acquire the appendages during G2/M-phase of the following cell cycle, is called the “daughter” (Vorobjev and Chentsov YuS, 1982). In vertebrates, the cartwheel is lost from the proximal part of the newborn centrioles at the end of the cell cycle, generating a stable ‘‘cartwheel-less’’ mother centriole that can serve as a template for new daughter centriole assembly (Arquint and Nigg, 2014; Arquint et al., 2012; Fong et al., 2014; Strnad et al., 2007; Tang et al., 2011; Vorobjev and Chentsov YuS, 1982; Vorobjev and Chentsov, 1980).

The centrioles of *Drosophila melanogaster* are relatively simple and exhibit significant variability in their length and architecture during different developmental stages (Callaini et al., 1997; González et al., 1998; Gottardo et al., 2015b; Gupta and Kitagawa, 2018). The centrioles in embryos and most somatic cells of *Drosophila* are composed of MT singlets or doublets rather than triplets and do not have distinct distal or sub-distal appendages (Callaini et al., 1997; Jana et al., 2016a; Nigg and Raff, 2009) (Figure 1.2B). The cartwheel structure in *Drosophila* centrioles extends throughout the length of the centriole, and is not lost when daughter centrioles are converted to mother centrioles (Lattao et al., 2017). This feature of *Drosophila* centrioles will be important for the work described in the last two Chapters of this thesis.

In most vertebrate quiescent cells, the linked mother and daughter centrioles move to the plasma membrane where the mother centriole docks via distal appendages to serve as a basal body to initiate cilia or flagella formation. The basal bodies of cilia or flagella contain 9 MT triplets, whereas the extended ciliary axonemes consist of 9 outer MT doublets (extensions of the A and B tubules of the basal body) and two central MT singlets (a “9+2” arrangement) (Figure 1.1C). Motile cilia can be used to generate liquid flow, such as in respiratory epithelium or the fallopian tubes, while flagella that are present in unicellular “ciliates” or in many vertebrate sperm cells are often used for locomotion. In contrast, axonemes of immotile cilia are usually made of the same 9 MT doublets, but they lack the central pair of MTs (a “9+0” arrangement; (Fliegauf et al., 2007). Non-motile or primary/sensory cilia are used for sensing of the extracellular environment, and intercellular signalling (Goetz and Anderson, 2010; Wheway et al., 2018).

1.3: Centriole ultrastructure

The cartwheel is the first structure that can be observed to form during centriole duplication (Dippell, 1968), and it was first observed by EM in the centriole of unicellular termite symbiont *Trichonympha*, which have very long centrioles, with a cartwheel that essentially extends throughout the length of the centriole (Gibbons and Grimstone, 1960). This elongated structure recently allowed Guichard, et al. to obtain relatively high-resolution Cryo-EM tomography reconstructions of the cartwheel structure, together with its associated triplet MTs (Figure 1.3D, top view) (Guichard et al., 2017; 2010; 2012; 2013; 2018). The cartwheel comprises a central hub, 20–25 nm in diameter, and nine 40–45 nm-long spokes that emanate radially outwards from this hub (Allen, 1969). At the end of each spoke, and just before the MT triplets, culminates the pinhead (Guichard et al., 2013; Hiraki et al., 2007; Hirono,

2014). The central hub of the cartwheel comprises a stack of rings exhibiting a vertical periodicity of 8.5 nm and the spokes from two rings merge vertically, two by two, to form a “double ring” repeating unit with 17nm periodicity (Guichard et al., 2010). A pinbody and two more peripheral pinfeet-1 and -2, both contact the A-MT (Figure 1.3C and D). Furthermore, a Cartwheel Inner Density (CID), also exhibiting a radial nine-fold symmetry, was found within the confines of the central hub and the native structure of the A-C linker that connects adjacent MT triplets is also polarized along the proximal-distal centriole axis (Guichard et al., 2017; 2018).

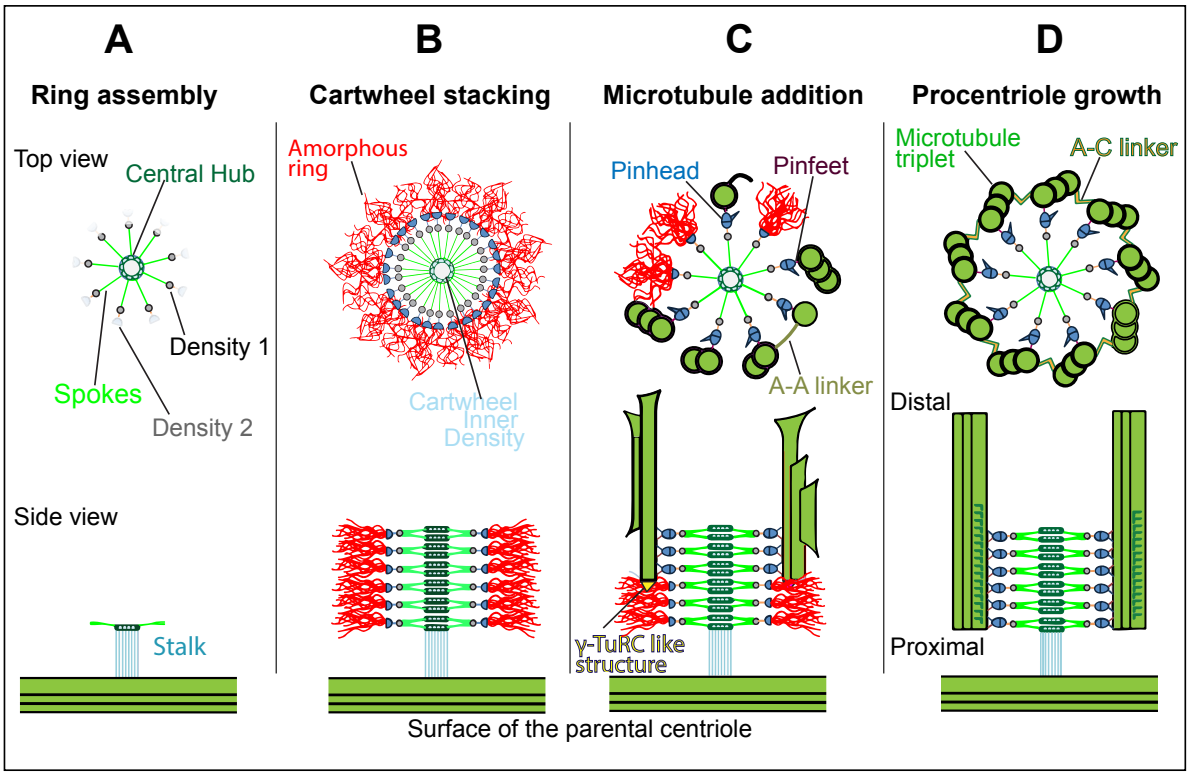

Figure 1.3: A model of cartwheel and procentriole assembly in *Chlamydomonas*. (A) SAS-6 homodimers self-assemble into rings through interactions of their N-terminal domains, and they initially attach to the mother centriole through a stalk structure. **(B)** Interaction of SAS-6 with the C-terminal domain of Bld10/Cep135 promotes stacking of the SAS-6 rings. In the absence of MTs, the Bld10/Cep135 N-terminal domain is disorganised, generating an amorphous ring around the SAS-6 rings. **(C)** The N-terminal domain of Bld10/Cep135 interacts with an A-MT and this stabilises the connecting pinhead structure. The B- and C- MTs assemble stochastically at the surface of the A- and B- MTs, respectively. **(D)** Eventually a fully built procentriole with cartwheel, pinhead elements and A-C linkers connecting the MT triplets is assembled. Model is modified from (Guichard et al., 2018).

A recent Cryo-ET analysis of isolated *Chlamydomonas reinhardtii* (Cr) procentrioles was able to infer a structural map of procentriole structure during the growth process

(Figure 1.3). This analysis revealed that the most proximal region of the daughter centriole initially harbours an amorphous ring surrounding the core cartwheel with no pinhead or MTs (Figure 1.3B); the middle region contains a cartwheel and pinhead attached to a mixed number of MTs (singlets, doublets or triplets) (Figure 1.3C); the distal region lacks a cartwheel, but harbours pinheads and MTs (Guichard et al., 2017; 2018) (Figure 1.3D). According to Guichard et al., cartwheel and procentriole assembly begins with the homo-dimerization and self assembly of nine monomers of Cr Spindle ASsembly abnormal-6 (SAS-6) proteins to the ring, via it's N-terminus domains (Figure 1.3, step A). Thereafter, the C-terminus of CrSAS-6 and Bld10p (or Centrosomal protein of 135 kDa, Cep135) promotes the formation of stacks to generate the amorphous ring (Figure 1.3, step B). Subsequently, the N-terminal domain of Bld10/Cep135 helps assemble the A-MT and triggers a conformational change to form the pinhead (Figure 1.3, step C). Finally, the B- and C- MTs are added along with A-C linkers connecting the MT triplets, completing the assembly of the procentriole around the cartwheel (Guichard et al., 2018) (Figure 1.3, step D).

1.4: Core centriole duplication factors in *C. elegans*, humans and *Drosophila*

Forward genetic and RNA interference (RNAi)-based functional genomic screens in *Caenorhabditis elegans* (*C. elegans*) identified five core proteins that are essential for centriole duplication (Dammermann et al., 2004; Delattre et al., 2004; Kemp et al., 2004; Kirkham et al., 2003; Leidel and Gönczy, 2003; Leidel et al., 2005; O'Connell et al., 2001; Pelletier et al., 2006; 2004) (Figure 1.4A). The coiled-coil protein SPindle Defective 2 (SPD-2), recruits the ZYGote defective embryonic lethal (ZYG-1) protein kinase that, in turn, recruits the Spindle ASsembly abnormal (SAS) proteins SAS-6

and SAS-5 to form the central tube (a structure equivalent to the cartwheel in other organisms). The central tube then elongates and increases in diameter. SAS-4 is then required to assemble or maintain nine singlet MTs onto the central tube.

These five proteins form a conserved “core” of centriole assembly proteins that are evolutionarily conserved in many species including humans and *Drosophila* (Conduit et al., 2015a; Dong, 2015) (Figure 1.4B). In flies, Asterless (Asl), rather than SPD-2, initiates the recruitment of the protein kinase Plk4/Sak (hereafter Plk4) to the side of the mother centriole (Blachon et al., 2008; Dzhindzhev et al., 2010). In vertebrates, homologues of both proteins—Cep192/SPD-2 and Cep152/Asl—play a part in this process (Hatch et al., 2010; Kim et al., 2013; Park et al., 2014; Sonnen et al., 2013). The Plk4 kinase family seems to play a widely conserved role in initiating centriole assembly, but they appear to have evolved independently of ZYG-1, making them functional orthologues, rather than homologues (Dong, 2015; Jana et al., 2012). Plk4 then recruits Anastral Spindle 2 (Ana2) in flies, or its homologue SCL/TAL1 interrupting locus (STIL) in humans—which are both distantly related to SAS-5 (Stevens et al., 2010a)—and Sas-6, which forms the structural core of the cartwheel structure (Hilbert et al., 2013; Kitagawa et al., 2011b; van Breugel et al., 2011; 2014). Finally Sas-4/human centrosomal P4.1-associated protein (CPAP) (Basto et al., 2006; Dammermann et al., 2008; Delattre et al., 2006; Hung et al., 2000; Kirkham et al., 2003; Kohlmaier et al., 2009; Leidel and Gönczy, 2003; Pelletier et al., 2006) is recruited to the outer region of the cartwheel where, perhaps together with Cep135/Bld10 (Hiraki et al., 2007; Hirono, 2014; Matsuura et al., 2004), it helps to recruit the centriole MTs. I discuss what is known about the structure of these core proteins and their role in the assembly process in more detail below.

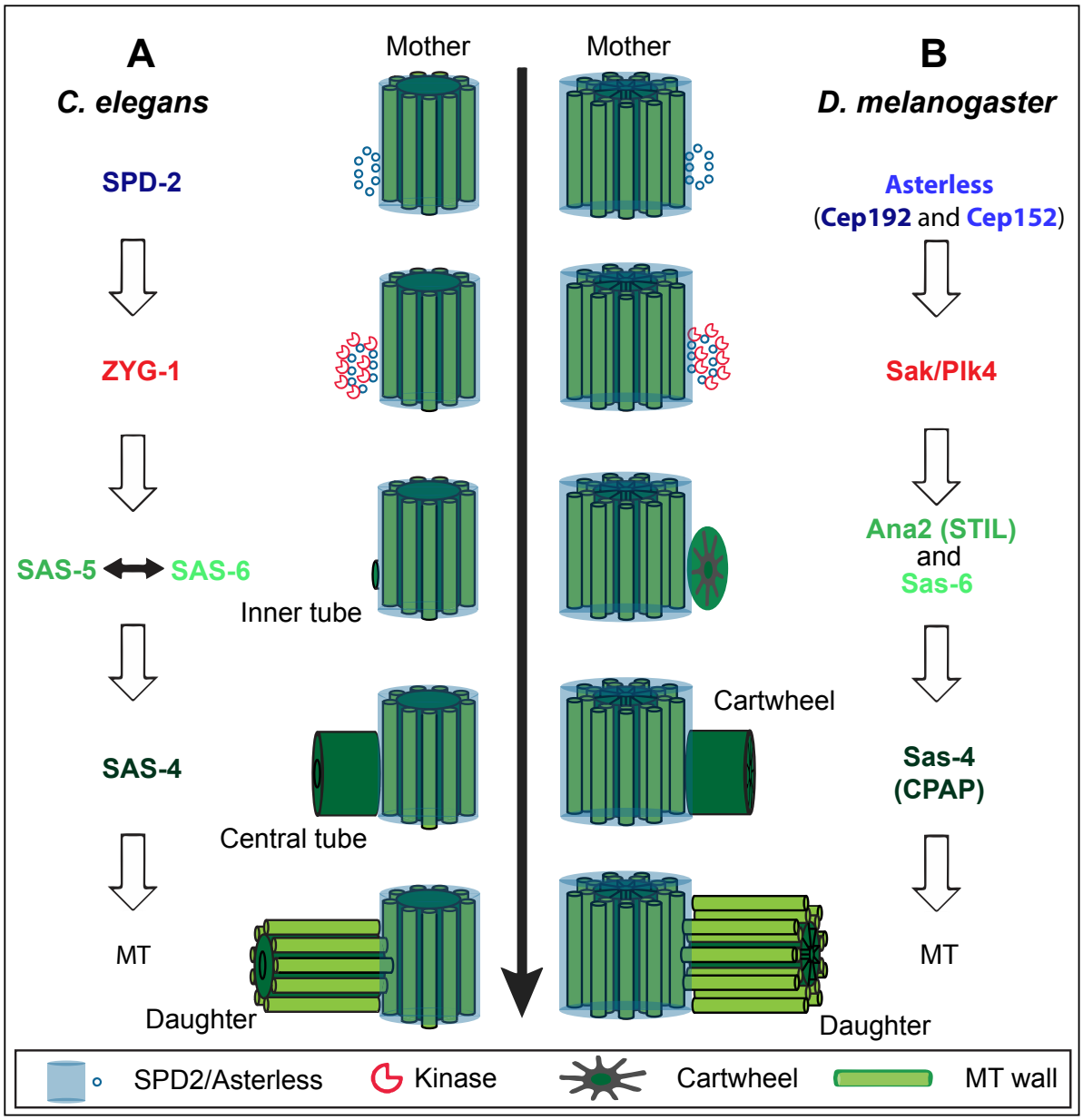

Figure 1.4: The centriole assembly pathway in *C. elegans* and *D. melanogaster*. (A) In *C. elegans*, centriole assembly is initiated when SPD-2 is recruited to the mother centriole (illustrated as a "haze" around the centriole, with molecules at the single site of daughter centriole assembly shown individually). SPD-2 then recruits ZYG-1 to the site of daughter centriole assembly, which in turn recruits SAS-5/SAS-6 to form the inner tube (the worm equivalent of the cartwheel). SAS-5/SAS-6 promotes SAS-4 recruitment and generation of the outer tube called central tube. Finally, the nine singlet MTs are assembled around the outer tube generating the MT wall. This pathway is well defined genetically in worms (Leidel and Gönczy, 2005; Pelletier et al., 2006). **(B)** The centriole assembly pathway in *D. melanogaster*. A very similar pathway can be inferred with functional homologues of the worm proteins, although flies use Asterless to recruit Plk4. In humans, homologues of both proteins—Cep192/SPD-2 and Cep152/Asl (shown in brackets)—play a part in this process. Plk4 then recruits Ana2, a distantly related protein to SAS-5 (STIL in humans, shown in brackets) and Sas-6, that forms the cartwheel structure. Finally, Sas-4 (CPAP in humans, shown in brackets) helps to recruit the MT wall. The protein with the same colour are homologues or orthologous.

1.4.1: ZYG-1/Sak/Plk4

ZYG-1/Sak/Plk4 are serine/threonine protein kinases that are widely believed to be the master regulators of the centriole assembly pathway (Bettencourt-Dias et al., 2005; Habedanck et al., 2005; Kleylein-Sohn et al., 2007; O'Connell et al., 2001; Pelletier et al., 2006). Plk4 contains a conserved N-terminal kinase domain, followed by two central tandem polo-boxes (PB1 and PB2), and then a third polo box (PB3) towards its C-terminus (Figure 1.5). In most Plk family members PB1 and PB2 form the Polo-Box-Domain (PBD) that targets them to different subcellular locations by interacting with phosphorylated epitopes in other proteins (Cizmecioglu et al., 2010; Dzhindzhev et al., 2010; Hatch et al., 2010; Kim et al., 2013; Klebba et al., 2015b; Sonnen et al., 2013). The PBD in Plk4 is divergent (and was originally referred to as a “cryptic” PB), and it does not seem to bind to phosphorylated target proteins (Lowery et al., 2005; Park et al., 2014), although this domain is required for the interaction with Asl/Cep152 and SPD-2/Cep192 (Delattre et al., 2006; Dzhindzhev et al., 2010; Kim et al., 2013; Park et al., 2014; Pelletier et al., 2006; Shimanovskaya et al., 2014; Slevin et al., 2012; Sonnen et al., 2013).

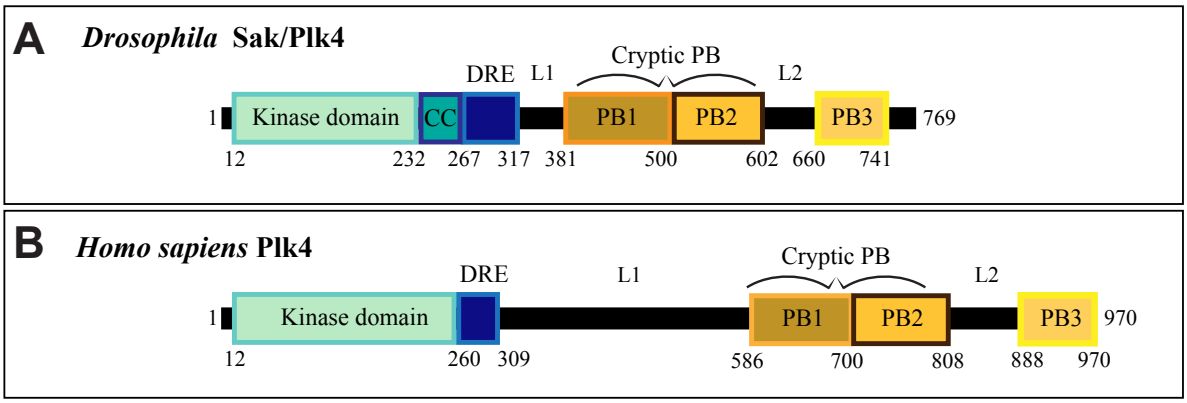

Figure 1.5: Plk4 protein domains in *Drosophila* and humans. (A) Schematic showing the topology of *Drosophila* Plk4 (Sak), indicating the N-terminal kinase domain, a coiled-coil domain, a downstream regulatory element (DRE), linker 1 (L1), two central tandem polo-boxes (PB1 and PB2), linker 2 (L2), and a third polo box (PB3) towards its C-terminus. **(B)** Schematic showing the topology of human Plk4 with the conserved domains as in (A).

Plk4 is a low abundance, short-lived protein, whose stability is controlled by a downstream regulatory element (DRE) that functions as a phospho-degron (Fu et al., 2015; Klebba et al., 2015a; 2013). Plk4 can form homodimers, and trans auto-phosphorylation of the phospho-degron sequence targets the protein for SCF (Skp/Cullin/F-box) E3 ligase mediated destruction by the proteasome (Cunha-Ferreira et al., 2013; Guderian et al., 2010; Holland et al., 2012; Lopes et al., 2015; Rogers et al., 2009; Sillibourne et al., 2010). This ability of Plk4 to catalyse its own destruction seems to be essential for preventing centriole over-duplication.

Plk4 seems to promote centriole duplication through an interaction with STIL/Ana2 via PB3 and its Linker 1 (L1) region (Ohta et al., 2018). Binding to STIL/Ana2 allows Plk4 to undergo conformational changes through trans auto-phosphorylation that lead to activation of its kinase activity (Arquint et al., 2015; Lopes et al., 2015; Moyer et al., 2015; Ohta et al., 2018). Activated PLK4 can then phosphorylate STIL within the conserved STIL/Ana2 (STAN) domain, which then promotes Sas6 recruitment at the centriole to initiate cartwheel assembly (Dzhindzhev et al., 2014; Kratz et al., 2015; Moyer et al., 2015; Ohta et al., 2018; 2014). In *C. elegans*, ZYG-1 interacts directly with SAS-6, and SAS-6 interacts directly with SAS-5; both interactions are required for the formation of centriole central tube (Lettman et al., 2013). In other species, it is not clear if Plk4 directly interacts with Sas-6, and the interaction between Sas-6 and STIL/Ana2 remains poorly defined (Arquint et al., 2012; Tang et al., 2011). Plk4 can phosphorylate CPAP (Chang et al., 2010) and Cep152 (Hatch et al., 2010) in *in vitro* assays, but the significance of these phosphorylation remains to be determined.

Plk4 dysfunction has been linked to several human diseases. Most convincingly, mutations in Plk4 lead to microcephaly and growth failure (Dinçer et al., 2017; Martin

et al., 2014; Shaheen et al., 2014), a feature shared with several other key centriole assembly proteins (Duerinckx and Abramowicz, 2018; Naveed et al., 2018; Patwardhan et al., 2018). How centriole dysfunction leads to these pathologies remains uncertain (Jayaraman et al., 2018; Nigg and Holland, 2018). A lack of Plk4 leads to loss of centrioles and overexpression can lead to the *de novo* formation and over-duplication of centrioles (Bettencourt-Dias et al., 2005; Habedanck et al., 2005; Kleylein-Sohn et al., 2007; Peel et al., 2007; Rodrigues-Martins et al., 2007). Centrosome amplification has been linked to chromosome mis-segregation (Ganem et al., 2009; Silkworth et al., 2009) and can drive tumourogenesis in fly and mouse models (Basto et al., 2008; Levine et al., 2017; Raff and Basto, 2017). Plk4 is overexpressed in human colorectal, liver, breast, brain and certain paediatric tumours as well as melanomas, and this is correlated with poor clinical prognosis (Chan, 2011; Denu et al., 2018; Kawakami et al., 2018; Levine et al., 2017; Marina and Saavedra, 2014; Pezuk et al., 2017; Sredni and Tomita, 2017). Recently, Plk4 has been evaluated as a potential therapeutic target for various cancers. Depletion of Plk4 by RNAi hinders centriole duplication and causes the death of breast cancer cells *in vitro* and inhibits breast cancer xenograft growth *in vivo* (Mason et al., 2014). Treatment of melanoma cells with a selective small-molecule Plk4 inhibitor (centrinone B) significantly decreased cell proliferation (Denu et al., 2018). Additionally, the Plk4 inhibitor CFI-400945 is reported to exert marked antineoplastic effects against lung cancers (Kawakami et al., 2018). Taken together, targeting Plk4 for inhibition alone, or as part of a combination regime, may be a promising way to combat various cancers.

1.4.2: SAS-6/Sas-6

Sas-6 proteins appear to be the main structural building blocks of the centriole cartwheel (Guichard et al., 2012; 2018). They broadly contain three domains: an N-terminal globular “Present in SAS-6” (PISA) domain, a long coiled-coiled region, and an unstructured C-terminal region (Leidel et al., 2005) (Figure 1.6). SAS-6 proteins homodimerize in the cytoplasm via their coiled-coil regions, and these homodimers can undergo higher-order oligomerization through their N-terminal globular head-regions to form ring-like assemblies that have a striking structural similarity to the cartwheel, with the N-terminal regions forming a central hub in the middle from which the coiled-coil regions radiate as spokes (Cottee et al., 2015; Guichard et al., 2012; 2018; Hilbert et al., 2013; Keller et al., 2014; Kitagawa et al., 2011b; Qiao et al., 2012; van Breugel et al., 2011; 2014). Sas-6 molecules can form rings with varying symmetries *in vitro*, although 9-fold symmetric rings tend to be favoured (Kitagawa et al., 2011b). It is not clear how the invariant 9-fold symmetry of the cartwheel is enforced *in vivo* (Dong, 2015). The C-terminal region of human SAS-6 has been suggested to bind MTs and to favour their polymerization, raising the possibility that SAS-6 proteins extend all the way up to the bordering centriole MTs (Gupta et al., 2015). Interestingly, crystallographic and biophysical analyses indicate that *C. elegans* Sas-6 adopts a continuous helical structure rather than a discrete set of stacked rings, possibly explaining why a central tube is observed in this organism *in vivo* instead of a canonical cartwheel (Hilbert et al., 2013; Pelletier et al., 2006).

The levels of human SAS-6 are regulated during the cell cycle by protein degradation at the onset of anaphase (mediated by APC/C:Cdh1, and also SCF/FBXW5), and vertebrate Sas-6 proteins contain a KEN box at their C-terminus, potentially explaining why the cartwheel is removed from the daughter centriole as it is converted

into a mother centriole during mitosis (Strnad et al., 2007). Interestingly, there is no KEN box in *Drosophila* Sas6, and the cartwheel is maintained at mother centrioles in flies (Cottee et al., 2011; Loncarek and Khodjakov, 2009). Recently, it has been proposed that the non-apoptotic caspase-dependent proteolysis of Sas-6 may also destabilise the cartwheel (Seo and Rhee, 2018).

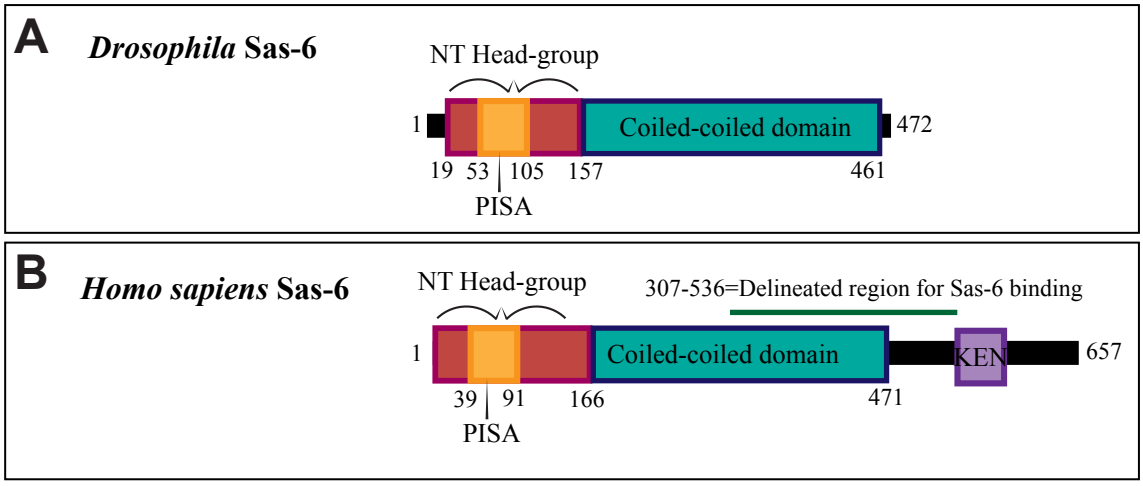

Figure 1.6: Sas-6 protein domains in *Drosophila* and humans. (A) Schematic showing the topology of *Drosophila* Sas-6, indicating the N-terminal globular domain containing the "Present in SAS-6" (PISA) domain, followed by a long coiled-coil domain **(B)** Schematic showing the topology of human Sas-6 with the conserved domains as in (A). Human Sas-6 also contains a KEN box at its C-terminus.

In humans, mutations in Sas-6 have been linked to microcephaly. A missense mutation was identified within the PISA domain converting Isoleucine 62 to Threonine (Khan et al., 2014). This mutation lead to the partial impairment of centriole formation in tissue culture cells, which could result in defective asymmetric cell divisions—reducing brain development and so causing the primary autosomal recessive microcephaly (Khan et al., 2014).

1.4.3: SAS-5/Ana2/STIL

SAS-5/Ana2/STIL protein is essential for centriole formation in *C. elegans* (Delattre et al., 2004), *Drosophila* (Cottee et al., 2013; Stevens et al., 2010a) and humans (Arquint et al., 2012; Tang et al., 2011). Ana2 contains a short, N-terminal proline-rich Sas4/CPAP binding motif (Cottee et al., 2013; Hatzopoulos et al., 2013), a central coiled-coil domain (CCCD) that is crucial for its oligomerization (Cottee et al., 2015; 2017; David et al., 2016; Rogala et al., 2015; Shimanovskaya et al., 2013; Slevin et al., 2014), a well-conserved STil/ANa2 (STAN) domain that modulates the interaction with Sas-6 proteins, and a Truncated In Microcephaly (TIM) domain at the C-terminus (Cottee et al., 2015; Slevin et al., 2014) (Figure 1.7). A novel direct interaction between SAS-5 and MTs has been recently proposed that relies on SAS-5 higher-order oligomerization that is required for centriole duplication (Bianchi et al., 2018).

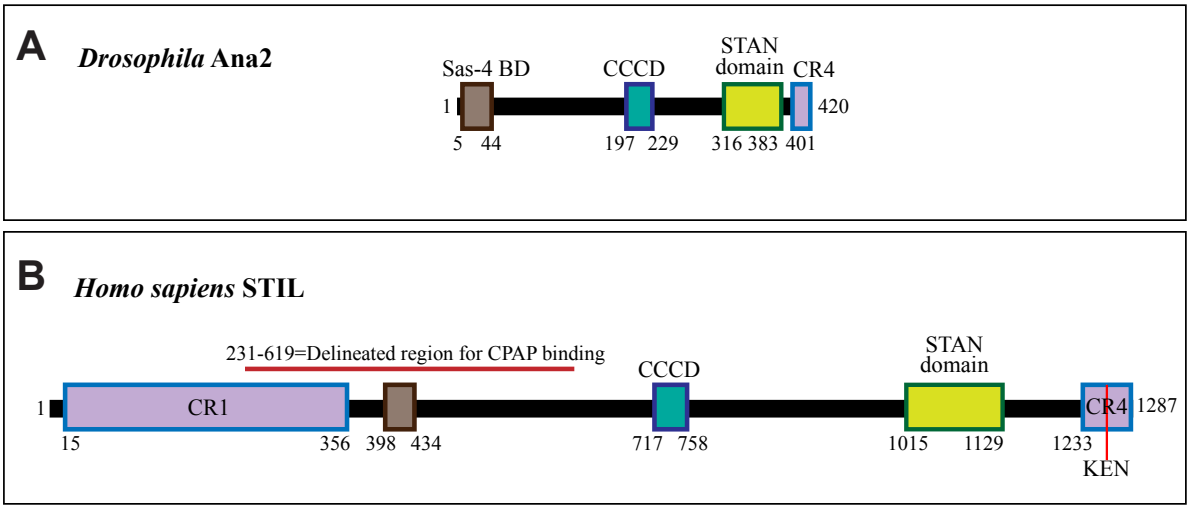

Figure 1.7: Ana2/STIL protein domains in *Drosophila* and humans. (A) Schematic showing the topology of *Drosophila* Ana2, indicating the N-terminal Sas4/CPAP binding motif, a central coiled-coil domain (CCCD), a well-conserved STil/ANa2 (STAN) domain that interacts with Sas-6 proteins. **(B)** Schematic showing the topology of human STIL with the conserved domains as in (A). The delineated region for CPAP binding is shown above by the bar along with a KEN box destruction motif at the C-terminus.

The recruitment of Ana2/STIL to centrioles, and its interaction with, and phosphorylation by, Plk4 appears to be a complicated process, potentially regulated

by multiple different domains and phosphorylation events. In humans, STIL is recruited to centrioles via its CCCD through an interaction with the PB3 domain of Plk4—an interaction that does not appear to be conserved in the *Drosophila* proteins (Cottee et al., 2017)—and an additional CC domain located adjacent to the kinase domain called linker (L1) region (Arquint et al., 2015; Cottee et al., 2015; Moyer et al., 2015; Ohta et al., 2014). In *Drosophila* , the CCCD is essential for all aspects of Ana2 function, but this appears to be mainly because it allows Ana2 to oligomerize into a stable tetramer (Cottee et al., 2015). The CCCD is also essential for higher-order oligomerisation in other species, although a stable tetramer does not appear to be formed: for example SAS-5 forms trimers, while the STIL CCCD mainly forms dimers and has only only a weak tendency to form tetramers (Arquint et al., 2015; Cottee et al., 2015; 2017; Rogala et al., 2015).

The binding of Plk4 to STIL appears to activate the kinase, allowing it to phosphorylate Ana2/STIL at the STAN domain, which promotes Sas6 binding and so cartwheel assembly (Dzhindzhev et al., 2014; Kratz et al., 2015; Moyer et al., 2015; Ohta et al., 2014). Recently, however, it was shown that Plk4 phosphorylates *Drosophila* Ana2 in an ordered pattern at multiple other sites, and this is required for the efficient phosphorylation of the STAN domain, and the subsequent release of the Ana2 from Plk4 (McLamarrah et al., 2018). Moreover, it was recently shown that the CCCD region of STIL binds to Plk4 and seems to protect it from degradation, while at the same time the TIM domain promotes the auto-phosphorylation and degradation of nearby Plk4 molecules, potentially helping to explain how Plk4 localisation becomes restricted to a single site on the side of the mother centriole (see below) (Ohta et al., 2018). Vertebrate STIL contains a KEN box, a common degradation motif that could

be responsible for STIL degradation in the cytoplasm after centriole assembly is complete, although *Drosophila* Ana2 lacks this domain (Arquint and Nigg, 2014).

Eight mutations of STIL are known to be associated with severe microcephaly producing truncated proteins or missense substitutions that do not result in a complete loss-of-function or are partially compensated by other genes (Bennett et al., 2014; Kakar et al., 2015; Kumar, 2009). Two such mutations— Valine 1219 and Glutamine 1239 that are converted into premature stop —resulting in the loss of the KEN box, accumulation of the mutant protein and subsequent centrosome amplification and microcephaly (Arquint and Nigg, 2014; Kumar, 2009). Another mutation— converting Glycine 717 to Glutamic Acid —appears to reduce STIL function and results in microcephaly (Kumar, 2009). STIL has been found to be up-regulated in lung cancer, colon carcinoma, prostate adenocarcinoma and ovarian cancers with metastatic potential (Erez et al., 2004; Patwardhan et al., 2018; Rabinowicz et al., 2017; Ramaswamy et al., 2003).

1.4.4: SAS-4/Sas-4/CPAP

Sas-4 is recruited to centrioles downstream of Ana2/STIL and Sas-6 and is thought to be at least partially responsible for linking the centriole cartwheel to the centriole MTs (Basto et al., 2006; Dammermann et al., 2008; Delattre et al., 2006; Hung et al., 2000; Kirkham et al., 2003; Kohlmaier et al., 2009; Leidel and Gönczy, 2003; Pelletier et al., 2006). Sas-4/CPAP proteins contain a conserved N-terminal domain that interacts with Cep152/Asl proteins (Cizmecioglu et al., 2010; Dzhindzhev et al., 2010; Hatch et al., 2010; Sonnen et al., 2013) and a conserved C-terminal T complex 10 (TCP) domain that interacts with Ana2/STIL proteins (Cottee et al., 2013; Hatzopoulos et al., 2013; Zheng et al., 2014) (Figure 1.8). Thus, it seems to have an important

function linking the central cartwheel to the more peripheral regions of the centriole. In addition, the protein contains two N-terminal domains that bind tubulin, a PN2-3 domain that destabilises MTs and an A5N domain, also called microtubule-binding domain (MBD), that binds and stabilises MTs (Cormier et al., 2009; Hsu et al., 2008; Hung et al., 2004; Sharma et al., 2016). PN2-3 is further divided into PN2-3N and PN2-3C containing the LID and "Similar in SAS-4 and CPAP" (SAC) domains respectively (Hsu et al., 2008; Kitagawa et al., 2011a; Leidel and Gönczy, 2003; Sharma et al., 2016). SAS-4/CPAP caps MT plus ends, where it dampens MT growth, functioning as a molecular "lid" that ensures the centriole MTs grow slowly (Sharma et al., 2016). This is puzzling, however, as in vertebrates the overexpression of SAS-4/CPAP leads to the growth of overly long centrioles (Cottee et al., 2013; Hatzopoulos et al., 2013; Sharma et al., 2016; Zheng et al., 2016) (discussed in Section 1.5.2).

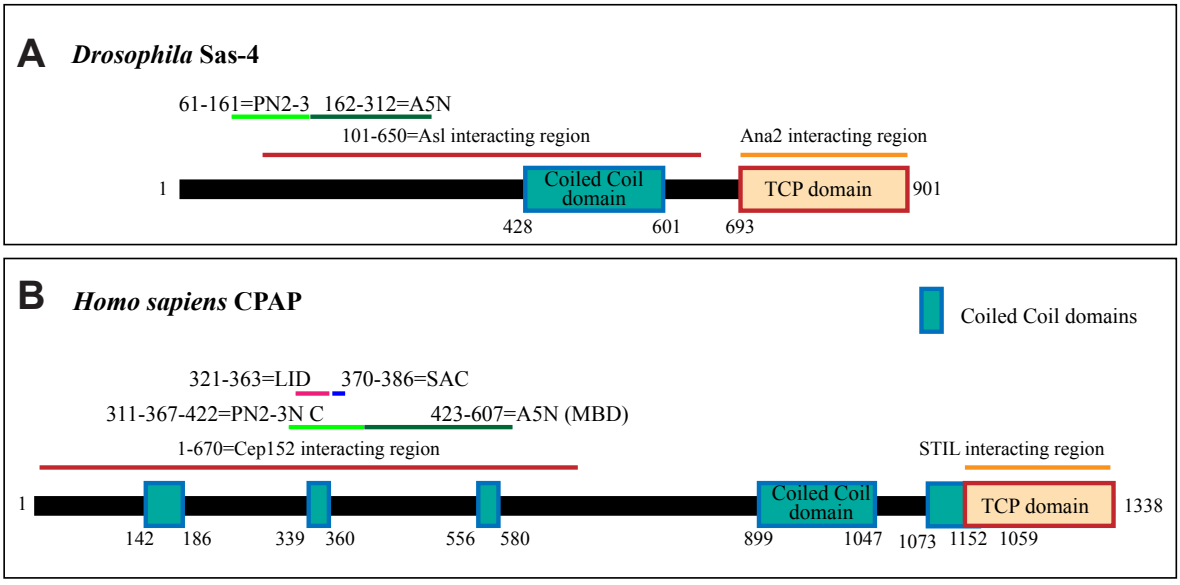

Figure 1.8: Sas-4/CPAP protein domains in *Drosophila* and humans. (A) Schematic showing the topology of *Drosophila* Sas-4, indicating the conserved N-terminal domain that interacts with Cep152/Asl proteins and a conserved C-terminal TCP (T complex 10) domain that interacts with Ana2/STIL proteins. The protein also contains two N-terminal domains that bind tubulin, a PN2-3 domain and an A5N domain, also called microtubule-binding domain (MBD). **(B)** Schematic showing the topology of human CPAP with the conserved domains as in (A). The PN2-3 is further divided into PN2-3N and PN2-3C, which contain the LID and "Similar in SAS-4 and CPAP" (SAC) domains, respectively.

A Glutamic Acid 1235 to Valine conversion mutation in the TCP domain of CPAP drastically reduced neuron numbers and brain size, causing microcephaly in humans (Al-Dosari et al., 2010; Bond et al., 2005). The mutant protein did not localize efficiently to the centriole, was defective in recruiting PCM components and failed in centriole duplication in cultured cells (Tang et al., 2011; Zheng et al., 2014). MCPH associated mutations of CPAP/CenpJ in mice have been shown to impair centriole biogenesis leading to abnormal spindle orientation during mitosis and thus reducing brain size two-fold (Garcez et al., 2015; McIntyre et al., 2012). The deletion of the fifth predicted coiled-coil region of CPAP was found in a patient with Seckel Syndrome, a disease similar to microcephaly, however with added characteristics like dwarfism, growth retardation, mental retardation and 'bird-headed' facial appearance (Gabriel et al., 2016; O'Neill et al., 2018). Interestingly, however, patient-derived fibroblasts exhibited no detectable defects in centriole duplication or centrosome assembly, but showed defective ciliary disassembly, leading to a delay in cilia resorption and the premature differentiation of neuronal cells (Gabriel et al., 2016; O'Neill et al., 2018).

1.4.5: Asl/Cep152

Cep152 is the Asl homolog in vertebrates, however there is no homolog of Asl in worms (Andersen et al., 2003; Blachon et al., 2008; Bonaccorsi et al., 1998; Cizmecioglu et al., 2010; Dobbelaere et al., 2008; Dzhindzhev et al., 2010; Goshima et al., 2007; Hatch et al., 2010; Varmark et al., 2007). Asl/Cep152 is predicted to be a highly coiled-coil protein with conserved region 1 (CR1) at it’s N-terminus (Dzhindzhev et al., 2010) (Figure 1.9). Cep152 has some additional domains such as Structural Maintenance of Chromosome-like domains (SMC-A and SMC-B) and a CR2 conserved region that is absent in Asl (Guernsey et al., 2010). CR1 is known to interact with PB1-PB2 of Plk4/Sak while C-terminal region of Asl interacts with Sas4

(Dzhindzhev et al., 2010; Klebba et al., 2015b; Novak et al., 2014). The Asl/Cep152, C-terminus is known to localise at the centriole wall with the N-terminus extending into the PCM (Mennella et al., 2012; Sonnen et al., 2012).

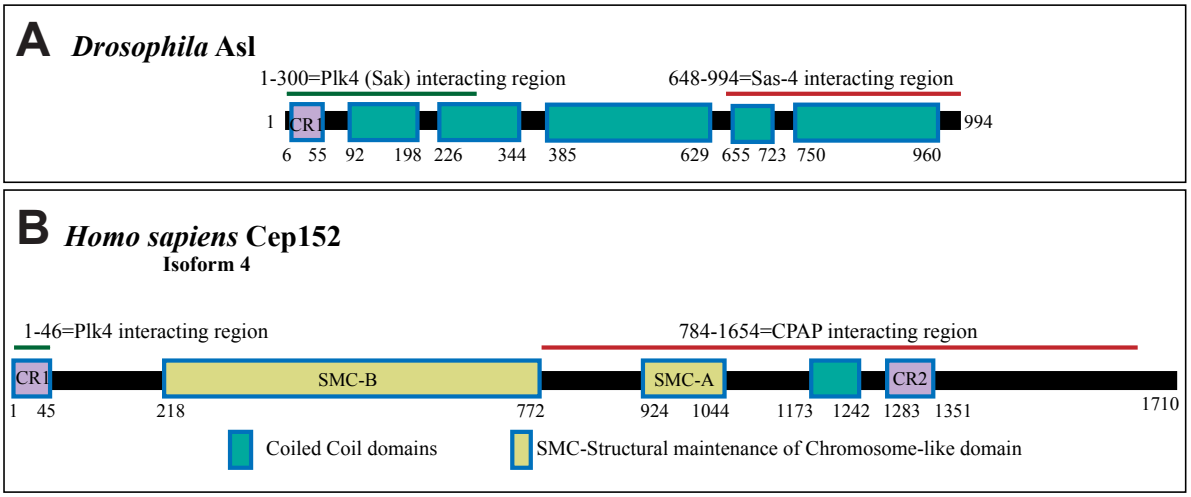

Figure 1.9: Asl/Cep152 protein domains in *Drosophila* and humans. (A) Schematic showing the topology of *Drosophila* Asl, indicating the conserved N-terminal domain that interacts with Plk4 proteins and a conserved C-terminal domain that interacts with Sas-4 proteins **(B)** Schematic showing the topology of human Cep152 with the conserved domains as in (A). Human Cep152 has an extra Structural maintenance of Chromosome-like domains- SMC-A and SMC-B.

In flies, the Cdk1 dependent phosphorylation of Sas-4 is required to initiate the recruitment Asl to new-born centrioles once they disengage from their mothers at the end of mitosis (Novak et al., 2014; 2016). The new centrioles mature into mother centrioles and are capable of supporting new rounds of centriole duplication and thus Asl “licenses” centrioles for their first duplication (Novak et al., 2014). Asl is suggested to recruit and stabilise Plk4 at the proximal part of the centriole for centriole duplication (Blachon et al., 2008; Cizmecioglu et al., 2010; Dzhindzhev et al., 2010; Hatch et al., 2010; Kim et al., 2013; Sonnen et al., 2013; Varmark et al., 2007). Asl/Cep152 along with Spd-2/Cep192 are proposed to act as a scaffold to recruit various PCM components on the mother centriole during mitosis (Bonaccorsi et al., 1998; Conduit et al., 2014b; Dzhindzhev et al., 2010; Varmark et al., 2007). Although, other reports oppose the PCM recruitment hypothesis (Blachon et al., 2008; Galletta et al., 2016a).

The loss of Asl leads to loss of centrosomes and its overexpression induces centriole over-duplication and de novo centriole assembly (Dobbelaere et al., 2008; Goshima et al., 2007; Varmark et al., 2007). Asl overexpression in cells lacking centrioles leads to the formation of acentriolar MT organising centres (aMTOCs), suggesting Asl involvement in the initiation of PCM assembly (Baumbach et al., 2015). Asl is suggested to negatively regulate the centriole length partly via Cep97 (Galletta et al., 2016b) (discussed in more detail in Section 1.5.3). Thus Asl appears to have multiple functions during centriole and centrosome assembly.

In humans, a Glutamine 265 to Proline mutation in the SMC domain of Cep152 disrupts the structure of the potential coiled-coiled domain and results in reduction of the brain size leading to microcephaly (Guernsey et al., 2010). An additional mutation of Cep152 that converts Arginine 987 to a premature stop, was carried recessively in the same family and this mutant form did not localise to the centrosomes in tissue culture cells (Guernsey et al., 2010). Cep152 is also linked to Seckel syndrome in humans where several mutations such as Lysine 667 to Arginine , Tyrosine 678 to premature stop, Isoleucine 899 to Leucine, Valine 1404 to premature stop and Valine 86, Asparagine 87 deletion of Cep152 are known to be associated with the disease (Kalay et al., 2011).

1.4.6: Cep135/Bld10

Cep135/Bld10 is usually not considered a core duplication protein as no homologue has been identified in worms, and several early studies in flies indicated that it was not essential for centriole duplication (Blachon et al., 2009; Carvalho-Santos et al., 2012; Mottier-Pavie and Megraw, 2009; Roque et al., 2012). Nevertheless, in *Chlamydomonas* and *Paramecium* Bld10 appears to be essential for proper cartwheel

assembly (Hiraki et al., 2007; Matsuura et al., 2004; Strnad and Gönczy, 2008), and it has been argued that the allele used in the *Drosophila* studies may not be a functional null (Fu et al., 2016). Cep135 protein is predicted to contain several coiled-coil domains with two conserved regions—CR1 and CR2—(Carvalho-Santos et al., 2012; 2010; Matsuura et al., 2004) (Figure 1.10). The N-terminal CR1 domain (1–190aa in human and 1–163 in *Drosophila*) of Cep135/Bld10p can bind to tubulin dimers and MTs and can stimulate the formation of MT bundles in cells, while the C-terminal CR2 domain in human (416-1140aa) interacts with the C-terminal part of Sas-6, suggesting a role to stabilise centrioles by interacting with their cartwheels and/or with their MT walls (Carvalho-Santos et al., 2012; Hilbert et al., 2016; Kraatz et al., 2016; Lin et al., 2013b). The N-terminus of human Cep135 (1-158aa) forms a very stable, parallel, two-stranded coiled-coil structure, while aa96-108 binds to MTs (Kraatz et al., 2016). Cep135/Bld10p localizes to the proximal lumen of the parental centriole and is absent from the lumen of the growing procentriole (Kleylein-Sohn et al., 2007; Sonnen et al., 2012). The protein localizes to the pinhead structure and may serve to bridge the cartwheel and MTs (Hiraki et al., 2007; Hirono, 2014; Matsuura et al., 2004).

Recent studies have indicated that Cep135 may have a role in stacking the Sas-6 rings within the cartwheel. Full-length *Chlamydomonas* SAS-6 protein can form large stacks of honeycomb arrays of cartwheel-like structures in the presence of a Bld10p C-terminal fragment (1061–1641aa, (Guichard et al., 2017). It is proposed that initially a twisted core cartwheel is formed with Sas-6 alone, and Bld10p then serves as a linker that locks the cartwheel in place with the outer MTs (Guichard et al., 2018). In human tissue culture cells, the depletion of Cep135/Bld10p causes a loss of centriolar MTs and reduction in centriole length (Dahl et al., 2015; Lin et al., 2013b). *Drosophila*

Cep135/Bld10p plays an important role in the asymmetric cell division of neuroblasts (Singh et al., 2014); *Cep135/Bld10p* mutant flies have short centrioles with an increase in centriole diameter and loss of central MTs of the sperm axoneme (Carvalho-Santos et al., 2012; Mottier-Pavie and Megraw, 2009; Roque et al., 2012). Recent experiments have suggested that Cep135 binds to Anastral Spindle 1 Ana1/Cep295 (discussed in section 3.2.8) to recruit Asl/Cep152 to centrioles, a study published during my studies that had major implications for my thesis work (Fu et al., 2016).

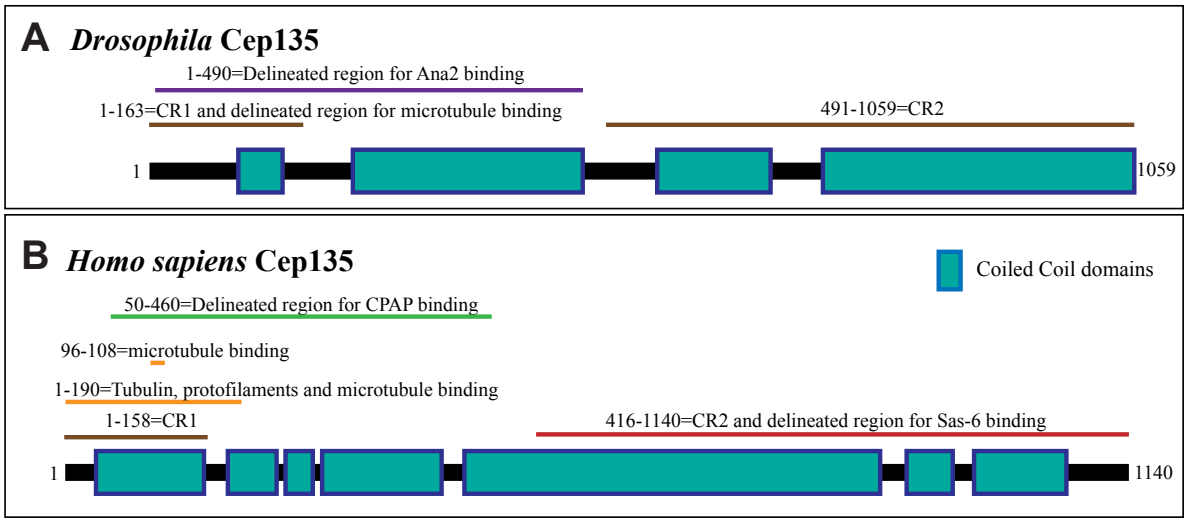

Figure 1.10: Cep135/Bld10 protein domains in *Drosophila* and humans. (A) Schematic showing the topology of *Drosophila* Cep135/Bld10, indicating the conserved N-terminal domain that interacts with Ana2 proteins and MTs and a conserved C-terminal domain (CR2). **(B)** Schematic showing the topology of human Cep135/Bld10 with the conserved domains as in (A). Human Cep135 is also thought to interact with Sas-6 at its C-terminus.

Cep135 mutations that introduce a frame shift and so a premature stop codon, fail to localise at centrosomes in tissue culture cells, exhibiting multiple centrosomes leading to multipolar spindle formation and autosomal-recessive primary microcephaly in humans (Farooq et al., 2016; Hussain et al., 2012). Another Cep135 Aspartic Acid 455 to Valine mutation has been shown to cause Multiple morphological abnormalities

of the sperm flagella (MMAF), where the mutated Cep135 protein mislocalises to form ectopic aggregates and cause the primary infertility in human males (Sha et al., 2017).

1.5: The regulation of Centriole length

Centriole length varies in different species and in different tissues but it is very consistent within any given cell type. There are at least two reasons why it is likely to be important to regulate centriole length. First, the size of the centriole influences the size of the mitotic centrosome (Kirkham et al., 2003). In flies this appears to be because the centrioles ultimately control the incorporation of the key mitotic PCM scaffolding proteins Spd-2 and Cnn into the mitotic PCM (Conduit et al., 2014b; 2010; 2015b). Thus, centrioles of different sizes will organise mitotic centrosomes of different sizes, and chromosomes often have trouble aligning on mitotic spindles that are organised by centrosomes that are unequal in size (Meraldi, 2016; Tan et al., 2015). Second, it has recently been shown that centriole over-elongation can be a significant cause of centriole over-amplification in cancer cells (Marteil et al., 2018) and this also appears to be the case in fly tissues where centriole MTs have been extended by the loss of the centriole capping protein CP110 (Franz et al., 2013), (described in more detail below). Several key centriole duplication proteins are expressed at low levels in cells (Bauer et al., 2016), and their overexpression can drive centriole over-duplication (Peel et al., 2007; Rodrigues-Martins et al., 2007; Stevens et al., 2010a; 2010b). Thus, the centriole duplication machinery is probably fine-tuned to function optimally at a certain centriole size (that may be different in different cell types).

How centriole size is determined is a question that has received very little attention, although it has been noted that centrioles are potentially an excellent system with

which to address the general question of organelle size control (Goehring and Hyman, 2012; Marshall, 2016). Centrioles duplicate once and only once during the cell cycle in a well-defined window, and the highly ordered structure of the growing daughter means that the complex 3-Dimension question of measuring organelle size can be simplified to a 1-Dimension question of measuring organelle length. While several models have been proposed to explain how centriole size is set, they remain largely untested because it has not been possible to obtain a quantitative description of centriole growth, as all data collected to date largely rely on inferring centriole growth progression from an EM analysis of a relatively small number of centrioles (Kuriyama and Borisy, 1981a; Shukla et al., 2015). In this section I describe what is known about the centriole growth process, and discuss the main proteins that have been implicated in influencing centriole length.

1.5.1: The Centriole elongation process

In vertebrate cells there appear to be two phases of centriole elongation: (1) Centriole assembly begins when a single procentriole of approximately 70-200nm in length is formed at the proximal end of the preexisting mother centriole during S phase (Figure 1.11A). (2) The procentriole then elongates during G2/M-phase until it reaches its final size of ~300nm-500nm in length sometime during mitosis (Marshall, 2001; Preble et al., 2000) (Figure 1.11B). In *Drosophila* (and many other species, such as worms), it is thought that only the first stage of centriole elongation occurs, as these centrioles lack the distal features of vertebrate centrioles (Greenan et al., 2018) (Figure 1.11).

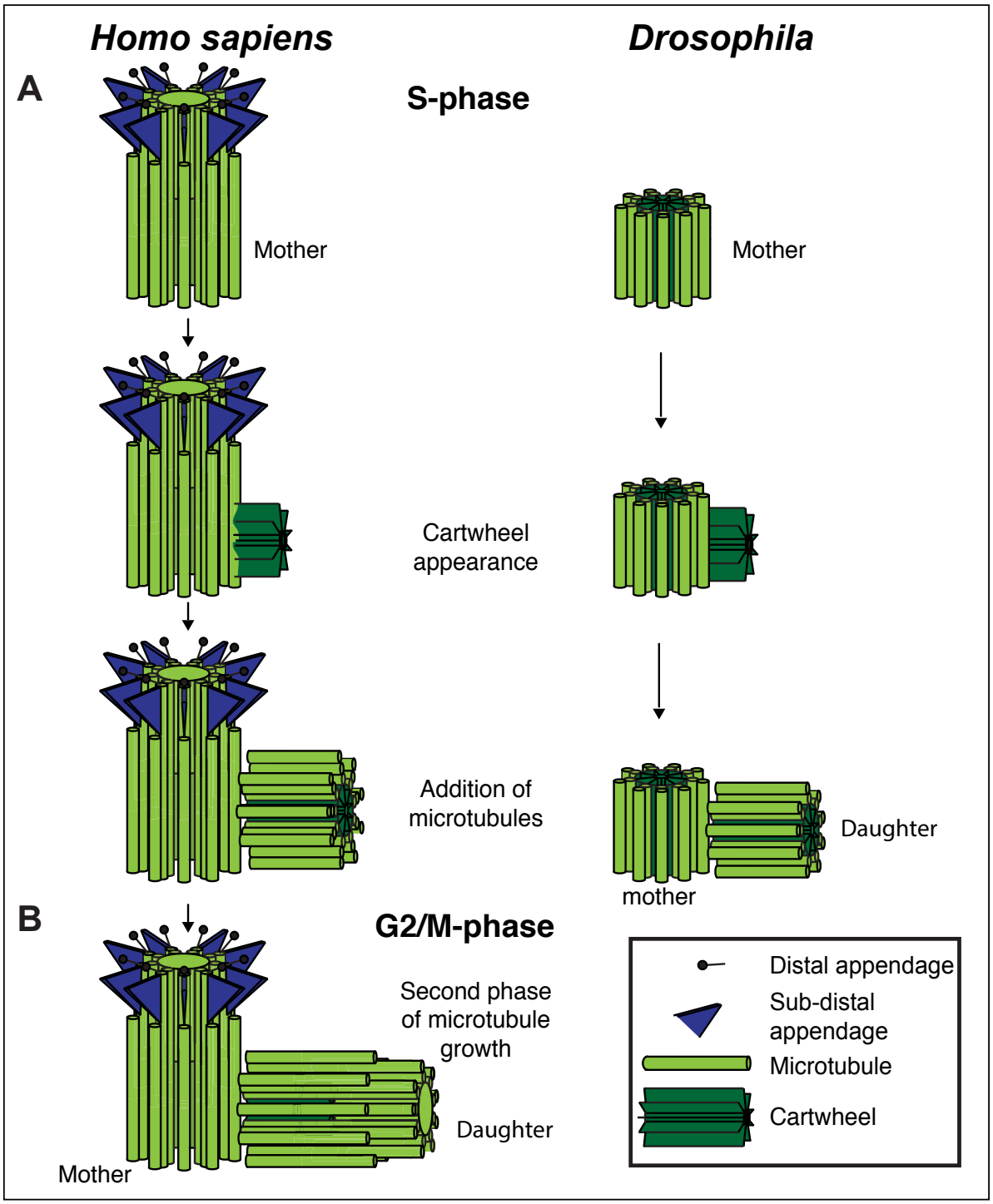

Figure 1.11: Schematic illustration of the Centriole elongation process in humans and *Drosophila*. (A) Centriole assembly begins when a single procentriole of approximately 70-200nm in length is formed at the proximal end of the pre-existing mother centriole during S phase. **(B)** The procentriole then elongates by extending its MTs past the cartwheel during G2/M-phase until it reaches its final size of ~300nm-500nm. In vertebrate cells (left panels) there appear to be two phases of centriole elongation (A and B). In *Drosophila* (and many other species such as worms, right panels), only the first stage of centriole elongation occurs (A only), as these centrioles lack the distal features of vertebrate centrioles (Greenan et al., 2018).

This first phase of centriole growth, which is common to all organisms, involves the elongation of two structures, the centriole cartwheel and the centriole MTs. In flies and worms, these two structures (the central cartwheel in flies, the central tube in worms) usually grow to the same size, suggesting that the cartwheel/tube—which forms first (Pelletier et al., 2006)—ultimately sets the size of the centriole MTs. In *Drosophila* spermatocytes, however, the centriole MTs extend well past the cartwheel structure (González et al., 1998), and this is also true in fly cells that lack the centriole capping protein CP110 (Franz et al., 2013).

1.5.2: Proteins that promote centriole growth

Sas-4/CPAP is essential for centriole duplication and it is thought to be required to recruit MTs to the growing centriole cartwheel (Delattre et al., 2006; Pelletier et al., 2006). CPAP overexpression in vertebrate cells leads to overly elongated centrioles, whereas its partial depletion give rise to asymmetric distribution of the PCM, that is proportional to centriole size and probably lead to shortened centrioles (Comartin et al., 2013; Kohlmaier et al., 2009; Lin et al., 2013b; Schmidt et al., 2009; Tang et al., 2009). In worms, the partial depletion of SAS-4 also leads to shortened centrioles (Kirkham et al., 2003), and this also appears to be the case when Sas-4 is partially inhibited by antibody injection in *Drosophila* embryos (Basto et al., 2006). SAS-4 overexpression has not been analysed in worms, but, perhaps surprisingly, it did not detectably lead to centriole over-elongation in fly cells (Franz et al., 2013). One possible interpretation of this result is that CPAP/SAS-4 proteins promote the second phase of MT growth that normally occurs in vertebrate cells during G2/M, but which does not occur in fly cells (Figure 1.11B).

In vertebrates, the overly elongated centrioles in U2OS cells overexpressing CPAP can reach up to 3.5μm in length and they promote the formation of supernumerary procentrioles (Kohlmaier et al., 2009). The length-regulating activity of CPAP is dependent on the presence of Cep135, whose depletion gives rise to shorter centrioles, and prevents CPAP recruitment to the centriole and CPAP-induced centriole over-elongation (Kleylein-Sohn et al., 2007; Lin et al., 2013b). Centrioles are also too short in *Cep135* mutant fly cells (Carvalho-Santos et al., 2012; Mottier-Pavie and Megraw, 2009; Roque et al., 2012). It is perhaps significant that both CPAP and Cep135 appear to directly interact with tubulin and/or MTs, strongly suggesting that they influence centriole length by promoting the growth and/or stability of the centriole MTs.

It has recently been shown that Centrobin—a protein often associated preferentially with daughter centrioles, and which in flies plays an important part in specifying the different function of mother and daughter centrioles (Gottardo et al., 2015d)—regulates CPAP levels in vertebrate cells, and so influences centriole length (Gudi et al., 2014; 2011). Centrobin interacts with CPAP and seems to protect ubiquitinated CPAP from proteasome-dependent degradation (Gudi et al., 2015).

1.5.3: Proteins that suppress centriole growth

Centrosomal protein of 110 kDa (CP110) was originally identified as a Cdk substrate that regulate centriole duplication in human cells (Chen et al., 2002). It was subsequently shown that the depletion of CP110, or its binding partner Centrosomal protein of 97 kDa (Cep97), led to the dramatic elongation of the centrioles and appearance of robust cilia-like acetylated tubulin positive extended filamentous structures (Spektor et al., 2007). Moreover, overexpression of CP110 suppresses

CPAP-induced centriole elongation, suggesting that these proteins have antagonistic roles in determining the extent of tubulin addition during centriole elongation, thereby controlling centriole length (Schmidt et al., 2009). CP110 also interacts with the kinesin superfamily protein 24 (Kif24), a Kinesin 13 family member that is thought to destabilise centriolar MTs at the distal ends (Kobayashi et al., 2011). The ubiquitin ligase complex SCF and the deubiquitinating enzyme USP33, tightly control CP110 levels during the cell cycle to allow centrioles to duplicate and elongate primarily in S and G2/M phases (Li et al., 2013). To promote ciliogenesis in a cell, Tau-tubulin kinase-2 (TTBK2) localizes to the distal appendages of the mother centriole where it phosphorylates Cep97 and removes CP110 from the mother centriole (Oda et al., 2014). Taken together, these data strongly suggest that CP110 and Cep97 cooperate to suppress cilia assembly and the growth of the centrioles, and they appear to do so, at least in part, by recruiting the MT depolymerizing Kif24 to the centriole MT plus-ends.

In *Drosophila*, CP110 also localizes to the distal end of the centrioles (Franz et al., 2013; Fu and Glover, 2012). Perhaps surprisingly, however, *CP110* mutant flies are viable and fertile, indicating that CP110 is not essential for centriole duplication. This also appears to be the case in CP110 knockout mice, that are viable, but die shortly after birth primarily it seems because of cilia defects caused by defects in the assembly of centriolar sub-distal appendages (Yadav et al., 2016). An EM study of centrioles in *Drosophila* larval wing discs revealed that centrioles were slightly elongated in the absence of CP110, but that dramatic singlet MT extensions emanated from the distal ends of the centrioles suggesting that CP110 must “cap” centriolar MTs to ensure that they do not extend beyond the distal end of the centriole.

Moreover, the overexpression of CP110 in *Drosophila* larval wing discs subtly, but significantly, shortened centriole length (Franz et al., 2013).

The *Drosophila* homologue of Kif24 is a Kinesin 13 called Klp10A, which regulates general MT stability both during interphase and mitosis (Goshima and Vale, 2005; Mennella et al., 2005; Rogers et al., 2004). Klp10A is localized on centrosomes, spindle poles, centromeres and the tips of astral MTs in *Drosophila* S2 cell, in agreement with the notion that this protein plays a general role in regulating MT stability (Mennella et al., 2009). It was recently shown that Klp10A also influences centriole behaviour: centrioles are significantly longer than normal in *Klp10A* mutant or depleted cells, and the centriole MTs are considerably longer than normal (Delgehyr et al., 2012; Franz et al., 2013). *Drosophila Klp10A* mutant adult males are sterile and the centrioles in spermatocytes are long and "frayed", sometimes with multiple short centrioles attached to them (Delgehyr et al., 2012). The testes centrioles of *Klp10A* mutants display an abnormal distribution of Plk4, Sas-4 and PLP along the length of the centrioles and display ectopic positioning of the daughter centrioles (Gottardo et al., 2016). RNAi-mediated Klp10A depletion in *Drosophila* male germline stem cells (GSCs) leads to abnormal elongation of the mother centriole which then organises a larger half spindle than the other centriole pair, yielding a smaller differentiating daughter cell at the end of mitosis (Chen et al., 2016).

Recently it has been suggested that in male germline stem cells (mGSCs), female germline stem cells (fGSCs) and larval wing discs, Asl negatively regulates centriole length (Galletta et al., 2016b). The centrioles in *asl* mutant GSCs and larval wing disc cells were overly elongated, up to 30-fold longer length than observed in WT cells, without any increase in centriole diameter (Galletta et al., 2016b). Such centrioles

display the proximally located centriole and PCM proteins such as Sas-6, Sas-4, Cnn, Spd2, and γ-tub along the full length of the centriole (Galletta et al., 2016b). Further, it has been suggested that Asl regulation of centriole length is partly via Cep97, as Asl C-terminus interacts with Cep97, and C*ep97* mutants also displayed the longer centriole phenotype in mGSC (Galletta et al., 2016b).

1.5.4: Other potential regulators of centriole length

Several other proteins have been implicated in centriole length regulation, although in most of these cases the evidence for such a role comes from only a small number of systems and/or reports. There is evidence, for example, that daughter centriole elongation is regulated by the proteasome, as proteasome inhibition leads to excess levels of several centriole proteins and the dramatic lengthening of the centrioles (Korzeniewski et al., 2010). Aurora A kinase may be involved in the control of centriole length during *Drosophila* male meiosis, as incubating testes with an Aurora A inhibitor (MNL8054) resulted in overly elongated centrioles in primary spermatocytes (Gottardo et al., 2015a). In *C. elegans*, Sas-1, a homologue of C2CD3 that can bind and stabilise MTs (Tobel et al., 2014), and Sas-7, which is required for daughter centrioles to become competent for duplication, has been shown to regulate centriole length (Sugioka et al., 2017).

1.6: The function of Ana1/Cep295 in centriole assembly

The initial focus of my thesis work was to study the function of *Drosophila* Ana1, so I describe what is known about this protein in this separate section. The *ana1* gene was first identified in an RNAi screen in *Drosophila* S2 cells, having the striking

phenotype (along with two other genes, *ana2* and *ana3*) of forming spindles that lacked astral MTs (Goshima et al., 2007). It was subsequently shown that this was because depleting any of these genes strongly reduced the number of centrioles in the depleted cells (Dobbelaere et al., 2008). Ana2 was found to be related to vertebrate STIL (a protein of unknown function at the time) and these proteins were the functional homologues of the worm core centriole assembly protein SAS-5 (Stevens et al., 2010a). Ana3 was subsequently shown to be essential for cilia function in flies, but it did not appear to be essential for centriole duplication (Dobbelaere et al., 2008; Stevens et al., 2009)—although it has very recently been shown that the vertebrate homologue of Ana3 (Rotatin) interacts with Ana2 (STIL) and does seem to function in centriole duplication (Chen et al., 2017). A mutation in fly *ana1* was identified and shown to exhibit several phenotypes that are typical of flies that lack centrioles (such as uncoordination and immotile sperm), although centriole numbers were not directly analysed (Blachon et al., 2009).

The human homologue of Ana1 is KIAA1731, now renamed as Centrosomal Protein 295 (Cep295) (Figure 1.12). Nagase et al., were the first to name KIAA1731 and clone the cDNA (Nagase et al., 2000). Further, Nagase et al., observed that highest expression of KIAA1731 was detected in adult brain, fetal brain, fetal liver, spinal cord, testis, ovary and spleen and lowest expression in adult lung (Nagase et al., 2000). Ana1/Cep295/KIAA1731 protein has several predicted coiled-coil domains and two conserved regions—one at the N-terminus called CR1 or DDC8-like domain (differential display clone 8) and another at the C-terminus called CR2 or recently named, Present In C-terminal of Ana-1 (PICA) motif (Knorz et al., 2010; Tsuchiya et al., 2016). The far C-terminus of Cep295 contains an extra motif called ALMS (Alstrom syndrome) motif of unknown function (Knorz et al., 2010), which is not present in

Drosophila Ana1. RNAi of KIAA1731 in human RPE1 and U2OS cells resulted in the loss of centrosomes (Knorz et al., 2010). A recent study has shown that the N-terminal DDC8-like domain is essential for Cep295 localisation, and the PICA motif is required for centrosome assembly (Tsuchiya et al., 2016).

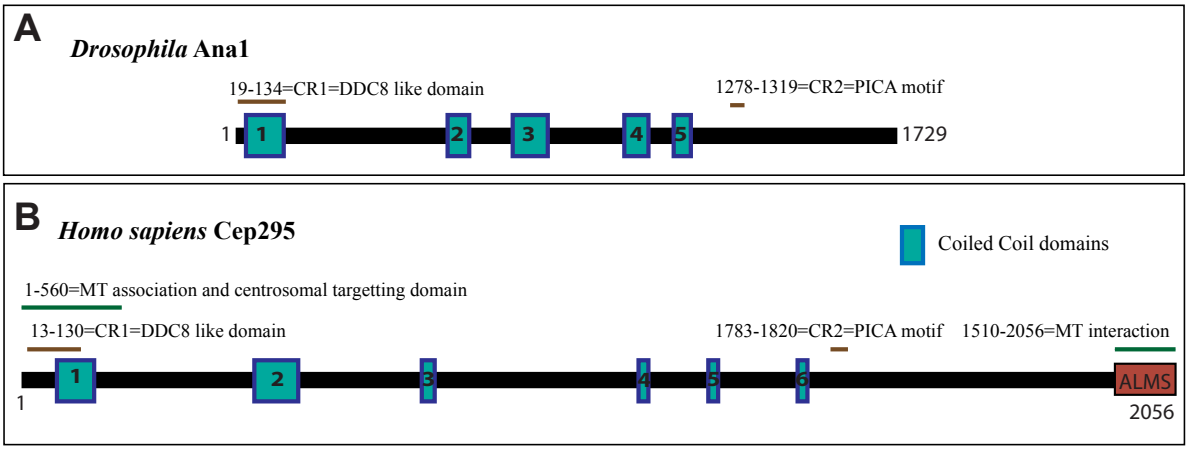

Figure 1.12: Ana1/Cep295 protein domains in *Drosophila* and humans. (A) Schematic showing the topology of *Drosophila* Ana1, indicating the conserved N-terminal domain CR1, also known as the DDC8-like domain (differential display clone 8), and the conserved C-terminal CR2 or PICA motif (present in C-terminal of Ana-1) **(B)** Schematic showing the topology of human Cep295 domains as in A. Human Cep295 also has a C-terminal ALMS (Alstrom syndrome) motif.

Cep295/KIAA1731 was identified in a screen for proteins enriched on new-born centrioles (Izquierdo et al., 2014). This study showed that new centrioles are still formed in the absence of Cep295, but, when the new centrioles mature into mothers and lose their associated cartwheel in mitosis, they failed to recruit PCM and disintegrated. Thus, it was proposed that when mother centrioles lose their cartwheels, they need to recruit PCM to remain stable: in the absence of Cep295, the new centrioles fail to recruit PCM during mitosis and so become destabilised (Izquierdo et al., 2014). Cep295 appears to allow the new-born cartwheel-less centrioles to recruit PCM during early mitosis, and so is required for “centriole-to-centrosome” conversion (Izquierdo et al., 2014). This model is attractive, but daughter centrioles do not lose their cartwheel as they mature into mothers in flies, suggesting that this model cannot fully explain the function of Ana1 in fly cells.

1.7: *Drosophila* embryo as a model system to study centrosome formation

Cell division in the early *Drosophila* embryo occurs in a common cytoplasm without cytokinesis, creating the syncytial blastoderm, a common feature during the early embryogenesis of several species. The syncytial embryo undergoes 13 rounds of extremely rapid and synchronized nuclear divisions comprising successive periods of S-phase and M-phase without intervening gap phases (Foe and Alberts, 1983). In cycle 8, the majority of nuclei start to migrate to the periphery of the embryo, the rest remain in the interior of embryo and become large, polyploid, yolk nuclei (Figure 1.13A). The yolk nuclei lose their centrosomes and are eventually lost later in embryo development (Foe and Alberts, 1983). During cycle 9, several nuclei arrive at the posterior pole of the embryo and form the pole cells that will give rise to the future germline (Cinalli and Lehmann, 2013). The remaining migrating nuclei arrive at the periphery of the embryo at nuclear cycle 10 and undergo four more divisions, leading to the formation of a syncytial blastoderm that contains ~6000 nuclei (Foe and Alberts, 1983)(Figure 1.13A). S-phase is lengthened incrementally and progressively from cycle 11 onwards, so that cycle 13 is 21 min long (interphase plus mitosis). After cycle 13, membranes grow between the nuclei to form the cellular blastoderm. A G2 phase becomes apparent, the genome is fully activated for transcription, and many maternal mRNAs are degraded (Farrell and O'Farrell, 2014).

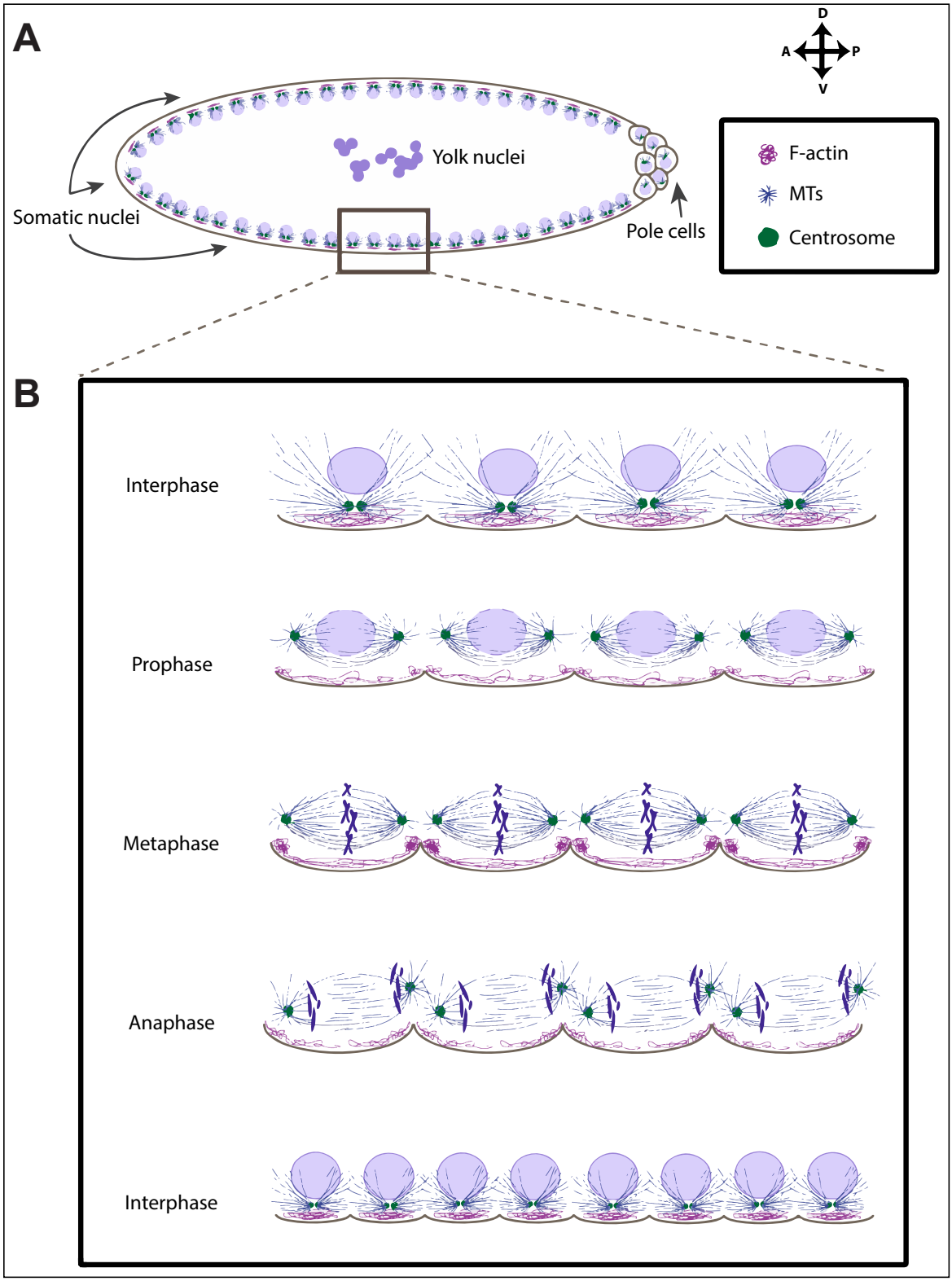

Figure 1.13: Schematic of a *Drosophila* embryo at the syncytial blastoderm stage. (A) A syncytial blastoderm stage *Drosophila* embryo with yolk nuclei in the middle, pole cells at the posterior end and the dividing nuclei at the cortex. **(B)** A magnified view of the cortical region of the embryo with nuclei, centrosomes, F-actin and the spindles at Interphase, Prophase, Metaphase and Anaphase. The centrosomes organize both the microtubule network and actin network accompanying each nucleus. The caps of F-actin between the nucleus and plasma membrane elongates in mitosis to form boundaries between the neighbouring nuclei and then divide along with the nuclear material. Illustrations are modified from original drawings of Dr. Zsofia Novak (a post-doctoral fellow in the Raff laboratory).

The syncytial *Drosophila* embryo offers several advantages for dissecting the molecular mechanisms of centrosome duplication. During nuclear cycles 10–14, the majority of nuclei form a monolayer at the cortex, centrosomes are found <5μm underneath the plasma membrane and are therefore easily imaged by fluorescence microscopy (Figure 1.13B) (Foe and Alberts, 1983; Warn et al., 1984). All the nuclei and all the centrosomes divide at the same time in the same cycle, allowing the simultaneous observation of many centrosomes, which is valuable for quantitative experiments (Figure 1.13B) (Foe and Alberts, 1983; Warn et al., 1984). I used confocal spinning disk microscopy throughout Chapter 4 and 5 for quantitative live imaging of centriole growth in the early *Drosophila* embryo. Further, in order to infer the function of a protein, *in vitro* transcribed mRNA encoding fluorescently-tagged (WT and mutant) proteins, or fluorescently-tagged antibodies, can be easily microinjected into syncytial *Drosophila* embryo to acutely inactivate protein function (Basto et al., 2006; Brust-Mascher et al., 2009; Buttrick et al., 2008; Conduit et al., 2010; Cottee et al., 2015; Gergely et al., 2000; Richens et al., 2015). This approach is particularly useful for studying centriole assembly pathway, as the chronic genetic mutation or knockdown of crucial centriolar proteins often prevents the formation of centrosomes altogether.

1.8: *Drosophila* testes as a model system to study centriole formation

The centrioles in *Drosophila* testes undergo a dramatic change in morphology during spermatogenesis (Figure 1.14). Initially, the male germ stem cell (mGSC) divides asymmetrically to generate another mGSC and a gonialblast. The centrioles in mGSCs display a combination of doublet and triplet microtubules (Gottardo et al.,

2015c). The gonialblast detaches from the stem cell hub and divides a further four times without undergoing cytokinesis to form a cyst of 16 primary spermatocytes. The primary spermatocytes then dramatically increase in size, and their centrioles grow significantly in size (growing up to 2.6μm in length) and they consist exclusively of triplet microtubules (González et al., 1998; Gottardo et al., 2015c). The centrioles migrate to the cell surface where they template a short axoneme inside a membrane covered protrusion sometimes called the cilium-like region (CLR) or the ciliary cap (Gottardo et al., 2013; Vieillard et al., 2016). At the initiation of meiotic division, the centrioles, together with their cilium-like region, migrate back into the cell close to the nucleus and organise the formation of the meiotic spindle. The centrioles do not duplicate after meiosis I, so only a single centriole is detected is at each meiosis II spindle pole. In this way, each primary spermatocyte generates four haploid spermatids with a single centriole that contains a small “proximal centriole-like” (PCL) structure on the side of the proximal end of each centriole (Blachon et al., 2009; Gottardo et al., 2015c). This centriole loses many of its characteristics (PCM, some centriole proteins, nine fold microtubules) via a process called centrosome reduction (Blachon et al., 2014; Khire et al., 2015; Manandhar et al., 2005; Wilson et al., 1997). The centriole in the spermatid becomes the basal body that nucleates the flagellar axoneme. The flagellum elongates to reach its full length and a fully mature 1.8mm long motile sperm (Noguchi et al., 2011). At fertilization, the sperm provides the paternal haploid DNA content and a single centriole to form the zygotic centrosome specifying the first mitotic spindle of the embryo (Baker et al., 2004; Loppin et al., 2015; Stetina and Orr-Weaver, 2011). I used confocal and 3D-SIM microscopy in Chapter 4 and 5 to image centrioles in *Drosophila* pupal and adult testes, as they form unusually large centrioles and are therefore ideal for localisation studies.

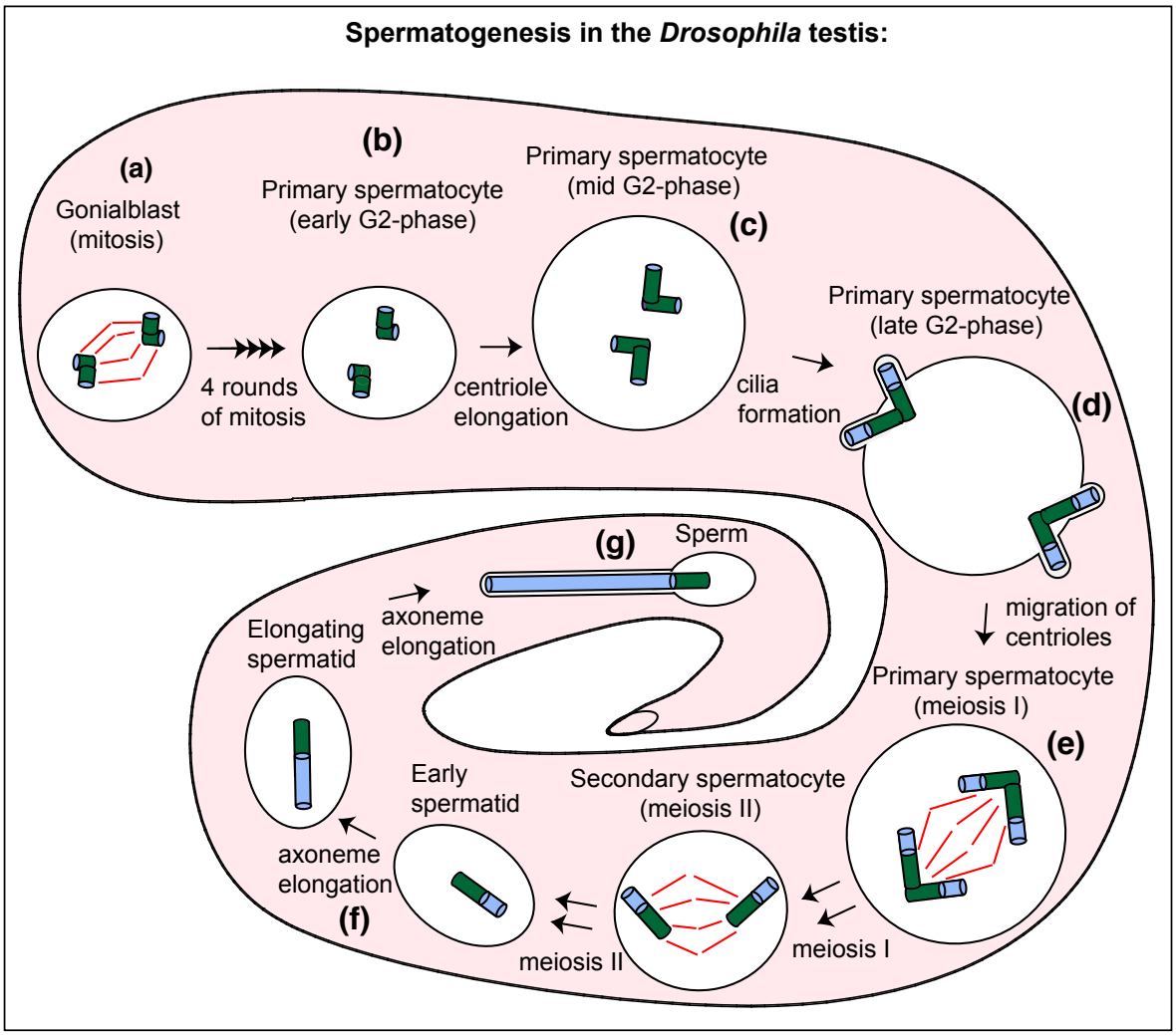

Figure 1.14: Schematic of centriole remodeling during different stages of *Drosophila* testis spermatogenesis. Male germ stem cells (mGSCs—not shown) at the testes hub divide asymmetrically to produce a gonialblast **(a).** After four rounds of mitosis each gonialblast forms a cyst of 16 primary spermatocytes, for simplicity only one primary spermatocyte is shown **(b).** The centrioles increase in length enormously as the primary spermatocytes grow during an extended G2-phase **(c).** The elongated centrioles then migrate to the cell surface and nucleate short cilia containing basal bodies and axonemes **(d).** The centrioles travel back to the cell cytoplasm in meiosis I and organise the meiotic spindle for cell division **(e).** After meiosis I and meiosis II, four spermatids are formed each containing one centriole at the base of the flagellum **(f).** The axoneme elongates to form fully mature sperm **(g).** The figure is modified from original drawings by Dr. Anna Franz (a former post-doctoral fellow in the Raff laboratory).

1.9: Thesis Summary

At the start of my thesis, I planned to investigate the function of Ana1 in flies and to try to establish how it interacted with the known core centriole assembly proteins. The bulk of this work is presented in **Chapter 3** and has been published (Saurya et al., 2016). During the course of my studies several publications came out (one of them back-to-back with my own research) that influenced our thinking and experiments; to keep these in proper context, I have only touched on these in this Introduction and discuss them in more detail in Chapter 3 (Chang et al., 2016; Fu et al., 2016; Saurya et al., 2016; Tsuchiya et al., 2016).

I discovered that Ana1 has a previously undescribed role in centriole length control (Saurya et al., 2016), and this was also shown to be the case for Cep295 in human cells (Chang et al., 2016). We realized that very little was known about centriole length control and that the early *Drosophila* embryo was an excellent model system with which to study this problem—as its rapid division cycle allows us to observe hundreds of centrioles as they rapidly and synchronously assemble during S-phase (section 1.7). In **Chapter 4** I describe how, in a collaborative effort with several other members of the laboratory, we developed methods to quantify the dynamics of centriole growth in early fly embryos (Aydogan et al., 2018). Unexpectedly, this work revealed that centriole growth is homeostatic: if centrioles grow slowly, they grow for a longer period of time, and so ultimately grow to a consistent size. We found that regulating Plk4 levels and activity is important for establishing this inverse relationship between the growth rate and growth period. I used these methods to probe the role of several factors that influence centriole length in regulating the dynamics of centriole growth.

In **Chapter 5** I describe how we used these methods to show that the dynamics of centriole growth are influenced by the basic cell cycle Cdk/Cyclin oscillator: as S-phase gets longer, centrioles grow more slowly, but they grow for a longer period. I investigate potential links between the basic cell cycle machinery and the centriole assembly pathway and provide preliminary evidence that several cell cycle regulators can influence the parameters of centriole growth.

Finally, in **Chapter 6** I summarize what we have learnt from my studies, and speculate about the mechanisms of centriole length control.

Chapter 2: Materials and Methods

2.1: Fly husbandry

2.1.1: Fly handling

Fly stocks and crosses were maintained at 25^{o}C or 18^{o}C on standard fly food (0.77% agar, 6.9% maize, 0.8% soya, 1.4% yeast, 6.9% malt, 1.9% molasses, 0.5% propionic acid, 0.03% orthophosphoric acid, 0.3% nipagin) in vials (9.5 cm X 2.5 cm) or in bottles (177ml) (Dutcher scientific). For embryo and unfertilized eggs collections, 25% cranberry-raspberry juice plates (2% sucrose and 1.8% agar) were used. Plates were supplemented with fresh yeast. Unless otherwise stated, all embryos/egg collections correspond to 0-3hr at 25°C. Standard fly handling techniques were used (Bewley, 1987). For analysis of SAPs in testes cell, mutant pupae were selected and transferred to a petri dish lined with moist paper. Once flies of correct genotype eclosed, they were manually fed for 2-3 days with 1% glucose solution to promote primary spermatocyte accumulation. Both pupae and uncoordinated flies were maintained at 25^{o}C.

2.1.2: *Drosophila* stocks

Standard WT lab stocks *OregonR* or w^{67} were used as indicated. Other fly stocks used are shown in Table 8.1 in the appendix.

2.1.2.1 Generation of Transgenic lines

In order to generate various fly transgenic lines, P element-mediated transformation vectors were created by cloning in the Gateway vectors (Basto et al., 2008). Constructs were injected, and transgenic fly lines were generated at Bestgene (USA) or the Department of Genetics, University of Cambridge (UK). Details of transgenic lines (existing or generated transgenic lines) used in this thesis are listed in Table 8.1 in the appendix.

2.1.2.2 Generation of Cilia rescue flies

Alan Wainman, a postdoctoral fellow in our laboratory, generated “cilia rescue” lines (Richens et al., 2015) in which all tissues overexpress GFP-Sas-6 and Ana2-GFP, but an Ana1 transgene expressed from a UASg promoter, is expressed only in the nervous system of the fly, allowing centrioles and cilia to assemble in the nervous system—so rescuing the uncoordinated phenotype of the *ana1* mutation. We generated flies of genotype: w; UASg-GFP-Ana1 ΔNT/Ubq-Ana2-GFP, elav-Gal4; Ubq-GFP-Sas-6, $ana1^{MecB}$/Df(*ana1*). See main text for details.

2.1.3: Assessing the hatching rate of embryos

WT, transgenic or mutant flies were kept in cages, and the flies were allowed to lay embryos on cranberry-raspberry juice plates, for 4-6hr at 25^{o}C. The embryos were then allowed to hatch on the plate, and the hatching rate of each genotype was measured by counting the number of empty egg cases left after 24-48hr. The experiment was repeated three times, and the average hatching rate was calculated.

2.1.4: Assessing the fertility of male adult flies

One WT or mutant adult male was mated with three WT virgin females in a tube. Three tubes per genotype were analysed. The male flies were considered infertile when no progeny was obtained.

2.2: Antibodies used in this thesis

All primary antibodies used and respective concentrations are shown in Table 2.1. For immuno-staining of various *Drosophila* tissues, Alexa 405, 488, 568 and 647 secondary antibodies (Molecular probes, Jackson Laboratories) were used at 1:1000 dilution. For immuno-staining of GFP or RFP tagged proteins, respective GFP and RFP booster antibody (nano bodies, Chromo Tek) were used at 1:1000 dilution. For western blotting experiments, HRP-conjugated secondary antibodies (GE Healthcare) were used at 1:3000dilution.

Table 2.1: Primary antibodies used in this thesis

Protein	Species	Source	Concentration	ID	Application
α-tubulin	Mouse	Sigma (DM1α)	1mg/ml (1:1000)	JR #141	Immunofluorescence
γ-tubulin	Mouse	Sigma (GTU-88*)	1mg/ml (1:1000)	JR #142	Immunofluorescence
Actin	Mouse	Sigma	1.5mg/ml (1:1000)	JR #221	Western blotting
Ana1 CT	Rabbit	(Stevens et al., 2009)	Serum (1:500)	JR #3	Antibody injection Western blotting
Ana1 Mid	Rabbit	(Conduit and Raff, 2010)	Serum (1:500)	JR #1	Antibody injection Western blotting
Ana1 CT	Guinea Pig	(Conduit et al., 2015b)	Serum (1:500)	JR #213	Western blotting
Ana1 CT	Rat	(Stevens et al., 2010a)	Serum (1:500)	JR #211	Western blotting

Ana2	Rabbit	(Stevens et al., 2010a)	Serum (1:500)	JR #6	Western blotting
Asl NT	Guinea Pig	(Roque et al., 2012)	Serum (1:500)	JR #199	Immunofluorescence
Asl NT	Rabbit	(Conduit and Raff, 2010)	Serum (1:500)	JR #11	Immunofluorescence
Asl NT	Rat	(Franz et al., 2013)	Serum (1:500)	JR #197	Immunofluorescence
Cnn	Sheep	(Conduit et al., 2014b)	Serum (1:500)	JR #193	Immunofluorescence
Cnn	Rabbit	(Lucas and Raff, 2007)	Serum (1:500)	JR #53	Immunofluorescence Western blotting
Sas-4 NT	Rabbit	(Basto et al., 2006)	Serum (1:500)	JR #63	Immunofluorescence
CP110	Rabbit	(Franz et al., 2013)	Serum (1:500)	JR #15	Western blotting
Cep97	Rabbit	Generated by Jeroen Dobbelaere	Serum (1:500)	JR #250	Western blotting
Sas-6	Rabbit	(Peel et al., 2007)	Serum (1:500)	JR #49	Western blotting
GFP	Mouse	Roche	1mg/ml (1:1000)	JR #186	Immunofluorescence and western blotting
Cep135	Rabbit	(Roque et al., 2012)	Serum (1:500)	JR #227	Immunofluorescence
Klp10A	Rabbit	Generated by Teresa Barros	Serum (1:500)	JR #77	Western blotting

2.3: Molecular Biology

2.3.1: Purification of genomic DNA from *Drosophila*

15 males and 15 females anaesthetized flies of the same genotype were frozen and homogenised on ice in 400μl of Buffer A (100mM Tris-HCl pH 7.5, 100mM EDTA, 100mM NaCl, 0.5% SDS). The mixture was incubated at 65°C for 30 min. 800μl of Buffer B (1:2.5 volume of 5M CH_3CO_2K and 6M LiCl respectively) was then added,

and the samples were incubated for 1hr on ice. Samples were centrifuged for 15 min at 12,000rpm at RT. 1ml of supernatant was transferred to a fresh 1.5ml tube, mixed with 600μl of isopropanol and centrifuged at 12,000rpm at RT for 15 min. The pellet was then washed with 70% ethanol twice, air dried and re-suspended in 150μl TE buffer or water.

2.3.2: Cloning of vectors to generate transgenic fly lines

Gateway cloning (Thermo Fisher Scientific) was used to generate vectors for p-element-mediated transformation. The primers were designed to incorporate attB sites into the PCR product. w^{67} genomic DNA or cDNA were used as a template and Phusion High Fidelity (NEB, #M0531) or Q5 Hot Start High-Fidelity (NEB, # M0494), 2X master mixes were used to generate PCR fragments using the following protocol:

PCR reaction

Component	Volume (μl)
2x master mix	25
Template (10-20ng/μl)	1
Forward primer 10μM	2
Reverse primer 10μM	2
DMSO (only for Phusion)	1.5
Distilled water	To final 50μl

PCR protocol

98°C	30 seconds	
98°C	10 seconds	} repeat 30 times
50-72°C	30 seconds	
72°C	30 seconds/kb	
72°C	5 minutes	

The resulting fragments were then introduced into the pDONR-Zeo vector (Gateway) according to the gateway BP reaction to generate an attL-containing entry vector. The resulting entry clones were recombined with the appropriate attR-containing destination vectors according to the Gateway LR reaction. The vectors used/ generated are listed in Table 8.2 in the appendix.

2.3.3: Plasmid mutagenesis

Point mutations and internal deletions were introduced within the full-length genomic DNA or cDNA using QuickChange II XL Site-Directed Mutagenesis (Agilent, #200522) or Q5 Site-Directed Mutagenesis Kit (NEB, #E0554). The primers used for the cloning, site-directed mutagenesis and Sequencing are listed in Table 8.3 in the appendix. The following PCR conditions were followed:

PCR reaction (**QuickChange II XL Site-Directed Mutagenesis)**

Component	Volume (μl)
10x reaction buffer	5
Template (10ng/μl)	1
Forward primer (125ng/μl)	1
Reverse primer (125ng/μl)	1
dNTP mix	1
'Quick Solution'	3
Distilled water	38μl

PCR protocol (**QuickChange II XL Site-Directed Mutagenesis)**

95°C	1 min	
95°C	50 seconds	repeat 18 times
60°C	50 seconds	
68°C	1min/kb	
68°C	7 minutes	

PCR reaction (Q5 Site-Directed Mutagenesis)

Component	Volume (μl)
2x master mix	12.5
Template (10ng/μl)	0.5
Forward primer (125ng/μl)	1
Reverse primer (125ng/μl)	1
Distilled water	10

PCR protocol (Q5 Site-Directed Mutagenesis)

98°C	30 seconds	
98°C	10 seconds	} repeat 30 times
50-72°C	30 seconds	
72°C	30 seconds/kb	
72°C	5 minutes	

The original template plasmid in the sample was degraded by adding 1μl of DpnI restriction enzyme (10U/μl) and incubated at 37°C for 1hr before transforming into XL10-Gold Ultracompetent Cells for QuickChange II XL Site-Directed Mutagenesis or into DH5α high efficiency competent cells (NEB) for Q5 Site-Directed Mutagenesis.

2.3.4: Construction of vectors for *in vitro* RNA production (for RNA-microinjection experiments)

To generate constructs for *in vitro* mRNA production, the complete coding region of a gene or cDNA was amplified from IP16240 (DGRC) for Ana1 or pENTR4-Klp10A (Radford et al.,2012) for Klp10A with att sites at either end of the cDNA and inserted into the Gateway pDONR-Zeo vector (Invitrogen). The missing 67bp of Ana1 DNA sequence in IP16240 (DGRC) was repaired by digesting and ligating Ana1 fragment from pDONR-Zeo-Ana1 genomic DNA into the pDONR-Zeo-cAna1. Ana1 or Klp10A deletions were generated by site-directed mutagenesis using the Quikchange II XL mutagenesis kit (Agilent) according to the manufacturer instructions. Deletions were

cloned via Gateway (Invitrogen) into the pRNA-(NT)-GFP or pRNA-GFP-(CT) destination vector (Conduit et al., 2014b; Cottee et al., 2015; Richens et al., 2015). cDNA clones of all the cell cycle regulators were obtained from DGRC and were cloned via Gateway into the pRNA-GFP (CT) as listed in Table 8.3 in the appendix. All plasmids were isolated using Qiagen mini or midi kits, and DNA sequencing was performed either by Sourcebioscience or Eurofinsgenomics. MacVector 14.5.2 software was used to generate plasmid maps, PCR and sequencing primers and DNA analysis. *In vitro* RNA synthesis was performed using a T3 mMESSAGE mMACHINE kit (Ambion) and the resultant capped mRNAs were purified using an RNeasy MinElute kit Clean up kit (Qiagen). All RNA constructs as listed in Table 2.2 were injected at a concentration of 2mg/ml into 0-30 min old embryos.

Table 2.2: Constructs generated for injecting into *Drosophila* embryos

Construct #	Construct name	Description
Ana1		
1	GFP-Ana1 (1-1729)	WT
2	GFP-Ana1 (640-1729)	Ana1ΔNT
3	GFP-Ana1 (756-1729)	Ana1ΔNT2
4	GFP-Ana1 (1-935)	ΔCT
5	GFP-Ana1 (Δ1282-1315)	Ana1ΔCR2
6	GFP-Ana1 (1-1282)	ΔCT2
7	GFP-Ana1 (1283-1729)	Ana1ΔNT3
8	GFP-Ana1 (Δ135-1282)	Ana1ΔMid1
9	GFP-Ana1 (Δ641-1282)	Ana1ΔMid2
10	GFP-Ana1 (Δ18-134)	Ana1ΔCR1
Klp10A		
1	Klp10A (1-805)-GFP	WT
2	Klp10A (66-805)-GFP	NTΔ
3	Klp10A (265-805)-GFP	NT & CC1Δ
4	Klp10A (611-805)-GFP	NT, CC1 & MDΔ
5	GFP-Klp10A (1-805)	WT
6	GFP-Klp10A (1-704)	CC2Δ
7	GFP-Klp10A (1-277)	MD & CC2Δ

8	GFP-Klp10A (1-204)	CC1, MD & CC2Δ
9	GFP-Klp10A (1-65)	Linker, CC1, MD & CC2Δ
10	Klp10A (Δ205-264)-GFP	CC1Δ
11	Klp10A (Δ278-610)-GFP	MDΔ
12	Klp10A (Δ205-610)-GFP	CC1 & MDΔ
Cell cycle regulators		
1	Myt1-GFP	From DGRC clone GH08848 after adding back first missing 4bp (#1)
2	Wee1-GFP	From DGRC clone_LD27552 after mutating back one bp to WT (#12)
3	Twine-GFP	From DGRC clone_LD19391 (#3)
4	String-GFP	From DGRC clone_LD47579 (#9)

2.4: Biochemistry

2.4.1: Preparation of *Drosophila* embryo, brain, wing disc and testes lysates for protein expression analysis

Drosophila embryos (0-3hr old) were collected and washed in PBS-0.05%Triton X-100, dechorionated in 60% bleach for 2 min. Dechorionated embryos were washed three times in PBS-0.05%Triton X-100. Embryos were then washed with 2ml heptane into a glass vial containing 2ml of methanol with or without 3% 0.5M EGTA, shaken for 30 secs and were left to fall into the lower, methanol-EGTA layer. After removing all the liquid from the vial, the embryos were washed three times with methanol and incubated overnight or up to several weeks in methanol at 4^{o}C. The methanol was then removed and embryos were washed three times for 15 min in PBS-0.2% Triton X-100. 50 pre cellularised staged embryos were selected in 20μl of PBS-0.2% Triton X-100, mixed with 30μl, 2xSDS loading dye. For other fly tissue sample lysates for

SDS-PAGE: twelve 3rd instar larval brains or twenty-four wing discs or twelve late pupae testes (seven testes for Klp10A blot) were dissected in PBS and transferred immediately into 36μl of 2xSDS loading dye. All samples were boiled for 10 min at 98°C and stored at -20°C until analysis. 5μl of each sample was analysed by SDS-PAGE followed by western blotting.

2.4.2: Electrophoresis and Western blotting

Protein lysates were run on 3-8% precast Nu-PAGE polyacrylamide gels (Thermo Fisher Scientific, #EA03785BOX) and Nu-PAGE tris-acetate SDS running buffer (Thermo Fisher Scientific # LA0041). Proteins were then transferred onto nitrocellulose membranes (Biorad, #162-0112) in western blot buffer (25% methanol, 1.13% glycine, 0.58% Tris, 0.01% SDS). The membranes were then quickly washed with distilled water, protein loading was checked using Ponceau staining (Sigma: P3504) and blocked in milk solution (PBS, 4% milk powder, 0.1% Tween-20) for 1hr at RT on the shaker. The protein blocked membranes were then incubated with primary antibody at RT for 1hr. After washing three times with TBST (TBS-0.1% tween 20), the membranes were then incubated with appropriate secondary antibody for 45 minutes to 1hr with anti-rabbit (NA934V, GE Healthcare) or anti-sheep (NA931V, GE Healthcare) or anti-guinea pig (AB7139, Abcam) or anti-mouse (NA931V, GE Healthcare) at a dilution of 1/3000 dilution. Afterwards, the membranes were washed three times with TBS-0.1% Tween-20 for 15 min each wash. Finally, the membranes were developed by enhanced chemiluminescence according to the manufacturer's instructions (Thermo Scientific Super Signal West Femto Maximum Sensitivity Substrate, #34095) or 2 or 3-fold dilution of the mixed chemiluminescence reagents and exposed to X-ray film.

2.4.3: Labelling of Antibody for microinjection

Affinity purified antibodies were desalted into C-buffer pH 8.6 (50mM HEPES, 50mM KCl+1mM MgCl, 1mM EGTA pH 7.5) on a P6 desalting column using an AKTA FPLC system (GE healthcare). 2ml of the peak protein fraction was then incubated with 2μl of 50μg/μl of N-hydroxysuccinaminde-Texas Red (Molecular Probes) at RT for 1hr. The uncoupled dye was removed by desalting on a P6 column into C-buffer pH 7.6 (50mM HEPES, 50mM KCl, 1mM MgCl, 1mM EGTA pH 7.5). Finally, the 2ml of peak protein fractions were concentrated using centrifugal concentrators (Amicore filter, Cut-off 50kDa, Millipore) at 4000rpm at 4^{o}C 2min bursts until a concentration of ~5mg/ml was achieved. 3μl aliquots were flash frozen in liquid nitrogen and stored at -80°C.

2.4.4: Fold increase calculation of the overexpressed proteins

To estimate the relative concentrations of overexpressed proteins, samples of the overexpressing tissue were serially diluted in 1XSDS loading buffer and then loaded onto a protein gel. After blotting, the band intensity of the serial dilution that most closely matched that of the WT endogenous protein was used as an approximate estimate of the level of overexpression.

2.5: Cell Biology

2.5.1: Preparation of embryos or fly testes for live imaging analysis

0-1 hr embryos were collected on cranberry and raspberry agar plates and aged at 25°C for 45 min to 1 hr. The embryos were then transferred on to the double-sided sticky tape and rolled gently with the tip of the forceps to dechorionate. The dechorionated embryos were mounted on a line of glue painted on a 35 mm glass bottom petri dish (MatTek, #P35G-1.5-14C) and were left to desiccate for 1 min at 25°C. After desiccation, the embryos were covered with Voltalef® grade H10S oil (ARKEMA) and imaged immediately.

Testes from GFP or mCherry tagged transgenic flies were dissected from early or late pupae or young adult flies in PBS and mounted on glass bottom microwell dishes (MatTek). A round glass coverslip was placed on top of the samples and sealed using Voltalef oil to prevent drying of the sample and imaged immediately.

2.5.2: Microinjection of antibodies or RNA into living embryos

For RNA injection experiments 0-20 min old embryos were dechorionated and desiccated for 5 min at 25^{o}C, covered with Voltalef® grade H10S oil (ARKEMA) before injecting the *in vitro* transcribed RNA constructs. The embryos were then allowed to develop further for 1hr before imaging. For antibody injection experiments, Texas Red™-X, Succinimidyl Ester (Thermofisher)-coupled antibodies were injected into 1.5hr old dechorionated embryos, and the embryos were imaged immediately. The

antibodies used for blocking the function of centrosomal proteins are described in Table 2.1.

2.5.3: Immunofluorescence staining of eggs or embryos

The embryos were fixed with Methanol as described in section 2.4.1. The methanol was then removed from the embryos and washed for three times for 30 min in PBS-0.2% Triton X-100-5% BSA at RT. Samples were then incubated with primary antibody overnight at 4^{o}C. The following day samples were washed 3X20 min in PBT-BSA and then incubated for 2 hrs with secondary antibody (Alexa Flour 488/568/647, Thermo Fisher Scientific; diluted in PBS-0.2% Triton X-100-5% BSA) at RT. Samples were then washed for 3X 15 min in PBT and mounted in mounting medium (85% glycerol, 2.5% n-propylgallate). For staining DNA, embryos were washed once in PBS-0.2% Triton X-100, followed by 15 min incubation in Hoeschst 33258 (Thermo Fisher Scientific), followed by a last wash of PBS-0.2% Triton X-100 before mounting in mounting medium (85% glycerol, 2.5% n-propylgallate) with high-precision glass coverslips (CellPath) onto the microscope slides.

2.5.4: Fixation and staining of *Drosophila* tissues for immunofluorescence analysis

3rd instar larval brains (or testes from early or late pupae or early adults) were dissected in PBS, incubated in 4% formaldehyde for 20 min (or 30 min for testes), then in 45% acetic acid for 15 s, and finally in 60% acetic acid for 3 min on a coverslip (the fly testes were cut open on the coverslip using tungsten needles). The acetic acid step was omitted if the slides were made to preserve GFP fluorescence. The slide (or silicon-dipped coverslips of thicknesses 1 for testes for 3D-SIM) was used to pick the

coverslip up and put between two pieces of Whatman paper (GE Healthcare), pressed with thumb, tapped vigorously with the tip of the pencil on the slide (tenderly in the case of testes or not at all for the samples prepared for 3D-SIM) and immediately flash frozen in liquid nitrogen. The slides (or coverslips) were removed from liquid nitrogen and the coverslips were flicked off with a razor blade. The slides (or coverslips) were incubated in cold 100% methanol at -20^{o}C for 5 min (or 8-15 min for testes). The slides (or coverslips) were washed 4 times with PBS-0.1% Triton X-100 for 10 min, air dried for 5 min and then samples were covered with 10μl primary antibody solution (diluted in PBS-0.1% Triton X-100, see Table 2.1), sealed with a coverslip (no coverslip for 3D-SIM sample preparation) and then incubated overnight at 4^{o}C in a humid chamber. The following day, the slides (or coverslips) were washed 3X5 min in PBS-0.1% Triton X-100. After air drying, the samples were covered with 10μl secondary antibody solution (Alexa Fluor 488/568/647, Thermo Fisher Scientific; diluted in PBS-0.1% Triton X-100), sealed with a coverslip (or no coverslip for 3D-SIM sample preparation) and then incubated at RT for 3hr in a humid chamber at 25^{o}C. The slides (or coverslips) were then washed 3X 15 min in PBS-0.1% Triton X-100, incubated in PBS-0.1% Triton X-100- 1/5000 V 10mg/ml Hoescht33258 (Thermo Fisher Scientific) for 10 min and washed in PBS-0.1% Triton X-100 for 5 min. Finally, the samples were covered with 10μl of mounting medium {85% glycerol, 2.5% n-propylgallate or ProLong gold anti-fade mounting medium (Invitrogen, Karlsruhe, Germany) or with VECTASHIELD® mounting medium with or without DAPI (Vector Laboratories)} onto the microscope slides with high precision glass coverslips (CellPath) for 3D-SIM sample preparation and sealed with a coverslip (or on slide). The sides of the coverslip were painted with nail polish to affix the coverslip onto a slide. The slides were stored at 4^{o}C in the dark until microscopic analysis.

2.6: Microscopy

2.6.1: Live confocal imaging of *Drosophila* embryos and testes

Dechorionated fly embryos or dissected testes were imaged on a Perkin Elmer ERS Spinning Disc confocal system on a Zeiss Axiovert 200M microscope, using a Zeiss plan-apochromat 63X/1.4NA, oil objective and a charge coupled device camera (Orca ER, Hamamatsu Photonics). All embryo collection was done at 25^{o}C, and all imaging was done at 22^{o}C. For imaging GFP tagged proteins alone, the UltraVIEW ERS fast sequential imaging mode was used (red/green dual pass-band filter: 525nm pass-band centre, 50nm half-power bandwidth and 640nm pass-band centre, 120nm half-power bandwidth, for imaging 488nm and /or 568nm emission). For imaging GFP tagged proteins together with RFP or mCherry tagged proteins or TexasRed labelled antibody, the UltraVIEW ERS emission discrimination imaging mode was used (green emission filter: 527nm pass-band centre, 55nm half-power bandwidth and blue/red emission filter: 445nm pass-band centre, 60nm half-power bandwidth and 615nm pass band centre, 70nm half-power bandwidth). Settings used were 2x2 bin, 100% laser power for GFP and 50% for RFP or mCherry or TexasRed, 200ms exposure time and slice spacing of 0.5µm. For all embryo imaging experiments, 13 confocal sections were collected every 20 or 30secs and the focus was occasionally re-adjusted in between the intervals.

2.6.2: Immunofluorescence imaging of fixed *Drosophila* eggs/embryos/brains/testes

Fixed *Drosophila* eggs/embryos, brains and testes samples were imaged on the inverted Olympus Fluoview FV1000 IX81 point scanning confocal system (Olympus) with UPlanSApo 60X/1.35NA oil objective and the FV1000 software. 0.5µm thick confocal sections were taken to cover the entire depth of the centriole, centrosome or SAP in a sample.

Some of the fixed samples were imaged on the epifluorescence (Zeiss Axioskope II) microscope equipped with a CoolSnapHQ camera (Photometrics) with Zeiss plan-neoflour 60X/1.25NA oil objective and MetaMorph software (Molecular Devices). All images were Z-Stacks of 0.5µm steps.

2.6.3: Super-resolution imaging of fixed *Drosophila* testes

For super-resolution imaging of fixed *Drosophila* testes, images were taken at 21°C on an OMX-V3 system (GE Healthcare) with a 60x/1.42 NA oil UPlanSApo objective (Olympus), 405nm, 488nm, 593nm diode lasers. 20-23 optical sections were collected (0.125µm steps) with five phases and three angles, to create each image using the OMX Deltavision software. SIM reconstruction was performed with SoftWorx software (Applied Precision). Different image channels were aligned using 200nm TetraSpeck bead (Thermo Fisher scientific) slides as a reference for the transformation in the OMX Editor software.

2.6.4: Transmission electron microscopy

Wing-discs from 3rd instar larvae or testes from late pupae were dissected in PBS and fixed in 2.5% glutaraldehyde, 4% paraformaldehyde in 0.1M cacodylate (or in PIPES) buffer (pH7.2) for 2hr at RT and left overnight at 4^{o}C. Samples were washed in 0.1M cacodylate (or in PIPES) buffer and post-fixed in 1% OsO4 for 2hr at RT, followed by extensive washing in distilled water. Samples were then stained with 0.5% uranyl acetate overnight at 4^{o}C, washed in distilled water, dehydrated in an ethanol series and embedded in Agar100 (Agar Scientific). Blocks were polymerised at 60^{o}C for 42hr. Semi-thin serial sections (100 nm) were obtained in a Leica EM UC7 ultramicrotome (Leica Microsystems, Austria) and stained in lead citrate. Images of centrioles in longitudinal orientation were taken on a TECNAI T12 transmission microscope (FEI, Netherlands) at 11,000x or 18,500x magnification, to measure centriole length in interphase cells from wing-discs. Semi-thick serial sections (150nm) were obtained, and dual-axis tilt series (typically -55°-55°) were acquired in a TECNAI T12 transmission microscope (FEI) at 13,000x magnification with SerialEM, for observing the testes SAPs. Using the IMOD software package (Mastronarde, 2005) the images were aligned, and the tomograms were reconstructed.

2.7: Image analysis and statistics

2.7.1: Quantification of centrosomes in larval brain cells and centriole in pupal testes cells

The images acquired on an Olympus confocal microscope or Zeiss Axioskope II were processed in Volocity software (Perkin Elmer) for quantification of centrosomes in

larval brain and pupal testes cells. Prometaphase or metaphase brains cells were chosen by DNA staining, and the number of Asl and Cnn positive dots were counted in each cell. Brain cells were scored for the presence or absence of centrosomes and the percentage of cells falling into different categories was calculated for each brain separately, and these values per brain were finally averaged. The Asl and Cnn positive elongated centrioles were counted in late G2-phase or meiosis I primary spermatocytes. The average centriole number per cell and the percentage of cells falling into different categories was calculated for each testis.

2.7.2: Quantification of centriole length in testes

Images acquired on Olympus confocal microscope of meiosis II testes cells stained for DNA, Asl, Cep135 and α-tubulin or DNA, Asl, Spd2 and GTU88* were processed in the Volocity (Perkin Elmer) software. Centriole length was measured in the appropriate channel in the extended focus mode using the line tool of the Volocity software. The average centriole length was calculated for each testis. Data was analysed in Prism (version 7.0 for Mac OSX, GraphPad Software, Inc).

2.7.3: Quantification of *de novo* centriole formation in unfertilised eggs

0-4 hr old unfertilised eggs expressing a GFP-fusion protein under the UASg-Gal4 system were collected and stained for DNA and Cnn. They were then imaged using a 20X air objective on a Zeiss Axioskope II microscope. The unfertilised eggs containing more than four Cnn and α-tubulin positive asters were scored as containing *de novo* formation of centriole-like structures. The percentage of eggs falling into *de*

novo formation of centriole-like structures or no *de novo* formation of centriole-like structures were calculated.

2.7.4: Analysis of live imaging data, acquired on the Perkin Elmer ERS spinning Disc confocal system

In antibody-injection experiments in *Drosophila* embryos the total centrosomal fluorescence was measured by drawing a boxed region centred around the brightest centrosomal voxel in Volocity 6.1.1. The local cytoplasmic background fluorescence, measured in an identically sized nearby boxed region, was then subtracted. The fluorescence values of inhibited and control centrosomes were compared using a t-test (Mann-Whitney test), and the error bars represent s.e.m in GraphPad Prism 7 (GraphPad Software Inc.).

For high throughput centriole protein dynamics, the collected images were processed using Fiji (NIH, US). All images were maximum intensity projected and bleach-corrected with Fiji's exponential fit algorithm, to analyse the dynamics of centriole proteins. The backgrounds were subtracted with a rolling ball radius of 10 pixels and using the "Subtract Background" function of Fiji software. A plug-in of Fiji, TrackMate (Tinevez et al., 2017) was used to track the centrioles with the settings of track spot diameter size of 1.1µm, initial threshold of >0.02 and quality of >0.07. The collected values were transferred to GraphPad Prism 7 (GraphPad Software Inc.), and various centriole growth regression curves were tested, as described in Aydogan et al., (Aydogan et al., 2018). S-phase and mitosis are two different phases of the cell cycle, and hence the growth curves in each embryo were modelled discontinuously. The data for S-phase were modelled using two separate functions: (1) linear growth and

(2) linear growth followed by a plateau, which was the best fit for the Sas-6-GFP incorporation data. The final regression model curves were created by calculating the best-fit parameters such as means of growth rate, growth period and S-phase length. The origin of the curve was re-adjusted approximately 1-1.5 min after where the centrosomes from the earlier cycle and the point at which TrackMate's tracking algorithm could detect the centrosome separation with the threshold parameters. The mean intensity, the initial mean intensity values were normalized to zero and hence normalized the rest of the data accordingly.

2.7.5: Analysis of data acquired on the OMX V3 super-resolution imaging system

The images collected from OMX-V3 system (GE Healthcare) were processed in Fiji. The images with very uniform centrioles (>10) for each sample were selected for measuring the radial diameter of the centriole. Several z-slices of the images were taken and maximum intensity projected to obtain the final picture of the centrioles. Ten lines were drawn through each centriole in Fiji, to calculate the radial diameters of the GFP protein. Double Gaussian curves were fitted, and the average fluorescence intensity profile of each protein was obtained. The distance between the two peaks was measured in Fiji. For the proteins, where the two peaks were not resolved, the diameters were measured by fitting the intensity profile crossing the centriole centre to two Gaussian curves of equal heights and standard deviations. The radial diameter calculated is the distance between the centre positions of each Gaussian peak. The analysis was performed with GNU Octave version 4.0.0 and Octave-Forge-optim package version 1.4.1. Data was analysed in Prism.

2.7.6: Quantification of GFP or SAPs fluorescence in live embryo or laid eggs or pupal testes

Z-stacks of images collected on the Olympus FV1000 confocal microscope described in section 2.6.2, were merged and analysed with Volocity software (Perkin-Elmer) for GFP or SAP fluorescence quantification. For GFP fluorescence in live embryo or fixed laid eggs, the find-spots function in the GFP channel was used to find objects in the image. The intensity threshold for each image was adjusted to just above the level at which random spots were detected in the background. Any objects touching the edges of the images were excluded. The total fluorescence signal within each object was then quantified using the measurement function in Volocity. The ROI was drawn manually in the areas that did not include centrosomes, and the average background fluorescence was determined. Average background values for each channel were then subtracted from GFP fluorescent values. The total GFP or mCherry fluorescence was manually measured in a boxed region centred around the centrosomes and subtracted the cytoplasmic background fluorescence in the RNA injection experiments. The average WT signal was set to one, and then each value was normalised to the WT signal. For quantification of SAP number per testes cell or laid egg, SAP intensity and SAP area were calculated in Volocity by manually drawing a region of interest (ROI) around each SAP. Background fluorescence was subtracted before obtaining the final value.

2.7.7: Centriole length measurement in *Drosophila* wing disc cells

Images of centrioles in longitudinal orientation taken on a TECNAI T12 transmission microscope (FEI, Netherlands) from wing-disc cells were manually measured using the line tool in Fiji (ImageJ 1.48f). The length of the MT doublets of the centriole within the electron-dense area was measured in nm.

2.7.8: Statistical analysis

Graphs and statistical analysis of data were performed using either Microsoft Excel 15.19.1 for Mac or GraphPad Prism 7.0 statistical package. D'Agostino-Pearson omnibus normality test in the GraphPad Prism was applied to test whether the data was normally distributed (i.e. bell-shaped, of Gaussian). If so, a **Student's t-test** was performed to determine whether there is a significant difference between the **means** (parametric) of the two groups, assuming the two groups are unpaired (i.e. the values on the same row are not related to each other), using Welch's correction where it is not assumed that the means have equal standard deviations. When these assumptions are correct, a Student's t-test produces accurate and precise estimates. Alternatively, a **Mann-Whitney test** was performed to establish whether there is a significant difference between the **medians** (nonparametric) of two unpaired, two tailed groups, when the dataset within one or both groups was not normally distributed (as this test does not require the assumption of normal distributions). The Mann Whitney test is simple, robust and leaves less room for improper use and misunderstanding.

To test the variation of **means** among three or more unpaired group (each of which is normally distributed), and considering only one independent factor, a **One-way ANOVA test** (Analysis of variance test) was performed. ANOVA test is conceptually similar to multiple two-sample Student's t-tests, but is more conservative, relatively robust against violations of its assumptions and is suited to a wide range of practical problems. ANOVA test is computationally elegant and is probably the most useful technique in the field of statistical inference. Alternatively, a **Kruskal-Wallis test** was used if the dataset within one or more of the groups was not normally distributed.

2.7.9: Image manipulation and presentation

All images taken from upright light or con focal or spinning disc microscope were adjusted for colour, contrast and brightness for each channel using Volocity 6.1.1. The smooth zoom filter was applied to all images (this filter only affects the aesthetic appearances of images but does not alter quantification). Images were then exported as TIFF files and contrast was further adjusted, consistently across any set of experimental and control images, using Adobe Photoshop CS6 13.0.0, while movies were exported as AVI files from Volocity.

All super-resolution images obtained on the OMX V3 system in this study are maximum intensity projections unless otherwise stated in Fiji (ImageJ 1.48f). Contrast and brightness were adjusted for easier observation. All control and experimental images were altered in the same way.

Chapter 3: The role of Ana1 in centrosome assembly

3.1: Introduction

Anastral spindles 1 (Ana1) was identified as a potential centriole assembly protein in two genome-wide RNAi screens in *Drosophila* S2 cells (Dobbelaere et al., 2008; Goshima et al., 2007). An *ana1* mutation was identified in a genetic screen of potential mechanosensory mutants (Avidor-Reiss et al., 2004), and *ana1* mutant flies exhibit all the features of a ciliary mutant: adult flies are severely uncoordinated due to the lack of functional cilia, axonemes are missing in the sperm tails, and so the sperm are immotile (Blachon et al., 2009). These results suggest that Ana1 has an unknown, but essential role in centriole and cilium formation in flies.

Mammalian Cep295 (also called KIAA1731 or Ddc8) are Ana1 homologues (Catalano et al., 1997; Knorz et al., 2010; Nagase et al., 2000). In vertebrate cells, the newborn centrioles usually lose their cartwheel structures during early mitosis (Banterle and Gönczy, 2017; Fırat-Karalar and Stearns, 2014; Gönczy, 2012), and Cep295 seems to specifically stabilize such cartwheel-less centrioles (Izquierdo et al., 2014). The newly stabilized centrioles subsequently acquire the competence to recruit PCM and thereby function as a centrosome—a process termed centriole-to-centrosome conversion (Fırat-Karalar and Stearns, 2014; Gönczy, 2012). In the absence of Cep295, new centrioles are formed in S/G2-phase and lose their associated cartwheel in mitosis, but they cannot organize PCM correctly, and are not converted to centrosomes. The newly formed centrioles lack both a cartwheel and PCM and are destabilised and ultimately disintegrate (Izquierdo et al., 2014).

As described in Chapter 1, section 1.4, a largely conserved pathway of centriole assembly has been identified, but, at the time I started my studies, it was unclear how Ana1 might fit into this pathway. I therefore decided to better characterize the *in vivo* function of Ana1 in flies. In this chapter, I describe how *ana1* mutants have very few centrosomes in larval brain cells and pupal spermatocyte cells. I perform a structure-function analysis of Ana1 using a medium-throughput embryo RNA injection assay and find that Ana1 plays a critical role in maintaining the key centriole and centrosome assembly protein Asl at centrioles. I provide evidence that Ana1 is not essential for centriole duplication, but is required to stabilise centrioles once they are formed. Unexpectedly, I also show that Ana1 promotes centriole elongation in a dose-dependent manner: centrioles are shorter when the *ana1* dosage is reduced and are longer when the *ana1* dosage is increased. Importantly, the function of Ana1 in promoting centriole elongation appears to be mechanistically different to its role in promoting Asl recruitment, and so centrosome and cilium assembly. Much of the work presented in this chapter was published in 2016 (Saurya et al., 2016).

3.2: Results

3.2.1: Initial characterization of the *ana1* gene and generation of transgenic lines expressing GFP-Ana1 fusion proteins

At the time I initiated my studies, the *ana1* gene was thought to encode two polypeptides—a long form and a short form that lacked the N-terminal 639aa (Blachon et al., 2009) (Figure 3.1A). The more extended protein has two short conserved regions (CRs)—CR1 (18-134aa) and CR2 (1281-1315aa) (Blachon et al., 2009; Knorz et al., 2010) (*blue* lines, Figure 3.1A)—and an extended middle region that contained several predicted coiled-coils (*green* boxes, Figure 3.1A)—predicted using the COILs sever (Lupas et al., 1991). The short form is missing CR1 and the first two predicted coiled-coils. The most recent release of FlyBase, however, indicates that two transcripts are produced from the *ana1* gene that encode the same 1729-amino acid protein and differ only in their 5' UTR. I therefore refer to the long-form as wild-type (WT) Ana1, and the short form as N-terminally deleted Ana1 (Ana1 ΔNT [640-1729]—hereafter Ana1 ΔNT).

Naomi Stevens, a former PhD student in the laboratory, previously generated transgenic lines expressing Ana1 ΔNT (as at that time a cDNA was available only for this form) under the control of the Ubq promoter (Stevens et al., 2010a). I generated transgenic fly lines expressing full-length Ana1 (from genomic DNA) tagged with GFP at either its N-terminus or C-terminus under the control of the Ubq- or UAS- (upstream activation sequence) promoter. I also generated a line expressing a GFP-Ana1 fusion from the Ubq-promoter in which the N-terminal Conserved Region 1 was deleted (GFP-Ana1 ΔCR1). The Ubq-promoter drives moderate levels of protein expression

in all tissues (Lee et al., 1988) while the UAS promoter binds the yeast Gal4 transcriptional activator and can be used to induce high-level protein overexpression in a tissue-specific manner (Brand and Perrimon, 1993; Rørth, 1998). I also obtained a published transgenic line expressing WT Ana1-GFP from its endogenous promoter (eAna1-GFP) (Blachon et al., 2009). A western blot analysis of pupal testes tissue probed with anti-Ana1 antibodies (generated by Naomi Stevens) revealed that the GFP-Ana1, GFP-Ana1 ΔNT and GFP-Ana1 ΔCR1 fusion proteins expressed from the Ubq promoter (uGFP-Ana1, uGFP-Ana1 ΔNT and uGFP-Ana1 ΔCR1) were all overexpressed by ~5 fold compared to the endogenous Ana1 (see Materials and Methods), while Ana1-GFP expressed transgenically from its endogenous promotor (eAna1-GFP) also seemed to be slightly overexpressed (Figure 3.1B). Interestingly, the endogenous WT Ana1 protein appeared as a prominent band of ~195kD with a "smear" of slower migrating forms (that were all absent in *ana1* mutant testes), indicating that Ana1 may be extensively post-translationally modified in testes.

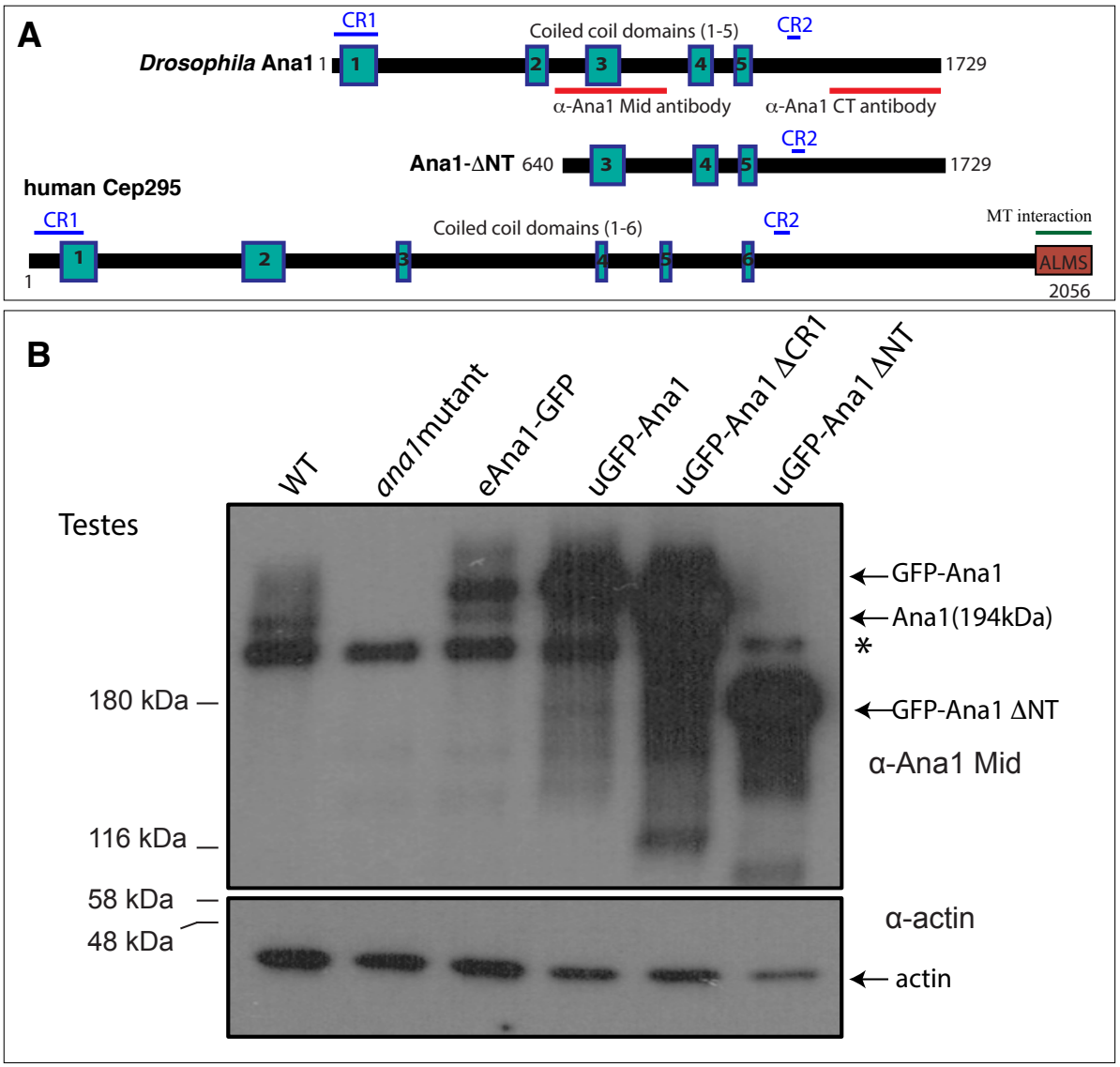

Figure 3.1: Initial characterization of the *ana1* gene and generation of transgenic lines expressing GFP-Ana1 fusion proteins. (A) A schematic illustration of *Drosophila* Ana1, Ana1 ΔNT, and human Cep295 proteins. Two conserved regions (CR1 and CR2—*blue* lines), several predicted coiled-coil domains (*green* boxes) and the recognition site of the two antibodies (*red*) are indicated. **(B)** Panels show Western blots of *Drosophila* late pupal testes from WT, *ana1* mutant, Ana1-GFP expressed under endogenous promoter (eAna1-GFP) or Ubiquitin promoter (uGFP-Ana1 or uGFP-Ana1 ΔCR1 or uGFP-Ana1 ΔNT) in an *ana1* mutant background. Blots are probed with either anti-Ana1-Mid antibody or anti-actin antibody (loading control). The expression level of the uGFP-Ana1, uGFP-Ana1 ΔCR1 and uGFP-Ana1 ΔNT proteins are ~5-10X more than that of the endogenous Ana1 protein (as judged by serial dilution experiments—see Chapter 2, section 2.4.4). Note the non specific band underneath the Ana1 band represented by *. Comparable results were obtained when similar blots were probed with the anti-Ana1-CT antibodies (data not shown).

3.2.2: Ana1 is required for the assembly and/or maintenance of centrioles and centrosomes

To analyse the function of *Drosophila* Ana1, I obtained the published *ana1*^{mecB} mutant fly line (Blachon et al., 2009) and the deficiency *Df(3R)Exel7357* (stock #7948, Bloomington stock centre), which uncovers the *ana1* gene. The *ana1*^{mecB} mutation is a C-to-T nonsense mutation at position 3358 (relative to the initiating ATG) that changes the Q1120 codon to a stop codon. I generated flies that were trans-heterozygous for *ana1*^{mecB} and the deficiency *Df(3R)Exel7357* (hereafter simply referred to as *ana1* mutants).

Although previous studies had indicated that Ana1 plays an important role in centriole and cilia function (Blachon et al., 2009; Dobbelaere et al., 2008; Goshima et al., 2007), the ability of *ana1* mutant cells to form centrioles and/or centrosomes had not been quantified *in vivo*. I therefore collected homozygous 3rd instar larvae and quantified the number of centrosomes in *ana1* mutant larval brain cells by immunofluorescence (IF). I found that *ana1* mutant cells have a dramatic reduction in centrosome number that is comparable to the reduction observed in brain cells that are mutant for the essential centriole assembly pathway genes *Sas-4* (Basto et al., 2006; Cottee et al., 2015) and *Sas-6* (Peel et al., 2007) indicating that Ana1 plays a crucial part in centrosome assembly and/or maintenance (Figure 3.2A).

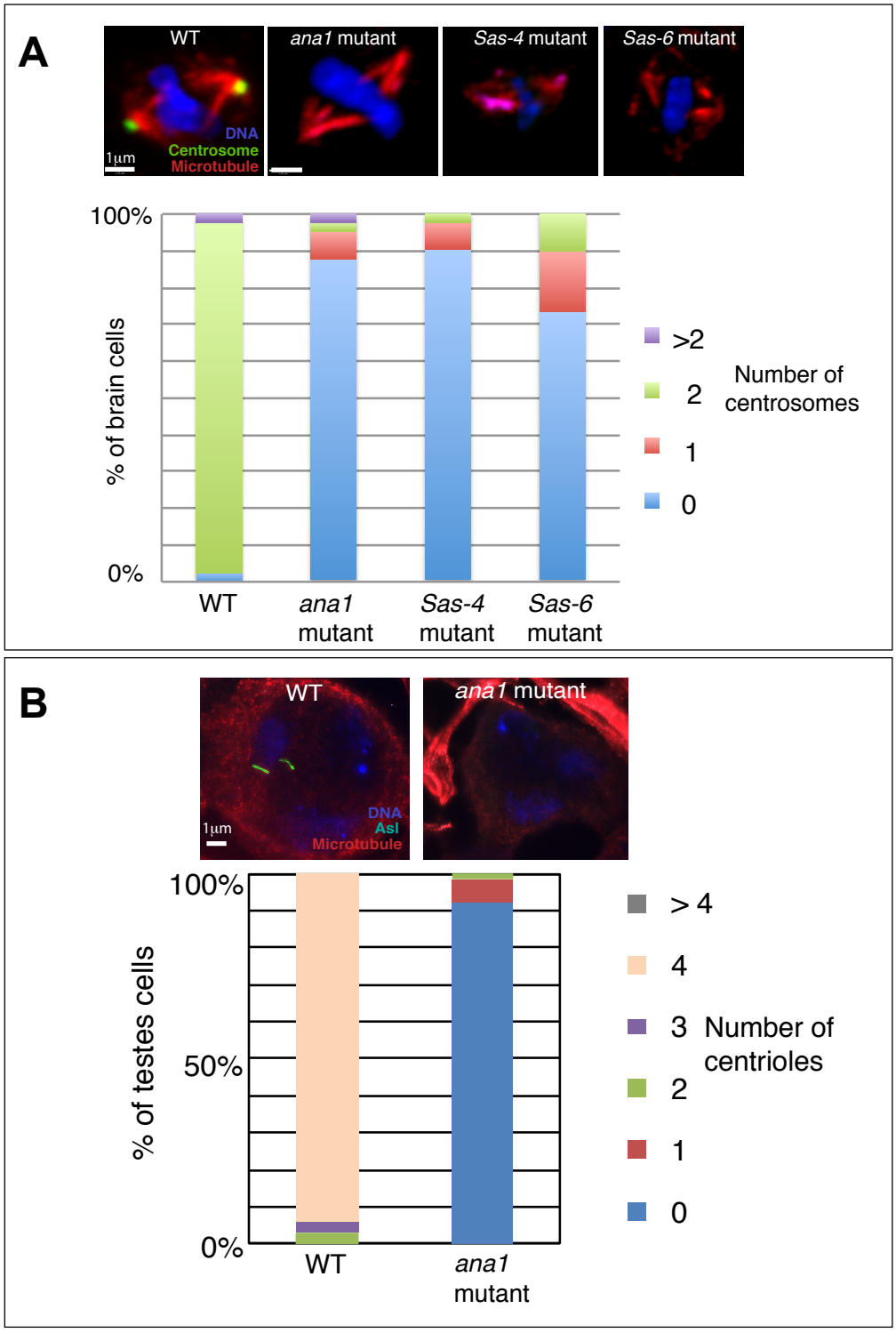

Figure 3.2: Ana1 is required for the assembly and/or maintenance of centrioles and centrosomes. (A) Micrographs show images of 3rd instar larval brain cells stained for DNA (*blue*), MTs (*red*) and the centrosome marker Asl (green) in WT or various mutant backgrounds (as indicated). Graphs show the quantification of the percentage of cells for each genotype exhibiting different numbers of centrosomes (n=30-42 cells in total, counted from 5 brains). Centrosomes were scored as dots in mitotic cells that were positive for both the centriole/centrosome protein Asl and the centrosome protein Cnn (Conduit et al., 2014b). **(B)** Micrographs show images of WT and *ana1* mutant primary spermatocytes of *Drosophila* late pupal testes stained for DNA (*blue*), MTs (*red*) and the centrosome marker Asl (*green*). Graphs show the quantification of the percentage of cells for each genotype exhibiting different numbers of centrioles (n=62 total cells from 5 different testes). Note that in WT primary spermatocytes there are normally four elongated centrioles per cell, however there are none in *ana1* mutant spermatocytes.

To test if Ana1 is required for centriole assembly and/or maintenance, I examined the centrioles in *ana1* mutant pupal testes. In this tissue, a cyst of 16 primary spermatocytes undergo an extended G2 phase during which the cell volume increases ~25X and the centrioles increase in length to ~2.6μm (González et al., 1998), forming a large, V-shaped, pair of centrioles at the end of G2 that can easily be visualized by standard confocal microscopy as described in section 1.8. Hence, testes are an excellent system with which to study centrioles due to their large size in the mature spermatocytes. I quantified the number of centrioles in *ana1* mutant spermatocytes by IF, and I found that centriole numbers were dramatically reduced in *ana1* mutant primary spermatocytes (Figure 3.2B). From the brain and testes data, I conclude that Ana1 has an essential role in the assembly and/or maintenance of centrioles and centrosomes in flies *in vivo*.

3.2.3: The N-terminal region of Ana1 does not appear to be essential for centriole assembly and/or maintenance

Surprisingly, the defect in centrosome numbers in *ana1* mutant brain cells appeared to be efficiently rescued not only by the WT eAna1-GFP and uGFP-Ana1 fusion proteins but also by the uGFP-Ana1 ΔNT and uGFP-Ana1 ΔCR1 fusion proteins (Figure 3.3A and B). Moreover, I noticed that GFP-Ana1, GFP-Ana1 ΔNT and GFP-Ana1 ΔCR1, all qualitatively rescued the severe un-coordinated defect in *ana1* mutant flies to approximately similar extents (data not shown). Interestingly, however, *ana1* mutant flies rescued by GFP-Ana1 ΔNT were both male and female sterile, whereas mutant flies rescued by GFP-Ana1 or GFP-Ana1 ΔCR1 were both male and female fertile (data not shown). Thus, the N-terminal region of Ana1 is not essential for

centriole and cilia assembly and/or maintenance (as flies expressing only this version of the protein appear to have centrioles, centrosomes and cilia), but it is essential for male and female fertility.

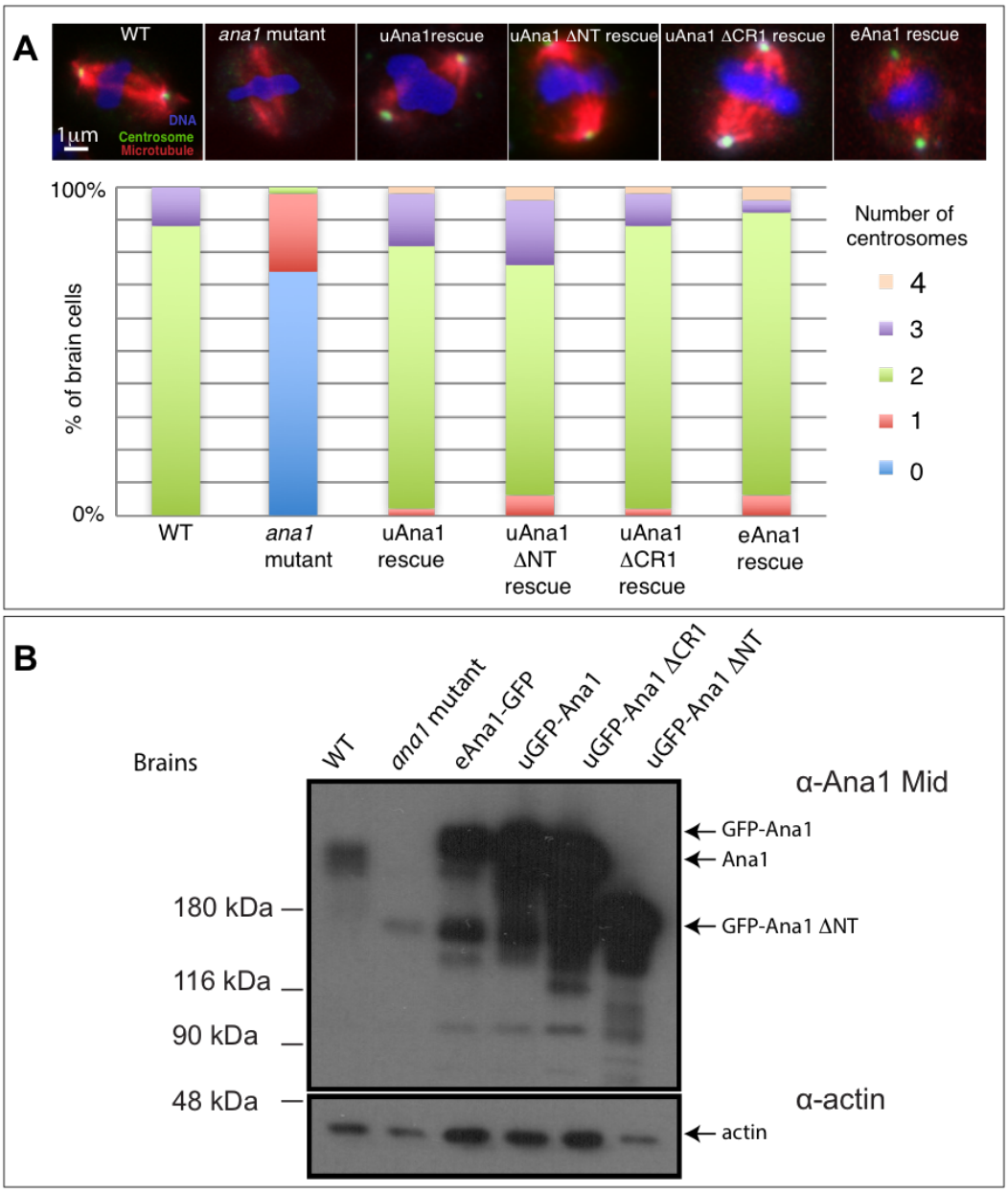

Figure 3.3: The N-terminal region of Ana1 does not appear to be essential for centriole assembly and/or maintenance in brain cells. (A) Micrographs show images of 3rd instar larval brain cells stained for DNA (*blue*), MTs (*red*) and the centrosome marker Asl (*green*) in WT, *ana1* mutant or *ana1* mutant rescued by different transgenes (as indicated). Graphs show the quantification of the percentage of cells for each genotype exhibiting different numbers of centrosomes (n=30-50 total cells counted from 5 brains). Centrosomes were scored as dots in mitotic cells that were positive for both the centriole/centrosome protein Asl and the centrosome protein Cnn (Conduit et al., 2014b). **(B)** Western blots of *Drosophila* third instar larval brains from WT, *ana1* mutant or WT brains expressing Ana1-GFP from its endogenous promoter (eAna1-GFP) or GFP-Ana1 or GFP-Ana1 ΔCR1 or GFP-Ana1 ΔNT from the ubiquitin promoter (uGFP-Ana1 or uGFP-Ana1 ΔCR1 or uGFP-Ana1 ΔNT). Blots were probed with anti-Ana1 Mid or anti-actin antibodies (loading control). The GFP-fusions are overexpressed relative to the endogenous Ana1 by ~2-4X (eAna1-GFP), 3-5X (uGFP-Ana1 or uGFP-Ana1 ΔCR1) or 5-10X (uGFP-Ana1 ΔNT).

I examined the centrosomal localization of GFP-Ana1 and GFP-Ana1 ΔNT in living early fly embryos. The centrosomal localisation of GFP-Ana1 ΔNT was markedly reduced compared to GFP-Ana1 (Figure 3.4A), and I confirmed this observation by quantitatively measuring the centriolar fluorescence of each fusion protein at various stages of the cell cycle (Figure 3.4B). Thus, although GFP-Ana1 ΔNT is only weakly localized to centrioles, it can rescue the centriole assembly/maintenance defect in *ana1* mutants. These points will be examined in more detail later on in this Chapter.

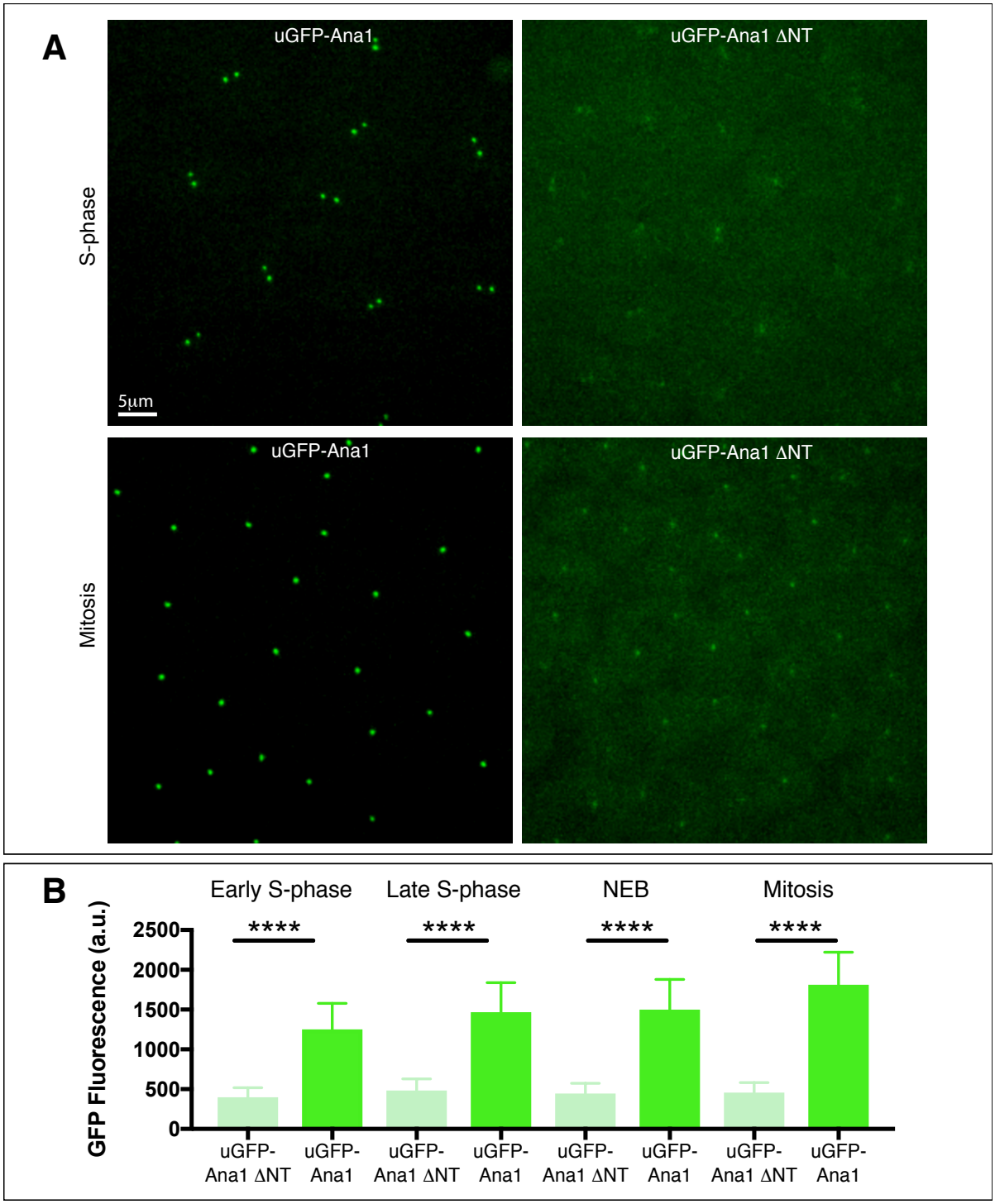

Figure 3.4: The N-terminal region of Ana1 does not appear to be essential for centriole assembly and/or maintenance in embryos. (A) Micrographs show representative images of live *Drosophila* embryos expressing uGFP-Ana1 (left panels) or uGFP-Ana1 ΔNT (right panels) in a WT background in S-phase (top panels) or in mitosis (bottom panels). **(B)** The graphs show the centrosomal fluorescence of uGFP-Ana1 ΔNT (light *green*) or uGFP-Ana1 (Fluorescent *green*) at indicated time points, averaged from 20-291 centrosomes/embryo from four different embryos. Note that the fluorescence intensity of uGFP-Ana1 increases over time, however, it remains stable in the case of uGFP-Ana1 ΔNT. Statistical significance was calculated using Mann-Whitney t-test for comparison. Error bars represent SD. (P-values: ****=<0.00001).

3.2.4: The overexpression of Ana1 does not detectably drive *de novo* centriole assembly or centriole over-duplication

Previous studies have shown that the high-level overexpression of UAS-driven GFP-fusions to all the "core" centriole assembly proteins (GFP-Sak, GFP-Sas-6, GFP-Ana2, Sas-4-GFP and Asl-GFP) could drive the *de novo* formation of centriole-like structures in unfertilized eggs (Dzhindzhev et al., 2010; Peel et al., 2007; Rodrigues-Martins et al., 2007; Stevens et al., 2010a; 2010b). I, therefore, used the UAS-GFP-Ana1 and UAS-GFP-Ana1 ΔNT transgenic lines to drive the high-level overexpression of Ana1 or Ana1 ΔNT in unfertilized eggs (Figure 3.5A). Neither fusion protein was able to induce the *de novo* formation of centriole-like structures in unfertilised eggs (Figure 3.5B).

GFP-fusions to most of the core centriole assembly proteins can also induce centriole over-duplication when overexpressed from the Ubq-promoter in various tissues (Peel et al., 2007; Rodrigues-Martins et al., 2007; Stevens et al., 2010a; 2010b). However, neither GFP-Ana1 or GFP-Ana1 ΔNT detectably induced centriole over-duplication in embryos (data not shown) or brain cells (Figure 3.3A). Thus, although *ana1* mutant flies lack detectable centrioles and centrosomes in a manner that is very similar to flies carrying mutations in any of the core centriole assembly genes, Ana1 appears to be different from the core centriole assembly proteins in that it cannot drive the *de novo* formation of centriole-like structures in eggs, or the formation of extra centrioles in any of the tested fly tissues.

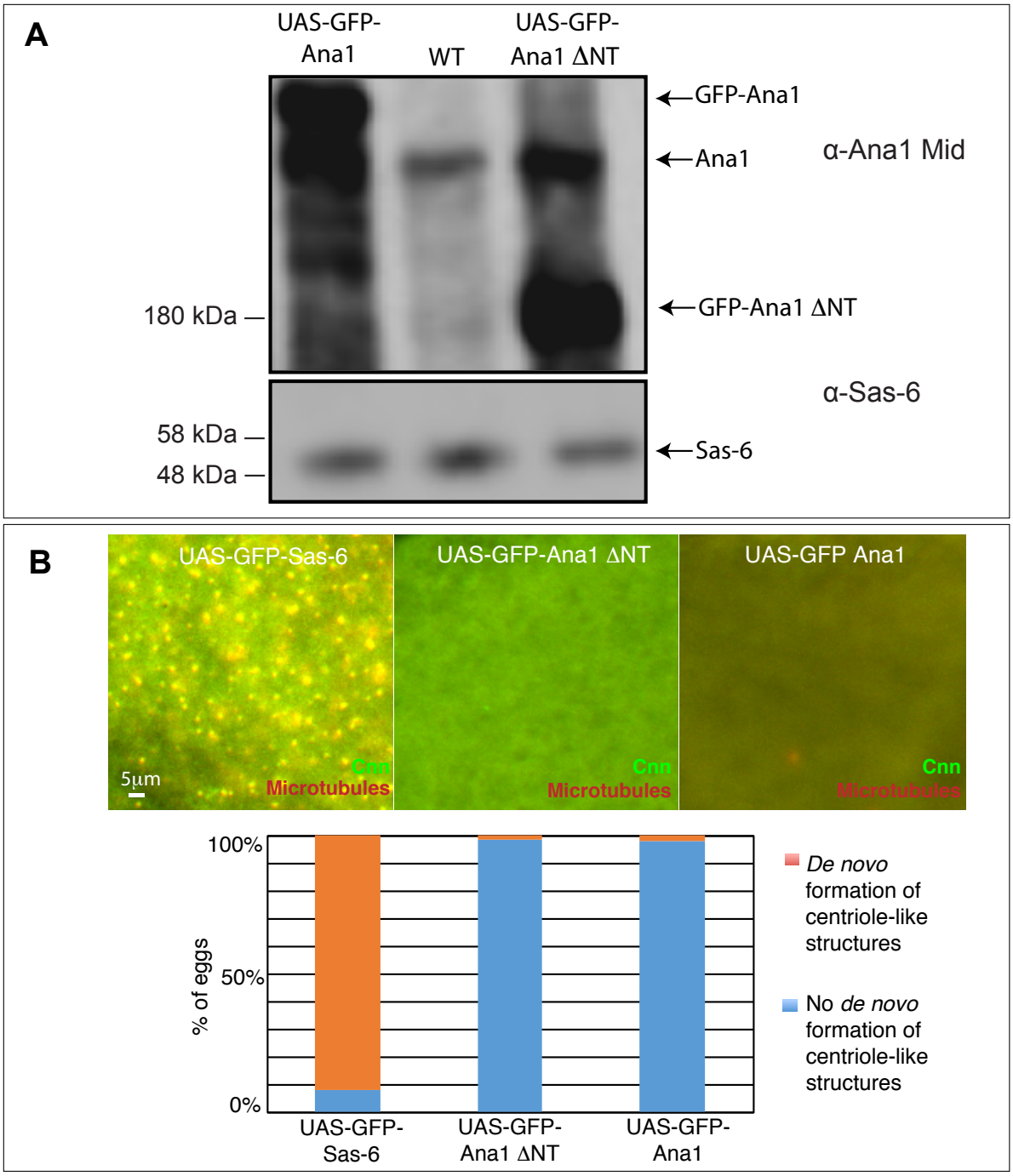

Figure 3.5: The overexpression of Ana1 does not detectably drive *de novo* centriole assembly or centriole over-duplication. (A) Western blots of WT (2nd lane), UAS-GFP-Ana1 (1st lane) and UAS-GFP-Ana1-ΔNT (3rd lane) embryos probed with the anti-Ana1 Mid antibodies or anti-Sas-6 antibodies (loading control). Note that the GFP-fusions are overexpressed by ~10-20X relative to endogenous Ana1 by using the UAS/Gal4 system. **(B)** Top panels: representative fluorescent images of unfertilized eggs laid by mothers expressing UAS-GFP-Sas-6, UAS-GFP-Ana1 ΔNT or UAS-GFP-Ana1 (as indicated) stained for Cnn and α-tubulin (MTs). Overexpression of Sas-6 drives the *de novo* formation of centriole-like structures (Peel et al., 2007) while overexpression of GFP-Ana1 ΔNT or GFP-Ana1 does not. Lower panel: graph quantifies the percentage of unfertilized eggs laid by mothers of the given genotype that contained centriole-like structures (n=50–70 eggs counted from each genotype).

3.2.5: Ana1 does not appear to be essential for the assembly of the central cartwheel

I wondered whether Ana1 might have a role in assembling and/or stabilizing the central cartwheel of the centriole. This question is difficult to address in *bona fide* centrioles, as these structures are missing in *ana1* mutants. It has previously been shown, however, that when GFP-Sas-6 and Ana2-GFP are co-overexpressed in wild-type spermatocytes, they assemble into **S**as-6/**A**na2 **P**article**s** (SAPs) that are composed of elongated tubules (SAStubules) that are structurally very similar to the cartwheel (Stevens et al., 2010b). I, therefore, tested whether Ana1 might have a role in assembling or stabilising SAStubules by co-overexpressing GFP-Sas-6 and Ana2-GFP in *ana1* mutant spermatocytes. GFP-Sas-6 and Ana2-GFP still formed SAPs in the mutant cells, but these were less abundant, although they appeared to be larger and brighter than in WT cells (Figure 3.6). Thus, a lack of Ana1 protein clearly influences SAP behaviour.

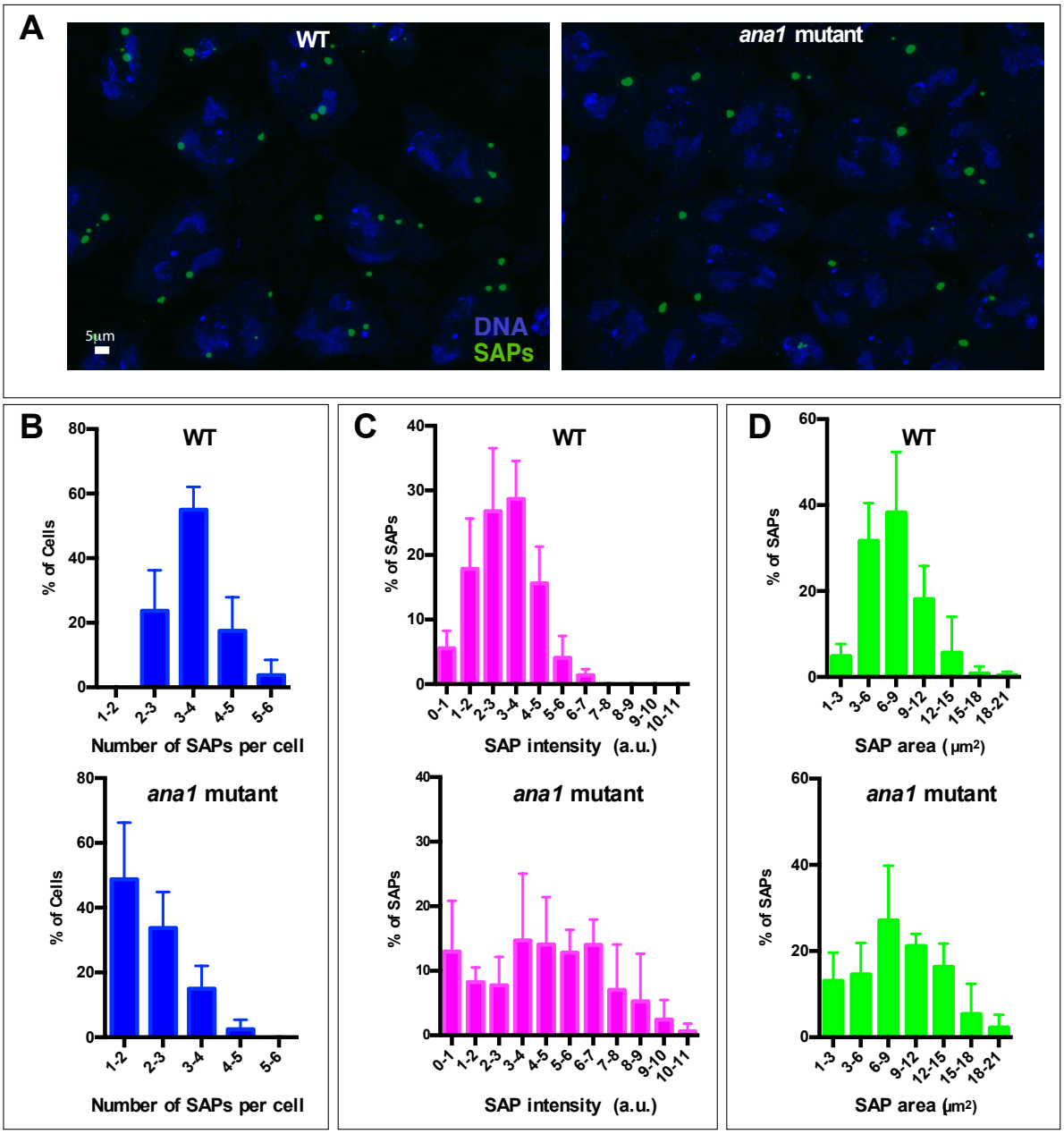

Figure 3.6: Ana1 is not required for the assembly of SAPs. (A) Micrographs show SAPs (*green*) in primary spermatocytes from WT (left panel) or *ana1* mutant (right panel) *Drosophila* late pupal testes. The tissue was stained with Hoechst to stain the DNA (*blue*). **(B-D)** Graphs quantify the number of SAPs per cell (B), SAP fluorescence intensity (C), and the average area of SAPs per cell in WT (top graphs) or *ana1* mutant (bottom graphs) spermatocytes. SAPs appear to be less abundant, but larger than normal, in *ana1* mutant spermatocytes. Error bars represent SD. N=20 spermatocytes per testis and four testes per genotype.

To examine SAP structure in the absence of Ana1, in more detail I performed an Electron Tomography (ET) analysis in collaboration with a post-doctoral fellow in the laboratory, Helio Roque (I prepared all samples, and he performed the ET analysis). Although the SAPs were generally less well ordered, structures resembling the

cartwheel central hub were still clearly visible (black arrowheads, Figure 3.7A). Thus, although the absence of Ana1 subtly alters SAP structure and behaviour, it does not appear to be essential for the assembly of a central cartwheel-like structure.

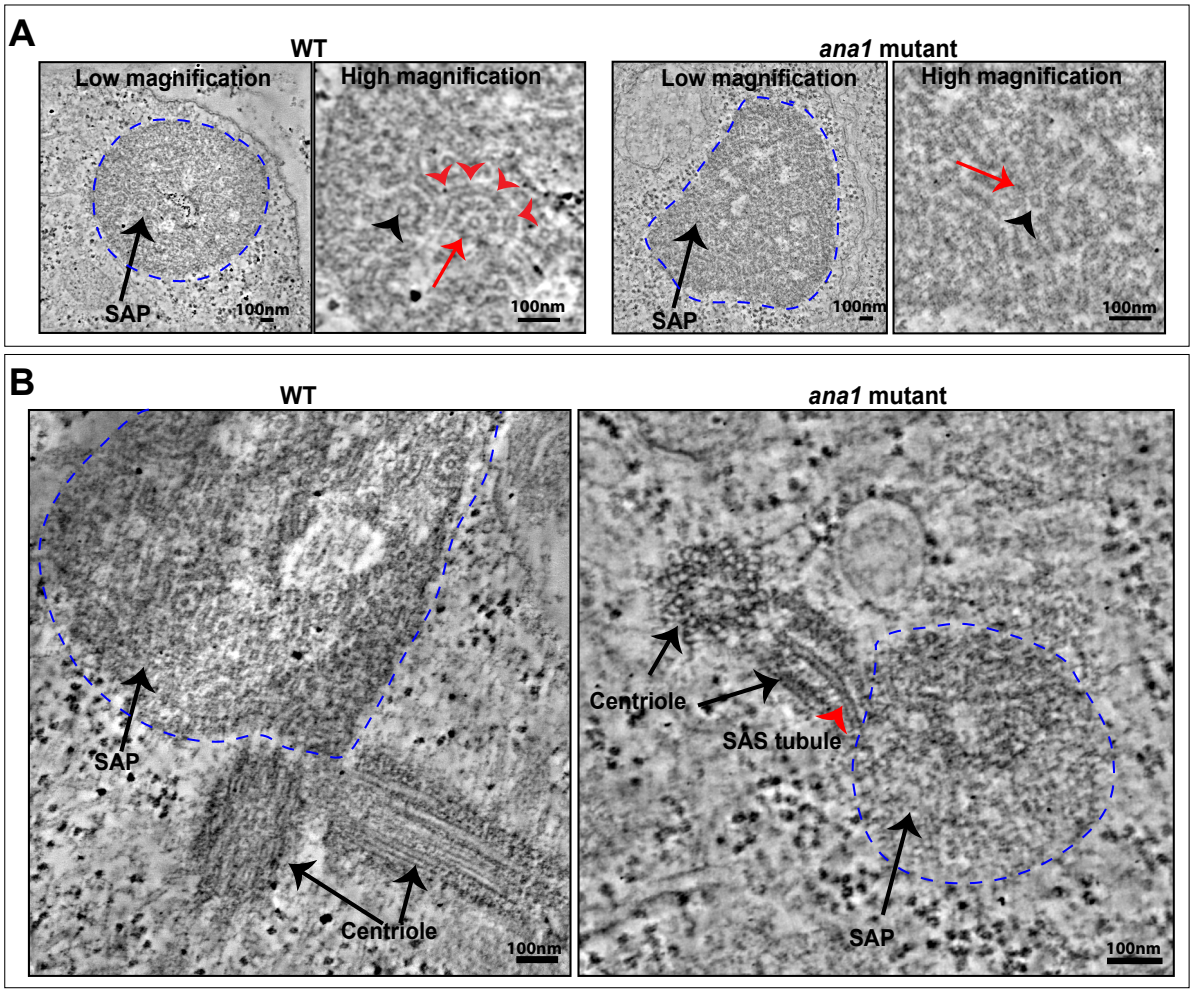

Figure 3.7: Ana1 does not appear to be essential for the assembly of the central cartwheel. (A) Micrographs show low- and high-magnification views of an EM tomogram of a SAP particle (dotted *blue* line) in either a WT (left panels) or *ana1* mutant (right panels) spermatocyte. The SAP in the WT cell is highly structured and consists of well-organised ‘‘SAStubules’’ that resemble the hub of the inner cartwheel of the centriole (Stevens et al., 2010b). The black arrow-head highlights an end-on view of a SAStubule, and *red* arrowheads highlight the transverse view. Spokes (*red* arrow) link the SAStubules to an electron-dense, fibrous outer ring. In *ana1* mutants, the SAP structures are less well defined, but hub-like SAStubules are still easily detected, especially in an end on view (black arrow-head), and these are surrounded by less well defined spokes (*red* arrow). **(B)** In WT spermatocytes, SAPs usually connect to the centrioles. In 7/11 of the *ana1* mutant SAPs, we could detect small centriole-like structures that appeared to comprise 9 MT-triplet blades surrounding a central cartwheel. Note that in this example the SAStubule of the SAPs extends directly from the cartwheel of the centriole-like structure (*red* arrowhead). All micrographs are courtesy of H. Roque.

Surprisingly, we noticed that structures resembling *bona fide* centrioles were detectable closely associated with the SAPs in 7/11 of the *ana1* mutant spermatocytes examined, suggesting that centrioles can still assemble and/or be maintained in mutant spermatocytes if Sas-6 and Ana2 are overexpressed (Figure 3.7B). Interestingly, in one of these structures, we observed the central cartwheel of a centriole directly connected to a SAStubule emanating from the SAP (*red* arrowhead, Figure 3.7B), supporting the conclusion that these tubules are closely related to central cartwheels, and that central cartwheel structures can still assemble in the absence of Ana1. Moreover, while SAPs are often associated with the very large centrioles in WT spermatocytes (Stevens et al., 2010b), the centriole-like structures associated with the SAPs in the *ana1* mutant spermatocytes were much shorter than normal, indicating that Ana1 may promote centriole elongation in these cells, an issue I will return to later in this Chapter.

3.2.6: Ana1 is required to recruit Asl to SAPs

The SAPs formed by the co-overexpression of GFP-Sas-6 and Ana2-GFP in WT spermatocytes do not recruit PCM or organize MTs, but when these proteins are co-overexpressed in eggs or early embryos they form SAPs that recruit several PCM markers, and that organize robust MT asters (Stevens et al., 2010b). Unfortunately, it is not possible to test how SAPs assemble in *ana1* mutant eggs or embryos as these mutant flies are uncoordinated and so female flies cannot mate or lay eggs. To overcome this limitation, Alan Wainman, a postdoctoral fellow in our laboratory, generated what we term “cilia rescue” lines (Richens et al., 2015) in which all tissues overexpress GFP-Sas-6 and Ana2-GFP, but the Ana1 transgene—under the control of a UASg promoter—is expressed only in the nervous system of the fly, allowing centrioles and cilia to assemble in the nervous system—so rescuing the

uncoordinated phenotype of the *ana1* mutation. UASg is a leaky promoter, and we were worried that full-length Ana1 would also be expressed in the embryos even without gal4. To circumvent this problem, we used UASg-GFP-Ana1 ΔNT lines instead of UASg-GFP-Ana1. We generated flies of genotype: w; UASg-GFP-Ana1 ΔNT/Ubq-Ana2-GFP, elavGal4; Ubq-GFP-Sas-6, $ana1^{mecB}$ / Df(*ana1*). The *ana1* mutant cilia rescue females can, therefore, lay eggs.

A western blot analysis of eggs or embryos probed with anti-Ana1 antibodies or anti-GFP revealed that cilia rescue embryos lack GFP-Ana1 or GFP-Ana1 ΔNT and overexpress GFP-Sas-6 and Ana2-GFP (Figure 3.8). Further, I found that these eggs still formed SAPs (Figure 3.9A). The mutant SAPs were slightly less abundant than WT SAPs (although this difference was not statistically significant) and were slightly brighter (Figure 3.9B), mimicking the behaviour of the SAPs in *ana1* mutant testes (Figure 3.6). I quantified the levels of GFP, Sas-4, Asl and MTs in the WT and mutant SAPs and found that the mutant SAPs were brighter, had higher levels of Sas-4, but much lower levels of Asl and MTs (Figure 3.10). It is unclear why Sas-4 levels increase in *ana1* mutant cilia rescue SAPs (see Discussion), but it is striking that Asl- and MT-levels are dramatically reduced. In flies, Asl is only recruited to new centrioles once they separate from their mothers at the end of mitosis, and it plays a crucial role in centriole-to-centrosome conversion as it is required to allow new centrioles to both duplicate for the first time and recruit PCM for the first time (Novak et al., 2014). Thus, a role for Ana1 in recruiting Asl to centrioles could potentially explain why Ana1 is not essential for centriole assembly *per se*, but is required to allow new centrioles to mature so that they can duplicate and recruit PCM.

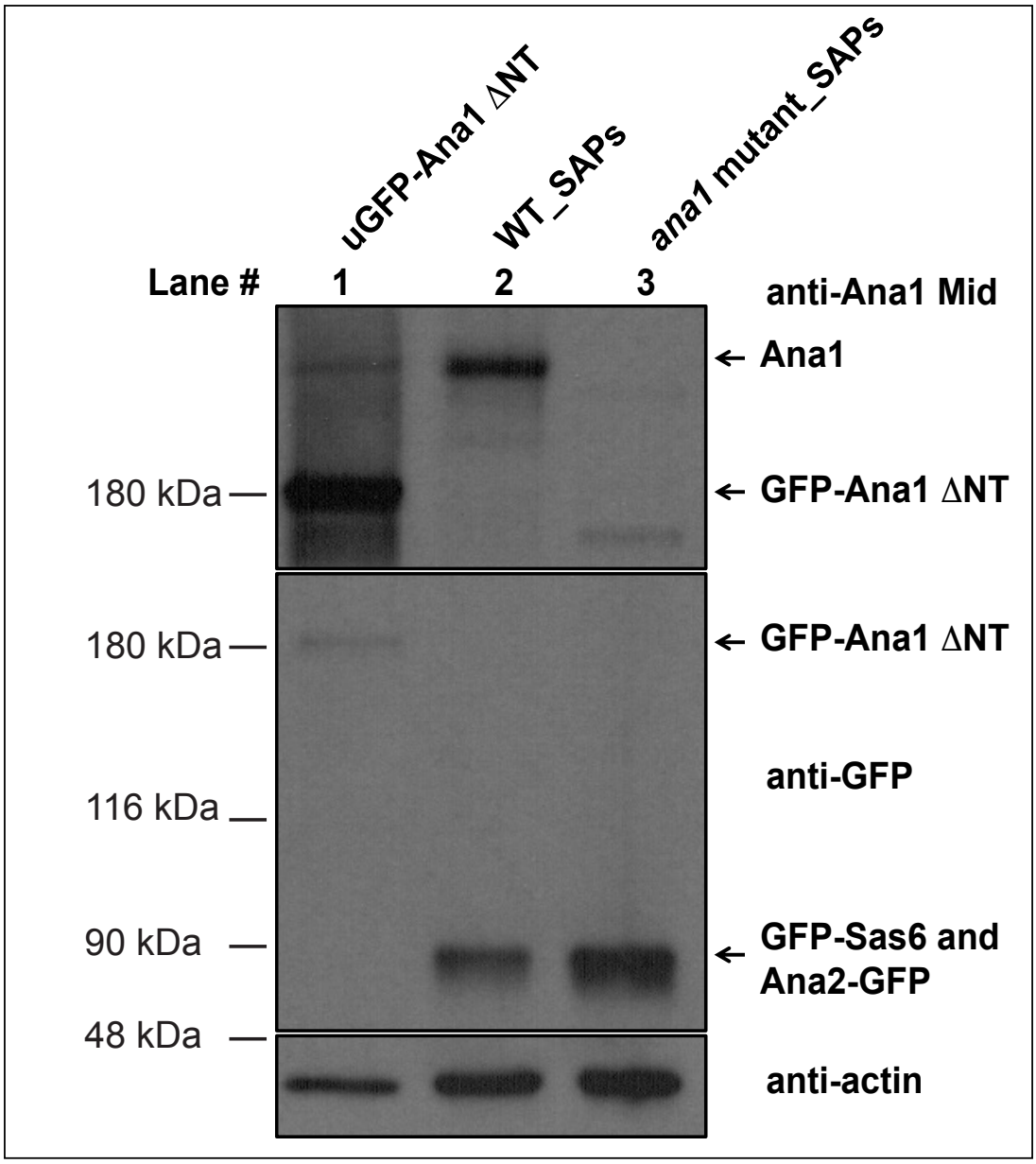

Figure 3.8: Generating SAPs in *ana1* mutant eggs. Panels show Western blots of *Drosophila* eggs laid by females over-expressing GFP-Ana1 ΔNT from the Ubq promoter (as a positive control to show the position of the GFP-Ana1 ΔNT fusion protein—Lane 1), or by WT females co-overexpressing GFP-Sas-6 and Ana2-GFP (Lane 2) or by *ana1* mutant cilia rescue females co- overexpressing GFP-Sas-6 and Ana2-GFP (Lane 3). The genotype of the *ana1* mutant cilia rescue flies is: w; UASg-GFP-Ana1 ΔNT / Ubq-Ana2-GFP, elavGal4; Ubq-GFP-Sas-6, $ana1^{mecB}$ / Df(*ana1*). The GFP-Ana1 ΔNT is overexpressed only in the neural tissue and therefore the *ana1* mutant cilia rescue females are not uncoordinated and can lay unfertilized eggs. The GFP-Ana1 ΔNT is undetectable in the eggs. Blots were probed with anti-Ana1 Mid (top panel), anti-GFP (middle panel) or anti-actin antibodies (loading control, bottom panel). Note the absence of Ana1 or GFP-Ana1 ΔNT bands in the *ana1* mutant cilia rescue unfertilized egg SAPs (Lane 3), indicating that there is no detectable "leaky" expression of GFP-Ana1 ΔNT in the mutant eggs. Also note that GFP-Sas-6 and Ana2-GFP are of similar sizes and so are detected as a single band.

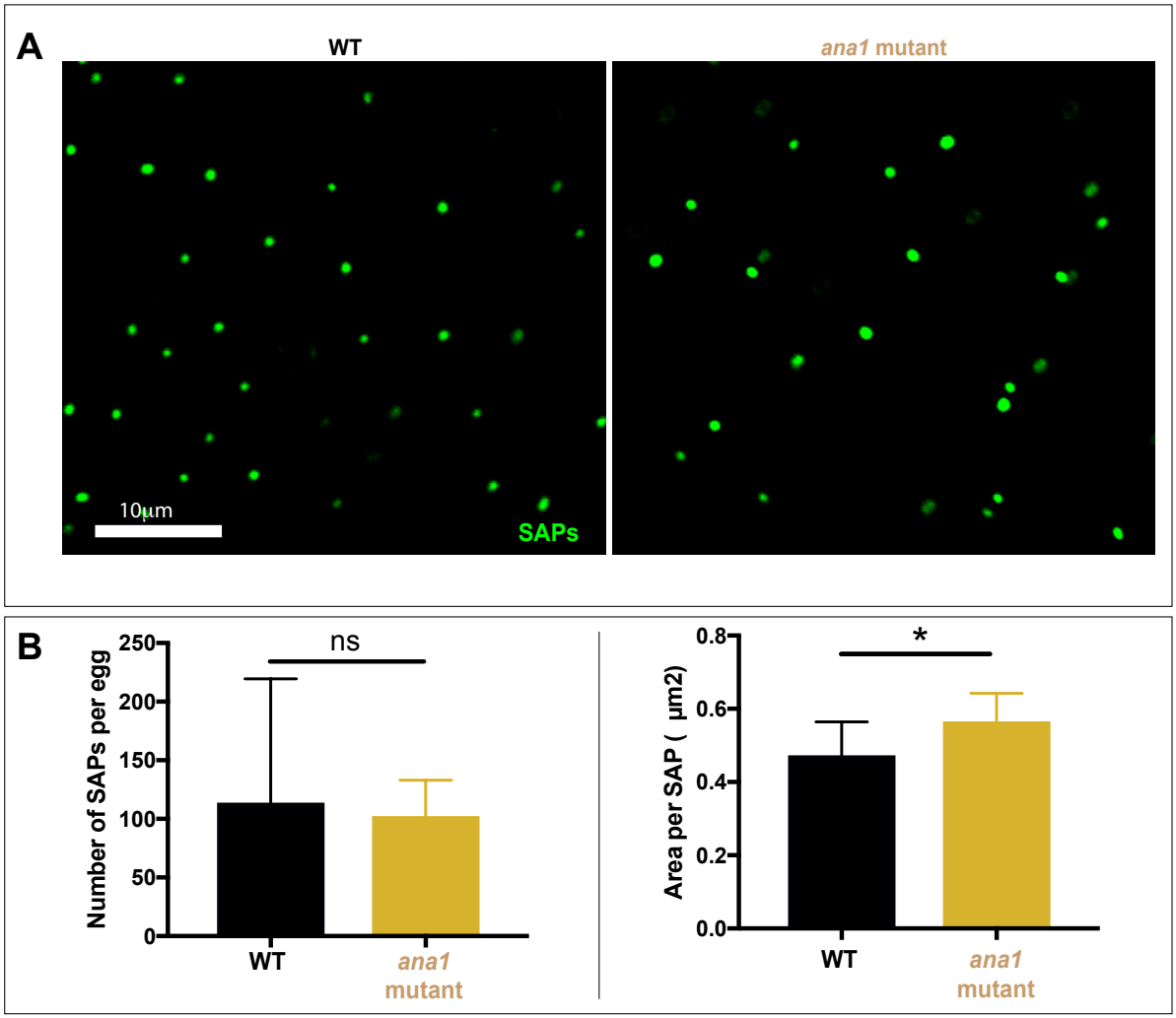

Figure 3.9: Ana1 is not required to form SAPs in unfertilized eggs. (A) Micrographs show SAPs (*green*) in unfertilized eggs from WT (left panel) or *ana1* mutant cilia rescue flies (right panel) stained for GFP (so recognizing both Sas-6-GFP and Ana2-GFP). **(B)** Graphs quantify the number of SAPs per egg (left panel) and the average area of SAPs per egg in WT or *ana1* mutant eggs. Note that SAPs are less abundant and larger than normal in *ana1* mutant eggs. Quantifications were performed on 2D-maximum intensity projections of the z-stacked images. N=14-290 SAPs from 10 eggs per genotype. Error bars represent SD. Statistical significance was calculated using Mann-Whitney t-test for comparison. (P-values: *=<0.05; ns=not significant).

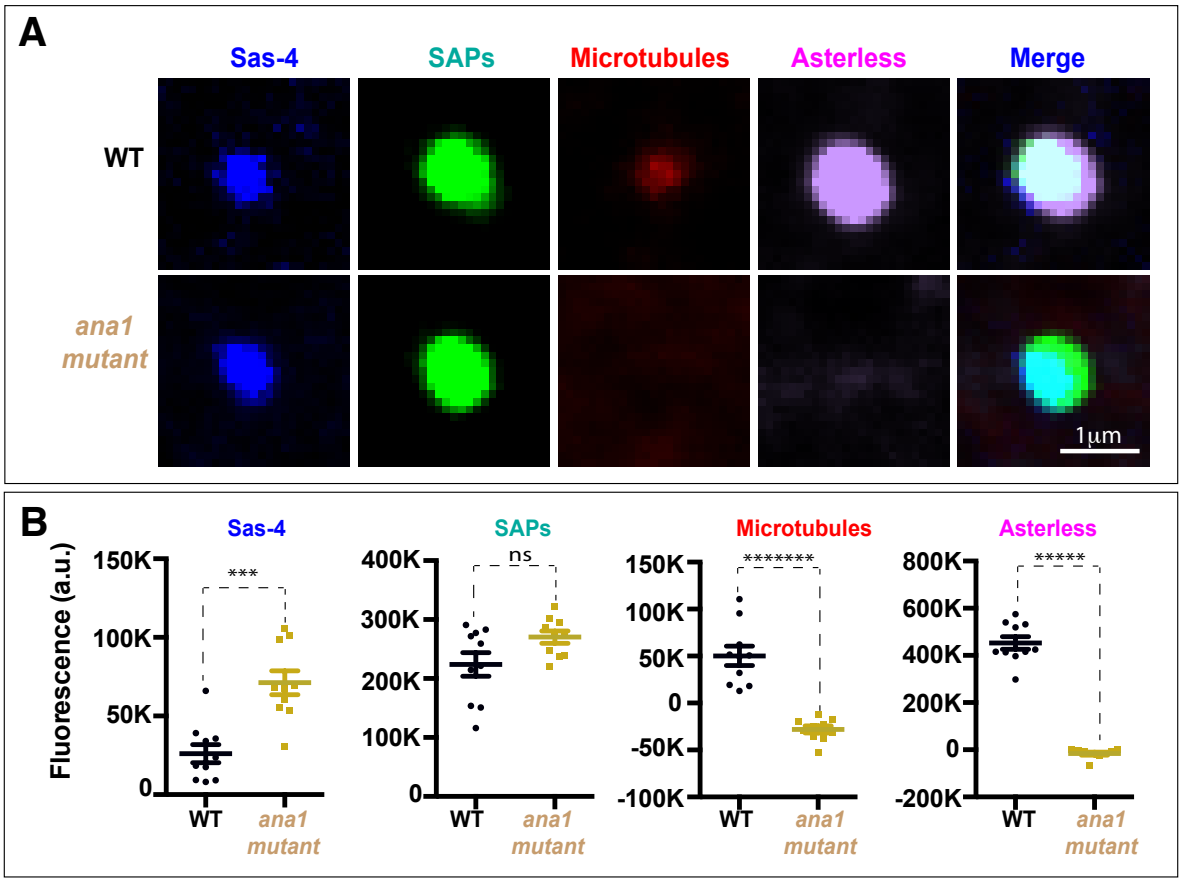

Figure 3.10: Ana1 is required to recruit Asl to SAPs. (A) Representative fluorescent images of WT (top panels) or *ana1 mutant* (bottom panels) SAPs in eggs of the cilia rescue flies stained for anti-Sas-4, anti-GFP (Ana2-GFP and GFP-Sas-6), anti-MTs and anti-Asterless antibodies. **(B)** The graph quantifies the fluorescent intensities of Sas-4, GFP (SAPs), MTs and Asterless in the SAPs of the WT or *ana1* mutant eggs from the upper panels (n=10 eggs, 20 SAPs each). Note the statistically significant reduced levels of MTs and Asterless in *ana1 mutant* SAPs indicating Asterless is downstream of Ana1 in the SAP assembly pathway. Statistical significance was calculated using Student's t-test for comparison (P values: ***=<0.0001; *****=<0.000001; *******=<0.00000001; ns=not significant). Error bars represent SD.

3.2.7: Antibody injection experiments suggest that Ana1 helps recruit Asl specifically to newly forming mother centrioles

To more directly test whether Ana1 might help recruit Asl to new mother centrioles I turned to antibody injection, a technique that the laboratory used very successfully in the past to study the function of several centrioles and centrosome components (Conduit et al., 2010; 2014a; Gergely et al., 2000; Novak et al., 2014). In this technique, purified antibodies raised against a protein of interest are labelled with a red-fluorophore and injected into one side of a developing syncytial embryo expressing a GFP-fusion protein that labels the centrioles or centrosomes—usually during nuclear cycles 10-11 when the nuclei (and their associated centrioles and centrosomes) are organized in a monolayer at the embryo cortex (Foe and Alberts, 1983). The injected antibody often binds to its cognate protein and interferes with its function, but it does not spread to the centrioles/centrosomes on the other side of the embryo, which then serve as a control with which to monitor the effect of the injected antibody.

I injected the Texas-Red conjugated purified antibodies raised against the C-terminal region of Ana1 into cycle 10 or 11 embryos expressing Asl-GFP (Figure 3.11A). The antibodies bound to the centrioles close to the injection site (top left of embryo shown in Figure 3.11A—a typical centriole pair is highlighted by a *red* arrow and shown at higher magnification in the *red* box), but were essentially not detectable at centrioles further away from the injection site (a typical centriole pair is highlighted by a *blue* arrow and shown at higher magnification in the *blue* box). Normally in these syncytial embryos, Asl is more strongly localized to the old mother centriole because new mother centrioles only start to recruit Asl when they separate from their mothers

(Novak et al., 2014). This normal asymmetry was apparent in separating mother centriole pairs that were far away from the injection site (*blue* box, Figure 3.11A), but was often much more exaggerated at centriole pairs that were close to the injection site (*red* box, Figure 3.11A). Quantification of centriolar fluorescence revealed that this difference was due to a failure to properly recruit Asl-GFP to the new (dimmer) mother: although the anti-Ana1 antibodies bound equally well to both mother centrioles (Figure 3.11B, right panel), the binding of the antibodies did not affect Asl levels at old mother centrioles (Figure 3.11B, middle panel), but led to a dramatic reduction in Asl levels at the new mother centrioles (Figure 3.11B, left panel). Similar results were obtained when embryos were injected with Texas-Red conjugated antibody raised against a different part of Ana1 (Ana1 Mid, Figure 3.11C). These data suggest that anti-Ana1 antibodies can block the ability of newly forming mother centrioles to recruit Asl, but these antibodies do not seem to perturb the ability of older mother centrioles (formed before the injection of the anti-Ana1 antibodies) to recruit or maintain Asl.

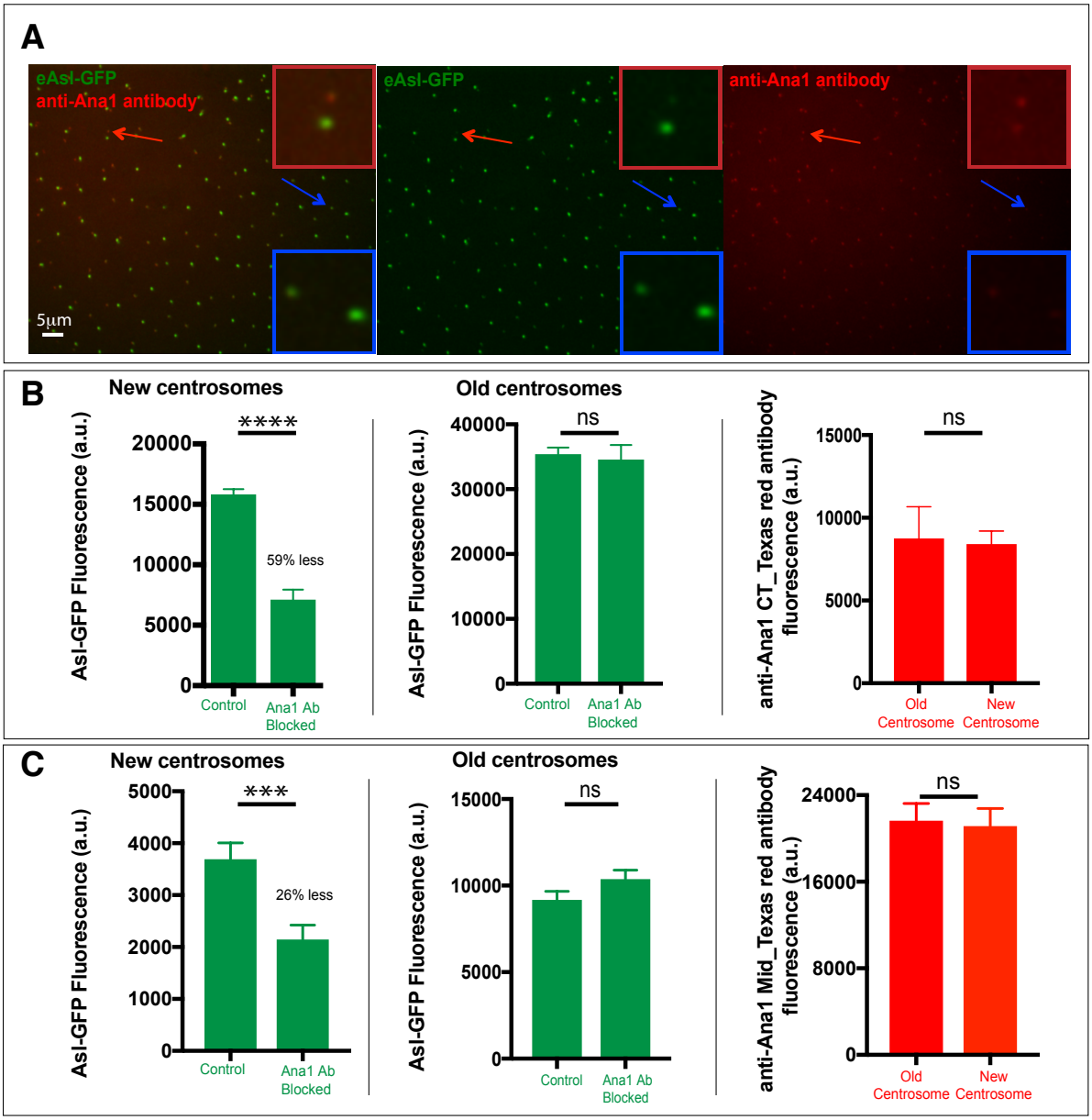

Figure 3.11: Antibody injection experiments suggest that Ana1 helps recruit Asl specifically to newly forming mother centrioles. (A) Images show an example of an embryo antibody injection experiment. The embryo shown here expressed Asl-GFP (*green*) and was injected with Texas-Red-labelled anti-Ana1 CT antibodies (*red*) in the top left corner. The centrosomes that are close to the injection site are exposed to a high concentration of the antibodies, which binds to the centrosomes; the centrosomes further away show very low antibody signal and serve as internal controls. As the centrosomes separate in S-phase, Asl-GFP is detectable on the young centrosomes in the control area (*blue* arrow) but is at a lower level (*red* arrow) near the injection site. **(B)** Graphs quantify Asl-GFP (*green* bars) or anti-Ana1 CT antibody (*red* bar) levels at either new or old centrosomes (as indicated) that are either far from the injection site (control), or close to the injection site (Ana1-Ab blocked) (n=7-11 centrosomes from one embryo). Note incorporation of Asl into new centrosomes is perturbed in the presence of high concentrations of the anti-Ana1 antibodies, however, it is not abolished, and the small amount of Asl that did incorporate was usually able to support another round of centriole duplication (not shown). **(C)** All graphs as in B, but this experiment was performed with the anti-Ana1 Mid antibody (n=50 centrosomes from five embryos). (Statistical significance was calculated using Mann-Whitney t-test for comparison. Error bars represent standard error of the mean (SEM). (P values: ***=<0.0001; ****=<0.00001; ns=not significant).

3.2.8: Ana1 molecules are asymmetrically oriented within the centriole, and the C-terminal regions of Asl and Ana1 are in close proximity

Previous studies using 3D-structured illumination super-resolution microscopy (3D-SIM) have revealed that several centriole proteins, including Asl, are organized in an oriented fashion around the centriole (Fu and Glover, 2012; Mennella et al., 2012). These studies have provided important information about the relative position of these molecules within the centriole and so about potential protein interacting domains. I used 3D-SIM to investigate whether Ana1 molecules were also asymmetrically organized at centrioles and whether the position of these molecules overlapped with other centriole proteins, most notably Asl. I used fixed spermatocytes expressing various N- or C-terminally tagged GFP fusions for this analysis, staining the cells with a GFP-nanobody to label the GFP-moiety and an antibody raised against the N-terminal region of Asl to label the outer region of the centrioles (Fu and Glover, 2012). I generated the GFP-Ana1 and Ana1-GFP stocks (as described above) and also Cep135-GFP and Sas-6-GFP stocks (all expressed from the Ubq-promoter). I also used existing laboratory stocks of GFP-Sas-6, GFP-Ana2, Ana2-GFP, GFP-Cep135, and Asl-GFP (all expressed from the Ubq-promoter) (Figure 3.12A).

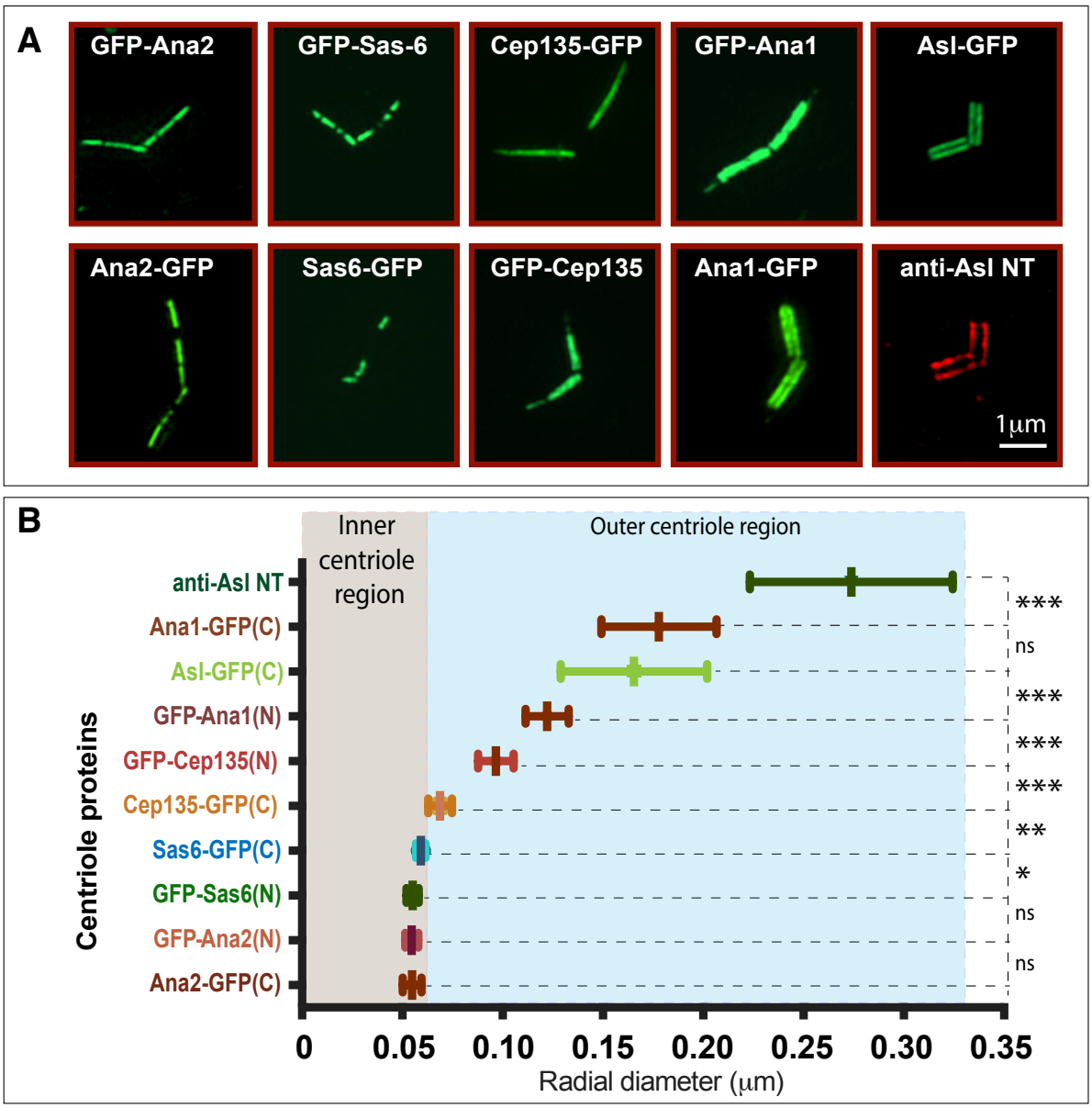

Figure 3.12: Ana1 molecules are asymmetrically oriented within the centriole, and the C-terminal regions of Asl and Ana1 are in close proximity. (A) Micrographs show 3D-structured illumination super-resolution microscopy (3D-SIM) images of centrioles in primary spermatocytes expressing various centriole proteins tagged with GFP at either their N- or C-termini and stained for GFP (*green*). Bottom right image shows a centriole stained with anti-Asl NT antibodies (*red*). **(B)** The graph shows the radial diameter of each centriole marker (as indicated—see Materials and Methods) (n=10-53 centrioles). Statistical significance of the different radial diameters between successive proteins—moving from the innermost (Ana2-GFP) to the outermost (Anti-Asl NT)—was calculated using Mann-Whitney t-test (P-values: *=<0.05; **=<0.001; ***=<0.0001; ns=not significant). Error bars indicate the standard deviation of the mean (SD). Note that the radial diameters of the N-terminal region of Cep135 and the N-terminal region of Ana1-that can directly interact with one another *in vitro* (Fu et al., 2016) are significantly different.

I quantitatively compared the radial distributions of the GFP-moiety on the various centriolar components averaged over many centrioles (see Materials and Methods, section 2.7.5). The position of the N- and C-terminal regions of the inner cartwheel

components Sas-6 and Ana2 could not be resolved in this analysis, but the average centriole-radii for the N- and C-terminal regions of Cep135, Ana1, and Asl appeared to be resolvable (Figure 3.12B). Interestingly, the Cep135, Ana1 and Asl molecules are all asymmetrically localised within the spermatocyte centriole, with the C-terminal regions of Ana1 and Asl being located quite close to each other, supporting the idea that these regions could interact with one another and so allow Ana1 to help recruit Asl to centrioles (Figure 3.12B).

At this stage in my studies, a paper was published from the Glover lab (Fu et al., 2016) showing very similar 3D-SIM localization data for N- and C-terminally tagged GFP-fusions of Ana1, Cep135 and Asl in spermatocytes and S2 cells. Moreover, these authors identified several interactions and localization dependencies indicating that the N-terminal region of Cep135 interacts with the N-terminal region of Ana1 to recruit Ana1 to centrioles and this then allows the C-terminal region of Ana1 to recruit Asl to centrioles via an interaction the Asl C-terminal region (summarized schematically in Figure 3.13). These conclusions are largely consistent with several of my experiments described above indicating a potential role for Ana1 in recruiting Asl to centrioles. However, there are several potentially interesting differences: (1) Although my localization data is largely consistent with that of Fu et al., in my studies the N-terminal regions of Cep135 and Ana1 do not overlap, raising the possibility that a direct interaction between these regions may not be the only way in which Ana1 is recruited to and/or maintained at centrioles. I also noted that the Cep135 staining at the proximal end is thicker than at the distal end, and the measurements could vary depending upon the locations taken for quantifications. The other explanation could be that the GFP moiety and the Nanobody that I used in my experiments has separated the signal further apart, as Glover lab used the signal from GFP only; (2)

Fu et al. conclude that the N-terminal region of Ana1 (defined in their experiments as aa1-755) is required to target Ana1 to centrioles through its interaction with Cep135 and that the deletion of this N-terminal fragment renders Ana1 non-functional. My Ana1 ΔNT deletion (in which aa1-639 are deleted) is still weakly recruited to centrioles and is largely functional regarding its ability to form centrioles, centrosomes and cilia.

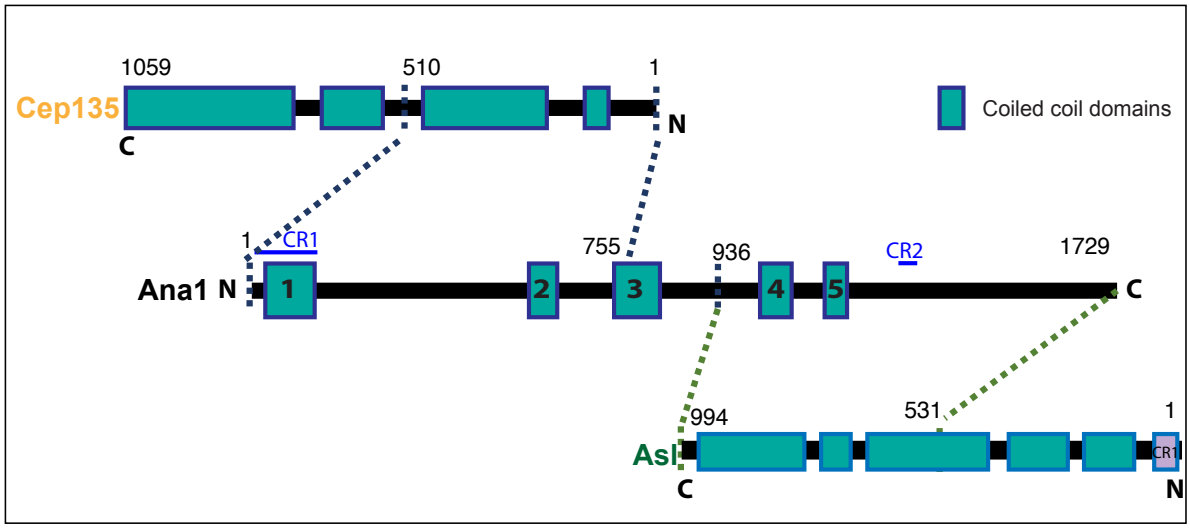

Figure 3.13: Summary of the putative interactions between Cep135, Ana1 and Asl. A schematic illustration of *Drosophila* Cep135, Ana1 and Asl proteins and their interacting regions as defined by Fu et al (Fu et al., 2016). Two conserved regions of Ana1 (CR1 and CR2—*blue* lines) and several predicted coiled-coil domains (*green* boxes) are indicated. N and C indicate the N- and C-termini of each protein. Super-resolution imaging suggests that the C-terminus of Cep135 is located closest to the centriole wall.

3.2.9: A structure/function analysis of Ana1

The discrepancies described above are not, however, irreconcilable. It is clearly possible, for example, that aa1-639 of Ana1 are not essential for its localization of function, but that aa 640-756 are essential. In an attempt to resolve some of these issues I decided to undertake a detailed structure/function analysis of Ana1 using a mRNA injection assay to assess the ability of various Ana1-GFP truncations and deletions to localize to centrosomes and to recruit an Asl-mCherry fusion protein to

centrosomes. In this assay, *in vitro* transcribed mRNA encoding various GFP-Ana1 fusion proteins is injected into early syncytial embryos (that contain endogenous but unlabelled, Ana1) expressing Asl-mCherry. The mRNA is gradually translated so that the GFP-Ana1 fusions first start to compete with the endogenous protein, and can then often eventually overwhelm the endogenous protein (as so much more of the mutant protein is produced). The centriole localization of the GFP-fusion and Asl-mCherry are then analysed and quantified (see Chapter 2, section 2.7.6). The laboratory has had great success using this assay to perform structure/function analyses with several centriole/centrosome proteins (Cottee et al., 2015; Richens et al., 2015). However, there are two important caveats to these types of studies: (1) The injection assay is much more variable than experiments performed with transgenic lines (largely due to differences in the timing and relative volume of mRNA injection); (2) these experiments are performed in the presence of the WT endogenous protein, which may, or may not, interact with some or all of the mutant constructs tested.

In an initial set of experiments, I compared the behaviour of my GFP-Ana1 ΔNT construct (that contains a deletion of aa1-639) to the Ana1 constructs analysed by Fu et al.: an N-terminal deletion of aa1-755 (that I term GFP-Ana1 ΔNT2) and a C-terminal deletion of aa936-1729 (GFP-Ana1 ΔCT) (Figure 3.14A). This analysis confirmed that low levels of GFP-Ana1 ΔNT can still be recruited to centrioles, and revealed that similar low levels of GFP-Ana1 ΔNT2 can also still be recruited (Figure 3.14B) (although these localizations could rely on interactions with endogenous WT Ana1). Interestingly, the recruitment of Asl to both old and new mother centrioles was strongly suppressed in the presence of either of these fusion proteins. This is surprising, as the C-terminal region of Ana1 (that is thought to recruit Asl) is still

present in these deleted fusions. Thus, if these fusions were being recruited to centrioles via multimerization with the endogenous WT protein, the recruitment of Asl to centrioles would not be expected to be perturbed. Alternatively, perhaps the overexpressed fusions can still bind to Asl in the cytoplasm, potentially sequestering the Asl in a form that cannot be recruited efficiently to centrioles by Ana1 at the centrioles.

The GFP-Ana1ΔC construct exhibited a markedly reduced localisation at centrosomes (Figure 3.14A and B). This is surprising, as this construct contains the entire N-terminal domain that interacts with Cep135 and is sufficient to recruit Ana1 to centrosomes in S2 cells (Fu et al., 2016). Moreover, although GFP-Ana1 ΔCT expression strongly perturbs the centrosomal localisation of Asl-mCherry (as expected because GFP-Ana1ΔCT should not be able to recruit Asl), it more strongly affected Asl localisation at the old centrosome than at the new centrosome. As a result, there was a significant reduction in the asymmetry of Asl accumulation at the old and new centrosome. The ratio of Asl-mCherry fluorescence at old/young centrosomes was 2.6 ± 0.3; 2.6 ± 0.5 and 2.7 ± 0.3 (mean ± SD.) in embryos expressing WT GFP-Ana1, GFP-Ana1 ΔNT and GFP-Ana1 ΔNT2, respectively, but only 1.5 ± 0.1 in embryos expressing GFP-Ana1 ΔCT ($p<0.001$; Student's t-test). Thus, GFP-Ana1 ΔCT preferentially perturbs the localisation of Asl-mCherry at old centrosomes, rather than at the recently converted new centrosomes. These findings support the idea that Ana1 is involved in recruiting Asl to centrioles, but they suggest that the model proposed by Fu et al. (where Asl is only recruited to centrioles by its interaction with Ana1) may be an oversimplification (see Discussion).

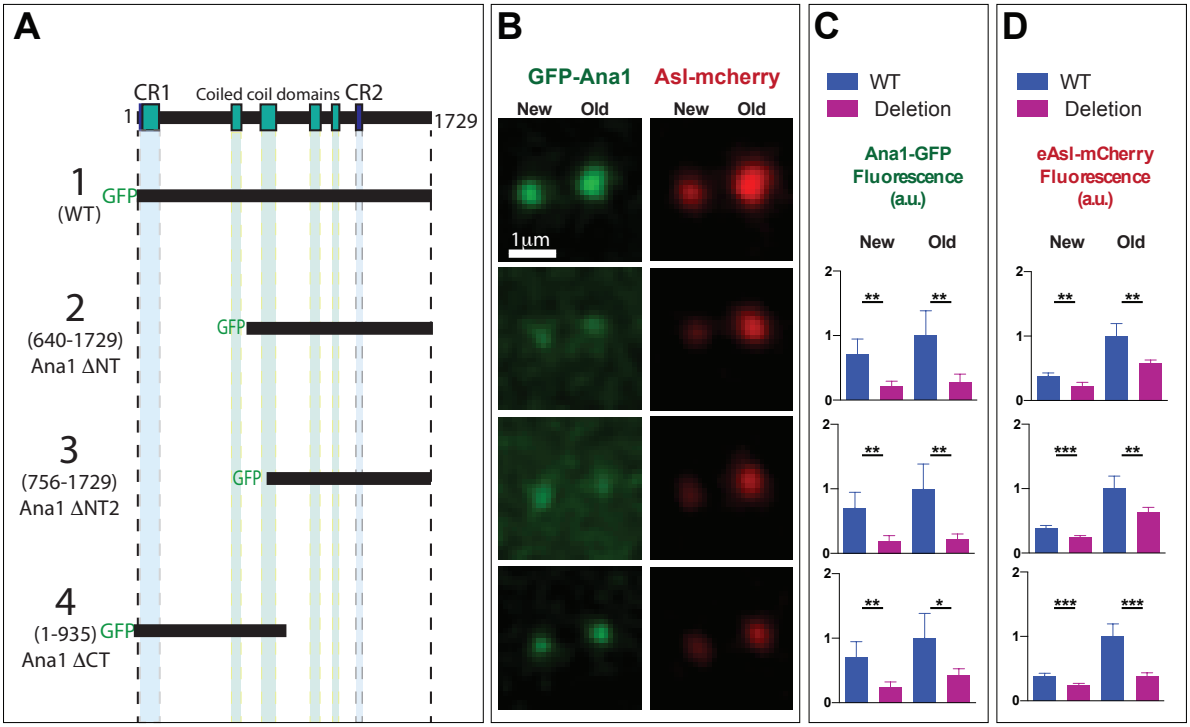

Figure 3.14: An initial structure/function analysis of Ana1. (A) A schematic representation of the various GFP-Ana1 deletion constructs analysed. **(B)** Micrographs show the localisation of the GFP-Ana1 fusion protein (*green*) and Asl-mCherry (*red*) in embryos injected with the Ana1 constructs as shown in (A) at new and old centrosomes in *S*-phase. **(C, D)** Bar graphs show the average centrosomal Ana1-GFP (C) or Asl-mCherry (D) fluorescence levels at new and old centrosomes. All values were normalized to the average fluorescence level of WT GFP-Ana1, or Asl-mCherry observed at old centrosomes in contemporaneous controls injected with WT GFP-Ana1 (construct 1) (arbitrarily given a value of 1). Note that the preferential asymmetric localization of Asl-mCherry to the old centrosome was consistently reduced in embryos expressing GFP-Ana1 ΔCT (construct 4). Error bars represent the standard deviation (SD) from 5 embryos for each construct. Statistical significance was calculated using Student's t-test (P-values: *=<0.05; **=<0.001; ***=<0.0001).

3.2.10: Attempts to narrow down the regions of Ana1 required for its centriolar localization and its ability to recruit Asl

I next tried to narrow down the region of Ana1 involved in recruiting Asl to the centrosome. As the interaction between Ana1/Cep295 and Asl/Cep152 appears to be conserved (Fu et al., 2016) I wondered whether the small conserved CR2 domain might be required (Figure 3.13A). Constructs lacking CR2 (GFP-Ana1 ΔCR2) or the entire C-terminal region from the CR2 domain (GFP-Ana1 ΔCT2) (Figure 3.15, constructs #5 and #6) localised to centrosomes slightly less strongly than full-length GFP-Ana1 but, perhaps surprisingly, did not significantly influence the levels of Asl significantly at the centrosome. It is highly likely that CR2 and the region of Ana1 C-terminal to CR2 are not vital for Asl recruitment to the centrosome.

I also tested the effect of expressing constructs that contained only the C-terminal region of Ana1 (GFP-Ana1 ΔNT3, construct #7, Figure 3.15), and that contained a fusion of the N- and C-terminal region of Ana1 (GFP-Ana1 ΔMid1, construct #8, Figure 3.15). Both fusion proteins were barely detectable at centrioles, but the centriolar localisation of Asl was slightly reduced. This effect was not statistically significant, but it was very consistent, so I suspect that the lack of statistical significance is due to the intrinsic variability of the mRNA injection assay. If this is the case, this observation would support the idea that the C-terminal region of Ana1 can to some extent bind to and sequester Asl in the cytoplasm, lowering the efficiency of Asl recruitment to centrioles.

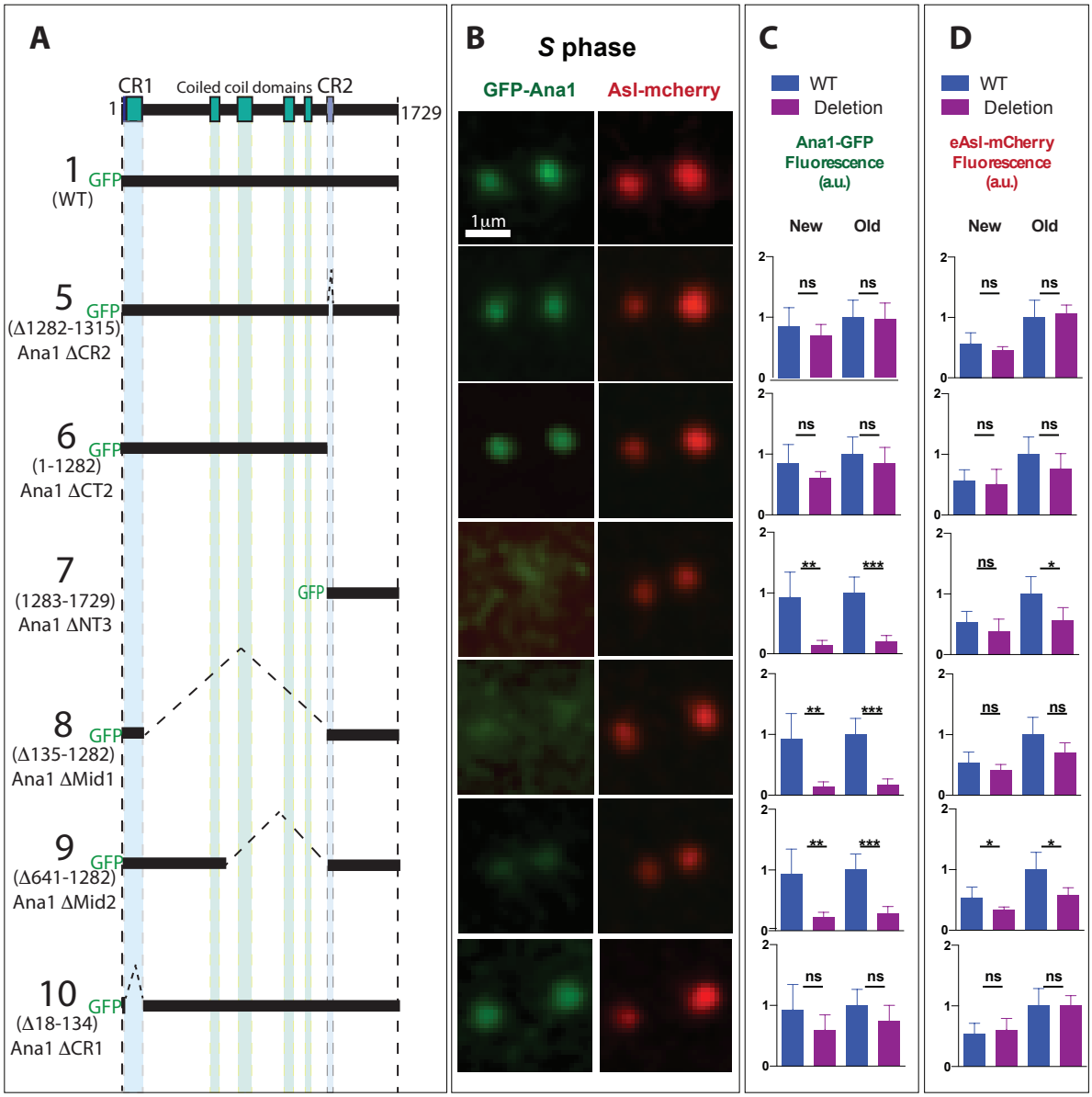

Figure 3.15: A more detailed structure/function analysis of Ana1. (A) A schematic representation of the various GFP-Ana1 deletion constructs analysed. **(B)** Micrographs show the localisation of the GFP-Ana1 fusion protein (*green*) and Asl-mCherry (*red*) in embryos injected with the Ana1 constructs as shown in (A) at new and old centrosomes in *S*-phase. **(C, D)** Bar graphs show average centrosomal Ana1-GFP (C) or Asl-mCherry (D) fluorescence levels at new and old centrosomes. All values were normalized to the average fluorescence level of WT GFP-Ana1, or Asl-mCherry observed at old centrosomes in contemporaneous controls injected with WT GFP-Ana1 (construct 1) (arbitrarily given a value of 1). Note that the constructs containing ΔCR1, ΔCR2 and ΔCT2 do not perturb the Asl levels at new or old centrosomes and suggests that they are not essential for Asl localization at the centrosomes. Middle coiled-coil regions of Ana1 are highly likely to be involved in the localization of Ana1 and hence Asl recruitment at the centriole. Error bars represent the standard deviation (SD) from 5 embryos for each construct. Statistical significance was calculated using Student's t-test (P-values: *=<0.05; **=<0.001; ***=<0.0001).

Interestingly, a smaller deletion of the middle region of Ana1, that removed three of the four central predicted coiled-coil domains (GFP-Ana1 ΔMid2, construct #9, Figure 3.15), also localized poorly to centrioles (although not as poorly as the GFP-Ana1 ΔNT3 and GFP-Ana1 ΔMid1 constructs) and consistently, but not statistically significantly, reduced the centriolar recruitment of Asl. Taken together, these findings suggest that the middle region of Ana1 containing the predicted coiled-coil regions play an important part in recruiting Ana1 to centrioles in this assay.

Finally, I tested whether the N-terminal conserved domain CR1 has any role in Ana1 recruitment. GFP-Ana1 ΔCR1 (construct #10, Figure 3.15) localised to centrosomes less strongly than full-length GFP-Ana1, although this difference was not statistically significant. As expected, the GFP-Ana1 ΔCR1 construct didn't influence the centriolar levels of Asl significantly.

Overall, the above experiments suggest that the CR1, the 1st and 2nd predicted coiled-coil regions (CC) and CR2 are neither essential for localization of Ana1 nor recruitment of Asl at the centrosome. The middle CCs regions are likely to be crucial for the Ana1 localization and Asl recruitment. The presence of endogenous Ana1 could influence these results as Ana1 could be interacting with itself and with other centriolar protein via it's CC regions and targeting it to the centrosome. Transgenic flies of the above-mentioned constructs in the *ana1* mutant background will reveal if that is the case.

3.2.11: Ana1 levels influence centriole length, and this activity requires the N-terminal region

During the course of my experiments I noticed that, qualitatively, the V-shaped centrioles in primary spermatocytes overexpressing GFP-Ana1 seemed significantly longer than normal (data not shown). In contrast, the centrioles we observed associated with the *ana1* mutant SAPs in spermatocytes overexpressing GFP-Sas-6 and Ana2-GFP were shorter than WT SAPs (Figure 3.7B). I wondered, therefore, whether Ana1 might have a previously unsuspected role in determining centriole length. As an initial test of this hypothesis, I compared the length of the long centrioles found in pupal testes in WT flies, flies expressing only a half-dose of Ana1 (*ana1*$^{1/2}$ i.e. flies trans-heterozygous for the *ana*^{mecB} mutation) and flies overexpressing either GFP-Ana1 or GFP-Ana1 ΔNT from the Ubq-promoter. Because the length of the centrioles in primary spermatocytes can vary depending on the stage of spermatocyte development, I examined the centrioles just after meiosis II, when each spermatid contains a single centriole, which becomes the basal body that nucleates the flagellar axoneme. The centrioles were significantly shorter than normal when the gene dosage of *ana1* was halved (*ana1*$^{1/2}$), and were significantly longer than normal when GFP-Ana1 was overexpressed, but not when GFP-Ana1 ΔNT was overexpressed (Figure 3.16A, B). I confirmed this result with four different centriole markers—Asl, GTU88*, Spd2 and Cep135. Thus, in spermatocytes at least, Ana1 seems to promote centriole growth in a dose-dependent manner. To my knowledge, Ana1 is the first protein shown to effect centriole length in this way. Moreover, the N-terminal region of Ana1, which in my hands is not essential for centriole, centrosome or cilia function in flies, seems to be required to promote centriole growth in spermatocytes.

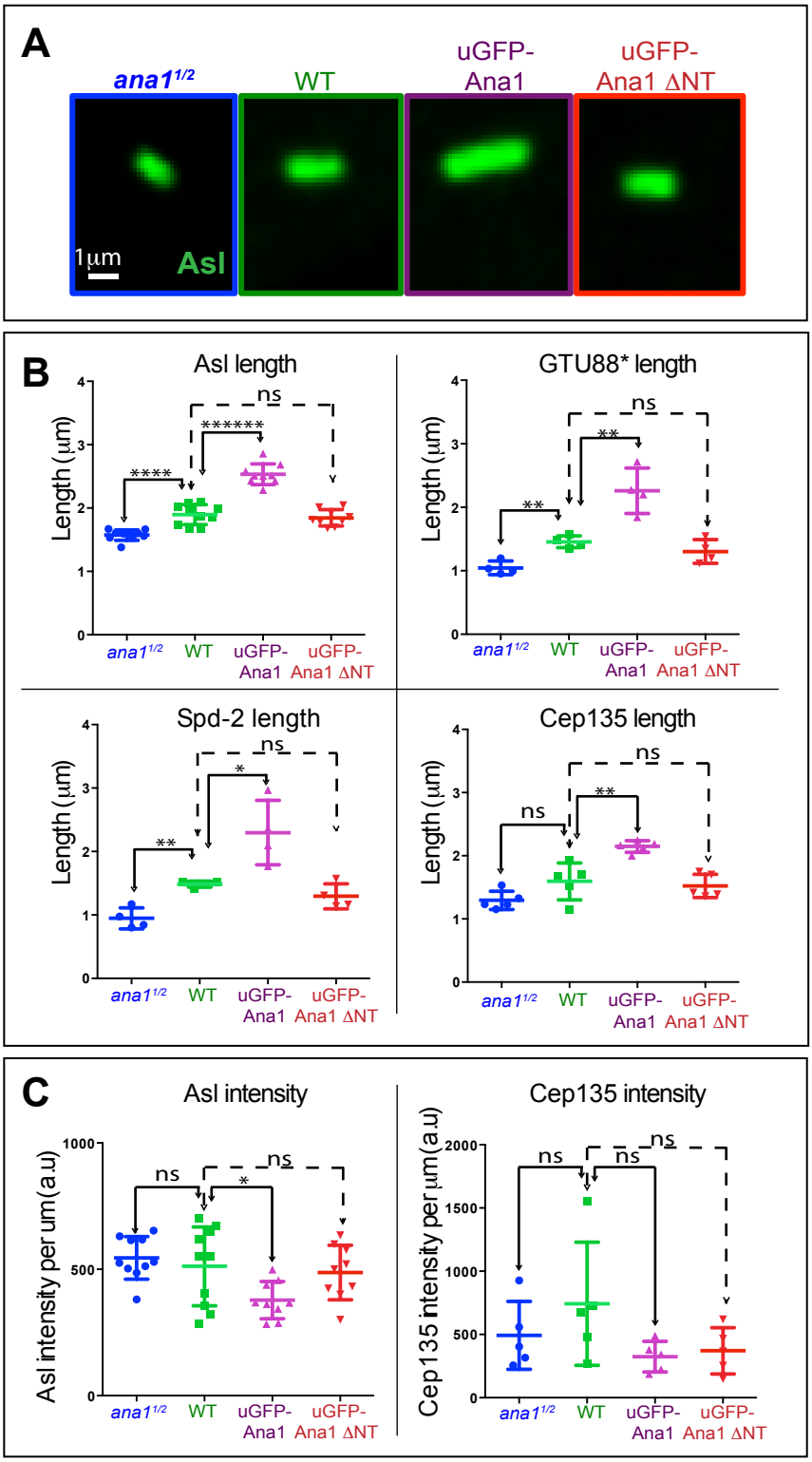

Figure 3.16: Ana1 levels influence centriole length in spermatocytes, and this activity requires the N-terminal region. (A) Micrographs show meiosis II centrioles in pupal testes of the indicated genotype, stained for Asl. **(B)** Graphs show the quantification of meiosis II centriole length using four different centriole markers for each indicated genotype. **(C)** Graphs show the quantification of Asl or Cep135 fluorescence intensity (per unit length of centriole) for each genotype. In (B) and (C), each point on the graph designates the average fluorescence intensity measured from 20-40 centrioles in a single testis (4-11 testes per genotype). Statistical significance was calculated using student's t-test (where n=number of testes analysed) (P values: *=<0.05; **=<0.001; ****=<0.00001; ******=<0.0000001; and ns=not significant). Error bars represent SD.

Given the previously described interactions between Ana1, Cep135 and Asl, I wanted to check if the levels of Ana1 changed the levels of Asl or Cep135 (per unit length of centriole). Surprisingly, reducing the genetic dose of *ana1* did not lead to an apparent reduction in the levels of Cep135 or Asl localised at centrioles per unit length of the centriole (Figure 3.16C). Interestingly, overexpressing, GFP-Ana1 led to a slight decrease in the amount of Asl and Cep135 recruited to the centrioles per unit length, although this difference was not statistically significant for Cep135 (Figure 3.16C). I conclude that Ana1 can promote centriole elongation in spermatocytes without recruiting more Cep135 or Asl (per unit length) to the centrioles.

Although the overexpression of GFP-Ana1 ΔNT in a WT background does not promote centriole elongation in spermatocytes (Figure 3.16 A, B), I wanted to test whether it could rescue the lack of centrioles in *ana1* mutant spermatocytes (as was the case in mutant brains—Figure 3.3). Interestingly, the centrioles in *ana1* mutant spermatocytes rescued by Ana1-GFP appeared abnormally elongated (although I did not quantify this phenotype), while those in mutant spermatocytes rescued by GFP-Ana1 ΔNT were invariably extremely short, and I could not measure the length of these centrioles as I could only distinguish them as dots, rather than elongated centrioles (Figure 3.17). The short centrioles in the *ana1* mutant spermatocytes rescued by GFP-Ana1 ΔNT could still be detected at the base of developing Stage 13 sperm, and they went on to to form tiny basal bodies at the base of the maturing sperm nuclei—although these often appeared somewhat disorganised (Figure 3.18). When I observed freshly dissected testes under the light microscope, *ana1* mutant sperm rescued by WT GFP-Ana1 were motile, while the mutant sperm rescued by GFP-Ana1 ΔNT were invariably immotile—presumably explaining why these flies are

male sterile (see Section 3.2.3). Thus, although GFP-Ana1 ΔNT can rescue the centrosome assembly defect in *ana1* mutant spermatocytes (Figure 3.18B) and brain cells (Figure 3.3A), it cannot support the dramatic elongation of the centrioles that normally occurs during spermatogenesis.

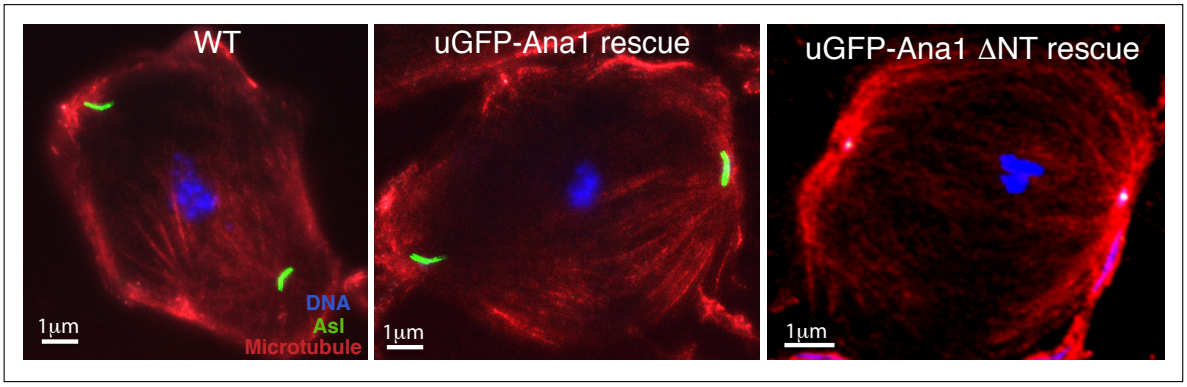

Figure 3.17: The N-terminal region of Ana1 is required to promote the normal elongation of centrioles in spermatocytes. Micrographs show Meiosis I primary spermatocyte cells, stained for Asl (*green*), MTs (*red*) and DNA (*blue*) of various indicated genotypes. Note the dot-like structures in the *ana1* mutant cells rescued by GFP-Ana1 ΔNT indicating that these centrioles have not elongated properly.

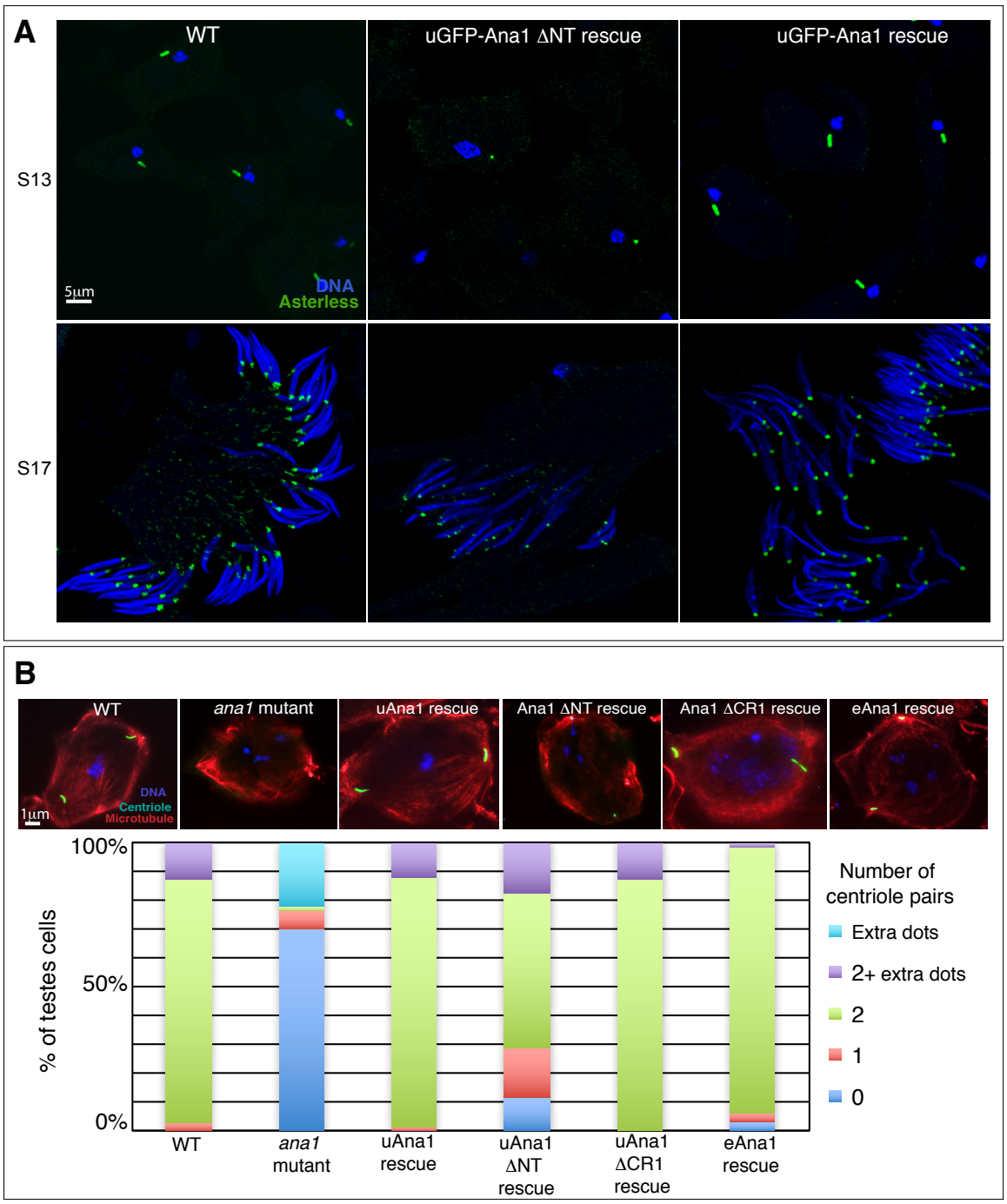

Figure 3.18: The small centrioles in *ana1* mutant testes rescued by GFP-Ana1 ΔNT can localise to the basal body region, but they do not appear to be functional. (A) Micrographs show *Drosophila* early S13 spermatids (top panels) at the onion stage (before axoneme formation) or S17 spermatids (bottom panels) during the process of axoneme elongation. Cells were stained for DNA (*blue*) and Asterless (centriole/basal body marker, *green*) from WT (left panels) or *ana1* mutant rescued with either uGFP-Ana1 ΔNT (middle panels) or uGFP-Ana1 (right panels). Note the non-elongated dot-like centrioles/basal bodies in the mutant cells rescued with uGFP-Ana1 ΔNT. **(B)** Micrographs show images of primary spermatocytes of *Drosophila* late pupal testes stained for DNA (*blue*), MTs (*red*) and the centrosome marker Asl (*green*) in WT, *ana1* mutant, *ana1* mutant rescued by different transgenes (as indicated). Graphs quantify the percentage of cells for each genotype exhibiting different numbers of centrosomes (n=>60 total cells from 5 different testes for each genotype). Note that in primary spermatocytes there are normally four elongated centrioles (2 pairs) per cell, but in the *ana1* mutants rescued by GFP-Ana1 ΔNT the centrioles were so short that the centriole pair could no longer be resolved, and so I counted these as two centrosomes per cell. Note also that I scored for the presence of occasional dot-like structures ("extra dots") that were stained with both Asl and Cnn antibodies.

3.2.12: Ana1 levels influence centriole length in wing disc cells

The centrioles in spermatocytes are much longer than those found in most fly tissues, so I wanted to test whether the length of more typical centrioles was also influenced by the dosage of *ana1*. I therefore examined centriole length by electron microscopy (EM) using fly wing disc cells, as this tissue is very amenable to this type of analysis (Franz et al., 2013; Roque et al., 2018). I took longitudinal images of multiple centrioles (usually >10 centrioles per wing disc), measured their length, and calculated an average centriole length for each wing disc, usually measuring five wing discs per genotype. Importantly, this analysis was scored blindly. GFP-Ana1 (but not GFP-Ana1 ΔNT) overexpression led to an increase in centriole length while halving the gene dosage of endogenous *ana1* (*ana1*$^{1/2}$) led to a decrease in centriole length (Figure 3.19). Thus, as in spermatocytes, Ana1 can influence centriole elongation in wing discs in a dose-dependent manner, and this activity requires the N-terminal 639aa of Ana1.

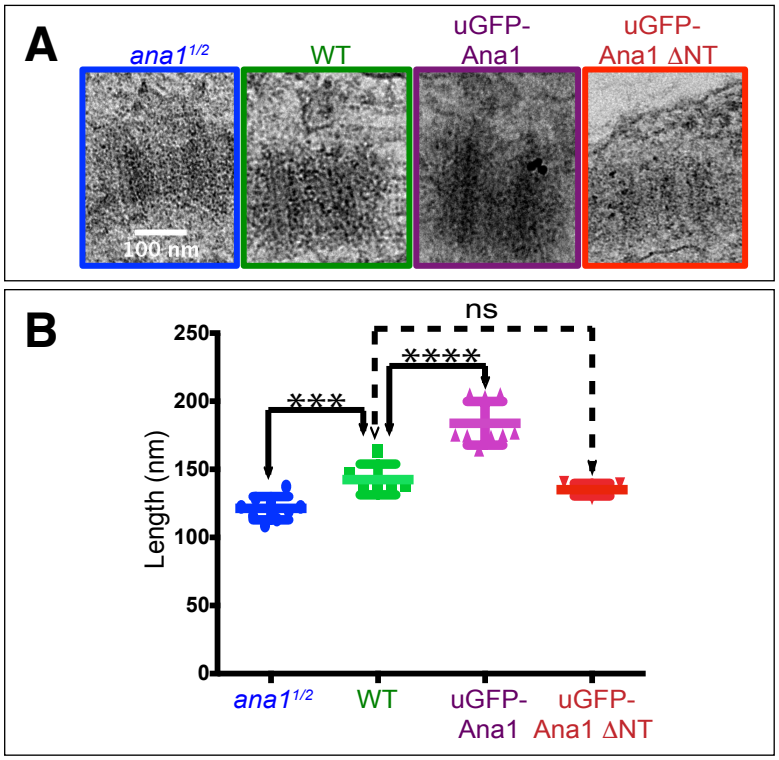

Figure 3.19: Ana1 levels influence centriole length in wing disc cells. (A) Electron micrographs show images of centrioles viewed in longitudinal section in wing disc cells of the indicated genotype. **(B)** Graph quantifies centriole length from the EM images (scored blindly). Note the similar pattern of centriole length variation as observed in spermatocyte centrioles (Figure 3.16). Each point on the graph denotes the average centriole length of >10 centrioles in a single wing disc. n=9, 6, 9 and 5 wing-discs respectively. Statistical significance was calculated using student's t-test (where n=number of wing discs) (P values: ***= <0.0001, ****=<0.00001 and ns=not significant). Error bars represent SD.

3.3: Discussion

When I began my studies, it was clear that Ana1 was important for centriole, centrosome and cilia assembly, but its precise role was not known. In particular, it was unclear whether Ana1 was part of the conserved centriole assembly pathway comprising Asl, Plk4, Sas-6, Ana2 and Sas-4. I found that, as was the case for mutations in the genes encoding these "core" proteins, *ana1* mutants essentially lacked detectable centrosomes. But, in contrast to these other proteins, the overexpression of Ana1 was unable to drive the assembly of centriole-like structures in eggs, or the over-duplication of centrioles in various proliferating tissues. At about this time, it was shown that Cep295, the human homologue of Ana1, was required for centriole-to-centrosome conversion, and that Cep295 was required to stabilize mother centrioles (Izquierdo et al., 2014). This was suggested because mother centrioles in vertebrates normally lose their inner cartwheels and, in the absence of Cep295, these centrioles could not recruit PCM: as a result, these mother centrioles lacked both a cartwheel and PCM, and so were destabilized. The idea that Cep295/Ana1 might be required to stabilize centriole structure was consistent with my data indicating that Ana1 did not appear to be a core component of the centriole assembly pathway, but that centrioles were nevertheless essentially absent from cells lacking Ana1.

In flies, however, mother centrioles do not lose their cartwheel structure, so I continued to investigate how Ana1 might function to stabilize centrioles in flies. My analysis of Sas-6/Ana2 Particles (SAPs) in *ana1* mutant testes suggested that Ana1 is not required for cartwheel hub assembly, but SAP ultrastructure was subtly perturbed. Most importantly, SAPs formed in *ana1* mutant eggs recruited excess Sas-4, but much less Asl and, as a result, they organized far fewer MTs—as Asl is known to be essential to allow centrioles to recruit PCM (Conduit et al., 2010; 2014a; 2014b;

Dzhindzhev et al., 2010; Gopalakrishnan et al., 2011; Varmark et al., 2007). It is currently unclear why SAPs lacking Ana1 recruit more Sas-4, but one possible explanation is that Sas-4 and Ana1 are recruited and/or maintained at centrioles/SAPs by the same protein so that, in the absence of Ana1, this protein can recruit more Sas-4. An obvious candidate is Cep135/Bld10, which helps recruit Ana1/Cep295 to centrioles (Fu et al., 2016), and which can interact with Sas-4/CPAP (Lin et al., 2013b). Further experiments will be required to determine if this is the case.

My antibody injection experiments confirmed and extended these findings, suggesting that Ana1 helps to recruit Asl to newly maturing mother centrioles. This observation was potentially very exciting, because Asl lies at the very heart of centriole and centrosome biogenesis—as it is required to recruit Plk4 to centrioles to initiate centriole duplication, and to recruit Spd-2 to centrioles to initiate the recruitment of the mitotic PCM (Conduit et al., 2010; 2014a; 2014b). Importantly, Asl is not initially recruited to growing daughter centrioles, but is only recruited to new centrioles as they separate from their mothers and mature into new mothers (Novak et al., 2014), potentially explaining why the acute inhibition of Ana1 function (by antibody injection) mainly perturbs the recruitment of Asl to the new mother centriole.

At about this time a paper was published that used RNAi to address the function of Ana1 in cultured fly cells (Fu et al., 2016). These authors concluded that the N-terminal regions of Cep135 and Ana1 interacted (allowing Cep135 to recruit Ana1 to centrioles) and the C-terminal regions of Ana1 and Asl also interacted (allowing Ana1 to recruit Asl to centrioles). Thus, Ana1 functioned as a “bridge” between Cep135 and Asl (see Figure 3.13). Moreover, this module appeared to be conserved in human

cells (Fu et al., 2016). Clearly these results were consistent with my observation that Ana1 helps recruit Asl to centrioles, but several aspects of this model were puzzling.

First, this module should be essential for centriole duplication: as discussed above, Asl is essential for all aspects of centriole and centrosome biogenesis as it recruits both Plk4 (for duplication) and Spd-2 (for mitotic PCM recruitment), so if centrioles cannot recruit Asl they cannot duplicate. Yet, I observed that in *ana1* mutant spermatocytes very short centrioles were often observed when Sas-6 and Ana2 were co-overexpressed to form SAPs. Moreover, several previous studies in flies had concluded that Cep135 is not essential for centriole duplication (Blachon et al., 2009; Carvalho-Santos et al., 2010; 2012; Mottier-Pavie and Megraw, 2009; Roque et al., 2012). Fu et al., argued that this was because the mutant allele used for these studies was not a null, but they did not test this by generating a null mutation. Second, there is strong evidence that the core centriole duplication protein Sas-4/CPAP can interact directly with Asl/Cep152 and that this interaction is conserved (Cizmecioglu et al., 2010; Dzhindzhev et al., 2010; Galletta et al., 2016a; Hatch et al., 2010) and plays some role in recruiting Asl to centrioles (Conduit et al., 2014b; Novak et al., 2014). This interaction is ignored in the Fu et al., model. Third, dynamic studies indicate that the recruitment of Asl to centrioles is likely to be complex, as ~50% of the protein is recruited irreversibly, while ~50% turns-over. This complexity cannot be accounted for in the Fu et al. model. Finally, my 3D-SIM studies indicate that the position of the N-termini of Cep135 and Ana1 within spermatocyte centrioles do not overlap, whereas, using the same technique but in S2 cells, Fu et al. concluded that they do overlap. None of these issues disproves the Fu et al. model, but I wondered whether this model was perhaps oversimplified.

I used a relatively high-throughput mRNA injection assay to undertake a classic structure/function analysis to try to better understand how Ana1 was recruited to centrioles, and how it helped recruit Asl to centrioles. Although, I feel these studies generally support my contention that these processes may not be as simple as proposed by Fu et al., an important caveat to these studies is that they were performed in the presence of the endogenous WT protein. As I started to analyse these results I realized that this made it very difficult to draw firm conclusions. This issue therefore remains unresolved. Clearly it will be important to generate a true null allele of *Cep135*, and this is currently underway in the Raff laboratory (although *Cep135* is a complicated gene, making this non-trivial). It will also be important to better understand the detailed kinetics of how Cep135, Ana1 and Asl are recruited to centrioles; these studies are also currently underway in the Raff laboratory, using some of the quantitative imaging techniques I discuss in the next Chapter.

Perhaps most importantly, I have found that Ana1 promotes centriole elongation in a dose-dependent manner: centrioles are too long when Ana1 is over-expressed and too short when Ana1 is under-expressed. Interestingly, Ana1 requires its N-terminal 639aa to promote centriole elongation, even though this region does not appear to be essential for Ana1's function in promoting centriole, centrosome and cilium assembly/maintenance. The Tang lab has also concluded that Cep295 is required for centriole elongation in human cells, and they show that the first 560aa and last 546aa of Cep295 can interact with tubulin, providing a potential mechanism for how Cep295 might regulate centriole length; this study was published back to back with our study of Ana1 function (Chang et al., 2016). At the N-terminus, Ana1 (19-134aa) protein shares sequence homology with Cep295/KIAA1731 (13-130aa) protein (Andersen et al., 2003). Perhaps surprisingly, Ana1 depletion does not appear to lead to a decrease

in centriole length in S2 cells (Fu et al., 2016). The reason for this discrepancy is unclear.

To my knowledge, Ana1 is the first protein that has been shown to affect centriole length in a dosage dependent manner. This observation led several of us in the Raff laboratory to start thinking about the problem of how centriole length is controlled. This area is explored further in the next Chapter.

Chapter 4: The regulation of centriole length

4.1: Introduction

Centriole assembly begins with the formation of a single procentriole next to a pre-existing centriole (Brownlee and Rogers, 2013). The procentriole then elongates until it reaches its final predetermined length (Azimzadeh and Marshall, 2010; Bornens, 2012; Gönczy, 2012; Jana et al., 2014). Significant progress has been made during the past few years towards understanding the mechanism of centriole assembly (Arquint and Nigg, 2016; Banterle and Gönczy, 2017; Fırat-Karalar and Stearns, 2014). However, it remains unclear how centriole length is measured and how it is rigorously enforced. Overly long centrioles can lead to the formation of extra centrioles (Godinho and Pellman, 2014; Marteil et al., 2018) that in turn can lead to errors in chromosome segregation (Basto et al., 2008; Godinho and Pellman, 2014; Marteil et al., 2018), and also potentially to the formation of too many cilia (Mahjoub and Stearns, 2012).

In a study of centriole behaviour during tumourigenesis, overly long centrioles were found to be over-active as centrosomes, forming ectopic procentriole nucleation sites and probably contributing to centriole amplification (Marteil et al., 2018). These excessively long centrioles were unstable at their distal ends, resulting in centriole fragmentation (Marteil et al., 2018). This type of phenotype could result from the deregulation of the expression of centriole length regulators or the loss of cell cycle control.

Thus, it appears that regulating centriole length plays an important part in various cellular processes, so it is vital to understand how centriole length is controlled. Recent results, largely from vertebrate cell lines and *Drosophila*, suggest that, as is the case for centriole assembly, a relatively small set of proteins may be necessary for setting centriole length.

In human cultured cells, the overexpression of centriole wall-proteins such as CPAP/ Sas-4, Cep135, Cep120, POC5, Centrobin, SPICE1 (spindle and centriole associated protein 1), C2CD3 (calcium-dependent lipid-binding domain of protein kinase C) and Cep295 results in overly long centrioles (Azimzadeh et al., 2009; Banterle and Gönczy, 2017; Chang et al., 2016; Comartin et al., 2013; Dahl et al., 2015; Dantas et al., 2013; Gudi et al., 2011; 2014; Jeffery et al., 2013; Keller et al., 2009; Kleylein-Sohn et al., 2007; Kohlmaier et al., 2009; Lin et al., 2013a; Thauvin-Robinet et al., 2014; Venoux et al., 2013). Conversely, the overexpression of distal end "capping" proteins—such as CP110 and Cep97, which bind to the distal end of the centriole—seems to restrict centriole growth (Kohlmaier et al., 2009; Schmidt et al., 2009; Spektor et al., 2007; Tang et al., 2009). Interestingly, CP110 and Cep97 may cooperate with a MT-depolymerizing kinesin Kif24 to ensure that the centriole MTs do not extend beyond the centriole itself (Kobayashi et al., 2011). OFD1 (Orofaciodigital Syndrome1), another distal end protein, has been shown to inhibits the activity of C2CD3 and control the length of the centriole (Thauvin-Robinet et al., 2014).

In *Drosophila* several proteins have been implicated in regulating centriole length (Figure 4.1). I showed in Chapter 3, sections 3.2.11 and 3.2.12 that *ana1* overexpression or *ana1* under-expression influences centriole length (Saurya et al., 2016). Cep135 also seems to promote centriole growth and *Cep135* mutant flies have

short centrioles in spermatocytes (Carvalho-Santos et al., 2012; Mottier-Pavie and Megraw, 2009), but there is no data on how the overexpression of *Cep135* influences centriole length. Unlike the situation in vertebrates (Alvarez-Cabrera et al., 2017; Comartin et al., 2013; Kohlmaier et al., 2009; Lin et al., 2013a; Schmidt et al., 2009; Sharma et al., 2016; Tang et al., 2009; Zheng et al., 2016), *Sas-4/CPAP* overexpression in flies does not appear to result in overly long centrioles (Franz et al., 2013). As in humans, fly CP110, Cep97 and Klp10A, seem to inhibit centriole growth, as flies with mutations in these genes exhibit overly-long centrioles, and an even more dramatic extension of the centriole MTs (Delgehyr et al., 2012; Franz et al., 2013). Interestingly, the core centriole duplication protein Asl, that functions in both centriole duplication and mitotic PCM recruitment, seems to inhibit centriole growth in wing disc, male and female germline stem cell (GSC) centrioles, and it requires Cep97 and, to a lesser extent, CP110 for this activity (Galletta et al., 2016b).

Although several molecules involved in regulating centriole length have been identified, it is not well understood how these proteins function in this process. This is in part because the current data is mostly derived from static EM images of the centrioles (Kuriyama and Borisy, 1981a; Shukla et al., 2015) and there is little information available on whether these proteins influence centriole size by altering the kinetics of daughter centriole growth, or by perturbing processes that maintain the length of the mother centrioles. In *asl* mutant wing disc cells, male and female GSCs there is some evidence that mother centrioles gradually elongate as they progress through successive rounds of division, indicating that Asl normally helps to maintain the length of the mother centriole (Galletta et al., 2016b).

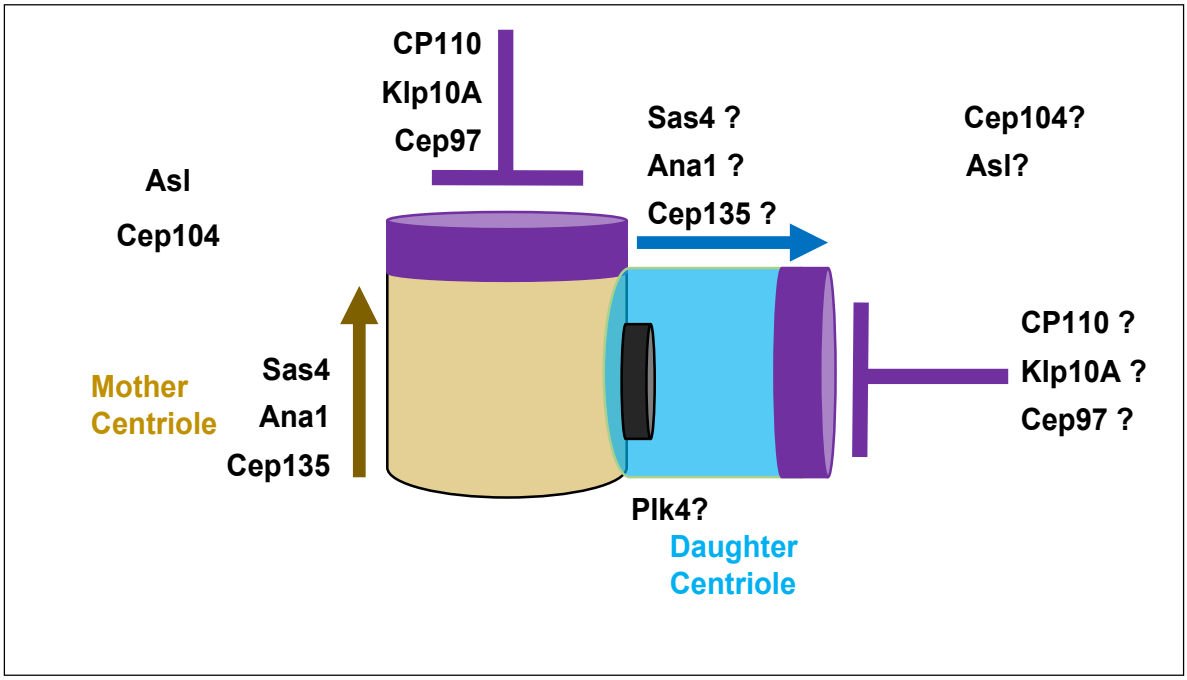

Figure 4.1: A summary of some of the proteins that have been implicated in centriole length control. The Schematic illustration shows the mother centriole (*light brown*) and several centriole proteins that are known to influence centriole length in *Drosophila*. The core centriole proteins Sas-4 (Tang et al., 2009), Ana1 (Chang et al., 2016; Saurya et al., 2016) and Cep135 (Mottier-Pavie and Megraw, 2009) appear to promote mother centriole elongation, while the "capping" proteins CP110, Cep97 and Klp10A (Kif24 in vertebrates) bind to the distal end of the mother centriole (*dark purple*) where they appear to inhibit mother centriole elongation. In flies there is evidence that Asl also inhibits mother centriole elongation in wing disc cells, male and female GSCs, at least in part through an interaction with Cep97 and/or CP110 (Galletta et al., 2016a). The loss of Asl in such tissues allows mother centrioles to gradually get larger over time, suggesting that Asl helps maintain the correct length of mother centrioles (Galletta et al., 2016a). In several other systems Cep104 has also been shown to influence centriole and cilia growth (Al-Jassar et al., 2017; Jiang et al., 2012; Rezabkova et al., 2016; Satish Tammana et al., 2013). Most measurements of centriole length come from an EM analysis of mother centrioles (that have either separated from their daughters, or where their engaged daughters were not measured), so it is unclear whether these proteins influence mother centriole length by effecting their growth when they were daughters—as illustrated here with the daughter centriole (*blue*)—or by effecting the dynamics of fully grown mother centrioles, that could in theory grow or shrink in size after they have matured into mother centrioles.

This lack of information is in part due to two major technical problems: (1) Centrioles in most cell types are tiny, making it difficult to directly measure their size during the growth process accurately, even with modern super-resolution microscopy; (2) Daughter centrioles initially grow during S-phase (Callaini and Riparbelli, 1990), but cultured cells are difficult to precisely synchronise, and they usually contain only two

duplicating centrioles, making it difficult to obtain a quantitative description of the kinetics of centriole growth.

In this chapter, I describe the development of several techniques that have allowed us to measure the kinetics of daughter centriole growth in the early syncytial *Drosophila* embryo, using the incorporation of the cartwheel component Sas6-GFP as a proxy to measure centriole length. These studies reveal that, most unexpectedly, daughter centriole growth is “homeostatic”: centrioles that grow quickly tend to grow for a shorter period of time, while centrioles that grow slowly tend to grow for a longer period of time—thus ensuring that centrioles ultimately grow to a consistent length. Moreover, we found that the amount and the activity of the key centriole duplication protein Plk4 seem to influence both the rate and period of daughter centriole growth. Perhaps surprisingly, I show that Ana1 and Sas-4 do not appear to effect the rate or period of daughter centriole growth, while Cep135, CP110, Cep97 and Klp10A do so. The work described in the next two Chapters touches on a large body of ongoing work that has been developed in collaboration with several members of the Raff laboratory, in particular, Mustafa G. Aydogan, Alan Wainman, Thomas L. Steinacker and Zsofia A. Novak. A first paper describing some of these findings was recently published (Aydogan et al., 2018) and I am the third of nine authors on this paper. Several more papers are in the pipeline. As a result of this collaborative effort, I present here some experiments that I did not directly perform myself—although in all cases I helped to develop reagents and methodologies that contributed to these experiments; these instances are clearly indicated in the text.

4.2: Results

4.2.1: Measuring the dynamics of daughter centriole growth in living fly embryos using a Sas-6-GFP incorporation assay

The *Drosophila* embryo is a well-established system with which to study centriole duplication (Lattao et al., 2017), and it is potentially an attractive system for measuring the kinetics of daughter centriole growth. It is a multinucleated syncytium that undergoes 13 rounds of nearly synchronous, rapid nuclear divisions as described in section 1.7 (Foe and Alberts, 1983). During nuclear cycles 10–14, the majority of nuclei form a monolayer at the cortex, allowing the simultaneous observation of many centrioles as they rapidly and synchronously progress through repeated rounds of S-phase and M-phase without intervening Gap-phases (Foe and Alberts, 1983). Moreover, centrioles in flies are structurally simpler than those in vertebrates (Callaini and Riparbelli, 1990; Callaini et al., 1997; Moritz et al., 1995). All centrioles start to assemble around the cartwheel in S-phase, but vertebrate centrioles often exhibit a second phase of growth during G2/M, when the centriolar MTs extend past the cartwheel (Chrétien et al., 1997; Kuriyama and Borisy, 1981b; Shukla et al., 2015). Fly centrioles usually do not exhibit this second phase of growth, so the centrioles are relatively short and, crucially for my studies, the cartwheel extends throughout the length of the daughter centriole (González et al., 1998; Lattao et al., 2017). We reasoned, therefore, that the fluorescence incorporation of the cartwheel components Sas-6-GFP or Ana2-GFP could be used as a proxy to measure daughter centriole length in these embryos.

Transgenic lines expressing eSas6-GFP under the control of the endogenous Sas-6 promoter were generated by a former Post Doctoral fellow in our Laboratory, Nadine Muschalik. A 3D-SIM-FRAP analysis of Sas6-GFP performed by Alan Wainman and Mustafa Aydogan revealed that Sas6-GFP is stably and irreversibly incorporated in the growing daughter in S-phase (Aydogan et al., 2018), making it an appropriate marker to monitor the daughter centriole growth kinetics. In collaboration with (Aydogan et al., 2018), we developed methods to track the incorporation of Sas-6-GFP into growing daughter centrioles, using spinning disk confocal microscopy and the Fiji software plugin Trackmate (Tinevez et al., 2017) (Figure 4.2A-C).

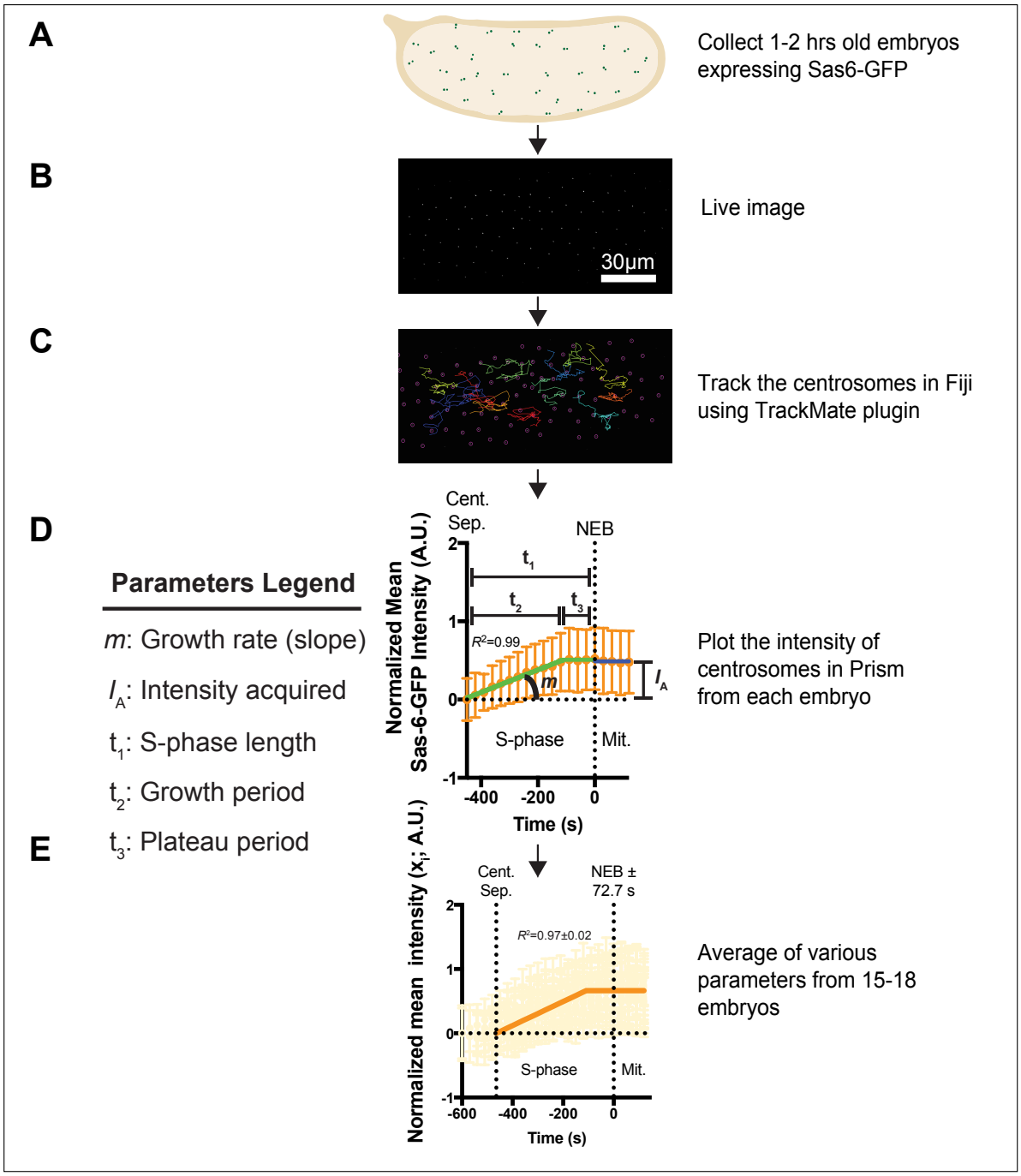

Figure 4.2: A schematic illustration of the daughter centriole growth assay in *Drosophila* embryos. (A-C) One to two hour old embryos expressing Sas-6-GFP were collected and imaged on a Perkin Elmer ERS Spinning Disk confocal system from early S-phase (when the centrosome first separate), through NEB and into mitosis. The centriole pairs are tracked in Fiji using the TrackMate plugin. **(D)** Graph shows the mean ± SD fluorescence intensity of the Sas-6-GFP tracks measured from the start of S-phase (when the centrioles first separate—Cent. Sep.) and into early mitosis—mitotic entry was scored as nuclear envelope breakdown (NEB). This data was tested against several growth models using mathematical regression, and was best fit by a "linear growth followed by plateau" model (Aydogan et al., 2018). Several growth parameters for an individual embryo can be extracted from the fitted graphs (as indicated). **(E)** Graph shows the regressed average centriole growth profile calculated from ≥ 15 individual embryos (the underlying data is shown in reduced opacity). Illustrations B-E are courtesy of M. Aydogan.

At the start of S-phase, each Sas-6-GFP focus comprises a mother and growing daughter centriole, but these cannot be resolved on spinning disk confocal microscope system. The Sas6-GFP intensities were measured from early S-phase (when the two separating mother centrioles first become visible as distinct entities), through nuclear envelope breakdown (NEB—the start of mitosis), until the two mother centrioles separate at the end of mitosis (Figure 4.2A-C). Sas6-GFP intensities of nearly 100 centriole pairs from the same embryo during nuclear cycle 12 were measured and plotted in Prism 7 (Figure 4.2D). Regression analysis was used to fit the data from each embryo during S-phase and early mitosis, and this fitted data was used to calculate mean values for several parameters that describe the kinetics of centriole growth in an individual embryo (Figure 4.2D). We then used these parameter values to generate an “average” centriole growth profile derived from ~1000 individual centrioles tracked throughout S-phase in 15 individual embryos (Figure 4.2E). As we developed these methods we realised that the data were more reproducible if they were collected and analysed by a single experimenter in a single continuous batch of experiments (sometimes over several days, and always alternating the analysis of a batch of experimental and control embryos). The data shown in Figure 4.2 was therefore collected and analysed by Mustafa Aydogan.

These studies reveal that Sas-6-GFP fluorescence increased steadily during S-phase but plateaued before the entry into mitosis, presumably when centrioles reached their correct size; levels then remained constant during early mitosis (Figure 4.2D). Interestingly, in early worm embryos, GFP: SAS-6 shows a similar incorporation profile, suggesting this pattern of approximately linear growth during S-phase followed by a plateau into mitosis may be a conserved feature of Sas-6 incorporation into the cartwheel (Dammermann et al., 2008).

4.2.2: Plk4 influences the rate and period of daughter centriole growth in living fly embryos

In experiments that I was not involved in, Mustafa Aydogan and Alan Wainman showed that Sas-6 is incorporated into the proximal end of the growing daughter centriole (Aydogan et al., 2018), not the distal end, as had been widely presumed (Gönczy, 2012; Guichard et al., 2010). This suggested to us that Plk4, the master regulator of centriole duplication that determines the site of daughter centriole assembly (Arquint and Nigg, 2016; Banterle and Gönczy, 2017), might also influence the parameters of centriole growth. We therefore monitored Sas-6-GFP incorporation in early embryos in which the genetic dose of *Plk4* was halved (hereafter, *Plk4*$^{1/2}$ embryos). The daughter centrioles in these embryos grew at a slower rate but, most unexpectedly, they also grew for a longer period, and so the centrioles ultimately grew to the same size as in WT controls (Figure 4.3A, B). The data for this Figure was also generated by Mustafa Aydogan.

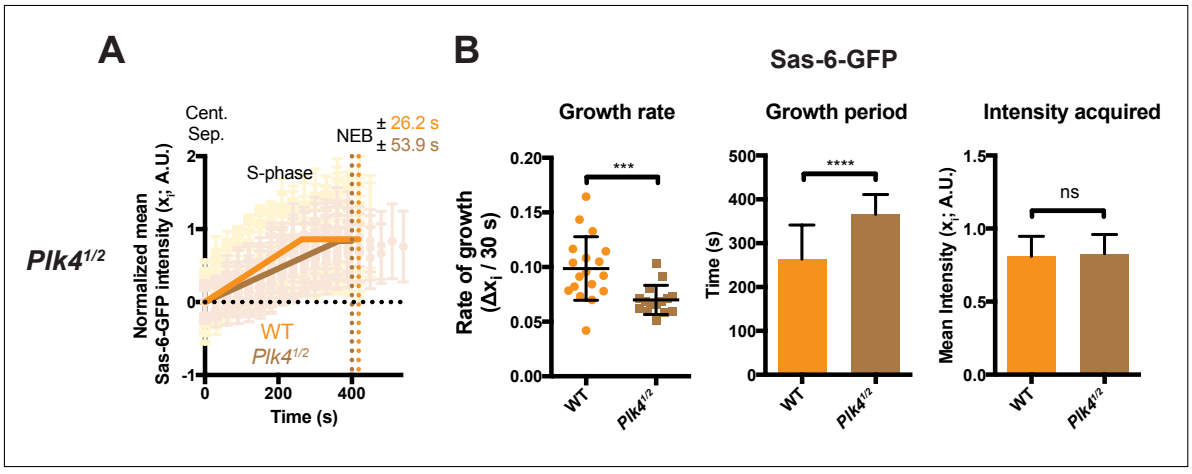

Figure 4.3: Plk4 influences the rate and period of daughter centriole growth in living fly embryos. (A) Graphs compare the average Sas-6-GFP incorporation profile in WT embryos (*orange*) and in *Plk4*$^{1/2}$ embryos (*brown*) during nuclear cycle 12. **(B)** Charts quantify various parameters of centriole growth that are calculated from the Sas-6-GFP incorporation profiles in (A). Data presented as mean ± SD (N≥15 embryos for each group). Statistical significance was measured using either Student's t-test (for Gaussian-distributed data) or Mann-Whitney test (*P<0.05; ***P<0.001; ****P<0.0001; ns, not significant). N≥15 embryos for each group. All Illustrations are courtesy of M. Aydogan.

This result was very surprising, so I used EM to directly confirm that centrioles really were of the same size in WT and *Plk4*$^{1/2}$ embryos. Unfortunately, after several attempts, I was unable to accurately measure centriole length by EM in embryos. I therefore turned to wing-disc tissue, which I had already successfully used to measure centriole length in my previous experiments (Chapter 3). I acquired images of centrioles in WT and *Plk4*$^{1/2}$ wing-discs (4-6 wing discs from each genotype, 12-27 centrioles per wing disc, Figure 4.4A). These images were then coded and randomised, and I then measured the length of the centrioles in each image, blindly. This analysis confirmed that centrioles were of the same size in WT and *Plk4*$^{1/2}$ wing-discs (Figure 4.4B). Taken together, these data raise the intriguing possibility that there is a homeostatic relationship between the daughter centriole growth rate and growth period that ensures daughter centrioles grow to a consistent size, and that Plk4 plays an important part in establishing this homeostatic relationship.

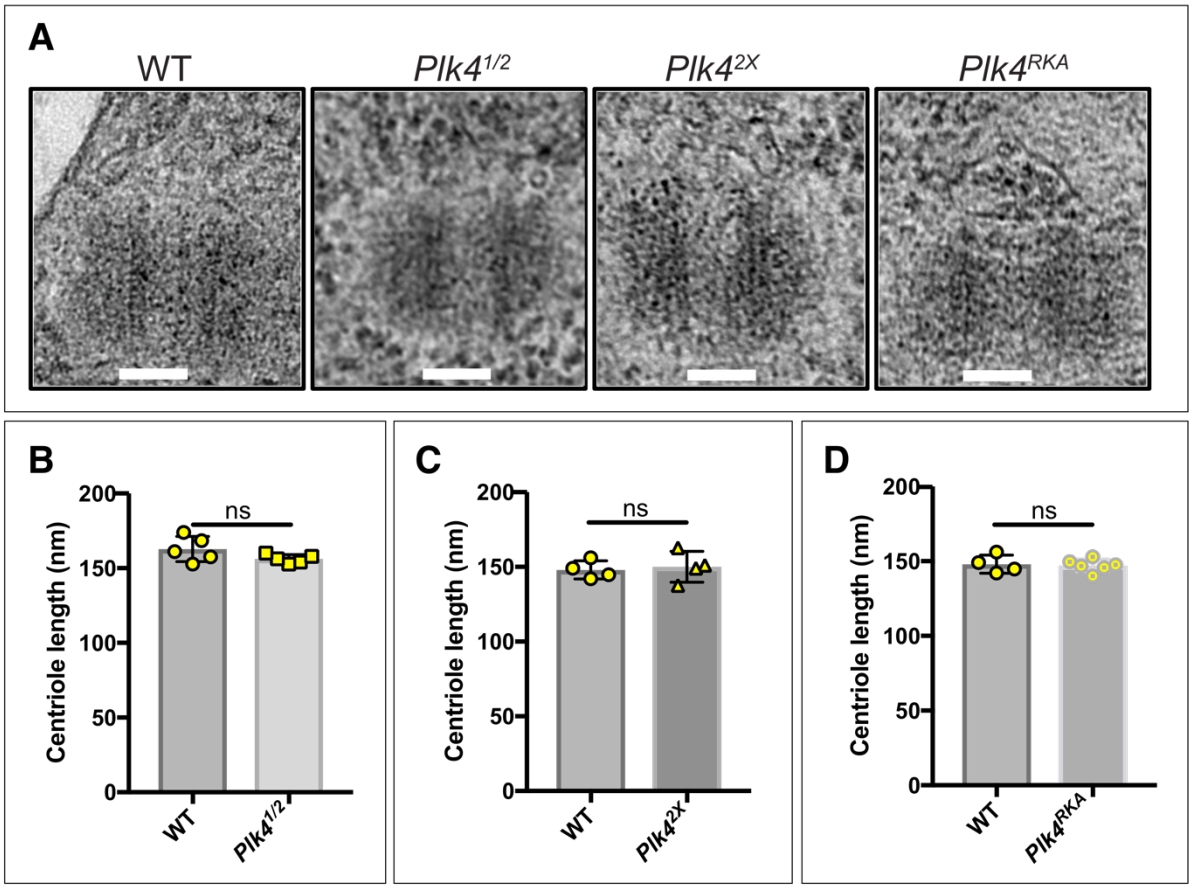

Figure 4.4: Plk4 does not detectably influence centriole length in fly wing disc cells. (A) Electron micrographs show images of centrioles viewed in longitudinal section in wing disc cells of the indicated genotype. **(B-D)** Graph quantifies the centriole length from the EM images (scored blindly). Each point on the graph denotes the average centriole length of 12-27 centrioles in a single wing disc. n= 4-6 wing-discs. Statistical significance was calculated using Mann-Whitney test (where n=number of wing discs) (P values: ns=not significant). Error bars represent SD. Scale bar, 100nm.

4.2.3: Overexpressing Plk4 increases the period of daughter centriole growth, but does not alter the rate of growth

We next wondered whether overexpressing Plk4 would perturb the parameters of centriole growth. We knew from previous studies that overexpressing Plk4 using the UAS-Gal4 system (so presumably at very high levels compared to the endogenous protein, which is expressed at very low levels—Thomas Steinacker, personal communication), lead to the *de novo* formation of centriole-like structures in eggs and embryos (Peel et al., 2007; Rodrigues-Martins et al., 2007). I therefore generated

transgenic lines expressing *Plk4* from its endogenous promoter (the 2kb region upstream of the endogenous Plk4 transcription initiation site). I used these lines to generate flies expressing Sas-6-GFP with 4 copies of the *Plk4* gene (hereafter $Plk4^{2X}$ flies). Mustafa Aydogan then analysed the embryos laid by these females and found that the growth rate was not significantly altered, but the growth period was shortened; as a result, the centrioles appeared to be smaller than normal (Figure 4.5A and C). This suggests that altering the amount of Plk4 can change the growth period without changing the growth rate, indicating that Plk4 can influence these parameters independently. Moreover, they show that the homeostatic mechanism can be broken, leading to an alteration in centriole size.

I again performed an EM analysis to compare the length of the centrioles in WT and $Plk4^{2X}$ wing-discs. Surprisingly, this revealed that the centrioles were of the same length in these tissues (Figure 4.4A and C). I discuss in more detail later how I rationalise these apparently contradictory findings (see Section 4.3) but, briefly, I believe that in the EM images I am measuring the electron-dense region of the centriole (that is usually bounded by the centriole MTs), while the Sas-6-GFP assay measures the length of the centriole cartwheel (which is usually not visible in my EM images): in WT embryos and wing discs these are normally the same length, but perhaps in the $Plk4^{2X}$ tissues the electron dense part of the centriole may be of normal length (Figure 4.4A and C), while the cartwheel may be too short (Figure 4.5A and B).

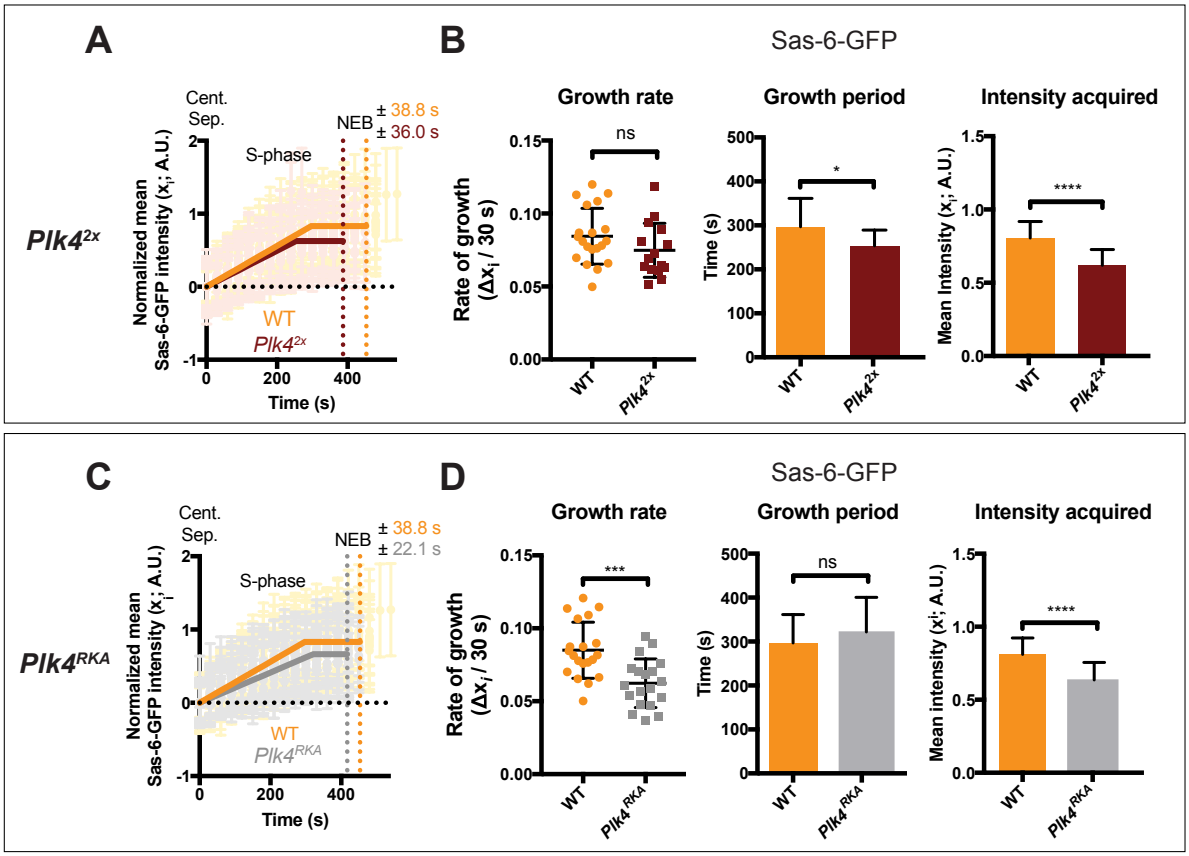

Figure 4.5: Overexpressing Plk4 increases the period of daughter centriole growth while reducing the kinase activity of Plk4 reduces the rate of daughter centriole growth (A) Graphs compare the average Sas-6-GFP incorporation profile in WT embryos (orange) and in *Plk4*^{2x} (*dark brown*) during nuclear cycle 12. **(B)** Charts quantify various parameters of centriole growth that are calculated from the Sas-6-GFP incorporation profiles in (A). (**C-D)** Graphs and charts show the identical analysis for *Plk4*^{RKA} embryos (grey) as in A and B. Data presented as mean ± SD (N≥15 embryos for each group). Statistical significance was measured using either Student's t-test (for Gaussian-distributed data) or Mann-Whitney test (*P<0.05; ***P<0.001; ****P<0.0001; ns, not significant). N≥15 embryos for each group. All Illustrations are courtesy of M. Aydogan.

4.2.4: Reducing the kinase activity of Plk4 reduces the rate of daughter centriole growth, but does not alter the period of growth

We next wanted to test whether altering the kinase activity of Plk4 effected the parameters of daughter centriole growth. It has previously been shown that an amino-acid substitution within the kinase domain of Plk4—changing Leucine 89 to Glycine (L89G)— lead to a ~10-fold reduction in its kinase activity, measured *in vitro* (Holland et al., 2010; Zitouni et al., 2016). I therefore mutated the equivalent residue (L89G) in

Drosophila melanogaster Plk4 and and generated transgenic fly lines expressing this form of *Plk4*, which should have Reduced Kinase Activity (hereafter $Plk4^{RKA}$), linked to the endogenous Plk4 promoter. I then generated fly lines expressing Sas-6-GFP and one copy of the $Plk4^{RKA}$ transgene in an otherwise WT background (i.e. in the presence of two copies of the endogenous *Plk4* gene). Mustafa Aydogan analysed the embryos laid by these females and found that the cartwheel growth period was not significantly altered, but the growth rate was slowed; as a result, the centrioles appeared to be smaller than normal (Figure 4.5C and D). Thus, lowering the kinase activity of Plk4 reduces the centriole growth rate, but does not alter the growth period and so again this homeostatic relationship is broken, leading to an alteration in centriole size. I again performed an EM analysis to compare the length of the centrioles in WT and $Plk4^{RKA}$ wing-discs, and this again revealed that the centrioles were the same length in these tissues (Figure 4.4A and D). Nevertheless, these striking findings have allowed us to propose a relatively simple model for how the levels and kinase activity of Plk4 might regulate the length of the centriole cartwheel in embryos (see Section 4.3).

4.2.5: Examining the potential role of centriole growth promoting factors in cartwheel growth dynamics.

With this cartwheel elongation assay in hand, I next wanted to test whether the two factors that have been shown to promote centriole elongation in flies—Ana1 (Saurya et al., 2016) and Cep135 (Mottier-Pavie and Megraw, 2009)—alter the parameters of cartwheel growth in embryos. I also included Sas-4/CPAP in my analysis, as this protein promotes the elongation of centrioles in vertebrate systems (Alvarez-Cabrera et al., 2017; Chang et al., 2016; Comartin et al., 2013; Dahl et al., 2015; Dantas et al., 2013; Gudi et al., 2014; Kohlmaier et al., 2009; Lin et al., 2013a; Schmidt et al., 2009;

Sharma et al., 2016; Tang et al., 2009; Thauvin-Robinet et al., 2014; Venoux et al., 2013; Zheng et al., 2016), but not in fly wing disc cells (Franz et al., 2013). To perform these experiments, I generated females expressing Sas-6-GFP in a background that was heterozygous for a null or strongly hypomorphic mutation in each of these genes (so lowering the genetic dosage of each gene by half): *ana1*$^{1/2}$, *Cep135*$^{1/2}$ or *Sas-4*$^{1/2}$ respectively. Unlike the Plk4 experiments described above, I performed all the data collection and analysis for this set of experiments. Perhaps surprisingly, the Sas6-GFP incorporation parameters in *ana1*$^{1/2}$ embryos did not differ significantly from WT, indicating that lowering the dose of *ana1* does not affect the growth of the cartwheel in the early embryos (Figure 4.6A and B). This result is perhaps unexpected, as I showed in the previous Chapter that halving the genetic dose of *ana1* leads to a decrease in centriole size in wing disc cells. I discuss the potential reasons for this apparent discrepancy in more detail in Section 4.3 but, as described above, I think it is possible that Ana1 may influence the growth of the centriole MTs, whereas the Sas-6-GFP assay measures the growth of the cartwheel.

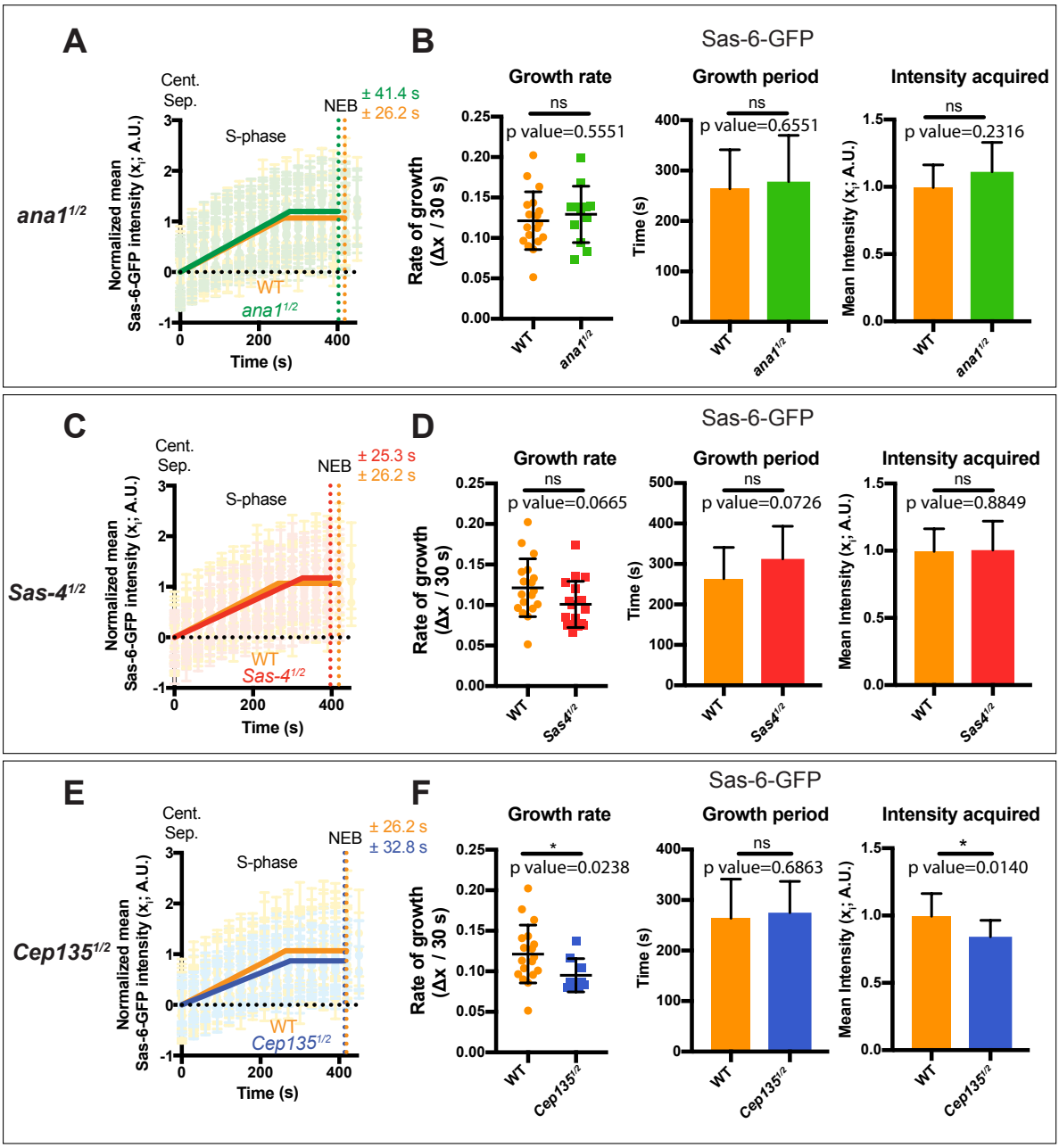

Figure 4.6: Examining the role of Ana1, Sas-4 and Cep135 in regulating the parameters of cartwheel growth. (A) Graphs compare the average Sas-6-GFP incorporation profile in WT embryos (orange) and in *ana1*$^{1/2}$ embryos (*green*) during nuclear cycle 12. **(B)** Charts quantify various parameters of centriole growth that are calculated from the Sas-6-GFP incorporation profiles in A. (**C-F)** Graphs and charts show the same analysis for *Sas-4*$^{1/2}$ (*red*) and *Cep135*$^{1/2}$ embryos (*blue*) in A and B. The data is from ≥40 centrioles per embryo. Number of embryos taken for WT =18, *ana1*$^{1/2}$=12, *Cep135*$^{1/2}$=9 *and Sas-4*$^{1/2}$=18. Data presented as mean ± SD. Statistical significance was measured using either Student's t-test (for Gaussian distributed data) or Mann-Whitney test (*P<0.05; ns, not significant).

The Sas-6-GFP incorporation parameters in *Sas-4*$^{1/2}$ embryos also did not differ significantly from WT, although here there was a trend that might be interesting: the growth rate was slightly slower, but the growth period was slightly longer, and so centrioles grew to the correct size (Figure 4.6C and D). These changes were small and were not statistically significant. Sas-4 is a *bona fide* component of the centriole cartwheel, however, so I suspect that these subtle differences might be real. It will be necessary to repeat this experiment with larger numbers of embryos to test this possibility.

Interestingly, halving the dose of *Cep135* led to a small decrease in the centriole growth rate, but it did not effect the centriole growth period; as a result, the cartwheel appeared to be slightly shorter (Figure 4.6E and F). Unfortunately, at the time of writing I have not had time to analyse centriole length in *Cep135*$^{1/2}$ wing discs by EM. It is also worth noting that I was unable to analyse as many *Cep135*$^{1/2}$ embryos in this experiment, so my numbers are quite low. I therefore view this result as preliminary, although potentially very interesting (see Section 4.3).

4.2.6: Examining the potential role of centriole distal-end binding proteins in regulating cartwheel growth

It has previously been shown that several proteins that bind to the distal end of the centriole can influence centriole length in flies. Mutations in the genes encoding CP110 and Klp10A lead to a slight elongation of the centrioles, and a dramatic elongation of the centriolar MTs, in wing-disc cells (Franz et al., 2013), and a similar phenotype has been found in *Cep97* mutant wing-disc cells (Anna Franz and Jeroen Dobbelaere, personal communication). In vertebrates, Cep104 also binds to the distal end of centrioles, and appears to influence their length (Al-Jassar et al., 2017; Jiang

et al., 2012; Rezabkova et al., 2016; Satish Tammana et al., 2013). Although the centriole cartwheel grows from the proximal end of the centriole (Aydogan et al., 2018), I wanted to test whether any of these distal-end proteins might influence the parameters of cartwheel growth.

As a first step, I wanted to confirm that GFP-fusions to all of these proteins localised to the distal end of the large centrioles in spermatocytes using 3D-SIM, and to compare their distributions. Transgenic lines expressing CP110-GFP and Cep97-GFP had already been generated and analysed by Anna Franz (Dobbelaere et al., 2008; Franz et al., 2013), and I obtained a line expressing Cep104-GFP from Metta Pratt (a former student in the lab). Together with Rachel Humphrey (an Oxford undergraduate project student I supervised), I generated transgenic lines expressing a Klp10A-GFP fusion and the expression of Klp10A-GFP in testes was confirmed via Western blotting. All of these fusion proteins are expressed from the Ubq-promoter and appear to be overexpressed by ~5-10-fold (Franz et al., 2013; Lee et al., 1988) (Metta Pratt, personal communication).

WT Spermatocytes expressing the various GFP-fusions were fixed and stained with a GFP-nanobody to label the GFP-moiety, and Asl to mark the outer region of the centriole wall (Fu and Glover, 2012) (Figure 4.7). All fusion proteins were detected at the distal-end of elongating centrioles as either a dot in young spermatocytes, or as an elongated fibre in maturing spermatocytes (Figure 4.7). Interestingly, the Klp10A fibres looked different to others, often having the appearance of “rings” or a “pair of rings” stacked together. The reason for this unusual localisation is presently unclear. The localisation of CP110-GFP to this elongated fibre has been reported previously, and this structure seems to be related to the small cilium that is formed by these centrioles, although it is unclear what these proteins are binding to within the cilium

(Franz et al., 2013). This localisation appears to be a consequence of overexpression (Franz et al., 2013), but it is nonetheless striking that CP110-GFP, Cep97-GFP and Cep104-GFP exhibit such a similar localisation to this structure, perhaps suggesting a common mode of binding to the distal end. In support of this possibility, there is compelling data from vertebrate systems that these proteins can interact with one another (Jiang et al., 2012; Kobayashi et al., 2011; Spektor et al., 2007).

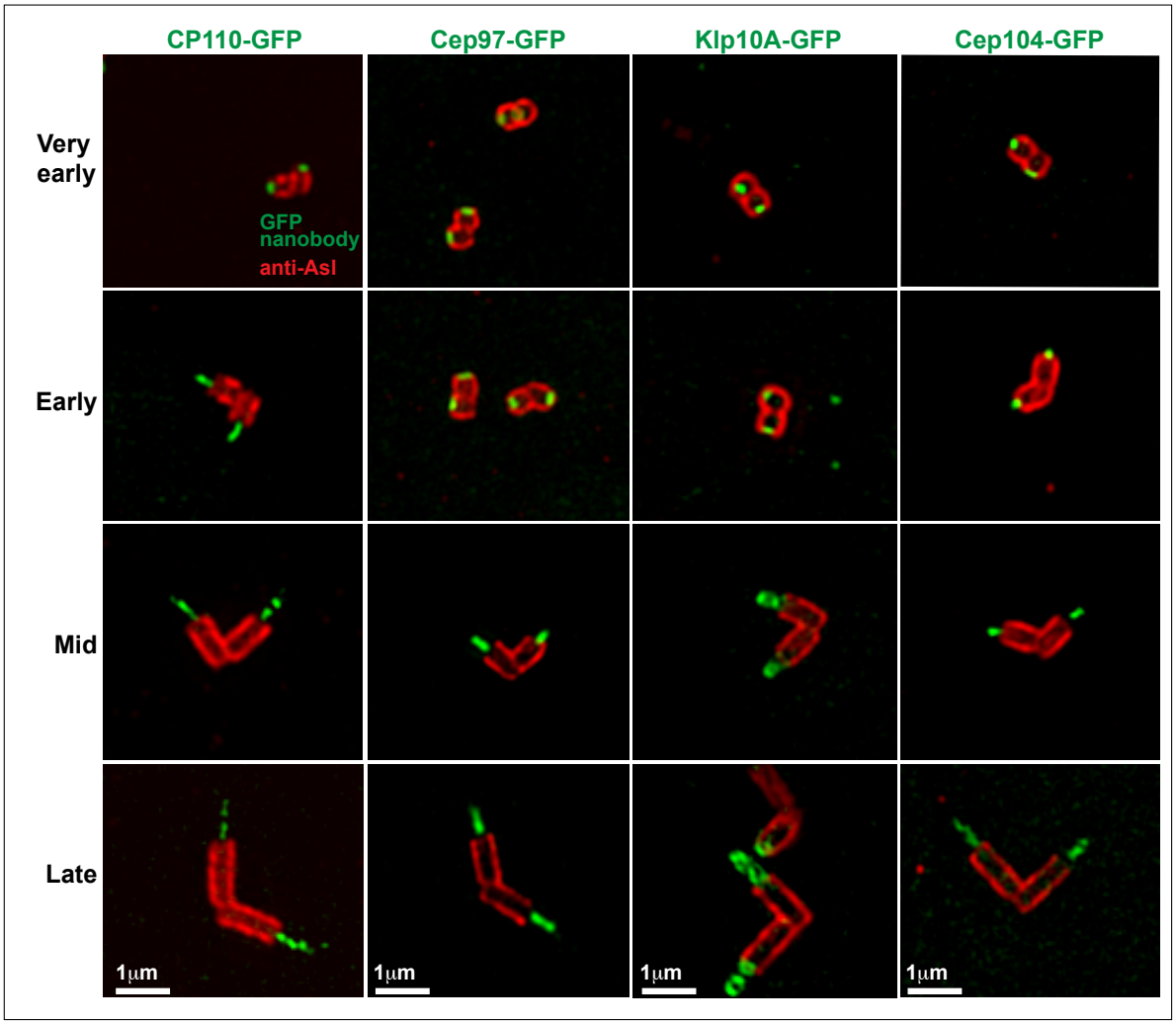

Figure 4.7: Localization of CP110, Cep97, Klp10A and Cep104 at the centriole in testes spermatocytes. Micrographs show 3D-SIM images of centrioles in primary spermatocytes at different developmental stages (as indicated) that overexpress GFP tagged distal-end centriole proteins (as indicated). Tissues were fixed and stained with an anti-GFP nanobody (*green*) and with anti-Asl antibodies (*red*) to reveal the outer centriole wall. Note that all GFP-fusions (*green*) are detected as a dot at the distal-end of the centriole pairs in young spermatocytes, but as more elongated structures at the distal end of the growing centriole pairs in maturing spermatocytes. Interestingly, Klp10A is detected as an elongated ring, or a pair of rings, rather than an elongating fibre.

4.2.7: Reducing the levels of CP110 and Klp10A changes the parameters of cartwheel growth

CP110, Cep97 and Klp10A appear to negatively regulate centriole size in part by blocking excessive growth of centriole MTs at the distal-end (Delgehyr et al., 2012; Franz et al., 2013; Schmidt et al., 2009; Spektor et al., 2007). Interestingly, however, EM analyses reveal that the electron dense centriole core is also slightly elongated in wing-disc cells lacking CP110, and is slightly shortened in such cells when CP110 is overexpressed, suggesting that CP110 influences more than just centriole MTs (Franz et al., 2013). To test whether these distal end proteins can influence cartwheel growth, I used previously described mutants of *CP110* (Franz et al., 2013) and *Klp10A* (Delgehyr et al., 2012) and a new unpublished *Cep97* null mutant (*Cep97*$^{-/-}$) generated by Jeroen Dobbelaere (IMP Vienna) using ends-out, or replacement, gene targeting (Gong and Golic, 2003).

I monitored Sas-6-GFP incorporation in early embryos in nuclear cycle 12 in which the genetic dose of *CP110* or *Cep97* or *Klp10A* was halved (hereafter, *CP110*$^{1/2}$ or *Cep97*$^{1/2}$ or *Klp10A*$^{1/2}$ embryos, respectively) (Figure 4.8). Surprisingly, the cartwheel grew slightly faster than normal in all of these half-dose embryos, although this increase was not statistically significant in *Cep97*$^{1/2}$ embryos. Nevertheless, this trend is striking and, if correct, it is remarkable—as it suggests that halving the dose of factors that normally suppress centriole MT growth at the distal end can also somehow suppress centriole cartwheel growth at the proximal end. Interestingly, the period of cartwheel growth was not altered in *CP110*$^{1/2}$ embryos, so cartwheels were too long (Figure 4.8A and B), whereas the growth period was dramatically reduced in *Klp10A*$^{1/2}$ embryos, so compensating for the increased growth rate and allowing the cartwheels to reach the correct size (Figure 4.8E and F). Moreover, the length of S-

phase was not altered in *CP110*$^{1/2}$ or *Cep97*$^{1/2}$ embryos, but was significantly shortened in *Klp10A*$^{1/2}$ embryos (Figure 4.8G). Taken together, these results indicate that cartwheel growth parameters are altered in potentially complicated ways when the genetic dosage of *CP110* or *Cep97* or *Klp10A* is halved.

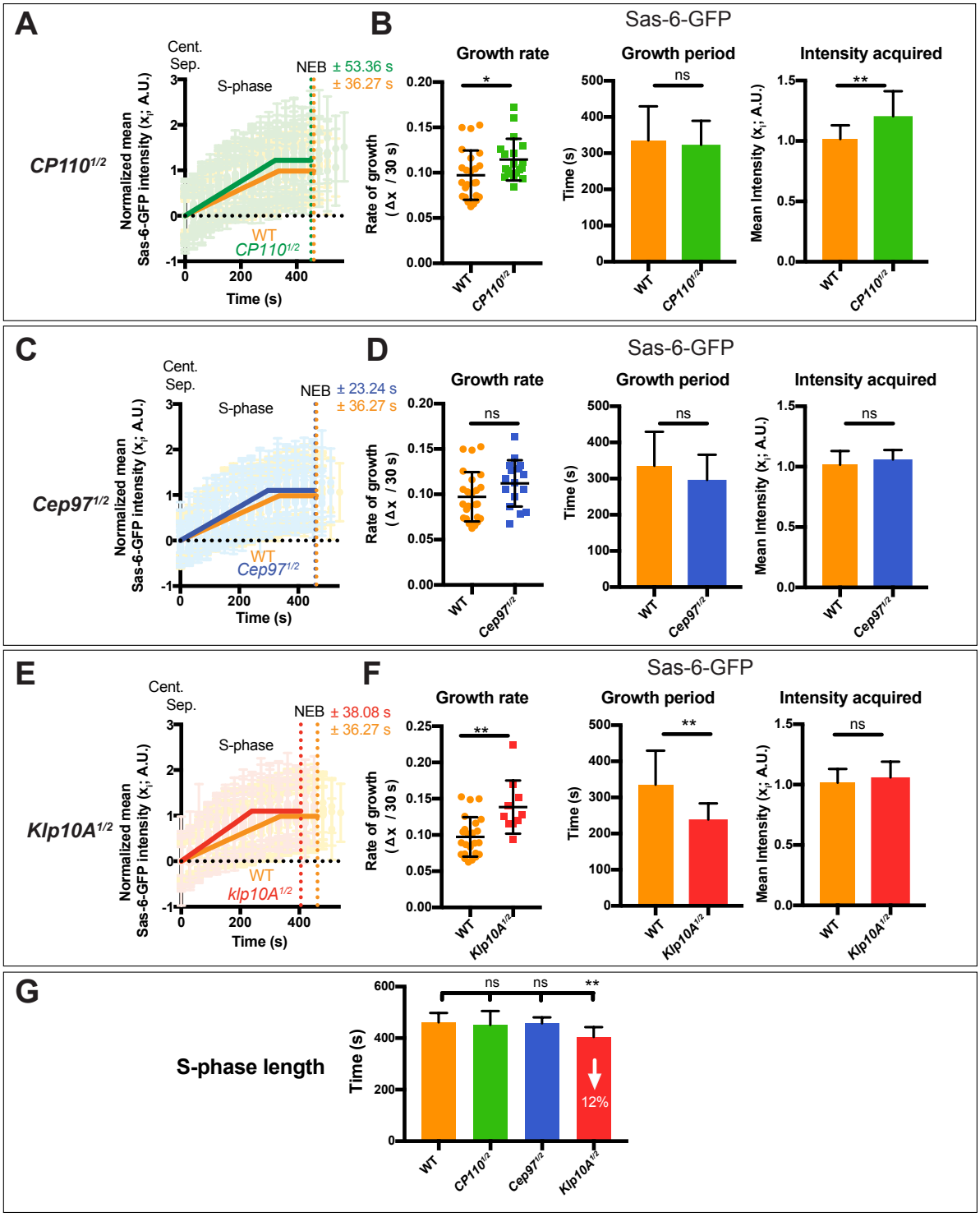

Figure 4.8: Examining the role of CP110, Cep97 and Klp10A in regulating the parameters of cartwheel growth. (A) Graphs compare the average Sas-6-GFP incorporation profile in WT embryos (*orange*) and in *CP110*$^{1/2}$ embryos (*green*) during nuclear cycle 12. **(B)** Charts quantify various parameters of centriole growth that are calculated from the Sas-6-GFP incorporation profiles in A. (**C-F)** Graphs and charts show the identical analysis for *Cep97*$^{1/2}$ (*blue*) and *Klp10A*$^{1/2}$ (*red*) embryos as in A and B. **(G)** Charts quantify the S-phase length of cartwheel growth for WT (*orange*), *CP110*$^{1/2}$ (*green*) *Cep97*$^{1/2}$ (*blue*) and *Klp10A*$^{1/2}$ (*red*) embryos that are calculated from the Sas-6-GFP incorporation profiles in (A, C and E). Data represents as mean ± SD. Statistical significance was measured using either Student's t-test (for Gaussian distributed data) or Mann-Whitney test (*P<0.05; **P<0.01; ns, not significant). From ≥40 centrioles per embryo. Number of embryos =24, 19, 16 and 10 from WT, *CP110*$^{1/2}$, *Cep97*$^{1/2}$ and *Klp10A*$^{1/2}$ respectively.

4.2.8: CP110 and Cep97 levels influence centriole cartwheel growth rate and growth period

These results are extremely surprising, but it must be noted that the effects I observed in these experiments were quite subtle. I therefore decided to collaborate with Mustafa Aydogan, the most experienced experimenter with this type of analysis, to examine the parameters of centriole growth in embryos that either completely lacked CP110 or Cep97 (as these stocks are viable and fertile as homozygous nulls—which is not the case for Klp10A), or that overexpressed CP110 or Cep97. To this end, I generated transgenic lines overexpressing untagged CP110 or Cep97 from the Ubq-promoter and crossed these into the Sas-6-GFP background (Figure 4.9A and B). I also generated similar lines overexpressing either Klp10A or Cep104, but have not had time to analyse these. Mustafa Aydogan generated fly lines expressing Sas-6-GFP in *CP110* or *Cep97* homozygous null mutant backgrounds (*CP110*$^{-/-}$ or *Cep97*$^{-/-}$) and he analysed Sas-6-GFP incorporation in all of these embryos (Figure 4.10).

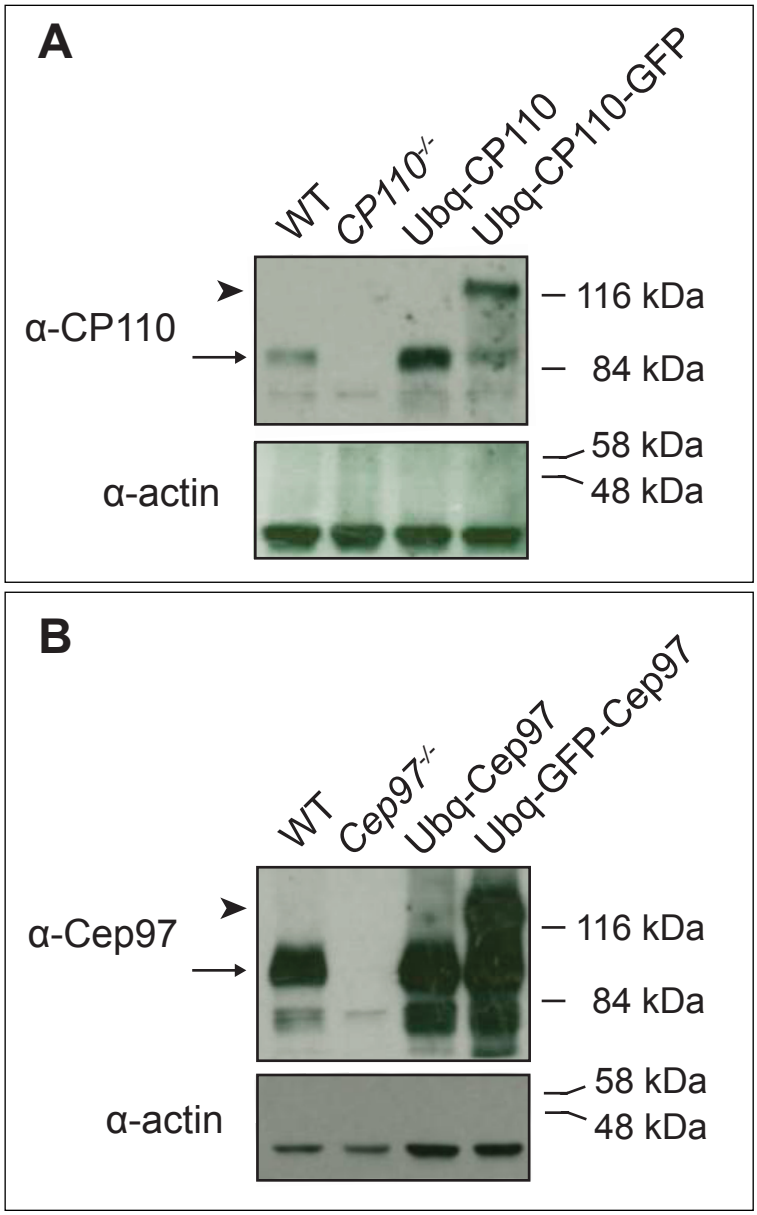

Figure 4.9: Examining CP110L-GFP or Cep97-GFP expression in fly embryos. (A) Western blots show CP110 protein levels in embryos of the following genotypes: WT, *CP110*$^{-/-}$, Ubq-CP110 and Ubq-CP110-GFP. A protein of ~93kDa corresponding to CP110 (arrow) is detected in the WT, Ubq-CP110 and Ubq-CP110-GFP embryos but not in the *CP110*$^{-/-}$ embryos. The anti-CP110 antibody also recognises the larger CP110-GFP protein (arrow head) **(B)** Western blots show Cep97 protein levels in embryos of the following genotypes: WT, *Cep97*$^{-/-}$, Ubq-Cep97 and Ubq-GFP-Cep97 and an α-actin antibody (loading control). A protein of ~97kDa corresponding to Cep97 (arrow) is detected in the WT, Ubq-Cep97 and Ubq-GFP-Cep97 embryos but not in *Cep97*$^{-/-}$ embryos. The anti-Cep97 antibody also recognises larger GFP-Cep97 protein (arrow head) and several prominent nonspecific bands. Blots were probed with anti-actin antibody, as a loading control. All Illustrations are courtesy of M. Aydogan.

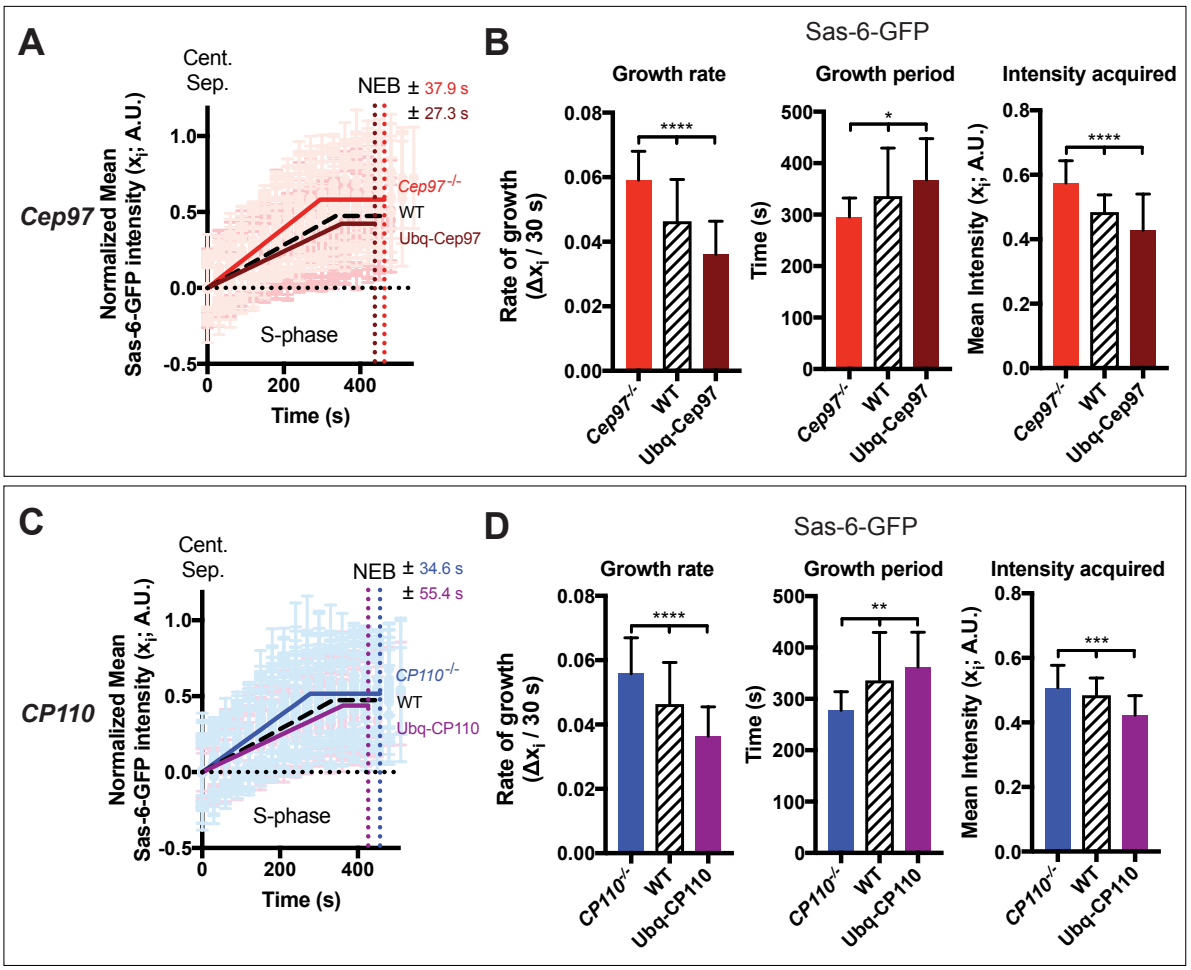

Figure 4.10: CP110 and Cep97 levels influence the centriole cartwheel growth rate and growth period. (A) Graphs compare the average Sas-6-GFP incorporation profiles in WT embryos (*black*), in *Cep97*$^{-/-}$ embryos (*red*) and in Ubq-Cep97 embryos (*brown*) during nuclear cycle 12. **(B)** Charts quantify various parameters of centriole growth calculated from the Sas-6-GFP incorporation profiles in A. (**C,D)** Graphs and charts show the same analysis for *CP110*$^{-/-}$ (*red*) and Ubq-CP110 embryos (*brown*) as shown in (A,B). Data presented as mean ± SD (N≥15 embryos for each group). Statistical significance was measured using either Student's t-test (for Gaussian distributed data) or Mann-Whitney test (*P<0.05; ***P<0.001; ****P<0.0001; ns, not significant). N≥15 embryos for each group; ≥39 centrioles from each WT, *Cep97*$^{-/-}$, Ubq-Cep97, *CP110*$^{-/-}$ and Ubq-CP110 embryo respectively. All Illustrations are courtesy of M. Aydogan.

Astonishingly, the cartwheels grew faster than normal in both *CP110*$^{-/-}$ and *Cep97*$^{-/-}$ embryos, and slower than normal in embryos overexpressing either CP110 or Cep97. In all cases, the homeostatic compensation rule of growth was obeyed: if the cartwheels grew faster, they grew for a shorter period of time, and *vice versa*. However, the adjustment in the growth period was not sufficient to compensate for the changes to the growth rate, so centrioles lacking CP110 or Cep97 appeared to be slightly longer than normal (as observed previously for centrioles in wing-discs lacking

CP110), and were slightly shorter than normal in embryos overexpressing CP110 or Cep97 (as observed previously for centrioles in wing-discs overexpressing CP110). Thus, the relatively modest changes in cartwheel length observed when CP110 or Cep97 levels are reduced or increased are very likely due to changes in the rate of cartwheel growth during the assembly of the daughter centriole. These unexpected results were obtained just as I started to write up my thesis. While I have been writing up, significant progress has been made by Laura Hankins (a new PhD student in the laboratory) and Mustafa Aydogan in understanding how CP110 and Cep97 might influence the parameters of cartwheel growth (see Discussion, Section 4.3).

4.2.9: Structure/function analysis of Klp10A

I did not have time during my thesis to follow up on my interesting observation that halving the genetic dose of *Klp10A* appears to change the centriole growth rate, growth period and S-phase length (Figure 4.8G). However, as mentioned above, I supervised an Oxford undergraduate project student, Rachel Humphrey, who performed a classical structure/function analysis of Klp10A, using an mRNA injection assay that has been used previously in the lab to perform similar analyses (Cottee et al., 2015; Feng et al., 2017; Novak et al., 2016; Richens et al., 2015; Saurya et al., 2016). Rachel carried out the majority of the fly husbandry, RNA microinjections, and microscopy work for these experiments under my supervision, although she broke her arm eight weeks before the end of her project, so I had to perform most of the mRNA injections. Rachel first performed a Basic Local Alignment Search Tool (BLAST) analysis to identify homologues of Klp10A. A PSI-blast based secondary structure PREDiction (PSIPRED) was also used to predict regions of secondary structure from the Klp10A primary sequence, and the COILs server (Lupas et al., 1991) was used to

predict coiled-coil regions. Together these data allowed predicted conserved domain boundaries to be defined (Figure 4.11A, top diagram).

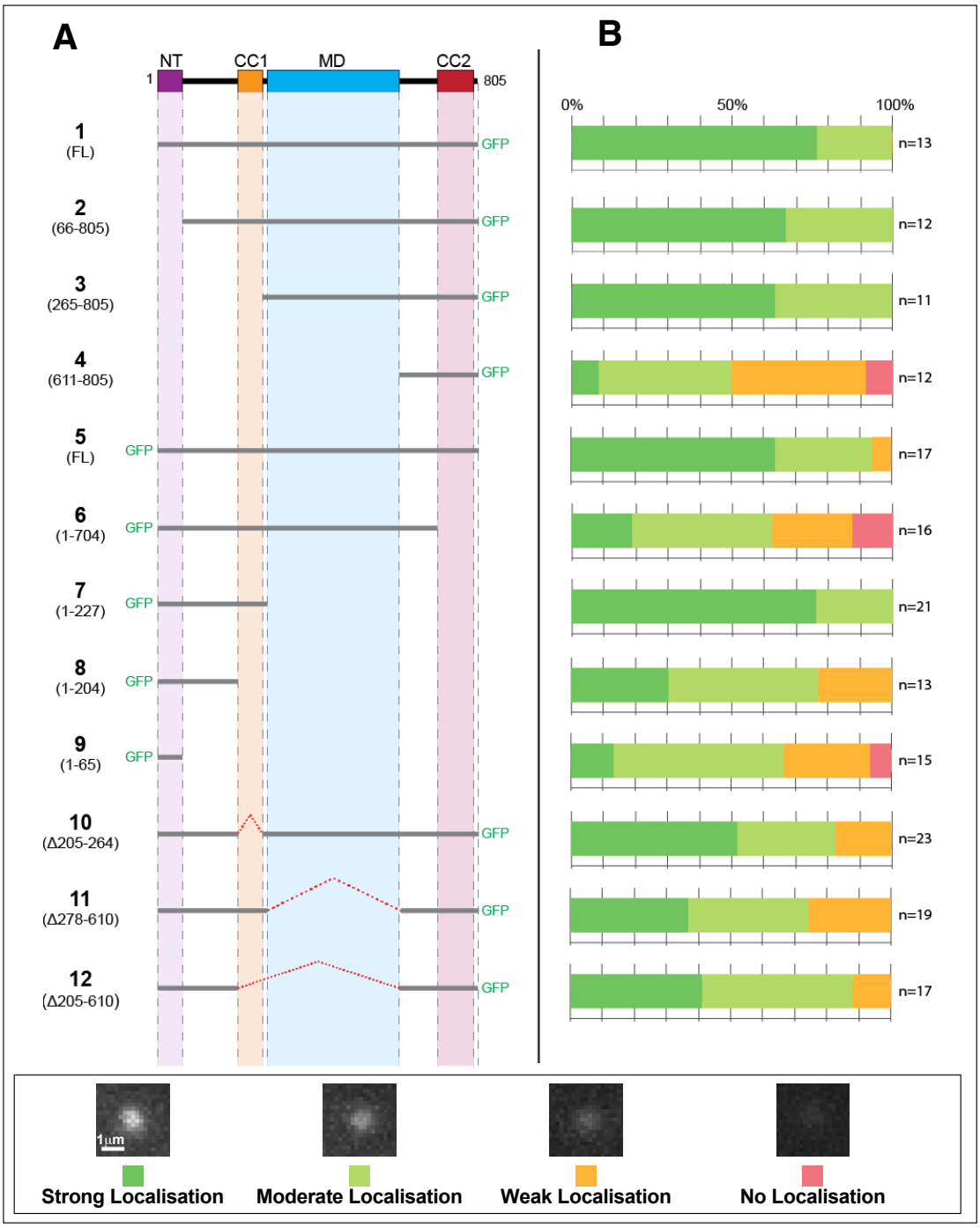

Figure 4.11: Structure/function analysis of Klp10A in living *Drosophila* embryos. (A) A schematic representation of Klp10A highlighting the conserved domains and illustrating the various constructs analysed as GFP fusions in this study: NT=conserved N-terminal domain; CC= conserved predicted coiled-coil domains; MD=conserved Motor Domain (although Klp10A does not seem to be an active motor). Embryos expressing RFP-Cnn (not shown) as a centrosomal marker were injected with mRNA encoding the GFP-fusion constructs and were imaged ~60-90mins after mRNA injection. Images were collected and manually scored on the centrosomal localisation of the GFP-fusion construct. **(B)** Bars show the percentage of embryos displaying the different localisation behaviours for each GFP-fusion constructs. The total number of embryos injected (n) per construct is indicated. Representative individual centrosomes images and the colour key are shown in the inset below. All Illustrations are courtesy of Rachel Humphrey, a part II student that I supervised in the laboratory.

RNA constructs were then designed that encoded various truncated or internally deleted forms of Klp10A fused with GFP either at the N- or C- terminus (Figure 4.11A, constructs 1-12). *In vitro* synthesized RNAs were injected into the embryos of transgenic lines expressing the centrosomal marker RFP-Cnn. The centrosomal localization of each Klp-10A construct was then analysed and quantified blindly, by randomizing all the images and assigning the centrosomal localisation qualitatively by eye as either strong, moderate, or weak (Figure 4.11B). As expected, full-length Klp10A tagged with GFP either at the N- or C-terminus localised strongly as a spot at the centre of the centrosomes (Figure 4.11) in the majority of embryos within a more diffuse PCM labelled by RFP-Cnn (Images not shown). Surprisingly, all of the deletion constructs localised to the centrosome, at least to some extent, and no discrete domain could be identified as being essential for the localisation of Klp10A to the centrosome.

It must be noted that these experiments were all carried out in the presence of endogenous wild-type (WT) Klp10A protein (as *Klp10A* mutants are non-viable), so the deleted proteins could be localised to centrosomes if they were able to multimerise with the endogenous protein. Thus, it is difficult to draw firm conclusions from this analysis. Nevertheless, I include them here as they may be useful to anyone in the lab who continues the project to investigate how Klp10A influences the parameters of centriole cartwheel growth.

4.3: Discussion

In the previous Chapter, I discovered that centriole length in wing-disc cells and spermatocytes was influenced by the levels of Ana1 protein: centrioles were shorter if Ana1 levels were reduced, and longer if Ana1 levels were increased. In thinking about this result, we realised that very little is known about how centriole length is regulated, and that centrioles are potentially an attractive model with which to study the more general problem of organelle-size control (Goehring and Hyman, 2012; Marshall, 2015; 2016).

Working as a team with several other members of the lab, we developed methods that allow us to accurately measure the rate of cartwheel growth in the early fly embryo. We used the incorporation of the centriole cartwheel protein Sas-6-GFP as a proxy for centriole size, as in fly embryos the cartwheel extends throughout the length of the centriole (Figure 1.2). By measuring the rate of increase in Sas-6-GFP fluorescence levels at multiple centrioles as they synchronously proceed through S-phase, we were able to show that centrioles grow at an approximately linear rate during early-mid S-phase, and then co-ordinately stop growing sometime prior to the entry into mitosis—presumably as they reach their final size. This approximately linear growth is informative, as it seems to rule out several models of centriole growth that have been proposed previously: (1) It suggests that centriole size is not determined by the availability of a key limiting component that is incorporated until its supply is exhausted (Goehring and Hyman, 2012); (2) It suggests size is not determined by a mechanism that somehow measures the length of the centriole and slows growth as the size increases. In both of these models, the rate of centriole growth would be expected to gradually slow as centrioles grow, which is not what we observe.

Instead, our studies suggest that centriole growth is “homeostatic”: centrioles that grow quickly tend to grow for shorter periods, while centrioles that grow slowly tend to grow for longer periods (Aydogan et al., 2018). (Note that in this paper we report several additional lines of evidence supporting this model that I have not discussed here as I was not directly involved in this work). Most importantly, and in collaboration with Mustafa Aydogan, I showed that Plk4 is intimately involved in this homeostatic mechanism. If we halve the dose of Plk4, centrioles grow slowly, but for a longer period, and so they grow to the correct size. Interestingly, if we increase the dose of Plk4 the centrioles do not grow faster, but grow for a shorter period, and so the centrioles appear to be too short; if we lower the kinase activity of Plk4 the period of centriole growth is unchanged, but the centrioles grow too slowly and so the centrioles again appear to be too short. Plk4 is a “suicide kinase” that can form a dimer that auto-phosphorylates itself in trans to promote its own degradation via the proteasome (Cunha-Ferreira et al., 2013; Guderian et al., 2010; Holland et al., 2010; Klebba et al., 2013; 2015a; Rogers et al., 2009). Thus, a plausible explanation for our findings is that Plk4 itself functions as a homeostatic clock: the higher the activity of Plk4, the faster the centrioles grow, but the faster Plk4 is degraded, so switching off the growth process (Aydogan et al., 2018).

While the Sas-6-GFP incorporation assay suggested that centrioles were too small when Plk4 was overexpressed or its kinase activity was reduced, my EM studies suggested that, at least in wing-disc cells, centriole size was not affected. I believe that the most likely explanation for this apparent discrepancy is that Sas-6-GFP incorporation assay measures the size of the centriole cartwheel, while in my EM measurements the cartwheel is rarely visible and I am instead measuring the length of the entire electron-dense centriole “core” encased by the centriole MTs. While in

flies and worms the cartwheel usually runs throughout the length of the centriole structure (so the cartwheel and the electron-dense core are approximately the same size), this is not true in many other species (Gottardo et al., 2015b; Gupta and Kitagawa, 2018; Jana et al., 2016b) —and it is also not true in fly spermatocytes, where the very long centrioles extend well beyond the central cartwheel structure (González et al., 1998; Roque et al., 2012). Perhaps Plk4 primarily regulates cartwheel growth from the proximal end, while a separate mechanism regulates the length of the centriole MTs and centriole core from the distal end (and there is some data to support this model—discussed below). Thus, in the embryos overexpressing Plk4, or expressing Plk4 with reduced kinase activity, the cartwheel may be too short (as observed in the Sas-6-GFP incorporation assay), but the centriole MTs and core may grow to the correct length (as observed in my EM images). An alternative explanation is that the very rapid cycles of the early embryo do not allow enough time for the homeostatic mechanism to properly adjust to these changes in Plk4 levels or overexpression, while there is enough time to adjust in the slower cycling wing-disc cells.

While writing this thesis, Mustafa Aydogan developed methods to follow the centriolar levels of a Plk4-NeonGreen fusion protein, revealing that these levels oscillate through the embryonic cell cycle, and that the amplitude and period of this oscillation appear to set the rate and period of centriole growth. It is currently unclear how Plk4 oscillates, and how this oscillation influences centriole growth, but oscillators are a common feature of several biological systems—such as the circadian clock (Cohen and Golden, 2015) and vertebrate segmentation clock (Pais-de-Azevedo et al., 2018)—so this is clearly a very exciting avenue for future research. In particular, it will

be interesting to see if some form of homeostatic oscillator might function to set the size of other organelles.

I used the Sas-6-GFP incorporation assay to test whether Ana1 influenced centriole size by changing the parameters of daughter centriole growth, but found that this was not the case, at least in embryos. This result is perhaps surprising, as I showed in the previous Chapter that halving the genetic dose of *ana1* leads to a decrease in centriole size in wing disc cells. There are at least two possible explanations for this apparent discrepancy: (1) Ana1 levels may influence the steady-state length of the mother centriole without influencing the growth of the daughter centriole; (2) As discussed above, in my EM analyses I measure the length of the electron-dense core of the centriole, while in the Sas-6-GFP assay I measure the length of the cartwheel: Ana1 could influence the former, without affecting the latter. I currently cannot distinguish between these possibilities, although it is interesting to note that human Cep295 (the homologue of Ana1) binds to MTs (Chang et al., 2016), consistent with the possibility that this family of proteins might regulate the growth of the centriole MTs, rather than of the central cartwheel.

In contrast to Ana1, I found that halving the dose of *Cep135* did lead to a modest reduction in the cartwheel growth rate. Like Ana1, Cep135 is also thought to interact with MTs (Carvalho-Santos et al., 2012; Kraatz et al., 2016; Lin et al., 2013b), but evidence suggests that the Cep135/Bld10 family of proteins also interact with inner cartwheel proteins (Guichard et al., 2018; Hatzopoulos et al., 2013; Lin et al., 2013b), and this is consistent with my localisation data shown in the previous Chapter (Figure 3.12). Moreover, in *Chlamydomonas*, Bld10 influences the number of spokes in the cartwheel (Hiraki et al., 2007; Hirono, 2014). Thus, it could be that Cep135 directly

stabilises the growing cartwheel, so that when its dose is reduced the cartwheel appears to grow more slowly. Alternatively, as discussed extensively in the previous Chapter, Cep135 plays an important part in recruiting Asl to centrioles, and Asl is required to recruit Plk4 to centrioles. Perhaps reducing the levels of Cep135 reduces the levels of Asl, which in turn reduces the levels of Plk4 and so slows cartwheel growth. Now that we have developed methods to measure centriolar levels of Plk4 it should be straightforward to test whether Cep135 levels (and/or Ana1 levels) influence centriolar Plk4 levels.

I also tested the ability of a group of centriole distal-end binding proteins to influence the parameters of cartwheel growth in the embryo. These proteins were known to influence centriole length, although there has been some controversy over whether they also cap centrioles to prevent cilia assembly (Kobayashi et al., 2014; Oda et al., 2014; Song et al., 2014; Spektor et al., 2007; Tsang and Dynlacht, 2013). In flies, however, the situation seems clear, as flies lacking CP110 have slightly longer centrioles, but greatly extended centriolar MTs, while overexpressing CP110 leads to a modest reduction in centriole length. No defect in cilia assembly or function was noted in these mutant flies. It was unclear, however, why CP110 levels modestly influenced centriole length, but dramatically influenced the length of the centriole MTs (Franz et al., 2013). My studies appear to answer this question as I found that in the absence of CP110 (or its binding partner Cep97) the cartwheel grows too quickly, while if either protein is overexpressed the cartwheel grows too slowly; as a result, the centriole cartwheel is either too long, or too short, respectively.

At the time we initiated these studies, this result would not have been too surprising, as we assumed that the cartwheel and centriole MTs both grew from the distal-end,

so would be likely to influence one another. It was recently shown in the lab, however, that the cartwheel grows from the proximal end (Aydogan et al., 2018), making it unclear how CP110 and Cep97, which are concentrated at the distal end of the centriole, could influence cartwheel assembly at the proximal end. While writing this thesis, this project was continued by Laura Hankins and Mustafa Aydogan, and they have found that levels of CP110 and Cep97 at the distal end of the growing daughter centriole also oscillate during the embryonic cell cycle; this oscillation is in synchrony, but out of phase, with the Plk4 oscillation at the proximal end of the growing daughter. Moreover, CP110/Cep97 levels influence the period and amplitude of the Plk4 oscillator, while the levels of Plk4 influence the period and amplitude of the CP110/Cep97 oscillator. In other words, it seems that there is cross-talk between two independent oscillators that regulate the growth of the centriole from both its proximal and distal ends. Thus, my initial observations have led to some potentially very interesting discoveries. It has recently been found that in human cells Plk4 can phosphorylate CP110 (Lee et al., 2017), suggesting at least one potential “crosstalk” mechanism.

Finally, I also showed that the MT depolymerising kinesin Klp10A influences both the cartwheel growth rate and growth period, although my numbers are relatively small so I would view this result as somewhat preliminary. I plan to repeat this analysis, and I have also generated tools that will allow me to assess the effect of overexpressing Klp10A (and also Cep104) on cartwheel growth parameters. Like CP110, the depletion of Klp10A leads to a relatively modest elongation of the centrioles, but a very dramatic elongation of the centriole MTs (Franz et al., 2013; Gottardo et al., 2016). It seems likely, therefore, that Klp10A cooperates with CP110 and Cep97 to influence centriole length from both the distal and proximal ends. It will be fascinating

to test whether, like CP110/Cep97, Klp10A influences cartwheel growth by influencing the Plk4 oscillator. Clearly there is much work to be done to understand how these two oscillators cooperate to regulate centriole size, and whether multiple oscillators may cooperate to regulate the size of other organelles. My observation that reducing the levels of Klp10A influences S-phase length is potentially very interesting, but it is probably not worthwhile discussing potential mechanisms (which would be very speculative) until this result is confirmed, and until it has been shown that overexpressing Klp10A has the opposite effect.

Chapter 5: The potential influence of cell cycle regulators on centriole cartwheel growth

5.1: Introduction

The effective cross-talk between DNA, kinetochores, centrosomes, the spindle midbody and potentially other sites are a prerequisite for faithful chromosome duplication, segregation and cytokinesis during the cell division cycle. Cyclin-dependent kinases (Cdks), together with their various Cyclin-binding partners, are key regulators of the cell cycle, and are known to phosphorylate multiple target proteins to promote the orderly progression through each phase of the cell cycle in eukaryotes (Beach et al., 1982; Evans et al., 1983; Fung and Poon, 2005; Nurse et al., 1976). In general, Cdk2 bound to Cyclin E or Cyclin A appears to be the major regulator of S-phase events (Dulić et al., 1992; Geng et al., 1996; Reed, 1997), while Cdk1 bound to Cyclins A or Cyclin B appears to be the major regulator of M-phase events (Fung and Poon, 2005; Pagano et al., 1992).

Importantly, however, studies suggest there is considerable redundancy between the different Cyclins and Cdks (Berthet et al., 2003; Bourouh et al., 2016; Caldon and Musgrove, 2010; Kalaszczynska et al., 2009; Lim and Kaldis, 2013; Ortega et al., 2003). In *Drosophila melanogaster*, for example, *CyclinB* is not essential for viability, however *CyclinB*, *CyclinB3* double mutants are embryonic lethal (Jacobs et al., 1998). CyclinB is the primary mediator of nuclear envelope breakdown (NEB) and CyclinB3 appears to promote APC/C activity and is the most significant driver of anaphase

(McCleland and O'Farrell, 2008; McCleland et al., 2009; Yuan and O'Farrell, 2015). CyclinA functions redundantly with CyclinB and CyclinB3 and is required in G2 to inhibit the activity of the APC/C and thus allow itself, CyclinB, and CyclinB3 (and other mitotic regulators) to accumulate and drive mitotic entry (Jacobs et al., 1998; Knoblich and Lehner, 1993; Reber et al., 2006).

It has long been known that centriole duplication is only initiated during S-phase. Cyclin-dependent kinase 2 (Cdk2) in partnership with Cyclin A and Cyclin E appears to be essential for this process (Arquint et al., 2018; Hinchcliffe and Sluder, 2001; Lacey et al., 1999; Matsumoto et al., 1999; Meraldi et al., 1999). The activity, levels and auto-phosphorylation of Plk4, the action of other kinases, type 2 phosphatase and the amount of PCM around the mother centrioles are all thought to limit the availability of essential centriolar components, so that centriole assembly is only initiated at a single site on the side of the mother centriole at the G1 to S transition (Dammermann et al., 2004; Guderian et al., 2010; Holland et al., 2010; Kim et al., 2013; Loncarek et al., 2008; Sillibourne et al., 2010). Active Cdk2 prevents SCF-βTrCP-mediated degradation of STIL, possibly by direct phosphorylation, and is suggested to allow the initial recruitment of STIL to the mother centriole (Arquint et al., 2018). Once at the centriole, STIL can bind and activate Plk4, which then phosphorylates STIL, allowing it to recruit Sas-6 and so initiate cartwheel assembly (Arquint et al., 2015; Dzhindzhev et al., 2014; Kratz et al., 2015; McLamarrah et al., 2018; Moyer et al., 2015; Ohta et al., 2014).

The core Cdk/Cyclin machinery is subject to multiple levels of regulation (Lim and Kaldis, 2013; Morgan, 1995). Wee1 kinase and Myt1 kinase, for example, inhibit Cdk1 activity by phosphorylating conserved Thr and Tyr residues (T14 and Y15 in human

Cdk1) and are part of conserved checkpoint mechanisms that function during interphase to ensure that DNA replication and repair is concluded before the cell initiates mitosis (Atherton-Fessler et al., 1993; Jin et al., 2005; 2008; Pavletich, 1999). Myt1 moves between the cytoplasm in S-phase, and the Golgi apparatus and endoplasmic reticulum in Mitosis (Jin et al., 2008); overexpression of Myt1 delays G2/M, as excessive Myt1 inhibits Cdk1 activity in the cytoplasm and extends S and G2 phase (Jin et al., 2008; Liu et al., 1999; Price et al., 2002). The inhibitory phosphorylation of Cdk1 by Wee1/Myt1 kinases is countered by the Cdc25 phosphatase, of which there are two in *Drosophila*, String and Twine. In M-phase Cdc25 dephosphorylates T14 and to activate Cdk1 probably in the nucleus (Coulonval et al., 2011; Timofeev et al., 2010). Active Cdk1 in complex with CyclinB or CyclinA can phosphorylate and inactivate Wee1 in the nucleus, thus creating a “switch-like” activation of Cdk1 (Honda et al., 1995). Cdk1-CyclinB complex is transported to the cytoplasm, where Cdk1 binds and phosphorylates many proteins to promote the entry into mitosis. Interestingly, Cdk1 can bind to and phosphorylate STIL to prevent its association with Plk4, and this is thought to help ensure that centriole duplication does not occur during mitosis (Zitouni et al., 2016). During mitosis, STIL is released from the centriole into the cytoplasm, where it is degraded by APC/C (Arquint and Nigg, 2014). After mitotic exit, Cdk1 activity is low, STIL is free to bind and activate Plk4 at the centriole. Plk4 phosphorylates STIL, allowing it to recruit Sas6 and so initiate centriole duplication (Dzhindzhev et al., 2014).

As described in the previous Chapter, we have developed methods to measure the kinetics of centriole assembly during the syncytial blastoderm divisions in the early *Drosophila* embryo. We discovered that centrioles grow at an approximately linear rate through early-mid S-phase, but then abruptly stop growing, presumably when

they reach their correct size. These studies focused on nuclear cycle 12, but S-phase gets progressively longer during nuclear cycles 11-14 (Foe and Alberts, 1983). We wondered whether the parameters of centriole growth would change in response to the lengthening of S-phase, and, if so, how these changes might be regulated to ensure that centriole duplication is always properly coordinated with the rapid nuclear cycles in these embryos.

In this chapter, I describe a collaboration with Mustafa Aydogan that revealed how the centriole growth rate slows, but the growth period increases, as S-phase lengthens. Surprisingly, however, genetically manipulating S-phase length did not affect the parameters of centriole growth significantly. I then investigate whether halving the genetic dose of several cell cycle regulators influences the parameters of centriole growth. I find that halving the genetic dose of either *Myt1*, *Wee1* or *string* modulates centriole growth parameters, but in different ways, but halving the genetic dose of either *Cdk1*, *CyclinA*, *CyclinB3*, *CyclinD1*, *CyclinE* or *dacapo* does not. I also show that GFP-fusions to Myt1, Wee1, String or Twine are not detectable at centrioles in the early *Drosophila* embryo. Part of the work presented in this chapter was recently published (Aydogan et al., 2018).

5.2: Results

5.2.1: Centriole growth parameters appear to be influenced by the basic cell cycle oscillator in early *Drosophila* embryos

As shown in the previous Chapter, Plk4 helps to set centriole size by ensuring an inverse relationship between the centriole growth rate and growth period in syncytial *Drosophila* embryos (Aydogan et al., 2018). In these embryos, the nuclear cycles gradually slows down during nuclear cycles 11-14, and this is primarily due to an increase in the length of S-phase (Foe and Alberts, 1983). It is still unclear exactly how this gradual slowing of S-phase is regulated, but there is strong evidence that as the nuclear/cytoplasmic ratio increases, the competition for limiting DNA replication components leads to a delay in DNA replication, activating Chk1 kinase (Grapes in flies), which then helps to delay the entry into mitosis (Sibon et al., 1997). We wondered how the kinetics of centriole growth would change in response to the gradual lengthening of S-phase at successive nuclear cycles. As described in the previous Chapter, some of the initial experiments described below were performed by me, but for reasons of consistency, the final dataset was generated and analysed by Mustafa Aydogan.

We tracked the incorporation of Sas-6-GFP foci during nuclear cycles 11-13 (Figure 5.1A) and found that, as S-phase length increased (Figure 5.1Bi), so centriole growth rate slowed (Figure 5.1Bii) but the growth period increased (Figure 5.1Biii), and so the daughter centrioles ultimately grew to the same length (Figure 5.1Biv, (Aydogan et al., 2018). These findings confirm the “homeostatic” relationship between the

growth rate and period discussed in the previous Chapter, and also indicate that centriole growth parameters appear to be influenced by the basic cell cycle oscillator of the early embryo. Perhaps surprisingly, however, we found that shortening S-phase—by halving the genetic dose of *grapes* (Sibon et al., 1997)—or lengthening S-phase—by halving the genetic dose of *Cyclin B* (Ji et al., 2004)—did not significantly alter the parameters of centriole growth (Aydogan et al., 2018) (Figure 5.2). Thus, it is unclear how the basic embryonic cell cycle oscillator might influence the parameters of centriole cartwheel growth: it does not seem that the length of S-phase directly sets the rate or period of centriole growth, although these are clearly correlated.

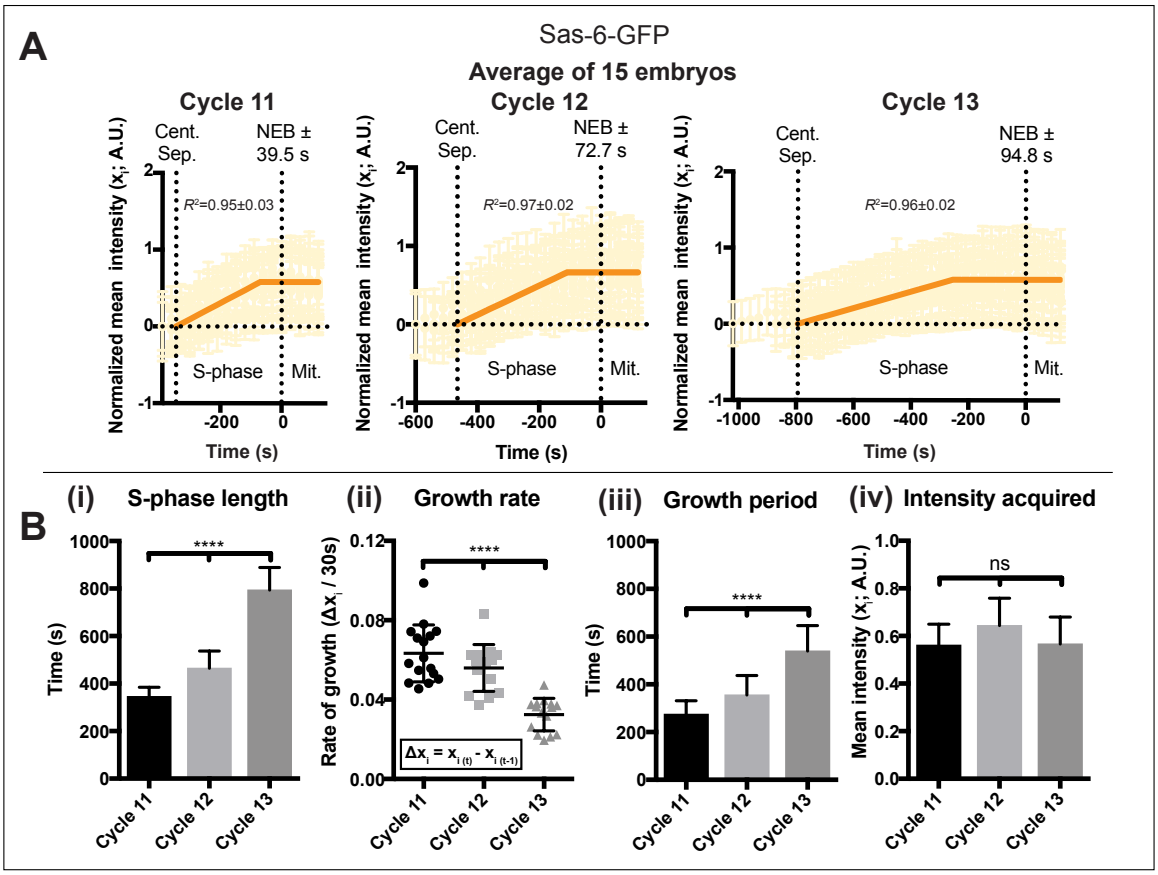

Figure 5.1: Centriole growth parameters appear to be influenced by the basic cell cycle oscillator in early *Drosophila* embryos. (A) Graphs show an "average" Sas-6-GFP incorporation profile (orange line, N≥15 embryos) at nuclear cycles 11, 12 or 13. The data from each embryo are shown in partial opacity. The "±" associated with NEB represents the SD from the mean value. **(B)** Bar charts measure several parameters of centriole growth derived from the average Sas-6-GFP incorporation profiles shown in A. Statistical significance was assessed using either an ordinary one-way ANOVA test (for Gaussian-distributed data) or a Kruskal-Wallis test; (****p<0.0001; ns=not significant). N≥15 embryos for each cell cycle; n=96; 174; 326 centrioles on average per embryo in each cycle respectively. All Illustrations are courtesy of M. Aydogan.

5.2.2: Assessing the role of the basic cell cycle machinery in regulating the parameters of cartwheel growth

One way that the cell cycle oscillator could regulate centriole growth is that Cdk1 has been shown to bind directly to STIL/Ana2 in human cells, and this binding seems to block the ability of STIL/Ana2 to interact with Plk4 (Zitouni et al., 2016). This interaction is thought to help prevent centriole duplication during M-phase, but it indicates that Cdk1/Cyclins can directly interact with at least one key player in the centriole assembly pathway. Moreover, it has recently been shown in our lab that Ana2 is phosphorylated on two conserved Cdk1 sites and this seems to inhibit (but does not block) the incorporation of Ana2 into the growing daughter centrioles (Lisa Gartenmann, personal communication).

Although halving the dose of *Cyclin B* does not appear to affect the parameters of centriole assembly (Figure 5.2), I decided to test whether halving the genetic dose of *Cdk1* or any one of several other Cyclin genes could influence these parameters. I also included the gene encoding the Cdk inhibitor *dacapo* in this analysis, as it was present in our stock collection. I monitored Sas-6-GFP incorporation in nuclear cycle 12 of early embryos in which the genetic dose of either *Cdk1*, *CyclinA*, *CyclinB3*, *CyclinD1*, *CyclinE* or *dacapo* was halved (hereafter, $Cdk1^{1/2}$ or $CyclinA^{1/2}$ or $CyclinB3^{1/2}$ or $CyclinD1^{1/2}$ or $CyclinE^{1/2}$ or $dacapo^{1/2}$ embryos) (Figure 5.3A-D). Halving the genetic dose of *CyclinB3* or *CyclinE* led to a significant decrease and halving the genetic dose of *Cdk1* led to a significant increase in S-phase length and, but none of these genetic manipulations led to a significant change in the parameters of centriole growth.

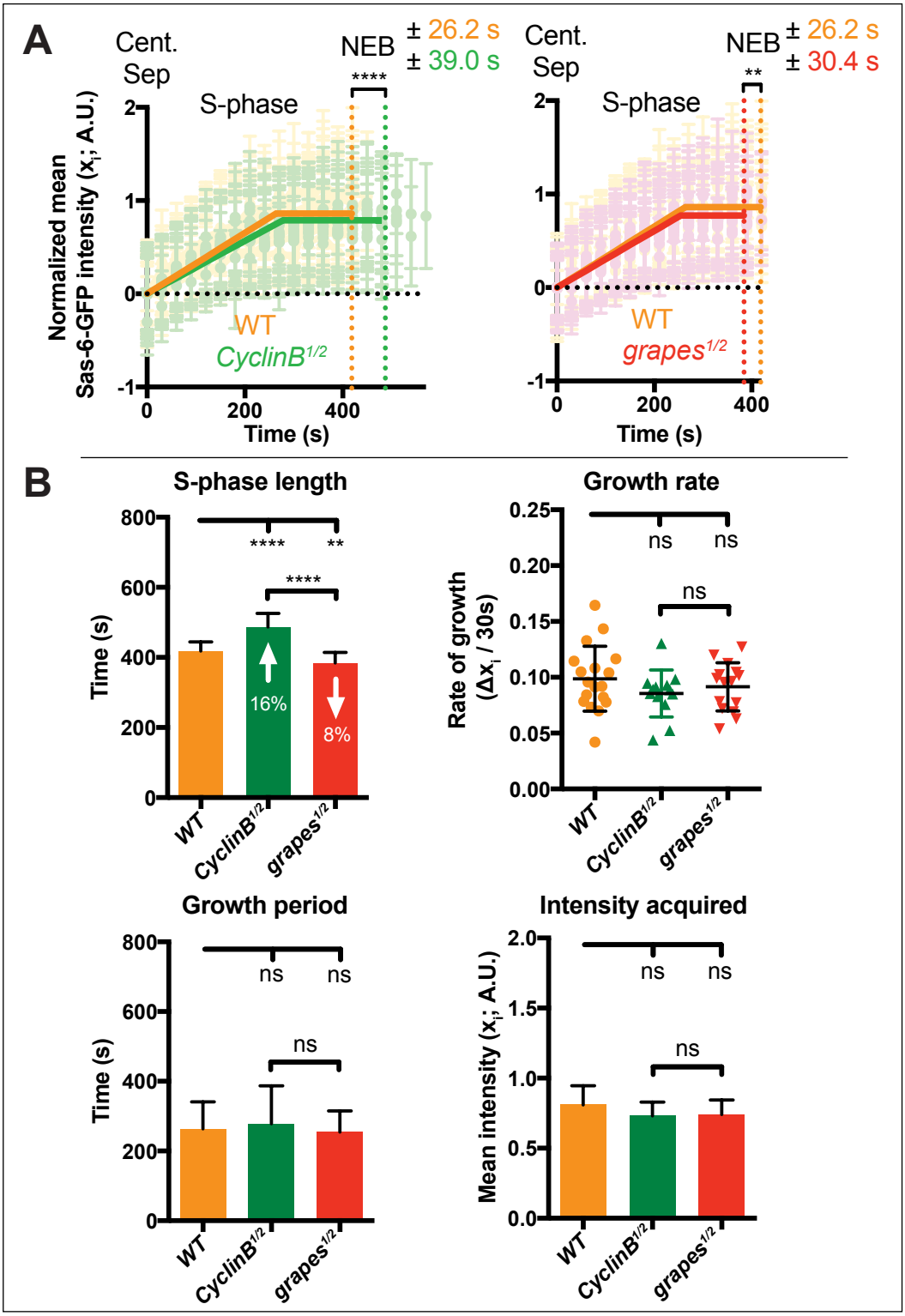

Figure 5.2: CyclinB and Grapes (Chk1 or Rad27) influence the S-phase length but not the centriole growth. (A and B) Graphs and charts illustrate and quantify centriole growth parameters in WT embryos, and embryos in which either the genetic dose of *Cyclin B* has been halved *(CyclinB$^{1/2}$* embryos) that increases the length of S-phase (Ji et al., 2004) or the genetic dose of the S-phase checkpoint protein *grapes* (Chk1 in vertebrates) has been halved (*grapes$^{1/2}$* embryos) and that decrease the length of S-phase (Sibon et al., 1997); Although S-phase is ~24% longer in *CyclinB$^{1/2}$* embryos compared to *grapes$^{1/2}$* embryos, the parameters of centriole growth are mostly the same in all three types of embryos. Statistical significance was calculated using either Student's t-test (for Gaussian distributed data) or Mann-Whitney test (**P<0.01; ****P<0.0001; ns, not significant). N≥13 embryos for each group; 184; 140; 122 centrioles on average from WT, *CyclinB$^{1/2}$*, and *grapes$^{1/2}$* embryos, respectively. All Illustrations are courtesy of M. Aydogan.

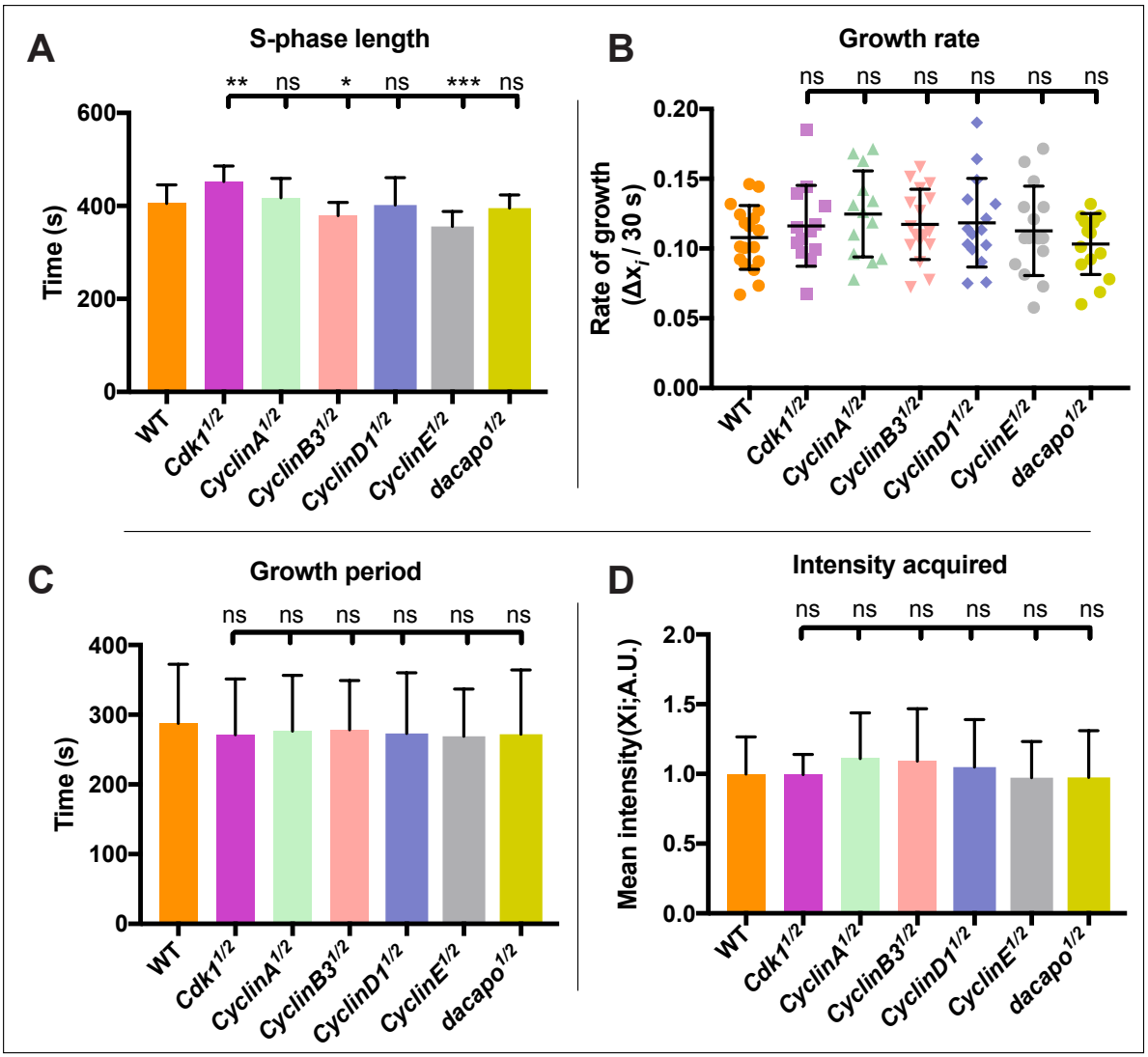

Figure 5.3: Assessing the role of the basic cell cycle machinery in regulating the parameters of cartwheel growth (A-D). Charts quantify various parameters of centriole growth that is resulted from the Sas-6-GFP incorporation profiles in WT embryos (*orange*), *Ckd1*$^{1/2}$(*purple*), *CyclinA*$^{1/2}$(*blue green*), *CyclinB*$^{1/2}$(*peach*), *CyclinD*$^{1/2}$(*violet*), *CyclinE*$^{1/2}$ (*grey*), and *dacapo*$^{1/2}$ (*light green*) embryos during nuclear cycle 12. Data represents as mean ± SD (N≥15 embryos for each group). Statistical significance was measured using Student's t-test (*P<0.05; ***P<0.001; ns, not significant). N≥15 embryos for each group; n>49 centrioles on average from each set of WT, *Cdk1*$^{1/2}$, *CyclinA*$^{1/2}$, *CyclinB*$^{1/2}$, *CyclinD*$^{1/2}$, *CyclinE*$^{1/2}$, and *dacapo*$^{1/2}$ embryos respectively.

Although these results did not look promising, I decided to test whether any of the key proteins that are thought to directly regulate Cdk/Cyclin activity in embryos might also influence centriole growth. As described in Section 5.1, Cdk/Cyclin activity is suppressed by Wee1- and/or Myt1-dependent phosphorylation, and activated by String- and/or Twine-dependent dephosphorylation. I monitored Sas-6-GFP incorporation in nuclear cycle 12 of early embryos in which genetic dose of *Wee1* or *Myt1* or *string* was halved (hereafter, *Wee1*$^{1/2}$ or *Myt1*$^{1/2}$ or *string*$^{1/2}$ embryos, Figure 5.4A-D). Unfortunately, at the time I was not able to obtain a *twine* mutant allele to test. As expected, S-phase was significantly shorter in *Wee1*$^{1/2}$ embryos (presumably because mitotic Cdk/Cyclin activity is now activated prematurely in these embryos), but, unexpectedly, S-phase was also significantly shorter in *string*$^{1/2}$ embryos. Most strikingly, however, S-phase length was not affected in *Myt1*$^{1/2}$ embryos, but the centriole cartwheel grew at a slower rate, but for a normal period of time, and so cartwheels appeared to be too short. Thus, it seems that Myt1 normally enhances the rate of cartwheel growth, but does not influence the growth period.

Puzzlingly, in *string*$^{1/2}$ embryos the cartwheel growth rate and growth period were both slightly, but not statistically significantly, reduced, yet cartwheel size (measured by Sas-6-GFP intensity acquired) was significantly smaller than in controls. My only explanation for this is that the effects of the *slightly* slower growth rate and *slightly* shorter growth period (neither of which on their own are statistically significant) are additive, and so produce a significant decrease in the amount of Sas-6-GFP incorporated into the growing daughter centriole. If this interpretation is correct, it potentially highlights the potential power of this assay, as even very modest differences in the measured parameters of centriole growth appear to have real biological consequences.

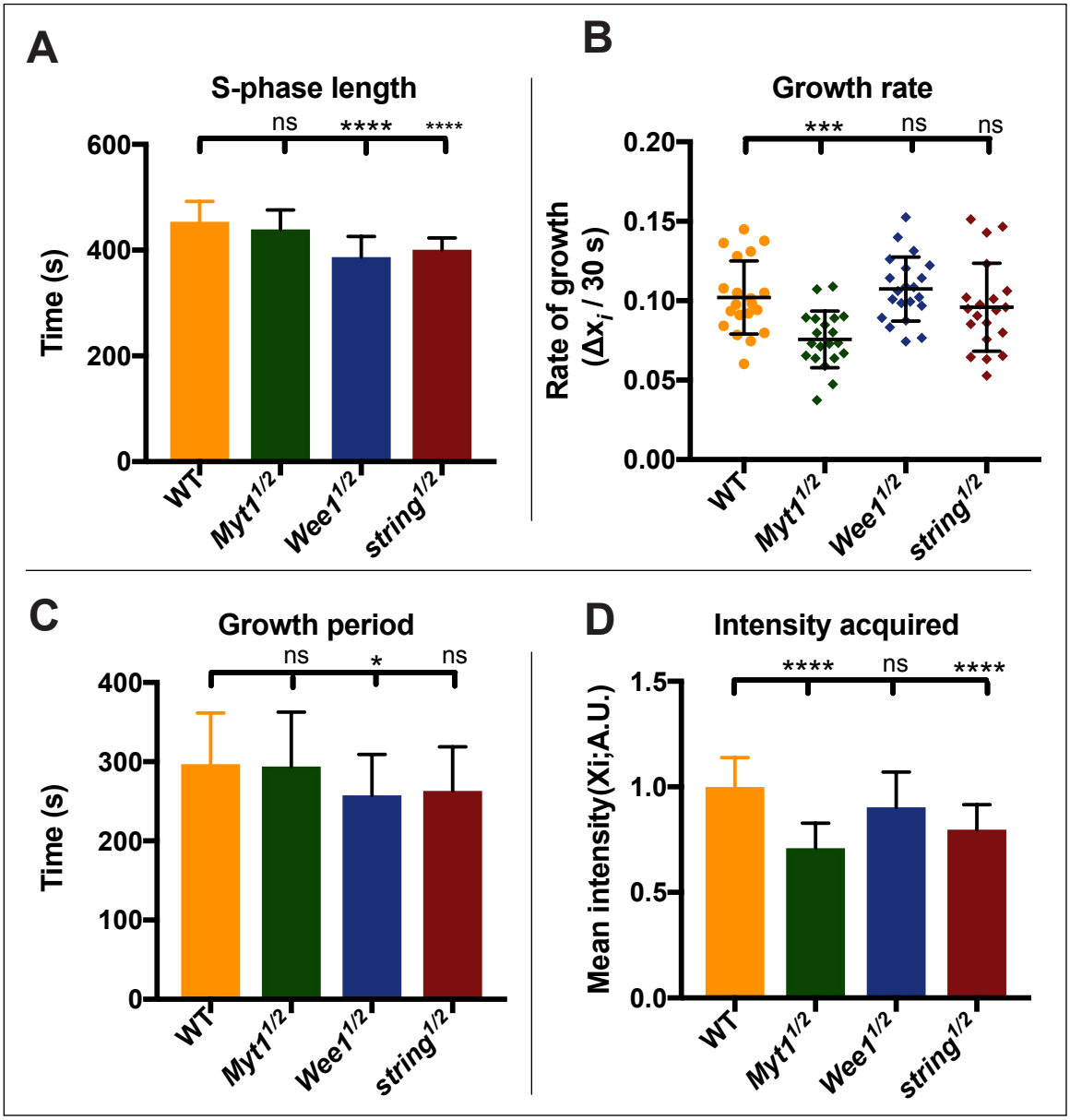

Figure 5.4: Myt1 effects the size and growth rate, String(cdc25) effects the size and S-phase length, while Wee1 effects the growth period and S-phase length of the centriole growth. (A-D) Charts quantify various parameters of centriole growth that has resulted from the average Sas-6-GFP incorporation profile in WT embryos (orange) and *Myt1$^{1/2}$(dark green), Wee1$^{1/2}$(dark blue) and String$^{1/2}$(dark red)* embryos during nuclear cycle 12. Data represents as mean ± SD (N≥15 embryos for each group). Statistical significance was measured using Student's t-test (*P<0.05; ***P<0.001; ****P<0.0001; ns, not significant). N≥15 embryos for each group; n> 39 centrioles on average from each WT, *Myt1$^{1/2}$, Wee1$^{1/2}$, String$^{1/2}$*and *CyclinE$^{1/2}$* embryos respectively.

Taken together, my findings suggest that halving the genetic dose of *Myt1*, and perhaps *Wee1* and/or *string*, alters the parameters of centriole cartwheel growth (Figure 5.4). Some of these effects are relatively subtle, however, so I wanted to test whether increasing the levels of any of these cell cycle regulators would have the opposite effect on cartwheel assembly. To this end I generated transgenic lines expressing either untagged *Myt1*, *Wee1*, *twine*, *string* or *Cdk1* under the control of the ubiquitin promoter. Interestingly, the Ubq-Myt1, Ubq-Twine and Ubq-String lines were all dominant male sterile (data not show). This makes these lines hard to work with and maintain, and I unfortunately did not have time prior to writing this thesis, to test how they might influence Sas-6-GFP incorporation.

Reducing the genetic dosage of *Myt1* or *Wee1* alters the parameters of centriole growth (Figure 5.4). Both proteins phosphorylate Cdk1 to inhibit its activity, so I wanted to test whether their effect on centriole growth kinetics depended on their ability to regulate Cdk1 activity, or whether these proteins might directly phosphorylate centriole assembly proteins. It has previously been shown that a form of Cdk1 in which Thr14 has been mutated to Ala, and Tyr15 has been mutated to Phe (Cdk1AF) cannot be phosphorylated by Myt1 or Wee1 (Coulonval et al., 2011; Jin et al., 2005; Timofeev et al., 2010). I attempted to generate fly lines expressing Cdk1AF from the Ubq promoter, but such lines could not be generated. I therefore injected mRNA encoding Cdk1AF into early embryos expressing Sas-6-GFP, and attempted to monitor Sas-6-GFP incorporation 1-1.5hrs later (Figure 5.5A). Only 5/50 injected embryos survived to syncytial stages; qualitatively, this is significantly less embryo survival than I usually get in this type of experiment (usually >70% of injected embryos survive long enough to be imaged), indicating that the expression of Cdk1AF is very likely toxic to the embryo.

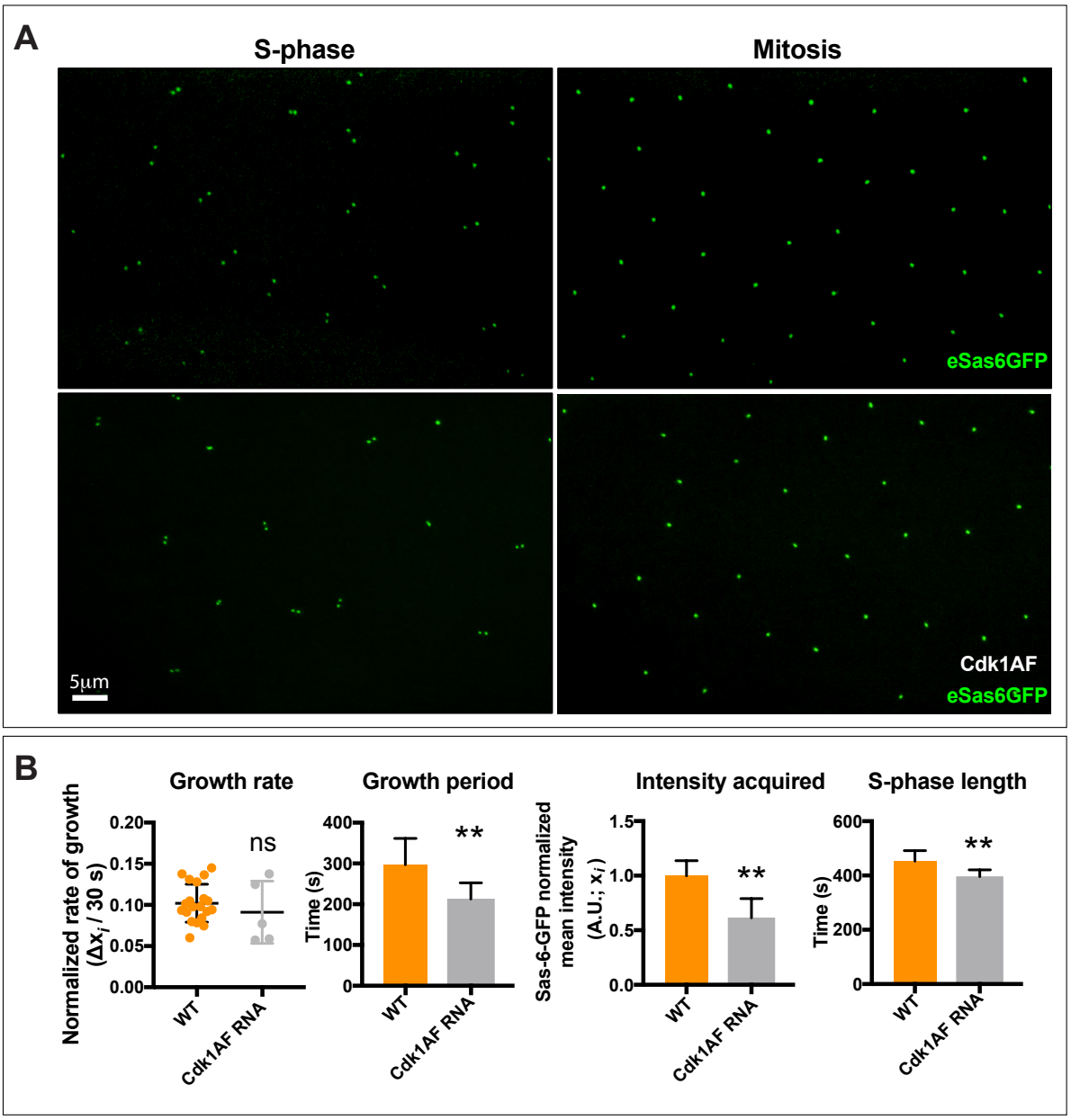

Figure 5.5: Constitutively active Cdk1AF could influence the parameters of centriole growth. **(A)** Micrographs show representative images of live *Drosophila* embryos showing the localisation of the eSas6-GFP (*green*) in embryos injected (bottom panel) or non-injected (top panels) with *in vitro* transcribed untagged Cdk1AF RNA in *S*-phase (left panels) or mitosis (right panels). **(B)** Charts quantify various parameters of centriole growth that resulted from the Sas-6-GFP incorporation profiles in A. Data represents as mean ± SD. Statistical significance was measured using Student's t-test (*P<0.05; ***P<0.001; ****P<0.0001; ns, not significant). N=5-15 embryos for each group; n=92; centrioles on average from each WT and Cdk1AF embryo respectively.

Nevertheless, I was able to measure the kinetics of Sas-6-GFP incorporation in these 5 embryos (Figure 5.5B). As expected, S-phase was shorter in these embryos, presumably because Cdk1 is prematurely activated to push the embryos into mitosis. Strikingly, although the centriole growth rate did not appear to be affected, the growth period was significantly reduced and, as a result, centriole cartwheels were too short. This result should be treated with great caution: the number of embryos analysed is low and, more importantly, I did not perform the proper control of injecting mRNA encoding WT Cdk1.

5.2.3: Myt1, Wee1, Twine and String are not detectably concentrated at the centrioles in early *Drosophila* embryos

To better understand how these cell cycle regulators might influence centriole cartwheel growth I wanted to test if any of them were concentrated at centrioles in early embryos. To test this in an efficient and consistent manner I used an mRNA injection approach (Cottee et al., 2015; Richens et al., 2015). I obtained cDNAs of these cell cycle regulators from DGRC and cloned them into a pRNA vector fused with GFP at their C- terminus, using the Gateway cloning system. I then individually injected the *in vitro* synthesized mRNAs into early syncytial embryos expressing the centrosomal marker Asl-mcherry. The localization of the GFP-fusion and Asl-mCherry were then analysed in living syncytial embryos (Figure 5.6).

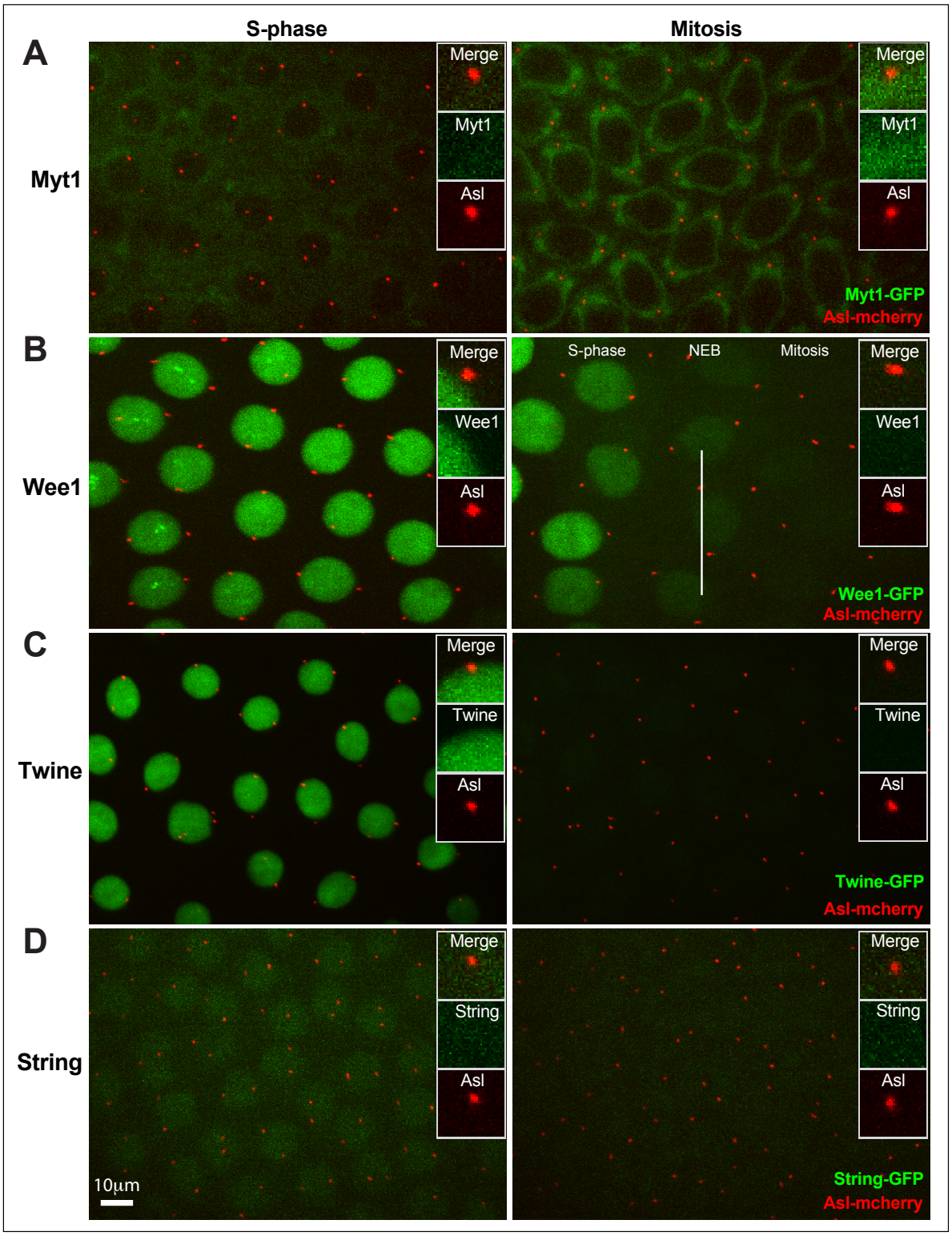

Figure 5.6: Myt1, Wee1, Twine and String are not detectably concentrated at the centrioles in early *Drosophila* embryos. Micrographs show representative images of live *Drosophila* embryos showing the localisation of the Myt1-GFP **(A)**, Wee1-GFP **(B)**, Twine-GFP **(C)** and **(D)** String-GFP fusion protein (*green*) and Asl-mCherry (red) in embryos injected with *in vitro* transcribe RNA in *S*-phase (left panel) and mitosis (right panel). Note that the preferential localization of Myt1 in the cytoplasm, Wee1 and Twine in the nucleus and no String in the nucleus in early S-phase. In mitosis, Myt1 is in the Golgi and ER, Wee1 nowhere, Twine and String are in the nucleus.

Myt1, the protein that seemed to have the most significant effect on the cartwheel growth rate, was primarily localised in the cytoplasm during S-phase, but it then seemed to concentrate in a region around the centrosomes and nuclear envelope (that is only partially broken-down during mitosis in these embryos (De Magistris and Antonin, 2018; Fernández-Álvarez et al., 2016; Liu et al., 1997) that is very likely the Golgi and/or ER (Figure 5.6A), as has been reported previously in *Drosophila*, *Xenopus* and other metazoans (Booher et al., 1997; Jin et al., 2005; Liu et al., 1997; Mueller et al., 1995; Villeneuve et al., 2013). No obvious co-localisation with centriolar Asl-mCherry was apparent, although this localization could have been somewhat obscured by the localization at the Golgi/ER. Wee1 and Twine both rapidly accumulated in the interphase nucleus at the start of S-phase, where they remained strongly concentrated until being rapidly released into the cytoplasm as the embryos entered mitosis (Figure 5.6B and C), as reported previously for Wee1 (Price et al., 2000; 2002). String was more slowly incorporated into the interphase nucleus during S-phase, and it was only ever moderately concentrated there before being released back into the cytoplasm during mitosis (Figure 5.6D). As with Myt1, none of these proteins were detectably concentrated at centrioles/centrosomes. Thus, although some of these proteins appear to influence the dynamics of centriole cartwheel growth, none of them are detectably enriched at centrioles in the early *Drosophila* embryo.

5.3: Discussion

Several cell cycle regulators are known to influence the centriole duplication cycle (Hinchcliffe and Sluder, 2001; Lacey et al., 1999; Matsumoto et al., 1999; Meraldi et al., 1999). How such protein regulates centriole growth, however, has remained unclear. Using live-imaging of the early *Drosophila* embryo, and in collaboration with Mustafa Aydogan, I showed that as S-phase length increases at successive nuclear cycles, so the centriole growth rate slowed and the growth period increased—so daughter centrioles eventually grew to the same size. However, genetically manipulating S-phase length did not significantly influence centriole growth parameters.

I found that halving the genetic dose of *Myt1*, *Wee1* and *string* altered these parameters (although in different ways), while halving the genetic dose of *Cdk1*, *CyclinA*, *CyclinB3*, *CyclinD1*, *CyclinE* and *dacapo* did not. It is important to stress that a negative result in this experiment does not prove that these proteins are incapable of influencing centriole growth: it could be, for example, that some of these proteins are in excess, and so halving their genetic dosage has little effect. Moreover, even in the cases where I found an effect, I view these data as preliminary: the effects were sometimes small, and I have only performed each analysis on one set of embryos (and sometimes only a relatively small number of embryos). Taken together, however, I believe these data strongly suggest that, perhaps not surprisingly, the machinery that establishes and regulates the basic cell cycle oscillator in these embryos also regulates the centriole assembly machinery, potentially explaining why centrioles grow slowly, but for a longer period, as S-phase lengthens during successive nuclear cycles.

Clearly, the key question is to understand how the embryonic cell cycle oscillator regulates centriole growth. As my data is preliminary, and sometimes contradictory (Wee1 and Myt1, for example, both phosphorylate Cdk1 to inhibit its activity, but halving their genetic dosage has very different effects on centriole growth kinetics), I have not attempted to construct a “model” of how this regulation might occur. These experiments are needed to be repeated, and I need to test whether increasing the levels of these proteins has the opposite effect to halving their genetic dosage (and I have generated lines to do this experiment). As reported in the previous chapter, this type of analysis was crucial for demonstrating that the relatively subtle effects of increasing and decreasing the levels of CP110 and Cep97 on centriole growth were likely to be biologically meaningful.

If my preliminary findings are confirmed, it will be important to distinguish whether cell cycle regulators like Wee1 and Myt1 influence centriole growth through their ability to regulate Cdk1 activity, or whether they might directly regulate key centriole assembly factors like Plk4 or Ana2. It seems worth testing whether Wee1 and/or Myt1 can phosphorylate Plk4, Ana2 or Sas-6 *in vitro*. There is strong evidence, however, that Cdk activity is indeed a crucial regulator of centriole biogenesis: it is well known that centriole duplication only occurs in S-phase, and Cdk2/Cyclin E activity appears to be essential—although its key targets remain unknown (Hinchcliffe and Sluder, 2001; Lacey et al., 1999; Matsumoto et al., 1999; Meraldi et al., 1999). Moreover, Cdk1/Cyclin B binds to STIL/Ana2 in human cells, and this blocks the ability of STIL to interact with Plk4, so inhibiting centriole assembly (Zitouni et al., 2016). The interaction between Cdk1 and STIL is not obviously regulated by phosphorylation: although Cdk1 can phosphorylate STIL, the significance of this is unclear. The interaction interface between Cdk1 and STIL in humans is not conserved in flies, but

Lisa Gartenmann in the lab has recently identified two conserved Cdk1 sites in Ana2 that can be phosphorylated by recombinant Cdk1/Cyclin B *in vitro*, and whose mutation to phospho-mimetic residues slows, but does not block, the rate of Ana2 incorporation into the cartwheel (mutation to non- phosphorylable Alanine residues has no discernable affect). In this scenario, Cdk1/Cyclin B appears to be acting to prevent cartwheel assembly in mitosis.

Clearly much work remains to be done to understand how the basic cell cycle machinery influences centriole assembly, a subject I return to in my final Discussion Chapter.

Chapter 6: Discussion

In this chapter I discuss some of the most interesting points that have arisen from my thesis work, focusing on two main areas: (1) The function of Ana1 in flies; (2) The regulation of centriole length in flies.

6.1: The function of Ana1 in flies

At the time I initiated my studies, it was clear that Ana1 had an important role in centriole assembly and/or maintenance (Avidor-Reiss et al., 2004; Blachon et al., 2009; Dobbelaere et al., 2008; Goshima et al., 2007), but it was unclear how Ana1 might fit into the canonical centriole duplication pathway that had recently emerged primarily from studies in worms and flies (Banterle and Gönczy, 2017; Conduit and Raff, 2015). Just as I started my studies a paper came out describing how Cep295, the human Ana1 homologue, was not essential for centriole duplication, but stabilised the new-born centrioles during early mitosis as they lost their cartwheels and were converted into centrosomes that recruited PCM (Izquierdo et al., 2014). In the absence of Cep295, the new centrioles were formed in S/G2 phase, but they were not converted to centrosomes and so could not recruit PCM (Izquierdo et al., 2014). It was proposed that these PCM-less centrioles were destabilised when they lost their cartwheel and so ultimately disintegrated (Izquierdo et al., 2014). This is an attractive model, but we realised that it could not completely explain the situation in flies, as fly centrioles do not lose their cartwheels when they mature into mother centrioles/centrosomes (González et al., 1998).

I found that Ana1 is not essential for centriole duplication, but that *ana1* mutants nevertheless have very few centrosomes in larval brain cells and pupal spermatocyte

cells. My studies also suggested that Ana1 plays an important part in recruiting and/or maintaining Asl to/at the newly maturing mother centrioles. These findings suggest that Ana1 is not essential for centriole duplication *per se*, but is essential for the conversion of daughter centrioles to mother centrioles/centrosomes. This is because the recruitment of Asl to the maturing daughter centriole is required to allow the new-born centriole to duplicate—as Asl is required to recruit Plk4 to centrioles (Blachon et al., 2008; Dzhindzhev et al., 2010; Novak et al., 2014)—and to organise mitotic PCM—as Asl is required to recruit Spd-2 to centrioles (Conduit et al., 2014b; 2015a). In this scenario, Ana1 is not required to stabilise new-born centrioles, as is thought to be the case for Cep295 in humans (Izquierdo et al., 2014), but it is required to allow the new-born centrioles to duplicate and organise mitotic PCM. This would explain why *ana1* mutant tissues largely lack centrioles/centrosomes.

As I was performing these studies, a second paper was published that also reported the function of Ana1 in recruiting Asl to centrioles in cultured fly cells (Fu et al., 2016). These authors concluded that Ana1 functioned as a “bridge” between Cep135 and Asl, and this module appeared to be conserved in human cells. While this paper comes to a similar conclusion to my own studies about Ana1 recruiting Asl to centrioles, several aspects of this study were puzzling.

First, several previous publications have concluded that Cep135 is not essential for centriole duplication in flies (Blachon et al., 2009; Carvalho-Santos et al., 2010; 2012; Mottier-Pavie and Megraw, 2009; Roque et al., 2012). Fu et al., argued that the *Cep135* allele used in all these studies may not be a null, and this is certainly plausible. The Cep135 gene is quite complicated in *D. melanogaster*, and it contains a large (>6kb) intron that essentially divides the N- and C-terminal halves of the

protein and that contains two other annotated genes. Anna Caballe in the Raff laboratory has used a CRISPR approach to successfully delete the C-terminal half of the gene (and a preliminary analysis suggests that this allele has a similar phenotype to the original allele used in the previous studies—personal communication). The Cabernard lab have also generated a *Cep135* allele in which they report the N-terminal part of the gene is deleted (Singh et al., 2014). In Anna's hands, this allele has a slightly stronger phenotype, but she has been unable to map the extent of the deletion, and it appears to be significantly larger than originally implied (the exact boundaries of the deletion were not reported). Clearly it will be important to generate a true *Cep135* null allele to determine whether Cep135 is essential for the recruitment of Asl to maturing centrioles, as suggested by Fu et al (Fu et al., 2016).

Second, the model proposed by Fu at al. ignores several previous reports of a conserved interaction between Sas-4/CPAP and Asl/Cep152, indicating that there may be at least one alternative pathway for recruiting Asl/Cep152 to centrioles (Blachon et al., 2008; Cizmecioglu et al., 2010; Dzhindzhev et al., 2010; Hatch et al., 2010). Indeed, studies from our laboratory suggest that Sas-4 must be phosphorylated by Cdk1 during mitosis to allow Sas-4 to recruit Polo and initiate Asl recruitment (although it is unclear if this phosphorylation promotes Asl recruitment by directly promoting the already characterised interaction between Sas-4/CPAP and Asl/Cep152, (Novak et al., 2016). This mechanism of Asl recruitment is attractive, as it explains why centrioles, born in S-phase, must first pass through mitosis before they mature into mothers that are competent for duplication and PCM recruitment. Moreover, several aspects of my structure/function studies of Ana1 suggested that the Fu et al. model is likely to be oversimplified, although none of my experiments were definitive on this point.

Finally, I collaborated with Alan Wainman to examine the dynamics of Ana1, Cep135 and Asl incorporation into new centrioles. I performed initial studies on Ana1, some of which were reported in our recent publication (Saurya et al., 2016). I did not report these experiments in this thesis, however, as Alan subsequently performed some 3D-SIM experiments that suggested that Ana1 was not being incorporated into the growing daughter centriole (as we had originally assumed), but rather was being incorporated into the new mother centriole once it had separated from its mother. Thus, at the time of writing this thesis, the interpretation of my original experiments was unclear. Alan has now shown that Asl, Ana1 and Cep135 are *all* only incorporated into the new centriole after it has separated from its mother. Moreover, all 3 proteins exhibit different kinetics, with Cep135 incorporation possibly not starting until after Asl and Ana1 have started to incorporate. These new data strongly suggest that Cep135 cannot be essential for the initial incorporation of Asl into new-born centrioles. Taken together, our analyses support the idea that Ana1 plays an important part in helping to recruit Asl to centrioles, but they suggest that the model proposed by Fu et al., is likely to be an oversimplification of how this occurs.

6.2: The regulation of centriole length in flies

Unexpectedly, I found that Ana1 promotes centriole elongation in a dose-dependent manner: centrioles are longer when Ana1 is over-expressed and shorter when Ana1 is under-expressed. The first N-terminal 639aa of Ana1 promotes centriole elongation, but this region is not essential for the function of Ana1 in promoting centriole, centrosome and cilium assembly/maintenance. This suggests that the function of Ana1 in promoting centriole growth is molecularly distinct from its function in promoting Asl recruitment to centrioles. Importantly, Chang et al. concluded that

human Ana1/Cep295 is also required for centriole elongation, and they showed that Cep295 can interact with tubulin, providing a potential mechanism; this study was published back to back with our study (Chang et al., 2016; Saurya et al., 2016).

These observations prompted me, and several others in the laboratory, to think about how centriole size is regulated. We realised that this was a fascinating question that was likely to be relevant to the problem of organelle size control more generally (Marshall, 2015). Indeed, it has been pointed out previously that centrioles are an attractive model with which to study this problem because, due to their highly ordered structure, the complex 3D-problem of organelle size regulation can be simplified to a 1D-problem of centriole length regulation (Goehring and Hyman, 2012; Marshall, 2016). We realised that it was difficult to test any models of centriole length regulation because a quantitative description of the growth process was lacking. This is probably due to two major technical challenges: (1) centrioles are very small, so it is hard to directly measure their length as they are growing; (2) cells contain only two growing centriole pairs, and these centrioles initiate growth in S-phase, and finish growth by M-phase, but it is difficult to know where in the growth cycle any particular cell is—thus, it is difficult to extract quantitative growth data from populations of cells.

We realised that we could potentially get around these problems using the early *Drosophila* embryo, where we can measure the incorporation of a centriole protein of interest in hundreds of centrioles as they synchronously assemble in just a few minutes during S-phase. Moreover, in these embryos the central cartwheel and centriole MTs grow to the same length, allowing us to use the growth of the cartwheel as a proxy to measure the growth of the centriole. In collaboration with Mustafa Aydogan, a student in the Raff laboratory, we developed methods to measure the

incorporation parameters of the cartwheel component Sas-6-GFP (Aydogan et al., 2018). This analysis revealed that centriole growth is homeostatic: if centrioles grow slowly, they grow for a longer period, if centrioles grow quickly, they grow for a shorter period—thus ensuring that centrioles grow to a consistent size. Moreover, we found that Plk4 influences both the centriole growth rate and growth period (Aydogan et al., 2018). More recently, Mustafa Aydogan extended these studies to show that Plk4 forms an oscillator at the base of the growing daughter centriole, raising the exciting and attractive possibility that organelle size control could be regulated by oscillators. A paper describing these findings is currently under review at *Science* (Aydogan et al., 2018B), and I am the fifth author (of eight), as I made several constructs and stocks that were crucial for these studies.

I used this assay to test whether several proteins that had been shown to influence centriole length (usually from an analysis of fixed EM images) influenced the rate of cartwheel growth in the embryo. Perhaps disappointingly, the three known positive promoters of centriole elongation that I tested, Ana1, Cep135 and Sas-4/CPAP, had relatively little effect on the parameters of centriole growth in the embryo (Figure 4.6), even though I had already shown that Ana1 levels clearly regulate centriole length in testes and wing disc cells (Figure 3.16 and Figure 3.19). In thinking about how to explain these apparently contradictory findings we realised that they highlighted an issue that we had not been thinking about properly. The cartwheel and centriole MTs grow to approximately the same length in *Drosophila* cells, so we had assumed that the length of the cartwheel (which is assembled first) determines the length of the centriole MTs. Moreover, we assumed that this would be true for the first phase of centriole growth that occurs in all species during S-phase, but that in some species

(such as vertebrates) a second phase of growth would allow the centriole MTs to extend past the cartwheel during G2/M.

Our results, however, suggested an alternative possibility: that the centriole cartwheel and centriole MTs grow independently of one another, and just happen to grow to approximately the same length in most fly cells. If this were the case, it could explain why Ana1 levels influence the growth of the centriole MTs (which is largely what I measured in my EM studies), but do not influence the growth of the cartwheel—which may have been of normal size in my Ana1 dosage EM studies, but I did not notice this as the cartwheel is difficult to discern in these images and my measurements were largely guided by the more prominent centriole MTs. In this scenario, cells would presumably normally coordinate the growth of the centriole cartwheel and centriole MTs to ensure a constant ratio between the length of these structures in the fully assembled centriole.

Importantly, I found some support for this hypothesis when I examined how several putative negative regulators of centriole length influenced the parameters of cartwheel growth in the embryo. CP110, Cep97 and Klp10A all localise to the distal end of the centriole where they are thought to form a cap that prevents the centriole and centriole MTs from elongating abnormally (Aydogan et al., 2018; Delgehyr et al., 2012; Franz et al., 2013; Fu and Glover, 2012; Galletta et al., 2016b; Kleylein-Sohn et al., 2007; Sonnen et al., 2012). In flies, the removal of this cap leads to a small increase in centriole size, but a dramatic increase in the size of the centriole MTs, that now extend well past the main body of the centriole (Franz et al., 2013; Galletta et al., 2016b). Remarkably, I discovered that the centriole cartwheel appeared to grow faster than normal if I reduced the genetic dosage of any of these proteins by half (Figure 4.8).

In collaboration with Mustafa Aydogan, we went on to show that the cartwheels grew slightly slower than normal when CP110 or Cep97 were overexpressed (Figure 4.10).

At this stage I stopped working in the laboratory to write up my thesis (although I continued my duties as lab-manager), so this line of investigation was continued by Mustafa and another student in the laboratory, Laura Hankins. They have very recently shown that CP110 and Cep97 levels oscillate at the distal end of the growing daughter centriole, and the peak of this oscillation appears to set the time at which the centriole MTs stop growing. Moreover, while Mustafa and I showed that CP110 and Cep97 levels influence the parameters of centriole cartwheel growth, Mustafa and Laura have now shown that Plk4 levels influence the CP110/Cep97 oscillation (personal communication). Thus, it appears that “cross-talk” between two spatially separated oscillators coordinates the growth of the centriole cartwheel (from the proximal end, regulated by Plk4) and the centriole MTs (from the distal end, regulated by CP110/Cep97) to ensure that the two structures grow to a consistent ratio within the centriole.

These findings are particularly exciting, as they raise the attractive possibility that coordinated oscillators could regulate organelle size to ensure that cells produce the correct amount of each organelle, in the correct ratio, that is optimal for any individual cell type. The early *Drosophila* embryo is a powerful system with which to tackle these issues, and there are plans within the Raff laboratory to investigate not only how oscillators regulate centriole (and potentially centrosome) assembly, but also how they might influence the biogenesis of other organelles. Thus, my initial studies of Ana1 have opened up several new areas of research for the laboratory that are likely to be productive for several years to come

Publications

© 2016. Published by The Company of Biologists Ltd | Journal of Cell Science (2016) 129, 2514-2525 doi:10.1242/jcs.186460

RESEARCH ARTICLE

Drosophila Ana1 is required for centrosome assembly and centriole elongation

Saroj Saurya[1], Hélio Roque[1], Zsofia A. Novak[1], Alan Wainman[1], Mustafa G. Aydogan[1], Adam Volanakis[1], Boris Sieber[1], David Miguel Susano Pinto[2] and Jordan W. Raff[1,*]

ABSTRACT

Centrioles organise centrosomes and cilia, and these organelles have an important role in many cell processes. In flies, the centriole protein Ana1 is required for the assembly of functional centrosomes and cilia. It has recently been shown that Cep135 (also known as Bld10) initially recruits Ana1 to newly formed centrioles, and that Ana1 then recruits Asl (known as Cep152 in mammals) to promote the conversion of these centrioles into centrosomes. Here, we show that *ana1* mutants lack detectable centrosomes *in vivo*, that Ana1 is irreversibly incorporated into centrioles during their assembly and appears to play a more important role in maintaining Asl at centrioles than in initially recruiting Asl to centrioles. Unexpectedly, we also find that Ana1 promotes centriole elongation in a dose-dependent manner: centrioles are shorter when Ana1 dosage is reduced and are longer when Ana1 is overexpressed. This latter function of Ana1 appears to be distinct from its role in centrosome and cilium function, as a GFP–Ana1 fusion lacking the N-terminal 639 amino acids of the protein can support centrosome assembly and cilium function but cannot promote centriole over-elongation when overexpressed.

KEY WORDS: Centriole, Centrosome, Ana1, Cep295, Centriole elongation, Centriole structure

INTRODUCTION

Centrioles are ancient cellular organelles that are required for the formation of centrosomes and cilia (Azimzadeh, 2014). These organelles play an important role in many cell processes, and their dysfunction has been linked to a diverse set of human pathologies (Bettencourt-Dias et al., 2011; Conduit et al., 2015a; Nigg and Raff, 2009). A better understanding of how these organelles are assembled is therefore an important goal of modern cell biology.

Recent studies have revealed that only a relatively small number of proteins are essential for centriole assembly (Conduit et al., 2015a; Fırat-Karalar and Stearns, 2014; Gönczy, 2012; Jana et al., 2014). These proteins form a conserved pathway in which the protein kinase ZYG-1 (in worms), Plk4 (in mammals) or Sak (in flies) (Bettencourt-Dias et al., 2005; Delattre et al., 2006; Habedanck et al., 2005; Pelletier et al., 2006) recruits SAS-5/Ana2/STIL (worms, flies and mammals, respectively) and Sas-6 to the side of the mother centriole to form a cartwheel structure that initiates the assembly of the new daughter centriole (Arquint et al., 2015; Dzhindzhev et al., 2014; Kitagawa et al., 2011; Kratz et al., 2015; Lettman et al., 2013; Moyer et al., 2015; Ohta et al., 2014; Qiao et al., 2012; Stevens et al., 2010b; van Breugel et al., 2011). These proteins then recruit Sas-4/CPAP (CPAP is also known as CENPJ), which in turn helps recruit the centriolar microtubules (Cottee et al., 2013; Hatzopoulos et al., 2013; Hsu et al., 2008; Pelletier et al., 2006; Tang et al., 2011). In worms, SPD-2 recruits ZYG-1 to the mother centrioles (Delattre et al., 2006; Pelletier et al., 2006), whereas this function is performed by Asterless (Asl) in flies (Dzhindzhev et al., 2010; Novak et al., 2014). Vertebrate cells appear to use a combination of these proteins (Cep192 and Cep152, respectively) (Kim et al., 2013; Park et al., 2014; Sonnen et al., 2013).

Genome-wide RNA interference (RNAi) screens in flies have identified Ana1 as a protein that is potentially required for centriole assembly (Dobbelaere et al., 2008; Goshima et al., 2007). Flies mutant for *ana1* are uncoordinated (a phenotype indicative of cilia defects) and exhibit reduced centrosome numbers in larval brain cells (Blachon et al., 2009), strongly suggesting that Ana1 has a role in centriole, centrosome and cilium assembly. A recent study on the human Ana1 homologue (Cep295) has suggested that this protein is not essential for centriole assembly, but rather is required for centriole-to-centrosome conversion (Izquierdo et al., 2014). New centrioles were not converted into centrosomes in the absence of Cep295 and so could not organise their pericentriolar material (PCM) properly: as a result, the new centrioles appeared to be destabilised once they lost their central cartwheel (as occurs normally in most vertebrate cells when the daughter centrioles are converted into mothers). Thus, vertebrate centrioles appear to be stabilised by both the central cartwheel and the PCM they organise. If newly formed centrioles cannot be converted into centrosomes (and so cannot organise any PCM) they are destabilised once they lose their central cartwheel – potentially explaining why Ana1/Cep295 proteins might be essential for both centrosome and cilium assembly. Like Cep295 in human cells, Ana1 appears to be required for centriole-to-centrosome conversion in fly cells (Fu et al., 2016). Ana1 is first recruited to centrioles by Cep135 (also known as Bld10) in late interphase and Ana1 subsequently recruits Asl to centrioles during mitosis (Fu et al., 2016). Asl plays a particularly important part in centriole-to-centrosome conversion in flies, as its incorporation is required to allow new centrioles to duplicate (Novak et al., 2014) and to recruit mitotic PCM for the first time (Conduit et al., 2014b).

Here, we investigated the function of Ana1 in flies *in vivo*. We show that *ana1* mutant flies have very few centrosomes, and that Ana1 appears to be irreversibly incorporated into centrioles throughout S-phase with unusual dynamics. A structure–function analysis suggests that the recruitment of Ana1 to centrioles, and the

[1]Sir William Dunn School of Pathology, University of Oxford, South Parks Road, Oxford OX1 3RE, UK. [2]Micron Oxford Advanced Bioimaging Unit, Department of Biochemistry, University of Oxford, South Parks Road, Oxford OX1 3QU, UK.

*Author for correspondence (jordan.raff@path.ox.ac.uk)

J.W.R., 0000-0002-4689-1297

This is an Open Access article distributed under the terms of the Creative Commons Attribution License (http://creativecommons.org/licenses/by/3.0), which permits unrestricted use, distribution and reproduction in any medium provided that the original work is properly attributed.

Received 18 January 2016; Accepted 11 May 2016

Journal of Cell Science

Journal of Cell Science (2016) 129, 2514-2525 doi:10.1242/jcs.186460

role of Ana1 in recruiting Asl to centrioles, might be more complicated than previously thought. Unexpectedly, we find that Ana1 also promotes centriole elongation in a dose-dependent manner, and this function appears to be mechanistically different to its role in promoting Asl recruitment, and centrosome and cilium assembly.

RESULTS

Fly tissues lacking Ana1 protein have very few centrosomes

It has been shown previously that Ana1 has a role in centriole, centrosome and cilium formation (Blachon et al., 2009; Dobbelaere et al., 2008; Goshima et al., 2007), and *ana1* mutant flies are severely uncoordinated due to the lack of functional cilia (Blachon et al., 2009). We found that *ana1* mutants have a dramatic reduction in centrosome numbers in third-instar larval brains that is comparable to that observed in brains mutant for the essential centriole assembly genes *Sas-4*, *Sas-6*, *ana2* and *asl* (Fig. 1A) (Basto et al., 2006; Baumbach et al., 2015; Cottee et al., 2015; Peel et al., 2007; Rodrigues-Martins et al., 2007). Thus, Ana1 has an important role in centrosome assembly *in vivo*.

The N-terminal region of Ana1 is not essential for centrosome assembly or cilium function

At the time we initiated our studies, the *ana1* gene was thought to encode two polypeptides – a long form and a shorter form that lacks the N-terminal 639 amino acids (Fig. 1C) (Blachon et al., 2009). The larger protein has two short conserved regions – an N-terminal region denoted CR1 and a more C-terminal region denoted CR2 – and an extended middle region comprising several predicted coiled-coils. The shorter form is missing CR1 and the first two predicted coiled-coils. The most recent release of Flybase, however, indicates that only the long polypeptide is produced *in vivo*, so we refer to the long-form as wild-type (WT) Ana1 and the short form as N-terminally deleted Ana1 [Ana1ΔNT (640–1729), hereafter Ana1ΔNT]. We obtained a transgenic line expressing WT Ana1–GFP from its endogenous promoter (eAna1–GFP) (Blachon et al., 2009), and we generated transgenic lines expressing WT GFP–Ana1 or GFP–Ana1ΔNT from the Ubiquitin promoter (uGFP–Ana1 or uGFP–Ana1ΔNT, respectively) (Stevens et al., 2010a).

Western blotting revealed that all these fusion proteins (including the one driven by the endogenous promoter) were overexpressed compared to the endogenous protein (Fig. 1D). Surprisingly, both GFP–Ana1 and GFP–Ana1ΔNT strongly rescued the severe uncoordination defect of *ana1* mutant flies to similar extents (data not shown), but mutant flies rescued by GFP–Ana1 were fertile, whereas mutant flies rescued by GFP–Ana1ΔNT were both male- and female-sterile. Moreover, both fusion proteins appeared to support centrosome assembly in third-instar larval brains to similar extents (Fig. 1B), and they both were recruited to centrosomes when expressed in embryos, although the centrosomal localisation of GFP–Ana1ΔNT was markedly reduced compared to GFP–Ana1 (Fig. 1E; see below). Taken together, these results suggest that the N-terminal 639 amino acids of Ana1 are not essential for centrosome assembly and cilium function, although flies surviving on the GFP–Ana1ΔNT fusion protein are male- and female-sterile.

A structure–function analysis of Ana1

The finding that GFP–Ana1ΔNT can support centrosome assembly *in vivo* is perhaps surprising, as a recent study has suggested that, in cultured cells, the N-terminal region of Ana1 (amino acids 1–935) is required to target Ana1 to centrioles through a direct interaction with Cep135, whereas the C-terminal region of Ana1 (amino acids 756–1729) interacts with Asl, but is not targeted to centrioles (even in the presence of the endogenous protein) (Fu et al., 2016). To analyse the potential function of the various regions of Ana1 in embryos in more detail, we synthesised mRNAs encoding GFP–Ana1, GFP–Ana1ΔNT or the N-terminal or C-terminal deletions analysed by Fu et al. (GFP–Ana1ΔNT2 or GFP–Ana1ΔCT, respectively) (Fig. 2A). We injected these into WT embryos (that therefore contain endogenous unlabelled Ana1) expressing Asl–mCherry; the injected mRNAs are then gradually translated and can compete for binding partners with the endogenous protein (Cottee et al., 2015; Richens et al., 2015). We then analysed the behaviour of the expressed proteins and their effect on Asl–mCherry localisation at 60–90 min after injection (Fig. 2B–D).

Full-length GFP–Ana1 strongly localised to centrosomes and had no discernible effect on the centrosomal localisation of Asl–mCherry, which is preferentially localised at ‘old’ centrosomes (that contain the older mother centrioles) because the ‘new’ centrosomes (that contain the younger mother centrioles) only start to recruit Asl at around the time the young mother centrioles separate from their mothers (Novak et al., 2014) (Fig. 2, construct 1). We noticed that GFP–Ana1 also often exhibited a slight asymmetry and was often slightly enriched on the old centrosome (see below). GFP–Ana1ΔNT and GFP–Ana1ΔNT2 both localised to centrioles, although much more weakly than WT GFP–Ana1 (Fig. 2, constructs 2 and 3). Moreover, the amount of Asl–mCherry localised to centrosomes was also significantly reduced. This is perhaps surprising because the C-terminal region of Ana1 is thought to recruit Asl to centrioles (Fu et al., 2016), so it is unclear why recruiting a C-terminal fragment of Ana1 to centrosomes should perturb Asl levels. Perhaps the cytoplasmic fractions of these proteins sequester cytoplasmic Asl–mCherry, preventing its recruitment to centrosomes.

Interestingly, GFP–Ana1ΔCT also exhibited a markedly reduced localisation to centrosomes, although its localisation appeared to be tighter and less diffuse than that observed with GFP–Ana1ΔNT or GFP–Ana1ΔNT2 (Fig. 2, construct 4). This reduction in centrosomal localisation is also perhaps surprising as GFP–Ana1ΔCT contains the entire N-terminal domain that interacts with Cep135, and that domain is both necessary and sufficient to recruit Ana1 to centrosomes in cultured cells (Fu et al., 2016). Moreover, although GFP–Ana1ΔCT expression strongly perturbed the centrosomal localisation of Asl–mCherry (as expected because GFP–Ana1ΔCT should not be able to recruit Asl), it more strongly affected the localisation at the old centrosome than at the new centrosome. As a result, the preferential accumulation of Asl at the old centrosome was greatly reduced: the ratio of Asl–mCherry fluorescence at old versus young centrosomes was 2.6±0.3; 2.6±0.5 and 2.7±0.3 (mean±s.d., n=5 embryos, 10 centrosomes per embryo) in embryos expressing WT GFP–Ana1, GFP–Ana1ΔNT and GFP–Ana1ΔNT2, respectively, but only 1.5±0.1 in embryos expressing GFP–Ana1ΔCT (P<0.001; two tailed t-test). Thus, most surprisingly, GFP–Ana1ΔCT preferentially perturbs the localisation of Asl–mCherry at old centrosomes, rather than at the recently converted new centrosomes (see Discussion).

Overexpressing Sas-6 and Ana2 can stabilise centrioles in the absence of Ana1

Ana1 is required for both centrosome and cilium function in flies, suggesting that it likely plays some part in centriole assembly. We wanted to test whether Ana1 might have a role in assembling

Journal of Cell Science (2016) 129, 2514-2525 doi:10.1242/jcs.186460

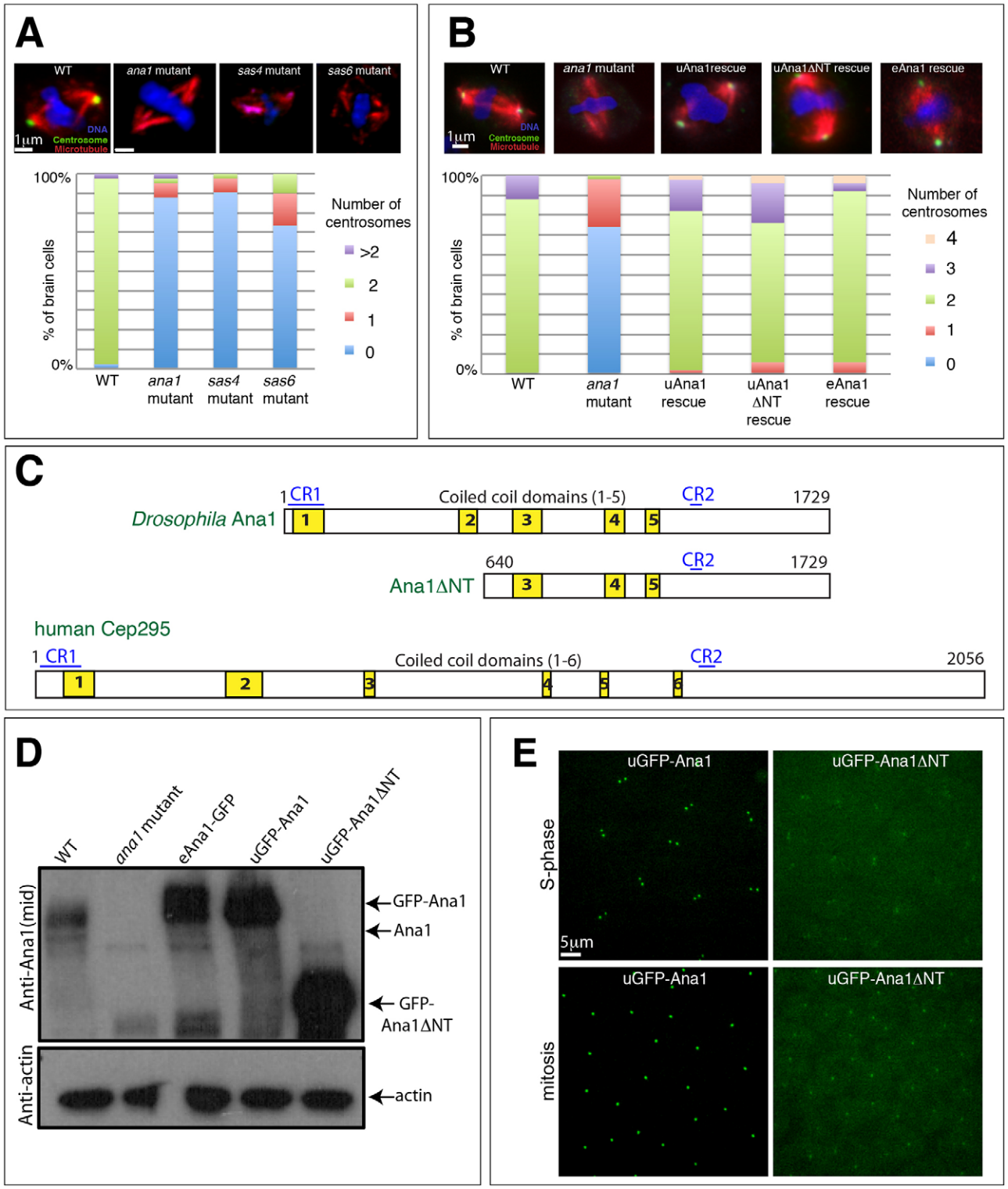

Fig. 1. Ana1 is required for efficient centrosome assembly and/or maintenance. (A,B) Micrographs showing images of third-instar larval brain cells stained for DNA (blue), microtubules (red) and the centrosome marker Asl (green) in WT, various mutants (as indicated), or the *ana1* mutant rescued by different transgenes (as indicated). Graphs quantify the percentage of cells of each genotype exhibiting different numbers of centrosomes (*n*=30–50 total cells counted from five brains). Centrosomes were scored as dots in mitotic cells that were positive for both the centriole and centrosome protein Asl and the centrosome protein Cnn (Conduit et al., 2014a). (C) A schematic representation of *Drosophila* Ana1, Ana1ΔNT and human Cep295 proteins. Two conserved regions (CR1 and CR2, blue lines) and several predicted coiled-coil domains (yellow boxes) are indicated. (D) Western blots of *Drosophila* third-instar larval brains from WT, *ana1* mutant or WT brains expressing Ana1–GFP from its endogenous promoter (eAna1–GFP), or GFP–Ana1 or GFP-Ana1-ΔNT from the ubiquitin promoter (uGFP–Ana1 or uGFP–Ana1ΔNT). Blots were probed with anti-Ana1 or anti-actin antibodies (loading control). Serial dilution blots (not shown) reveal that the GFP fusions are overexpressed relative to endogenous Ana1 by ~2–4× (eAna1–GFP), 3–5× (uGFP–Ana1) or 5–10× (uGFP–Ana1ΔNT). (E) Micrographs showing representative images of *Drosophila* embryos expressing uGFP–Ana1 (left panels) or uGFP–Ana1ΔNT (right panels) in a WT background in S-phase (top panels) or in mitosis (bottom panels).

Journal of Cell Science

Journal of Cell Science (2016) 129, 2514-2525 doi:10.1242/jcs.186460

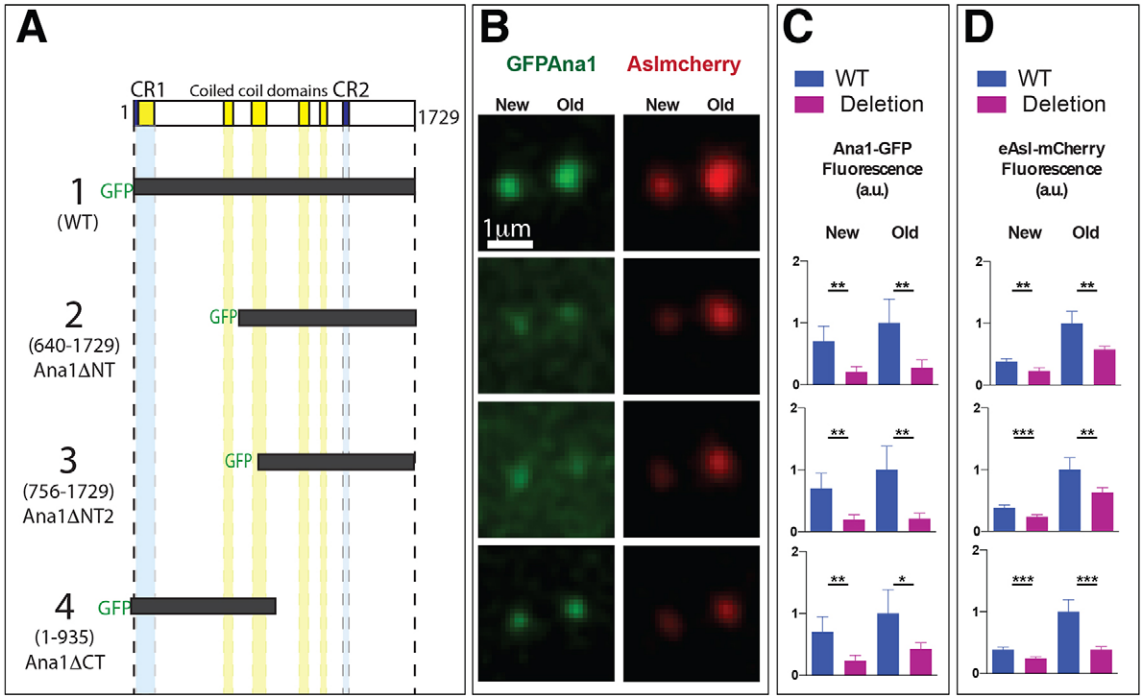

Fig. 2. A structure–function analysis of Ana1. (A) A schematic representation of the various GFP–Ana1 deletion constructs analysed. *In-vitro*-transcribed mRNA encoding each of these constructs was injected into WT embryos expressing eAsl–mCherry; the distribution of each fusion protein was analysed in living embryos in mid-S-phase (as judged by the separation of the centrosomes in the embryo). (B) Micrographs showing the typical localisation of each GFP–Ana1 fusion protein (green) and Asl–mCherry (red) at new and old centrosomes in embryos injected with the Ana1 constructs as shown in A. (C,D) The bar graphs show the mean±s.d. centrosomal Ana1–GFP fusion protein (C) or Asl–mCherry (D) fluorescence at new and old centrosomes. All values were normalised to the average fluorescence level of WT GFP–Ana1 or Asl–mCherry observed at old centrosomes in contemporaneous controls injected with WT GFP–Ana1 (construct 1) (arbitrarily given a value of 1). Note that the preferential asymmetric localisation of Asl–mCherry to the old centrosome was consistently reduced in embryos expressing Ana1ΔCT (construct 4). n=5 embryos for each construct. *P<0.05; **P<0.001; ***P<0.0001 (paired two-tailed t-test).

and/or stabilising the centriole central cartwheel structure. We have previously shown that the co-overexpression of Sas-6 and Ana2 in spermatocytes leads to the assembly of Sas-6 and Ana2 particles (SAPs) that are composed of long tubules (SAStubules) that resemble the central cartwheel (Stevens et al., 2010b). We therefore overexpressed Sas-6 and Ana2 in *ana1* mutant spermatocytes. SAPs still formed in these cells, but these were less abundant and larger than normal (Fig. S1). Electron microscopy tomography revealed that the SAPs were generally less well-ordered, but structures resembling the cartwheel central hub were still clearly visible (black arrowheads, Fig. 3A). Thus, SAP structure and behaviour is altered in the absence of Ana1 – supporting the idea that Ana1 influences centriole structure – but Ana1 does not appear to be essential for the assembly of a central cartwheel-like structure.

Surprisingly, we noticed that structures resembling centrioles that were closely associated with the SAPs were detected in seven of the 11 of the *ana1* mutant spermatocytes we examined, suggesting that centriole-like structures can still assemble in these spermatocytes under certain conditions (Fig. 3B). Interestingly, in one of these structures, we observed the central cartwheel of the centriole-like structure directly connected to a SAStubule emanating from the SAP (red arrowhead, Fig. 3B), supporting our conclusion that these tubules are closely related to central cartwheels. The centriole-like structures associated with the SAPs in *ana1* mutant cells appeared to be much shorter than the very large centrioles normally found in spermatocytes, indicating that Ana1 has a role in promoting centriole elongation in these cells (see below).

Ana1 is oriented within the centriole and is irreversibly incorporated into daughter centrioles as they assemble in S-phase

To gain insight into how Ana1 might function at centrioles, we used three-dimensional (3D) structured illumination super-resolution microscopy (3D-SIM) to investigate its localisation relative to other centriole proteins in the large centrioles found in *Drosophila* spermatocytes (Fig. 4A,B). We expressed N- or C-terminally tagged GFP fusion proteins to several centriole proteins in WT spermatocytes, and measured an average fluorescence intensity profile across ten lines drawn through each spermatocyte centriole (as indicated by the grill-like white lines in the GFP–Ana1 panel in Fig. 4A). This allowed us to calculate an average radial diameter for each protein (see Materials and Methods). As reported previously from studies on centrosomes in cultured fly cells, Cep135, Ana1 and Asl molecules were all asymmetrically localised within the centriole (Fu and Glover, 2012; Fu et al., 2016; Mennella et al., 2012) (Fig. 4A,B). All of these molecules were localised outside the cartwheel region occupied by Sas-6 and Ana2 (a region that is below the resolution of our 3D-SIM system). As in cultured cell centrosomes, the C-terminal regions of Ana1 and Asl – which directly interact *in vitro* – were essentially overlapping in the spermatocyte centrioles. In contrast to cultured cell centrosomes, however, the N-terminal regions of Cep135 and Ana1 – which also directly interact *in vitro* – were close to each other, but were essentially non-overlapping in the spermatocyte centrioles. As these studies report the localisation of the GFP moiety (rather than the actual N-termini of these proteins), it is difficult to interpret the importance of this observation.

Journal of Cell Science

Journal of Cell Science (2016) 129, 2514-2525 doi:10.1242/jcs.186460

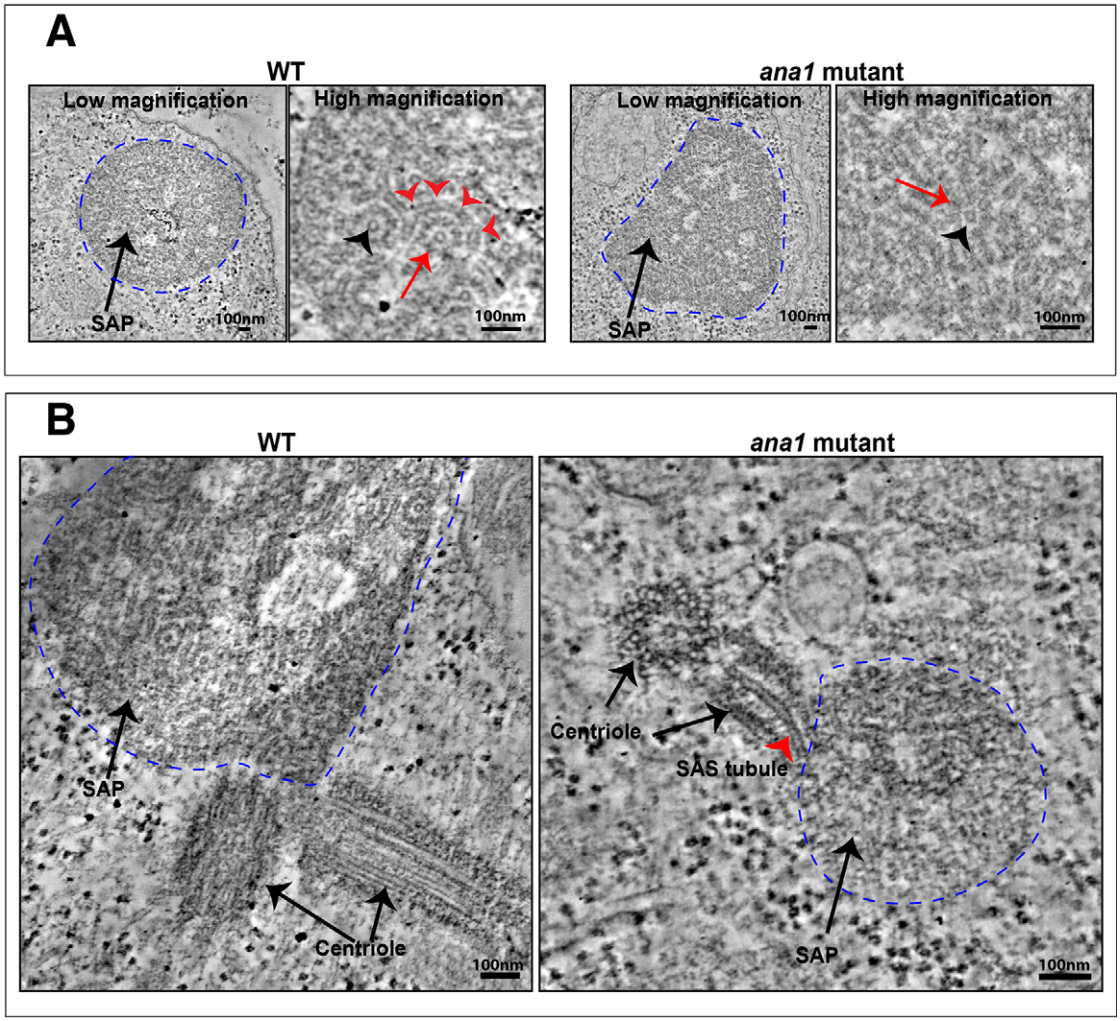

Fig. 3. Ana1 is not essential for SAP assembly. (A) Micrographs show low- and high-magnification views from electron microscopy tomographs of a SAP particle (dotted blue line) in a WT (left panels) or *ana1* mutant (right panels) spermatocyte. The SAP in the WT cell is highly structured and consists of well-organised 'SAStubules' that resemble the central cartwheel of the centriole (Stevens et al., 2010b). An end-on view of a SAStubule is highlighted by the black arrowhead, and a transverse view is highlighted with red arrowheads. The SAStubules are linked by spokes to an electron-dense outer ring (red arrow). In *ana1* mutants, the SAP structures are less well-defined, but the central cartwheel-like SAStubules are still easily discerned (red arrow), especially in an end-on view (black arrowhead). (B) The SAPs in WT spermatocytes are often directly connected to the centrioles, and we could detect small centriole-like structures associated with the SAPs in *ana1* mutants in seven out of 11 of the SAPs we examined: in this example the central cartwheel of one of the centriole-like structures appears to be directly connected to a SAStubule that extends into the SAP (red arrowhead).

We next examined how Ana1 incorporates into centrioles by following the dynamic behaviour of Ana1 in the early fly embryo. In these embryos, the nuclei exist in a common cytoplasm (the syncytium) and proceed nearly synchronously through rapid cycles of alternating S- and M-phases without intervening gap phases. Each mother centriole forms a daughter centriole early in S-phase that grows and reaches its full length by M-phase (Callaini and Riparbelli, 1990). We have previously shown that Sas-4 is incorporated at an approximately linear rate into the growing daughter centrioles throughout S-phase in these embryos (Conduit et al., 2015b; Novak et al., 2014), whereas Asl is not incorporated into the new daughter centriole during S-phase, but starts incorporating into new centrioles at an approximately linear rate when they separate from their mothers during mitosis (Novak et al., 2014). As GFP–Ana1 is slightly enriched on old centrosomes (Fig. 2C), we measured the incorporation profile of GFP–Ana1 at old (yellow boxes and lines, Fig. 5A) and new (purple boxes and lines, Fig. 5A) centrosomes independently. GFP–Ana1 exhibited an 'exponential' incorporation profile at both centrosomes, that is, incorporating at a rate that was low in early S-phase, but that gradually increased throughout S-phase and into mitosis, before plateauing in late mitosis (Fig. 5A). Clearly, more work will be required to understand the importance of this unexpected incorporation profile.

To test whether Ana1 is incorporated irreversibly into centrioles, we performed a fluorescence recovery after photobleaching (FRAP) analysis (Fig. 5B). We found that centrioles bleached in early S-phase exhibited a very similar incorporation profiled to non-bleached centrioles, strongly suggesting that the fluorescence recovery we observe is primarily driven by incorporation into the new daughter centrioles and that there is very little turnover of GFP–Ana1 at the mother centriole (see schematic interpretation, Fig. 5B). Thus, Ana1 appears to be stably incorporated into centrioles during their assembly. This might explain why GFP–Ana1 appears to be slightly enriched on old centrosomes: as GFP takes some time to mature and fluoresce, older centrioles will contain a higher

Journal of Cell Science

Journal of Cell Science (2016) 129, 2514-2525 doi:10.1242/jcs.186460

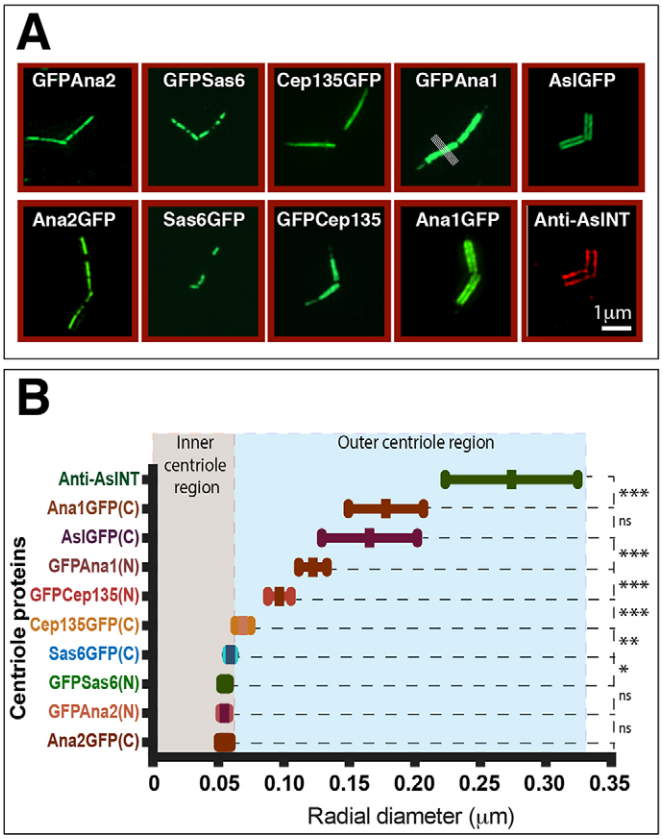

Fig. 4. Ana1, Cep135 and Asl molecules are oriented within spermatocyte centrioles. (A) Micrographs showing 3D-SIM images of centrioles in primary spermatocytes expressing various centriole proteins tagged with GFP at either their N- or C-termini and stained for GFP (green). The bottom-right image shows a centriole stained with anti-Asl-NT antibodies (red). The white lines in the GFPAna1 panel indicate example lines drawn through the centriole to calculate a fluorescence intensity distribution. (B) Graph showing the mean±s.d. radial diameter of each centriole marker (as indicated, see Materials and Methods) (n=10–53 centrioles). Statistical significance of the different radial diameters between successive proteins – moving from the innermost (Ana2–GFP) to the outermost (Asl-NT) – was calculated using a paired two-tailed t-test. *P<0.05; **P<0.001; ***P<0.0001; ns, not significant. Note that the radial diameters of the N-terminal region of Cep135 and the N-terminal region of Ana1 – which can directly interact with one another *in vitro* – are significantly different.

proportion of fluorescent GFP–Ana1 than newly formed centrioles. A similar phenomenon has been reported for GFP–PACT, a centriole protein that is also irreversibly incorporated into centrioles (Conduit et al., 2010).

Ana1 levels influence centriole length, and this requires its N-terminal region

During the course of our studies, we noticed that the elongated centrioles normally found in fly spermatocytes were significantly longer than normal when GFP–Ana1 was overexpressed, but not when GFP–Ana1ΔNT was overexpressed (Fig. 6A,B). The centrioles were also significantly shorter than normal in *ana1* heterozygous mutant spermatocytes (that have only one copy of the endogenous *ana1* gene) (Fig. 6A,B). We confirmed this result with four different spermatocyte centriole markers: Asl, GTU88* [a batch of an anti-γ-tubulin monoclonal antibody that cross reacts with spermatocyte centrioles (Martinez-Campos et al., 2004)], Spd-2 and Cep135. Interestingly, although the levels of Ana1 clearly influenced the length of spermatocyte centrioles, halving the dose of Ana1 did not lead to an obvious reduction in the levels of Cep135 or Asl localised at centrioles per unit length of centriole, whereas overexpressing GFP–Ana1 actually led to a slight decrease in the amount of Asl and Cep135 recruited to the centrioles per unit length (although this decrease was not statistically significant in the case of Cep135) (Fig. 6C). We conclude that Ana1 can promote centriole elongation in spermatocytes without recruiting more Cep135 or Asl (per unit length) to the centrioles.

Although the centrioles in *ana1* mutant spermatocytes rescued by Ana1–GFP usually appeared to be abnormally elongated, those in mutant spermatocytes rescued by GFP–Ana1ΔNT were invariably extremely short (Fig. 7). These centrioles were so short that it was impossible to measure their length in immunofluorescence experiments as we could only discern them as dots, rather than elongated centrioles (Fig. 7; Fig. S2A, stage13). Nevertheless, the short centrioles in the *ana1* mutant spermatocytes rescued by GFP–Ana1ΔNT often went on to form short basal bodies at the base of the sperm nuclei, although these often appeared disorganised (Fig. S2A, stage 17), and mutant sperm were invariably immotile, presumably explaining why these flies are male sterile. Thus, although Ana1ΔNT can rescue the centrosome assembly defect in *ana1* mutant spermatocytes (Fig. S2B) and brain cells (Fig. 1B), it cannot support the dramatic elongation of the centrioles that normally occurs in spermatocytes.

Because the centrioles in fly spermatocytes are much longer and more elaborate than those found in other fly tissues (Gonzalez et al., 1998), we examined centriole length by electron microscopy in fly wing disc cells, which contain centrioles more typical of those found in most *Drosophila* tissues. We found that GFP–Ana1 (but not GFP–Ana1ΔNT) overexpression led to an increase in centriole length, whereas halving the gene dosage of endogenous *ana1* led to a decrease in centriole length (Fig. 8A,B). Taken together, these observations demonstrate that Ana1 can promote centriole elongation in a dose-dependent manner, and that this activity appears to require the N-terminal 639 amino acids of Ana1.

DISCUSSION

Our results are consistent with recent reports that Ana1/Cep295 is required for centriole-to-centrosome conversion in flies and humans (Fu et al., 2016; Izquierdo et al., 2014), and we show that *ana1* mutant cells have very few centrosomes *in vivo*. Studies on fly cells in culture suggested a simple model of centriole-to-centrosome conversion whereby Cep135 is initially recruited to centrioles and this subsequently recruits Ana1 to centrioles in late interphase. In mitosis, Ana1 then recruits Asl to new centrioles; Asl recruitment is crucial for centriole-to-centrosome conversion, as Asl is required to allow newly formed centrioles to recruit PCM during mitosis (Conduit et al., 2014b) and to duplicate during the next S-phase (Novak et al., 2014). A similar molecular mechanism appears to operate in human cultured cells (Fu et al., 2016).

Our findings suggest, however, that the recruitment of Ana1 to centrioles might be more complicated. The N-terminal region of Ana1 (amino acids 1–935) interacts with Cep135 *in vitro* and is recruited to centrioles in cultured cells, whereas an N-terminally deleted fragment of Ana1 (amino acids 756–1729) cannot be recruited to centrioles in cultured cells, even in the presence of the endogenous WT Ana1 protein. In contrast, we find that the C-terminal region of Ana1 can be recruited to centrosomes (although quite weakly). Moreover, GFP–Ana1ΔNT (comprising amino acids 640–1729) can rescue the centrosome assembly defect in *ana1* mutant cells and the uncoordinated phenotype of *ana1* mutant flies, although this protein is clearly not fully functional

Journal of Cell Science (2016) 129, 2514-2525 doi:10.1242/jcs.186460

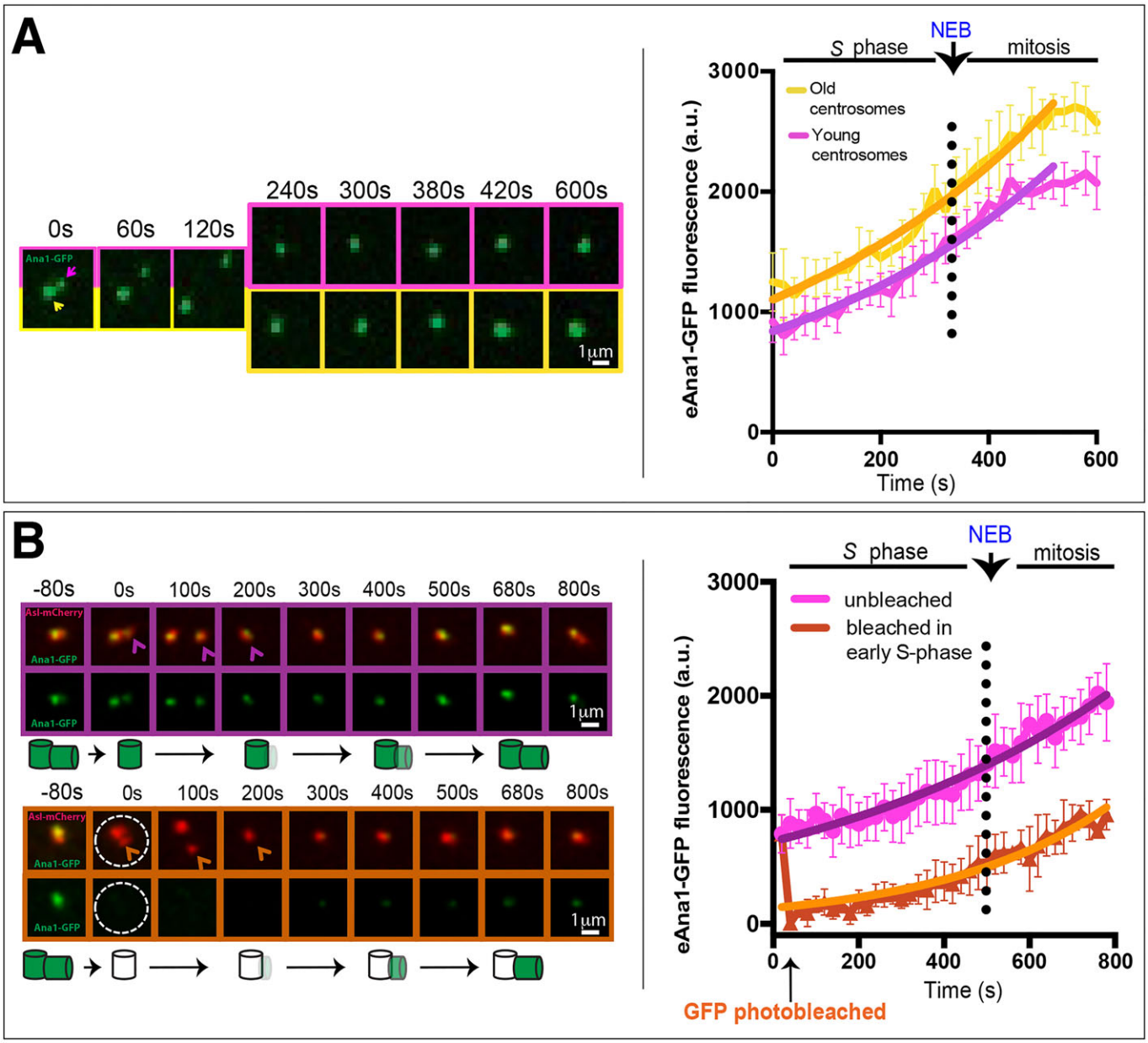

Fig. 5. Ana1 is stably incorporated into centrioles during S-phase and mitosis. (A) Micrographs showing images from a time-lapse movie following eAna1–GFP incorporation into newly separated centrosomes. The graphs show the mean±s.d. centrosomal eAna1–GFP fluorescence over time averaged from three embryos (10 centrosomes per embryo). Time (s) relative to centriole separation (t=0) is indicated. Old (yellow arrow, boxes and line on graph) and young centrosomes (purple arrow, boxes and line on graph) were measured independently. Non-linear regression analysis indicates that the pattern of Ana1–GFP incorporation is best fitted by an exponential function (solid line), with incorporation plateauing in late mitosis. (B) Micrographs showing images from a time-lapse movie of a FRAP experiment following GFP–Ana1 incorporation in control (purple arrow, boxes and line on graph) and photobleached (orange arrow, boxes and line on graph) centrosomes (both taken at the same time form the same embryo). A schematic of the interpretation of these results is shown beneath the images. The graphs show the mean±s.d. eAna1–GFP fluorescence over time averaged from three embryos (six photobleached or non-photobleached centrosomes per embryo). These embryos also expressed eAsl–mCherry (red) so that centrioles could be followed after photobleaching. Note that after the 100 s timepoint only the dimmer (younger) centrosome is shown in the micrographs. Time (s) relative to centriole photobleaching (which was performed at centriole separation, t=0) is indicated.

because it is only weakly recruited to centrosomes, and the rescued mutant flies are both male- and female-sterile. We do not know why this deletion construct appears to behave differently in embryos and cultured cells, but our findings suggest that several mechanisms help to localise Ana1 to centrioles in embryos. In particular, the middle region of Ana1 contains multiple predicted coiled-coil regions that could allow Ana1 to interact with itself (potentially complicating the analysis of protein localisation experiments performed in the presence of the WT endogenous protein) and also with other proteins such as Cep135.

Surprisingly, we also find that in the presence of GFP–Ana1ΔCT (a C-terminal Ana1 deletion that cannot interact with Asl) (Fu et al., 2016) the recruitment of Asl is more strongly reduced at old mother centrioles than at new mother centrioles. This is unexpected, and suggests that the process of recruiting Asl to mother centrioles might also be more complicated than originally thought. Indeed, mother

Journal of Cell Science

Journal of Cell Science (2016) 129, 2514-2525 doi:10.1242/jcs.186460

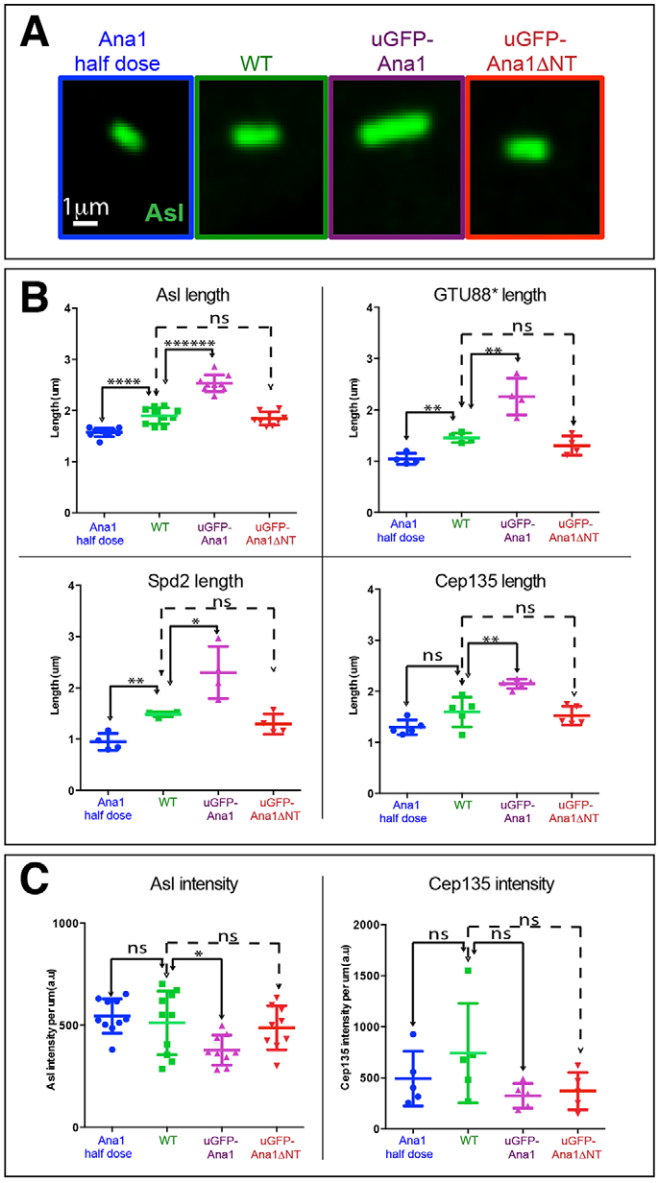

Fig. 6. Ana1 levels influence centriole length. (A) Micrographs showing typical examples of meiosis II centrioles (revealed by Asl staining) in pupal testes from *ana1* heterozygous mutants (containing only one copy of the WT gene), WT, WT overexpressing GFP–Ana1 and WT overexpressing GFP–Ana1ΔNT. (B) Graphs show the mean±s.d. quantification of meiosis II centriole length using four different centriole markers for each genotype. (C) Graphs show the mean±s.d. quantification of Asl or Cep135 fluorescence intensity (per unit length of centriole) for each genotype. Each point on the graphs represents the average length or fluorescence intensity measured from a single testis, and 20–40 centrioles were measured in each testis. **P*<0.05; ***P*<0.001; *****P*<0.00001; *******P*<0.0000001; ns, not significant (paired two-tailed *t*-test using number of testes analysed as the *n* value).

centrioles appear to contain at least two pools of Asl: ∼50% of the Asl protein is stably incorporated into centrioles, whereas ∼50% is in exchange with the cytoplasmic pool (Novak et al., 2014). Interestingly, Asl interacts directly with another centriole protein, Sas-4/CPAP, in both fly and human cells (Cizmecioglu et al., 2010; Dzhindzhev et al., 2010; Hatch et al., 2010), and we have shown that Sas-4 plays an important part in recruiting Asl to new mother centrioles, but is not required to maintain Asl at old mother centrioles (Novak et al., 2014; Novak et al., 2016). Perhaps Sas-4 plays a more important role in initially recruiting Asl to new mother centrioles, whereas Ana1 plays a more important role in maintaining Asl at mother centrioles.

In human cells, centrioles are destabilised in the absence of Cep295. This appears to be because the failure in centriole-to-centrosome conversion blocks the recruitment of the PCM, and the PCM is required to stabilise the centrioles after they lose their central cartwheels during the conversion process (as normally occurs in vertebrates) (Izquierdo et al., 2014). In flies, however, the centrioles do not usually lose their cartwheels during the conversion process (Gonzalez et al., 1998), so it is unclear why centrioles appear to be destabilised in the absence of Ana1 (as the permanent central cartwheel structure would presumably stabilise centrioles even when they cannot recruit PCM). We observed that centriole-like structures can be seen at the electron microscopy level in *ana1* mutant cells overexpressing Sas-6 and Ana2 (Fig. 3B), and some Sas-4-containing structures are visible in immunofluorescence images from early *ana1* mutant spermatocytes (Fu et al., 2016), suggesting that some residual centriole-like structures can persist in *ana1* mutant cells. If some residual centriole structures do persist in *ana1* mutant tissues, however, they are clearly not capable of supporting centrosome assembly (Fig. 1B) or cilium function (as *ana1* mutant flies are severely uncoordinated).

We find that Ana1 promotes centriole elongation in a dose-dependent manner: centrioles are slightly longer when Ana1 is overexpressed, and slightly shorter when *ana1* gene dosage is halved. This finding is in contrast to the observation that Ana1 depletion does not lead to a decrease in centriole length in S2 cells (Fu et al., 2016), perhaps because Ana1 depletion does not alter the length of centrioles that had already formed in the cell population prior to Ana1 depletion (and our dynamic analysis of Ana1 behaviour suggests that Ana1 is irreversibly incorporated into centrioles). Importantly, this function of Ana1 appears to have different molecular requirements to the function of Ana1 in centriole stabilisation, as the N-terminal 639 amino acids of Ana1 are not essential for centrosome assembly or cilium function, but are required to allow Ana1 to promote centriole elongation in spermatocytes and to promote centriole over-elongation when overexpressed.

Several centriole proteins can influence centriole length. Positive regulators such as Sas-4/CPAP, Cep135, Cep120 and SPICE can increase centriole length when overexpressed in human cells, and negative regulators such as CP110, Cep97 and Klp10A appear to act to suppress centriole elongation (Comartin et al., 2013; Delgehyr et al., 2012; Franz et al., 2013; Kohlmaier et al., 2009; Lin et al., 2013a,b; Mahjoub et al., 2010; Schmidt et al., 2009; Tang et al., 2009). Although it is unclear how Ana1 influences centriole length, it is intriguing that its N-terminal region, which is required to promote centriole elongation, can interact with Cep135 (Fu et al., 2016) as centrioles are shorter than normal in *Cep135* mutant spermatocytes (Mottier-Pavie and Megraw, 2009). Our data suggests, however, that Ana1 does not promote centriole elongation simply by recruiting extra Cep135 or Asl to the centrioles. Interestingly, Cep295, the human homologue of Ana1, also promotes centriole elongation in human cells (suggesting that this function is conserved), and it can interact with tubulin – potentially providing a molecular mechanism that can explain how Cep295 promotes centriole elongation (Chang et al., 2016). To our knowledge, Ana1 is the first protein shown to reduce centriole length when its gene dosage is halved, suggesting that Ana1 is a limiting factor that ensures proper centriole elongation in flies.

Journal of Cell Science (2016) 129, 2514-2525 doi:10.1242/jcs.186460

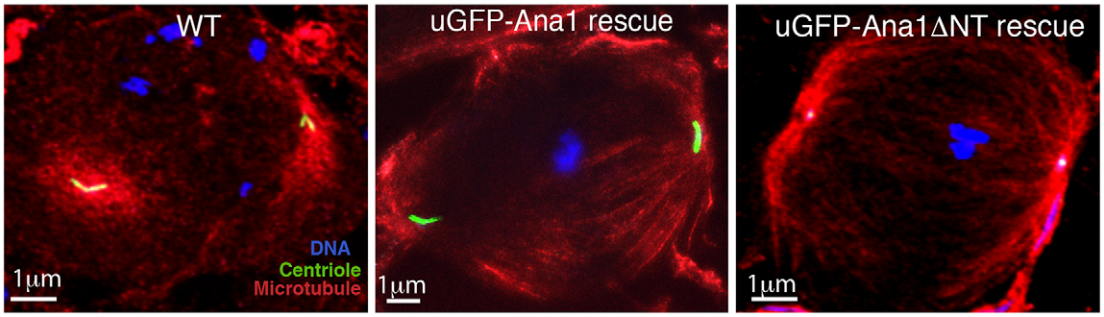

Fig. 7. GFP–Ana1ΔNT does not support centriole elongation in *ana1* mutant spermatocytes. (A) Micrographs showing *Drosophila* mature primary spermatocytes in meiosis I stained for DNA (blue), microtubules (red) and the centriole marker Asl (green) in WT cells or *ana1* mutant cells overexpressing either GFP–Ana1 or GFP–Ana1ΔNT (as indicated). Centrioles are detectable at the poles of the spindles in the *ana1* mutant cells rescued by GFP–Ana1ΔNT, but these appear dot-like and have failed to elongate.

MATERIALS AND METHODS

Fly stocks

The following fly lines were used in this study: OregonR flies (used as WT), flies expressing eAna1–GFP and eAsl–GFP at endogenous levels (Blachon et al., 2008), $ana1^{mecB}$ mutant flies (Avidor-Reiss et al., 2004), RFP–PACT-expressing flies (Lucas and Raff, 2007), flies expressing eAsl–mCherry at endogenous levels, and the asl^{B46} mutant (Baumbach et al., 2015). The transgenic lines contain GFP fusions expressed from the Ubq promoter, which drives moderate expression in all tissues (Lee et al., 1988): GFP–Ana1 (WT), Ana1(WT)–GFP, Sas-6–GFP and Cep135–GFP (this study); GFP–Sas-6 (Peel et al., 2007); Asl–GFP, GFP–Ana2 and Ana2–GFP, and GFP–Ana1ΔNT (Stevens et al., 2010a) and GFP-Cep135 (Roque et al., 2012). The *Df(3R)Exel7357* that uncovers the *ana1* gene was obtained from the Bloomington *Drosophila* Stock Center (BDSC). Throughout this study flies or cells referred to as '*ana1* mutant' have the genotype $ana1^{mecB}$/*Df(3R)Exe7357*.

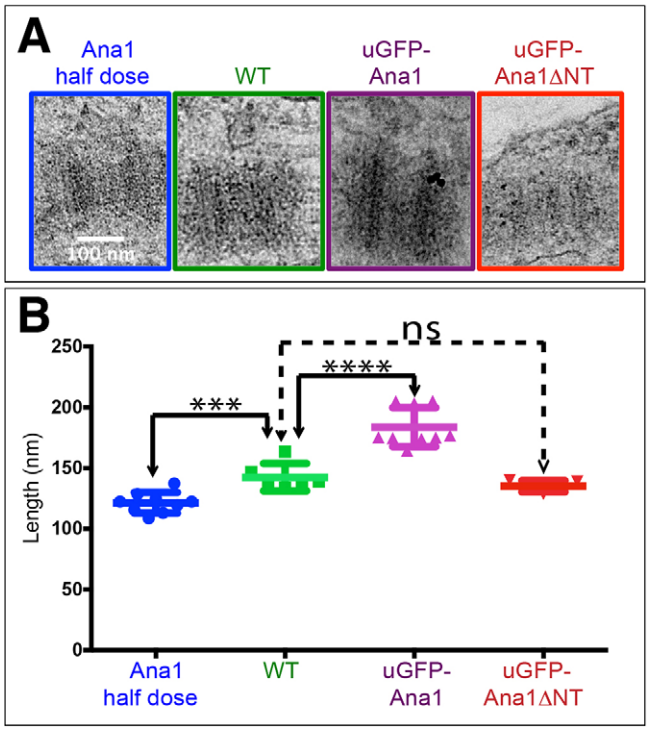

Fig. 8. Ana1 levels influence centriole length in wing disc cells. (A) Electron micrographs showing images of centrioles viewed in longitudinal cross section in wing discs from *ana1* heterozygous mutants (containing only one copy of the WT gene), WT, WT overexpressing GFP–Ana1 and WT overexpressing GFP–Ana1ΔNT. (B) Graph quantifying the mean±s.d. centriole length (determined from electron microscopy images that were scored blindly) showing that the pattern of centriole length variation observed in spermatocyte centrioles (see Fig. 6) is also observed in wing disc centrioles. Each point on the graph represents the average centriole length of ten centrioles in an individual wing disc (nine, six, nine, and five wing discs were scored, respectively). ***P<0.0001, ****P<0.00001; ns, not significant (paired two-tailed t-test using number of wing discs analysed as the n value).

Antibodies for immunofluorescence and western blotting

The following primary antibodies were used for immunofluorescence: rabbit anti-Asl (Conduit and Raff, 2010), guinea-pig anti-Asl (Roque et al., 2012), rat anti-Asl (Franz et al., 2013), mouse anti-GTU88* (Sigma-Aldrich), mouse anti-α-tubulin (DM1 α; Sigma-Aldrich), rabbit anti-Cnn (Lucas and Raff, 2007), sheep anti-Cnn (Conduit et al., 2014a), rabbit anti-Ana1CT (Stevens et al., 2010a), rabbit anti-Ana1Mid (Conduit and Raff, 2010), guinea-pig anti-Ana1 (Conduit et al., 2014b), rat anti-Ana1CT (this study), rabbit anti-Sas4 (Basto et al., 2006) and rabbit anti-Spd-2 (Dix and Raff, 2007) antibodies, all used at 1:500 (see details in Table S1). Secondary antibodies conjugated to Alexa Fluor 405, 488, 568, 594 (used for SIM) and 647 (Invitrogen) were used, all at 1:1000; GFP-booster–atto488 (ChromoTek) was used at 1:500. DNA was labelled with Hoechst 33342 (Invitrogen). Rabbit anti-Ana1 (Conduit et al., 2010) and mouse anti-actin (Sigma-Aldrich) antibodies, and appropriate horseradish peroxidase (HRP)-conjugated secondary antibodies (GE Healthcare) were used for western blotting (all 1:3000).

Generation of transgenic lines

P-element-mediated transformation vectors containing GFP fusions to Ana1 were generated by cloning the genomic region of *ana1* from the start codon up to the stop codon into the Ubq-GFP(NT) or pUAST-GFP(NT), or without the stop codon into Ubq-GFP(CT) or pUAST-GFP(CT) Gateway vectors as described previously (Basto et al., 2008). Similarly, GFP fusions to Sas6 or Cep135 at their C-terminal were generated from their respective cDNAs using the Ubq-GFPCT or pUAST-GFPCT Gateway vectors (full cloning details are available upon request). Constructs were injected and transgenic lines were generated at Bestgene (USA) or at the Department of Genetics, University of Cambridge (UK).

Immunofluorescence analysis of tissues

Drosophila brains from third-instar larvae or *Drosophila* testes from late pupae were dissected, fixed and stained as described previously (Franz et al., 2013). *Drosophila* eggs or embryos were collected, fixed and stained as described previously (Stevens et al., 2010a). Images were obtained on a confocal microscope system (Fluoview FV1000; Olympus) using a 60×1.4 NA oil objective and Fluoview software (Olympus), or on Zeiss Axioskop 2 microscope (Carl Zeiss, Ltd., UK) with a CoolSNAP HQ camera (Photometrics, Tucson, AZ) using a 63×1.25 NA objective (Zeiss) with Immersol oil (Zeiss) and MetaMorph software (Molecular Devices). All live-cell images acquired were analysed using Volocity software (Perkin

Journal of Cell Science

Elmer). Quantification of centriole length in spermatocytes by assessing immunofluorescence images was performed as described previously (Franz et al., 2013). Quantification of Asl and Cep135 mean intensities per µm of centriole length in spermatocytes by assessing immunofluorescence images was performed in Fiji (ImageJ 1.48f) using the line tool (line width=9). Background fluorescence was subtracted before obtaining the final value. Quantification of SAP numbers per cell, SAP intensity and SAP area was performed using Volocity software (Perkin Elmer) by manually drawing a region of interest (ROI) around each SAP. Data was analysed in Prism (version 6.0 for Mac OSX, GraphPad Software, Inc).

Live-cell imaging

Embryos (1–2-hours-old) were imaged, and individual centrosomes photobleached, on a Perkin Elmer ERS Spinning Disc confocal system on a Zeiss Axiovert microscope, using a 63×1.4 NA, oil-immersion objective. A total of 11 or 13 confocal sections were collected from each embryo (0.5-µm steps) every 20 or 30 s and were analysed using Volocity software (Perkin Elmer, USA) as described previously (Novak et al., 2014). Data was analysed and curve fitting performed in Prism (version 6.0 for Mac OSX, GraphPad Software, Inc).

3D-SIM and analysis

Preparation, fixation and staining of squashed late-pupal testes for 3D-SIM was as described previously (Franz et al., 2013). Images were taken at 21°C on an OMX-V3 system (GE Healthcare) with a 60×1.42 NA oil objective (Olympus) and SIM reconstruction was performed with SoftWorx software (Applied Precision). Different image channels were aligned using 200-nm TetraSpeck (Thermo Fisher Scientific) bead slides as reference for the transformation. Images shown are maximum intensity projections of several *z*-slices in the central area of the centrioles that were processed in Fiji (ImageJ 1.48f). GFP protein radial diameters were calculated by fitting a double-Gaussian curve to the average fluorescence intensity profile of each protein (obtained by drawing ten lines through each centriole and averaging the intensity profile of each line, as indicated by the white lines in the GFP–Ana1 panel in Fig. 4A); the distance between the two peaks was measured in Fiji (ImageJ 1.48f). Where it was not possible to resolve the two peaks, the diameters were measured by fitting the intensity profile crossing the centriole centre to two Gaussian curves of equal heights and standard deviations. The radial diameter calculated is the distance between the centre positions of each Gaussian peak. Analysis was performed with GNU Octave version 4.0.0 and Octave Forge optim package version 1.4.1. Data was analysed in Prism (version 6.0 for Mac OSX, GraphPad Software, Inc).

Western blotting

Protein extracts from embryos, brains, wing discs and testes were separated on protein gels as described previously (Novak et al., 2014). In brief, samples containing ten embryos, two brains, four wing discs or two testes were run on NuPAGE 3–8% Tris-acetate pre-cast gels (Life Technologies). The proteins were transferred onto Biorad nitrocellulose membrane and loading was initially checked using Ponceau staining. The membrane was then blocked with 4% milk powder, 0.1% Tween-20 in PBS and probed with antibodies against Ana1, and against actin as a loading control.

Transmission electron microscopy

Wing discs from third-instar larvae and testes from late pupae were dissected in PBS and prepared as described previously (Stevens et al., 2010b). Semi-thin serial sections (100 nm) were obtained by using a Reichert-Jung Ultracut E (Leica Microsystems, Austria) and stained in lead citrate. To measure centriole length in interphase cells from wing discs, images of centrioles in longitudinal orientation were taken on a TECNAI T12 transmission microscope (FEI, The Netherlands) at 11,000× or 18,500× magnification. The length of the microtubule doublets within the electron-dense area was measured using the line tool in Fiji (ImageJ 1.48f). Data were analysed in Prism (version 6.0 for Mac OSX, GraphPad Software, Inc). For measurement of the number of testes SAPs, semi-thick serial sections (150 nm) were obtained and dual-axis tilt series (typically −55°–55°) were acquired in a TECNAI T12 transmission microscope (FEI) at 13,000× magnification with SerialEM. Using the IMOD software package (Mastronarde, 2005) the images were aligned, and the tomograms were reconstructed.

In vitro mRNA production and injection

The complete coding region of Ana1 protein was amplified from cDNA IP16240 (DGRC) with att sites at either end, and inserted into the Gateway pDONR-Zeo vector (Invitrogen). Ana1 deletions were generated by site-directed mutagenesis of pDonor-Zeo-Ana1 (after repairing the missing 67 bp from the available Ana1 cDNA), using the Quikchange II XL mutagenesis kit (Agilent). Deletions were cloned in Gateway vectors (Invitrogen) into the pRNAGFP destination vector (Conduit et al., 2014a). WT or truncated versions of Ana1 fused to an N-terminal GFP mRNA were synthesised and injected into early embryos expressing eAsl–mCherry as described previously (Cottee et al., 2013; Richens et al., 2015). Syncytial stage embryos were imaged on a Perkin Elmer microscope and analysed using Volocity software (Perkin Elmer) as described previously (Novak et al., 2014). Briefly, we measured the total GFP or mCherry fluorescence in a boxed region centred around the centrosomes and subtracted the local cytoplasmic background fluorescence (n=10 centrosomes from five embryos for each construct). Each value was normalised to the averaged WT signal (set to one). The Fluorescence values were compared using a *t*-test (unpaired). Data was analysed in Prism (version 6.0 for Mac OSX, GraphPad Software, Inc).

Acknowledgements

We thank present and past members of the Raff laboratory for advice and comments on the manuscript, Matthew Cottee for his assistance in analysing the predicted coiled-coil domains of Ana1, the Micron Oxford Advanced Bioimaging Unit for access to the OMX 3D-SIM system, and Errin Johnson for electron microscopy assistance at the Dunn School Bioimaging Facility.

Competing interests

The authors declare no competing or financial interests.

Author contributions

S.S. designed and performed the majority of experiments and helped write the manuscript. H.R. performed electron tomography on SAPs. Z.A.N. and A.V. helped design and perform initial experiments on Ana1 dynamics, and M.G.A. helped with the analysis and curve fitting of these experiments. B.S. repaired and constructed the WT pRNA GFPAna1 vector. A.W. helped design the 3D-SIM experiments. D.M.S.P. wrote the program to calculate the radial diameter of the centriole markers. J.W.R. designed experiments and helped to write the manuscript.

Funding

S.S., H.R., Z.A.N., A.W. and J.W.R. were supported by a Wellcome Trust Senior Investigator Award [grant number 104575]; A.W. and D.M.S.P. were supported by a Wellcome Trust Strategic Award to the Micron Oxford Advanced Bioimaging Unit [grant number 091911]. M.G.A. was supported by an Edward Penley Abraham (EPA) Research Fund PhD studentship; A.V. was supported by a Wellcome Trust PhD studentship; and B.S. was supported by Excellence Master Fellowships, Faculty of Science, University of Geneva, Switzerland. Deposited in PMC for immediate release.

Supplementary information

Supplementary information available online at
http://jcs.biologists.org/lookup/doi/10.1242/jcs.186460.supplemental

References

Arquint, C., Gabryjonczyk, A.-M., Imseng, S., Böhm, R., Sauer, E., Hiller, S., Nigg, E. A. and Maier, T. (2015). STIL binding to Polo-box 3 of PLK4 regulates centriole duplication. *Elife* **4**, e07888.

Avidor-Reiss, T., Maer, A. M., Koundakjian, E., Polyanovsky, A., Keil, T., Subramaniam, S. and Zuker, C. S. (2004). Decoding cilia function: defining specialized genes required for compartmentalized cilia biogenesis. *Cell* **117**, 527-539.

Azimzadeh, J. (2014). Exploring the evolutionary history of centrosomes. *Philos. Trans. R. Soc. Lond. B Biol. Sci.* **369**, 20130453.

Basto, R., Lau, J., Vinogradova, T., Gardiol, A., Woods, C. G., Khodjakov, A. and Raff, J. W. (2006). Flies without centrioles. *Cell* **125**, 1375-1386.

Basto, R., Brunk, K., Vinadogrova, T., Peel, N., Franz, A., Khodjakov, A. and Raff, J. W. (2008). Centrosome amplification can initiate tumorigenesis in flies. *Cell* **133**, 1032-1042.

Baumbach, J., Novak, Z. A., Raff, J. W. and Wainmann, A. (2015). Dissecting the function and assembly of acentriolar microtubule organizing centers in Drosophila cells in vivo. *PLoS Genet.* **11**, e1005261.
Bettencourt-Dias, M., Rodrigues-Martins, A., Carpenter, L., Riparbelli, M., Lehmann, L., Gatt, M. K., Carmo, N., Balloux, F., Callaini, G. and Glover, D. M. (2005). SAK/PLK4 is required for centriole duplication and flagella development. *Curr. Biol.* **15**, 2199-2207.
Bettencourt-Dias, M., Hildebrandt, F., Pellman, D., Woods, G. and Godinho, S. A. (2011). Centrosomes and cilia in human disease. *Trends Genet.* **27**, 307-315.
Blachon, S., Gopalakrishnan, J., Omori, Y., Polyanovsky, A., Church, A., Nicastro, D., Malicki, J. and Avidor-Reiss, T. (2008). Drosophila asterless and vertebrate Cep152 Are orthologs essential for centriole duplication. *Genetics* **180**, 2081-2094.
Blachon, S., Cai, X., Roberts, K. A., Yang, K., Polyanovsky, A., Church, A. and Avidor-Reiss, T. (2009). A proximal centriole-like structure is present in Drosophila spermatids and can serve as a model to study centriole duplication. *Genetics* **182**, 133-144.
Callaini, G. and Riparbelli, M. G. (1990). Centriole and centrosome cycle in the early Drosophila embryo. *J. Cell Sci.* **97**, 539-543.
Chang, C.W., Hsu, W.B., Tsai, J.J., Tang, C.C. and Tang, T.K. (2016) CEP295 interacts with microtubules and is required for centriole elongation. *J. Cell Sci.* **129**, 2501-2513.
Cizmecioglu, O., Arnold, M., Bahtz, R., Settele, F., Ehret, L., Haselmann-Weiß, U., Antony, C. and Hoffmann, I. (2010). Cep152 acts as a scaffold for recruitment of Plk4 and CPAP to the centrosome. *J. Cell Biol.* **191**, 731-739.
Comartin, D., Gupta, G. D., Fussner, E., Coyaud, É., Hasegan, M., Archinti, M., Cheung, S. W. T., Pinchev, D., Lawo, S., Raught, B. et al. (2013). CEP120 and SPICE1 cooperate with CPAP in centriole elongation. *Curr. Biol.* **23**, 1360-1366.
Conduit, P. T. and Raff, J. W. (2010). Cnn dynamics drive centrosome size asymmetry to ensure daughter centriole retention in Drosophila neuroblasts. *Curr. Biol.* **20**, 2187-2192.
Conduit, P. T., Brunk, K., Dobbelaere, J., Dix, C. I., Lucas, E. P. and Raff, J. W. (2010). Centrioles regulate centrosome size by controlling the rate of Cnn incorporation into the PCM. *Curr. Biol.* **20**, 2178-2186.
Conduit, P. T., Feng, Z., Richens, J. H., Baumbach, J., Wainmann, A., Bakshi, S. D., Dobbelaere, J., Johnson, S., Lea, S. M. and Raff, J. W. (2014a). The centrosome-specific phosphorylation of Cnn by Polo/Plk1 drives Cnn scaffold assembly and centrosome maturation. *Dev. Cell* **28**, 659-669.
Conduit, P. T., Richens, J. H., Wainmann, A., Holder, J., Vicente, C. C., Pratt, M. B., Dix, C. I., Novak, Z. A., Dobbie, I. M., Schermelleh, L. et al. (2014b). A molecular mechanism of mitotic centrosome assembly in Drosophila. *Elife* **3**, e03399.
Conduit, P. T., Wainmann, A. and Raff, J. W. (2015a). Centrosome function and assembly in animal cells. *Nat. Rev. Mol. Cell Biol.* **16**, 611-624.
Conduit, P. T., Wainmann, A., Novak, Z. A., Weil, T. T. and Raff, J. W. (2015b). Re-examining the role of Drosophila Sas-4 in centrosome assembly using two-colour-3D-SIM FRAP. *Elife* **4**, 1032.
Cottee, M. A., Muschalik, N., Wong, Y. L., Johnson, C. M., Johnson, S., Andreeva, A., Oegema, K., Lea, S. M., Raff, J. W. and van Breugel, M. (2013). Crystal structures of the CPAP/STIL complex reveal its role in centriole assembly and human microcephaly. *Elife* **2**, e01071.
Cottee, M. A., Muschalik, N., Johnson, S., Leveson, J., Raff, J. W. and Lea, S. M. (2015). The homo-oligomerisation of both Sas-6 and Ana2 is required for efficient centriole assembly in flies. *Elife* **4**, e07236.
Delattre, M., Canard, C. and Gönczy, P. (2006). Sequential protein recruitment in C. elegans centriole formation. *Curr. Biol.* **16**, 1844-1849.
Delgehyr, N., Rangone, H., Fu, J., Mao, G., Tom, B., Riparbelli, M. G., Callaini, G. and Glover, D. M. (2012). Klp10A, a microtubule-depolymerizing kinesin-13, cooperates with CP110 to control Drosophila centriole length. *Curr. Biol.* **22**, 502-509.
Dix, C. I. and Raff, J. W. (2007). Drosophila Spd-2 recruits PCM to the sperm centriole, but is dispensable for centriole duplication. *Curr. Biol.* **17**, 1759-1764.
Dobbelaere, J., Josué, F., Suijkerbuijk, S., Baum, B., Tapon, N. and Raff, J. (2008). A genome-wide RNAi screen to dissect centriole duplication and centrosome maturation in Drosophila. *PLoS Biol.* **6**, e224.
Dzhindzhev, N. S., Yu, Q. D., Weiskopf, K., Tzolovsky, G., Cunha-Ferreira, I., Riparbelli, M., Rodrigues-Martins, A., Bettencourt-Dias, M., Callaini, G. and Glover, D. M. (2010). Asterless is a scaffold for the onset of centriole assembly. *Nature* **467**, 714-718.
Dzhindzhev, N. S., Tzolovsky, G., Lipinszki, Z., Schneider, S., Lattao, R., Fu, J., Debski, J., Dadlez, M. and Glover, D. M. (2014). Plk4 phosphorylates Ana2 to trigger Sas6 recruitment and procentriole formation. *Curr. Biol.* **24**, 2526-2532.
Fırat-Karalar, E. N. and Stearns, T. (2014). The centriole duplication cycle. *Philos. Trans. R. Soc. Lond. B Biol. Sci.* **369**, 20130460-20130460.
Franz, A., Roque, H., Saurya, S., Dobbelaere, J. and Raff, J. W. (2013). CP110 exhibits novel regulatory activities during centriole assembly in Drosophila. *J. Cell Biol.* **203**, 785-799.
Fu, J. and Glover, D. M. (2012). Structured illumination of the interface between centriole and peri-centriolar material. *Open Biol.* **2**, 120104.
Fu, J., Lipinszki, Z., Rangone, H., Min, M., Mykura, C., Chao-Chu, J., Schneider, S., Dzhindzhev, N. S., Gottardo, M., Riparbelli, M. G. et al. (2016). Conserved molecular interactions in centriole-to-centrosome conversion. *Nat. Cell Biol.* **18**, 87-99.
Gönczy, P. (2012). Towards a molecular architecture of centriole assembly. *Nat. Rev. Mol. Cell Biol.* **13**, 425-435.
Gonzalez, C., Tavosanis, G. and Mollinari, C. (1998). Centrosomes and microtubule organisation during Drosophila development. *J. Cell Sci.* **111**, 2697-2706.
Goshima, G., Wollman, R., Goodwin, S. S., Zhang, N., Scholey, J. M., Vale, R. D. and Stuurman, N. (2007). Genes required for mitotic spindle assembly in Drosophila S2 cells. *Science* **316**, 417-421.
Habedanck, R., Stierhof, Y.-D., Wilkinson, C. J. and Nigg, E. A. (2005). The Polo kinase Plk4 functions in centriole duplication. *Nat. Cell Biol.* **7**, 1140-1146.
Hatch, E. M., Kulukian, A., Holland, A. J., Cleveland, D. W. and Stearns, T. (2010). Cep152 interacts with Plk4 and is required for centriole duplication. *J. Cell Biol.* **191**, 721-729.
Hatzopoulos, G. N., Erat, M. C., Cutts, E., Rogala, K. B., Slater, L. M., Stansfeld, P. J. and Vakonakis, I. (2013). Structural analysis of the G-box domain of the microcephaly protein CPAP suggests a role in centriole architecture. *Structure* **21**, 2069-2077.
Hsu, W.-B., Hung, L.-Y., Tang, C.-J. C., Su, C.-L., Chang, Y. and Tang, T. K. (2008). Functional characterization of the microtubule-binding and -destabilizing domains of CPAP and d-SAS-4. *Exp. Cell Res.* **314**, 2591-2602.
Izquierdo, D., Wang, W.-J., Uryu, K. and Tsou, M.-F. B. (2014). Stabilization of cartwheel-less centrioles for duplication requires CEP295-mediated centriole-to-centrosome conversion. *Cell Rep.* **8**, 957-965.
Jana, S. C., Marteil, G. and Bettencourt-Dias, M. (2014). Mapping molecules to structure: unveiling secrets of centriole and cilia assembly with near-atomic resolution. *Curr. Opin. Cell Biol.* **26**, 96-106.
Kim, T.-S., Park, J.-E., Shukla, A., Choi, S., Murugan, R. N., Lee, J. H., Ahn, M., Rhee, K., Bang, J. K., Kim, B. Y. et al. (2013). Hierarchical recruitment of Plk4 and regulation of centriole biogenesis by two centrosomal scaffolds, Cep192 and Cep152. *Proc. Natl. Acad. Sci. USA* **110**, E4849-E4857.
Kitagawa, D., Vakonakis, I., Olieric, N., Hilbert, M., Keller, D., Olieric, V., Bortfeld, M., Erat, M. C., Flückiger, I., Gönczy, P. et al. (2011). Structural basis of the 9-fold symmetry of centrioles. *Cell* **144**, 364-375.
Kohlmaier, G., Loncarek, J., Meng, X., McEwen, B. F., Mogensen, M. M., Spektor, A., Dynlacht, B. D., Khodjakov, A. and Gönczy, P. (2009). Overly long centrioles and defective cell division upon excess of the SAS-4-related protein CPAP. *Curr. Biol.* **19**, 1012-1018.
Kratz, A.-S., Bärenz, F., Richter, K. T. and Hoffmann, I. (2015). Plk4-dependent phosphorylation of STIL is required for centriole duplication. *Biol. Open* **4**, 370-377.
Lee, H. S., Simon, J. A. and Lis, J. T. (1988). Structure and expression of ubiquitin genes of Drosophila melanogaster. *Mol. Cell. Biol.* **8**, 4727-4735.
Lettman, M. M., Wong, Y. L., Viscardi, V., Niessen, S., Chen, S.-H., Shiau, A. K., Zhou, H., Desai, A. and Oegema, K. (2013). Direct binding of SAS-6 to ZYG-1 recruits SAS-6 to the mother centriole for cartwheel assembly. *Dev. Cell* **25**, 284-298.
Lin, Y.-C., Chang, C.-W., Hsu, W.-B., Tang, C.-J. C., Lin, Y.-N., Chou, E.-J., Wu, C.-T. and Tang, T. K. (2013a). Human microcephaly protein CEP135 binds to hSAS-6 and CPAP, and is required for centriole assembly. *EMBO J.* **32**, 1141-1154.
Lin, Y.-N., Wu, C.-T., Lin, Y.-C., Hsu, W.-B., Tang, C.-J. C., Chang, C.-W. and Tang, T. K. (2013b). CEP120 interacts with CPAP and positively regulates centriole elongation. *J. Cell Biol.* **202**, 211-219.
Lucas, E. P. and Raff, J. W. (2007). Maintaining the proper connection between the centrioles and the pericentriolar matrix requires Drosophila centrosomin. *J. Cell Biol.* **178**, 725-732.
Mahjoub, M. R., Xie, Z. and Stearns, T. (2010). Cep120 is asymmetrically localized to the daughter centriole and is essential for centriole assembly. *J. Cell Biol.* **191**, 331-346.
Mastronarde, D. N. (2005). Automated electron microscope tomography using robust prediction of specimen movements. *J. Struct. Biol.* **152**, 36-51.
Martinez-Campos, M., Basto, R., Baker, J., Kernan, M. and Raff, J. W. (2004). The Drosophila pericentrin-like protein is essential for cilia/flagella function but appears to be dispensable for mitosis. *J. Cell Biol.* **165**, 673-683.
Mennella, V., Keszthelyi, B., McDonald, K. L., Chhun, B., Kan, F., Rogers, G. C., Huang, B. and Agard, D. A. (2012). Subdiffraction-resolution fluorescence microscopy reveals a domain of the centrosome critical for pericentriolar material organization. *Nat. Cell Biol.* **14**, 1159-1168.
Mottier-Pavie, V. and Megraw, T. L. (2009). Drosophila bld10 is a centriolar protein that regulates centriole, basal body, and motile cilium assembly. *Mol. Biol. Cell* **20**, 2605-2614.
Moyer, T. C., Clutario, K. M., Lambrus, B. G., Daggubati, V. and Holland, A. J. (2015). Binding of STIL to Plk4 activates kinase activity to promote centriole assembly. *J. Cell Biol.* **209**, 863-878.
Nigg, E. A. and Raff, J. W. (2009). Centrioles, centrosomes, and cilia in health and disease. *Cell* **139**, 663-678.

Journal of Cell Science

Novak, Z. A., Conduit, P. T., Wainmann, A. and Raff, J. W. (2014). Asterless licenses daughter centrioles to duplicate for the first time in Drosophila embryos. *Curr. Biol.* **24**, 1276-1282.

Novak, Z. A., Wainmann, A., Gartenmann, A., and Raff, J. W. (2016). Cdk1 phosphorylates Drosophila Sas-4 to recruit Polo to daughter centrioles and convert them to centrosomes. *Developmental Cell.*, in press. doi:10.1016/j.devcel.2016.05.022fc.

Ohta, M., Ashikawa, T., Nozaki, Y., Kozuka-Hata, H., Goto, H., Inagaki, M., Oyama, M. and Kitagawa, D. (2014). Direct interaction of Plk4 with STIL ensures formation of a single procentriole per parental centriole. *Nat. Commun.* **5**, 5267.

Park, S.-Y., Park, J.-E., Kim, T.-S., Kim, J. H., Kwak, M.-J., Ku, B., Tian, L., Murugan, R. N., Ahn, M., Komiya, S. et al. (2014). Molecular basis for unidirectional scaffold switching of human Plk4 in centriole biogenesis. *Nat. Struct. Mol. Biol.* **21**, 696-703.

Peel, N., Stevens, N. R., Basto, R. and Raff, J. W. (2007). Overexpressing centriole-replication proteins in vivo induces centriole overduplication and de novo formation. *Curr. Biol.* **17**, 834-843.

Pelletier, L., O'Toole, E., Schwager, A., Hyman, A. A. and Müller-Reichert, T. (2006). Centriole assembly in Caenorhabditis elegans. *Nature* **444**, 619-623.

Qiao, R., Cabral, G., Lettman, M. M., Dammermann, A. and Dong, G. (2012). SAS-6 coiled-coil structure and interaction with SAS-5 suggest a regulatory mechanism in C. elegans centriole assembly. *EMBO J.* **31**, 4334-4347.

Richens, J. H., Barros, T. P., Lucas, E. P., Peel, N., Pinto, D. M. S., Wainmann, A. and Raff, J. W. (2015). The Drosophila Pericentrin-like-protein (PLP) cooperates with Cnn to maintain the integrity of the outer PCM. *Biol. Open* **4**, 1052-1061.

Rodrigues-Martins, A., Bettencourt-Dias, M., Riparbelli, M., Ferreira, C., Ferreira, I., Callaini, G. and Glover, D. M. (2007). DSAS-6 organizes a tube-like centriole precursor, and its absence suggests modularity in centriole assembly. *Curr. Biol.* **17**, 1465-1472.

Roque, H., Wainmann, A., Richens, J., Kozyrska, K., Franz, A. and Raff, J. W. (2012). Drosophila Cep135/Bld10 maintains proper centriole structure but is dispensable for cartwheel formation. *J. Cell Sci.* **125**, 5881-5886.

Schmidt, T. I., Kleylein-Sohn, J., Westendorf, J., Le Clech, M., Lavoie, S. B., Stierhof, Y.-D. and Nigg, E. A. (2009). Control of Centriole Length by CPAP and CP110. *Curr. Biol.* **19**, 1005-1011.

Sonnen, K. F., Gabryjonczyk, A.-M., Anselm, E., Stierhof, Y.-D. and Nigg, E. A. (2013). Human Cep192 and Cep152 cooperate in Plk4 recruitment and centriole duplication. *J. Cell Sci.* **126**, 3223-3233.

Stevens, N. R., Dobbelaere, J., Brunk, K., Franz, A. and Raff, J. W. (2010a). Drosophila Ana2 is a conserved centriole duplication factor. *J. Cell Biol.* **188**, 313-323.

Stevens, N. R., Roque, H. and Raff, J. W. (2010b). DSas-6 and Ana2 coassemble into tubules to promote centriole duplication and engagement. *Dev. Cell* **19**, 913-919.

Tang, C.-J. C., Fu, R.-H., Wu, K.-S., Hsu, W.-B. and Tang, T. K. (2009). CPAP is a cell-cycle regulated protein that controls centriole length. *Nat. Cell Biol.* **11**, 825-831.

Tang, C.-J. C., Lin, S.-Y., Hsu, W.-B., Lin, Y.-N., Wu, C.-T., Lin, Y.-C., Chang, C.-W., Wu, K.-S. and Tang, T. K. (2011). The human microcephaly protein STIL interacts with CPAP and is required for procentriole formation. *EMBO J.* **30**, 4790-4804.

van Breugel, M., Hirono, M., Andreeva, A., Yanagisawa, H.-A., Yamaguchi, S., Nakazawa, Y., Morgner, N., Petrovich, M., Ebong, I.-O., Robinson, C. V. et al. (2011). Structures of SAS-6 suggest its organization in centrioles. *Science* **331**, 1196-1199.

Supplementary Material

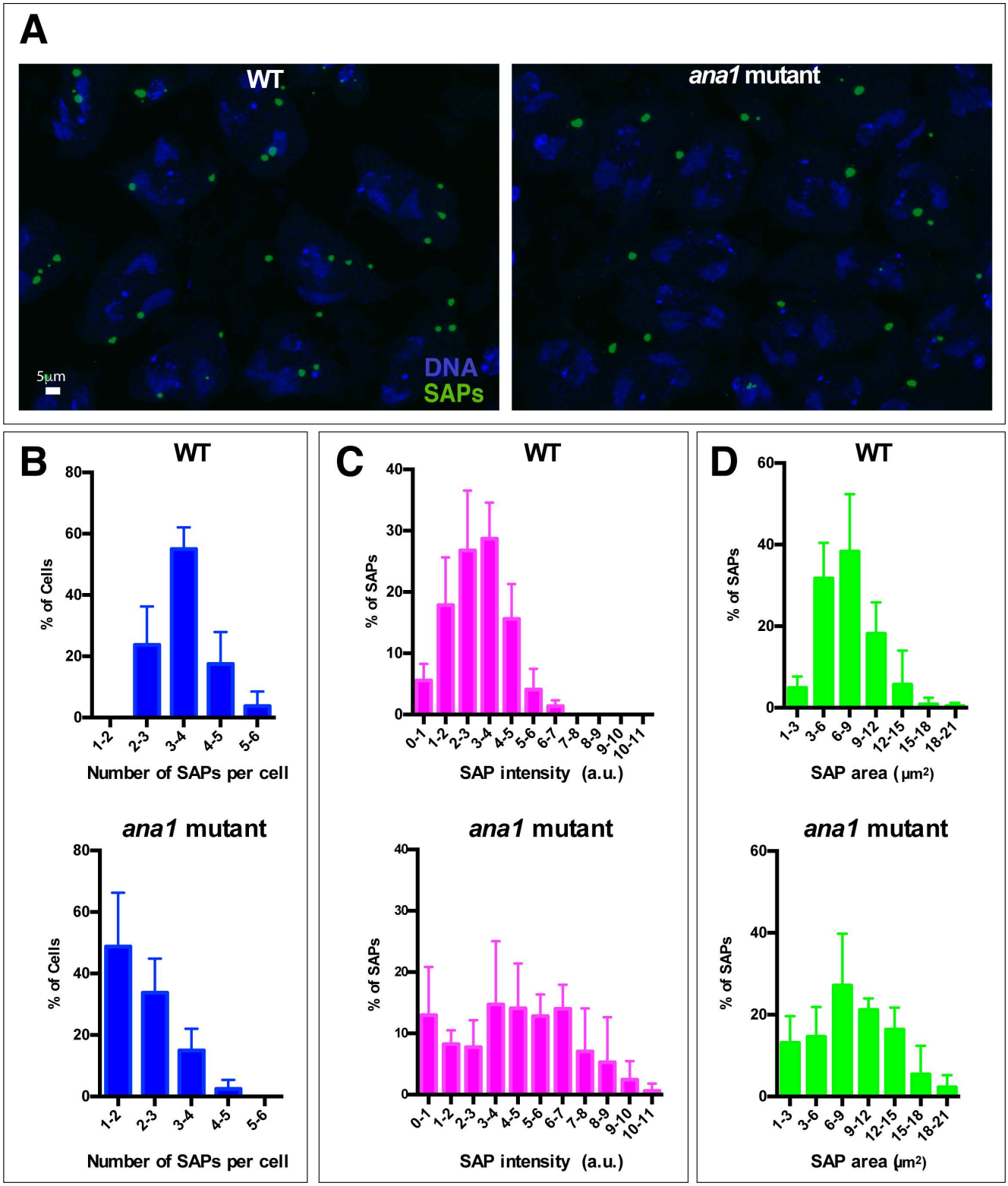

Journal of Cell Science • Supplementary information

Figure S1

SAP assembly is subtly altered in the absence of Ana1. (A) Micrographs show SAPs (*green*) in primary spermatocytes from WT (left panel) or *ana1* mutant (right panel) *Drosophila* late pupal testes. The tissue was stained with Hoechst to stain the DNA (*blue*)**. (B-D)** Graphs quantify the number of SAPs per cell (B), the sum SAP fluorescence intensity (C), and the average area of SAPs per cell in WT (top graphs) or *ana1* mutant (bottom graphs) spermatocytes. These data show that SAPs are less abundant and larger than normal in *ana1* mutant spermatocytes. Error bars represent SD. N=20 spermatocytes per testis and 4 testes per genotype.

Journal of Cell Science • Supplementary information

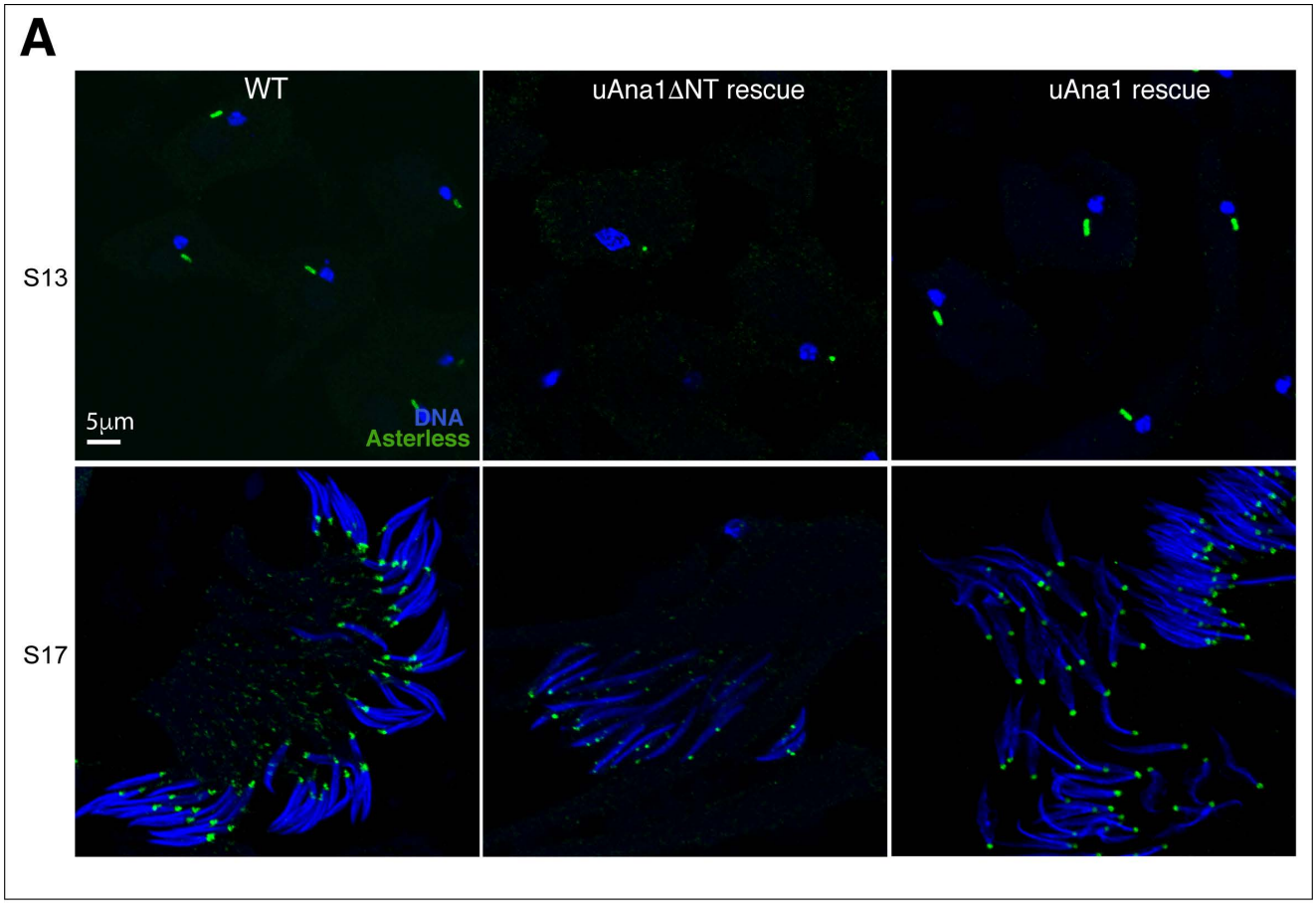

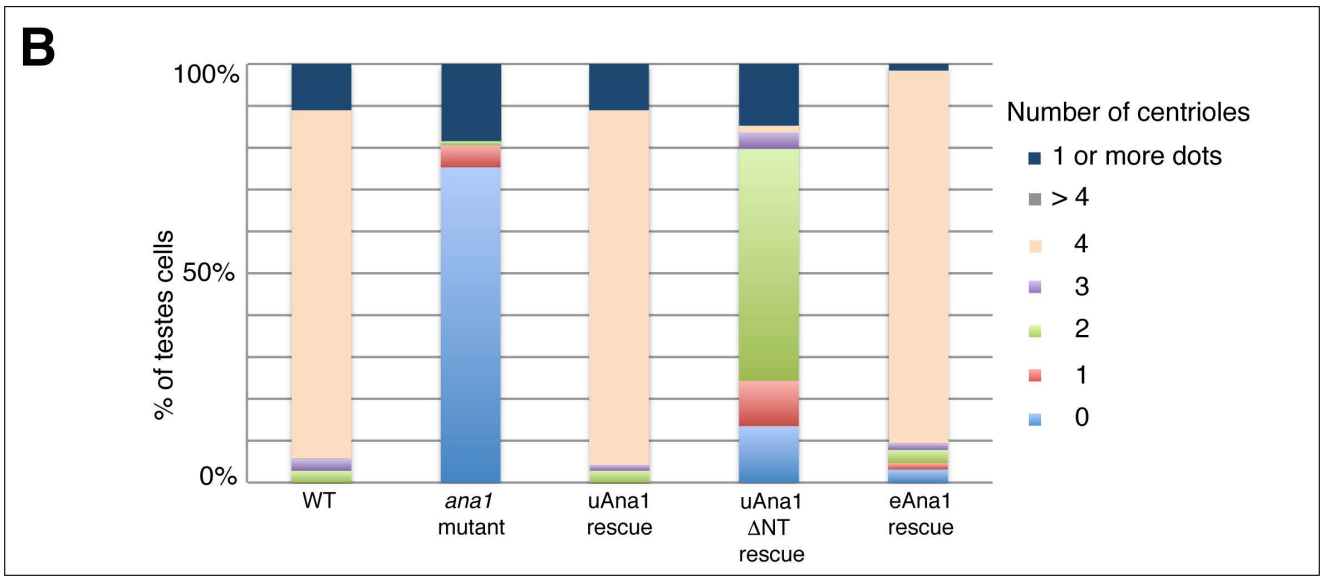

Journal of Cell Science • Supplementary information

Figure S2

Ana1 levels influence centriole length. (A) Micrographs show *Drosophila* early S13 spermatids (top panels) at the onion stage (before axoneme formation) or S17 spermatids (bottom panels) during the process of axoneme elongation. Cells were stained for DNA (*blue*) and Asterless (centriole/basal body marker) (*green*) from WT (left panels) or *ana1* mutant rescued with either uGFP-Ana1ΔNT (middle panels) or uGFP-Ana1 (right panels). Note the non-elongated dot-like centrioles/basal bodies in the mutant cells rescued with uGFP-Ana1ΔNT. **(B)** Graphs illustrate the quantification of the percentage of primary spermatocytes of *Drosophila* late pupal testes exhibiting different numbers of centrosomes (n=62 total cells from 5 different testes) in WT, *ana1* mutant, *ana1* mutant rescued by the different transgenes (as indicated). Note that in primary spermatocytes there are normally 4 elongated centrioles per cell, but in the ana1 mutants rescued by GFP-Ana1ΔNT the centrioles were so short that the centriole pair could no longer be resolved, and so we counted these as 2 centrioles per cell (see Figure 7). Note also that we scored for the presence of occasional dot-like structures (“dots”) that were stained by both Asl and Cnn antibodies.

Journal of Cell Science • Supplementary information

JCB Journal of Cell Biology

ARTICLE

A homeostatic clock sets daughter centriole size in flies

Mustafa G. Aydogan[1], Alan Wainman[1,2], Saroj Saurya[1], Thomas L. Steinacker[1], Anna Caballe[1], Zsofia A. Novak[1], Janina Baumbach[1], Nadine Muschalik[1], and Jordan W. Raff[1]

Centrioles are highly structured organelles whose size is remarkably consistent within any given cell type. New centrioles are born when Polo-like kinase 4 (Plk4) recruits Ana2/STIL and Sas-6 to the side of an existing "mother" centriole. These two proteins then assemble into a cartwheel, which grows outwards to form the structural core of a new daughter. Here, we show that in early *Drosophila melanogaster* embryos, daughter centrioles grow at a linear rate during early S-phase and abruptly stop growing when they reach their correct size in mid- to late S-phase. Unexpectedly, the cartwheel grows from its proximal end, and Plk4 determines both the rate and period of centriole growth: the more active the centriolar Plk4, the faster centrioles grow, but the faster centriolar Plk4 is inactivated and growth ceases. Thus, Plk4 functions as a homeostatic clock, establishing an inverse relationship between growth rate and period to ensure that daughter centrioles grow to the correct size.

Introduction

How organelles grow to the right size is a fundamental problem in cell biology (Marshall, 2016). For many organelles, however, this question is difficult to address: the number and distribution of an organelle within a cell can vary, and it can also be difficult to determine whether an organelle's surface area, volume, or perhaps the amount of a limiting component, best defines its size. Centrioles are highly structured organelles that form centrosomes and cilia (Nigg and Raff, 2009). Their length can vary by an order of magnitude between different species and tissues but is very consistent within a given cell type. Centrioles are potentially an attractive system with which to study organelle size control (Goehring and Hyman, 2012; Marshall, 2016), as their numbers are precisely regulated: most cells are born with a single centriole pair that is duplicated once per cell cycle, when a single daughter centriole grows outwards from each mother centriole during S-phase. Moreover, the highly ordered structure of the centriole means that the complex 3D question of organelle size control can be simplified to a 1D question of daughter centriole length control.

Much progress has been made recently in understanding the molecular mechanisms of centriole duplication (Fırat-Karalar and Stearns, 2014; Arquint and Nigg, 2016; Banterle and Gönczy, 2017). Polo-like kinase 4 (Plk4) initiates duplication and is first recruited in a ring surrounding the mother centriole; this ring ultimately resolves into a single "dot" that marks the site of daughter centriole assembly (Sonnen et al., 2012; Kim et al., 2013; Ohta et al., 2014). Plk4 recruits and phosphorylates Ana2/STIL, which helps recruit Sas-6 to initiate the assembly of the ninefold-symmetric cartwheel that forms the structural backbone of the growing daughter centriole (Kitagawa et al., 2011; van Breugel et al., 2011; Ohta et al., 2014; Dzhindzhev et al., 2014; Kratz et al., 2015). How Plk4 is ultimately localized to a single site on the side of the mother is unclear, but Plk4 can dimerize and autophosphorylate itself in trans to trigger its own destruction (Rogers et al., 2009; Guderian et al., 2010; Holland et al., 2010; Cunha-Ferreira et al., 2013). In addition, binding to Ana2/STIL activates Plk4's kinase activity (Moyer et al., 2015) and also appears to stabilize Plk4 (Ohta et al., 2014; Arquint et al., 2015). Thus, the binding of Plk4 to Ana2/STIL at a single site on the side of the mother could activate and protect the kinase at this site, whereas the remaining Plk4 around the mother centriole is degraded (Ohta et al., 2014; Moyer et al., 2015; Arquint and Nigg, 2016; Banterle and Gönczy, 2017).

Although these studies provide important insight into how mother centrioles grow only a single daughter, the question of how daughter centrioles subsequently grow to the correct length has been difficult to address (Winey and O'Toole, 2014). This is in part because centrioles are small structures (usually 100–500

[1]Sir William Dunn School of Pathology, University of Oxford, Oxford, England, UK; [2]Micron Oxford Advanced Bioimaging Unit, Department of Biochemistry, University of Oxford, Oxford, England, UK.

Correspondence to Jordan W. Raff: jordan.raff@path.ox.ac.uk; J. Baumbach's and N. Muschalik's present address is Medical Research Council Laboratory of Molecular Biology, University of Cambridge, Cambridge, England, UK.

© 2018 Aydogan et al. This article is available under a Creative Commons License (Attribution 4.0 International, as described at https://creativecommons.org/licenses/by/4.0/).

nm in length), making it hard to directly monitor the kinetics of centriole growth. Also, cells usually only assemble two daughter centrioles per cell cycle, and this makes it difficult to measure centriole growth in a quantitative manner. The early *Drosophila melanogaster* embryo is an established model for studying centriole and centrosome assembly (Lattao et al., 2017), and it is potentially an attractive system for measuring the kinetics of daughter centriole growth. First, it is a multinucleated single cell (a syncytium) that undergoes 13 rounds of nearly synchronous, rapid nuclear divisions (Foe and Alberts, 1983). During nuclear cycles 10–14, the majority of nuclei (and their associated centrioles) form a monolayer at the cortex, allowing the simultaneous observation of many centrioles as they rapidly and synchronously progress through repeated rounds of S-phase and mitoses without intervening gap phases (Foe and Alberts, 1983). Second, centrioles in flies are structurally simpler than those in vertebrates (Callaini and Riparbelli, 1990; Moritz et al., 1995; Callaini et al., 1997). All centrioles start to assemble around the cartwheel in S-phase, but vertebrate centrioles often exhibit a second phase of growth during G2/M, when the centriolar microtubules (MTs) extend past the cartwheel (Kuriyama and Borisy, 1981; Chrétien et al., 1997). Fly centrioles usually do not exhibit this second phase of growth, so the centrioles are relatively short, and the cartwheel extends throughout the length of the daughter centriole (González et al., 1998; Lattao et al., 2017). We reasoned, therefore, that the fluorescence incorporation of the cartwheel components Sas-6-GFP or Ana2-GFP could potentially be used as a proxy to measure daughter centriole length in *D. melanogaster* embryos.

We show here that this is the case, and we provide the first quantitative description of the kinetics of daughter centriole growth in a living cell. Our findings reveal an unexpected inverse relationship between the centriole growth rate and growth period: in embryos where daughter centrioles tend to grow slowly, they tend to grow for a longer period. Surprisingly, Plk4 influences both the centriole growth rate and growth period and helps coordinate the inverse relationship between them. Thus, Plk4 functions as a homeostatic clock that helps to ensure daughter centrioles grow to the correct size in fly embryos.

Results

The cartwheel protein Sas-6 is incorporated irreversibly into growing daughter centrioles

To establish an assay to monitor centriole growth kinetics, we tested whether Sas-6 and/or Ana2 are stably incorporated into growing daughter centrioles. We generated transgenic lines expressing either Sas-6-GFP or Ana2-GFP under the control of their own promoters and in their respective mutant backgrounds (Fig. S1, A and B). These fusion proteins significantly rescued the severe uncoordinated phenotype (caused by the lack of centrioles) in their respective mutant backgrounds (Fig. S1, C and D; and Videos 1 and 2). 3D structured illumination microscopy (SIM) FRAP (Conduit et al., 2015) revealed that Sas-6-GFP and Ana2-GFP were both incorporated into growing daughter centrioles during S-phase; but, whereas Ana2-GFP turned over at the mother centrioles, Sas-6-GFP did not (Fig. 1). Thus, during the time course of these experiments, Sas-6-GFP is incorporated exclusively and irreversibly into the growing daughter centriole, making it a suitable marker to monitor daughter centriole growth kinetics.

Centrioles grow approximately linearly during early S-phase but abruptly stop growing in mid-late S-phase

We analyzed the kinetics of Sas-6-GFP incorporation into daughter centrioles in individual *Sas-6* mutant embryos during nuclear cycle 12, using spinning-disk confocal microscopy to track Sas-6-GFP foci (comprising the mother and growing daughter centriole, which cannot be resolved on this microscope system) from early S-phase, when the two separating mother centrioles first become visible as distinct entities (Fig. 2 A and Video 3). When measured at a single centriole pair, Sas-6-GFP levels tended to increase over time, but the data were noisy and it was difficult to discern a consistent pattern (Fig. 2 B). When measurements from >100 centriole pairs from the same embryo were averaged, however, a clear pattern emerged (Fig. 2 C). We used regression analysis to fit the mean data from each embryo to several different growth models (Figs. S2 and S3; see Materials and methods): centriole growth was usually best described by a period of linear growth in early-S-phase that plateaued in mid-to-late S-phase, presumably when the growing centrioles had reached their correct size, and this plateau continued into mitosis. A similar pattern of "linear growth in S-phase followed by a plateau in mitosis" has been reported previously for GFP:SAS-6 in the early worm embryo, suggesting that the dynamics of Sas-6 incorporation are likely to be conserved (Dammermann et al., 2008). From the fitted data, we extracted several growth parameters (Fig. 2 D) and used these to generate an average centriole growth profile derived from ∼1,100 individual centrioles tracked throughout S-phase in 15 individual embryos (Figs. 3 and S3). [AQ2]

Centriole length is regulated by a homeostatic inverse relationship between growth rate and period

We wondered whether the parameters of centriole growth would change as S-phase length gradually increased during embryogenesis (Foe and Alberts, 1983), so we compared the parameters of centriole growth during nuclear cycles 11–13 (Fig. 3 A). As S-phase length increased (Fig. 3 Bi), the centriole growth rate slowed (Fig. 3 Bii), but this was precisely compensated for by an increase in the growth period (Fig. 3 Biii), and thus daughter centrioles ultimately incorporated the same amount of Sas-6-GFP during each nuclear cycle, indicating that they had grown to the same length (Fig. 3 Biv). Interestingly, a similar inverse relationship between growth rate and growth period was observed between embryos that were at the same nuclear cycle (Fig. 3 C). These observations raised the intriguing possibility that centriole growth in these embryos is regulated by a homeostatic mechanism, whereby an inverse relationship between the growth rate and period ensures that daughter centrioles grow to a consistent size.

The rate and period of centriole growth are not simply determined by S-phase length

Perhaps surprisingly, there was no significant correlation between the length of S-phase and the centriole growth rate or

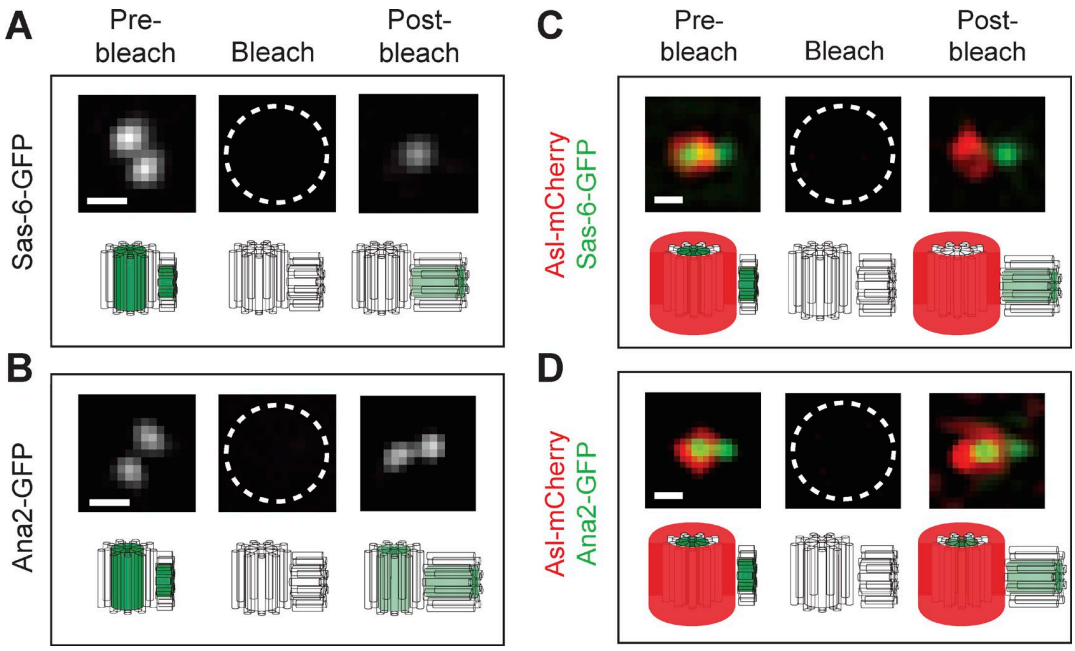

Figure 1. **Sas-6-GFP is incorporated irreversibly into the growing daughter centriole. (A and B)** Micrographs show a 3D-SIM-FRAP analysis of Sas-6-GFP (A) or Ana2-GFP (B) dynamics. A 3D-SIM image of a centriole pair was acquired in early S-phase (Pre-bleach); the centrioles were then photobleached (Bleach), and a post-bleach image was acquired 5–10 min later. **(C and D)** The same image acquisition protocol was followed in embryos that simultaneously express the mother centriole marker Asl-mCherry along with either Sas-6-GFP (C) or Ana2-GFP (D; note that bleaching the Sas-6- or Ana2-GFP, as an unintended consequence, also bleaches the Asl-mCherry fluorescence). Asl-mCherry fluorescence rapidly recovers at the mother centriole, as reported previously (Novak et al., 2014, 2016), as does Ana2-GFP fluorescence, indicating that both proteins turn over at the fully grown mother centrioles. In contrast, Sas-6-GFP does not detectably recover at the mother centriole, but does recover at the daughter. This suggests that once Sas-6-GFP molecules are incorporated into the cartwheel structure they do not turn over, at least not over the time course of these experiments. The underlying schematics illustrate our interpretation of the behavior of the GFP and mCherry fusions. Bars, 0.2 µm. *n* = 4 embryos; *n* = 15 centriole pairs for each protein in each experiment.

growth period in embryos at the same nuclear cycle (Fig. 4, A and B). To more directly test whether S-phase length influences the parameters of centriole growth, we genetically manipulated S-phase length by either halving the genetic dose of cyclin B, which leads to an increase in S-phase length (Ji et al., 2004), or by halving the genetic dose of the DNA checkpoint protein *Chk1* (*grapes* in flies), which leads to a decrease in S-phase length (Sibon et al., 1997; Fig. 4, C and D). Although there was a ∼24% difference in the length of S-phase between these two sets of embryos, the parameters of centriole growth were not significantly altered (Fig. 4 D), demonstrating that S-phase length does not directly determine the centriole growth rate or period.

Plk4 influences the rate and period of daughter centriole growth

Plk4 determines the site of daughter centriole assembly (Arquint and Nigg, 2016; Banterle and Gönczy, 2017), so we wondered whether it might also influence the parameters of daughter centriole growth. We generated a likely null allele of *Plk4* (Fig. 5 and Video 4), and then monitored Sas-6-GFP incorporation in early embryos in which we halved the genetic dose of *Plk4* (hereafter, $Plk4^{1/2}$ embryos; Fig. 6 A). $Plk4^{1/2}$ embryos hatched at normal rates (Fig. S4), and we observed no centriole duplication defects in our analysis of >1,300 duplication events. Compared with WT embryos, however, the daughter centrioles in $Plk4^{1/2}$ embryos grew more slowly, but for a longer period of time; as a result the centrioles ultimately grew to their normal size (Fig. 6, A and B). These findings support our conclusion that there is a homeostatic inverse relationship between the growth rate and growth period that ensures daughter centrioles grow to a consistent size. Moreover, they suggest that Plk4 influences both the rate and period of daughter centriole growth, and so helps to establish this inverse relationship.

We next tested the effect of either doubling the genetic dosage of *Plk4* ($Plk4^{2X}$) or expressing a previously described mutated form of Plk4 with reduced kinase activity (Holland et al., 2010; Zitouni et al., 2016; $Plk4^{RKA}$) in a WT background (Fig. 6, C–F). Both sets of embryos hatched at normal rates (Fig. S4), and we observed no centriole duplication defects in our analysis of >1,400 duplication events in each genotype. Surprisingly, however, both perturbations resulted in a significant decrease in daughter centriole size, but for different reasons: in $Plk4^{2X}$ embryos, the centrioles grew at a normal rate but for a shorter period (Fig. 6, C and D), whereas in $Plk4^{RKA}$ embryos, the centrioles grew at a slower rate but for a normal period (Fig. 6, E and F). Thus, Plk4 appears to influence the daughter centriole growth rate and growth period independently, with the extra Plk4 influencing the growth period and reduced Plk4 kinase activity influencing the growth rate.

A second assay to measure the parameters of daughter centriole growth

We wanted to confirm the kinetics of daughter centriole growth using an assay that was independent of Sas-6-GFP fluorescence

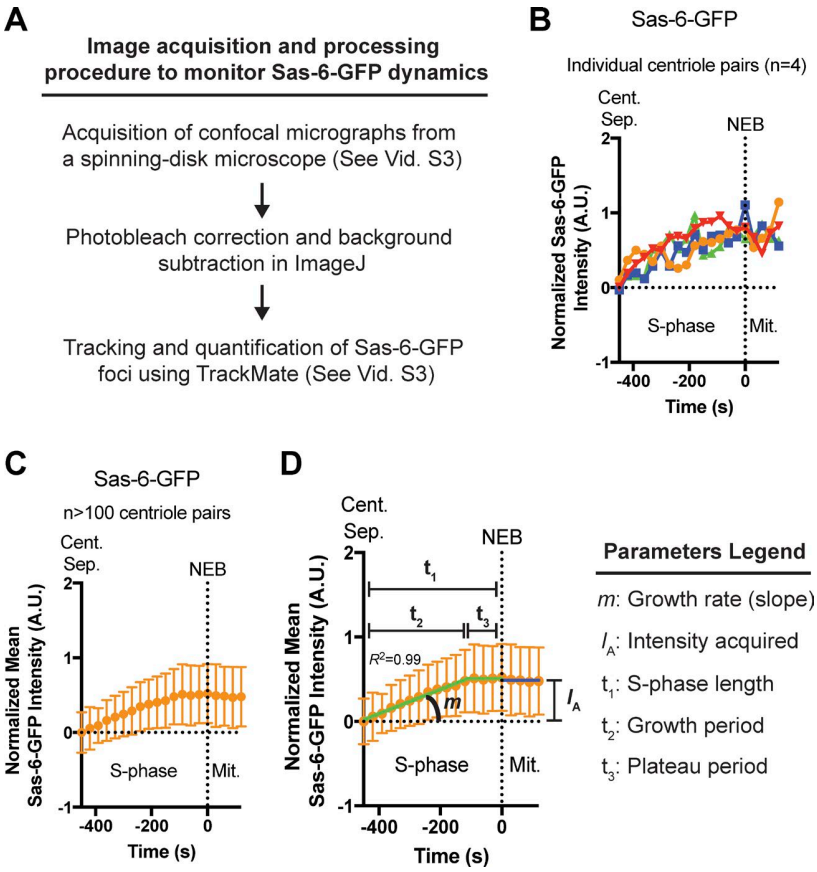

Figure 2. **Measuring the parameters of daughter centriole growth. (A)** Schematic summary of the Sas-6-GFP image acquisition and processing procedure used to monitor Sas-6-GFP dynamics over time (see also Video 3). **(B)** Graph shows the Sas-6-GFP fluorescence intensity over time measured from four different centriole-pair tracks during nuclear cycle 12 (A.U., arbitrary units; Cent. Sep., time centriole pair separation first detected at the start of S-phase; NEB, nuclear envelope breakdown). Note that when Sas-6-GFP is imaged using spinning-disk confocal microscopy, the mother and growing daughter centrioles cannot be resolved, and so they appear as a single fluorescent focus. Therefore, to measure the growth of the daughter centriole, all centriolar Sas-6-GFP intensities were normalized by subtracting the mean initial intensity of all the mother centrioles in that embryo at the start of S-phase (so that the mean Sas-6-GFP fluorescence at the start of S-phase is 0 in every embryo). **(C)** Same as in B, but the mean has been taken of the fluorescence intensity of >100 centriole pairs from the same embryo. **(D)** The S-phase (green line) and M-phase (dark blue line) data from C were fitted by regression analysis (see Fig. S2 for a summary of the models tested). R^2 is used as a measure of goodness-of-fit. From this model, several parameters of centriole growth were measured for each individual embryo (as indicated in the figure). Data are represented as mean ± SD.

incorporation. Our 3D-SIM analysis of the centrioles in early *D. melanogaster* embryos revealed that mother centrioles are usually oriented end-on to the cortex, so they appear as hollow rings (Fig. 7 A, Fig. S5, and Video 5). Thus, mother centrioles do not freely rotate in the *z*-axis, but rather adopt a relatively fixed orientation in reference to the cortex. We reasoned, therefore, that we could use the centriole distal-end binding protein GFP-Cep97 (Fig. 7 B) to measure the distance between the center of the mother centriole and the distal end of the growing daughter using Airyscan superresolution microscopy (Fig. 7 C).

We acquired superresolution images of embryos expressing GFP-Cep97, determined the center of mass (COM) of the mother and of the distal end of the growing daughter, and measured the distance between them as S-phase progressed (note that all scoring was performed blind; Fig. 7, C and D). This method produced centriole growth curves similar to the Sas-6-GFP incorporation assay in both WT and *Plk4*$^{1/2}$ embryos, confirming the kinetics of daughter centriole growth in WT embryos, and that daughter centrioles grow more slowly but for a longer period of time in *Plk4*$^{1/2}$ embryos, and so reach the same size as in WT embryos (Fig. 7 D).

Sas-6 incorporates into the proximal end of growing daughter centrioles

Our observation that Plk4 influences the parameters of daughter centriole growth led us to ask whether the centriole cartwheel grows by incorporating Sas-6 at its proximal or distal end or isotropically throughout its length (Fig. 8 A). We generated embryos expressing Sas-6-GFP and Asl-mCherry (a marker of the mother centriole; Novak et al., 2014) and allowed daughters to grow to approximately half their full size. We then acquired a superresolution fluorescence image (Fig. 8 A, T1), and measured the distance between the COM of the mother and daughter centrioles (Fig. 8 A, distance d_1). We photobleached the Sas-6-GFP (Fig. 8 A, T2)—which unintentionally also bleached the Asl-mCherry, but this fluorescence rapidly recovers (Novak et al., 2014)—allowing us to calculate the COM of the mother centriole at subsequent time points. We allowed the daughter centrioles to grow and incorporate Sas-6-GFP for 1min before acquiring a third superresolution image (Fig. 8 A, T3) and measuring the distance between the COM of the mother centriole and the newly incorporated Sas-6-GFP (Fig. 8 A, distance d_2). This analysis revealed that in nonbleached controls $d_2 > d_1$, as expected, because the daughter centriole has grown in the time between T1 and T3. In bleached centrioles, however, $d_2 < d_1$, indicating that Sas-6-GFP is incorporated into the proximal end of the growing daughter (Fig. 8 B).

As an additional control, we used the same strategy to assess whether the centriole distal-end binding protein GFP-Cep97 incorporated into the distal end of the centriole after bleaching (Fig. 8, C and D); this was the case, confirming that our methods are sensitive enough to distinguish proximal- and distal-end incorporation. It is currently unclear how Sas-6-GFP can incorporate into the proximal end of the growing cartwheel while the daughter centriole maintains an "engaged" connection to its mother.

[AQ7]

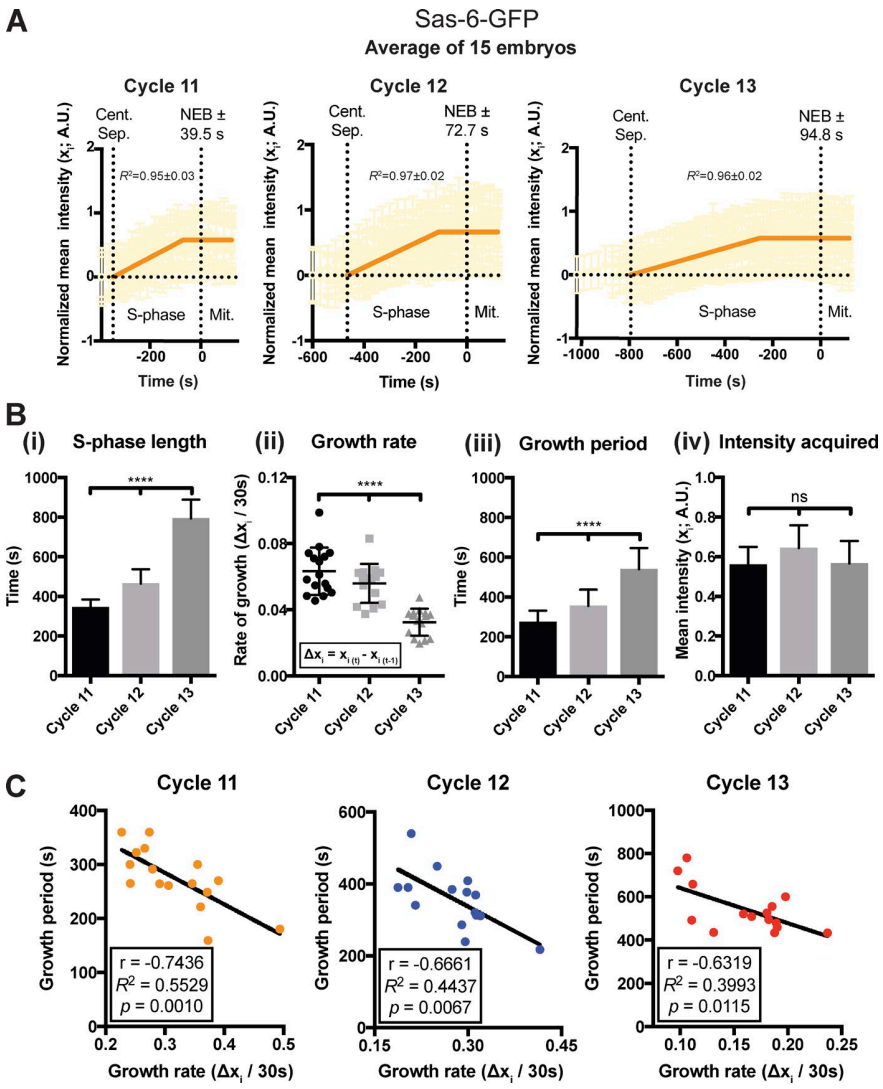

Figure 3. **An inverse relationship between the centriole growth rate and period sets daughter centriole size. (A)** Graphs show a "mean" centriolar Sas-6-GFP incorporation profile (orange line; $n \geq 15$ embryos) for embryos at nuclear cycles 11, 12, or 13. The underlying data from each embryo in this and all subsequent "mean" graphs are shown in partial opacity. The ± associated with NEB represents the SD from the mean value. A.U., arbitrary units. **(B)** Bar charts quantify several parameters of centriole growth derived from the mean Sas-6-GFP incorporation profiles shown in A. Statistical significance was assessed using either an ordinary one-way ANOVA test (for Gaussian-distributed data) or a Kruskal–Wallis test (****, $P < 0.0001$; ns, not significant). **(C)** Graphs show the inverse correlation between the centriole growth rate and growth period in individual embryos during each nuclear cycle. The data were extracted from the data shown in A. Correlation strength was examined using Pearson's correlation coefficient ($r < 0.40$ weak; $0.40 < r < 0.60$ moderate; $r > 0.6$ strong), and the significance of correlation was determined by the p-value ($P < 0.05$). $n \geq 15$ embryos for each cell cycle; $n = 96$, 174, and 326 centrioles (mean) per embryo in each cycle, respectively.

Plk4 levels oscillate at the centriole

To better understand how Plk4 might influence the parameters of centriole growth, we quantified its centriolar localization during the embryonic nuclear cycles. Plk4 is usually present at very low levels in cells (Bauer et al., 2016), and neither the localization of the endogenous protein nor its detection by Western blotting has been reported previously in flies. We therefore generated flies expressing Plk4-GFP under the control of endogenous *Plk4* promoter in the *Plk4* mutant background, where it rescued the uncoordinated fly phenotype (Fig. S1 E and Video 6) and the centriole duplication defects (Fig. 5, D and E) observed in the *Plk4* mutant.

Centriolar Plk4-GFP levels oscillated in cycling early embryos: levels were lowest at metaphase, increased during late mitosis and early S-phase, and then abruptly started to decline in early-to-mid S-phase (Fig. 9, A and B; and Video 7). This decline was not caused by photobleaching, as the level of centriolar Plk4-GFP fluorescence started to increase again after metaphase of the next mitosis. As we cannot detect endogenous Plk4 by immunofluorescence, we cannot confirm that this localization reflects the localization of the endogenous Plk4. These mutant embryos that lack endogenous Plk4 but express Plk4-GFP can survive, however, demonstrating that Plk4-GFP can support the very rapid cycles of centriole duplication that are essential for early embryo development (Stevens et al., 2007; Varmark et al., 2007; Rodrigues-Martins et al., 2008).

From these data, we infer that daughter centrioles can grow at a constant rate even as centriolar Plk4-GFP levels fluctuate (Fig. 9 B). This suggests that not all of the Plk4-GFP recruited to centrioles during S-phase directly promotes daughter centriole growth (see Discussion). Interestingly, slightly lower levels of Plk4-GFP were recruited to centrioles at each successive nuclear cycle (Fig. 9 C), potentially explaining, at least in part, why daughter centrioles grow more slowly but for a longer period of time at successive nuclear cycles. Moreover, the centriolar levels of Plk4-GFP at the start of S-phase appeared to influence the rate at which Plk4-GFP was recruited to, and then lost from, the centrioles: in nuclear cycle 11, for example, centriolar Plk4 levels were relatively high, and the rate of Plk4 recruitment to, and subsequent loss from, the centrioles was also relatively high; during nuclear cycle 13, centriolar Plk4 levels were relatively low, and the rate of Plk4 recruitment to, and subsequent loss from, the centrioles was also relatively low (Fig. 9 D). These findings

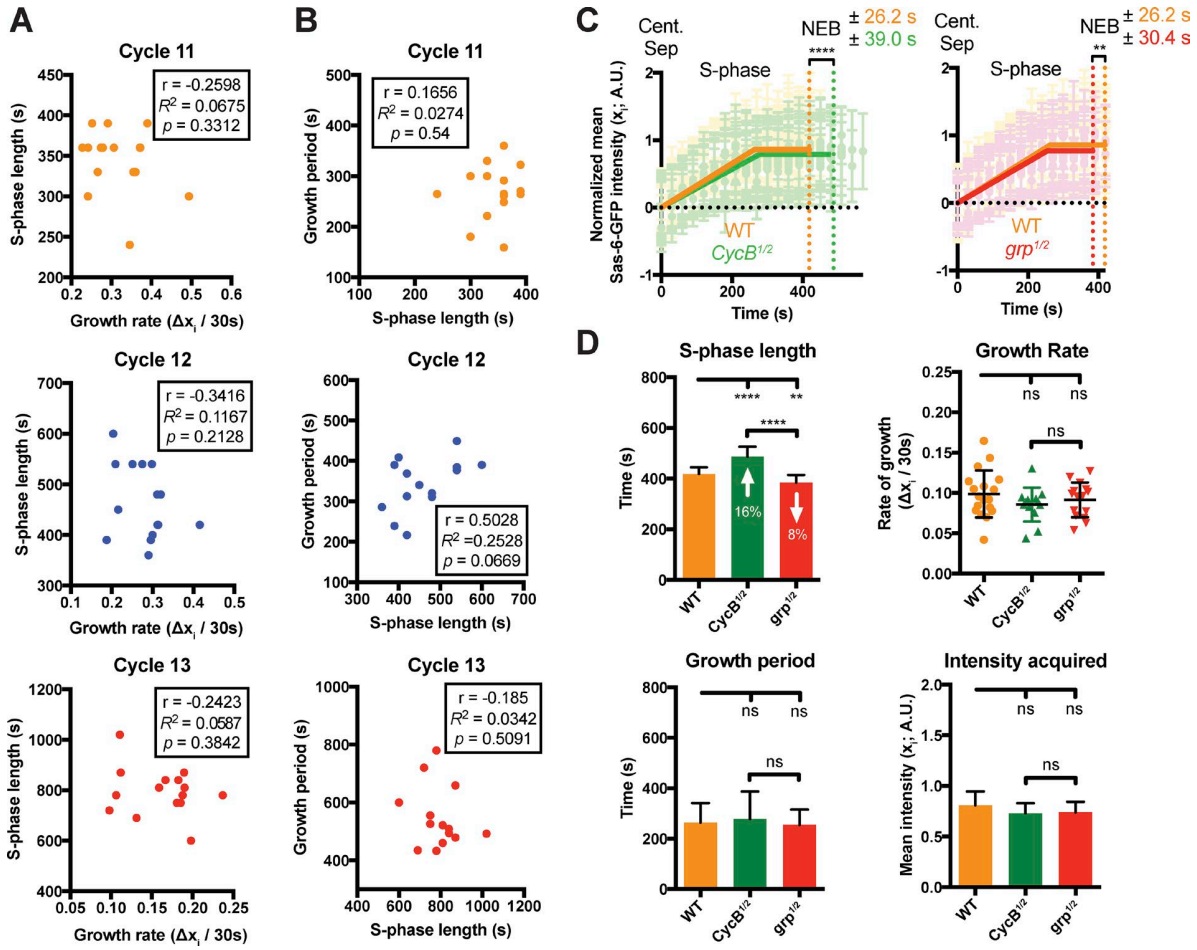

Figure 4. **The rate and period of daughter centriole growth are not directly determined by the length of S-phase. (A and B)** Graphs show the lack of a consistent correlation between the length of S-phase and either the centriole growth rate (A) or growth period (B), in each nuclear cycle. The data were extracted from the data shown in Fig. 3 A and analyzed as described in Fig. 3 C. **(C and D)** Graphs and charts illustrate and quantify centriole growth parameters in WT embryos and embryos in which either the genetic dose of Cyclin B has been halved to increase the length of S-phase (Ji et al., 2004; *CycB*$^{1/2}$ embryos) or the genetic dose of the S-phase checkpoint protein grapes (Chk1 in vertebrates) has been halved to decrease the length of S-phase (Sibon et al., 1997; *grp*$^{1/2}$ embryos); ≥13 embryos were analyzed in each case. Although S-phase is ∼24% longer in *CycB*$^{1/2}$ embryos compared with *grp*$^{1/2}$ embryos, the parameters of centriole growth are essentially the same in all three types of embryos. Statistical significance was assessed using either an unpaired *t* test with Welch's correction (for Gaussian-distributed data) or an unpaired Mann–Whitney test (**, P < 0.01; ****, P < 0.0001; ns, not significant). A.U., arbitrary units. *n* ≥ 13 embryos for each group; *n* = 184, 140, and 122 centrioles (mean) from WT, *CycB*$^{1/2}$, and *grp*$^{1/2}$ embryos, respectively.

suggest that the levels of centriolar Plk4 at the start of S-phase can influence how fast Plk4 is subsequently recruited to, and then lost from, the centrioles.

Discussion

Several models have been proposed to explain how daughter centrioles might grow to the correct size (Goehring and Hyman, 2012; Marshall, 2015, 2016; Banterle and Gönczy, 2017), but none of these have been tested, primarily because of the lack of a quantitative description of centriole growth kinetics. Our observations suggest an unexpected, yet relatively simple, model by which centriolar Plk4 might determine daughter centriole length in flies (Fig. 10).

We propose that a small fraction of centriolar Plk4, perhaps the fraction bound to both Asl and Ana2 (Fig. 10, pink stars), influences both the rate of cartwheel growth (by determining the rate of Sas-6 and Ana2 recruitment to the centriole) and the period of cartwheel growth (by determining the rate of Plk4 recruitment to the centriole, and so how quickly centriolar Plk4 accumulates to trigger its own destruction). This model is consistent with our observation that daughter centrioles grow at a relatively constant rate even as centriolar levels of Plk4 fluctuate (indicating that the majority of Plk4 located at the centriole during S-phase is not directly promoting daughter centriole growth) and that centriolar Plk4 levels appear to influence the rate at which Plk4 is accumulated at centrioles (suggesting that Plk4 can recruit itself, either directly or indirectly, to centrioles).

In this model, Plk4 functions as a homeostatic clock, regulating both the rate and period of daughter centriole growth, and ensuring an inverse relationship between them: the more "active" the Plk4, the faster the daughters grow, but the faster Plk4 is recruited and so inactivated. The activity of this Plk4 fraction is probably a function of both the total amount of Plk4

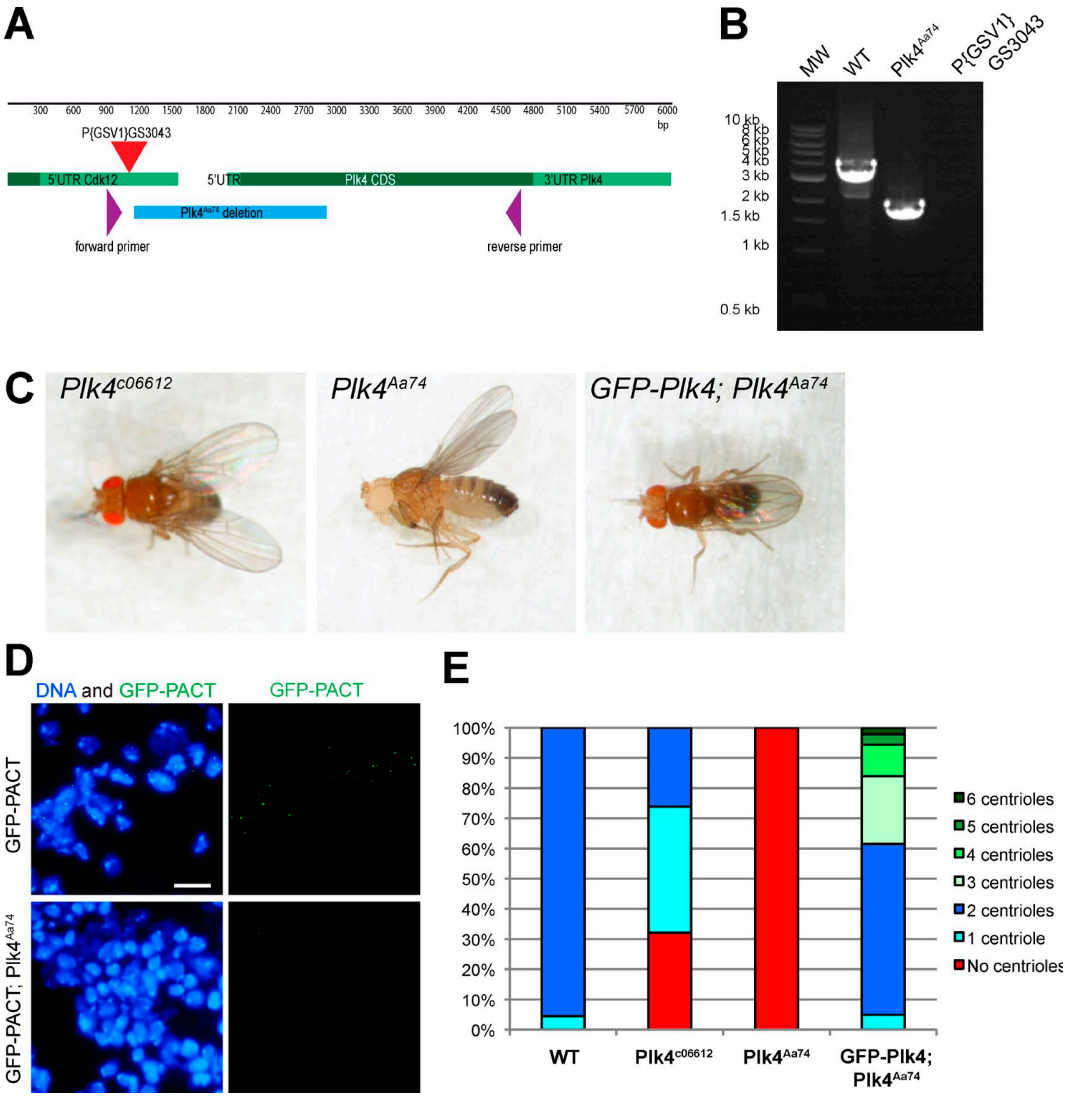

Figure 5. **Generation of the *Plk4^{Aa74}* mutant allele.** Previous studies of *Plk4* have used the weak hypomorphic *Plk4^{c06612}* allele (Bettencourt-Dias et al., 2005), so we generated a stronger allele (*Plk4^{Aa74}*) by imprecise excision of the *Plk4^{c06612}* P-element. **(A)** The schematic shows the *PLK4* genomic region, indicating the coding sequence (CDS; dark green), the UTRs (light green), the position of the original P{GSV1}GS3043 P-element insertion (red triangle), the position of the primers used to screen for imprecise excision of the P-element (purple), and the position of the Aa74 deletion (which deletes essentially the entire protein kinase domain; blue). **(B)** DNA gel shows the PCR products observed when these primers were used to amplify DNA from either WT flies or the homozygous *Plk4^{Aa74}* deletion flies. Sequencing of the PCR products confirmed deletion of the 1,751-bp region indicated in A. MW stands for molecular weight marker as a unit label. **(C)** Photographs of adult flies taken without anesthesia (see also Video 4): the original *Plk4^{c06612}* mutant flies can maintain a normal body posture and walk in a partially uncoordinated manner; *Plk4^{Aa74}* flies are highly uncoordinated and appear to lack all proprioception, as is typical of flies lacking centrioles (Basto et al., 2006); GFP-Plk4 expression rescues the uncoordinated phenotype of *Plk4^{Aa74}* mutant flies. **(D)** Micrographs show WT or *Plk4^{Aa74}* third-instar larval brains, with DNA stained with Hoechst (blue) and centrioles revealed with GFP-PACT staining (green). Bar, 10 µm. **(E)** Bar chart quantifies the number of centrioles in mitotic larval brain cells of various genotypes (as indicated). *n* = 12 brains; *n* = 264 cells *in toto* for WT; 5 brains, 237 cells for *Plk4^{c06612}*; 7 brains, 355 cells for *Plk4^{Aa74}*; 4 brains, 143 cells for GFP-Plk4; *Plk4^{Aa74}*. Collectively, these data indicate that the *Plk4^{Aa74}* allele behaves as a null or strong hypomorph.

in this fraction and its kinase activity. We speculate that this activity is determined before the start of S-phase by a complex web of interactions between Plk4, Ana2, Sas-6, and Asl that influence each other's recruitment and stability and also, directly or indirectly, Plk4's kinase activity (Ohta et al., 2014; Arquint et al., 2015; Klebba et al., 2015; Moyer et al., 2015). These interactions are likely to be regulated by external factors (such as the basic cell cycle machinery), allowing cells to set centriole growth parameters according to their needs. In cells with a G1 period, for example, Plk4 could be activated as cells progress from mitosis into G1, allowing the mother centriole to recruit an appropriate amount of Sas-6 and Ana2/STIL at this stage, which could then be incorporated into the cartwheel when cells enter S-phase. This could explain why in some somatic cells Plk4 levels appear to be higher during mitosis/G1 than in S-phase (Rogers et al., 2009; Sillibourne et al., 2010; Ohta et al., 2014), and why Plk4 kinase activity appears to be required primarily during G1, rather than S-phase (Zitouni et al., 2016).

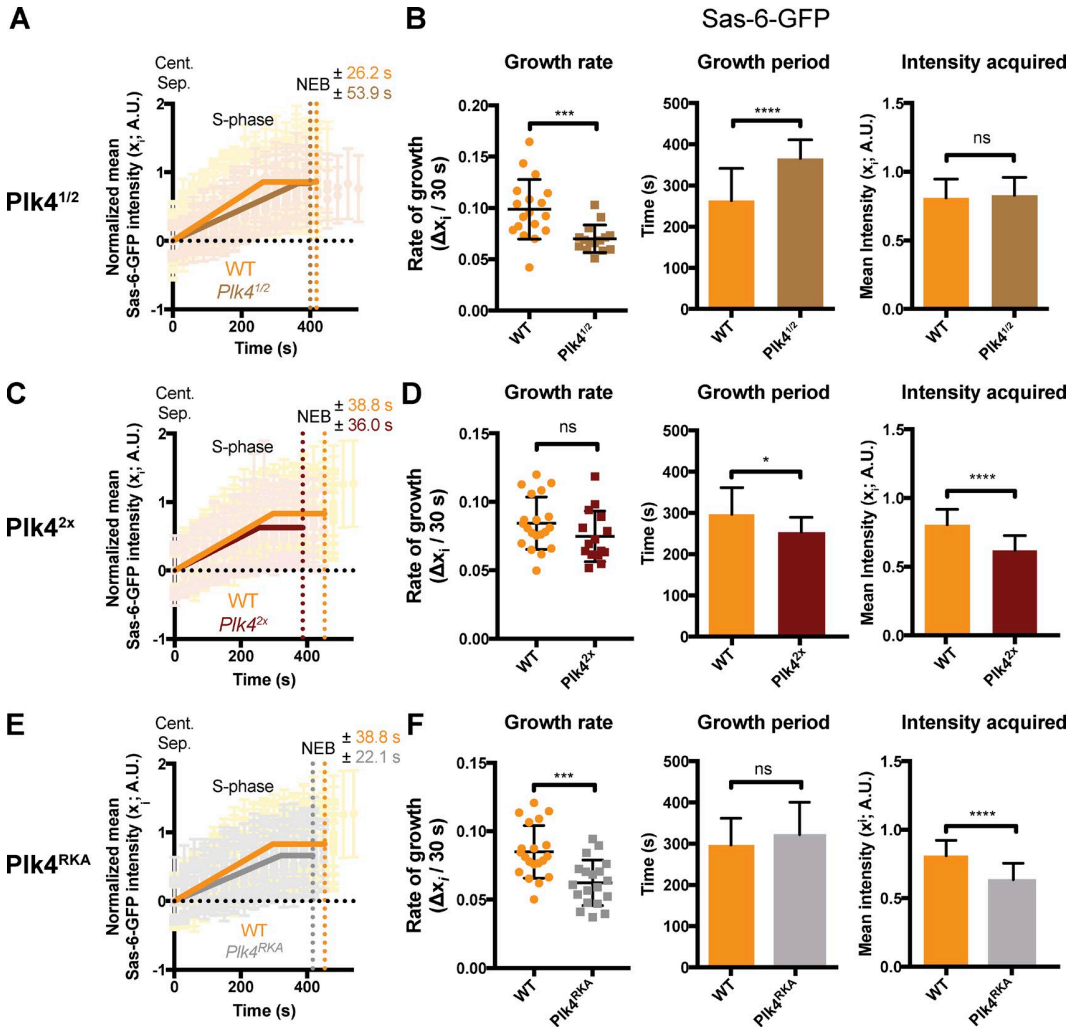

Figure 6. **Plk4 levels influence the rate and period of centriole growth. (A)** Graphs compare the mean Sas-6-GFP incorporation profile during nuclear cycle 12 in WT embryos (orange) and *Plk4*$^{1/2}$ embryos (brown). **(B)** Charts quantify parameters of centriole growth derived from the Sas-6-GFP incorporation profiles in A. **(C–F)** Graphs and charts show the same analysis for *Plk4*^{2x} (dark brown) and *Plk4*^{RKA} embryos (gray). Data are represented as mean ± SD ($n \geq 15$ embryos for each group). Statistical significance was assessed using either an unpaired *t* test with Welch's correction (for Gaussian-distributed data) or an unpaired Mann–Whitney test (*, P < 0.05; ***, P < 0.001; ****, P < 0.0001; ns, not significant). A.U., arbitrary units. $n \geq 15$ embryos for each group; n = 92, 84, 98, and 39 centrioles (mean) from each WT, *Plk4*$^{1/2}$, *Plk4*^{2x}, and *Plk4*^{RKA} embryo, respectively.

This model can explain why halving the dose of Plk4 leads to a decrease in the growth rate and an increase in the growth period: halving the dose of Plk4 would be predicted to lower both the kinase activity of centriolar Plk4 (so slowing the growth rate) and the amount of centriolar Plk4 (so increasing the growth period). It can also potentially explain why doubling the dose of Plk4 might change the growth period without changing the growth rate: increasing the dose could lead to an increased rate of Plk4 recruitment (because of its increased cytoplasmic concentration), without increasing the amount or kinase activity of the Plk4 fraction bound to Asl or Ana2 (if these were already near saturation). Finally, it could explain why decreasing the kinase activity of Plk4 decreases the rate of growth without changing the growth period: the decrease in Plk4 kinase activity might affect the rate at which it recruits Ana2/Sas-6 without affecting the amount of centriolar Plk4, and so the rate at which Plk4 recruits itself to centrioles (Fig. 10).

Importantly, although the cartwheel extends throughout the entire length of the daughter centriole in worms and flies, this is not the case in vertebrates, where centrioles exhibit a second phase of growth during G2/M and the centriolar MTs grow to extend beyond the cartwheel. We suspect that the homeostatic clock mechanism we describe here may regulate the initial phase of centriole/cartwheel growth in all species, but the subsequent extension of the daughter centriole beyond the cartwheel that occurs in vertebrates will likely require a separate regulatory network. [AQ3]

To our knowledge, the concept of a homeostatic clock regulating organelle size has not been proposed previously. This mechanism is plausible for Plk4, because it can behave as a "suicide" kinase: the more active it is, the faster it will trigger its own inactivation (Rogers et al., 2009; Guderian et al., 2010; Holland et al., 2010; Cunha-Ferreira et al., 2013). This mechanism relies on delayed negative feedback, a principle that helps set both the

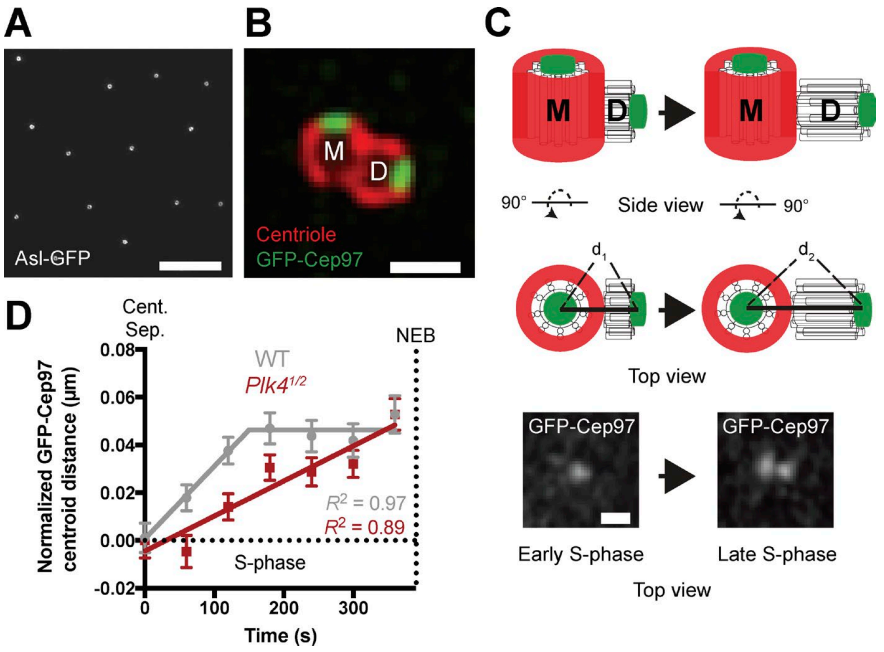

Figure 7. **A second assay to measure centriole growth using the centriole distal-end binding protein GFP-Cep97. (A)** Micrograph shows a 3D-SIM image of an embryo expressing Asl-GFP (a mother centriole marker), illustrating how mother centrioles in these embryos are preferentially oriented end-on to the cortex (so each mother centriole appears as a hollow ring; see also Fig. S5 and Video 5). Bar, 5 µm. **(B)** Micrograph shows a 3D-SIM image of a centriole pair in a fixed *D. melanogaster* spermatocyte expressing the distal-end-binding protein GFP-Cep97. These cells have unusually large centrioles (González et al., 1998), allowing one to easily distinguish the proximal and distal ends. The outer wall of the centriole is revealed by Asl-staining (red), which in spermatocytes is detected on both mother and daughter centrioles. GFP-Cep97 foci (green) are concentrated at the distal end of both the mother (M) and daughter (D) centriole. Bar, 0.5 µm. **(C)** Schematic shows how the distance between the GFP-Cep97 signal at the distal ends of the mother and daughter would be expected to increase as the centriole grows from early S-phase (d_1) to late S-phase (d_2). The schematic shows the centriole pair viewed both from the side and the top of the mother. The latter view resembles how the centrioles would usually be viewed in the early embryo, allowing us to measure daughter centriole growth in essentially 2D rather than 3D. Micrographs below show typical images of GFP-Cep97 in early and late S-phase, acquired on a Zeiss-880 Airyscan system. Bar, 0.25 µm. **(D)** Graph shows daughter centriole length over time, measured using this GFP-Cep97 assay in WT (n = 4 embryos; n = 69 centrioles in gray) and $Plk4^{1/2}$ embryos (n = 5 embryos; n = 84 centrioles in red). These daughter centriole growth profiles are similar to those obtained using the Sas-6-GFP incorporation assay (see Fig. 6 A). Note that centriolar GFP-Cep97 levels decrease toward the end of S-phase, so we cannot accurately track the GFP-Cep97 signal up to NEB. Data are shown as mean ± SEM; R^2 is used as a measure for goodness-of-fit.

circadian clock (Knippschild et al., 2005) and the somite segmentation clock (Lewis and Ozbudak, 2007). A similar mechanism might operate with other kinases that influence organelle biogenesis and whose activity accelerates their own inactivation, such as PKC, which regulates lysosome biogenesis (Feng and Hannun, 1998; Gould and Newton, 2008; Li et al., 2016). It will be interesting to determine whether homeostatic clock mechanisms that rely on delayed negative feedback could regulate organelle size more generally.

Materials and methods

D. melanogaster stocks and husbandry

The specific *D. melanogaster* stocks used in this study are listed in Table S1, and the lines generated and tested here are listed in Table S2. Sas-6-, Ana2-, and Plk4-GFP constructs were made by cloning the genetic region of *Sas-6*, *ana2*, and *PLK4*, respectively, from 2 kb upstream of the start codon up to (but excluding) the stop codon, into pDONR-Zeo vector (Thermo Fisher Scientific), which was then recombined with the pUAST-GFPCT vector (pTWG-1076; Drosophila Genomics Resource Centre) via Gateway technology (Thermo Fisher Scientific). To generate a Plk4 construct without any fluorescent tag, the endogenous Plk4 stop codon was introduced to the Plk4 pDONR (just described) by site-directed mutagenesis, using the Quikchange II XL mutagenesis kit (Agilent Technologies). To generate a Plk4 construct with reduced kinase activity ($Plk4^{RKA}$), the L89G substitution (Holland et al., 2010; Zitouni et al., 2016) was introduced into the Plk4 coding sequence by site-directed mutagenesis, using the Quikchange II XL mutagenesis kit (Agilent Technologies). Both constructs were then recombined with the pUAS-G-empty vector (this study; details available on request). The primer sequences used in the Gateway cloning for each gene are listed in Table S3. Transgenic lines were generated by the Fly Facility in the Department of Genetics, University of Cambridge (Cambridge, England, UK).

The $Plk4^{Aa74}$ allele was generated by inducing an imprecise excision of the P-element P{GSV1}GS3043 (Kyoto Stock Center, Kyoto Institute of Technology) located 996 bp upstream of the *PLK4* start codon. The resulting 1,751-bp deletion (Fig. 5 A) removed the first third of the coding sequence, including all sequences encoding the kinase domain (Fig. 5 B). $Plk4^{Aa74}$ mutant flies were viable but uncoordinated, unlike the hypomorphic $Plk4^{c06612}$ flies that retained some coordination (Fig. 5 C and Video 4). The uncoordinated phenotype of $Plk4^{Aa74}$ mutant flies was rescued by the expression GFP-Plk4 under the control of the Ubq promoter and by the expression of Plk4-GFP under the control of its own endogenous promoter (Fig. 5 C and Video 6). $Plk4^{Aa74}$ mutant third-instar larval brains expressing GFP-PACT had no detectable centrioles, a phenotype that was rescued by the expression of both GFP-Plk4 (Fig. 5, D and E) and Plk4-GFP (not depicted) under the control of Ubq promoter or of its endogenous promoter, respectively, whereas the hypomorphic $Plk4^{c06612}$ allele had reduced centriole numbers. Thus, the $Plk4^{Aa74}$ allele appears to be a null or a very strong hypomorph.

Flies were maintained at 18°C or 25°C on Drosophila culture medium (0.77% agar, 6.9% maize, 0.8% soya, 1.4% yeast, 6.9% malt,

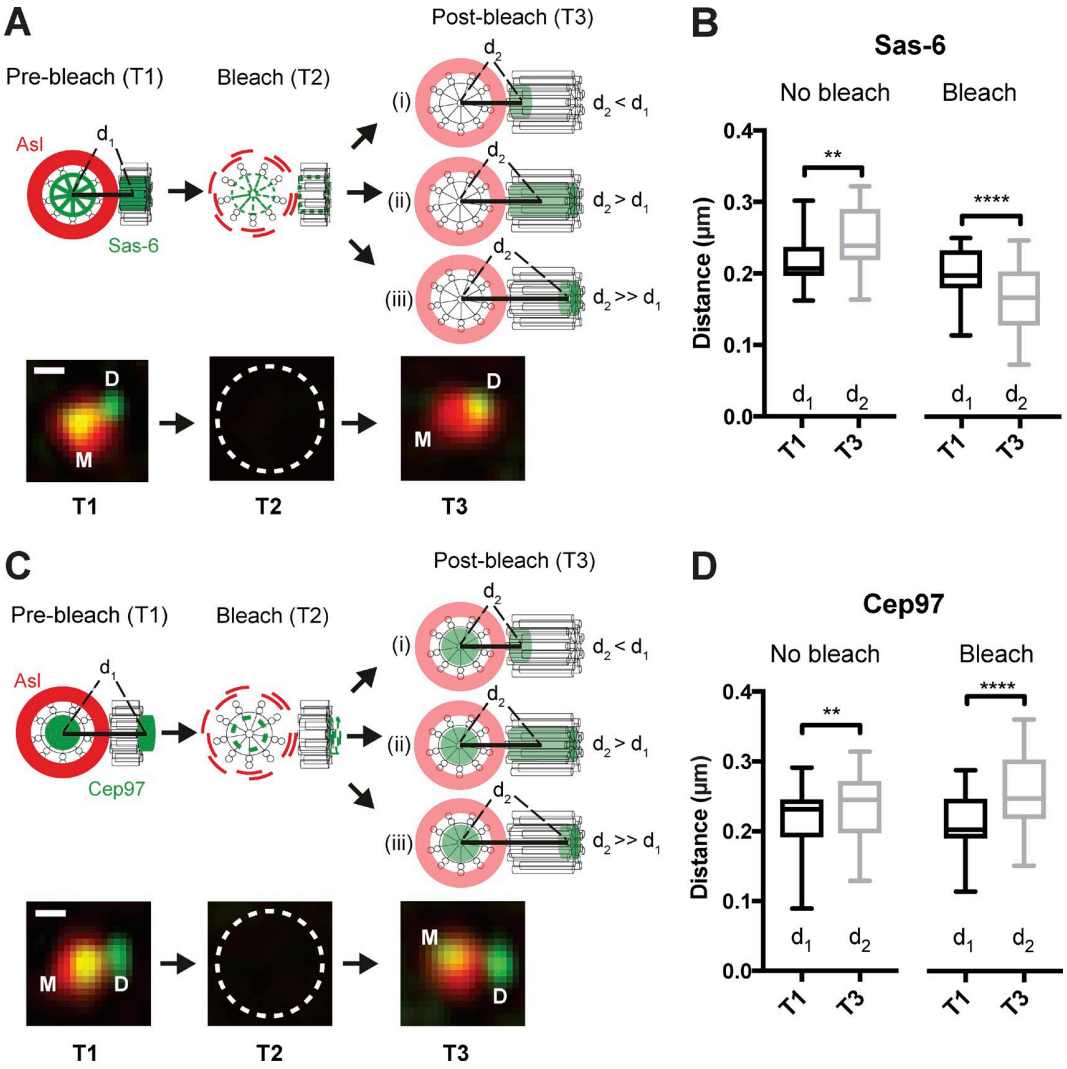

[AQ8]

Figure 8. **Sas-6-GFP is incorporated into the proximal end of the growing daughter centriole. (A)** Experimental scheme to test the site of centriolar Sas-6-GFP incorporation. Embryos expressing Sas-6-GFP and Asl-mCherry were allowed to proceed through S-phase until daughter centrioles were approximately halfway through their growth period. The distance (d_1) between the centroid of the mother (calculated using the Asl-mCherry signal) and daughter (calculated using the Sas-6-GFP signal) was measured (time = T1). The centriole pair was bleached (time = T2; note that bleaching the GFP fluorescence unintentionally also bleached the Asl-mCherry fluorescence, but Asl-mCherry fluorescence at the mother rapidly recovered), and a second image acquired 1 min later (time = T3), when the distance between the centroids was measured again (d_2). The difference between d_2 and d_1 will depend upon the site of Sas-6-GFP incorporation, as illustrated. Micrographs below the schematic illustrate examples of the images acquired at the corresponding time points. **(B)** Graph quantifies d_1 and d_2: in unbleached centrioles, which have grown slightly between T1 and T3, d_2 is greater than d_1; after bleaching d_2 is less than d_1, indicating that Sas-6-GFP is incorporated proximally. n = 10 embryos; n = 23 centriole pairs for control (unbleached) and 24 pairs for FRAP. **(C and D)** These panels show similar data to that shown in A and B, but for a control experiment examining where the distal-end-binding protein GFP-Cep97 is incorporated. n = 10 embryos; n = 25 centriole pairs for control (unbleached) and 28 pairs for FRAP. In this control, GFP-Cep97 appears to be incorporated distally, as expected, indicating that these methods are sensitive enough to distinguish between the proximal incorporation of Sas-6-GFP (B) and the distal incorporation of GFP-Cep97 (D). Midlines represent the median, whiskers mark the minimum to maximum, and bottom/top of the boxes indicate the first/third quartile of the distribution, respectively. Statistical significance was assessed using a paired t test (**, P < 0.01; ****, P < 0.0001).

1.9% molasses, 0.5% propionic acid, 0.03% ortho-phosphoric acid, and 0.3% nipagin) in vials or bottles. For embryo collections, 25% cranberry-raspberry juice plates (2% sucrose and 1.8% agar with a drop of yeast suspension) were used. Embryos studied in our imaging experiments were 0–1-h collections at 25°C, which were then aged at 25°C for 45–60 min. Before imaging, embryos were dechorionated by hand, mounted on a strip of glue painted on a 35-mm glass-bottom Petri dish with 14 mm micro-well (MatTek), and were left to desiccate for 1 min at 25°C. After desiccation, the embryos were covered with Voltalef grade H10S oil (Arkema).

Behavioral assays

Hatching experiments

To examine the quality of the embryonic development for various fly strains generated in this study, 0–1-h collected embryos were aged for 24 h, and the percentage of the embryos that had hatched

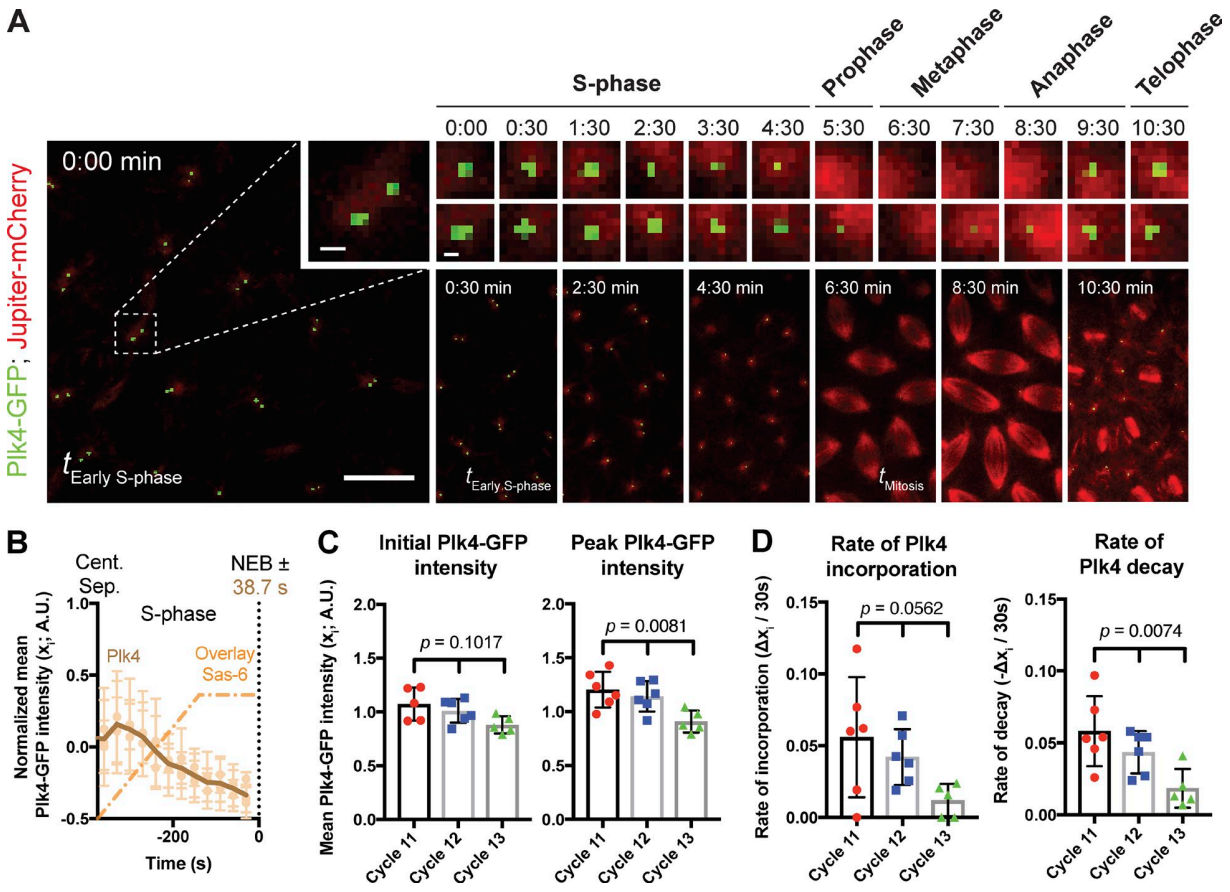

Figure 9. **An analysis of Plk4 centriolar dynamics. (A)** Micrographs show spinning-disk confocal fluorescence images taken from a time-lapse movie of an early embryo expressing Jupiter-mCherry (as a microtubule marker) and Plk4-GFP; time in minutes:seconds is indicated. At time *t* = 0:00, the embryo is in early S-phase, and the centrosomes have recently separated. Inset shows a single centriole pair (bar, 1 µm), which is then shown at 30-s or 1-min intervals (bar, 0.5 µm). The cell-cycle stage is indicated above each time interval. A series of lower-magnification views of the embryos are shown below the images of the individual centrioles to illustrate how MTs were used to determine the cell-cycle stage at each time point. Bar, 10 µm. **(B)** Graph shows the mean Plk4-GFP (brown) incorporation profile during S-phase of nuclear cycle 12 in WT embryos (n = 6 embryos). The mean incorporation profile of Sas-6-GFP is shown overlaid (dotted orange, same data shown in Fig. 3 A, but normalized for the length of S-phase). **(C and D)** Charts quantify parameters of Plk4-GFP behavior derived from mean Plk4-GFP profiles from embryos at nuclear cycles 11, 12, and 13 ($n \geq 5$ embryos for each cycle; n = 34, 31, and 33 centriole pairs [mean] per embryo, respectively). A.U., arbitrary units. Data are represented as mean ± SD. Statistical significance was assessed using either an ordinary one-way ANOVA test (for Gaussian-distributed data) or a Kruskal–Wallis test, and is shown above each chart.

out of their chorion was calculated. For this assay, six technical repeats were performed over several days.

Negative gravitaxis experiments

A standard negative gravitaxis assay (Ma and Jarman, 2011; Pratt et al., 2016) was used to assess the climbing reflexes of *Sas-6*, *ana2*, and *Plk4* null mutant flies rescued, respectively, with Sas-6-GFP, Ana2-GFP, and Plk4-GFP. In brief, three technical repeats of 1–4-d-old adult male flies (n = ∼15 for each technical repeat) were sharply tapped to the bottom of a cylinder, and the maximum distance climbed by individual flies within the first 10 s after tapping was measured. The distances were calculated using Fiji (ImageJ).

Immunoblotting

0–3-h embryos were collected at 25°C. They were chemically dechorionated and fixed with methanol as previously described (Stevens et al., 2010). Fixed embryos were preserved overnight at 4°C and rehydrated by washing in PBT (PBS and 0.1% Triton X-100) three times for 15 min. Using a bright-field dissecting microscope (with 50× magnification), 40 embryos were selected in a volume of 20 µl PBT, and this was mixed with 20 µl of 2× SDS loading buffer. The sample was lysed at 95°C for 10 min, and 10 µl suspension/sample was loaded onto 3–8% Tris-acetate precast gels for SDS-PAGE (Thermo Fisher Scientific). Proteins were then transferred to nitrocellulose membrane for Western blotting. Membrane was blocked using 4% milk powder in PBS and 0.1% Tween 20 for 1 h. Primary antibodies used in this study are as follows: anti–Sas-6 (rabbit; Peel et al., 2007), anti-Ana2 (rabbit; Stevens et al., 2010), anti-Cnn (rabbit; Dobbelaere et al., 2008), and anti-GFP (mouse; Roche) used 1:500 in blocking solution. The incubation period for primary antibodies was 1 h. Secondary antibody used for immunoblotting: HRPO-linked anti-rabbit IgG and HRPO-linked anti-mouse IgG (both GE Healthcare) diluted 1:3,000 in blocking solution. The incubation period for secondary antibody was 45 min, after which membranes were

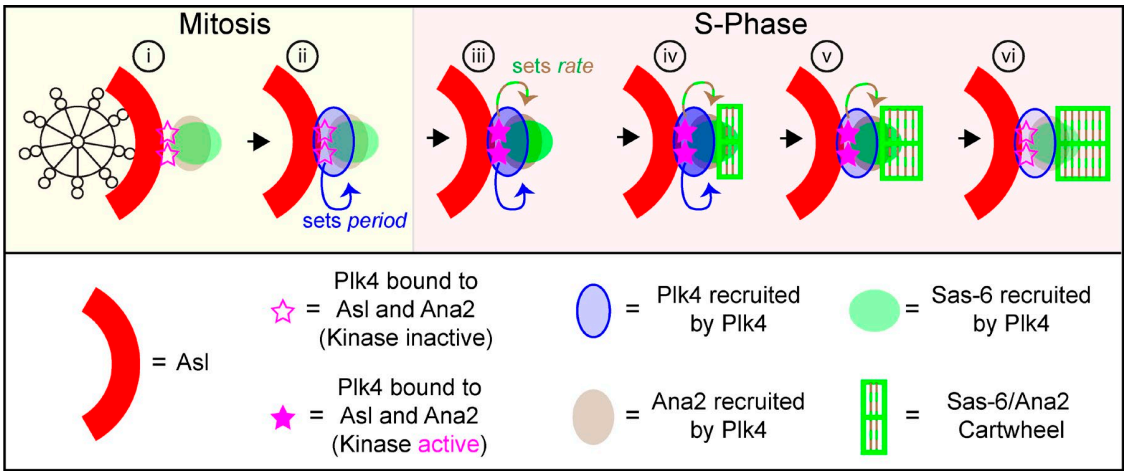

Figure 10. **Schematic illustration of how a Plk4-dependent homeostatic clock might set daughter centriole length in flies. (i)** The schematic shows an end-on view of a mother centriole (black skeleton) in mitosis, just after it has disengaged from its daughter. Plk4 starts to be recruited to mothers by the surrounding ring of Asl (red, only shown in part) but we speculate that a small fraction of Plk4 (pink star) is stabilized by binding to Ana2 (brown)—and potentially Sas-6 (green)—so defining the site where the daughter will form. **(ii)** This pool of Plk4 starts to recruit more Plk4 (blue arrow, recruiting to blue ellipse); the rate of this recruitment is dependent on the amount of Plk4 initially bound to Asl and Ana2, and it sets the period of daughter centriole growth by determining how quickly Plk4 will accumulate to trigger its own destruction. **(iii)** When the embryo enters S-phase, the Asl/Ana2-bound fraction of Plk4 is activated (filled pink stars), allowing it to recruit more Sas-6 and Ana2 (green/brown arrow); the kinase activity of the Plk4 influences the rate of Sas-6/Ana2 recruitment, and so the rate of centriole growth. **(iv)** Sas-6 and Ana2 levels reach a threshold that allows cartwheel assembly, whereas the local concentration of Plk4 continues to increase. **(v)** Centriolar Plk4 levels reach a critical concentration that triggers its destruction—centriolar Plk4 levels start to fall, but levels of the Asl/Ana2-bound Plk4 initially remain high enough that Sas-6 and Ana2 recruitment is not slowed, and cartwheel growth continues. **(vi)** Eventually, levels of the Asl/Ana2-bound Plk4 are too low to support Sas-6 and Ana2 recruitment, so their concentration falls below the threshold for cartwheel growth and the daughter centriole stops growing.

washed with three changes of TBST (TBS and 0.1% Tween 20) for 45 min. Membranes were incubated in SuperSignal West Femto Maximum Sensitivity Substrate (Thermo Fisher Scientific; 1:1 mix, diluted 1:2, 1:6, 1:10, and 1:5 in water for Sas-6, Ana2, Cnn, and GFP, respectively). Finally, membranes were exposed to film using exposure times that ranged from <1 to 30 s.

Immunofluorescence

Immunostaining on late pupal testes and larval brains

Late pupal testes from Ubq-GFP-CG3980 (GFP-Cep97) strain and the third instar larvae brains from GFP-PACT strain were dissected in PBS on a silicon dish and fixed by incubation in 4% formaldehyde in PBS for 20 min (for brains) or 30 min (for testes). As an additional step, fixed brains were transferred to a drop of 45% acetic acid for 15 s and then to a drop of 60% acetic acid for 3 min. This was followed by squashing the testes in between two coverslips of thicknesses 1 and 1.5 (silicon-dipped), which had been placed between two pieces of Whatman filter papers (GE Healthcare). In the case of brains, the squashing step was done using a 1.5-thickness coverslip and a slide. After squashing, the sample was snap-frozen in liquid nitrogen for 10 min. Once taken out of the liquid nitrogen, the 1-thickness coverslip was carefully removed from either the 1.5-thickness coverslip (for testes) or the slides (for brains) using a razor blade. The samples were incubated in 100% cold methanol at −20°C for 5 min (for brains) or 100% cold ethanol at −20°C for 15 min (for testes) and were transferred to a Petri dish containing PBST (1% Tween-20 [Sigma-Aldrich] in PBS) to be incubated for 10 min. For testes, this was followed by three washes in PBS for 5 min and by incubation in PBST containing 1:500 Guinea pig polyclonal anti-Asl primary antibody (Roque et al., 2012) overnight at 4°C in a humid chamber. The sample was then washed three times with PBS for 5 min and incubated in PBST containing 1:500 anti–guinea pig IgG Alexa Fluor 568 secondary antibody (Thermo Fisher Scientific) and 1:500 GFP-booster coupled to Atto 488 (ChromoTek) at room temperature for 3 h. For brains, the sample was stained for 10 min in Hoechst 33258 (Thermo Fisher Scientific). After washing three times in PBS for 15 min, the sample was mounted in mounting medium.

Immunostaining on embryos

For immunostaining on embryos, 0–2-h old *Oregon-R* WT samples were collected and dechorionated in 60% bleach for 2 min. This was followed by a wash in 0.05% Triton X-100 in distilled water. Embryos were then washed into small glass ampules containing 100% heptane and were shaken gently with 3% of 0.5 M EGTA in pure methanol. Samples were then stored in methanol at 4°C. Refrigerated samples were rehydrated by a wash in PBT (0.1% Triton X-100 in PBS) and blocked in 5% BSA (in PBS) for 1 h at room temperature. Blocking was followed by incubating the samples in 5% BSA (in PBS) containing 1:500 guinea pig anti-Asl (Roque et al., 2012) or 1:500 rabbit anti-PLP (Martinez-Campos et al., 2004) overnight at 4°C. Samples were then washed with PBT before 3-h incubation in 5% BSA (in PBS) containing 1:1,000 anti-guinea pig IgG Alexa Fluor 488 (Thermo Fisher Scientific) or 1:1,000 anti-rabbit IgG Alexa Fluor 594 (Thermo Fisher Scientific) secondary antibodies. After washing three times in PBT, each for 15 min, samples were mounted using Vectashield

mounting medium containing DAPI (Vector Laboratories) onto microscopy slides with high-precision glass coverslips (CellPath).

Image acquisition, processing, and analysis

3D SIM

Living embryos were imaged at 21°C using a DeltaVision OMX V3 Blaze microscope (GE Healthcare). The system was equipped with a 60×/1.42-NA oil UPlanSApo objective (Olympus Corp.), 488- and 593-nm diode lasers, and Edge 5.5 sCMOS cameras (PCO). Spherical aberration was reduced by matching the refractive index of the immersion oil (1.514) to that of the embryos. 3D-SIM image stacks consisting of six slices at 0.125-µm intervals were acquired in five phases and from three angles per slice. The raw acquisition was reconstructed using softWoRx 6.1 (GE Healthcare) with a Wiener filter setting of 0.006 and channel-specific optical transfer function. For two-color 3D-SIM, images from green and red channels were registered with the alignment coordination information obtained from the calibrations using 0.2-µm-diameter TetraSpeck beads (Thermo Fisher Scientific) in the OMX Editor software. The SIM-Check plug-in in ImageJ (National Institutes of Health) was used to assess the quality of the SIM reconstructions (Ball et al., 2015).

To carry out the FRAP experiments in 3D-SIM, the software development kit (GE Healthcare) was used. Settings for the sequence of events needed for FRAP experiments were as follows: (1) acquisition of a single *z*-stack in 3D-SIM (Fig. 1, pre-bleach); (2) multispot photobleaching (by the OMX galvo scanner TIRF/photo kinetics module); (3) acquisition of the photobleached image (Fig. 1, bleach); and (4) acquisition of the time-lapse images in 3D-SIM (Fig. 1, post-bleach).

Assessment of the mother centriole orientation in early embryos (Fig. S5) was performed by visually scoring the percentage of mother centrioles that formed clear hollow rings when stained with anti-Asl or anti-PLP antibodies.

Spinning disk confocal microscopy

Living embryos were imaged at 21°C using a PerkinElmer ERS Spinning Disk confocal system on a Zeiss Axiovert 200M microscope. The system was equipped with a Plan-Apochromat 63×/1.4-NA oil DIC lens. 488- and 568-nm lasers were used to excite GFP and mCherry, respectively (using fast-sequential mode for GFP only, and emission discrimination mode for GFP and mCherry together). Confocal sections of 13 slices with 0.5-µm-thick intervals were collected every 30 s. Focus was occasionally readjusted in between the 30-s intervals.

In embryos expressing Jupiter-mCherry and Plk4-GFP in a Plk4^{Aa74} homozygous background (data presented in Fig. 9 A), the fluorescent signal was too faint to be properly visualized on the system. We therefore used a system equipped with an EM-CCD Andor iXon+ camera on a Nikon Eclipse TE200-E microscopy using a Plan-Apochromat 60×/1.42-NA oil DIC lens, controlled with Andor IQ2 software. Confocal sections of 17 slices with 0.5-µm-thick intervals were collected every 30 s at 21°C.

Postacquisition image processing was performed using Fiji (National Institutes of Health). Maximum-intensity projections of the images were first bleach-corrected with Fiji's exponential fit algorithm, and then the backgrounds were subtracted using the subtract background function with a rolling ball radius of 10 pixels. Centrioles (Sas-6-GFP foci) were tracked using TrackMate (Tinevez et al., 2017), a plug-in of Fiji, with the following analysis settings: track spot diameter size of 1.1 µm, initial threshold of >0.02, and quality of >0.07. Centriole growth regression curves were made using Prism 7 (GraphPad Software), and the mathematical modeling was done using the nonlinear regression (curve fit) analysis function. Growth curves in S-phase and mitosis were modeled discontinuously, as we reasoned that these two phases of the cell cycle are two separate entities (when data were modeled continuously, there was no statistically significant difference between the two ways of modeling; unpublished data). For S-phase, the data were initially fitted against three different functions to assess the most suitable model: linearity (or linear growth followed by a plateau), one-phase association (parabola), and sigmoidal (Fig. S2); among these models, linearity (or linear growth followed by a plateau) best fit the data. Thus, the data were modeled using two separate functions for S-phase: (1) linear growth and (2) linear growth followed by a plateau (Fig. 2 C). The latter function is an in-house algorithm where a linear line is tested against having a point of inflection at any point in S-phase after which the growth is constant. The equation is described as follows, where b represents the first intercept that leads to the point of inflection (x_0, y_1) after x amount of time with a slope of m:

$$\begin{aligned} y_1 &= m * x + b \\ y_{x0} &= m * x_0 + b \\ y_2 &= y_{x0} \\ y &= \text{if}(x < x_0, y_1, y_2). \end{aligned}$$

The only constraint applied to this equation was the requirement of the condition that m and x_0 must be greater than 0. For mitosis, the data were fitted against two separate functions: (1) linear growth and (2) constant (Fig. 2 C). In both the S-phase and mitosis analysis, centrioles that come from a single embryo were reasoned as internal replicates, and thus the fitting was done based on considering only the mean y value of each time point (in contrast to considering each replicate y value as an individual point). To judge and control the quality and precision of regression (goodness-of-fit), we used the R^2 and absolute sum-of-square values as well as applying the runs test. To compare the fits, the extra sum-of-squares F test was applied, and the appropriate fit was chosen by selecting the simpler model unless the p-value was <0.05.

To create the final regression model curves of Sas-6-GFP, the best-fit parameters (means of growth rate, growth period [m and x_0, respectively, in the equations] and S-phase length; see Fig. 2 C for the visual definition of these parameters) were calculated and origin-adjusted against the time point, ∼1–1.5 min after where the centrosomes from the previous cycle had separated (this was the time point at which TrackMate's tracking algorithm could detect the centrosome separation with the threshold parameters). Plk4-GFP data were too noisy to predict a meaningful regression model; however, the regression analysis using linear increase and decrease functions in Prism 7 (taking the peak intensity value in Plk4-GFP's growth curves as the point of inflection) allowed us to compare the differences between the rates of incorporation and decay over successive cell cycles

(Fig. 9). To create the final nonregression model curve of Plk4-GFP, the raw curves from multiple embryos were averaged and plotted (Fig. 9 B, bold rown). The mean intensity values and the final model curves for all the proteins were normalized to zero by bringing the initial mean intensity values (just after centrosome separation) down to zero and normalizing the rest of the data accordingly. In all of these imaging experiments, the timing of nuclear envelope breakdown (NEB) in individual embryos was easily inferred from the sum intensity projections of *z*-slices, except in the case of Plk4-GFP, where we had to use the simultaneous expression of Jupiter-mCherry to determine the timing of NEB (Fig. 9 A and Video 7).

Airyscan superresolution microscopy

Living embryos in nuclear cycle 12 or cycle 14 were imaged at 21°C using an inverted Zeiss 880 microscope fitted with an Airyscan detector. The system was equipped with Plan-Apochromat 63×/1.4-NA oil lens. 488-nm argon and 561-nm diode lasers were used to excite GFP and mCherry, respectively (sequential excitation of each wavelength was switched per line to ensure green and red channels were aligned). Sections of five slices with 0.2-µm-thick intervals were collected every 1 min with a zoom value of 24.6 pixels/µm. Focus was readjusted between the 1-min intervals. Images were Airy-processed in 3D with a strength value of "auto" (~6) or 6.5.

To measure the distancing between GFP-Cep97 foci at the distal ends of mother and daughter centrioles, three serial stacks were rapidly acquired (over a period of ~10 s) at 1-min intervals through nuclear cycle 12. Multiple stacks were acquired at each time point to allow us to select the image that gave the best resolution of the two GFP-Cep97 foci at each centriole pair at each time point (as this varied, perhaps because of "wobbling" of the centriole pair). After acquisition, images were analyzed using their maximum-intensity projections in Fiji (see Fig. 7 C for an example). The GFP foci were thresholded to the extent that the threshold encapsulated only the entire intensity mass of the foci for each centriole. After thresholding, the COM for each GFP-Cep97 focus was calculated, and then the distance between COM of the foci on the daughter and mother was measured. The regression curves for GFP-Cep97 distancing were made and quality-controlled using the same methodology described in Spinning disk confocal microscopy. Although this methodology produces a daughter centriole growth profile similar to that seen with our Sas-6-GFP incorporation assay, we note that the data are very noisy, and this methodology may not be sensitive enough to detect subtle changes in centriole length in different conditions. We also note that the data from WT and half-dose embryos were scored blind.

We also used the Airyscan superresolution microscope to probe the site of incorporation of Sas-6-GFP and GFP-Cep97 into daughter centrioles (Fig. 8). Embryos were identified as they exited mitosis of nuclear cycle 13 and daughter centrioles were allowed to grow for 5 min into cycle 14 (where daughter centriole growth takes 10.7 ± 0.8 min [n = 4 embryos] in S-phase; unpublished data). This allowed centrioles to grow to roughly half of their final size, before the centrioles were photobleached. The following settings were used in terms of the sequence of events needed for FRAP experiments: (1) acquisition of a single *z*-stack using airy-scan (Fig. 8, T1); (2) multispot serial photo-bleaching (Fig. 8, T2); and (3) acquisition of the photobleached and the time-lapse images in Airyscan (Fig. 8, T3). To measure the distance between the COM of the mother centriole and the incorporated Sas-6-GFP or GFP-Cep97 (Fig. 8, A and C, distances d_1 and d_2), the center of Asl-mCherry focus was taken as the reference center of mother centriole for both pre- and postbleaching time points (Fig. 8, T1 and T3, respectively).

Quantification and statistical analysis

All the details for quantification, statistical tests, n, definitions of center, and dispersion and precision measures are described in the main text, relevant figure legends, or Materials and methods. Significance in statistical tests was defined by $P < 0.05$. To determine whether the data values came from a Gaussian distribution, D'Agostino–Pearson omnibus normality test was applied. Prism 7 was used for all the modeling and statistical analyses.

Online supplemental material

Fig. S1 compares the embryonic expression levels of Sas-6- and Ana2-GFP to their endogenous counterparts and quantifies the ability of Sas-6-GFP, Ana2-GFP, and Plk4-GFP transgenes to rescue the uncoordinated phenotype of their respective mutants. Fig. S2 illustrates the regression models tested to find the best-fit regression type for Sas-6-GFP dynamics. Fig. S3 shows the Sas-6-GFP model curves fitted to data from 15 different embryos in cycle 12. Fig. S4 compares the embryo hatching rates of embryos in which the genetic dosage or the activity of Plk4 was altered. Fig. S5 shows immunofluorescence data and quantification illustrating how mother centrioles are preferentially oriented end-on to the cortex in early fly embryos. Videos 1, 2, 4, and 6 compare the behavior of *Sas-6*, *Ana2*, or *Plk4* mutant flies to mutant flies rescued with their respective GFP-fusions. Video 3 shows an example of a time-lapse video of an embryo in nuclear cycle 12 expressing Sas-6-GFP and the tracks generated by TrackMate that were used to quantify Sas-6-GFP fluorescence levels through the cycle. Video 5 is a time-lapse 3D-SIM movie of Asl-GFP in early fly embryos, illustrating how mother centrioles remain oriented end-on with respect to the cortex through time. Video 7 illustrates the oscillating behavior of Plk4-GFP in cycle 12 of early embryogenesis. Table S1 lists the source of the *D. melanogaster* strains used in this study. Table S2 lists the *D. melanogaster* strains used in this study. Table S3 lists the sequences of the oligonucleotides used in this study.

Acknowledgments

We thank Drs. J. Richard McIntosh and Guangshuo Ou and the members of the Raff Laboratory for critically reading the manuscript, Dr. Omer Dushek for his advice on curve fitting, and Lisa Gartenmann for designing and sharing the primers used to generate the Plk4^{RKA} construct.

Superresolution microscopy was performed at the Micron Oxford Advanced Bioimaging Unit, funded by a Strategic Award from the Wellcome Trust (107457). The research was funded by a Wellcome Trust Senior Investigator Award (104575; A. Wainman,

S. Saurya, T.L. Steinacker, A. Caballe, Z.A. Novak, N.M., and J.W. Raff) and an Edward Penley Abraham Scholarship (to M.G. Aydogan and J. Baumbach).

The authors declare no competing financial interests.

Author contributions: M.G. Aydogan, A. Wainman, and J.W. Raff formulated the theory of this study and wrote and revised the article. M.G. Aydogan, A. Wainman, S. Saurya, and J.W. Raff contributed to experimental conception and design. M.G. Aydogan, A. Wainman, S. Saurya, T.L. Steinacker, A. Caballe, and J. Baumbach acquired and analyzed the data. M.G. Aydogan, A. Wainman, Z.A. Novak, J. Baumbach, and N. Muschalik created and provided critical reagents/materials.

Submitted: 3 January 2018
Revised: 23 January 2018
Accepted: 26 January 2018

References

Arquint, C., and E.A. Nigg. 2016. The PLK4-STIL-SAS-6 module at the core of centriole duplication. *Biochem. Soc. Trans.* 44:1253–1263. https://doi.org/10.1042/BST20160116

Arquint, C., A.-M. Gabryjonczyk, S. Imseng, R. Böhm, E. Sauer, S. Hiller, E.A. Nigg, and T. Maier. 2015. STIL binding to Polo-box 3 of PLK4 regulates centriole duplication. *eLife.* 4. https://doi.org/10.7554/eLife.07888

Ball, G., J. Demmerle, R. Kaufmann, I. Davis, I.M. Dobbie, and L. Schermelleh. 2015. SIMcheck: A toolbox for successful super-resolution structured illumination microscopy. *Sci. Rep.* 5:15915. https://doi.org/10.1038/srep15915

Banterle, N., and P. Gönczy. 2017. Centriole biogenesis: From identifying the characters to understanding the plot. *Annu. Rev. Cell Dev. Biol.* 33:23–49. https://doi.org/10.1146/annurev-cellbio-100616-060454

Basto, R., J. Lau, T. Vinogradova, A. Gardiol, C.G. Woods, A. Khodjakov, and J.W. Raff. 2006. Flies without centrioles. *Cell.* 125:1375–1386. https://doi.org/10.1016/j.cell.2006.05.025

Bauer, M., F. Cubizolles, A. Schmidt, and E.A. Nigg. 2016. Quantitative analysis of human centrosome architecture by targeted proteomics and fluorescence imaging. *EMBO J.* 35:2152–2166. https://doi.org/10.15252/embj.201694462

Bettencourt-Dias, M., A. Rodrigues-Martins, L. Carpenter, M. Riparbelli, L. Lehmann, M. Gatt, N. Carmo, F. Balloux, G. Callaini, and D. Glover. 2005. SAK/PLK4 is required for centriole duplication and flagella development. *Curr. Biol.* 15:2199–2207.

Callaini, G., and M.G. Riparbelli. 1990. Centriole and centrosome cycle in the early Drosophila embryo. *J. Cell Sci.* 97:539–543.

Callaini, G., W.G. Whitfield, and M.G. Riparbelli. 1997. Centriole and centrosome dynamics during the embryonic cell cycles that follow the formation of the cellular blastoderm in Drosophila. *Exp. Cell Res.* 234:183–190. https://doi.org/10.1006/excr.1997.3618

Chrétien, D., B. Buendia, S.D. Fuller, and E. Karsenti. 1997. Reconstruction of the centrosome cycle from cryoelectron micrographs. *J. Struct. Biol.* 120:117–133. https://doi.org/10.1006/jsbi.1997.3928

Conduit, P.T., A. Wainman, Z.A. Novak, T.T. Weil, and J.W. Raff. 2015. Re-examining the role of Drosophila Sas-4 in centrosome assembly using two-colour-3D-SIM FRAP. *eLife.* 4:1032. https://doi.org/10.7554/eLife.08483

Cunha-Ferreira, I., I. Bento, A. Pimenta-Marques, S.C. Jana, M. Lince-Faria, P. Duarte, J. Borrego-Pinto, S. Gilberto, T. Amado, D. Brito, et al. 2013. Regulation of autophosphorylation controls PLK4 self-destruction and centriole number. *Curr. Biol.* 23:2245–2254. https://doi.org/10.1016/j.cub.2013.09.037

Dammermann, A., P.S. Maddox, A. Desai, and K. Oegema. 2008. SAS-4 is recruited to a dynamic structure in newly forming centrioles that is stabilized by the γ-tubulin–mediated addition of centriolar microtubules. *J. Cell Biol.* 180:771–785. https://doi.org/10.1083/jcb.200709102

Dobbelaere, J., F. Josué, S. Suijkerbuijk, B. Baum, N. Tapon, and J. Raff. 2008. A genome-wide RNAi screen to dissect centriole duplication and centrosome maturation in Drosophila. *PLoS Biol.* 6:e224. https://doi.org/10.1371/journal.pbio.0060224

Dzhindzhev, N.S., G. Tzolovsky, Z. Lipinszki, S. Schneider, R. Lattao, J. Fu, J. Debski, M. Dadlez, and D.M. Glover. 2014. Plk4 phosphorylates Ana2 to trigger Sas6 recruitment and procentriole formation. *Curr. Biol.* 24:2526–2532.

Feng, X., and Y.A. Hannun. 1998. An essential role for autophosphorylation in the dissociation of activated protein kinase C from the plasma membrane. *J. Biol. Chem.* 273:26870–26874. https://doi.org/10.1074/jbc.273.41.26870

Fırat-Karalar, E.N., and T. Stearns. 2014. The centriole duplication cycle. *Philos. Trans. R. Soc. Lond. B Biol. Sci.* 369:20130460. https://doi.org/10.1098/rstb.2013.0460

Foe, V.E., and B.M. Alberts. 1983. Studies of nuclear and cytoplasmic behaviour during the five mitotic cycles that precede gastrulation in Drosophila embryogenesis. *J. Cell Sci.* 61:31–70.

Goehring, N.W., and A.A. Hyman. 2012. Organelle growth control through limiting pools of cytoplasmic components. *Curr. Biol.* 22:R330–R339. https://doi.org/10.1016/j.cub.2012.03.046

González, C., G. Tavosanis, and C. Mollinari. 1998. Centrosomes and microtubule organisation during Drosophila development. *J. Cell Sci.* 111:2697–2706.

Gould, C.M., and A.C. Newton. 2008. The life and death of protein kinase C. *Curr. Drug Targets.* 9:614–625. https://doi.org/10.2174/138945008785132411

Guderian, G., J. Westendorf, A. Uldschmid, and E.A.E. Nigg. 2010. Plk4 trans-autophosphorylation regulates centriole number by controlling betaTrCP-mediated degradation. *J. Cell Sci.* 123:2163–2169. https://doi.org/10.1242/jcs.068502

Holland, A.J., W. Lan, S. Niessen, H. Hoover, and D.W. Cleveland. 2010. Polo-like kinase 4 kinase activity limits centrosome overduplication by autoregulating its own stability. *J. Cell Biol.* 188:191–198. https://doi.org/10.1083/jcb.200911102

Ji, J.-Y., J.M. Squirrell, and G. Schubiger. 2004. Both cyclin B levels and DNA-replication checkpoint control the early embryonic mitoses in Drosophila. *Development.* 131:401–411. https://doi.org/10.1242/dev.00944

Kim, T.-S., J.-E. Park, A. Shukla, S. Choi, R.N. Murugan, J.H. Lee, M. Ahn, K. Rhee, J.K. Bang, B.Y. Kim, et al. 2013. Hierarchical recruitment of Plk4 and regulation of centriole biogenesis by two centrosomal scaffolds, Cep192 and Cep152. *Proc. Natl. Acad. Sci. USA.* 110:E4849–E4857. https://doi.org/10.1073/pnas.1319656110

Kitagawa, D., I. Vakonakis, N. Olieric, M. Hilbert, D. Keller, V. Olieric, M. Bortfeld, M.C. Erat, I. Flückiger, P. Gönczy, and M.O. Steinmetz. 2011. Structural basis of the 9-fold symmetry of centrioles. *Cell.* 144:364–375. https://doi.org/10.1016/j.cell.2011.01.008

Klebba, J.E., B.J. Galletta, J. Nye, K.M. Plevock, D.W. Buster, N.A. Hollingsworth, K.C. Slep, N.M. Rusan, and G.C. Rogers. 2015. Two Polo-like kinase 4 binding domains in Asterless perform distinct roles in regulating kinase stability. *J. Cell Biol.* 208:401–414. https://doi.org/10.1083/jcb.201410105

Knippschild, U., A. Gocht, S. Wolff, N. Huber, J. Löhler, and M. Stöter. 2005. The casein kinase 1 family: Participation in multiple cellular processes in eukaryotes. *Cell. Signal.* 17:675–689. https://doi.org/10.1016/j.cellsig.2004.12.011

Kratz, A.-S., F. Bärenz, K.T. Richter, and I. Hoffmann. 2015. Plk4-dependent phosphorylation of STIL is required for centriole duplication. *Biol. Open.* 4:370–377. https://doi.org/10.1242/bio.201411023

Kuriyama, R., and G.G. Borisy. 1981. Centriole cycle in Chinese hamster ovary cells as determined by whole-mount electron microscopy. *J. Cell Biol.* 91:814–821. https://doi.org/10.1083/jcb.91.3.814

Lattao, R., L. Kovács, and D.M. Glover. 2017. The centrioles, centrosomes, basal bodies, and cilia of Drosophila melanogaster. *Genetics.* 206:33–53. https://doi.org/10.1534/genetics.116.198168

Lewis, J., and E.M. Ozbudak. 2007. Deciphering the somite segmentation clock: Beyond mutants and morphants. *Dev. Dyn.* 236:1410–1415. https://doi.org/10.1002/dvdy.21154

Li, Y., M. Xu, X. Ding, C. Yan, Z. Song, L. Chen, X. Huang, X. Wang, Y. Jian, G. Tang, et al. 2016. Protein kinase C controls lysosome biogenesis independently of mTORC1. *Nat. Cell Biol.* 18:1065–1077. https://doi.org/10.1038/ncb3407

Ma, L., and A.P. Jarman. 2011. Dilatory is a Drosophila protein related to AZI1 (CEP131) that is located at the ciliary base and required for cilium formation. *J. Cell Sci.* 124:2622–2630. https://doi.org/10.1242/jcs.084798

Marshall, W.F. 2015. How cells measure length on subcellular scales. *Trends Cell Biol.* 25:760–768. https://doi.org/10.1016/j.tcb.2015.08.008

Marshall, W.F. 2016. Cell geometry: How cells count and measure size. *Annu. Rev. Biophys.* 45:49–64. https://doi.org/10.1146/annurev-biophys-062215-010905

Martinez-Campos, M., R. Basto, J. Baker, M. Kernan, and J.W. Raff. 2004. The *Drosophila* pericentrin-like protein is essential for cilia/flagella function, but appears to be dispensable for mitosis. *J. Cell Biol.* 165:673–683. https://doi.org/10.1083/jcb.200402130

Moritz, M., M.B. Braunfeld, J.C. Fung, J.W. Sedat, B.M. Alberts, and D.A. Agard. 1995. Three-dimensional structural characterization of centrosomes from early *Drosophila* embryos. *J. Cell Biol.* 130:1149–1159. https://doi.org/10.1083/jcb.130.5.1149

Moyer, T.C., K.M. Clutario, B.G. Lambrus, V. Daggubati, and A.J. Holland. 2015. Binding of STIL to Plk4 activates kinase activity to promote centriole assembly. *J. Cell Biol.* 209:863–878. https://doi.org/10.1083/jcb.201502088

Nigg, E.A., and J.W. Raff. 2009. Centrioles, centrosomes, and cilia in health and disease. *Cell.* 139:663–678. https://doi.org/10.1016/j.cell.2009.10.036

Novak, Z.A., P.T. Conduit, A. Wainman, and J.W. Raff. 2014. Asterless licenses daughter centrioles to duplicate for the first time in Drosophila embryos. *Curr. Biol.* 24:1276–1282. https://doi.org/10.1016/j.cub.2014.04.023

Novak, Z.A., A. Wainman, L. Gartenmann, and J.W. Raff. 2016. Cdk1 phosphorylates Drosophila Sas-4 to recruit polo to daughter centrioles and convert them to centrosomes. *Dev. Cell.* 37:545–557. https://doi.org/10.1016/j.devcel.2016.05.022

Ohta, M., T. Ashikawa, Y. Nozaki, H. Kozuka-Hata, H. Goto, M. Inagaki, M. Oyama, and D. Kitagawa. 2014. Direct interaction of Plk4 with STIL ensures formation of a single procentriole per parental centriole. *Nat. Commun.* 5:5267. https://doi.org/10.1038/ncomms6267

Peel, N., N.R. Stevens, R. Basto, and J.W. Raff. 2007. Overexpressing centriole-replication proteins in vivo induces centriole overduplication and de novo formation. *Curr. Biol.* 17:834–843.

Pratt, M.B., J.S. Titlow, I. Davis, A.R. Barker, H.R. Dawe, J.W. Raff, and H. Roque. 2016. Drosophila sensory cilia lacking MKS proteins exhibit striking defects in development but only subtle defects in adults. *J. Cell Sci.* 129:3732–3743. https://doi.org/10.1242/jcs.194621

Rodrigues-Martins, A., M. Riparbelli, G. Callaini, D.M. Glover, and M. Bettencourt-Dias. 2008. From centriole biogenesis to cellular function: Centrioles are essential for cell division at critical developmental stages. *Cell Cycle.* 7:11–16. https://doi.org/10.4161/cc.7.1.5226

Rogers, G.C., N.M. Rusan, D.M. Roberts, M. Peifer, and S.L. Rogers. 2009. The SCF Slimb ubiquitin ligase regulates Plk4/Sak levels to block centriole reduplication. *J. Cell Biol.* 184:225–239. https://doi.org/10.1083/jcb.200808049

Roque, H., A. Wainman, J. Richens, K. Kozyrska, A. Franz, and J.W. Raff. 2012. Drosophila Cep135/Bld10 maintains proper centriole structure but is dispensable for cartwheel formation. *J. Cell Sci.* 125:5881–5886. https://doi.org/10.1242/jcs.113506

Sibon, O.C., V.A. Stevenson, and W.E. Theurkauf. 1997. DNA-replication checkpoint control at the Drosophila midblastula transition. *Nature.* 388:93–97. https://doi.org/10.1038/40439

Sillibourne, J.E., F. Tack, N. Vloemans, A. Boeckx, S. Thambirajah, P. Bonnet, F.C.S. Ramaekers, M. Bornens, and T. Grand-Perret. 2010. Autophosphorylation of polo-like kinase 4 and its role in centriole duplication. *Mol. Biol. Cell.* 21:547–561. https://doi.org/10.1091/mbc.E09-06-0505

Sonnen, K.F., L. Schermelleh, H. Leonhardt, and E.A. Nigg. 2012. 3D-structured illumination microscopy provides novel insight into architecture of human centrosomes. *Biol. Open.* 1:965–976. https://doi.org/10.1242/bio.20122337

Stevens, N.R., A.A.S.F. Raposo, R. Basto, D. St Johnston, and J.W. Raff. 2007. From stem cell to embryo without centrioles. *Curr. Biol.* 17:1498–1503. https://doi.org/10.1016/j.cub.2007.07.060

Stevens, N.R., J. Dobbelaere, K. Brunk, A. Franz, and J.W. Raff. 2010. *Drosophila* Ana2 is a conserved centriole duplication factor. *J. Cell Biol.* 188:313–323. https://doi.org/10.1083/jcb.200910016

Tinevez, J.-Y., N. Perry, J. Schindelin, G.M. Hoopes, G.D. Reynolds, E. Laplantine, S.Y. Bednarek, S.L. Shorte, and K.W. Eliceiri. 2017. TrackMate: An open and extensible platform for single-particle tracking. *Methods.* 115:80–90. https://doi.org/10.1016/j.ymeth.2016.09.016

van Breugel, M., M. Hirono, A. Andreeva, H.-A. Yanagisawa, S. Yamaguchi, Y. Nakazawa, N. Morgner, M. Petrovich, I.-O. Ebong, C.V. Robinson, et al. 2011. Structures of SAS-6 suggest its organization in centrioles. *Science.* 331:1196–1199. https://doi.org/10.1126/science.1199325

Varmark, H., S. Llamazares, E. Rebollo, B. Lange, J. Reina, H. Schwarz, and C. González. 2007. Asterless is a centriolar protein required for centrosome function and embryo development in Drosophila. *Curr. Biol.* 17:1735–1745. https://doi.org/10.1016/j.cub.2007.09.031

Winey, M., and E. O'Toole. 2014. Centriole structure. *Philos. Trans. R. Soc. Lond. B Biol. Sci.* 369:20130457. https://doi.org/10.1098/rstb.2013.0457

Zitouni, S., M.E. Francia, F. Leal, S. Montenegro Gouveia, C. Nabais, P. Duarte, S. Gilberto, D. Brito, T. Moyer, S. Kandels-Lewis, et al. 2016. CDK1 prevents unscheduled PLK4-STIL complex assembly in centriole biogenesis. *Curr. Biol.* 26:1127–1137. https://doi.org/10.1016/j.cub.2016.03.055

Author: Read proofs carefully. This is your ONLY opportunity to make changes. NO further alterations will be allowed after this point.

Author Queries

[AQ1]: Please supply a condensed title of less than 90 characters (including space and punctuation) for incorporation in the running head.

[AQ2]: Journal style prefers "mean" to "average." It has been replaced throughout the paper; please confirm or edit further.

[AQ3]: References "41, 42" (as superscript numbers) were cited here; please advise which two reference citations should be inserted.

[AQ4]: Unpublished data is not permitted in Materials and methods. Please cite a published work, provide a revised sentence in which the methodology/data is described, or delete from the text.

[AQ5]: Unpublished data is not permitted in Materials and methods. Please cite a published work, provide a revised sentence in which the methodology/data is described, or delete from the text.

[AQ6]: Individuals who supply materials should be cited in Materials and methods. Please insert all people who provided materials into the Materials and methods, if possible, and provide the individuals' names, institution names, and the location (city and state/country). You may still thank them in the Acknowledgments, but first mention should be in Materials and methods.

[AQ7]: Please define error bars in Fig. 3, A and B, Fig. 4, C and D, Fig. 8, B and D, Fig. S1, and Fig. S3.

[AQ8]: Please give length of scale bars in A and C.

[AQ9]: Please define **** in Fig. S5 B.

https://doi.org/10.1083/jcb.201801014

Supplemental material

Aydogan et al., https://doi.org/10.1083/jcb.201801014

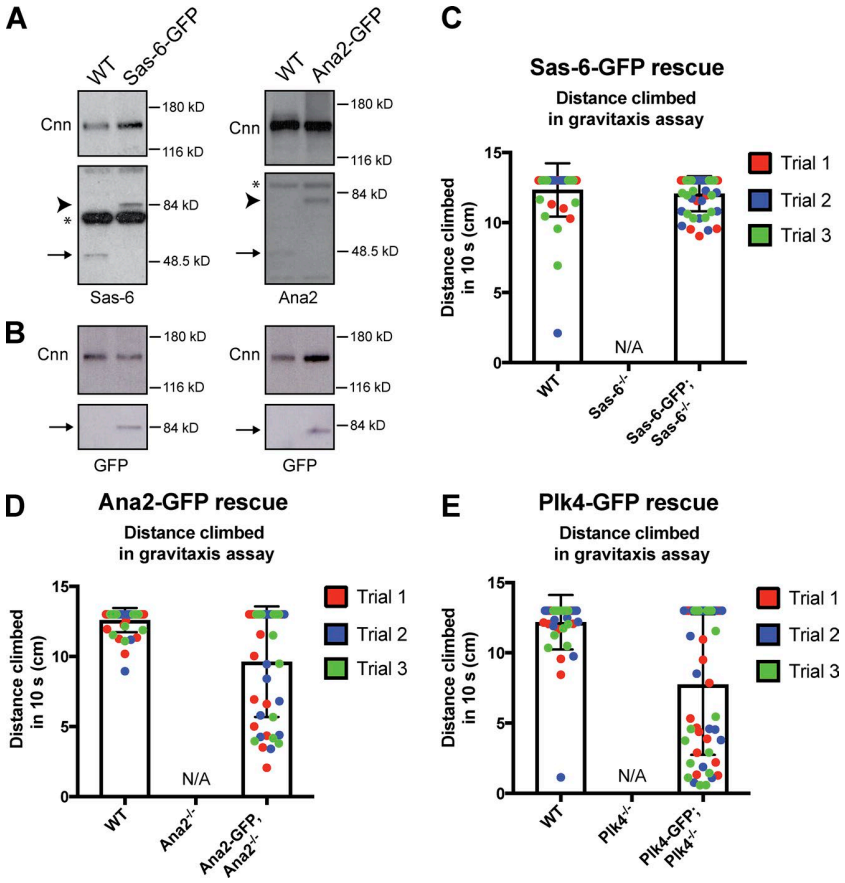

Figure S1. **Sas-6- and Ana2-GFP are expressed at similar levels as their endogenous proteins, and Sas-6-, Ana2-, and Plk4-GFP can at least partially rescue the uncoordinated phenotype of their respective adult mutant flies. (A)** Western blots show the protein levels of Sas-6-GFP (left) and Ana2-GFP (right; arrowheads) in transgenic embryos compared with their endogenous proteins in WT embryos (arrows). Cnn is shown as a loading control, and prominent nonspecific bands are indicated (*). **(B)** Similar blots were probed with anti-GFP antibodies to confirm that the GFP-fusion proteins were correctly identified. Cnn is shown as a loading control. Representative blots are shown from three technical repeats. **(C–E)** Graphs show the quantification of standard negative gravitaxis assays (Ma and Jarman, 2011; Pratt et al., 2016). In brief, three technical repeats of 1–4-d-old adult male flies (n ≈ 15 for each technical repeat) were sharply tapped to the bottom of a cylinder, and the maximum distance climbed by individual flies within the first 10 s after tapping was measured. Note that mutant flies were not scored in this assay, as it is difficult to keep them alive long enough to age them for the assay (as they are uncoordinated and have to be individually fed by hand to keep them alive). 100% of the mutant flies, however, were completely unable to climb (see Videos 1, 2, 4, and 6), so we show this bar as zero—marked with not/applicable (NA)—to give a reference of comparison for estimating the level of rescue for each transgene. Thus, although the Ana2-GFP and Plk4-GFP transgenes do not rescue the climbing activity of the mutant flies to the same level as WT flies, the level of rescue is appreciable.

N = 15 embryos*	Linear / Linear followed by a plateau	One phase association (Parabolic)	Sigmoidal
	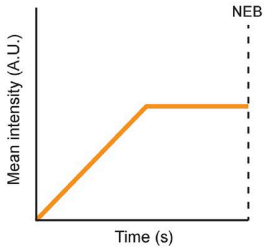	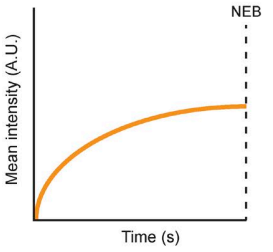	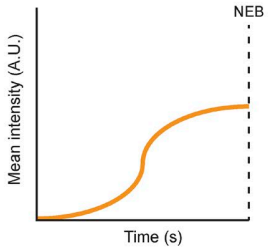
R^2 value	0.98 ± 0.02	0.97 ± 0.03	0.85 ± 0.02
SS_{Abs}	0.46 ± 0.43	0.41 ± 0.45	3.18 ± 1.66
% of fit preference	73.4%	26.6%	0%

*Reference data set: Cycle 12 in Figure 3

Figure S2. **The models tested in the regression analysis of Sas-6-GFP incorporation into the daughter centriole.** The Sas-6-GFP incorporation data for each individual embryo (see Fig. S3) was assessed using the nonlinear regression (curve fit) analysis function in GraphPad Prism 7. Growth curves in S-phase and mitosis were modeled discontinuously, as we reasoned that these two phases of the cell cycle are two separate entities. However, we also modeled the data continuously and found that there was no statistically significant difference between the two ways of modeling (not depicted). For S-phase, the data were initially fitted against three different functions (illustrated schematically in the graphs) to assess the most suitable model: linearity (or linear growth followed by a plateau), one-phase association (parabola), and sigmoid. Among these models, linear growth followed by a plateau was clearly the most preferable, and so all the data were fitted and analyzed with this model (as illustrated in Fig. S3). R^2 and absolute sum-of-squares values are used as a measure for goodness-of-fit. Sample size for modeling is indicated on the figure and in the legend of Fig. 3, from which the reference dataset (cycle 12) was obtained. A.U., arbitrary units.

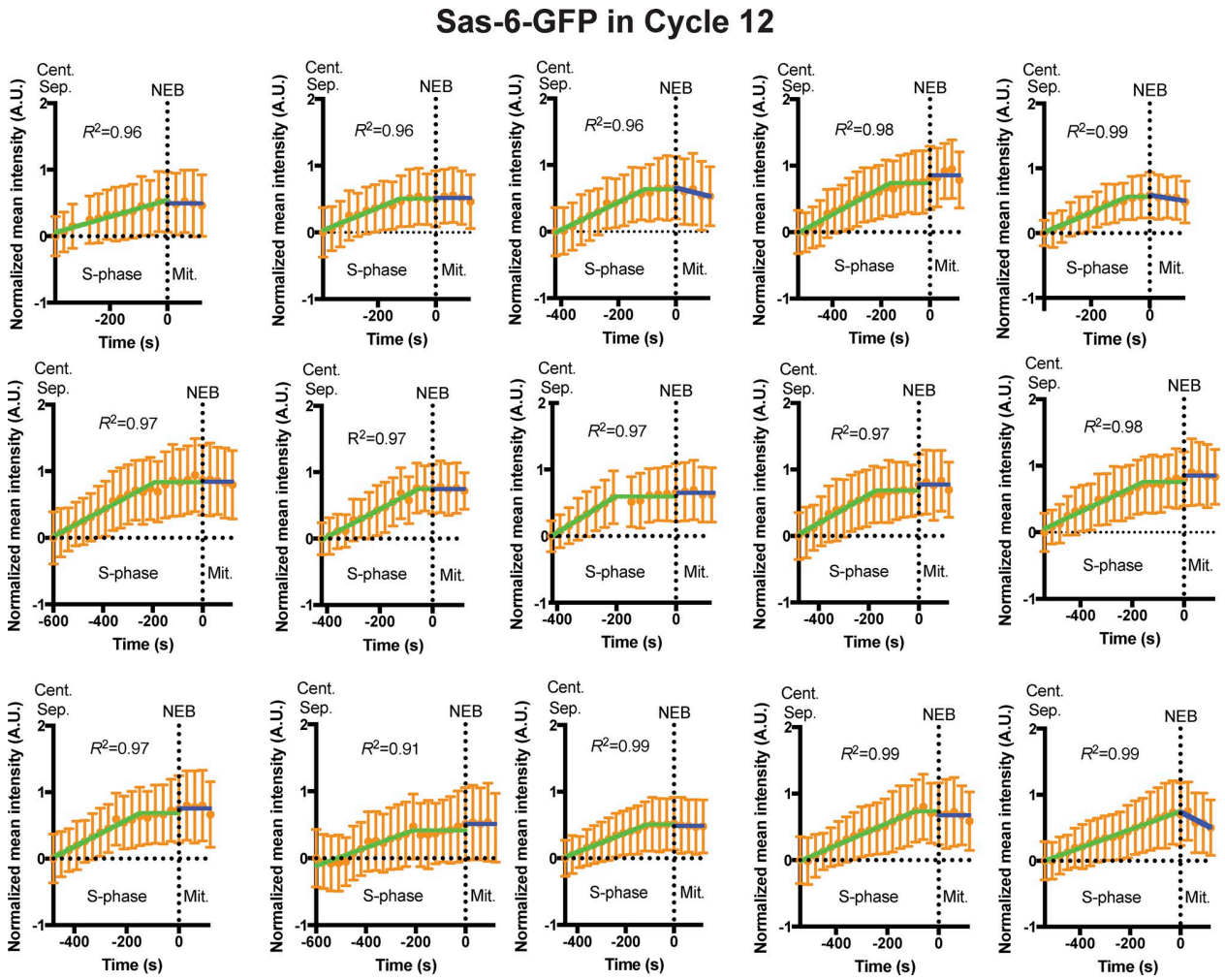

Figure S3. **Modeling Sas-6-GFP centriolar incorporation during nuclear cycle 12.** Graphs show the Sas-6-GFP incorporation profile from 15 different embryos at nuclear cycle 12. A regression analysis was performed independently on the S-phase (green line) and mitosis (blue line) data in each embryo using the model that best fit the overall data (linear growth followed by plateau, as described in Fig. S2). The R^2 value of the S-phase data is indicated in each graph. The full datasets for cycles 11 and 13 are not depicted. Note that, in a small number of embryos, Sas-6-GFP levels start to decrease as the embryos enter mitosis. We speculate that this is because in these embryos, some "excess" Sas-6-GFP might have been recruited to centrioles but is ultimately not incorporated into the cartwheel and then disperses back into the cytoplasm as the embryos enter mitosis. This finding is consistent with previous observations of SAS-6 dynamics in *Caenorhabditis elegans* embryos (Dammermann et al., 2008). A.U., arbitrary units.

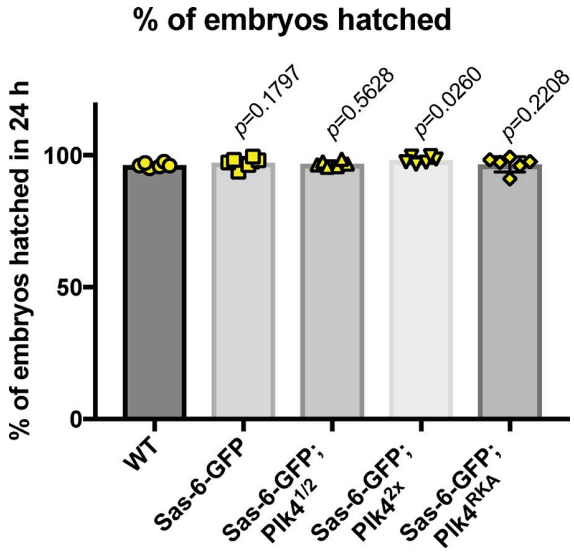

Figure S4. **Subtly altering the gene dosage or kinase activity of Plk4 does not detectably perturb embryo development.** Graph quantifies the hatching frequency of embryos laid by females of the indicated genotypes (which were all mated with WT males). The experimental lines expressed Sas-6-GFP (so we could measure the parameters of daughter centriole growth) and halved the genetic dose of *Plk4* (*Plk4*$^{1/2}$), doubled the dose of *Plk4* (*Plk4*^{2X}), or expressed a form of Plk4 with reduced kinase activity in an otherwise WT background (*Plk4*^{RKA}). None of these relatively subtle genetic changes detectably perturbed embryo development, as assessed by the hatching rate of the embryos. Data are represented as mean ± SD. Statistical significance was assessed using either an unpaired *t* test with Welch's correction (for Gaussian-distributed data) or an unpaired Mann–Whitney test, and is shown above each bar on the chart. *n* = 6 technical repeats for each group; per repeat *n* = 70 embryos in WT; *n* = 143 in Sas-6-GFP; *n* = 205 in Sas-6-GFP *Plk4*$^{1/2}$; *n* = 261 in Sas-6-GFP *Plk4*^{2x}; *n* = 193 in Sas-6-GFP *Plk4*^{RKA}.

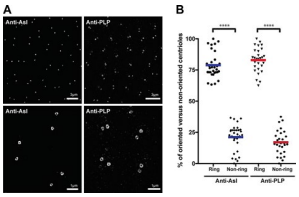

[AQ9]

Figure S5. **Mother centrioles are preferentially oriented end-on to the embryo cortex. (A)** Micrographs show 3D-SIM images that illustrate how the majority of mother centrioles in fixed embryos are oriented end-on to the embryo cortex, so that they appear as hollow rings. The mother centrioles here were recognized with either anti-Asl (Roque et al., 2012) or anti-PLP (Martinez-Campos et al., 2004) antibodies. **(B)** Graph quantifies the percentage of centrioles that were clearly recognizable/not recognizable as rings with each antibody. Note that we believe this analysis of fixed embryos probably underestimates the percentage of centrioles that are orientated end-on to the cortex, because the antibody staining varied somewhat between embryos: in embryos that were not as brightly stained, the reduced signal/noise ratio made the SIM reconstructions less reliable, and so fewer centrioles could be unambiguously scored as rings. *n* = 31 and 28 embryos, respectively, for anti-Asl and anti-PLP staining; *n* ≥ 70 centrioles (mean) per embryo.

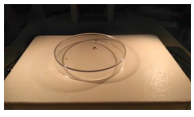

Video 1. ***Sas-6* mutant flies are uncoordinated, and this phenotype is rescued by the expression of Sas-6-GFP.** This montage shows short video clips of flies of the following genotypes: WT; *Sas-6* mutant (*Sas-6*$^{-/-}$); *Sas-6* mutant rescued by Sas-6-GFP flies (Sas-6-GFP; *Sas-6*$^{-/-}$). Like all flies that lack centrioles, the Sas-6 mutant is strongly uncoordinated because of the lack of cilia in its sensory neurons (Basto et al., 2006); this uncoordinated phenotype is strongly rescued by the expression of Sas-6-GFP. See also Fig. S1 C.

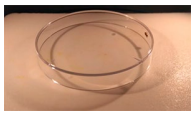

Video 2. ***Ana2* mutant flies are uncoordinated, and this phenotype is rescued by the expression of Ana2-GFP.** This video montage is similar to the one shown in Video 1 but shows the behavior of *Ana2* mutant flies and the rescue by Ana2-GFP. See also Fig. S1 D.

Video 3. **Monitoring Sas-6-GFP dynamics in early *D. melanogaster* embryos.** The first part of this video shows Sas-6-GFP foci followed through S-phase of nuclear cycle 12. The second part illustrates the dynamic tracking of Sas-6-GFP foci over time using the ImageJ plugin TrackMate. Note that TrackMate was set to generate "tracks" only for centriole pairs that were successfully monitored through every image of the S-phase period.

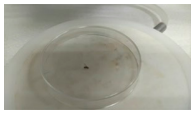

Video 4. **A comparison of the uncoordinated phenotype of the original *Plk4^{c06612}* mutant flies compared with the stronger *Plk4^{Aa74}* mutant flies we generate here.** This video montage shows short clips of flies of the following genotypes: the original *Plk4^{c06612}* mutation transheterozygous with a *Plk4* deficiency (*Plk4 hypomorph/Df*); the stronger *Plk4^{Aa74}* allele we generate in this study (*Plk4$^{-/-}$*); or the *Plk4^{Aa74}* mutant rescued by Plk4-GFP (Plk4-GFP; *Plk4$^{-/-}$*).

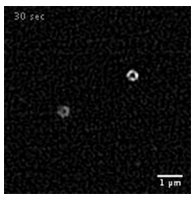

Video 5. **Mother centrioles are preferentially oriented end-on to the embryo cortex.** This short time-lapse video shows the behavior of the mother centriole marker Asl-GFP at two mother centrioles in mid-S-phase observed by 3D-SIM. Time in seconds is indicated. The centrioles are rapidly bleached over the 80-s time course of this video (with an image acquired every 10 s), so the images gradually degrade in quality as the movie proceeds; nevertheless, it can be seen that both centrioles maintain their end-on orientation relative to the embryo cortex.

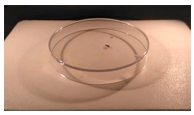

Video 6. ***Plk4* mutant flies are uncoordinated, and this phenotype is rescued by the expression of Plk4-GFP.** This video montage is similar to the one in Video 1 but shows the behavior of *Plk4* mutant flies and the rescue by Plk4-GFP. See also Fig. S1 E. Note that the video clip of the Plk4 mutant and the mutant rescued by Plk4-GFP are the same as those shown in Video 4.

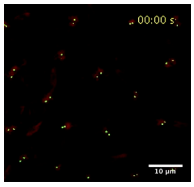

Video 7. **Centriolar Plk4-GFP levels fluctuate during the nuclear cycle.** This time-lapse video shows the behavior of Plk4-GFP (green) and Jupiter-mCherry (red), a marker of the microtubules, from early S-phase to late mitosis of nuclear cycle 12. The video was acquired on a spinning-disk confocal system.

Table S1. ***D. melanogaster*** strains used in this study

Allele[a]	Source	ID
Sas-6-GFP	This paper	NA
Sas-6^{c02901}	Peel et al., 2007	FlyBase ID: FBal0162156
Ana2-GFP	This paper	NA
ana2^{169}	Wang et al., 2011	FlyBase ID: Fbal0269126
ana2^{719}	Wang et al., 2011	FlyBase ID: Fbal0269127
Asl-mCherry	Conduit et al., 2015	NA
Ubq-GFP-CG3980 (GFP-Cep97)	Dobbelaere et al., 2008	NA
CycB^{2}	Jacobs et al., 1998	FlyBase ID: Fbal0094855
grp^{fsA4}	Sibon et al., 1997	FlyBase ID: Fbal0062815
Plk4^{Aa74}	This paper	NA
Plk4	This paper	NA
Plk4^{RKA}	This paper	NA
Asl-GFP	Blachon et al., 2008	FlyBase ID: FBtp0040947
asl^{B46}	Baumbach et al., 2015	NA
YFP-Asl	Varmark et al., 2007	FlyBase ID: FBtp0039668
Plk4-GFP	This paper	NA
Jupiter-mCherry	Callan et al., 2010	NA
Plk4^{c06612} (Hypomorph)	Bettencourt-Dias et al., 2005	FlyBase ID: FBal0159857
Plk4$^{Df(3L)Pc\text{-}2q}$ (Plk4^{Df})	Russell et al., 1996	FlyBase ID: FBab0022367
Ubq-GFP-Plk4	Basto et al., 2008	FlyBase ID: FBal0282567
Ubq-GFP-PACT	Martinez-Campos et al., 2004	FlyBase ID: FBal0190641

NA, not applicable.
[a]These alleles were expressed under their endogenous promoters unless ubiquitin expression is specified with the prefix *Ubq*.

Table S2. ***D. melanogaster*** strains generated and/or used in this study

Strain genotype	Tissue used	Experiment (figure, video)
Sas-6-GFP/Sas-6-GFP; Sas-6^{c02901}/Sas-6^{c02901}	Embryo	Figs. 1 A, 2 (B–D), 3, 4 (A and B), S1 (A–C), S2, and S3
Ana2-GFP, ana2^{169}/Ana2-GFP, ana2^{719}	Embryo	Figs. 1 B and S1 (A, B, and D)
Sas-6-GFP/Cyo	Embryo	Figs. 4 (C and D), 6, and S4
Sas-6-GFP/+; Plk4^{Aa74}/+	Embryo	Figs. 6 (A and B) and S4
Sas-6-GFP/Plk4; Plk4/+	Embryo	Figs. 6 (C and D) and S4
Sas-6-GFP/+; Plk4^{RKA}/+	Embryo	Figs. 6 (E and F) and S4
Asl-GFP/Asl-GFP; asl^{B46}/asl^{B46}	Embryo	Fig. 7 A
YFP-Asl/YFP-Asl	Embryo	Video 5
GFP-Cep97/+	Embryo; late pupal testis	Fig. 7 (B–D)
GFP-Cep97/+; Plk4^{Aa74}/+	Embryo	Fig. 7 D
Oregon-R (Wild-type)	Embryos; fly itself; third instar larval brain	Figs. 5 (B, D, and E), S1, S4, and S5; Videos 1, 2, 4, and 6
Asl-mCherry/Sas6-GFP	Embryo	Fig. 8 (A and B)
GFP-Cep97/+; Asl-mCherry/+	Embryo	Fig. 8 (C and D)
Plk4-GFP/+; Plk4^{Aa74}/Plk4^{Aa74}	Adult fly	Fig. S1 E; Videos 4 and 6
Plk4-GFP/+; Plk4^{Aa74}, Jupiter-mCherry/Plk4^{Aa74}	Embryo	Fig. 9; Video 7
Sas-6^{c02901}/Sas-6^{c02901}	Adult fly	Fig. S1 C; Video 1
ana2^{169}/ana2^{719}	Adult fly	Fig. S1 D; Video 2
Plk4^{Aa74}/Plk4^{Aa74}	Adult fly; third instar larval brain	Figs. 5 (B, C, and E) and S1 E; Videos 4 and 6
Asl-mCherry/Sas-6-GFP; Sas-6^{c02901}/Sas-6^{c02901}	Embryo	Fig. 1 C
Ana2-GFP, ana2^{169}/Ana2-GFP, ana2^{719}; Asl-mCherry/+	Embryo	Fig. 1 D
Sas-6-GFP/CycB^{2}	Embryo	Fig. 4 (C and D)
Sas-6-GFP/grp^{fsA4}	Embryo	Fig. 4 (C and D)
Plk4^{c06612}/Plk4^{c06612}	Adult fly; third instar larval brain	Fig. 5 (C and E)
Plk4^{c06612}/Plk4^{Df}	Adult fly	Video 4
Ubq-GFP-Plk4/+; Plk4^{Aa74}/Plk4^{Aa74}	Adult fly; third instar larval brain	Fig. 5 (C and E)
GFP-PACT/+	third instar larval brain	Fig. 5 D
GFP-PACT/+; Plk4^{Aa74}/+	third instar larval brain	Fig. 5 D

Table S3. **Oligonucleotides used in this study**

Oligonucleotide name	Sequence	Source
Primer for endogenous Plk4 (for GFP construct)	Forward: GCAGGCTTCAGACGACCTTTGGAGAACTGATTA	Thermo Fisher Scientific
Primer for endogenous Plk4 (for GFP construct)	Reverse: AGCTGGGTCAAGAAGCATGCGATTATAATAAGG	Thermo Fisher Scientific
Primer for endogenous Sas-6	Forward: GCAGGCTTCCTGTTTGATAACCACACAAAGCTTCGAAG	Thermo Fisher Scientific
Primer for endogenous Sas-6	Reverse: AGCTGGGTCTCGCCGATTTTCTTTGCCCGTG	IThermo Fisher Scientific
Primer for endogenous Ana2	Forward: GCAGGCTTCCTTTGTACAGGCTTCCCCATACGG	IThermo Fisher Scientific
Primer for endogenous Ana2	Reverse: AGCTGGGTCCAACAGCTTCGGCTGGTTCCTG	Thermo Fisher Scientific
Primer for Plk4^{Aa74}	Forward: TTGAAGTTCCGTTGGGTTGG	Thermo Fisher Scientific
Primer for Plk4^{Aa74}	Reverse: GCGAAAGTTCCAGGAAGTGG	Thermo Fisher Scientific
Primer to introduce stop codon into Plk4 pDONR by mutagenesis	Forward: CGCCTTATTATAATCGCATGCTTCTTTAAGACCCAGCTTTCTTGT ACAAAGTTGGC	Thermo Fisher Scientific
Primer to introduce stop codon into Plk4 pDONR by mutagenesis	Reverse: GCCAACTTTGTACAAGAAAGCTGGGTCTTAAAGAAGCATGCG ATTATAATAAGGCG	Thermo Fisher Scientific
Primer for Plk4^{RKA}	Forward: CAGCTCGAGCACCCCATACACATAGTTGGCGTCCTGAAAG	Thermo Fisher Scientific
Primer for Plk4^{RKA}	Reverse: CTTTCAGGACGCCAACTATGTGTATGGGGTGCTCGAGCTG	Thermo Fisher Scientific

References

Basto, R., J. Lau, T. Vinogradova, A. Gardiol, C.G. Woods, A. Khodjakov, and J.W. Raff. 2006. Flies without centrioles. *Cell.* 125:1375–1386. https://doi.org/10.1016/j.cell.2006.05.025

Basto, R., K. Brunk, T. Vinadogrova, N. Peel, A. Franz, A. Khodjakov, and J.W. Raff. 2008. Centrosome amplification can initiate tumorigenesis in flies. *Cell.* 133:1032–1042. https://doi.org/10.1016/j.cell.2008.05.039

Baumbach, J., Z.A. Novak, J.W. Raff, and A. Wainman. 2015. Dissecting the function and assembly of acentriolar microtubule organizing centers in Drosophila cells in vivo. *PLoS Genet.* 11:e1005261. https://doi.org/10.1371/journal.pgen.1005261

Bettencourt-Dias, M., A. Rodrigues-Martins, L. Carpenter, M. Riparbelli, L. Lehmann, M. Gatt, N. Carmo, F. Balloux, G. Callaini, and D. Glover. 2005. SAK/PLK4 is required for centriole duplication and flagella development. *Curr. Biol.* 15:2199–2207.

Blachon, S., J. Gopalakrishnan, Y. Omori, A. Polyanovsky, A. Church, D. Nicastro, J. Malicki, and T. Avidor-Reiss. 2008. Drosophila asterless and vertebrate Cep152 are orthologs essential for centriole duplication. *Genetics.* 180:2081–2094. https://doi.org/10.1534/genetics.108.095141

Callan, M.A., C. Cabernard, J. Heck, S. Luois, C.Q. Doe, and D.C. Zarnescu. 2010. Fragile X protein controls neural stem cell proliferation in the Drosophila brain. *Hum. Mol. Genet.* 19:3068–3079. https://doi.org/10.1093/hmg/ddq213

Conduit, P.T., A. Wainman, Z.A. Novak, T.T. Weil, and J.W. Raff. 2015. Re-examining the role of Drosophila Sas-4 in centrosome assembly using two-colour-3D-SIM FRAP. *eLife.* 4:1032. https://doi.org/10.7554/eLife.08483

Dammermann, A., P.S. Maddox, A. Desai, and K. Oegema. 2008. SAS-4 is recruited to a dynamic structure in newly forming centrioles that is stabilized by the γ-tubulin–mediated addition of centriolar microtubules. *J. Cell Biol.* 180:771–785. https://doi.org/10.1083/jcb.200709102

Dobbelaere, J., F. Josué, S. Suijkerbuijk, B. Baum, N. Tapon, and J. Raff. 2008. A genome-wide RNAi screen to dissect centriole duplication and centrosome maturation in Drosophila. *PLoS Biol.* 6:e224. https://doi.org/10.1371/journal.pbio.0060224

Jacobs, H.W., J.A. Knoblich, and C.F. Lehner. 1998. Drosophila Cyclin B3 is required for female fertility and is dispensable for mitosis like Cyclin B. *Genes Dev.* 12:3741–3751. https://doi.org/10.1101/gad.12.23.3741

Ma, L., and A.P. Jarman. 2011. Dilatory is a Drosophila protein related to AZI1 (CEP131) that is located at the ciliary base and required for cilium formation. *J. Cell Sci.* 124:2622–2630. https://doi.org/10.1242/jcs.084798

Martinez-Campos, M., R. Basto, J. Baker, M. Kernan, and J.W. Raff. 2004. The *Drosophila* pericentrin-like protein is essential for cilia/flagella function, but appears to be dispensable for mitosis. *J. Cell Biol.* 165:673–683. https://doi.org/10.1083/jcb.200402130

Peel, N., N.R. Stevens, R. Basto, and J.W. Raff. 2007. Overexpressing centriole-replication proteins in vivo induces centriole overduplication and de novo formation. *Curr. Biol.* 17:834–843.

Pratt, M.B., J.S. Titlow, I. Davis, A.R. Barker, H.R. Dawe, J.W. Raff, and H. Roque. 2016. Drosophila sensory cilia lacking MKS proteins exhibit striking defects in development but only subtle defects in adults. *J. Cell Sci.* 129:3732–3743. https://doi.org/10.1242/jcs.194621

Roque, H., A. Wainman, J. Richens, K. Kozyrska, A. Franz, and J.W. Raff. 2012. Drosophila Cep135/Bld10 maintains proper centriole structure but is dispensable for cartwheel formation. *J. Cell Sci.* 125:5881–5886. https://doi.org/10.1242/jcs.113506

Russell, S.R., G. Heimbeck, C.M. Goddard, A.T. Carpenter, and M. Ashburner. 1996. The Drosophila Eip78C gene is not vital but has a role in regulating chromosome puffs. *Genetics.* 144:159–170.

Sibon, O.C., V.A. Stevenson, and W.E. Theurkauf. 1997. DNA-replication checkpoint control at the Drosophila midblastula transition. *Nature.* 388:93–97. https://doi.org/10.1038/40439

Varmark, H., S. Llamazares, E. Rebollo, B. Lange, J. Reina, H. Schwarz, and C. González. 2007. Asterless is a centriolar protein required for centrosome function and embryo development in Drosophila. *Curr. Biol.* 17:1735–1745. https://doi.org/10.1016/j.cub.2007.09.031

Wang, C., S. Li, J. Januschke, F. Rossi, Y. Izumi, G. Garcia-Alvarez, S.S.L. Gwee, S.B. Soon, H.K. Sidhu, F. Yu, et al. 2011. An ana2/ctp/mud complex regulates spindle orientation in Drosophila neuroblasts. *Dev. Cell.* 21:520–533. https://doi.org/10.1016/j.devcel.2011.08.002

Appendix

Tables

Table 8.1: Fly stocks generated and/or used in this thesis		
Strain Genotype	**Description/ Notes**	**Origin**
eAna1-GFP/CyO	Ana1 under it's own endogenous promoter On 2nd Chromosome (T1085)	(Blachon et al., 2008)
eAsl-GFP/CyO	Asl under it's own endogenous promoter On 2nd Chromosome (T1083)	(Blachon et al., 2008)
ana1^{mecB}/TM6C	*ana1* mutation (T1089)	(Avidor-Reiss et al., 2004)
mRFP-PACT	On 2nd Chromosome (T842)	(Lucas and Raff, 2007)
eAsl-mcherry,*asl*^{B46}	Asl under it's own endogenous promoter in *asl* mutant background (T1236)	(Novak et al., 2014)
pUbq-GFP-Ana1	Full length Ana1 genomic DNA from start to stop codon from w^{67} flies	Generated by Saroj Saurya
pUbq-Ana1-GFP	3E, Ana1 from genomic DNA of w^{67} and site directed mutagenesis to remove the stop codon	Generated by Saroj Saurya
pUbq-Sas-6-GFP	5A, Sas-6 from cDNA (Peel et al., 2007) and site directed mutagenesis to remove the stop codon	Generated by Saroj Saurya
pUbq-Cep135-GFP	4B, Cep135 from cDNA (Roque et al., 2012) and site directed mutagenesis to remove the stop codon	Generated by Saroj Saurya
Ubq-GFP-Sas-6 /TM6C	Sas-6 cDNA tagged with GFP at the N-terminus (T928)	(Peel et al., 2007)
pUbq-Asl-GFP	Asl cDNA tagged with GFP at the C-terminus on X Chromosome (T1051)	(Stevens et al., 2010a)
pUbq-GFP-Ana2 /SM5	Ana2 cDNA tagged with GFP at the N-terminus (T091)	(Stevens et al., 2010a)
pUbq-Ana2-GFP /SM5	Ana2 cDNA tagged with GFP at the C-terminus (T098)	(Stevens et al., 2010a)
pUbq-GFP-Ana1 ΔNT	Short Ana1 lacking the first N-terminal 639aa tagged with GFP at the N-terminus (T105)	(Stevens et al., 2010a)
pUbq-GFP-Cep135	Cep135 cDNA tagged with GFP at the N-terminus (T104)	(Roque et al., 2012)
Df(3R)Exel7357	Deficiency covering *ana1* number 7948 (D336)	Bloomington stock centre
ana1^{mecB}*/ Df(3R)Exe7357*	Cross of *ana1*^{mecB}/TM6C (Avidor-Reiss et al., 2004) and *Df(3R)Exel7357* (Bloomington 7948)	Generated by Saroj Saurya
eAna1GFP; *ana1*^{mecB}*/Df*	Ana1 under it's own endogenous promoter (Blachon et al., 2008) rescuing *ana1* mutant (Avidor-Reiss et al., 2004) */ana1* deficiency	Generated by Saroj Saurya
pUASg-GFP-Ana1	Full length Ana1 genomic DNA from start to stop codon from w^{67} flies	Generated by Saroj Saurya
pUbq-CP110-GFP	CP110 from cDNA (RE33938) without stop codon (Franz et al., 2013) Long form, pUbq-CP110L-GFP	Generated by Saroj Saurya
pUASg-Sas-6	Sas-6 from cDNA (Peel et al., 2007) and UASg (Nadine Muschalik)	Generated by Saroj Saurya
pUASg-Ana2	Ana2 from cDNA (Peel et al., 2007) and UASg (Nadine Muschalik)	Generated by Saroj Saurya
pUASg-Ana1genomic	Full length Ana1 genomic DNA from start to stop codon from w^{67} flies in pUASg	Generated by Saroj Saurya
pUbq-GFP-Ana1 ΔCR1	First N-terminal 471bp deletion of Ana1 genomic DNA with stop codon, GFP tagged at the N-terminus	Generated by Saroj Saurya

pUbq-Ana1 ΔCR1-GFP	First N-terminal 471bp deletion of Ana1 genomic DNA without stop codon, GFP tagged at the C-terminus	Generated by Saroj Saurya
pUbq-Ana1	Ana1 cDNA from IP16240, after repairing the missing 67 bp using the Quikchange II XL mutagenesis kit	Generated by Saroj Saurya
pUbq-Klp10A	Klp10A cDNA (Radford et al., 2012) in pUbq without tag	Generated by Saroj Saurya
pUbq-Cep97	Full length Cep97 genomic DNA (Dobbelaere et al., 2008) from start to stop codon	Generated by Saroj Saurya
pUbq-Cep104	pDONR Cep104 cDNA (DGRC-GH24474) from (Roque et al., 2018)	Generated by Saroj Saurya
pUASg-Plk4	Full length genomic Plk4 with it's own promoter (Aydogan et al., 2018) and site directed mutagenesis to add the stop codon	Generated by Saroj Saurya
pUbq-Cep135	Full length Cep135 cDNA (Roque et al., 2012) and site directed mutagenesis to add the stop codon	Generated by Saroj Saurya
pUbq-CP110	Full length CP110 cDNA (Franz et al., 2013) and site directed mutagenesis to add the stop codon	Generated by Saroj Saurya
pUASg-eSas-4	Full length genomic Sas-4 with it's own promoter (Novak et al., 2014) and site directed mutagenesis to add the stop codon	Generated by Saroj Saurya
pUbq-Asl	Asl cDNA (Dobbelaere et al., 2008) and site directed mutagenesis to add the stop codon	Generated by Saroj Saurya
pUASg-eSas-6	Full length genomic Sas-6 with it's own promoter (Aydogan et al., 2018) and site directed mutagenesis to add the stop codon	Generated by Saroj Saurya
pUASg-eAna2	Full length genomic Ana2 with it's own promoter and site directed mutagenesis to repair the mutations	Generated by Saroj Saurya
pUASg-eCep135	Cep135 cDNA (Roque et al., 2012), added stop codon and then it's own promoter from w^{67} flies using NEBuilder	Generated by Saroj Saurya
pUASg-eAsl	Full length genomic Asl with it's own promoter (Novak et al., 2014) and site directed mutagenesis to add the stop codon	Generated by Saroj Saurya
pUASg-eAna1	Full length genomic Ana1 with it's own promoter and site directed mutagenesis to add stop codon	Generated by Saroj Saurya
pUbq-Sas-4	Full length genomic Sas-4 (Novak et al., 2014) and site directed mutagenesis to remove promoter and stop codon	Generated by Saroj Saurya
pUASg-ePlk4^{RKA} (L89G)	Full length genomic Plk4 with it's own promoter (Aydogan et al., 2018) and site directed mutagenesis to add the stop codon and change to L89G (shokat1)	Generated by Saroj Saurya
pUASg-ePlk4 (L89G, H190Y)	Full length genomic Plk4 with it's own promoter (Aydogan et al., 2018) and site directed mutagenesis to add the stop codon and change to L89G, H190Y (shokat2)	Generated by Saroj Saurya
pUASg-eSas-6 (F143D)	Full length genomic Sas-6 with it's own promoter (Aydogan et al., 2018) and site directed mutagenesis to add the stop codon and Change F143D	Generated by Saroj Saurya
pUASg-eAna2 2A (S318A, S373A)	Full length genomic Ana2 with it's own promoter and amplify fragments from Ana2 cDNA 2A (Boris Seiber) and assembled using NEB HiFi assembly	Generated by Saroj Saurya
pUASg-eAna2 2E (S318E, S373E)	Full length genomic Ana2 with it's own promoter and amplify fragments from Ana2cDNA 2E (Boris Seiber) and assembled using NEB HiFi assembly	Generated by Saroj Saurya

pUASg-eAna2 4A (S318A S365A, S370A, S373A)	Full length genomic Ana2 with it's own promoter and amplify fragments from Ana2cDNA 4A (Boris Seiber) and assembled using NEB HiFi assembly	Generated by Saroj Saurya
pUASg-eAna2 6A (S318A, S345A, S348A S365A, S370A, S373A)	Full length genomic Ana2 with it's own promoter and amplify fragments from Ana2cDNA 6A (Boris Seiber) and assembled using NEB HiFi assembly	Generated by Saroj Saurya
pUASg-eAna2 6E (S318E, S345E, S348E S365E, S370E, S373E)	Full length genomic Ana2 with it's own promoter and amplify fragments from Ana2cDNA 6E (Boris Seiber) and assembled using NEB HiFi assembly	Generated by Saroj Saurya
pUASg-eAna2 4E (S318E, S365E, S370E, S373E)	Full length genomic Ana2 with it's own promoter and amplify fragments from Ana2cDNA 4E (Boris Seiber) and assembled using NEB HiFi assembly	Generated by Saroj Saurya
pUbq-Cdk1	Cdk1 cDNA (DGRC_LD38718) in pUbq without tag and site directed mutagenesis to add the stop codon	Generated by Saroj Saurya
pUbq-Cdk1 AF(T14A,Y15F)	Cdk1 cDNA (DGRC_LD38718) and site directed mutagenesis to change T14A and Y15F	Generated by Saroj Saurya
pUbq-Cdk1 F(Y15F)	Cdk1 cDNA (DGRC_LD38718) and site directed mutagenesis to change Y15F	Generated by Saroj Saurya
pUbq-Ana2 (S284A,T301A)	From cDNA (Peel et al., 2007) mutations S284A,T301A (Lisa Gartenmann) and Q5 site directed mutagenesis to add the stop codon	Generated by Saroj Saurya
pUbq-Ana2 (S284E,T301E)	From cDNA (Peel et al., 2007) mutations S284A,T301A (Lisa Gartenmann) and Q5 site directed mutagenesis to add the stop codon	Generated by Saroj Saurya
pUbq-Myt1	Myt1 cDNA (DGRC_GH08848) after adding the first 4bp in the primer during the PCR and Q5 site directed mutagenesis to add the stop codon	Generated by Saroj Saurya
pUbq-Twine	Twine cDNA (DGRC_LD19391) in pUbq without tag and Q5 site directed mutagenesis to add the stop codon	Generated by Saroj Saurya
pUbq-String	String cDNA (DGRC_LD47579) in pUbq without tag and Q5 site directed mutagenesis to add the stop codon	Generated by Saroj Saurya
pUbq-Wee1	Wee1 cDNA (DGRC_LD27552) in pUbq without tag and Q5 site directed mutagenesis to add the stop codon	Generated by Saroj Saurya
eSas-6-GFP	Sas-6 genomic DNA under it's own endogenous promoter tagged with GFP at the C-terminus	(Aydogan et al., 2018)
Sas-6c02901	FBal0162156	(Peel et al., 2007)
Asl-mCherry	Asl tagged with mCherry at the C-terminus	(Conduit et al., 2015b)
Ubq-GFP-Cep97	Cep97 tagged with GFP at the N-terminus (Ubq-GFP-CG3980)	(Dobbelaere et al., 2008)
Cep135 ΔN /TM6B	*Cep135* mutant (L612)	(Singh et al., 2014)
l(3)S2214/TM3 Sb	*Sas-4* mutant (L396)	(Basto et al., 2006)
CP110 mutant	*CP110* mutant (L465)	(Franz et al., 2013)
Cep97 mutant	Cep97 (11-6), using ends-out, or replacement, gene targeting (T1239), M170 *Cep97* mutant on 2nd Chromosome	Generated by Jeroen Dobbelaere
$Plk4^{Aa74}$	L556	(Aydogan et al., 2018)
$CyclinB^{2}$	FlyBase ID: Fbal0094855 (F200)	(Jacobs et al., 1998)
$grapes^{fsA4}$	FlyBase ID: Fbal0062815, Grapes (Chk1) (F204)	(Sibon et al., 1997)
Wee1/CyO	F504, Shelagh Campbell (Price et al., 2000)	Cleaned by Saroj
w; $Myt1^{R6}$/TM6B Tb	From Shelagh Campbell $Myt1^{R6}$ is the homozygous viable recombinant derived from the original $myt1^{1}$ allele (Jin et al., 2005) .(F500)	(Jin et al., 2008)

w*; *Cdk1*^{B47} cn1 bw1/CyO, P{ftz/lacB}E3	EMS mutated gene *Cdc2* ^{B47}/CyO, Bloomington 6643 LacZ is with CyO balancer	(Stern et al., 1993)
CyclinB3^{2}	Female sterile on 3rd Chromosome Stamm Number 722, from Christian Lehner (F495)	(Jacobs et al., 1998)
CyclinE^{AR95}	Lethal, on 2nd Chromosome, Stamm Number 223 from Christian Lehner (L605)	(Knoblich et al., 1994)
CyclinD^{1}	Homozygous viable, on X Chromosome, BDSC_55125 Stamm Number 448, from Christian Lehner (F496)	(Emmerich et al., 2004)
dacapo^{4}	Lethal on 2nd Chromosome,Stamm Number 673 dacapo, dap, from Christian Lehner (L606)	(Lane et al., 1996)
string (Cdc25^{7B}*)*	Lethal, on 3rd Chromosome, Stamm Number 68, from Christian Lehner, String/cdc25 (L608)	(Edgar and O'Farrell, 1989)
w; *CyclinA*/TM6B	From Shelagh Campbell, Bloomington stock 17699 is a homozygous lethal pBAC(w+) insertion into the *CyclinA* gene (presumably null, FBrf0179797). (L611)	(Knoblich and Lehner, 1993)
pUbq-mGFP-Klp10A-CT, 4-1/TM6c	cDNA from pENTR4-Klp10A_LD29208 cDNA (Radford et al., 2012) pUbq-mGFP-Klp10A-CT, 4-1/TM6c	Generated by Rachel Humphrey under Saroj Saurya's supervision
pUbq-Cep104-GFP#8/TM3	T1244, Generated by Metta Pratt	(Roque et al., 2018)

Table 8.2 : Construct list		
Plasmid ID	**Construct**	**Notes**
33	pDONR-Ana1 cDNA (IP16240)	Ana 1 cdna in pDONR (IP16240). This has some bp missing Ana1 at c terminus. Generated by Saroj Saurya.
34	pDONR-CP110 cDNA -no stop (RE33938)	CP110 cdna for C-terminal GFP fusion (RE33938 in pDONR-Zeo no stop codon and amino acid T 301 is P (it was already in the clone). It is not a conserved amino acid. Generated by Saroj Saurya.
35	pDONR-Ana1 genomic DNA-FL	Ana1-Genomic DNA. Full genomic DNA with all the introns and exons (5.5KB). Generated by Saroj Saurya.
36	pUbq-Ana1 genomic DNA-FL	Ana1-Genomic DNA (# 35). Full genomic DNA with all the introns and exons (5.5KB) in pUbq (# 1100). Generated by Saroj Saurya.
37	pUbq-GFP-Ana1 genomic DNA-FL	Ana1-Genomic DNA (# 35). Full genomic DNA with all the introns and exons (5.5KB) in pUbq-GFP-N-terminus. Generated by Saroj Saurya.
38	pUASg-GFP-Ana1 genomic DNA-FL	Ana1-Genomic DNA (# 35). Full genomic DNA with all the introns and exons (5.5KB) in pUASg-GFP-N-terminus. Generated by Saroj Saurya.
39	pUbq-CP110 cDNA -no stop (RE33938)	pDONR-CP110 (# 34) cdna no stop codon and amino acid T 301 is P (it was already in the clone). It is not a conserved amino acid In pUbq (# 1100). Generated by Saroj Saurya.
40	pUbq-CP110-GFP	pDONR-CP110 (# 34) in pUbq-GFP- c-term. (Franz et al., 2013) Generated by Saroj Saurya.
41	pUASg-CP110-GFP	pDONR-CP110 (# 34) in pUASg- c-term. Generated by Saroj Saurya.
64	pUASg-Sas-6	pDONR-Sas-6(# 26) in pUASg empty. Generated by Saroj Saurya.
65	pUASg-Ana2	pDONR-Ana2(# 396) in pUASg empty. Generated by Saroj Saurya.
68	pUbq-mGFP-NT-DEST	GFP gateway cassette inserted with KpnI & SacII. Jeroen's plasmids # 1
69	pUbq-mGFP-CT-DEST	GFP gateway cassette inserted with KpnI & SacII Jeroen's plasmids # 2
70	pDONR-ENTRY	Jeroen's plasmids # 23
71	pUbq-RFP-NT-DEST	for NT fusions, tag sequenced cloned with KpnI/SpeI, clone 1, Jeroen's plasmids # 147
72	pUbq-RFP-CT-DEST	for CT gateway fusions, clone1, Jeroen's plasmids # 188
74	pUASt-GFP-NT-DEST	Terence Murphy pTGW, Jeroen's plasmids # 711
75	pUASt-GFP-CT-DEST	Terence Murphy pTWG. Jeroen's plasmids # 712
76	pUASg-GFP-NT-DEST	Terence Murphy pPGW. Also called UAS-P, Jeroen's plasmids # 713
77	pUASg-GFP-CT-DEST	Terence Murphy pPWG, also called UAS-P Jeroen's plasmids # 714

78	pUbq-empty-DEST	Gateway Reading frame cassette C1 (attR1-chloramphenicol-ccdB gene-attR2) cloned at Not1 site (now disrupted) in pWUbq (146)-Generated by Saroj Saurya.
79	pUbq-Cherry-NT-DEST	KpnI- SacII fragment, 238, Jeroen's plasmids # 355
80	pUbq-Cherry-CT-DEST	KpnI- SacII fragment, 242, Jeroen's plasmids # 359
83	pUASg-empty-DEST	Gateway Reading frame cassette C1 (attR1-chloramphenicol-ccdB gene-attR2) cloned at Not1 site (now disrupted) in pUASg. Made by Nadine Ampicillin resistant
92	pDONR-Sas-6 for C-term tag	Generated by Saroj Saurya. Sas-6 cdna without stop codon for C-terminal tags.
93	pDONR-Ana1 ΔCR1 for N-term tag	Generated by Saroj Saurya. Ana1genomic DNA but missing 471bp at the N-terminus
94	pDONR-Ana1 ΔCR1for C-term tag	Generated by Saroj Saurya. Ana1genomic DNA but missing 471bp at the N-terminus missing stop codon to have C-terminal tag
95	pDONR-Ana1 for C-term tag	Generated by Saroj Saurya. Ana1genomic DNA, missing stop codon to have C-terminal tag
96	pDONR-Cep135 for C-term tag	Generated by Saroj Saurya. Cep135 cDNA, missing stop codon to have C-terminal tag (original plasmid from Matt Cottee)
97	pUbq-CP110-GFP	pDONR-Sas-6 (# 92) in pUbq-GFP- c-term. Generated by Saroj Saurya.
98	pUASg-Ana1genomic	pDONR-Ana1(# 35) in pUASg -empty vector. Generated by Saroj Saurya.
99	pUbq-GFP-Ana1 ΔCR1	pDONR-Ana1 ΔCR1 (# 93) in pUbq-GFP- n-term. Ana1genomic DNA but missing 471bp at the N-terminus. Generated by Saroj Saurya.
100	pUbq-Ana1 ΔCR1-GFP	pDONR-Ana1 ΔCR1(# 94) in pUbq-GFP- c-term. Ana1genomic DNA but missing 471bp at the N-terminus. Generated by Saroj Saurya.
101	pUbq-Ana1-GFP	pDONR-Ana1 (# 95) in pUbq-GFP- c-term. Full length Ana1genomic DNA, GFP at C-terminal. Generated by Saroj Saurya.
102	pUbq-Cep135-GFP	pDONR-Cep135 (# 96) in pUbq-GFP- c-term. Full length Cep135 cDNA GFP at C-terminal. Generated by Saroj Saurya.
103	pRNA-GFP-CT-DEST	Made by Jenny and Nadine from Janina's pRNA and corrected by Matt
104	pRNA-GFP-NT-DEST	Made by Jenny and Nadine from Janina's pRNA
105	pDONR-Ana1 cDNA	Generated by Saroj and Boris from plasmid # 33. Digesting out the wrong fragment and ligating the right fragment from # plasmid # 35
106	pDONR-Ana1 cDNA ΔCR1	Generated by Saroj and Zsofi from plasmid # 105 by using site directed mutagenesis (deleted 56-402bp from Ana1 gene)

107	pDONR-Ana1 cDNA ΔCR2	Generated by Saroj and Zsofi from plasmid # 105 by using site directed mutagenesis (deleted 3845-3944bp from Ana1 gene)
108	pUbqGFP-Ana1 cDNA ΔCR1	Generated by Saroj Saurya from plasmid # 106 and # 68 (deleted 56-402bp from Ana1 gene)
109	pUbqGFP-Ana1 cDNA ΔCR2	Generated by Saroj Saurya from plasmid # 107 and # 68 (deleted 56-402bp from Ana1 gene)
113	pUbq-Ana1-cDNA full length	LR of # 78 (raff Lab) and # 105 (Raff Lab) Generated by Saroj and Thomas
114	pUbq-Klp10A-cDNA full length	LR of # 78 (raff Lab) and # 5 (Rachel) Generated by Saroj and Thomas
115	pUbq-Cep97-genomicDNA full length	LR of # 78 (raff Lab) and # 377 (Jeroen's plasmid) Generated by Saroj and Thomas
116	pUbq-Cep104-cDNA	LR of # 78 (raff Lab) and plasmid (Roque et al., 2018), Generated by Saroj and Thomas
117	pDONR-ePlk4	Stop codon added to pDONR-ePlk4 (Made by Zsofi) by quick change. Generated by Saroj and Thomas
118	pUASg-ePlk4	LR from # 117 and # 83 Generated by Saroj and Thomas To make flies without tag
119	pDONR-Cep135	Made from # 96 by putting back stop codon using quick change kit. Generated by Saroj and Thomas
120	pDONR-CP110	Made from # 34 by putting back stop codon using quick change kit. Generated by Saroj and Thomas
121	pDONR-eSas-4-genomic	Made from Zsofi's pDONR by putting back stop codon using quick change kit. Generated by Saroj and Thomas
122	pDONR-Asl	Made from Jeroen"s # 373, pDONR-Asl(ct) by putting back stop codon using quick change kit. Generated by Saroj and Thomas
123	pDONR-eAna2-genomic-Mut	Generated by Saroj Saurya. and Thomas by Amplifying genomic DNA with Promoter from W67 flies DNA. Has some changes A299T compared to fly base and lab cDNA
124	pDONR-eCyclinB-genomic	Generated by Saroj and Thomas by Amplifying genomic DNA with Promoter from W67 fly DNA.
125	pDONR-eWee1-genomic-Mut	Generated by Saroj and Thomas by Amplifying genomic DNA with Promoter from W67 fly DNA. There are some changes compared to flybase (P56T and D72G)
126	pUbq-Cep135 full length	LR from # 119 and # 78. Generated by Saroj and Thomas. To make flies without tag
127	pUbq-CP110	LR from # 120 and # 78. Generated by Saroj and Thomas. To make flies without tag
128	pUASg-eSas-4-genomic	LR from # 121 and # 83. Generated by Saroj Saurya. and Thomas. To make flies without tag
129	pUbq-Asl	LR from # 122 and # 78. Generated by Saroj and Thomas To make flies without tag
130	pDONR-eSas-6-genomic	QuickChanged to put stop codon from Nadine's pDONR-eSas-6M183R. This vector and Nadine's vector has extra S110T compared to lab cDNA. Generated by Saroj Saurya.
131	pDONR-eAna2-genomic	QuickChanged # 123 (pDONR-eAna2-genomic-MutT299A-full length) back to WT. Generated by Saroj Saurya.
132	pDONR-Cep135-SacII	QuickChanged # 119 to put SacII RE site in front of Cep135 cDNA, to put endo promoter in the front Generated by Saroj Saurya.

133	pDONR-eAsl-genomic	Made from Zsofi's pDONR by putting back stop codon using quick change kit. Generated by Saroj Saurya.
134	pDONR-eAna1-genomic	Made from Generated by Saroj Saurya. pDONR by putting back stop codon using quick change kit. Generated by Saroj Saurya.
135	pDONR-Sas-4-genomic	Made from # 121 (pDONR-eSas-4-genomic- full length) using quick change kit to delete endo promoter. Generated by Saroj Saurya.
136	pDONR-ePlk4 L89G (shokat1)	Made from # 117 (pDONR-ePlk4 full length) using quick change kit to add L89G (shokat1) using Lisa's primers. Generated by Saroj Saurya.
137	pDONR-eCep135	2KB upstream promoter was amplified from W67 genomic DNA using Phusion, gel purified, assembled with NE builder with SacII digested and gel purified Cep135 cDNA # 132. Generated by Saroj Saurya.
138	pUASg-eSas-6-genomic	LR from # 130 and # 83 Generated by Saroj Saurya.To make flies without tag
139	pUASg-eAna2-genomic	LR from # 131 and # 83 Generated by Saroj Saurya. To make flies without tag
140	pUASg-eCep135	LR from # 137 and # 83 Generated by Saroj Saurya. To make flies without tag
141	pUASg-eAsl-genomic	LR from # 133 and # 83 Generated by Saroj Saurya. To make flies without tag
142	pUASg-eAna1-genomic	LR from # 134 and # 83. Generated by Saroj Saurya. To make flies without tag
143	pUbq-Sas-4-genomic	LR from # 135 and # 78. Generated by Saroj Saurya. To make flies without tag
144	pUASg-ePlk4^{RKA} (L89G)	LR from # 136 and # 83. Generated by Saroj Saurya. To make flies without tag (shokat1)
145	pUASg-ePlk4 (L89G, H190Y)	LR from pDONR-ePlk4 L89G-H190Y (shokat2) made by Lisa and # 83. Generated by Saroj Saurya. To make flies without tag
146	pDONR-eSas-6 (F143D)	Quick Changed to change F143D (head group mutation) in # 130. Generated by Saroj Saurya.
147	pDONR-eAna2-genomic -2A (S318A, S373A)	PCR the insert from Boris plasmid # 61 and PCR the vector # 131. Assemble with NEB HiFi assembly. Generated by Saroj Saurya.
148	pDONR-eAna2-genomic -2E (S318E, S373E)	PCR the insert from Boris plasmid # 62 and PCR the vector # 131. Assemble with NEB HiFi assembly. Generated by Saroj Saurya.
149	pDONR-eAna2-genomic -4A (S318A S365A, S370A, S373A)	PCR the insert from Boris plasmid # 19 and PCR the vector # 131. Assemble with NEB HiFi assembly. Generated by Saroj Saurya.
150	pUASg-eSas-6 (F143D)-genomic	LR from # 146 and # 83. Generated by Saroj Saurya. To make flies without tag
151	pUASg-eAna2-genomic-2A (S318A, S373A)	LR from # 147 and # 83. Generated by Saroj Saurya. To make flies without tag
152	pUASg-eAna2-genomic-2E (S318E, S373E)	LR from # 148 and # 83. Generated by Saroj Saurya. To make flies without tag
153	pUASg-eAna2-genomic-4A (S318A S365A, S370A, S373A)	LR from # 149 and # 83. Generated by Saroj Saurya. To make flies without tag
154	pDONR-eAna2-genomi-6A (S318A, S345A, S348A S365A, S370A, S373A)	PCR the insert from Boris plasmid # 17 and PCR the vector # 131. Assemble with NEB HiFi assembly. Generated by Saroj Saurya.

155	pDONR-eAna2-genomic - 6E (S318E, S345E, S348E S365E, S370E, S373E)	PCR the insert from Boris plasmid # 18 and PCR the vector # 131. Assemble with NEB HiFi assembly. Generated by Saroj Saurya.
156	pDONR-eAna2-genomic - 4E (S318E, S365E, S370E, S373E)	PCR the insert from Boris plasmid # 20 and PCR the vector # 131. Assemble with NEB HiFi assembly. Generated by Saroj Saurya.
157	pUASg-eAna2-genomic-6A (S318A, S345A, S348A S365A, S370A, S373A)	LR from # 154 and # 83. Generated by Saroj Saurya. To make flies without tag
158	pUASg-eAna2-genomic-6E (S318E, S345E, S348E S365E, S370E, S373E)	LR from # 155 and # 83. Generated by Saroj Saurya. To make flies without tag
159	pUASg-eAna2-genomic-4E (S318E, S365E, S370E, S373E)	LR from # 156 and # 83. Generated by Saroj Saurya. To make flies without tag
160	GH08848-Myt1-fist 4bp missing	Stock # 7426 https://dgrc.bio.indiana.edu/product/View?product=7426
161	RE12958-Dacapo	Stock #: 1085642 https://dgrc.bio.indiana.edu/product/View?product=1085642,
162	LD19391-Twine	Stock #: 3518 https://dgrc.bio.indiana.edu/product/View?product=3518,
163	LD22957-CyclinD	Stock #: 7400 https://dgrc.bio.indiana.edu/product/View?product=7400
164	LD23613-CyclinB	Stock #: 7418 https://dgrc.bio.indiana.edu/product/View?product=7418
165	LD25083-Cdc6	Stock #: 2245 https://dgrc.bio.indiana.edu/product/View?product=2245
166	LD31205-Cdk4	Stock #: 2039 https://dgrc.bio.indiana.edu/product/View?product=2039
167	LD44443-CyclinA	Stock #: 2574 https://dgrc.bio.indiana.edu/product/View?product=2574
168	LD47579-String	Stock #: 2623 https://dgrc.bio.indiana.edu/product/View?product=2623
169	LD22351-Cdk2(Cdc2c)	Stock #: 4666 https://dgrc.bio.indiana.edu/product/View?product=4666
170	LD22682-CyclinE-some bp changes	Stock #: 5318 https://dgrc.bio.indiana.edu/product/View?product=5318
171	LD27552-Wee1-one bp changes	Stock #: 12506 https://dgrc.bio.indiana.edu/product/View?product=12506
172	LD42896-Grapes(chk1)	Stock #: 2416 https://dgrc.bio.indiana.edu/product/View?product=2416
173	LD11626-Orc1	Stock #: 4974 https://dgrc.bio.indiana.edu/product/View?product=4974
174	LD38718-Cdk1(Cdc2c)	Stock #: 6778 https://dgrc.bio.indiana.edu/product/View?product=6778
175	LD35784-Cdt (dup)	Stock #: 12620 https://dgrc.bio.indiana.edu/product/View?product=12620

176	pDONR-Myt1-no stop	PCR, gel extract and BP reaction from plasmid # 160 and pDONR plasmid # 70, without stop codon for C-terminal tags. Generated by Saroj Saurya.
177	pDONR-Dacapo-no stop	PCR, gel extract and BP reaction from plasmid # 161 and pDONR plasmid # 70, without stop codon for C-terminal tags. Generated by Saroj Saurya.
178	pDONR-Twine-no stop	PCR, gel extract and BP reaction from plasmid # 162 and pDONR plasmid # 70, without stop codon for C-terminal tags. Generated by Saroj Saurya.
179	pDONR-CyclinD-some changes-no stop	PCR, gel extract and BP reaction from plasmid # 163 and pDONR plasmid # 70, without stop codon for C-terminal tags. Generated by Saroj Saurya, 24bp missing in the middle
180	pDONR-CyclinB-no stop	PCR, gel extract and BP reaction from plasmid # 164 and pDONR plasmid # 70, without stop codon for C-terminal tags. Generated by Saroj Saurya.
181	pDONR-Cdc6-no stop	PCR, gel extract and BP reaction from plasmid # 165 and pDONR plasmid # 70, without stop codon for C-terminal tags. Generated by Saroj Saurya.
182	pDONR-Cdk4-no stop	PCR, gel extract and BP reaction from plasmid # 166 and pDONR plasmid # 70, without stop codon for C-terminal tags. Generated by Saroj Saurya.
183	pDONR-CyclinA-no stop	PCR, gel extract and BP reaction from plasmid # 167 and pDONR plasmid # 70, without stop codon for C-terminal tags. Generated by Saroj Saurya.
184	pDONR-String-no stop	PCR, gel extract and BP reaction from plasmid # 168 and pDONR plasmid # 70, without stop codon for C-terminal tags. Generated by Saroj Saurya.
185	pDONR-Cdk2-no stop	PCR, gel extract and BP reaction from plasmid # 169 and pDONR plasmid # 70, without stop codon for C-terminal tags. Generated by Saroj Saurya.
186	pDONR-CyclinE-some bp changes-no stop	PCR, gel extract and BP reaction from plasmid # 170 and pDONR plasmid # 70, without stop codon for C-terminal tags. Generated by Saroj Saurya. 24bp changes in the beginning
187	pDONR-Wee1-no stop	PCR, gel extract and BP reaction from plasmid # 171 and pDONR plasmid # 70, without stop codon for C-terminal tags. Generated by Saroj Saurya.
188	pDONR-Grapes-no stop	PCR, gel extract and BP reaction from plasmid # 172 and pDONR plasmid # 70, without stop codon for C-terminal tags. Generated by Saroj Saurya.
189	pDONR-Orc1-no stop	PCR, gel extract and BP reaction from plasmid # 173 and pDONR plasmid # 70, without stop codon for C-terminal tags. Generated by Saroj Saurya.
190	pDONR-Cdk1(Cdc2c)-no stop	PCR, gel extract and BP reaction from plasmid # 174 and pDONR plasmid # 70, without stop codon for C-terminal tags. Generated by Saroj Saurya.
191	pDONR-Cdt1(dup)-no stop	PCR, gel extract and BP reaction from plasmid # 175 and pDONR plasmid # 70, without stop codon for C-terminal tags. Generated by Saroj Saurya.
192	pRNA-Myt1-GFP (CT)	LR from # 103 and # 176. Generated by Saroj Saurya. To make RNA with GFP tagged at the C-terminus and inject in the embryos
193	pRNA-Dacapo-GFP (CT)	LR from # 103 and # 177. Generated by Saroj Saurya. To make RNA with GFP tagged at the C-terminus and inject in the embryos
194	pRNA-Twine-GFP (CT)	LR from # 103 and # 178. Generated by Saroj Saurya. To make RNA with GFP tagged at the C-terminus and inject in the embryos

195	pRNA-CyclinB-GFP (CT)	LR from # 103 and # 180. Generated by Saroj Saurya. To make RNA with GFP tagged at the C-terminus and inject in the embryos
196	pRNA-Cdc6-GFP (CT)	LR from # 103 and # 181. Generated by Saroj Saurya. To make RNA with GFP tagged at the C-terminus and inject in the embryos
197	pRNA-Cdk4-GFP (CT)	LR from # 103 and # 182. Generated by Saroj Saurya. To make RNA with GFP tagged at the C-terminus and inject in the embryos
198	pRNA-CyclinA-GFP (CT)	LR from # 103 and # 183. Generated by Saroj Saurya. To make RNA with GFP tagged at the C-terminus and inject in the embryos
199	pRNA-String-GFP (CT)	LR from # 103 and # 184. Generated by Saroj Saurya. To make RNA with GFP tagged at the C-terminus and inject in the embryos
200	pRNA-Cdk2(Cdc2c)-GFP (CT)	LR from # 103 and # 185. Generated by Saroj Saurya. # 10A1 (22.06.2017) To make RNA with GFP tagged at the C-terminus and inject in the embryos
201	pRNA-Wee1-GFP (CT)	LR from # 103 and # 187. Generated by Saroj Saurya. To make RNA with GFP tagged at the C-terminus and inject in the embryos
202	pRNA-Grapes(chk1)-GFP (CT)	LR from # 103 and # 188. Generated by Saroj Saurya. To make RNA with GFP tagged at the C-terminus and inject in the embryos
203	pRNA-Orc1-GFP (CT)	LR from # 103 and # 189. Generated by Saroj Saurya. To make RNA with GFP tagged at the C-terminus and inject in the embryos
204	pRNA-Cdk1(Cdc2c)-GFP (CT)	LR from # 103 and # 190 Generated by Saroj Saurya. To make RNA with GFP tagged at the C-terminus and inject in the embryos
205	pRNA-Cdt1(dup)-GFP (CT)	LR from # 103 and # 191. Generated by Saroj Saurya. To make RNA with GFP tagged at the C-terminus and inject in the embryos
206	pDONR-CyclinD-no stop	Q5 mutagenesis on plasmid # 179, added back 24bp. Without stop codon for C-terminal tags Generated by Saroj Saurya., Corrected
207	pDONR-CyclinE-no stop	Q5 mutagenesis on plasmid # 186, added back all the changes. Without stop codon for C-terminal tags Generated by Saroj Saurya., Corrected
208	pRNA-CyclinD-GFP corrected	Generated by Saroj Saurya. from #179 corrected using Q5 mutagenesis kit. For making RNA and inject in the embryos. Generated by Saroj Saurya.
209	pRNA-CyclinE-GFP corrected	Generated by Saroj Saurya. from #186 corrected using Q5 mutagenesis kit. For making RNA and inject in the embryos. Generated by Saroj Saurya.
210	pRNA-Ana2 (S284A, T301A)	Generated by Saroj Saurya. from Lisa's pRNA-Ana2 (S284A, T301A)-neongreen. Removed Neon green and added Stop codon using Q5 mutagenesis kit. For making RNA without Tag and inject in the embryos Generated by Saroj Saurya.
211	pRNA-Ana2 (S284E, T301E)	Generated by Saroj Saurya. from Lisa's pRNA-Ana2 (S284E, T301E)-neongreen. Removed Neon green and added Stop codon using Q5 mutagenesis kit. For making RNA without Tag and inject in the embryos Generated by Saroj Saurya.

212	pRNA-Cdk1(Cdc2c) AF(T14A and Y15F)-GFP (CT)	From # 204. used Q5 mutagenesis kit and changed T14A and Y15F.For making RNA and inject in the embryos. Generated by Saroj Saurya.
213	pRNA-Cdk1(Cdc2c) Y15F-GFP (CT)	From # 204. used Q5 mutagenesis kit and changed Y15F. For making RNA and inject in the embryos Generated by Saroj Saurya.
214	pRNA-DEST	Generated by Saroj Saurya. from #103 removed GFP using Q5 mutagenesis kit. For making RNA without Tag and inject in the embryos. Generated by Saroj Saurya.
215	pRNA-Cdk1	Generated by Saroj Saurya. from #204 removed GFP and added Stop codon using Q5 mutagenesis kit 2a For making RNA without Tag and inject in the embryos Generated by Saroj Saurya.
216	pDONR-Ana2-(S284E,T301E)	Q5 mutagenesis on Lisa's pDONR plasmid # to add stop codon for N-terminal tags or to make without tag. Generated by Saroj Saurya.
217	pDONR-Cdk1	Q5 mutagenesis on pDONR plasmid # 190 to add stop codon for N-terminal tags or to make without tag. Generated by Saroj Saurya.
218	pDONR-Cdk1AF(T14A,Y15F)-no stop	Q5 mutagenesis on pDONR plasmid # 190 to mutate AF(T14A,Y15F) for C-terminal tags. Generated by Saroj Saurya.
219	pDONR-Cdk1F(Y15F)-no stop	Q5 mutagenesis on pDONR plasmid # 190 to mutate Y15F for C-terminal tags. Generated by Saroj Saurya.
220	pRNA-Ana2	Generated by Saroj Saurya., LR of Jeroen's plasmid # 396 into plasmid # 214. For making RNA without Tag and inject in the embryos. Generated by Saroj Saurya.
221	pRNA-Ana2-GFP	Matt's plasmid # 168 (transformed, miniprep and re sequenced) . For making RNA with GFPTag and inject in the embryos. Generated by Saroj Saurya.
222	pRNA-Ana2 (S284E, T301E)-GFP	Generated by Saroj Saurya. LR of pDONR Lisa's plasmid into plasmid # 103. For making RNA with GFP (CT) and inject in the embryos. Generated by Saroj Saurya.
223	pRNA-Cdk1AF(T14A,Y15F)	Generated by Saroj Saurya from #212 removed GFP and added Stop codon using Q5 mutagenesis kit For making RNA without Tag and inject in the embryos Generated by Saroj Saurya.
224	pRNA-Cdk1F(Y15F)	Generated by Saroj Saurya from #213 removed GFP and added Stop codon using Q5 mutagenesis kit For making RNA without Tag and inject in the embryos Generated by Saroj Saurya.
225	pDONR-Ana2 (S284A,T301A)	Q5 mutagenesis on Lisa's pDONR (plasmid # 2) to add stop codon for N-terminal tags or to make without tag. Generated by Saroj Saurya.
226	pRNA-Ana2 (S284A, T301A)-GFP	Generated by Saroj Saurya. LR of pDONR Lisa's plasmid (# 2) into plasmid # 103. For making RNA with GFP (CT) and inject in the embryos. Generated by Saroj Saurya.
227	pDONR-Cdk1AF(T14A,Y15F)	Q5 mutagenesis on pDONR plasmid # 218 to add stop codon. Generated by Saroj Saurya.
228	pDONR-Cdk1F(Y15F)	Q5 mutagenesis on pDONR plasmid # 219 to add stop codon. Generated by Saroj Saurya.
229	pUbq-Cdk1	LR from # 217 and # 78. Generated by Saroj Saurya. To make flies without tag
230	pUbq-Cdk1AF (T14A,Y15F)	LR from # 227 and # 78. Generated by Saroj Saurya. To make flies without tag
231	pUbq-Cdk1F (Y15F)	LR from # 228 and # 78. Generated by Saroj Saurya. To make flies without tag

232	pUbq-Ana2 (S284A,T301A)	LR from # 225 and # 78. Generated by Saroj Saurya. To make flies without tag
233	pUbq-Ana2 (S284E,T301E)	LR from # 216 and # 78. Generated by Saroj Saurya. To make flies without tag
234	pDONR-Myt1	Q5 mutagenesis on pDONR plasmid # 176 to add stop codon for N-terminal tags or to make without tag. Generated by Saroj Saurya.
235	pDONR-Dacapo	Q5 mutagenesis on pDONR plasmid # 177 to add stop codon for N-terminal tags or to make without tag. Generated by Saroj Saurya.
236	pDONR-Twine	Q5 mutagenesis on pDONR plasmid # 178 to add stop codon for N-terminal tags or to make without tag. Generated by Saroj Saurya.
237	pDONR-CyclinD	Q5 mutagenesis on pDONR plasmid # 206 to add stop codon for N-terminal tags or to make without tag. Generated by Saroj Saurya.
238	pDONR-CyclinB	Q5 mutagenesis on pDONR plasmid # 180 to add stop codon for N-terminal tags or to make without tag. Generated by Saroj Saurya.
239	pDONR-Cdc6	Q5 mutagenesis on pDONR plasmid # 181 to add stop codon for N-terminal tags or to make without tag. Generated by Saroj Saurya.
240	pDONR-Cdk4	Q5 mutagenesis on pDONR plasmid # 182 to add stop codon for N-terminal tags or to make without tag. Generated by Saroj Saurya.
241	pDONR-CyclinA	Q5 mutagenesis on pDONR plasmid # 183 to add stop codon for N-terminal tags or to make without tag. Generated by Saroj Saurya.
242	pDONR-String	Q5 mutagenesis on pDONR plasmid # 184 to add stop codon for N-terminal tags or to make without tag. Generated by Saroj Saurya.
243	pDONR-Cdk2 (Cdc2c)	Q5 mutagenesis on pDONR plasmid # 185 to add stop codon for N-terminal tags or to make without tag. Generated by Saroj Saurya.
244	pDONR-CyclinE	Q5 mutagenesis on pDONR plasmid # 207 to add stop codon for N-terminal tags or to make without tag. Generated by Saroj Saurya.
245	pDONR-Wee1	Q5 mutagenesis on pDONR plasmid # 187 to add stop codon for N-terminal tags or to make without tag. Generated by Saroj Saurya.
246	pDONR-Grapes (chk1)	Q5 mutagenesis on pDONR plasmid # 188 to add stop codon for N-terminal tags or to make without tag. Generated by Saroj Saurya.
247	pDONR-Orc1	Q5 mutagenesis on pDONR plasmid # 189 to add stop codon for N-terminal tags or to make without tag. Generated by Saroj Saurya.
248	pDONR-Cdt1 (dup)	Q5 mutagenesis on pDONR plasmid # 191 to add stop codon for N-terminal tags or to make without tag. Generated by Saroj Saurya.
249	pUbq-Myt1	LR from # 234 and # 78. Generated by Saroj Saurya. To make flies without tag
250	pUbq-Dacapo	LR from # 235 and # 78. Generated by Saroj Saurya. To make flies without tag
251	pUbq-Twine	LR from # 236 and # 78. Generated by Saroj Saurya. To make flies without tag
252	pUbq-CyclinD	LR from # 237 and # 78. Generated by Saroj Saurya. To make flies without tag
253	pUbq-CyclinB	LR from # 238 and # 78. Generated by Saroj Saurya. To make flies without tag

254	pUbq-Cdc6	LR from # 239 and # 78. Generated by Saroj Saurya. To make flies without tag
255	pUbq-Cdk4	LR from # 240 and # 78. Generated by Saroj Saurya. To make flies without tag
256	pUbq-CyclinA	LR from # 241 and # 78. Generated by Saroj Saurya. To make flies without tag
257	pUbq-String	LR from # 242 and # 78. Generated by Saroj Saurya. To make flies without tag
258	pUbq-Cdk2 (Cdc2c)	LR from # 243 and # 78. Generated by Saroj Saurya. To make flies without tag
259	pUbq-CyclinE	LR from # 244 and # 78. Generated by Saroj Saurya. To make flies without tag
260	pUbq-Wee1	LR from # 245 and # 78. Generated by Saroj Saurya. To make flies without tag
261	pUbq-Grapes (chk1)	LR from # 246 and # 78. Generated by Saroj Saurya. To make flies without tag
262	pUbq-Orc1	LR from # 247 and # 78. Generated by Saroj Saurya. To make flies without tag
263	pUbq-Cdt1 (dup)	LR from # 248 and # 78. Generated by Saroj Saurya. To make flies without tag
	pENTR4-Klp10A	Klp10A cDNA (Radford et al.,2012)

Table 8.3: Primers list		
Primer name	**Sequence**	**Notes**
16_Saroj_Ana1 F1	GCAGGCTTCATGGCTCTGCAGCTAACA GTAAATG	For cloning Ana1 genomic, Saroj Saurya
17_Saroj_Ana1 R1	AGCTGGGTCTCATTTTCGGGGCGACTTT CGATG	For cloning Ana1 genomic, Saroj Saurya
70_Saroj_Ana1 F15	GGGGACAAGTTTGTACAAAAAAGCAGG CTTCATGGCTCTGCAGCTAACAGT AAATG	For cloning Ana1 genomic, Saroj Saurya
69_Saroj_Ana1_CT_R12	GGGGACCACTTTGTACAAGAAAGCTGG GTCTTTTCGGGGCGACTTTCGATG	For cloning Ana1 genomic without Stop codon, Saroj Saurya
88_Saroj_Ana1 D1921_3846F	GCCATCGGTACGCGGATGCAGCTGCCA GGCGAGAGCAAAAGCCGGCCACGATTC GTCGGTATAGTCCTCAACTAAACGC	For Making internal deletions in Ana1 cDNA, Saroj Saurya
89_Saroj_Ana1 D1921_3846R	GCGTTTAGTTGAGGACTATACCGACGAA TCGTGGCCGGCTTTTGCTCTCGCCGGC AGCTGCATCCGC GTACCGATGGC	For Making internal deletions in Ana1 cDNA, Saroj Saurya
90_Saroj_Ana1 D4_3846F	GCCACCATGATCAAACAAGTTTGTACAA AAAAGCAGGCTTCATGCCGGCCACGATT CGTCGGTATAGTCCTCAACTAAACGCCG	For Making internal deletions in Ana1 cDNA, Saroj Saurya
91_Saroj_Ana1 D4_3846R	CGGCGTTTAGTTGAGGACTATACCGACG AATCGTGGCCGGCATGAAGCCTGCTTTT TTGTACAAACTTGTTTGATCATGGTG GC	For Making internal deletions in Ana1 cDNA, Saroj Saurya
92_Saroj_Ana1 D403_3846F	CGACAAAATCCGAAGGTGTCGCAAGCA GGCCTTGAAACCGGCCACGATTCGTCG GTATAGTCCTCAACTAAACG	For Making internal deletions in Ana1 cDNA, Saroj Saurya
93_Saroj_Ana1 D403_3846R	CGTTTAGTTGAGGACTATACCGACGAAT CGTGGCCGGTTTCAAGGCCTGCTTGCG ACACCTTCGGATTTTGTCG	For Making internal deletions in Ana1 cDNA, Saroj Saurya
94_Saroj_Ana1 D4_3846NF	GCTGTACAAGACTAGATCAACAAGTTTG TACAAAAAAGCAGGCTTCATGCCGGCCA CGATTCGTCGGTATAGTCCTCAACTAAA CGCCG	For Making internal deletions in Ana1 cDNA, Saroj Saurya
95_Saroj_Ana1 D4_3846NR	CGGCGTTTAGTTGAGGACTATACCGACG AATCGTGGCCGGCATGAAGCCTGCTTTT TTGTACAAACTTGTTGATCTAGTCTTGTA CAGC	For Making internal deletions in Ana1 cDNA, Saroj Saurya
98_Saroj_Ana1 Primer D936-1729aaF	GCTCCCCCTTCTGCTCCATTACATCCCA TGGT GGTTCAATGAGACCCA GCTTTCTTGTACAAAGT GGTTGATGGCCG	For Making internal deletions in Ana1 cDNA, Saroj Saurya
99_Saroj_Ana1 Primer D936-1729aaR	CGGCCATCAACCACTTTGTACAAGAAAG CTGGGTCTCATTGAACCACCATGGGATG TAATGGAG CAGAAGGGGGAGC	For Making internal deletions in Ana1 cDNA, Saroj Saurya
100_Saroj_Ana1 Primer D1-755aaF	GCTGTACAAGACTAGATCAACAAGTTTG TACAAAAAAGCAGGCTTCGGTGCATCAA AGGGTGAC AATGCACAGGAATTGA ATAATATACG	For Making internal deletions in Ana1 cDNA, Saroj Saurya
101_Saroj_Ana1 Primer D1-755aaR	CGTATATTATTCAATTCCTGTGCATTGTC ACCCTTTGATGCACCGAAGCCTGCTTTT TTGTACAAACTTGTTGATCTAGTCTT GTACAGC	For Making internal deletions in Ana1 cDNA, Saroj Saurya
102_Saroj_Ana1 Primer D1144-1729aaF	GCCCCCGAAAAATCGAAAGCACTATCCA CCAGTGAGGATGAGACCCAGCTTTCTTG TACAAAGTGGTTGATGGCCGCG	For Making internal deletions in Ana1 cDNA, Saroj Saurya
103_Saroj_Ana1 Primer D1144-1729aaR	CGCGGCCATCAACCACTTTGTACAAGAA AGCTGGGTCTCATCCTCACTGGTGGATA GTGCTTTCGATTTTTCGGGGGC	For Making internal deletions in Ana1 cDNA, Saroj Saurya

104_Saroj_Ana1 Primer D1008-1729aaF	GCATCGCATGGAGCGGGTGCAAACCTTTATTGCCGACAATGAGACCCAGCTTTCTTGTACAAAGTGGTTGATGGCCGC	For Making internal deletions in Ana1 cDNA, Saroj Saurya
105_Saroj_Ana1 Primer D1008-1729aaR	GCGGCCATCAACCACTTTGTACAAGAAAGCTGGGTCTCATTGTCGGCAATAAAGGTTTGCACCCGCTCCATGCGATGC	For Making internal deletions in Ana1 cDNA, Saroj Saurya
oZN228_Ana1 DCR2	CGCAGAATAATACAGCACGCGGACGAGTAAGGGCAATTGTGGCCGCCACACCGGTGCCCAAGCC	For Making internal deletions in Ana1 cDNA, Zsofia Novak
oZN229_Ana1 DCR2	GGCTTGGGCACCGGTGTGGCGGCCACAATTGCCCTTACTCGTCCGCGTGCTGTATTATTCTGCG	For Making internal deletions in Ana1 cDNA, Zsofia Novak
144_Saroj_Ana1_qc_TAG_for	CGAAAGTCGCCCCGAAAATGAGACCCAGCTTTCTTGTAC	For adding stop codon in Ana1 cDNA, Saroj Saurya
145_Saroj_Ana1_qc_TAG_rev	GTACAAGAAAGCTGGGTCTCATTTTCGGGGCGACTTTCG	For adding stop codon in Ana1 cDNA, Saroj Saurya
20_Saroj_Ana1 F2	AATCCGAAGGTGTCGCAAG	Ana1 Sequencing primer, Saroj Saurya
21_Saroj_Ana1 F3	CGCCCAGAAAATGTGTAG	Ana1 Sequencing primer, Saroj Saurya
22_Saroj_Ana1 F4	AAGCCCAGTTTCCACAACC	Ana1 Sequencing primer, Saroj Saurya
23_Saroj_Ana1 F5	CTGTTGGAGGAACTGAAGG	Ana1 Sequencing primer, Saroj Saurya
24_Saroj_Ana1 F6	TGACAGCACACCAAGAGAC	Ana1 Sequencing primer, Saroj Saurya
25_Saroj_Ana1 F7	CGTAGAACTCAAGAAGGGGAC	Ana1 Sequencing primer, Saroj Saurya
26_Saroj_Ana1 F8	GAGGAAACGCAACTGAGAC	Ana1 Sequencing primer, Saroj Saurya
27_Saroj_Ana1 F9	GGAGCAACAAACGACAGAC	Ana1 Sequencing primer, Saroj Saurya
28_Saroj_Ana1 R2	TGGTCTCGGTTTTTCTTACC	Ana1 Sequencing primer, Saroj Saurya
29_Saroj_Ana1 R3	CAGGTGATAATGGCTGGTC	Ana1 Sequencing primer, Saroj Saurya
30_Saroj_Ana1 R4	CTCTTTGTTGGTTTGCTGAC	Ana1 Sequencing primer, Saroj Saurya
31_Saroj_Ana1 R5	ATCCTCGGCGTTTAGTTG	Ana1 Sequencing primer, Saroj Saurya
32_Saroj_Ana1 R6	AGCCGTCAATGTGGTCTCAG	Ana1 Sequencing primer, Saroj Saurya
33_Saroj_Ana1 R7	CACAGTGGAATCGTCCTTAG	Ana1 Sequencing primer, Saroj Saurya
86_Saroj_Ana1_F19	TGTGAGTTCCTCGTGTGTG	Ana1 Sequencing primer, Saroj Saurya
87_Saroj_Ana1_F20	TTCAAGACCCGCCACAACATCG	Ana1 Sequencing primer, Saroj Saurya
oZN220_Ana1 Seq 1	CATAGTGGAGGACAAAGAAAACCG	Ana1 Sequencing primer, Zsofi Novak
oZN221_Ana1 Seq 2	GATAGATGCGGGAATACACAGAGG	Ana1 Sequencing primer, Zsofi Novak
oZN222_Ana1 Seq 3	GGAACAGGAACTGGACAAACTGAGG	Ana1 Sequencing primer, Zsofi Novak
oZN223_Ana1 Seq 4	CAGGAATTGAATAATATACGTCAGG	Ana1 Sequencing primer, Zsofi Novak
oZN224_Ana1 Seq 5	CATTGAGAAACGTAACCCCTTGTCC	Ana1 Sequencing primer, Zsofi Novak

oZN225_Ana1 Seq 6	CGAACTTACAGAGCTGATCACG	Ana1 Sequencing primer, Zsofi Novak
oZN226_Ana1 Seq 7	ACTGACTACCGTGAGTTTCCTAGC	Ana1 Sequencing primer, Zsofi Novak
oZN227_Ana1 Seq 8	AGCACAACAATAGGTCTAAGGACG	Ana1 Sequencing primer, Zsofi Novak
58_Saroj_attb1	GGGGACAAGTTTGTACAAAAAAGCAGGCTTC	For nest PCR to clone into pDONR, Saroj Saurya
59_Saroj_attb2	GGGGACCACTTTGTACAAGAAAGCTGGGTC	For nest PCR to clone into pDONR, Saroj Saurya
71_Saroj_Cep135 F1	GGGGACAAGTTTGTACAAAAAAGCAGGCTTCATGAATATCAACGATGGTGACTTTA	For cloning Cep135 genomic, Saroj Saurya
72_Saroj_Cep135 CT_R1	GGGGACCACTTTGTACAAGAAAGCTGGGTCAAGAGTCTTCGATGGCACCCGGGGGCTA	For cloning Cep135 genomic without Stop codon, Saroj Saurya
133_Saroj_Cep135 qc_TAA_for	GTGCCATCGAAGACTCTTTAAGACCCAGCTTTCTTGTAC	For adding stop codon in Cep135 cDNA, Saroj Saurya
134_Saroj_Cep135 qc_TAA_rev	GTACAAGAAAGCTGGGTCTTAAAGAGTCTTCGATGGCAC	For adding stop codon in Cep135 cDNA, Saroj Saurya
148_Saroj_Cep135 DONARSacIIF	GTACAAAAAAGCAGGCTTCCCGCGGATGAATATCAACGATGGTG	For adding Cep135 endogenous promoter in front of Cep135cDNA, Saroj Saurya
149_Saroj_Cep135 DONARSacIIR	CACCATCGTTGATATTCATCCGCGGGAAGCCTGCTTTTTTGTAC	For adding Cep135 endogenous promoter in front of Cep135cDNA, Saroj Saurya
161_Saroj_Cep135 promoter_for	TGTACAAAAAAGCAGGCTTCCTGCTCCCGCTGTGGACTG	For adding Cep135 endogenous promoter in front of Cep135cDNA, Saroj Saurya
162_Saroj_Cep135 promoter_rev	AGTCACCATCGTTGATATTCATGGGAAAACACTAATAACAGCAAAAAAATC	For adding Cep135 endogenous promoter in front of Cep135cDNA, Saroj Saurya
183_Cep135 FP1	GACAGCTGGCATTGGACGTC	Cep135 Sequencing primer, Matthew Cottee
184_Cep135 FP2	CTGCGTTGCAAGTGGAACAG	Cep135 Sequencing primer, Matthew Cottee
185_Cep135 FP3	CCACAGCTTCATCCATTACC	Cep135 Sequencing primer, Matthew Cottee
186_Cep135 FP4	CCAACTCCGCATGGACTTAG	Cep135 Sequencing primer, Matthew Cottee
187_Cep135 FP5	GGGCCAAGCTACACTGGAGG	Cep135 Sequencing primer, Matthew Cottee
156_Saroj_Cep135 Seq 1	GAGAGTTGCTCCTATTTCCAC	Cep135 Sequencing primer Saroj Saurya
157_Saroj_Cep135 Seq 2	CTCTTCCTGCTCCACATAAC	Cep135 Sequencing primer Saroj Saurya
158_Saroj_Cep135 Seq 3	GCCCCATCGTAGTTACTTC	Cep135 Sequencing primer Saroj Saurya
159_Saroj_Cep135 Seq 4	GGTAACTTCTTTTCGGTTGC	Cep135 Sequencing primer Saroj Saurya
160_Saroj_Cep135 Seq 5	ATGGGTTTCACACAGACGC	Cep135 Sequencing primer Saroj Saurya
73_Saroj_Sas-6F1	GGGGACAAGTTTGTACAAAAAAGCAGGCTTCATGTGGCCTCCAGGGAGCGAGGATA	For cloning Sas-6 genomic, Saroj Saurya
74_Saroj_Sas-6_CT_R1	GGGGACCACTTTGTACAAGAAAGCTGGGTCTCGCCGATTTTCTTTGCCCGTGGGTA	For cloning Sas-6 genomic without Stop codon, Saroj Saurya

139_Saroj_eSas-6_qc_TAG_for	GGGCAAAGAAAATCGGCGATAGGACCCAGCTTTCTTGTAC	For adding stop codon in Sas-6 genomic cDNA, Saroj Saurya
140_Saroj_eSas-6_qc_TAG_rev	GTACAAGAAAGCTGGGTCCTATCGCCGATTTTCTTTGCCC	For adding stop codon in Sas-6 genomic cDNA, Saroj Saurya
46_Sas-6_F143D_FP	CAGTTTGTTGAAATTCGGTCCGACAAGAACCTAGTTCACCTTAG	For generating head group mutation in Sas-6 genomic DNA, Matthew Cottee
47_Sas-6_F143D_RP	CTAAGGTGAACTAGGTTCTTGTCGGACCGAATTTCAACAAACTG	For generating head group mutation in Sas-6 genomic DNA, Matthew Cottee
106_eSas-6_R183M g548t	CAATATATTCTCGAGCAAAGTATGCAGCAAATGCAGGC	Cloning eSas-6 aa exchange in pDONR sequence, change back from R to M as in WT Sas-6_Nadine Muschalik
107_eSas-6_R183M_antisense g548t	GCCTGCATTTGCTGCATACTTTGCTCGAGAATATATTG	Cloning eSas-6 aa exchange in pDONR sequence, change back from R to M as in WT Sas-6_Nadine Muschalik
2_Saroj_Sas-6F1	GGTCTTTTTGAGGTTGAGC	Sas-6 Sequencing primer, Saroj Saurya
3_Saroj_Sas-6R1	ACGATGTCAAACCCTGTC	Sas-6 Sequencing primer, Saroj Saurya
4_Saroj_Sas-6F2	AACGACAAGGCAGGCTAAG	Sas-6 Sequencing primer, Saroj Saurya
51_stein_eSas-6_Seq 1_for	GGGGACCTGTTTGATAACC	Sas-6 Sequencing primer, Thomas Steinacker
52_stein_eSas-6_Seq 2_for	GCGATGATTGGGGTTAGTG	Sas-6 Sequencing primer, Thomas Steinacker
53_stein_eSas-6_Seq 3_for	TCTACAGGCAGGGCAAATC	Sas-6 Sequencing primer, Thomas Steinacker
54_stein_eSas-6_Seq 4_for	CCACCTTGAACTGAGGATG	Sas-6 Sequencing primer, Thomas Steinacker
55_stein_eSas-6_Seq 5_for	TGGAGATGGACAACTGTGC	Sas-6 Sequencing primer, Thomas Steinacker
56_stein_eSas-6_Seq _rev	GGGGACAACTATCGTTATCG	Sas-6 Sequencing primer, Thomas Steinacker
135_Saroj_CP110 qc_TAG_for	CAAACATCGCCGATTGGATTAGGACCCAGCTTTCTTGTAC	For adding stop codon in CP110 cDNA, Saroj Saurya
136_Saroj_CP110 qc_TAG_rev	GTACAAGAAAGCTGGGTCCTAATCCAATCGGCGATGTTTG	For adding stop codon in CP110 cDNA, Saroj Saurya
37_Saroj_CP110 F1	AAACAGTTGCCCACCATAC	CP110 Sequencing primer, Saroj Saurya
38_Saroj_CP110 F2	CCATCGCCACTAAAACCAC	CP110 Sequencing primer, Saroj Saurya
39_Saroj_CP110 F3	GCAAGAGGCTGTTTAGTCC	CP110 Sequencing primer, Saroj Saurya
40_Saroj_CP110 F4	CCAAACCATCAGAGACACC	CP110 Sequencing primer, Saroj Saurya
41_Saroj_CP110 R1	TGGAACCGAAAGGAGACAGG	CP110 Sequencing primer, Saroj Saurya
42_Saroj_CP110 R2	ATTCATTCGCTCCCGATG	CP110 Sequencing primer, Saroj Saurya
43_Saroj_CP110 R3	GCTGCGGTGATTGTTTTTAC	CP110 Sequencing primer, Saroj Saurya
141_Saroj_Sas-4 qc_TAG_for	CACAGACTATGCCAAGTATTAGGACCCAGCTTTCTTGTAC	For adding stop codon in Sas-4 cDNA, Saroj Saurya
142_Saroj_Sas-4 qc_TAG_rev	GTACAAGAAAGCTGGGTCCTAATACTTGGCATAGTCTGTG	For adding stop codon in Sas-4 cDNA, Saroj Saurya

oZN14_Sas-4	CGCGATACAAGTTCGC	Sas-4 Sequencing primer, Zsofia Novak
oZN15_Sas-4	ATTCAGCTCTTTGAACAG	Sas-4 Sequencing primer, Zsofia Novak
oZN16_Sas-4	CAACAGCAAGATGCTGC	Sas-4 Sequencing primer, Zsofia Novak
146_Saroj_Asl qc_TAA_for	GGCAATGGTCACAGCTAAGACCCAGCTTTCTTG	For adding stop codon in Asl cDNA, Saroj Saurya
147_Saroj_Asl qc_TAA_rev	CAAGAAAGCTGGGTCTTAGCTGTGACCATTGCC	For adding stop codon in Asl cDNA, Saroj Saurya
59_stein_eSak_qc_TAA_for	CGCCTTATTATAATCGCATGCTTCTTTAAGACCCAGCTTTCTTGTACAAAGTTGGC	For adding stop codon in eSak/Plk4, Thomas Steinacker
60_stein_eSak_qc_TAA_rev	GCCAACTTTGTACAAGAAAGCTGGGTCTTAAAGAAGCATGCGATTATAATAAGGCG	For adding stop codon in eSak/Plk4, Thomas Steinacker
261_oLG_SAKcDNA_L89G_F	CAGCTCGAGCACCCCATACACATAGTTGGCGTCCTGAAAG	For generating Sak/Plk4 Shokat L89G (SK1), Lisa Gartenmann
262_oLG_SAKcDNA_L89G_R	CTTTCAGGACGCCAACTATGTGTATGGGGTGCTCGAGCTG	For generating Sak/Plk4 Shokat L89G (SK1), Lisa Gartenmann
265_oLG_SAKcDNA_H190Y_F	GGCAGTCCGTAAGACGTTCGCGATACCACC	For generating Sak/Plk4 Shokat compensation H190Y (SK2), Lisa Gartenmann
266_oLG_SAKcDNA_H190Y_R	GGTGGTATCGCGAACGTCTTACGGACTGCC	For generating Sak/Plk4 Shokat compensation H190Y (SK2), Lisa Gartenmann
Jbaumbach_S10	GGAAGCACTTGTTGTGGTCC	Plk4/Plk4 Sequencing primer Janina Baumbach
Jbaumbach_S11	ATGGAAAGTGGCGATAGTGG	Sak/Plk4 Sequencing primer Janina Baumbach
Jbaumbach_S12	GTCACAATCGGACGAAGACC	Sak/Plk4 Sequencing primer Janina Baumbach
Jbaumbach_P7R	GGGTGAAACACTCGTTTCCG	Sak/Plk4 Sequencing primer Janina Baumbach
63_stein_eAna2 for_attb1	GGGGACAAGTTTGTACAAAAAAGCAGGCTTCCTTTGTACAGGCTTCCCCATACGG	For cloning of genomic Ana2, Thomas Steinacker
64_stein_eAna2 rev_attb2	GGGGACCACTTTGTACAAGAAAGCTGGGTCTCACAACAGCTTCGGCTGGTTCC	For cloning of genomic Ana2, Thomas Steinacker
255_Saroj_Ana2 stop_Q5_R1	TCACAACAGCTTCGGCTGGTTC	To put stop and take off GFP from pRNA, Saroj Saurya
163_Saroj_Ana2 Gib_for	CAGGTAGACGCTTGTCTCCC	Ana2 Gibson cloning primer, Saroj Saurya
164_Saroj_Ana2 Gib_rev	GCTGGTTCCTGATATTCTCCAAG	Ana2 Gibson cloning primer, Saroj Saurya
165_Saroj_Ana2 Gib_rev1	GGGAGACAAGCGTCTACCTG	Ana2 Gibson cloning primer, Saroj Saurya
166_Saroj_Ana2 Gib_for1	CTTGGAGAATATCAGGAACCAGC	Ana2 Gibson cloning primer, Saroj Saurya
11_Saroj_Ana2 1	ATGCTCTTCTCGGTGTTGG	Ana2 Sequencing primer, Saroj Saurya
12_Saroj_Ana2 2	CGGGGCATTACTTGGTATTC	Ana2 Sequencing primer, Saroj Saurya
13_Saroj_Ana2 1	CCAGGTTGTCTATTCCGAC	Ana2 Sequencing primer, Saroj Saurya
65_stein_eAna2 Seq 1_for	AGGCGGGAAGTTAGGATAGC	Ana2 Sequencing primer, Thomas Steinacker
66_stein_eAna2 Seq 2_for	AAGTGGATACACACCCAAAC	Ana2 Sequencing primer, Thomas Steinacker

67_stein_eAna2 Seq 3_for	CGCTACAGACCAAAAAGACG	Ana2 Sequencing primer, Thomas Steinacker
68_stein_eAna2 Seq 4_for	CCAGGAGCGATTTGAGAAG	Ana2 Sequencing primer, Thomas Steinacker
1-Saroj_pWR_R	GTAACCGGACCGGATCATTA	Ubquitin promter Sequencing primer, Saroj Saurya
5_Saroj_UbqF2	CATCTCTATTTTGCCCGC	Ubquitin promter Sequencing primer, Saroj Saurya
6_Saroj_UbqF	CAACAAAGTTGGCGTCGATA	Ubquitin promter Sequencing primer, Saroj Saurya
7_Saroj_UbqF3	TTGGTTTTGAAGGCGACC	Ubquitin promter Sequencing primer, Saroj Saurya
8_Saroj_UbqF4	GTTTATTTTCGCAGAGCCC	Ubquitin promter Sequencing primer, Saroj Saurya
9_Saroj_UbqR1	GAAATCCTCATTCAGCCG	Ubquitin promter Sequencing primer, Saroj Saurya
10_Saroj_UbqR2	CCATTTTGCTTTCGGTGC	Ubquitin promter Sequencing primer, Saroj Saurya
135_pUbqCTGFP-midGFP-RP	CTCTTGAAGAAGTCGTGCCG	Ubquitin promter Sequencing primer, Matthew Cottee
136_pUbqCTGFP-ORF-FP2	TCTCTATTTTGCCCGCAGAATAATC	Ubquitin promter Sequencing primer, Matthew Cottee
60_Jbaumbach_pRNA_F	GTTGTGTGGAATTGTGAGCG	pRNA Sequencing primer Janina Baumbach
60_Jbaumbach_pRNA_R	GAACTTCAGGGTCAGCTTGC	pRNA Sequencing primer Janina Baumbach
130_Saroj_pRNA_EGFP_F1	TGAGCAAAGACCCCAACGAG	pRNA GFP Sequencing primer Saroj Saurya
131_Saroj_pRNA_T7_R1	CTCAAGAACACCCGAATGG	pRNA T7 Sequencing primer Saroj Saurya
132_Saroj_pRNA_T7_R2	GAGCAGATACGAATGGCTAC	pRNA T Sequencing primer Saroj Saurya
248_Saroj_pRNA_For_Q5_R1	GCTAGATCGAACCACTTTGTACAAG	To take off GFP from pRNA vector, Saroj Saurya
249_Saroj_pRNA_Rev_Q5_F1	TAAGCGGCCGCGGATC	To take off GFP from pRNA vector, Saroj Saurya
259_Saroj_pDNR_For_Q5_F2	GACCCAGCTTTCTTGTACAAAGTTGGCATTATAAG	Forward primer to amplify pDNOR to be used along with primer at the end of the gene , Saroj Saurya
41_stein_Cep104_Seq _rev	TTCGCCATCCGTGAACTGTG	Cep104 Sequencing primer, Thomas Steinacker
HR297	AACTCTGGCTGCACTACTCG	Cep104 Sequencing primer, Helio Roque
HR298	CAGCTTTAAGGACTGCCGGA	Cep104 Sequencing primer, Helio Roque
HR299	CAACAAGAGCGTTCCACGAA	Cep104 Sequencing primer, Helio Roque
HR300	TCCATCTGCTCGATTGCACA	Cep104 Sequencing primer, Helio Roque
HR301	CACCAGCTCAGATGCCTCTC	Cep104 Sequencing primer, Helio Roque
HR302	GCTCGATGTCCCCTTTGTCA	Cep104 Sequencing primer, Helio Roque
42_stein_Cep97_Seq 1_for	TTGGGATTTGCGTGCTGAC	Cep97 Sequencing primer, Thomas Steinacker
43_stein_Cep97_Seq 2_for	ACGAAAGTGGCGAGGAGAAG	Cep97 Sequencing primer, Thomas Steinacker

44_stein_Cep97_Seq 3_for	AGCATTGGCAGCATTTCGG	Cep97 Sequencing primer, Thomas Steinacker
45_stein_Cep97_Seq 4_for	GGGCTTGGCAAAATACCTAAG	Cep97 Sequencing primer, Thomas Steinacker
46_stein_Cep97_Seq 5_for	ACGATGGCGAAGGCTTTAG	Cep97 Sequencing primer, Thomas Steinacker
47_stein_Cep97_Seq 6_for	TTGCCAAGAGTGCGAAGTCC	Cep97 Sequencing primer, Thomas Steinacker
48_stein_Cep97_Seq 7_for	AACAAGGACATAGCCGAGC	Cep97 Sequencing primer, Thomas Steinacker
49_stein_Cep97_Seq 8_for	ACACACGCCGCAAATAGAGG	Cep97 Sequencing primer, Thomas Steinacker
50_stein_Cep97_Seq _rev	ACAGTCAGCACGCAAATCC	Cep97 Sequencing primer, Thomas Steinacker
23_stein_Cdk1_for_attb1	GGGGACAAGTTTGTACAAAAAAGCAGG CTTCATGGAGGATTTTGAGAAAATTGAG	For Cloning Cdk1 cDNA, Thomas Steinacker
166_Saroj_Cdk1_rev_attb2_CT	GGGGACCACTTTGTACAAGAAAGCTGG GTCATTTCGAACTAAGCCCGATTG	For Cloning Cdk1 cDNA without stop codon, Saroj Saurya
250_Saroj_Cdk1AF_For_Q5_R 1	GCCCTCGCCAATCTTCTC	To mutagesise Cdk1 to AF (T14Y15), Myt1 sites, Saroj Saurya
251_Saroj_Cdk1AF_Rev_Q5_F 1	GCATTTGGCGTGGTGTATAAG	To mutagesise Cdk1 to AF (T14Y15), Myt1 sites, Saroj Saurya
252_Saroj_Cdk1_stop_For_Q5_ R1	TTAATTTCGAACTAAGCCCGATTG	To put stop and take off GFP from pRNA, Saroj Saurya
254_Saroj_Cdk1Y15F_Rev_Q5 _F1	ACATTTGGCGTGGTGTATAAG	To mutagesise Cdk1 to Y15F , Saroj Saurya
25_stein_Cdk1_Seq 1_for	TTGAGAAGATTGGCGAGGG	Cdk1 Sequencing primer, Thomas Steinacker
26_stein_Cdk1_Seq 2_for	AGCCGCAGAACTTACTAATC	Cdk1 Sequencing primer, Thomas Steinacker
27_stein_Cdk1_Seq 3_for	TCTGAAAACACCTACCGAAG	Cdk1 Sequencing primer, Thomas Steinacker
28_stein_Cdk1_Seq _rev	ATGTGCCCTCGCCAATCTTC	Cdk1 Sequencing primer, Thomas Steinacker
35_stein_String for_attb1	GGGGACAAGTTTGTACAAAAAAGCAGG CTTCATGCTGTGGGAAACTATTGTGGAG G	For Cloning String cDNA, Thomas Steinacker
167_Saroj_String rev_attb2_CT	GGGGACCACTTTGTACAAGAAAGCTGG GTCCAGCATCAGTCGCGAGCGCGACTT C	For Cloning String cDNA without stop codon, Saroj Saurya
295_Saroj_String stop_For_Q5_R1	CTACAGCATCAGTCGCGAGCGC	To put stop codon in String, used 259 as forward primer, Saroj Saurya
37_stein_String Seq 1_for	GCTGTGGGAAACTATTGTGG	String Sequencing primer, Thomas Steinacker
38_stein_String Seq 2_for	TTCCGCATCTTCAACAGCC	String Sequencing primer, Thomas Steinacker
92_stein_String Seq 3_for	ATCGGCGACTTCAGCAAAG	String Sequencing primer, Thomas Steinacker
39_stein_String Seq 4_for	AAAATGTCCCGCTTCCTG	String Sequencing primer, Thomas Steinacker
40_stein_String Seq _rev	CGAACTGCTGGTGTTATTACTG	String Sequencing primer, Thomas Steinacker
1_stein_Wee1 for_attb1	GGGGACAAGTTTGTACAAAAAAGCAGG CTTCATGGCATTCCGCCAGTCGGAGCA CG	For Cloning Wee1 cDNA, Thomas Steinacker
168_Saroj_Wee1 rev_attb2_CT	GGGGACCACTTTGTACAAGAAAGCTGG GTCGATATTGGTGATAACGTTCTTG	For Cloning Wee1 cDNA without stop codon, Saroj Saurya

298_Saroj_Wee1 stop_For_Q5_R1	TCAGATATTGGTGATAACGTTCTTGTTG CGATC	To put stop codon in Wee1, used 259 as forward primer, Saroj Saurya
3_stein_Wee1 Seq 1_for	CACTCCAAAGACCATCCTG	Wee1 Sequencing primer, Thomas Steinacker
4_stein_Wee1 Seq 2_for	GTTCCAATGCGTCAATCG	Wee1 Sequencing primer, Thomas Steinacker
5_stein_Wee1 Seq 3_for	CAGCAGACCAAAGATGACG	Wee1 Sequencing primer, Thomas Steinacker
6_stein_Wee1 Seq 4_for	CTGTTGACTCCAAGAGCAAG	Wee1 Sequencing primer, Thomas Steinacker
20_stein_Wee1 Seq _rev	CTTGTCAAAGTCATCATCGG	Wee1 Sequencing primer, Thomas Steinacker
14_stein_Grapes for_attb1	GGGGACAAGTTTGTACAAAAAAGCAGG CTTCATGGCTGCAACGCTGACGGAAGC G	For Cloning Grapes cDNA, Thomas Steinacker
169_Saroj_Grapes rev_attb2_CT	GGGGACCACTTTGTACAAGAAAGCTGG GTCAGGCACCGAATTTGTAGCAATC	For Cloning Grapes cDNA without stop codon, Saroj Saurya
299_Saroj_Grapes stop_For_Q5_R1	TCAAGGCACCGAATTTGTAGCAATCG	To put stop codon in Grapes, used 259 as forward primer, Saroj Saurya
16_stein_Grapes Seq 1_for	TCGGTGCGAAAGGAGGTATG	Grapes/grp Sequencing primer, Thomas Steinacker
17_stein_Grapes Seq 2_for	GAAAATCTGCTGCTTGACG	Grapes/grp Sequencing primer, Thomas Steinacker
18_stein_Grapes Seq 3_for	TTCCTATGACCTGGTGGACTCG	Grapes/grp Sequencing primer, Thomas Steinacker
19_stein_Grapes Seq 4_for	CACGATGGGATGACACTATC	Grapes/grp Sequencing primer, Thomas Steinacker
22_stein_Grapes Seq _rev	CCTGGAGCATCTTCTGTATG	Grapes/grp Sequencing primer, Thomas Steinacker
7_stein_CyclinB for_attb1	GGGGACAAGTTTGTACAAAAAAGCAGG CTTCATGGTGGGCACAACACTGAAAATG C	For Cloning CyclinB cDNA, Thomas Steinacker
170_Saroj_CyclinB rev_attb2_CT	GGGGACCACTTTGTACAAGAAAGCTGG GTCTTTCCTCTGGCTCTGGCCCAC	For Cloning CyclinB cDNA without stop codon, Saroj Saurya
291_Saroj_CyclinB stop_For_Q5_R1	CTATTTCCTCTGGCTCTGGCCCAC	To put stop codon in CyclinB, used 259 as forward primer, Saroj Saurya
9_stein_CyclinB Seq 1_for	GGGCACAACACTGAAAATG	CyclinB Sequencing primer, Thomas Steinacker
10_stein_CyclinB Seq 2_for	TCCGACCAAGACCACTGTAG	CyclinB Sequencing primer, Thomas Steinacker
11_stein_CyclinB Seq 3_for	CCAATGACAAGGAGAACCTG	CyclinB Sequencing primer, Thomas Steinacker
12_stein_CyclinB Seq 4_for	TCATCACGGACGACACCTAC	CyclinB Sequencing primer, Thomas Steinacker
13_stein_CyclinB Seq 5_for	TACAGGATTCAACGACCG	CyclinB Sequencing primer, Thomas Steinacker
21_stein_CyclinB Seq _rev	CCACGCATTTTCAGTGTTG	CyclinB Sequencing primer, Thomas Steinacker
245_Saroj_Myt1 For_attb2	GGGGACAAGTTTGTACAAAAAAGCAGG CTTCATGGAAAAGCATCATCGCCTGCCC	For Cloning Myt1 cDNA, Saroj Saurya
172_Saroj_Myt1 Rev_attb2_CT	GGGGACCACTTTGTACAAGAAAGCTGG GTCCTCGTCGTCATATTCCAGGACG	For Cloning Myt1 cDNA without stop codon, Saroj Saurya
287_Saroj_Myt1 stop_For_Q5_R1	TCACTCGTCGTCATATTCCAGGACGAAG	To put stop codon in Myt1, used 259 as forward primer, Saroj Saurya
173_Saroj_Myt1 Seq 1_F	ATCCTTCGGCGAGGTATTC	Myt1 Sequencing primer Saroj Saurya

174_Saroj_Myt1 Seq 2_F	CAGACTTTGGACTGGTCATC	Myt1 Sequencing primer Saroj Saurya
175_Saroj_Myt1 Seq 3_F	AGCCGCCTTTCGTTACCTTC	Myt1 Sequencing primer Saroj Saurya
176_Saroj_Myt1 Seq 4_F	CCCGTCTGGATTTGCTAAAG	Myt1 Sequencing primer Saroj Saurya
177_Saroj_Myt1 Seq 5_F	ACGACGACAAACACAGAC	Myt1 Sequencing primer Saroj Saurya
184_Saroj_CyclinE For_attb1	GGGGACAAGTTTGTACAAAAAAGCAGGCTTCATGGGTTTAAATGCCAAGAGTG	For Cloning short CyclinE cDNA, Saroj Saurya
185_Saroj_CyclinE Rev_attb2_CT	GGGGACCACTTTGTACAAGAAAGCTGGGTCGGGATTGCTTCTACTGCTGCAGC	For Cloning short CyclinE cDNA without stop codon, Saroj Saurya
186_Saroj_CyclinE For_Q5_F1	CCGCTTACTAGAAGTGTTTGTTCTACCAGC	For mutagenize mutant CyclinE back to WT, Saroj Saurya
187_Saroj_CyclinE Rev_Q5_R1	AAAAATGCTTAACATGAAGCCTGCTTTTTTGTAC	For mutagenize mutant CyclinE back to WT, Saroj Saurya
297_Saroj_CyclinE stop_For_Q5_R1	TCAGGGATTGCTTCTACTGCTGCAGC	To put stop codon in CyclinE, used 259 as forward primer, Saroj Saurya
178_Saroj_CyclinE Seq F1	TTCTACCAGCAGCACTGAG	CyclinE Sequencing primer Saroj Saurya
179_Saroj_CyclinE Seq F2	GCGACTTCCAATGGCAATAAAC	CyclinE Sequencing primer Saroj Saurya
180_Saroj_CyclinE Seq F3	AAGACGGAGGATGATGACC	CyclinE Sequencing primer Saroj Saurya
181_Saroj_CyclinE Seq F4	CGAGGTCTGTGAAGTTTACAAG	CyclinE Sequencing primer Saroj Saurya
182_Saroj_CyclinE Seq F5	CAACTATTCCTACTCGGTGC	CyclinE Sequencing primer Saroj Saurya
183_Saroj_CyclinE Seq F6	AAAGTCTTCTGACGCCTCCC	CyclinE Sequencing primer Saroj Saurya
192_Saroj_CyclinA For_attb1	GGGGACAAGTTTGTACAAAAAAGCAGGCTTCATGGCCAGTTTCCAGATCCACCAAG	For Cloning CyclinA cDNA, Saroj Saurya
193_Saroj_CyclinA Rev_attb2_CT	GGGGACCACTTTGTACAAGAAAGCTGGGTCAAACTTATAAAACAAATTC	For Cloning CyclinA cDNA without stop codon, Saroj Saurya
294_Saroj_CyclinA stop_For_Q5_R1	TTAAAACTTATAAAACAAATTCACGTTCGATTTAG	To put stop codon in CyclinA, used 259 as forward primer, Saroj Saurya
188_Saroj_CyclinA Seq F1	GGAAAAGCGGAGAAAAATGC	CyclinA Sequencing primer Saroj Saurya
189_Saroj_CyclinA Seq F2	CCAACTGGAAGAGTCAAGG	CyclinA Sequencing primer Saroj Saurya
190_Saroj_CyclinA Seq F3	GTCTTCATCAACACCTATGCTG	CyclinA Sequencing primer Saroj Saurya
191_Saroj_CyclinA Seq F4	AAGAGGATGAGCACCAGCAG	CyclinA Sequencing primer Saroj Saurya
198_Saroj_CyclinD For_attb1	GGGGACAAGTTTGTACAAAAAAGCAGGCTTCATGGATCTTTTATGCTCGGAAATC	For Cloning CyclinD cDNA, Saroj Saurya
199_Saroj_CyclinD Rev_attb2_CT	GGGGACCACTTTGTACAAGAAAGCTGGGTCAAATGTAACGTCTTGTATCTCG	For Cloning CyclinD cDNA without stop codon, Saroj Saurya
246_Saroj_CyclinD For_Q5_F1	CGCCACCACCACCGACAGCGACCCAATCAATCC	To mutagenize mutant CyclinD back to WT, Saroj Saurya
247_Saroj_CyclinD Rev_Q5_R1	GCGGTGGTGGAGGTGGCGGAGGCGGCTCC	To mutagenize mutant CyclinD back to WT, Saroj Saurya

290_Saroj_CyclinD stop_For_Q5_R1	TCAAAATGTAACGTCTTGTATCTCGTTTTGAGC	To put stop codon in CyclinD, used 259 as forward primer, Saroj Saurya
194_Saroj_CyclinD Seq F1	GCTCGGAAATCATAGTCTACG	CyclinD Sequencing primer Saroj Saurya
195_Saroj_CyclinD Seq F2	TCACATTGCCAACGACTC	CyclinD Sequencing primer Saroj Saurya
196_Saroj_CyclinD Seq F3	TATGTGCTAAGTCGCTTGGGCTGG	CyclinD Sequencing primer Saroj Saurya
197_Saroj_CyclinD Seq F4	ACATCAATCGCAGCATCTC	CyclinD Sequencing primer Saroj Saurya
214_Saroj_Cdk4 For_attb1	GGGGACAAGTTTGTACAAAAAAGCAGGCTTCATGTCATATGTACGCCAGC	For Cloning Cdk4 cDNA, Saroj Saurya
215_Saroj_Cdk4 Rev_attb2_CT	GGGGACCACTTTGTACAAGAAAGCTGGGTCTAGGGGTTCCTGCTGAAAGTAATCG	For Cloning Cdk4 cDNA without stop codon, Saroj Saurya
293_Saroj_Cdk4 stop_For_Q5_R1	CTATAGGGGTTCCTGCTGAAAGTAATCGTGC	To put stop codon in Cdk4, used 259 as forward primer, Saroj Saurya
211_Saroj_Cdk4 Seq F1	TCCGTTCAACTACCAGGAG	Cdk4 Sequencing primer Saroj Saurya
212_Saroj_Cdk4 Seq F2	CTCACACCGTATCATCCATC	Cdk4 Sequencing primer Saroj Saurya
213_Saroj_Cdk4 Seq F3	GCATCCAAAGAGACCAAAAGAC	Cdk4 Sequencing primer Saroj Saurya
219_Saroj_Cdk2 For_attb1	GGGGACAAGTTTGTACAAAAAAGCAGGCTTCATGACCACCATTCTAGATAAC	For Cloning Cdk2 cDNA, Saroj Saurya
220_Saroj_Cdk2 Rev_attb2_CT	GGGGACCACTTTGTACAAGAAAGCTGGGTCGACGAGCCGCGTTAGACG	For Cloning Cdk2 cDNA without stop codon, Saroj Saurya
296_Saroj_Cdk2 stop_For_Q5_R1	TCAGACGAGCCGCGTTAGACGC	To put stop codon in Cdk2, used 259 as forward primer, Saroj Saurya
216_Saroj_Cdk2 Seq F1	AAAAGATTGGCGAGGGCACC	Cdk2 Sequencing primer Saroj Saurya
217_Saroj_Cdk2 Seq F2	AACCTTCTCGTAGACACGGC	Cdk2 Sequencing primer Saroj Saurya
218_Saroj_Cdk2 Seq F3	ACGCTTACTTCCGCAATG	Cdk2 Sequencing primer Saroj Saurya
209_Saroj_Twine For_attb1	GGGGACAAGTTTGTACAAAAAAGCAGGCTTCATGGCGAGCAAGCGGCTAATGC	For Cloning Twine cDNA, Saroj Saurya
210_Saroj_Twine Rev_attb2_CT	GGGGACCACTTTGTACAAGAAAGCTGGGTCCTCGGCGTAGAGCAGTCGTGAACG	For Cloning Twine cDNA without stop codon, Saroj Saurya
289_Saroj_Twine_stop_For_Q5_R1	TCACTCGGCGTAGAGCAGTCGTG	To put stop codon in Twine, used 259 as forward primer, Saroj Saurya
205_Saroj_Twine Seq F1	GGAGGAAGAAGATGATGAAAGTGG	Twine/Twe Sequencing primer Saroj Saurya
206_Saroj_Twine Seq F2	CCAACAAAAAAGGCTCCCTG	Twine/Twe Sequencing primer Saroj Saurya
207_Saroj_Twine Seq F3	CAGATACAGGAGGCGTTTC	Twine/Twe Sequencing primer Saroj Saurya
208_Saroj_Twine Seq F4	AAGACCAAGTCCTGGCAATGTGGC	Twine/Twe Sequencing primer Saroj Saurya
203_Saroj_Dacapo For_attb1	GGGGACAAGTTTGTACAAAAAAGCAGGCTTCATGGTCAGTGCCCGAGTCCTG	For Cloning Dacapo cDNA, Saroj Saurya
204_Saroj_Dacapo Rev_attb2_CT	GGGGACCACTTTGTACAAGAAAGCTGGGTCGTTGTGGCGCGGCCGCTTCAAC	For Cloning Dacapo cDNA without stop codon, Saroj Saurya
288_Saroj_Dacapo stop_For_Q5_R1	TTAGTTGTGGCGCGGCCGC	To put stop codon in Dacapo, used 259 as forward primer, Saroj Saurya

200_Saroj_Dacapo Seq F1	GAGTCCTGAATCCTGTGATG	Dacapo/Dap Sequencing primer Saroj Saurya
201_Saroj_Dacapo Seq F2	TGGACATTTTGGTCAACGAG	Dacapo/Dap Sequencing primer Saroj Saurya
202_Saroj_Dacapo Seq F3	ACACTTTGGGGCGATGTTG	Dacapo/Dap Sequencing primer Saroj Saurya
226_Saroj_Cdc6 For_attb1	GGGGACAAGTTTGTACAAAAAAGCAGGCTTCATGGCTGCCGTACGCCGCTCCACG	For Cloning Cdc6 cDNA, Saroj Saurya
227_Saroj_Cdc6 Rev_attb2_CT	GGGGACCACTTTGTACAAGAAAGCTGGGTCCTTGCTCAGGCAGGCGGTATCG	For Cloning Cdc6 cDNA without stop codon, Saroj Saurya
292_Saroj_Cdc6 stop_For_Q5_R1	TCACTTGCTCAGGCAGGCGGTATC	To put stop codon in Cdc6, used 259 as forward primer, Saroj Saurya
221_Saroj_Cdc6 Seq F1	GCCGAAAAAAGTGCTTGC	Cdc6 Sequencing primer Saroj Saurya
222_Saroj_Cdc6 Seq F2	ACACAAGACTGAAACGGC	Cdc6 Sequencing primer Saroj Saurya
223_Saroj_Cdc6 Seq F3	CAGCATAGCAAGTGTAGGAG	Cdc6 Sequencing primer Saroj Saurya
224_Saroj_Cdc6 Seq F4	ATCAGTGGAGATGTGCGAAGGG	Cdc6 Sequencing primer Saroj Saurya
225_Saroj_Cdc6 Seq F5	AGGTCTACAGGAGAGTGTGC	Cdc6 Sequencing primer Saroj Saurya
235_Saroj_Orc1 For_attb1	GGGGACAAGTTTGTACAAAAAAGCAGGCTTCATGGTTAATAAAGAGAACGCCCGCAG	For Cloning Orc1 cDNA, Saroj Saurya
236_Saroj_Orc1 Rev_attb2_CT	GGGGACCACTTTGTACAAGAAAGCTGGGTCGTTGACCATCTCTTCCACTCTG	For Cloning Orc1 cDNA without stop codon, Saroj Saurya
300_Saroj_Orc1 stop_For_Q5_R1	TTAGTTGACCATCTCTTCCACTCTGAGGGC	To put stop codon in Orc1, used 259 as forward primer, Saroj Saurya
228_Saroj_Orc1 Seq F1	TAAAGAGAACGCCCGCAGTGTG	Orc1 Sequencing primer Saroj Saurya
229_Saroj_Orc1 Seq F2	ACGACACGCCAACAAACTG	Orc1 Sequencing primer Saroj Saurya
230_Saroj_Orc1 Seq F3	CCGCAACCTAAATCTCAGC	Orc1 Sequencing primer Saroj Saurya
231_Saroj_Orc1 Seq F4	TATCCACTCCGAAAAGGGG	Orc1 Sequencing primer Saroj Saurya
232_Saroj_Orc1 Seq F5	ACTGTCACTGGCGTCATAC	Orc1 Sequencing primer Saroj Saurya
233_Saroj_Orc1 Seq F6	TTACCCGTCTCACATTCCAGCC	Orc1 Sequencing primer Saroj Saurya
234_Saroj_Orc1 Seq F7	ATCAGTGAACATTCCCGC	Orc1 Sequencing primer Saroj Saurya
243_Saroj_Dup For_attb1	GGGGACAAGTTTGTACAAAAAAGCAGGCTTCATGGCCCAGCCATCGGTAGCTG	For Cloning dup cDNA, Saroj Saurya
244_Saroj_Dup Rev_attb2_CT	GGGGACCACTTTGTACAAGAAAGCTGGGTCATTGCTCTTGGCGTTAGCCACG	For Cloning dup cDNA without stop codon, Saroj Saurya
301_Saroj_Dup cdt1_stop_For_Q5_R1	CTAATTGCTCTTGGCGTTAGCCACGC	To put stop codon in Dup, used 259 as forward primer, Saroj Saurya
237_Saroj_Dup Seq F1	ATCAGTATCAAGAACAGGCG	Dup/Cdt1 Sequencing primer Saroj Saurya
238_Saroj_Dup Seq F2	CGACGAGGTAAAAACGAAGGTATC	Dup/Cdt1 Sequencing primer Saroj Saurya
239_Saroj_Dup Seq F3	GCAAGGAGACCATCACATTC	Dup/Cdt1 Sequencing primer Saroj Saurya

240_Saroj_Dup Seq F4	CGCAGTTTGATTTGGAGAGTTGTC	Dup/Cdt1 Sequencing primer Saroj Saurya
241_Saroj_Dup Seq F5	AAGGCTTTGGAGGCGATGAC	Dup/Cdt1 Sequencing primer Saroj Saurya
242_Saroj_Dup Seq F6	CGCATCTGAAACTACTTGCC	Dup/Cdt1 Sequencing primer Saroj Saurya

References

Al-Dosari, M.S., Shaheen, R., Colak, D., and Alkuraya, F.S. (2010). Novel CENPJ mutation causes Seckel syndrome. J. Med. Genet. *47*, 411–414.

Al-Jassar, C., Andreeva, A., Barnabas, D.D., McLaughlin, S.H., Johnson, C.M., Yu, M., and van Breugel, M. (2017). The Ciliopathy-Associated Cep104 Protein Interacts with Tubulin and Nek1 Kinase. Structure *25*, 146–156.

Allen, R.D. (1969). The morphogenesis of basal bodies and accessory structures of the cortex of the ciliated protozoan Tetrahymena pyriformis. J. Cell Biol. *40*, 716–733.

Alvarez-Cabrera, A.L., Delgado, S., Gil-Carton, D., Mortuza, G.B., Montoya, G., Sorzano, C.O.S., Tang, T.K., and Carazo, J.M. (2017). Electron Microscopy Structural Insights into CPAP Oligomeric Behavior: A Plausible Assembly Process of a Supramolecular Scaffold of the Centrosome. Front Mol Biosci *4*, 17.

Andersen, J.S., Wilkinson, C.J., Mayor, T., Mortensen, P., Nigg, E.A., and Mann, M. (2003). Proteomic characterization of the human centrosome by protein correlation profiling. Nature *426*, 570–574.

Arquint, C., and Nigg, E.A. (2014). STIL microcephaly mutations interfere with APC/C-mediated degradation and cause centriole amplification. Curr. Biol. *24*, 351–360.

Arquint, C., and Nigg, E.A. (2016). The PLK4-STIL-SAS-6 module at the core of centriole duplication. Biochem. Soc. Trans. *44*, 1253–1263.

Arquint, C., Cubizolles, F., Morand, A., Schmidt, A., and Nigg, E.A. (2018). The SKP1-Cullin-F-box E3 ligase βTrCP and CDK2 cooperate to control STIL abundance and centriole number. Open Biol *8*, 170253.

Arquint, C., Gabryjonczyk, A.-M., Imseng, S., Böhm, R., Sauer, E., Hiller, S., Nigg, E.A., and Maier, T. (2015). STIL binding to Polo-box 3 of PLK4 regulates centriole duplication. Elife *4*, 1948.

Arquint, C., Sonnen, K.F., Stierhof, Y.-D., and Nigg, E.A. (2012). Cell-cycle-regulated expression of STIL controls centriole number in human cells. J. Cell. Sci. *125*, 1342–1352.

Atherton-Fessler, S., Hannig, G., and Piwnica-Worms, H. (1993). Reversible tyrosine phosphorylation and cell cycle control. Semin. Cell Biol. *4*, 433–442.

Avidor-Reiss, T., Maer, A.M., Koundakjian, E., Polyanovsky, A., Keil, T., Subramaniam, S., and Zuker, C.S. (2004). Decoding Cilia Function. Cell *117*, 527–539.

Aydogan, M.G., Wainman, A., Saurya, S., Steinacker, T.L., Caballe, A., Novak, Z.A., Baumbach, J., Muschalik, N., and Raff, J.W. (2018). A homeostatic clock sets daughter centriole size in flies. J. Cell Biol. *217*, 1233–1248.

Azimzadeh, J. (2014). Exploring the evolutionary history of centrosomes. Philos. Trans. R. Soc. Lond., B, Biol. Sci. *369*, 20130453–20130453.

Azimzadeh, J., and Marshall, W.F. (2010). Building the centriole. Curr. Biol. *20*, R816–R825.

Azimzadeh, J., Hergert, P., Delouvée, A., Euteneuer, U., Formstecher, E., Khodjakov, A., and Bornens, M. (2009). hPOC5 is a centrin-binding protein required for assembly of full-length centrioles. J. Cell Biol. *185*, 101–114.

Baker, J.D., Adhikarakunnathu, S., and Kernan, M.J. (2004). Mechanosensory-defective, male-sterile unc mutants identify a novel basal body protein required for ciliogenesis in Drosophila. Development *131*, 3411–3422.

Banterle, N., and Gönczy, P. (2017). Centriole Biogenesis: From Identifying the Characters to Understanding the Plot. Annu. Rev. Cell Dev. Biol. *33*, 23–49.

Basto, R., Brunk, K., Vinadogrova, T., Peel, N., Franz, A., Khodjakov, A., and Raff, J.W. (2008). Centrosome amplification can initiate tumorigenesis in flies. Cell *133*, 1032–1042.

Basto, R., Lau, J., Vinogradova, T., Gardiol, A., Woods, C.G., Khodjakov, A., and Raff, J.W. (2006). Flies without centrioles. Cell *125*, 1375–1386.

Bauer, M., Cubizolles, F., Schmidt, A., and Nigg, E.A. (2016). Quantitative analysis of human centrosome architecture by targeted proteomics and fluorescence imaging. Embo J. *35*, 2152–2166.

Baumbach, J., Novak, Z.A., Raff, J.W., and Wainman, A. (2015). Dissecting the function and assembly of acentriolar microtubule organizing centers in Drosophila cells in vivo. PLoS Genet. *11*, e1005261.

Beach, D., Durkacz, B., and Nurse, P. (1982). Functionally homologous cell cycle control genes in budding and fission yeast. Nature *300*, 706–709.

Bennett, H., Presti, A., Adams, D., Rios, J., Benito, C., and Cohen, D. (2014). A prenatal presentation of severe microcephaly and brain anomalies in a patient with novel compound heterozygous mutations in the STIL gene found postnatally with exome analysis. Pediatr. Neurol. *51*, 434–436.

Berthet, C., Aleem, E., Coppola, V., Tessarollo, L., and Kaldis, P. (2003). Cdk2 knockout mice are viable. Current Biology *13*, 1775–1785.

Bettencourt-Dias, M., Rodrigues-Martins, A., Carpenter, L., Riparbelli, M., Lehmann, L., Gatt, M.K., Carmo, N., Balloux, F., Callaini, G., and Glover, D.M. (2005). SAK/PLK4 is required for centriole duplication and flagella development. Current Biology *15*, 2199–2207.

Bettencourt-Dias, M., Hildebrandt, F., Pellman, D., Woods, G., and Godinho, S.A. (2011). Centrosomes and cilia in human disease. Trends Genet. *27*, 307–315.

Bewley, G.C. (1987). Drosophila: A practical approach. Edited by D.B. Roberts Oxford-Washington, DC: IRL Press, 1986. 295 pp. Developmental Genetics *8*, 59–60.

Bianchi, S., Rogala, K.B., Dynes, N.J., Hilbert, M., Leidel, S.A., Steinmetz, M.O., Gönczy, P., and Vakonakis, I. (2018). Interaction between the Caenorhabditis elegans centriolar protein SAS-5 and microtubules facilitates organelle assembly. Mol. Biol. Cell *29*, 722–735.

Blachon, S., Cai, X., Roberts, K.A., Yang, K., Polyanovsky, A., Church, A., and Avidor-Reiss, T. (2009). A Proximal Centriole-Like Structure Is Present in Drosophila Spermatids and Can Serve as a Model to Study Centriole Duplication. Genetics *182*, 133–144.

Blachon, S., Gopalakrishnan, J., Omori, Y., Polyanovsky, A., Church, A., Nicastro, D., Malicki, J., and Avidor-Reiss, T. (2008). Drosophila asterless and vertebrate Cep152 Are orthologs essential for centriole duplication. Genetics *180*, 2081–2094.

Blachon, S., Khire, A., and Avidor-Reiss, T. (2014). The origin of the second centriole in the zygote of Drosophila melanogaster. Genetics *197*, 199–205.

Bonaccorsi, S., Giansanti, M.G., and Gatti, M. (1998). Spindle self-organization and

cytokinesis during male meiosis in asterless mutants of Drosophila melanogaster. J. Cell Biol. *142*, 751–761.

Bond, J., Roberts, E., Springell, K., Lizarraga, S.B., Lizarraga, S., Scott, S., Higgins, J., Hampshire, D.J., Morrison, E.E., Leal, G.F., et al. (2005). A centrosomal mechanism involving CDK5RAP2 and CENPJ controls brain size. Nat. Genet. *37*, 353–355.

Booher, R.N., Holman, P.S., and Fattaey, A. (1997). Human Myt1 is a cell cycle-regulated kinase that inhibits Cdc2 but not Cdk2 activity. J. Biol. Chem. *272*, 22300–22306.

Bornens, M. (2002). Centrosome composition and microtubule anchoring mechanisms. Current Opinion in Cell Biology *14*, 25–34.

Bornens, M. (2012). The centrosome in cells and organisms. Science *335*, 422–426.

Bourouh, M., Dhaliwal, R., Rana, K., Sinha, S., Guo, Z., and Swan, A. (2016). Distinct and Overlapping Requirements for Cyclins A, B and B3 in Drosophila Female Meiosis. G3 (Bethesda).

Brand, A.H., and Perrimon, N. (1993). Targeted gene expression as a means of altering cell fates and generating dominant phenotypes. Development *118*, 401–415.

Braun, D.A., and Hildebrandt, F. (2017). Ciliopathies. Cold Spring Harb Perspect Biol *9*, a028191.

Brownlee, C.W., and Rogers, G.C. (2013). Show me your license, please: deregulation of centriole duplication mechanisms that promote amplification. Cellular and Molecular Life Sciences *70*, 1021–1034.

Brust-Mascher, I., Sommi, P., Cheerambathur, D.K., and Scholey, J.M. (2009). Kinesin-5-dependent poleward flux and spindle length control in Drosophila embryo mitosis. Mol. Biol. Cell *20*, 1749–1762.

Buttrick, G.J., Beaumont, L.M.A., Leitch, J., Yau, C., Hughes, J.R., and Wakefield, J.G. (2008). Akt regulates centrosome migration and spindle orientation in the early Drosophila melanogaster embryo. J. Cell Biol. *180*, 537–548.

Caldon, C.E., and Musgrove, E.A. (2010). Distinct and redundant functions of cyclin E1 and cyclin E2 in development and cancer. Cell Div *5*, 2.

Callaini, G., and Riparbelli, M.G. (1990). Centriole and centrosome cycle in the early Drosophila embryo. J. Cell. Sci. *97 (Pt 3)*, 539–543.

Callaini, G., Whitfield, W.G., and Riparbelli, M.G. (1997). Centriole and centrosome dynamics during the embryonic cell cycles that follow the formation of the cellular blastoderm in Drosophila. Exp. Cell Res. *234*, 183–190.

Carvalho-Santos, Z., Azimzadeh, J., Pereira-Leal, J.B., and Bettencourt-Dias, M. (2011). Evolution: Tracing the origins of centrioles, cilia, and flagella. J. Cell Biol. *194*, 165–175.

Carvalho-Santos, Z., Machado, P., Alvarez-Martins, I., Gouveia, S.M., Jana, S.C., Duarte, P., Amado, T., Branco, P., Freitas, M.C., Silva, S.T.N., et al. (2012). BLD10/CEP135 is a microtubule-associated protein that controls the formation of the flagellum central microtubule pair. Developmental Cell *23*, 412–424.

Carvalho-Santos, Z., Machado, P., Branco, P., Tavares-Cadete, F., Rodrigues-Martins, A., Pereira-Leal, J.B., and Bettencourt-Dias, M. (2010). Stepwise evolution of the centriole-assembly pathway. J. Cell. Sci. *123*, 1414–1426.

Catalano, R.D., Vlad, M., and Kennedy, R.C. (1997). Differential display to identify and isolate novel genes expressed during spermatogenesis. Mol. Hum. Reprod. *3*, 215–221.

Chan, J.Y. (2011). A clinical overview of centrosome amplification in human cancers. Int. J. Biol. Sci. *7*, 1122–1144.

Chang, C.-W., Hsu, W.-B., Tsai, J.-J., Tang, C.-J.C., and Tang, T.K. (2016). CEP295 interacts with microtubules and is required for centriole elongation. J. Cell. Sci. *129*, 2501–2513.

Chang, J., Cizmecioglu, O., Hoffmann, I., and Rhee, K. (2010). PLK2 phosphorylation is critical for CPAP function in procentriole formation during the centrosome cycle. Embo J. *29*, 2395–2406.

Chavali, P.L., Pütz, M., and Gergely, F. (2014). Small organelle, big responsibility: the role of centrosomes in development and disease. Philos. Trans. R. Soc. Lond., B, Biol. Sci. *369*, 20130468–20130468.

Chen, C., Inaba, M., Venkei, Z.G., and Yamashita, Y.M. (2016). Klp10A, a stem cell centrosome-enriched kinesin, balances asymmetries in Drosophila male germline stem cell division. Elife *5*, 91.

Chen, H.-Y., Wu, C.-T., Tang, C.-J.C., Lin, Y.-N., Wang, W.-J., and Tang, T.K. (2017). Human microcephaly protein RTTN interacts with STIL and is required to build full-length centrioles. Nature Communications *8*, 247.

Chen, Z., Indjeian, V.B., McManus, M., Wang, L., and Dynlacht, B.D. (2002). CP110, a cell cycle-dependent CDK substrate, regulates centrosome duplication in human cells. Developmental Cell *3*, 339–350.

Chrétien, D., Buendia, B., Fuller, S.D., and Karsenti, E. (1997). Reconstruction of the centrosome cycle from cryoelectron micrographs. J. Struct. Biol. *120*, 117–133.

Cinalli, R.M., and Lehmann, R. (2013). A spindle-independent cleavage pathway controls germ cell formation in Drosophila. Nat. Cell Biol. *15*, 839–845.

Cizmecioglu, O., Arnold, M., Bahtz, R., Settele, F., Ehret, L., Haselmann-Weiss, U., Antony, C., and Hoffmann, I. (2010). Cep152 acts as a scaffold for recruitment of Plk4 and CPAP to the centrosome. J. Cell Biol. *191*, 731–739.

Cohen, S.E., and Golden, S.S. (2015). Circadian Rhythms in Cyanobacteria. Microbiol. Mol. Biol. Rev. *79*, 373–385.

Comartin, D., Gupta, G.D., Fussner, E., Coyaud, E., Hasegan, M., Archinti, M., Cheung, S.W.T., Pinchev, D., Lawo, S., Raught, B., et al. (2013). CEP120 and SPICE1 cooperate with CPAP in centriole elongation. Curr. Biol. *23*, 1360–1366.

Conduit, P.T., and Raff, J.W. (2010). Cnn dynamics drive centrosome size asymmetry to ensure daughter centriole retention in Drosophila neuroblasts. Curr. Biol. *20*, 2187–2192.

Conduit, P.T., and Raff, J.W. (2015). Different Drosophila cell types exhibit differences in mitotic centrosome assembly dynamics. Curr. Biol. *25*, R650–R651.

Conduit, P.T., Brunk, K., Dobbelaere, J., Dix, C.I., Lucas, E.P., and Raff, J.W. (2010). Centrioles regulate centrosome size by controlling the rate of Cnn incorporation into the PCM. Curr. Biol. *20*, 2178–2186.

Conduit, P.T., Feng, Z., Richens, J.H., Baumbach, J., Wainman, A., Bakshi, S.D., Dobbelaere, J., Johnson, S., Lea, S.M., and Raff, J.W. (2014a). The centrosome-specific

phosphorylation of Cnn by Polo/Plk1 drives Cnn scaffold assembly and centrosome maturation. Developmental Cell *28*, 659–669.

Conduit, P.T., Richens, J.H., Wainman, A., Holder, J., Vicente, C.C., Pratt, M.B., Dix, C.I., Novak, Z.A., Dobbie, I.M., Schermelleh, L., et al. (2014b). A molecular mechanism of mitotic centrosome assembly in Drosophila. Elife *3*, e03399.

Conduit, P.T., Wainman, A., and Raff, J.W. (2015a). Centrosome function and assembly in animal cells. Nature Publishing Group *16*, 611–624.

Conduit, P.T., Wainman, A., Novak, Z.A., Weil, T.T., and Raff, J.W. (2015b). Re-examining the role of Drosophila Sas-4 in centrosome assembly using two-colour-3D-SIM FRAP. Elife *4*, 15915.

Cormier, A., Clément, M.-J., Knossow, M., Lachkar, S., Savarin, P., Toma, F., Sobel, A., Gigant, B., and Curmi, P.A. (2009). The PN2-3 domain of centrosomal P4.1-associated protein implements a novel mechanism for tubulin sequestration. J. Biol. Chem. *284*, 6909–6917.

Cottee, M.A., Johnson, S., Raff, J.W., and Lea, S.M. (2017). A key centriole assembly interaction interface between human PLK4 and STIL appears to not be conserved in flies. Biol Open *6*, 381–389.

Cottee, M.A., Muschalik, N., Johnson, S., Leveson, J., Raff, J.W., and Lea, S.M. (2015). The homo-oligomerisation of both Sas-6 and Ana2 is required for efficient centriole assembly in flies. Elife *4*, e07236.

Cottee, M.A., Muschalik, N., Wong, Y.L., Johnson, C.M., Johnson, S., Andreeva, A., Oegema, K., Lea, S.M., Raff, J.W., and van Breugel, M. (2013). Crystal structures of the CPAP/STIL complex reveal its role in centriole assembly and human microcephaly. Elife *2*, e01071.

Cottee, M.A., Raff, J.W., Lea, S.M., and Roque, H. (2011). SAS-6 oligomerization: the key to the centriole? Nat. Chem. Biol. *7*, 650–653.

Coulonval, K., Kooken, H., and Roger, P.P. (2011). Coupling of T161 and T14 phosphorylations protects cyclin B-CDK1 from premature activation. Mol. Biol. Cell *22*, 3971–3985.

Cunha-Ferreira, I., Bento, I., Pimenta-Marques, A., Jana, S.C., Lince-Faria, M., Duarte, P., Borrego-Pinto, J., Gilberto, S., Amado, T., Brito, D., et al. (2013). Regulation of autophosphorylation controls PLK4 self-destruction and centriole number. Curr. Biol. *23*, 2245–2254.

Dahl, K.D., Sankaran, D.G., Bayless, B.A., Pinter, M.E., Galati, D.F., Heasley, L.R., Giddings, T.H., and Pearson, C.G. (2015). A Short CEP135 Splice Isoform Controls Centriole Duplication. Curr. Biol. *25*, 2591–2596.

Dammermann, A., Maddox, P.S., Desai, A., and Oegema, K. (2008). SAS-4 is recruited to a dynamic structure in newly forming centrioles that is stabilized by the gamma-tubulin-mediated addition of centriolar microtubules. J. Cell Biol. *180*, 771–785.

Dammermann, A., Müller-Reichert, T., Pelletier, L., Habermann, B., Desai, A., and Oegema, K. (2004). Centriole assembly requires both centriolar and pericentriolar material proteins. Developmental Cell *7*, 815–829.

Dantas, T.J., Daly, O.M., Conroy, P.C., Tomas, M., Wang, Y., Lalor, P., Dockery, P., Ferrando-May, E., and Morrison, C.G. (2013). Calcium-binding capacity of centrin2 is required for linear POC5 assembly but not for nucleotide excision repair. PLoS ONE *8*,

e68487.

David, A., Amartely, H., Rabinowicz, N., Shamir, M., Friedler, A., and Izraeli, S. (2016). Molecular basis of the STIL coiled coil oligomerization explains its requirement for de-novo formation of centrosomes in mammalian cells. Sci Rep *6*, 24296.

De Magistris, P., and Antonin, W. (2018). The Dynamic Nature of the Nuclear Envelope. Curr. Biol. *28*, R487–R497.

Delattre, M., and Gönczy, P. (2004). The arithmetic of centrosome biogenesis. J. Cell. Sci. *117*, 1619–1630.

Delattre, M., Canard, C., and Gönczy, P. (2006). Sequential protein recruitment in C. elegans centriole formation. Current Biology *16*, 1844–1849.

Delattre, M., Leidel, S., Wani, K., Baumer, K., Bamat, J., Schnabel, H., Feichtinger, R., Schnabel, R., and Gönczy, P. (2004). Centriolar SAS-5 is required for centrosome duplication in C. elegans. Nat. Cell Biol. *6*, 656–664.

Delgehyr, N., Rangone, H., Fu, J., Mao, G., Tom, B., Riparbelli, M.G., Callaini, G., and Glover, D.M. (2012). Klp10A, a microtubule-depolymerizing kinesin-13, cooperates with CP110 to control Drosophila centriole length. Curr. Biol. *22*, 502–509.

Denu, R.A., Shabbir, M., Nihal, M., Singh, C.K., Longley, B.J., Burkard, M.E., and Ahmad, N. (2018). Centriole Overduplication is the Predominant Mechanism Leading to Centrosome Amplification in Melanoma. Mol. Cancer Res. *16*, 517–527.

Dinçer, T., Yorgancıoğlu-Budak, G., Ölmez, A., Er, İ., Dodurga, Y., Özdemir, Ö.M., Toraman, B., Yıldırım, A., Sabir, N., Akarsu, N.A., et al. (2017). Analysis of centrosome and DNA damage response in PLK4 associated Seckel syndrome. Eur. J. Hum. Genet. *25*, 1118–1125.

Dippell, R.V. (1968). The development of basal bodies in paramecium. Proc. Natl. Acad. Sci. U.S.a. *61*, 461–468.

Dobbelaere, J., Josué, F., Suijkerbuijk, S., Baum, B., Tapon, N., and Raff, J. (2008). A genome-wide RNAi screen to dissect centriole duplication and centrosome maturation in Drosophila. PLoS Biol. *6*, e224.

Dong, G. (2015). Building a ninefold symmetrical barrel: structural dissections of centriole assembly. Open Biol *5*, 150082.

Duerinckx, S., and Abramowicz, M. (2018). The genetics of congenitally small brains. Seminars in Cell and Developmental Biology *76*, 76–85.

Dulić, V., Lees, E., and Reed, S.I. (1992). Association of human cyclin E with a periodic G1-S phase protein kinase. Science *257*, 1958–1961.

Dzhindzhev, N.S., Tzolovsky, G., Lipinszki, Z., Schneider, S., Lattao, R., Fu, J., Debski, J., Dadlez, M., and Glover, D.M. (2014). Plk4 phosphorylates Ana2 to trigger Sas6 recruitment and procentriole formation. Curr. Biol. *24*, 2526–2532.

Dzhindzhev, N.S., Yu, Q.D., Weiskopf, K., Tzolovsky, G., Cunha-Ferreira, I., Riparbelli, M., Rodrigues-Martins, A., Bettencourt-Dias, M., Callaini, G., and Glover, D.M. (2010). Asterless is a scaffold for the onset of centriole assembly. Nature *467*, 714–718.

Edgar, B.A., and O'Farrell, P.H. (1989). Genetic control of cell division patterns in the Drosophila embryo. Cell *57*, 177–187.

Emmerich, J., Meyer, C.A., la Cruz, de, A.F.A., Edgar, B.A., and Lehner, C.F. (2004). Cyclin D does not provide essential Cdk4-independent functions in Drosophila. Genetics *168*, 867–875.

Erez, A., Perelman, M., Hewitt, S.M., Cojacaru, G., Goldberg, I., Shahar, I., Yaron, P., Muler, I., Campaner, S., Amariglio, N., et al. (2004). Sil overexpression in lung cancer characterizes tumors with increased mitotic activity. Oncogene *23*, 5371–5377.

Evans, T., Rosenthal, E.T., Youngblom, J., Distel, D., and Hunt, T. (1983). Cyclin: a protein specified by maternal mRNA in sea urchin eggs that is destroyed at each cleavage division. Cell *33*, 389–396.

Farooq, M., Fatima, A., Mang, Y., Hansen, L., Kjaer, K.W., Baig, S.M., Larsen, L.A., and Tommerup, N. (2016). A novel splice site mutation in CEP135 is associated with primary microcephaly in a Pakistani family. J. Hum. Genet. *61*, 271–273.

Farrell, J.A., and O'Farrell, P.H. (2014). From egg to gastrula: how the cell cycle is remodeled during the Drosophila mid-blastula transition. Annu. Rev. Genet. *48*, 269–294.

Feng, Z., Caballe, A., Wainman, A., Johnson, S., Haensele, A.F.M., Cottee, M.A., Conduit, P.T., Lea, S.M., and Raff, J.W. (2017). Structural Basis for Mitotic Centrosome Assembly in Flies. Cell *169*, 1078–1089.e13.

Fernández-Álvarez, A., Bez, C., O'Toole, E.T., Morphew, M., and Cooper, J.P. (2016). Mitotic Nuclear Envelope Breakdown and Spindle Nucleation Are Controlled by Interphase Contacts between Centromeres and the Nuclear Envelope. Developmental Cell *39*, 544–559.

Fliegauf, M., Benzing, T., and Omran, H. (2007). When cilia go bad: cilia defects and ciliopathies. Nature Publishing Group *8*, 880–893.

Foe, V.E., and Alberts, B.M. (1983). Studies of nuclear and cytoplasmic behaviour during the five mitotic cycles that precede gastrulation in Drosophila embryogenesis. J. Cell. Sci. *61*, 31–70.

Fong, C.S., Kim, M., Yang, T.T., Liao, J.-C., and Tsou, M.-F.B. (2014). SAS-6 assembly templated by the lumen of cartwheel-less centrioles precedes centriole duplication. Developmental Cell *30*, 238–245.

Franz, A., Roque, H., Saurya, S., Dobbelaere, J., and Raff, J.W. (2013). CP110 exhibits novel regulatory activities during centriole assembly in Drosophila. J. Cell Biol. *203*, 785–799.

Fu, J., and Glover, D.M. (2012). Structured illumination of the interface between centriole and peri-centriolar material. Open Biol *2*, 120104–120104.

Fu, J., Hagan, I.M., and Glover, D.M. (2015). The centrosome and its duplication cycle. Cold Spring Harb Perspect Biol *7*, a015800.

Fu, J., Lipinszki, Z., Rangone, H., Min, M., Mykura, C., Chao-Chu, J., Schneider, S., Dzhindzhev, N.S., Gottardo, M., Riparbelli, M.G., et al. (2016). Conserved molecular interactions in centriole-to-centrosome conversion. Nat. Cell Biol. *18*, 87–99.

Fung, T.K., and Poon, R.Y.C. (2005). A roller coaster ride with the mitotic cyclins. Seminars in Cell and Developmental Biology *16*, 335–342.

Fırat-Karalar, E.N., and Stearns, T. (2014). The centriole duplication cycle. Philos. Trans. R. Soc. Lond., B, Biol. Sci. *369*, 20130460–20130460.

Gabriel, E., Wason, A., Ramani, A., Gooi, L.M., Keller, P., Pozniakovsky, A., Poser, I., Noack,

F., Telugu, N.S., Calegari, F., et al. (2016). CPAP promotes timely cilium disassembly to maintain neural progenitor pool. Embo J. *35*, 803–819.

Galletta, B.J., Fagerstrom, C.J., Schoborg, T.A., McLamarrah, T.A., Ryniawec, J.M., Buster, D.W., Slep, K.C., Rogers, G.C., and Rusan, N.M. (2016a). A centrosome interactome provides insight into organelle assembly and reveals a non-duplication role for Plk4. Nature Communications *7*, 12476.

Galletta, B.J., Jacobs, K.C., Fagerstrom, C.J., and Rusan, N.M. (2016b). Asterless is required for centriole length control and sperm development. J. Cell Biol. *213*, 435–450.

Ganem, N.J., Godinho, S.A., and Pellman, D. (2009). A mechanism linking extra centrosomes to chromosomal instability. Nature *460*, 278–282.

Garcez, P.P., Diaz-Alonso, J., Crespo-Enriquez, I., Castro, D., Bell, D., and Guillemot, F. (2015). Cenpj/CPAP regulates progenitor divisions and neuronal migration in the cerebral cortex downstream of Ascl1. Nature Communications *6*, 6474.

Geng, Y., Eaton, E.N., Picón, M., Roberts, J.M., Lundberg, A.S., Gifford, A., Sardet, C., and Weinberg, R.A. (1996). Regulation of cyclin E transcription by E2Fs and retinoblastoma protein. Oncogene *12*, 1173–1180.

Gergely, F., Kidd, D., Jeffers, K., Wakefield, J.G., and Raff, J.W. (2000). D-TACC: a novel centrosomal protein required for normal spindle function in the early Drosophila embryo. Embo J. *19*, 241–252.

Gibbons, I.R., and Grimstone, A.V. (1960). On flagellar structure in certain flagellates. J Biophys Biochem Cytol *7*, 697–716.

Godinho, S.A., and Pellman, D. (2014). Causes and consequences of centrosome abnormalities in cancer. Philos. Trans. R. Soc. Lond., B, Biol. Sci. *369*, 20130467–20130467.

Goehring, N.W., and Hyman, A.A. (2012). Organelle growth control through limiting pools of cytoplasmic components. Curr. Biol. *22*, R330–R339.

Goetz, S.C., and Anderson, K.V. (2010). The primary cilium: a signalling centre during vertebrate development. Nat. Rev. Genet. *11*, 331–344.

Gong, W.J., and Golic, K.G. (2003). Ends-out, or replacement, gene targeting in Drosophila. Proc. Natl. Acad. Sci. U.S.a. *100*, 2556–2561.

González, C., Tavosanis, G., and Mollinari, C. (1998). Centrosomes and microtubule organisation during Drosophila development. J. Cell. Sci. *111 (Pt 18)*, 2697–2706.

Gopalakrishnan, J., Mennella, V., Blachon, S., Zhai, B., Smith, A.H., Megraw, T.L., Nicastro, D., Gygi, S.P., Agard, D.A., and Avidor-Reiss, T. (2011). Sas-4 provides a scaffold for cytoplasmic complexes and tethers them in a centrosome. Nature Communications *2*, 359.

Goshima, G., and Vale, R.D. (2005). Cell cycle-dependent dynamics and regulation of mitotic kinesins in Drosophila S2 cells. Mol. Biol. Cell *16*, 3896–3907.

Goshima, G., Wollman, R., Goodwin, S.S., Zhang, N., Scholey, J.M., Vale, R.D., and Stuurman, N. (2007). Genes required for mitotic spindle assembly in Drosophila S2 cells. Science *316*, 417–421.

Gottardo, M., Callaini, G., and Riparbelli, M.G. (2015a). Aurora A inhibition by MNL8054 promotes centriole elongation during Drosophila male meiosis. Cell Cycle *14*, 2844–2852.

Gottardo, M., Callaini, G., and Riparbelli, M.G. (2013). The cilium-like region of the Drosophila spermatocyte: an emerging flagellum? J. Cell. Sci. *126*, 5441–5452.

Gottardo, M., Callaini, G., and Riparbelli, M.G. (2015b). The Drosophila centriole - conversion of doublets into triplets within the stem cell niche. J. Cell. Sci. *128*, 2437–2442.

Gottardo, M., Callaini, G., and Riparbelli, M.G. (2015c). Structural characterization of procentrioles in Drosophila spermatids. Cytoskeleton (Hoboken) *72*, 576–584.

Gottardo, M., Callaini, G., and Riparbelli, M.G. (2016). Klp10A modulates the localization of centriole-associated proteins during Drosophila male gametogenesis. Cell Cycle *15*, 3432–3441.

Gottardo, M., Pollarolo, G., Llamazares, S., Reina, J., Riparbelli, M.G., Callaini, G., and Gonzalez, C. (2015d). Loss of Centrobin Enables Daughter Centrioles to Form Sensory Cilia in Drosophila. Curr. Biol. *25*, 2319–2324.

Gönczy, P. (2012). Towards a molecular architecture of centriole assembly. Nature Publishing Group *13*, 425–435.

Gönczy, P. (2015). Centrosomes and cancer: revisiting a long-standing relationship. Nat. Rev. Cancer *15*, 639–652.

Greenan, G.A., Keszthelyi, B., Vale, R.D., and Agard, D.A. (2018). Insights into centriole geometry revealed by cryotomography of doublet and triplet centrioles. Elife *7*, 351.

Guderian, G., Westendorf, J., Uldschmid, A., and Nigg, E.A. (2010). Plk4 trans-autophosphorylation regulates centriole number by controlling betaTrCP-mediated degradation. J. Cell. Sci. *123*, 2163–2169.

Gudi, R., Haycraft, C.J., Bell, P.D., Li, Z., and Vasu, C. (2015). Centrobin-mediated regulation of the centrosomal protein 4.1-associated protein (CPAP) level limits centriole length during elongation stage. J. Biol. Chem. *290*, 6890–6902.

Gudi, R., Zou, C., Dhar, J., Gao, Q., and Vasu, C. (2014). Centrobin-centrosomal protein 4.1-associated protein (CPAP) interaction promotes CPAP localization to the centrioles during centriole duplication. J. Biol. Chem. *289*, 15166–15178.

Gudi, R., Zou, C., Li, J., and Gao, Q. (2011). Centrobin-tubulin interaction is required for centriole elongation and stability. J. Cell Biol. *193*, 711–725.

Guernsey, D.L., Jiang, H., Hussin, J., Arnold, M., Bouyakdan, K., Perry, S., Babineau-Sturk, T., Beis, J., Dumas, N., Evans, S.C., et al. (2010). Mutations in centrosomal protein CEP152 in primary microcephaly families linked to MCPH4. Am. J. Hum. Genet. *87*, 40–51.

Guichard, P., Hamel, V., Le Guennec, M., Banterle, N., Iacovache, I., Nemčíková, V., Flückiger, I., Goldie, K.N., Stahlberg, H., Lévy, D., et al. (2017). Cell-free reconstitution reveals centriole cartwheel assembly mechanisms. Nature Communications *8*, 14813.

Guichard, P., Chrétien, D., Marco, S., and Tassin, A.-M. (2010). Procentriole assembly revealed by cryo-electron tomography. Embo J. *29*, 1565–1572.

Guichard, P., Desfosses, A., Maheshwari, A., Hachet, V., Dietrich, C., Brune, A., Ishikawa, T., Sachse, C., and Gönczy, P. (2012). Cartwheel architecture of Trichonympha basal body. Science *337*, 553–553.

Guichard, P., Hachet, V., Majubu, N., Neves, A., Demurtas, D., Olieric, N., Flückiger, I., Yamada, A., Kihara, K., Nishida, Y., et al. (2013). Native architecture of the centriole proximal

region reveals features underlying its 9-fold radial symmetry. Curr. Biol. *23*, 1620–1628.

Guichard, P., Hamel, V., and Gönczy, P. (2018). The Rise of the Cartwheel: Seeding the Centriole Organelle. Bioessays *40*, e1700241.

Gupta, A., and Kitagawa, D. (2018). Ultrastructural diversity between centrioles of eukaryotes. J. Biochem. *164*, 1–8.

Gupta, H., Badarudeen, B., George, A., Thomas, G.E., Gireesh, K.K., and Manna, T.K. (2015). Human SAS-6 C-Terminus Nucleates and Promotes Microtubule Assembly in Vitro by Binding to Microtubules. Biochemistry *54*, 6413–6422.

Habedanck, R., Stierhof, Y.-D., Wilkinson, C.J., and Nigg, E.A. (2005). The Polo kinase Plk4 functions in centriole duplication. Nat. Cell Biol. *7*, 1140–1146.

Hatch, E.M., Kulukian, A., Holland, A.J., Cleveland, D.W., and Stearns, T. (2010). Cep152 interacts with Plk4 and is required for centriole duplication. J. Cell Biol. *191*, 721–729.

Hatzopoulos, G.N., Erat, M.C., Cutts, E., Rogala, K.B., Slater, L.M., Stansfeld, P.J., and Vakonakis, I. (2013). Structural analysis of the G-box domain of the microcephaly protein CPAP suggests a role in centriole architecture. Structure *21*, 2069–2077.

Hilbert, M., Erat, M.C., Hachet, V., Guichard, P., Blank, I.D., Flückiger, I., Slater, L., Lowe, E.D., Hatzopoulos, G.N., Steinmetz, M.O., et al. (2013). Caenorhabditis elegans centriolar protein SAS-6 forms a spiral that is consistent with imparting a ninefold symmetry. Proc. Natl. Acad. Sci. U.S.a. *110*, 11373–11378.

Hilbert, M., Noga, A., Frey, D., Hamel, V., Guichard, P., Kraatz, S.H.W., Pfreundschuh, M., Hosner, S., Flückiger, I., Jaussi, R., et al. (2016). SAS-6 engineering reveals interdependence between cartwheel and microtubules in determining centriole architecture. Nat. Cell Biol. *18*, 393–403.

Hinchcliffe, E.H., and Sluder, G. (2001). Centrosome duplication: three kinases come up a winner! Current Biology *11*, R698–R701.

Hiraki, M., Nakazawa, Y., Kamiya, R., and Hirono, M. (2007). Bld10p constitutes the cartwheel-spoke tip and stabilizes the 9-fold symmetry of the centriole. Current Biology *17*, 1778–1783.

Hirono, M. (2014). Cartwheel assembly. Philos. Trans. R. Soc. Lond., B, Biol. Sci. *369*, 20130458–20130458.

Holland, A.J., Fachinetti, D., Zhu, Q., Bauer, M., Verma, I.M., Nigg, E.A., and Cleveland, D.W. (2012). The autoregulated instability of Polo-like kinase 4 limits centrosome duplication to once per cell cycle. Genes Dev. *26*, 2684–2689.

Holland, A.J., Lan, W., Niessen, S., Hoover, H., and Cleveland, D.W. (2010). Polo-like kinase 4 kinase activity limits centrosome overduplication by autoregulating its own stability. J. Cell Biol. *188*, 191–198.

Honda, R., Tanaka, H., Ohba, Y., and Yasuda, H. (1995). Mouse p87wee1 kinase is regulated by M-phase specific phosphorylation. Chromosome Res. *3*, 300–308.

Hsu, W.-B., Hung, L.-Y., Tang, C.-J.C., Su, C.-L., Chang, Y., and Tang, T.K. (2008). Functional characterization of the microtubule-binding and -destabilizing domains of CPAP and d-SAS-4. Exp. Cell Res. *314*, 2591–2602.

Hung, L.Y., Tang, C.J., and Tang, T.K. (2000). Protein 4.1 R-135 interacts with a novel

centrosomal protein (CPAP) which is associated with the gamma-tubulin complex. Mol. Cell. Biol. *20*, 7813–7825.

Hung, L.-Y., Chen, H.-L., Chang, C.-W., Li, B.-R., and Tang, T.K. (2004). Identification of a novel microtubule-destabilizing motif in CPAP that binds to tubulin heterodimers and inhibits microtubule assembly. Mol. Biol. Cell *15*, 2697–2706.

Hussain, M.S., Baig, S.M., Neumann, S., Nürnberg, G., Farooq, M., Ahmad, I., Alef, T., Hennies, H.C., Technau, M., Altmüller, J., et al. (2012). A truncating mutation of CEP135 causes primary microcephaly and disturbed centrosomal function. Am. J. Hum. Genet. *90*, 871–878.

Ishikawa, H., Kubo, A., Tsukita, S., and Tsukita, S. (2005). Odf2-deficient mother centrioles lack distal/subdistal appendages and the ability to generate primary cilia. Nat. Cell Biol. *7*, 517–524.

Izquierdo, D., Wang, W.-J., Uryu, K., and Tsou, M.-F.B. (2014). Stabilization of cartwheel-less centrioles for duplication requires CEP295-mediated centriole-to-centrosome conversion. CellReports *8*, 957–965.

Jacobs, H.W., Knoblich, J.A., and Lehner, C.F. (1998). Drosophila Cyclin B3 is required for female fertility and is dispensable for mitosis like Cyclin B. Genes Dev. *12*, 3741–3751.

Jana, S.C., Bazan, J.F., and Bettencourt-Dias, M. (2012). Polo Boxes Come out of the Crypt: A New View of PLK Function and Evolution. Structure *20*, 2191.

Jana, S.C., Bettencourt-Dias, M., Durand, B., and Megraw, T.L. (2016a). Drosophila melanogaster as a model for basal body research. Cilia *5*, 22.

Jana, S.C., Marteil, G., and Bettencourt-Dias, M. (2014). Mapping molecules to structure: unveiling secrets of centriole and cilia assembly with near-atomic resolution. Current Opinion in Cell Biology *26*, 96–106.

Jana, S.C., Mendonça, S., Werner, S., and Bettencourt-Dias, M. (2016b). Methods to Study Centrosomes and Cilia in Drosophila. Methods Mol. Biol. *1454*, 215–236.

Jayaraman, D., Bae, B.-I., and Walsh, C.A. (2018). The Genetics of Primary Microcephaly. Annu Rev Genomics Hum Genet *19*, 177–200.

Jeffery, J.M., Grigoriev, I., Poser, I., van der Horst, A., Hamilton, N., Waterhouse, N., Bleier, J., Subramaniam, V.N., Maly, I.V., Akhmanova, A., et al. (2013). Centrobin regulates centrosome function in interphase cells by limiting pericentriolar matrix recruitment. Cell Cycle *12*, 899–906.

Ji, J.-Y., Squirrell, J.M., and Schubiger, G. (2004). Both cyclin B levels and DNA-replication checkpoint control the early embryonic mitoses in Drosophila. Development *131*, 401–411.

Jiang, K., Toedt, G., Montenegro Gouveia, S., Davey, N.E., Hua, S., van der Vaart, B., Grigoriev, I., Larsen, J., Pedersen, L.B., Bezstarosti, K., et al. (2012). A Proteome-wide screen for mammalian SxIP motif-containing microtubule plus-end tracking proteins. Curr. Biol. *22*, 1800–1807.

Jin, Z., Homola, E.M., Goldbach, P., Choi, Y., Brill, J.A., and Campbell, S.D. (2005). Drosophila Myt1 is a Cdk1 inhibitory kinase that regulates multiple aspects of cell cycle behavior during gametogenesis. Development *132*, 4075–4085.

Jin, Z., Homola, E., Tiong, S., and Campbell, S.D. (2008). Drosophila myt1 is the major cdk1 inhibitory kinase for wing imaginal disc development. Genetics *180*, 2123–2133.

Kakar, N., Ahmad, J., Morris-Rosendahl, D.J., Altmüller, J., Friedrich, K., Barbi, G., Nürnberg, P., Kubisch, C., Dobyns, W.B., and Borck, G. (2015). STIL mutation causes autosomal recessive microcephalic lobar holoprosencephaly. Hum. Genet. *134*, 45–51.

Kalaszczynska, I., Geng, Y., Iino, T., Mizuno, S.-I., Choi, Y., Kondratiuk, I., Silver, D.P., Wolgemuth, D.J., Akashi, K., and Sicinski, P. (2009). Cyclin A is redundant in fibroblasts but essential in hematopoietic and embryonic stem cells. Cell *138*, 352–365.

Kalay, E., Yigit, G., Aslan, Y., Brown, K.E., Pohl, E., Bicknell, L.S., Kayserili, H., Li, Y., Tüysüz, B., Nürnberg, G., et al. (2011). CEP152 is a genome maintenance protein disrupted in Seckel syndrome. Nat. Genet. *43*, 23–26.

Kawakami, M., Mustachio, L.M., Zheng, L., Chen, Y., Rodriguez-Canales, J., Mino, B., Kurie, J.M., Roszik, J., Villalobos, P.A., Thu, K.L., et al. (2018). Polo-like kinase 4 inhibition produces polyploidy and apoptotic death of lung cancers. Proc. Natl. Acad. Sci. U.S.a. *115*, 1913–1918.

Keller, D., Orpinell, M., Olivier, N., Wachsmuth, M., Mahen, R., Wyss, R., Hachet, V., Ellenberg, J., Manley, S., and Gönczy, P. (2014). Mechanisms of HsSAS-6 assembly promoting centriole formation in human cells. J. Cell Biol. *204*, 697–712.

Keller, L.C., Geimer, S., Romijn, E., Yates, J., Zamora, I., and Marshall, W.F. (2009). Molecular architecture of the centriole proteome: the conserved WD40 domain protein POC1 is required for centriole duplication and length control. Mol. Biol. Cell *20*, 1150–1166.

Kemp, C.A., Kopish, K.R., Zipperlen, P., Ahringer, J., and O'Connell, K.F. (2004). Centrosome maturation and duplication in C. elegans require the coiled-coil protein SPD-2. Developmental Cell *6*, 511–523.

Khan, M.A., Rupp, V.M., Orpinell, M., Hussain, M.S., Altmüller, J., Steinmetz, M.O., Enzinger, C., Thiele, H., Höhne, W., Nürnberg, G., et al. (2014). A missense mutation in the PISA domain of HsSAS-6 causes autosomal recessive primary microcephaly in a large consanguineous Pakistani family. Hum. Mol. Genet. *23*, 5940–5949.

Khire, A., Vizuet, A.A., Davila, E., and Avidor-Reiss, T. (2015). Asterless Reduction during Spermiogenesis Is Regulated by Plk4 and Is Essential for Zygote Development in Drosophila. Curr. Biol. *25*, 2956–2963.

Kim, T.-S., Park, J.-E., Shukla, A., Choi, S., Murugan, R.N., Lee, J.H., Ahn, M., Rhee, K., Bang, J.K., Kim, B.Y., et al. (2013). Hierarchical recruitment of Plk4 and regulation of centriole biogenesis by two centrosomal scaffolds, Cep192 and Cep152. Proc. Natl. Acad. Sci. U.S.a. *110*, E4849–E4857.

Kirkham, M., Müller-Reichert, T., Oegema, K., Grill, S., and Hyman, A.A. (2003). SAS-4 is a C. elegans centriolar protein that controls centrosome size. Cell *112*, 575–587.

Kitagawa, D., Kohlmaier, G., Keller, D., Strnad, P., Balestra, F.R., Flückiger, I., and Gönczy, P. (2011a). Spindle positioning in human cells relies on proper centriole formation and on the microcephaly proteins CPAP and STIL. J. Cell. Sci. *124*, 3884–3893.

Kitagawa, D., Vakonakis, I., Olieric, N., Hilbert, M., Keller, D., Olieric, V., Bortfeld, M., Erat, M.C., Flückiger, I., Gönczy, P., et al. (2011b). Structural basis of the 9-fold symmetry of centrioles. Cell *144*, 364–375.

Klebba, J.E., Buster, D.W., McLamarrah, T.A., Rusan, N.M., and Rogers, G.C. (2015a). Autoinhibition and relief mechanism for Polo-like kinase 4. Proc. Natl. Acad. Sci. U.S.a. *112*, E657–E666.

Klebba, J.E., Buster, D.W., Nguyen, A.L., Swatkoski, S., Gucek, M., Rusan, N.M., and

Rogers, G.C. (2013). Polo-like kinase 4 autodestructs by generating its Slimb-binding phosphodegron. Curr. Biol. *23*, 2255–2261.

Klebba, J.E., Galletta, B.J., Nye, J., Plevock, K.M., Buster, D.W., Hollingsworth, N.A., Slep, K.C., Rusan, N.M., and Rogers, G.C. (2015b). Two Polo-like kinase 4 binding domains in Asterless perform distinct roles in regulating kinase stability. J. Cell Biol. *208*, 401–414.

Kleylein-Sohn, J., Westendorf, J., Le Clech, M., Habedanck, R., Stierhof, Y.-D., and Nigg, E.A. (2007). Plk4-induced centriole biogenesis in human cells. Developmental Cell *13*, 190–202.

Knoblich, J.A., and Lehner, C.F. (1993). Synergistic action of Drosophila cyclins A and B during the G2-M transition. Embo J. *12*, 65–74.

Knoblich, J.A., Sauer, K., Jones, L., Richardson, H., Saint, R., and Lehner, C.F. (1994). Cyclin E controls S phase progression and its down-regulation during Drosophila embryogenesis is required for the arrest of cell proliferation. Cell *77*, 107–120.

Knorz, V.J., Spalluto, C., Lessard, M., Purvis, T.L., Adigun, F.F., Collin, G.B., Hanley, N.A., Wilson, D.I., and Hearn, T. (2010). Centriolar association of ALMS1 and likely centrosomal functions of the ALMS motif-containing proteins C10orf90 and KIAA1731. Mol. Biol. Cell *21*, 3617–3629.

Kobayashi, T., Kim, S., Lin, Y.-C., Inoue, T., and Dynlacht, B.D. (2014). The CP110-interacting proteins Talpid3 and Cep290 play overlapping and distinct roles in cilia assembly. J. Cell Biol. *204*, 215–229.

Kobayashi, T., Tsang, W.Y., Li, J., Lane, W., and Dynlacht, B.D. (2011). Centriolar kinesin Kif24 interacts with CP110 to remodel microtubules and regulate ciliogenesis. Cell *145*, 914–925.

Kohlmaier, G., Loncarek, J., Meng, X., McEwen, B.F., Mogensen, M.M., Spektor, A., Dynlacht, B.D., Khodjakov, A., and Gönczy, P. (2009). Overly long centrioles and defective cell division upon excess of the SAS-4-related protein CPAP. Curr. Biol. *19*, 1012–1018.

Korzeniewski, N., Cuevas, R., Duensing, A., and Duensing, S. (2010). Daughter centriole elongation is controlled by proteolysis. Mol. Biol. Cell *21*, 3942–3951.

Kraatz, S., Guichard, P., Obbineni, J.M., Olieric, N., Hatzopoulos, G.N., Hilbert, M., Sen, I., Missimer, J., Gönczy, P., and Steinmetz, M.O. (2016). The Human Centriolar Protein CEP135 Contains a Two-Stranded Coiled-Coil Domain Critical for Microtubule Binding. Structure *24*, 1358–1371.

Kratz, A.-S., Bärenz, F., Richter, K.T., and Hoffmann, I. (2015). Plk4-dependent phosphorylation of STIL is required for centriole duplication. Biol Open *4*, 370–377.

Kumar, R.A. (2009). STIL on my small brain: a new gene for microcephaly. Clin. Genet. *76*, 501–502.

Kuriyama, R., and Borisy, G.G. (1981a). Centriole cycle in Chinese hamster ovary cells as determined by whole-mount electron microscopy. J. Cell Biol. *91*, 814–821.

Kuriyama, R., and Borisy, G.G. (1981b). Microtubule-nucleating activity of centrosomes in Chinese hamster ovary cells is independent of the centriole cycle but coupled to the mitotic cycle. J. Cell Biol. *91*, 822–826.

Lacey, K.R., Jackson, P.K., and Stearns, T. (1999). Cyclin-dependent kinase control of centrosome duplication. Proc. Natl. Acad. Sci. U.S.a. *96*, 2817–2822.

Lane, M.E., Sauer, K., Wallace, K., Jan, Y.N., Lehner, C.F., and Vaessin, H. (1996). Dacapo, a cyclin-dependent kinase inhibitor, stops cell proliferation during Drosophila development. Cell *87*, 1225–1235.

Lattao, R., Kovács, L., and Glover, D.M. (2017). The Centrioles, Centrosomes, Basal Bodies, and Cilia of Drosophila melanogaster. Genetics *206*, 33–53.

Lee, H.S., Simon, J.A., and Lis, J.T. (1988). Structure and expression of ubiquitin genes of Drosophila melanogaster. Mol. Cell. Biol. *8*, 4727–4735.

Lee, M., Seo, M.Y., Chang, J., Hwang, D.S., and Rhee, K. (2017). PLK4 phosphorylation of CP110 is required for efficient centriole assembly. Cell Cycle *16*, 1225–1234.

Leidel, S., and Gönczy, P. (2003). SAS-4 is essential for centrosome duplication in C elegans and is recruited to daughter centrioles once per cell cycle. Developmental Cell *4*, 431–439.

Leidel, S., and Gönczy, P. (2005). Centrosome duplication and nematodes: recent insights from an old relationship. Developmental Cell *9*, 317–325.

Leidel, S., Delattre, M., Cerutti, L., Baumer, K., and Gönczy, P. (2005). SAS-6 defines a protein family required for centrosome duplication in C. elegans and in human cells. Nat. Cell Biol. *7*, 115–125.

Lettman, M.M., Wong, Y.L., Viscardi, V., Niessen, S., Chen, S.-H., Shiau, A.K., Zhou, H., Desai, A., and Oegema, K. (2013). Direct binding of SAS-6 to ZYG-1 recruits SAS-6 to the mother centriole for cartwheel assembly. Developmental Cell *25*, 284–298.

Levine, M.S., Bakker, B., Boeckx, B., Moyett, J., Lu, J., Vitre, B., Spierings, D.C., Lansdorp, P.M., Cleveland, D.W., Lambrechts, D., et al. (2017). Centrosome Amplification Is Sufficient to Promote Spontaneous Tumorigenesis in Mammals. Developmental Cell *40*, 313–322.e315.

Li, J., D'Angiolella, V., Seeley, E.S., Kim, S., Kobayashi, T., Fu, W., Campos, E.I., Pagano, M., and Dynlacht, B.D. (2013). USP33 regulates centrosome biogenesis via deubiquitination of the centriolar protein CP110. Nature *495*, 255–259.

Lim, S., and Kaldis, P. (2013). Cdks, cyclins and CKIs: roles beyond cell cycle regulation. Development *140*, 3079–3093.

Lin, Y.-N., Wu, C.-T., Lin, Y.-C., Hsu, W.-B., Tang, C.-J.C., Chang, C.-W., and Tang, T.K. (2013a). CEP120 interacts with CPAP and positively regulates centriole elongation. J. Cell Biol. *202*, 211–219.

Lin, Y.-C., Chang, C.-W., Hsu, W.-B., Tang, C.-J.C., Lin, Y.-N., Chou, E.-J., Wu, C.-T., and Tang, T.K. (2013b). Human microcephaly protein CEP135 binds to hSAS-6 and CPAP, and is required for centriole assembly. Embo J. *32*, 1141–1154.

Linck, R.W., and Stephens, R.E. (2007). Functional protofilament numbering of ciliary, flagellar, and centriolar microtubules. Cell Motil. Cytoskeleton *64*, 489–495.

Liu, F., Rothblum-Oviatt, C., Ryan, C.E., and Piwnica-Worms, H. (1999). Overproduction of human Myt1 kinase induces a G2 cell cycle delay by interfering with the intracellular trafficking of Cdc2-cyclin B1 complexes. Mol. Cell. Biol. *19*, 5113–5123.

Liu, F., Stanton, J.J., Wu, Z., and Piwnica-Worms, H. (1997). The human Myt1 kinase preferentially phosphorylates Cdc2 on threonine 14 and localizes to the endoplasmic reticulum and Golgi complex. Mol. Cell. Biol. *17*, 571–583.

Loncarek, J., and Khodjakov, A. (2009). Ab ovo or de novo? Mechanisms of centriole duplication. Mol. Cells *27*, 135–142.

Loncarek, J., Hergert, P., Magidson, V., and Khodjakov, A. (2008). Control of daughter centriole formation by the pericentriolar material. Nat. Cell Biol. *10*, 322–328.

Lopes, C.A.M., Jana, S.C., Cunha-Ferreira, I., Zitouni, S., Bento, I., Duarte, P., Gilberto, S., Freixo, F., Guerrero, A., Francia, M., et al. (2015). PLK4 trans-Autoactivation Controls Centriole Biogenesis in Space. Developmental Cell *35*, 222–235.

Loppin, B., Dubruille, R., and Horard, B. (2015). The intimate genetics of Drosophila fertilization. Open Biol *5*, 150076.

Lowery, D.M., Lim, D., and Yaffe, M.B. (2005). Structure and function of Polo-like kinases. Oncogene *24*, 248–259.

Lucas, E.P., and Raff, J.W. (2007). Maintaining the proper connection between the centrioles and the pericentriolar matrix requires Drosophila centrosomin. J. Cell Biol. *178*, 725–732.

Lupas, A., Van Dyke, M., and Stock, J. (1991). Predicting coiled coils from protein sequences. Science *252*, 1162–1164.

Mahjoub, M.R., and Stearns, T. (2012). Supernumerary centrosomes nucleate extra cilia and compromise primary cilium signaling. Curr. Biol. *22*, 1628–1634.

Manandhar, G., Schatten, H., and Sutovsky, P. (2005). Centrosome reduction during gametogenesis and its significance. Biol. Reprod. *72*, 2–13.

Marina, M., and Saavedra, H.I. (2014). Nek2 and Plk4: prognostic markers, drivers of breast tumorigenesis and drug resistance. Front Biosci (Landmark Ed) *19*, 352–365.

Marshall, W.F. (2001). Centrioles take center stage. Current Biology *11*, R487–R496.

Marshall, W.F. (2015). How Cells Measure Length on Subcellular Scales. Trends Cell Biol. *25*, 760–768.

Marshall, W.F. (2016). Cell Geometry: How Cells Count and Measure Size. Annu Rev Biophys *45*, 49–64.

Marteil, G., Guerrero, A., Vieira, A.F., de Almeida, B.P., Machado, P., Mendonça, S., Mesquita, M., Villarreal, B., Fonseca, I., Francia, M.E., et al. (2018). Over-elongation of centrioles in cancer promotes centriole amplification and chromosome missegregation. Nature Communications *9*, 1258.

Martin, C.-A., Ahmad, I., Klingseisen, A., Hussain, M.S., Bicknell, L.S., Leitch, A., Nürnberg, G., Toliat, M.R., Murray, J.E., Hunt, D., et al. (2014). Mutations in PLK4, encoding a master regulator of centriole biogenesis, cause microcephaly, growth failure and retinopathy. Nat. Genet. *46*, 1283–1292.

Mason, J.M., Lin, D.C.-C., Wei, X., Che, Y., Yao, Y., Kiarash, R., Cescon, D.W., Fletcher, G.C., Awrey, D.E., Bray, M.R., et al. (2014). Functional characterization of CFI-400945, a Polo-like kinase 4 inhibitor, as a potential anticancer agent. Cancer Cell *26*, 163–176.

Matsumoto, Y., Hayashi, K., and Nishida, E. (1999). Cyclin-dependent kinase 2 (Cdk2) is required for centrosome duplication in mammalian cells. Current Biology *9*, 429–432.

Matsuura, K., Lefebvre, P.A., Kamiya, R., and Hirono, M. (2004). Bld10p, a novel protein essential for basal body assembly in Chlamydomonas: localization to the cartwheel, the first

ninefold symmetrical structure appearing during assembly. J. Cell Biol. *165*, 663–671.

McCleland, M.L., and O'Farrell, P.H. (2008). RNAi of mitotic cyclins in Drosophila uncouples the nuclear and centrosome cycle. Current Biology *18*, 245–254.

McCleland, M.L., Farrell, J.A., and O'Farrell, P.H. (2009). Influence of cyclin type and dose on mitotic entry and progression in the early Drosophila embryo. J. Cell Biol. *184*, 639–646.

McIntyre, R.E., Lakshminarasimhan Chavali, P., Ismail, O., Carragher, D.M., Sanchez-Andrade, G., Forment, J.V., Fu, B., Del Castillo Velasco-Herrera, M., Edwards, A., van der Weyden, L., et al. (2012). Disruption of mouse Cenpj, a regulator of centriole biogenesis, phenocopies Seckel syndrome. PLoS Genet. *8*, e1003022.

McLamarrah, T.A., Buster, D.W., Galletta, B.J., Boese, C.J., Ryniawec, J.M., Hollingsworth, N.A., Byrnes, A.E., Brownlee, C.W., Slep, K.C., Rusan, N.M., et al. (2018). An ordered pattern of Ana2 phosphorylation by Plk4 is required for centriole assembly. J. Cell Biol. *217*, 1217–1231.

Mennella, V., Keszthelyi, B., McDonald, K.L., Chhun, B., Kan, F., Rogers, G.C., Huang, B., and Agard, D.A. (2012). Subdiffraction-resolution fluorescence microscopy reveals a domain of the centrosome critical for pericentriolar material organization. Nat. Cell Biol. *14*, 1159–1168.

Mennella, V., Rogers, G.C., Rogers, S.L., Buster, D.W., Vale, R.D., and Sharp, D.J. (2005). Functionally distinct kinesin-13 family members cooperate to regulate microtubule dynamics during interphase. Nat. Cell Biol. *7*, 235–245.

Mennella, V., Tan, D.-Y., Buster, D.W., Asenjo, A.B., Rath, U., Ma, A., Sosa, H.J., and Sharp, D.J. (2009). Motor domain phosphorylation and regulation of the Drosophila kinesin 13, KLP10A. J. Cell Biol. *186*, 481–490.

Meraldi, P., Lukas, J., Fry, A.M., Bartek, J., and Nigg, E.A. (1999). Centrosome duplication in mammalian somatic cells requires E2F and Cdk2-cyclin A. Nat. Cell Biol. *1*, 88–93.

Meraldi, P. (2016). Centrosomes in spindle organization and chromosome segregation: a mechanistic view. Chromosome Res. *24*, 19–34.

Morgan, D.O. (1995). Principles of CDK regulation. Nature *374*, 131–134.

Moritz, M., Braunfeld, M.B., Fung, J.C., Sedat, J.W., Alberts, B.M., and Agard, D.A. (1995). Three-dimensional structural characterization of centrosomes from early Drosophila embryos. J. Cell Biol. *130*, 1149–1159.

Mottier-Pavie, V., and Megraw, T.L. (2009). Drosophila bld10 is a centriolar protein that regulates centriole, basal body, and motile cilium assembly. Mol. Biol. Cell *20*, 2605–2614.

Moyer, T.C., Clutario, K.M., Lambrus, B.G., Daggubati, V., and Holland, A.J. (2015). Binding of STIL to Plk4 activates kinase activity to promote centriole assembly. J. Cell Biol. *209*, 863–878.

Mueller, P.R., Coleman, T.R., Kumagai, A., and Dunphy, W.G. (1995). Myt1: a membrane-associated inhibitory kinase that phosphorylates Cdc2 on both threonine-14 and tyrosine-15. Science *270*, 86–90.

Nagase, T., Kikuno, R., Hattori, A., Kondo, Y., Okumura, K., and Ohara, O. (2000). Prediction of the coding sequences of unidentified human genes. XIX. The complete sequences of 100 new cDNA clones from brain which code for large proteins in vitro. DNA Res. *7*, 347–355.

Naveed, M., Kazmi, S.K., Amin, M., Asif, Z., Islam, U., Shahid, K., and Tehreem, S. (2018). Comprehensive review on the molecular genetics of autosomal recessive primary microcephaly (MCPH). Genet Res (Camb) *100*, e7.

Nigg, E.A., and Holland, A.J. (2018). Once and only once: mechanisms of centriole duplication and their deregulation in disease. Nature Publishing Group *19*, 297–312.

Nigg, E.A., and Raff, J.W. (2009). Centrioles, centrosomes, and cilia in health and disease. Cell *139*, 663–678.

Noguchi, T., Koizumi, M., and Hayashi, S. (2011). Sustained elongation of sperm tail promoted by local remodeling of giant mitochondria in Drosophila. Curr. Biol. *21*, 805–814.

Novak, Z.A., Conduit, P.T., Wainman, A., and Raff, J.W. (2014). Asterless licenses daughter centrioles to duplicate for the first time in Drosophila embryos. Curr. Biol. *24*, 1276–1282.

Novak, Z.A., Wainman, A., Gartenmann, L., and Raff, J.W. (2016). Cdk1 Phosphorylates Drosophila Sas-4 to Recruit Polo to Daughter Centrioles and Convert Them to Centrosomes. Developmental Cell *37*, 545–557.

Nurse, P., Thuriaux, P., and Nasmyth, K. (1976). Genetic control of the cell division cycle in the fission yeast Schizosaccharomyces pombe. Mol. Gen. Genet. *146*, 167–178.

O'Connell, K.F., Caron, C., Kopish, K.R., Hurd, D.D., Kemphues, K.J., Li, Y., and White, J.G. (2001). The C. elegans zyg-1 gene encodes a regulator of centrosome duplication with distinct maternal and paternal roles in the embryo. Cell *105*, 547–558.

O'Neill, R.S., Schoborg, T.A., and Rusan, N.M. (2018). Same but different: pleiotropy in centrosome-related microcephaly. Mol. Biol. Cell *29*, 241–246.

Oda, T., Chiba, S., Nagai, T., and Mizuno, K. (2014). Binding to Cep164, but not EB1, is essential for centriolar localization of TTBK2 and its function in ciliogenesis. Genes Cells *19*, 927–940.

Ohta, M., Ashikawa, T., Nozaki, Y., Kozuka-Hata, H., Goto, H., Inagaki, M., Oyama, M., and Kitagawa, D. (2014). Direct interaction of Plk4 with STIL ensures formation of a single procentriole per parental centriole. Nature Communications *5*, 5267.

Ohta, M., Watanabe, K., Ashikawa, T., Nozaki, Y., Yoshiba, S., Kimura, A., and Kitagawa, D. (2018). Bimodal Binding of STIL to Plk4 Controls Proper Centriole Copy Number. CellReports *23*, 3160–3169.e3164.

Ortega, S., Prieto, I., Odajima, J., Martín, A., Dubus, P., Sotillo, R., Barbero, J.L., Malumbres, M., and Barbacid, M. (2003). Cyclin-dependent kinase 2 is essential for meiosis but not for mitotic cell division in mice. Nat. Genet. *35*, 25–31.

Pagano, M., Pepperkok, R., Verde, F., Ansorge, W., and Draetta, G. (1992). Cyclin A is required at two points in the human cell cycle. Embo J. *11*, 961–971.

Pais-de-Azevedo, T., Magno, R., Duarte, I., and Palmeirim, I. (2018). Recent advances in understanding vertebrate segmentation. F1000Res *7*, 97.

Park, S.-Y., Park, J.-E., Kim, T.-S., Kim, J.H., Kwak, M.-J., Ku, B., Tian, L., Murugan, R.N., Ahn, M., Komiya, S., et al. (2014). Molecular basis for unidirectional scaffold switching of human Plk4 in centriole biogenesis. Nat. Struct. Mol. Biol. *21*, 696–703.

Patwardhan, D., Mani, S., Passemard, S., Gressens, P., and Ghouzzi, El, V. (2018). STIL balancing primary microcephaly and cancer. Cell Death and Disease *9*, 65.

Pavletich, N.P. (1999). Mechanisms of cyclin-dependent kinase regulation: structures of Cdks, their cyclin activators, and Cip and INK4 inhibitors. J. Mol. Biol. *287*, 821–828.

Peel, N., Stevens, N.R., Basto, R., and Raff, J.W. (2007). Overexpressing centriole-replication proteins in vivo induces centriole overduplication and de novo formation. Current Biology *17*, 834–843.

Pelletier, L., O'Toole, E., Schwager, A., Hyman, A.A., and Müller-Reichert, T. (2006). Centriole assembly in Caenorhabditis elegans. Nature *444*, 619–623.

Pelletier, L., Ozlü, N., Hannak, E., Cowan, C., Habermann, B., Ruer, M., Müller-Reichert, T., and Hyman, A.A. (2004). The Caenorhabditis elegans centrosomal protein SPD-2 is required for both pericentriolar material recruitment and centriole duplication. Current Biology *14*, 863–873.

Pezuk, J.A., Brassesco, M.S., de Oliveira, R.S., Machado, H.R., Neder, L., Scrideli, C.A., and Tone, L.G. (2017). PLK1-associated microRNAs are correlated with pediatric medulloblastoma prognosis. Childs Nerv Syst *33*, 609–615.

Preble, A.M., Giddings, T.M., and Dutcher, S.K. (2000). Basal bodies and centrioles: their function and structure. Curr. Top. Dev. Biol. *49*, 207–233.

Price, D., Rabinovitch, S., O'Farrell, P.H., and Campbell, S.D. (2000). Drosophila wee1 has an essential role in the nuclear divisions of early embryogenesis. Genetics *155*, 159–166.

Price, D.M., Jin, Z., Rabinovitch, S., and Campbell, S.D. (2002). Ectopic expression of the Drosophila Cdk1 inhibitory kinases, Wee1 and Myt1, interferes with the second mitotic wave and disrupts pattern formation during eye development. Genetics *161*, 721–731.

Qiao, R., Cabral, G., Lettman, M.M., Dammermann, A., and Dong, G. (2012). SAS-6 coiled-coil structure and interaction with SAS-5 suggest a regulatory mechanism in C. elegans centriole assembly. Embo J. *31*, 4334–4347.

Rabinowicz, N., Mangala, L.S., Brown, K.R., Checa-Rodriguez, C., Castiel, A., Moskovich, O., Zarfati, G., Trakhtenbrot, L., Levy-Barda, A., Jiang, D., et al. (2017). Targeting the centriolar replication factor STIL synergizes with DNA damaging agents for treatment of ovarian cancer. Oncotarget *8*, 27380–27392.

Radford, S.J., Harrison, A.M., and McKim, K.S. (2012). Microtubule-depolymerizing kinesin KLP10A restricts the length of the acentrosomal meiotic spindle in Drosophila females. Genetics *192*, 431–440.

Raff, J.W., and Basto, R. (2017). Centrosome Amplification and Cancer: A Question of Sufficiency. Developmental Cell *40*, 217–218.

Ramaswamy, S., Ross, K.N., Lander, E.S., and Golub, T.R. (2003). A molecular signature of metastasis in primary solid tumors. Nat. Genet. *33*, 49–54.

Reber, A., Lehner, C.F., and Jacobs, H.W. (2006). Terminal mitoses require negative regulation of Fzr/Cdh1 by Cyclin A, preventing premature degradation of mitotic cyclins and String/Cdc25. Development *133*, 3201–3211.

Reed, S.I. (1997). Control of the G1/S transition. Cancer Surv. *29*, 7–23.

Rezabkova, L., Kraatz, S.H.W., Akhmanova, A., Steinmetz, M.O., and Kammerer, R.A. (2016). Biophysical and Structural Characterization of the Centriolar Protein Cep104 Interaction Network. J. Biol. Chem. *291*, 18496–18504.

Richens, J.H., Barros, T.P., Lucas, E.P., Peel, N., Pinto, D.M.S., Wainman, A., and Raff, J.W. (2015). The Drosophila Pericentrin-like-protein (PLP) cooperates with Cnn to maintain the integrity of the outer PCM. Biol Open *4*, 1052–1061.

Rodrigues-Martins, A., Bettencourt-Dias, M., Riparbelli, M., Ferreira, C., Ferreira, I., Callaini, G., and Glover, D.M. (2007). DSAS-6 organizes a tube-like centriole precursor, and its absence suggests modularity in centriole assembly. Current Biology *17*, 1465–1472.

Rogala, K.B., Dynes, N.J., Hatzopoulos, G.N., Yan, J., Pong, S.K., Robinson, C.V., Deane, C.M., Gönczy, P., and Vakonakis, I. (2015). The Caenorhabditis elegans protein SAS-5 forms large oligomeric assemblies critical for centriole formation. Elife *4*, e07410.

Rogers, G.C., Rogers, S.L., Schwimmer, T.A., Ems-McClung, S.C., Walczak, C.E., Vale, R.D., Scholey, J.M., and Sharp, D.J. (2004). Two mitotic kinesins cooperate to drive sister chromatid separation during anaphase. Nature *427*, 364–370.

Rogers, G.C., Rusan, N.M., Roberts, D.M., Peifer, M., and Rogers, S.L. (2009). The SCF Slimb ubiquitin ligase regulates Plk4/Sak levels to block centriole reduplication. J. Cell Biol. *184*, 225–239.

Roque, H., Saurya, S., Pratt, M.B., Johnson, E., and Raff, J.W. (2018). Drosophila PLP assembles pericentriolar clouds that promote centriole stability, cohesion and MT nucleation. PLoS Genet. *14*, e1007198.

Roque, H., Wainman, A., Richens, J., Kozyrska, K., Franz, A., and Raff, J.W. (2012). Drosophila Cep135/Bld10 maintains proper centriole structure but is dispensable for cartwheel formation. J. Cell. Sci. *125*, 5881–5886.

Rørth, P. (1998). Gal4 in the Drosophila female germline. Mechanisms of Development *78*, 113–118.

Satish Tammana, T.V., Tammana, D., Diener, D.R., and Rosenbaum, J. (2013). Centrosomal protein CEP104 (Chlamydomonas FAP256) moves to the ciliary tip during ciliary assembly. J. Cell. Sci. *126*, 5018–5029.

Saurya, S., Roque, H., Novak, Z.A., Wainman, A., Aydogan, M.G., Volanakis, A., Sieber, B., Pinto, D.M.S., and Raff, J.W. (2016). Drosophila Ana1 is required for centrosome assembly and centriole elongation. J. Cell. Sci. *129*, 2514–2525.

Schatten, H., and Sun, Q.-Y. (2015). Centrosome and microtubule functions and dysfunctions in meiosis: implications for age-related infertility and developmental disorders. Reprod. Fertil. Dev. *27*, 934–943.

Schmidt, T.I., Kleylein-Sohn, J., Westendorf, J., Le Clech, M., Lavoie, S.B., Stierhof, Y.-D., and Nigg, E.A. (2009). Control of centriole length by CPAP and CP110. Curr. Biol. *19*, 1005–1011.

Seo, M.Y., and Rhee, K. (2018). Caspase-mediated cleavage of the centrosomal proteins during apoptosis. Cell Death and Disease *9*, 571.

Sha, Y.-W., Xu, X., Mei, L.-B., Li, P., Su, Z.-Y., He, X.-Q., and Li, L. (2017). A homozygous CEP135 mutation is associated with multiple morphological abnormalities of the sperm flagella (MMAF). Gene *633*, 48–53.

Shaheen, R., Tala, Al, S., Almoisheer, A., and Alkuraya, F.S. (2014). Mutation in PLK4, encoding a master regulator of centriole formation, defines a novel locus for primordial dwarfism. J. Med. Genet. *51*, 814–816.

Sharma, A., Aher, A., Dynes, N.J., Frey, D., Katrukha, E.A., Jaussi, R., Grigoriev, I., Croisier, M., Kammerer, R.A., Akhmanova, A., et al. (2016). Centriolar CPAP/SAS-4 Imparts Slow Processive Microtubule Growth. Developmental Cell *37*, 362–376.

Shimanovskaya, E., Qiao, R., Lesigang, J., and Dong, G. (2013). The SAS-5 N-terminal domain is a tetramer, with implications for centriole assembly in C. elegans. Worm *2*, e25214.

Shimanovskaya, E., Viscardi, V., Lesigang, J., Lettman, M.M., Qiao, R., Svergun, D.I., Round, A., Oegema, K., and Dong, G. (2014). Structure of the C. elegans ZYG-1 cryptic polo box suggests a conserved mechanism for centriolar docking of Plk4 kinases. Structure *22*, 1090–1104.

Shukla, A., Kong, D., Sharma, M., Magidson, V., and Loncarek, J. (2015). Plk1 relieves centriole block to reduplication by promoting daughter centriole maturation. Nature Communications *6*, 8077.

Sibon, O.C., Stevenson, V.A., and Theurkauf, W.E. (1997). DNA-replication checkpoint control at the Drosophila midblastula transition. Nature *388*, 93–97.

Silkworth, W.T., Nardi, I.K., Scholl, L.M., and Cimini, D. (2009). Multipolar spindle pole coalescence is a major source of kinetochore mis-attachment and chromosome mis-segregation in cancer cells. PLoS ONE *4*, e6564.

Sillibourne, J.E., Tack, F., Vloemans, N., Boeckx, A., Thambirajah, S., Bonnet, P., Ramaekers, F.C.S., Bornens, M., and Grand-Perret, T. (2010). Autophosphorylation of polo-like kinase 4 and its role in centriole duplication. Mol. Biol. Cell *21*, 547–561.

Singh, P., Ramdas Nair, A., and Cabernard, C. (2014). The Centriolar Protein Bld10/Cep135 Is Required to Establish Centrosome Asymmetry in Drosophila Neuroblasts. Current Biology *24*, 1548–1555.

Slevin, L.K., Nye, J., Pinkerton, D.C., Buster, D.W., Rogers, G.C., and Slep, K.C. (2012). The structure of the plk4 cryptic polo box reveals two tandem polo boxes required for centriole duplication. Structure *20*, 1905–1917.

Slevin, L.K., Romes, E.M., Dandulakis, M.G., and Slep, K.C. (2014). The mechanism of dynein light chain LC8-mediated oligomerization of the Ana2 centriole duplication factor. J. Biol. Chem. *289*, 20727–20739.

Song, R., Walentek, P., Sponer, N., Klimke, A., Lee, J.S., Dixon, G., Harland, R., Wan, Y., Lishko, P., Lize, M., et al. (2014). miR-34/449 miRNAs are required for motile ciliogenesis by repressing cp110. Nature *510*, 115–120.

Sonnen, K.F., Gabryjonczyk, A.-M., Anselm, E., Stierhof, Y.-D., and Nigg, E.A. (2013). Human Cep192 and Cep152 cooperate in Plk4 recruitment and centriole duplication. J. Cell. Sci. *126*, 3223–3233.

Sonnen, K.F., Schermelleh, L., Leonhardt, H., and Nigg, E.A. (2012). 3D-structured illumination microscopy provides novel insight into architecture of human centrosomes. Biol Open *1*, 965–976.

Spektor, A., Tsang, W.Y., Khoo, D., and Dynlacht, B.D. (2007). Cep97 and CP110 suppress a cilia assembly program. Cell *130*, 678–690.

Sredni, S.T., and Tomita, T. (2017). The polo-like kinase 4 gene (PLK4) is overexpressed in pediatric medulloblastoma. Childs Nerv Syst *33*, 1031–1031.

Stern, B., Ried, G., Clegg, N.J., Grigliatti, T.A., and Lehner, C.F. (1993). Genetic analysis of

the Drosophila cdc2 homolog. Development *117*, 219–232.

Stetina, Von, J.R., and Orr-Weaver, T.L. (2011). Developmental control of oocyte maturation and egg activation in metazoan models. Cold Spring Harb Perspect Biol *3*, a005553–a005553.

Stevens, N.R., Dobbelaere, J., Brunk, K., Franz, A., and Raff, J.W. (2010a). Drosophila Ana2 is a conserved centriole duplication factor. J. Cell Biol. *188*, 313–323.

Stevens, N.R., Dobbelaere, J., Wainman, A., Gergely, F., and Raff, J.W. (2009). Ana3 is a conserved protein required for the structural integrity of centrioles and basal bodies. J. Cell Biol. *187*, 355–363.

Stevens, N.R., Roque, H., and Raff, J.W. (2010b). DSas-6 and Ana2 coassemble into tubules to promote centriole duplication and engagement. Developmental Cell *19*, 913–919.

Strnad, P., and Gönczy, P. (2008). Mechanisms of procentriole formation. Trends Cell Biol. *18*, 389–396.

Strnad, P., Leidel, S., Vinogradova, T., Euteneuer, U., Khodjakov, A., and Gönczy, P. (2007). Regulated HsSAS-6 levels ensure formation of a single procentriole per centriole during the centrosome duplication cycle. Developmental Cell *13*, 203–213.

Sugioka, K., Hamill, D.R., Lowry, J.B., McNeely, M.E., Enrick, M., Richter, A.C., Kiebler, L.E., Priess, J.R., and Bowerman, B. (2017). Centriolar SAS-7 acts upstream of SPD-2 to regulate centriole assembly and pericentriolar material formation. Elife *6*, 555.

Tan, C.H., Gasic, I., Huber-Reggi, S.P., Dudka, D., Barisic, M., Maiato, H., and Meraldi, P. (2015). The equatorial position of the metaphase plate ensures symmetric cell divisions. Elife *4*, 731.

Tang, C.-J.C., Fu, R.-H., Wu, K.-S., Hsu, W.-B., and Tang, T.K. (2009). CPAP is a cell-cycle regulated protein that controls centriole length. Nat. Cell Biol. *11*, 825–831.

Tang, C.-J.C., Lin, S.-Y., Hsu, W.-B., Lin, Y.-N., Wu, C.-T., Lin, Y.-C., Chang, C.-W., Wu, K.-S., and Tang, T.K. (2011). The human microcephaly protein STIL interacts with CPAP and is required for procentriole formation. Embo J. *30*, 4790–4804.

Thauvin-Robinet, C., Lee, J.S., Lopez, E., Herranz-Pérez, V., Shida, T., Franco, B., Jego, L., Ye, F., Pasquier, L., Loget, P., et al. (2014). The oral-facial-digital syndrome gene C2CD3 encodes a positive regulator of centriole elongation. Nat. Genet. *46*, 905–911.

Timofeev, O., Cizmecioglu, O., Settele, F., Kempf, T., and Hoffmann, I. (2010). Cdc25 phosphatases are required for timely assembly of CDK1-cyclin B at the G2/M transition. J. Biol. Chem. *285*, 16978–16990.

Tinevez, J.-Y., Perry, N., Schindelin, J., Hoopes, G.M., Reynolds, G.D., Laplantine, E., Bednarek, S.Y., Shorte, S.L., and Eliceiri, K.W. (2017). TrackMate: An open and extensible platform for single-particle tracking. Methods *115*, 80–90.

Tobel, von, L., Mikeladze-Dvali, T., Delattre, M., Balestra, F.R., Blanchoud, S., Finger, S., Knott, G., Müller-Reichert, T., and Gönczy, P. (2014). SAS-1 is a C2 domain protein critical for centriole integrity in C. elegans. PLoS Genet. *10*, e1004777.

Tsang, W.Y., and Dynlacht, B.D. (2013). CP110 and its network of partners coordinately regulate cilia assembly. Cilia *2*, 9.

Tsuchiya, Y., Yoshiba, S., Gupta, A., Watanabe, K., and Kitagawa, D. (2016). Cep295 is a

conserved scaffold protein required for generation of a bona fide mother centriole. Nature Communications *7*, 12567.

Uzbekov, R., and Alieva, I. (2018). Who are you, subdistal appendages of centriole? Open Biol *8*, 180062.

Uzbekov, R., and Prigent, C. (2007). Clockwise or anticlockwise? Turning the centriole triplets in the right direction! FEBS Letters *581*, 1251–1254.

van Breugel, M., Hirono, M., Andreeva, A., Yanagisawa, H.-A., Yamaguchi, S., Nakazawa, Y., Morgner, N., Petrovich, M., Ebong, I.-O., Robinson, C.V., et al. (2011). Structures of SAS-6 suggest its organization in centrioles. Science *331*, 1196–1199.

van Breugel, M., Wilcken, R., McLaughlin, S.H., Rutherford, T.J., and Johnson, C.M. (2014). Structure of the SAS-6 cartwheel hub from Leishmania major. Elife *3*, e01812.

Varmark, H., Llamazares, S., Rebollo, E., Lange, B., Reina, J., Schwarz, H., and Gonzalez, C. (2007). Asterless is a centriolar protein required for centrosome function and embryo development in Drosophila. Current Biology *17*, 1735–1745.

Venoux, M., Tait, X., Hames, R.S., Straatman, K.R., Woodland, H.R., and Fry, A.M. (2013). Poc1A and Poc1B act together in human cells to ensure centriole integrity. J. Cell. Sci. *126*, 163–175.

Vieillard, J., Paschaki, M., Duteyrat, J.-L., Augière, C., Cortier, E., Lapart, J.-A., Thomas, J., and Durand, B. (2016). Transition zone assembly and its contribution to axoneme formation in Drosophila male germ cells. J. Cell Biol. *214*, 875–889.

Villeneuve, J., Scarpa, M., Ortega-Bellido, M., and Malhotra, V. (2013). MEK1 inactivates Myt1 to regulate Golgi membrane fragmentation and mitotic entry in mammalian cells. Embo J. *32*, 72–85.

Vorobjev, I.A., and Chentsov YuS (1982). Centrioles in the cell cycle. I. Epithelial cells. J. Cell Biol. *93*, 938–949.

Vorobjev, I.A., and Chentsov, Y.S. (1980). The ultrastructure of centriole in mammalian tissue culture cells. Cell Biol. Int. Rep. *4*, 1037–1044.

Warn, R.M., Magrath, R., and Webb, S. (1984). Distribution of F-actin during cleavage of the Drosophila syncytial blastoderm. J. Cell Biol. *98*, 156–162.

Wheway, G., Nazlamova, L., and Hancock, J.T. (2018). Signaling through the Primary Cilium. Front Cell Dev Biol *6*, 8.

Wilson, P.G., Zheng, Y., Oakley, C.E., Oakley, B.R., Borisy, G.G., and Fuller, M.T. (1997). Differential expression of two gamma-tubulin isoforms during gametogenesis and development in Drosophila. Developmental Biology *184*, 207–221.

Winey, M., and O'Toole, E. (2014). Centriole structure. Philos. Trans. R. Soc. Lond., B, Biol. Sci. *369*, 20130457–20130457.

Yadav, S.P., Sharma, N.K., Liu, C., Dong, L., Li, T., and Swaroop, A. (2016). Centrosomal protein CP110 controls maturation of the mother centriole during cilia biogenesis. Development *143*, 1491–1501.

Yuan, K., and O'Farrell, P.H. (2015). Cyclin B3 is a mitotic cyclin that promotes the metaphase-anaphase transition. Curr. Biol. *25*, 811–816.

Zheng, X., Gooi, L.M., Wason, A., Gabriel, E., Mehrjardi, N.Z., Yang, Q., Zhang, X., Debec, A., Basiri, M.L., Avidor-Reiss, T., et al. (2014). Conserved TCP domain of Sas-4/CPAP is essential for pericentriolar material tethering during centrosome biogenesis. Proc. Natl. Acad. Sci. U.S.a. *111*, E354–E363.

Zheng, X., Ramani, A., Soni, K., Gottardo, M., Zheng, S., Ming Gooi, L., Li, W., Feng, S., Mariappan, A., Wason, A., et al. (2016). Molecular basis for CPAP-tubulin interaction in controlling centriolar and ciliary length. Nature Communications *7*, 11874.

Zitouni, S., Francia, M.E., Leal, F., Montenegro Gouveia, S., Nabais, C., Duarte, P., Gilberto, S., Brito, D., Moyer, T., Kandels-Lewis, S., et al. (2016). CDK1 Prevents Unscheduled PLK4-STIL Complex Assembly in Centriole Biogenesis. Curr. Biol. *26*, 1127–1137.